

Transactions

of the

ASME

A New High-Yield-Strength Alloy Steel for Welded Structures	269
. <i>L. C. Bibber, J. M. Hodge, R. C. Altman, and W. D. Doty</i>	
Fatigue Tests of Piping Components	287
. <i>A. R. C. Marhl</i>	
Analysis of Some Corrosion Problems in Petroleum Refineries.	305
. <i>J. F. Mason, Jr.</i>	
Stresses in a Pressure Vessel With a Conical Head	315
. <i>G. W. Watts and H. A. Lang</i>	
Recommended Practices for the Cleaning of Turbine Lubricating Systems After Service	327
Line-Reversal Techniques in the Determination of Temperature of Gun Flash or Other Rapid Transient Phenomena	333
. <i>J. T. Agnew</i>	
Distribution of Heat-Transfer Coefficients Around Circular Cylinders in Crossflow at Reynolds Numbers From 20 to 500	343
. <i>E. R. G. Eckert and E. Soehngen</i>	
Peculiar Behavior of Steel Beams Under Dead Loads That Produce Inelastic Strains	349
. <i>H. T. Corten, M. E. Clark, and O. M. Sidebottom</i>	
An Experimental Investigation of Over-Straining in Mild-Steel Thick-Walled Cylinders by Internal Fluid Pressure	355
. <i>M. C. Steele and John Young</i>	
Dynamic Properties of Nodular Cast Iron—Part 1.	365
. <i>Harry Majors, Jr.</i>	
Relaxation of Stress in a Heat-Exchanger Tube of Ideal Material	381
. <i>E. A. Davis</i>	
Notes on a Theoretical Basis for Design of Tube Sheets of Triangular Layout	387
. <i>J. I. Malkin</i>	
Analysis of Stresses and Displacements in Heat-Exchanger Expansion Joints	397
. <i>Glenn Murphy</i>	
Strain-Hardening and Softening With Time in Reference to Creep and Relaxation in Metals	403
. <i>A. Nadai</i>	
Automatic Flight Control—Analysis and Synthesis of Lateral-Control Problem	415
. <i>R. N. Broto</i>	

APRIL, 1952

VOL. 74, No. 3

Transactions

of The American Society of Mechanical Engineers

Published on the tenth of every month, except March, June, September, and December

OFFICERS OF THE SOCIETY:

R. J. S. PEDOTT, *President*

JOSEPH L. KOFF, *Treasurer*

BIGGS J. KATZ, *Asst. Treasurer*

C. E. DAVIES, *Secretary*

COMMITTEE ON PUBLICATIONS:

C. B. CAMPBELL, *Chairman*

GEORGE R. RICH

PAUL T. NORDEN, JR.

OTTO DE LORENZO

COLIN CAMERON

MORRIS GEAR } *Junior Advisory Members*
JOSEPH SCHMIDLER }

GEORGE A. STETSON, *Editor*

K. W. CAMDENHORN, *Managing Editor*

REGIONAL ADVISORY BOARD OF THE PUBLICATIONS COMMITTEE:

KERR AYERHEDD—I

J. DE S. COOTNER—II

W. H. RAE—III

F. C. SMITH—IV

HENDLEY BLACKMON—V

CHAS. R. BAILEY—VI

R. G. ROMOND—VII

M. A. DURLAND—VIII

Published monthly by The American Society of Mechanical Engineers. Publication office at 20th and Northampton Streets, Easton, Pa. The editorial department is located at the headquarters of the Society, 39 West Thirty-Ninth Street, New York 18, N. Y. Cable address, "Dynamic," New York. Price \$1.50 a copy, \$12.00 a year for Transactions and the *Journal of Applied Mechanics* to members and affiliates, \$1.00 a copy, \$6.00 a year. Changes of address must be received at Society headquarters four weeks before they are to be effective on the mailing list. Please send old as well as new address. . . . By-Laws: The Society shall not be responsible for statements or opinions advanced in papers or . . . printed in its publications (B13, Par. 2). . . . Entered as second-class matter March 2, 1928, at the Post Office at Easton, Pa., under the Act of August 24, 1912. . . . Copyrighted, 1952, by The American Society of Mechanical Engineers. Reprints from this publication may be made on condition that full credit be given the Transactions of the ASME and the author, and that date of publication be noted.

A New High-Yield-Strength Alloy Steel for Welded Structures

By L. C. BIBBER,¹ J. M. HODGE,¹ R. C. ALTMAN,² AND W. D. DOTY,¹ PITTSBURGH, PA.

This paper concerns a new kind of steel, its development, its metallurgical characteristics, its welding and gas-cutting characteristics, its low-temperature toughness, its applications, and its engineering potentialities. This steel was developed by the United States Steel Company to offer to industry a plate steel having a unique combination of properties, such as a far higher strength than has hitherto been available, superior toughness, and good weldability. As will be evident from the test results which will be described in detail, these rather formidable goals have been achieved. This new USS "Carilloy" steel has been designated "T-1." It is characterized by yield-strength levels of 100,000 psi and above. At these high strengths it retains its toughness to much lower temperatures than ordinary structural steels. In addition, welds which develop the full strength of the base metal can be made in T-1 steel without preheating or postheating.

METALLURGICAL CONSIDERATIONS

THE most important metallurgical characteristics of USS Carilloy T-1 steel are its microstructure and its carbon content. The microstructure is tempered martensite, and the carbon content is low, less than 0.20 per cent. The superiority of this steel in strength, weldability, and toughness is largely a reflection of these two factors.

Tempered martensitic microstructures are characteristically tough; that is, they are highly resistant to brittle behavior under adverse conditions. This toughness is furthermore most pronounced at low carbon levels. Tempered martensite also permits the attainment of higher strength levels with this low carbon content than would be possible with any other microstructure. The low carbon content is essential for good weldability, and in addition, permits the use of water-quenching to obtain the martensitic structure without danger of cracking.

Thus, in the development of this composition, the first consideration was hardenability in relation to the attainment of a microstructure having at least 95 per cent martensite on water-quenching. The alloying elements employed to obtain this hardenability are manganese, nickel, chromium, molybdenum, and boron. This last element, boron, is particularly effective at the low carbon level of this steel, and permits using relatively small percentages of the other alloying elements which are less available and more expensive. For example, at present the composition contains less than 1 per cent of nickel, manganese, or chromium, and the molybdenum is between 0.4 to 0.6 per cent.

In the laboratory research and development work on this steel the hardenabilities of a wide variety of compositions involving variations in manganese, silicon, nickel, chromium, molybdenum,

and boron were measured. It was found possible to arrive at multiplying factors expressing the individual hardenability effects of each of these elements. These factors then could be used to predict the hardenability of any combination of these elements at the 0.20 per cent carbon level in terms of a microstructure of 95 per cent martensite. The correlation between these calculated hardenability values and the actual measured hardenability values of a large number of steels of this type was found to be excellent. The final composition was then determined by selecting that combination of elements which would give a hardenability sufficient to permit the attainment of a 95 per cent martensitic microstructure in plate thicknesses of 2 in. on water-quenching. Also, those alloying elements least available or most expensive were held to a minimum.

Throughout the development of this steel, the emphasis has been on toughness. To obtain maximum toughness it has been the practice to temper at as high a temperature as possible without exceeding the lower critical temperature. In order to minimize the loss in strength at these high tempering temperatures, a small amount of vanadium has been incorporated into the composition. This element retards the rate of tempering at high temperatures, thus maintaining the high-yield-strength characteristic of this steel.

The high toughness of this steel is extremely important in that it minimizes the likelihood that brittle behavior will occur under such adverse conditions as (1) stress concentrations at notches, sharp angles, or abrupt changes in section; (2) rapid rates of loading; or (3) low temperatures. Such brittle behavior in service is characterized by failure with almost no manifestation of ductility. One method of evaluating the resistance of steel to this type of behavior is the Charpy (keyhole) impact test carried out over a range of temperatures. This was the type of test used in the development of T-1 steel.

When Charpy keyhole impact specimens are tested at various temperatures, a temperature range is found at which the performance changes from reasonably tough behavior, with considerable energy absorption, to extremely brittle behavior with very low energy absorption. At a given temperature within this range, considerable scatter in energy absorption occurs, some specimens showing high impact values and some low values, with generally very few specimens breaking at intermediate levels. The temperature at the middle of this "scatter band" is known as the "ductility transition temperature" and is the criterion of toughness which is used in evaluating the toughness of this new material. This ductility transition temperature thus is the temperature below which fracture will occur with very little ductility and at low energy levels under the conditions of this test.

The ductility transition temperature furnishes a quantitative evaluation of the effect of temperature under these particular conditions of notch severity and rate of loading, and a qualitative indication of the resistance to brittle behavior under adverse conditions in general. Decreasing temperature of testing is known to have qualitatively the same effect as increasing the rate of loading, increasing the severity of the notch, or intensifying the stress concentration.

In studies of brittle failures of ship plates a relationship has been found between the behavior at low energy levels in the Charpy

¹ Research and Development, United States Steel Company.

² Metallurgical Division, United States Steel Company.

Presented at the Petroleum Mechanical Engineering Conference, Tulsa, Okla., September 24-26, 1951, of THE AMERICAN SOCIETY OF MECHANICAL ENGINEERS.

NOTE: Statements and opinions advanced in papers are to be understood as individual expressions of their authors and not those of the Society. Manuscript received at ASME Headquarters, July 6, 1951. Paper No. 51-PET-5.

impact test and the susceptibility to brittle failure in service. Furthermore, these service failures have occurred with almost no manifestations of ductility. The authors therefore feel that the ductility transition temperature is a very significant evaluation of toughness in relation to performance in service. Other types of ductility transition-temperature measurements will be described in the section on welding.

A typical Charpy (keyhole) performance curve for a commercial plate of T-1 steel is shown in Fig. 1. The relatively high room-temperature values, the small decrease in these values as

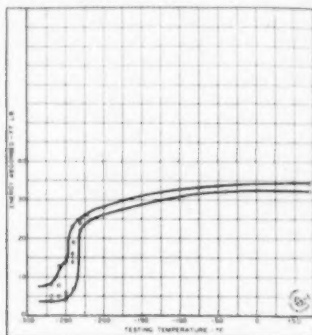


FIG. 1 TYPICAL CHARPY (KEYHOLE) TRANSITION-TEMPERATURE CURVE FOR A COMMERCIAL PLATE OF CARILLO T-1 STEEL

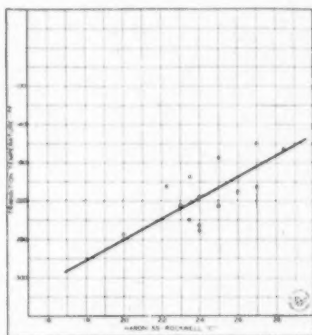


FIG. 2 CHARPY (KEYHOLE) TRANSITION TEMPERATURE VERSUS HARDNESS FOR COMMERCIAL HEATS OF CARILLO T-1 STEEL

the temperature is lowered, and the very low temperature of the scatter band at the ductility transition temperature are all characteristic of T-1 steel, and all serve to emphasize its remarkable toughness.

In the research and development work on this composition such transition-temperature determinations were made on samples rolled from laboratory heats incorporating variations in manganese from 0.20 to 1.50 per cent, in nickel from 0.50 to 2.50 per cent, and smaller variations in silicon, chromium, molybdenum, vanadium, and boron. It was found that in all cases in which the as-quenched microstructures were at least 95 per cent martensite, the transition temperatures varied only with hardness and were not a function of alloy content. The transition tem-

peratures, of course, were lower with the steels of lower hardness, but all transition temperatures were below -200°F .

The toughness has likewise been evaluated by transition-temperature measurements on heat-treated plates from many production heats. Transition temperatures of these plates are shown as a function of hardness in Fig. 2. It will be noted that the transition temperatures range between -150 and -250°F , depending upon the hardness. Such low transition temperatures should minimize the likelihood that this material will behave in a brittle manner in any but the most severe of service applications.

Since the high strength of T-1 steel will permit the use of lighter plates in many applications, resistance to atmospheric corrosion is important. Accordingly, about 0.30 per cent of copper has been included in the composition to augment the resistance of T-1 steel to atmospheric corrosion.

As a result of the development work described in the foregoing, it has been established that T-1 steel can be furnished to the mechanical properties given in Table 1.

TABLE 1 MECHANICAL PROPERTIES OF T-1 STEEL

	Thickness 1/4 in. to 2 in., incl.	Over 2 in. to 4 in., incl.	Over 4 in. to 6 in., incl.
Yield strength, 0.2 per cent offset (min), psi	100000	90000	90000
Tensile strength (min), psi	115000	105000	105000
Elongation in 2 in., per cent (min)	18	17	16
Reduction of area, per cent (min)	55	50	43
Cold bend	1/4 in. to 1 1/2 in. incl.	Over 1 1/2 in. to 2 in. incl.	Over 2 in. to 6 in. incl.
	180° D = 1/2	180° D = 2	180° D = 3

NOTE: Testing in accord with ASTM recommended practices.

WELDING AND GAS-CUTTING CHARACTERISTICS

The use of steels with yield strengths higher than 50,000 psi has heretofore been restricted by the special precautions, such as preheat, the use of austenitic electrodes, and post-heat-treatment, often required for the welding of such materials. Preheating is a very desirable practice in connection with welding. In some instances preheating is religiously carried out; in others, particularly in the case of field welding, the inspection necessary to insure the proper use of preheat is difficult, if not impossible. When austenitic electrodes are used to weld high-yield-strength alloy steels, joints of only 65-75 per cent efficiency are obtained. Also, repairs to such welds are very costly and difficult to make.

Recently new high-strength ferritic electrodes capable of making welds which can develop the yield and ultimate strengths of the quenched and tempered base metal have become available. Such electrodes, and the weld metals they deposit, will be discussed in detail in a later section.

Let us consider for the present the testing to determine the effect of manual metal-arc welding on the properties and characteristics of T-1 steel. The tensile properties of the particular steel tested are given in Table 2.

Many types of joinability and performance tests were carried out, as follows:

- 1 Underbead cracking test.
- 2 Kinzel-type bead-weld notch-bend test.
- 3 Tee-bend test.
- 4 Transverse butt-weld tensile test.
- 5 Longitudinal butt-weld tensile test.
- 6 Fillet-weld tensile test.
- 7 Butt-weld bend test.

Underbead Cracking Test. Underbead cracking tests were made on the new steel to determine its susceptibility to cracking during fabrication. For this test, bead-cracking specimens, as

TABLE 2 TENSILE PROPERTIES OF STEELS TESTED: AVERAGE OF THREE TESTS

Plate thickness, in.	Condition	Orientation of specimen	Yield strength (0.2% offset), psi	Tensile strength, psi	Elong. in 2 in., per cent	Elong. in 8 in., per cent	Reduction in area, per cent
1/2	Quenched and tempered ^a	Long.	112300	119800	31.3	13.1	56.1
1	Quenched and tempered ^a	Long.	118000	125000	39.7	14.8	59.6

^a Quenched in water from 1700 F, tempered at 1200 F.

shown in Fig. 3, were made from 1-in. plates. Using the conditions given in Fig. 3, welds were deposited at each of three temperatures, 0 F, 70 F, and 212 F. These temperatures are those of the specimens before welding and of the bath in which the specimens are partially immersed during and after welding. The cooling media used were as follows:

Temperature, deg F	Medium
0.....	Ethylene glycol and dry ice
70.....	Water
212.....	Water

In this particular test two kinds of electrodes were used, the ordinary mild-steel E6010 electrode, and the E12015. These numbers are ASTM-AWS electrode classifications. The first two or three digits show the strength of the deposited metal and the last two indicate the operating characteristics of the rod. The cellulose coating on the E6010 electrodes breaks down in the heat of the arc to form considerable quantities of hydrogen. The mineral coating on E12015 electrodes, on the other hand, contains a minimum of organic substances and hence evolves very little hydrogen. It has been shown² that when using the E6010 electrodes, some of the hydrogen evolved is absorbed by the base metal immediately beneath the weld, and upon cooling, the base metal, particularly the harder metals, will crack. The deposition of a small bead at high speed results in such drastic cooling rates that even ordinary low-carbon steel may crack. In evaluating the susceptibility of a steel to cracking, it is necessary to use such welding conditions, because only by causing

² "Cold Cracking in the Heat Affected Zone," by C. B. Voldrich, *The Welding Journal*, vol. 26, 1947, pp. 153-8-169-8.

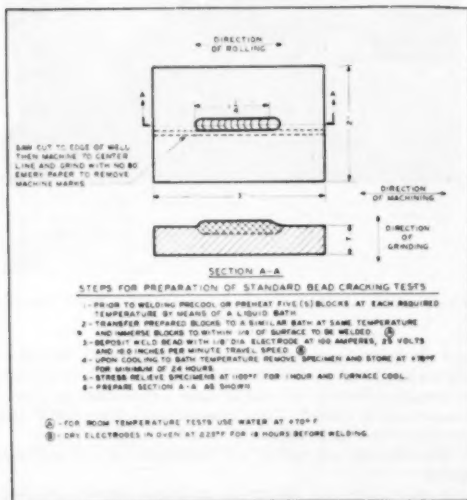


FIG. 3 STANDARD BEAD-CRACKING TEST

cracking can the degree of cracking be determined. Although the welding conditions are perhaps more drastic than those used for the average weld in actual practice, they are still within the range of conditions encountered in production welding, particularly tack-welding.

The appearance of a typical bead-cracking specimen from 1-in. plate welded with an E6010 electrode is shown in Fig. 4. The

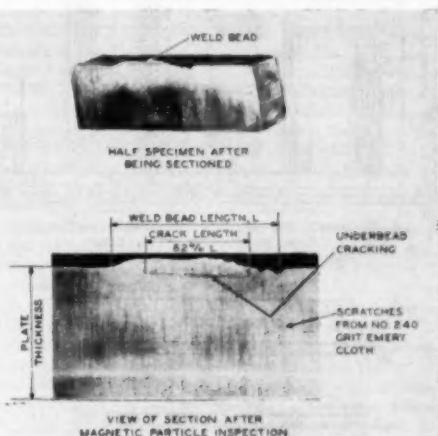


FIG. 4 TYPICAL UNDERBEAD CRACKING SPECIMEN OF 1-IN. QUENCHED-AND-TEMPERED T-1 STEEL WELDED WITH E6010 ELECTRODE

projected length of crack, or the total of the projected lengths of many cracks, if more than one occur, is divided by the length of the bead to provide a per cent of cracking for that individual specimen. The specimens are tested in groups of five, and the individual percentages are averaged to give an average per cent of cracking for one condition of welding. The results are shown graphically in Fig. 5; the solid black lines show the per cent cracking for individual specimens; the hatched areas show the averages for the groups.

It will be seen that at least 20 per cent average cracking occurs under practically all the conditions investigated. In one case the average cracking was as high as 78 per cent.

The effectiveness of the change in coating in minimizing underbead cracking is remarkable, for no underbead cracking was obtained when the steel was welded with E12015 electrodes. Accordingly, it is suggested that only low-hydrogen electrodes be used for the welding of Carilloy T-1.

Notch-Bend Tests. Kinzel-type notch-bend tests were made on welded and unwelded plate to determine the effect of welding on the notch toughness of the steel. Details of the welded specimen are shown in Fig. 6. The unwelded specimens were identical to the welded, except for the omission of the weld. The dimensions of the specimens and the welding conditions employed are essen-

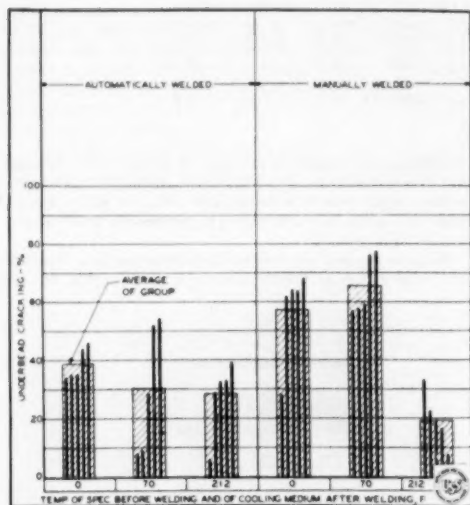
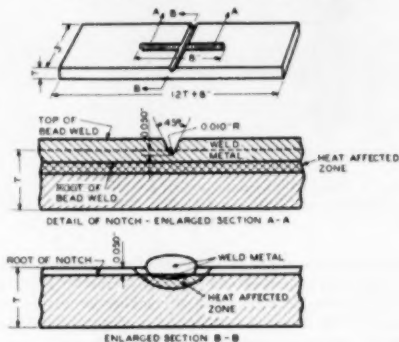


FIG. 5 SUSCEPTIBILITY OF 1-IN. QUENCHED-AND-TEMPERED T-1 STEEL TO UNDERBEAD CRACKING (E6010 electrode with various welding conditions.)



WELDING CONDITIONS

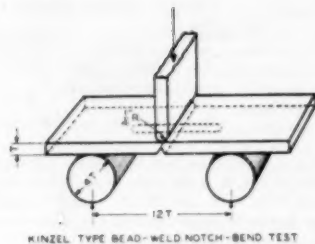
ELECTRODE DIAMETER	3/16"
CURRENT (AMPS)	180
VOLTAGE	27
SPEED OF TRAVEL (IN./MIN.)	8.0
HEAT INPUT (WATT SEC./IN.)	48,800

FIG. 6 DETAILS OF KINZEL-TYPE BEAD-WELD NOTCH-BEND SPECIMEN

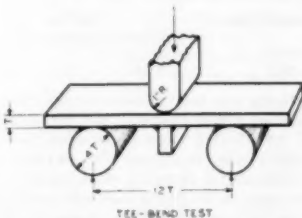
tially the same as those used by Kinzel.⁴ The plate temperature prior to welding was 70 F and no postheating was employed. After welding, the specimens were aged at 50–80 F for a minimum of 3 weeks. They were then bent at various temperatures with the weld bead in tension, as shown in the upper half of Fig. 7.

Fig. 8 shows a general view of the universal testing machine,

⁴ "Ductility of Steels for Welded Structures," by A. B. Kinzel, *The Welding Journal*, vol. 27, 1948, pp. 217-S–234-S.



KINZEL-TYPE BEAD-WELD NOTCH-BEND TEST



TEE-BEND TEST

FIG. 7 DETAILS OF TESTING JIG USED FOR NOTCH-BEND AND TEE-BEND TESTS



FIG. 8 GENERAL VIEW OF LOW-TEMPERATURE BEND TESTING EQUIPMENT

and the low-temperature bend-testing equipment. Details of the insulated box and deflectionometer are shown in Fig. 9. A bath of acetone and dry ice was used to obtain temperatures from room temperature to -100 F. Test temperatures below -100 F were obtained with a bath of Freon 12 cooled with liquid nitrogen.

The following information was determined for each specimen tested:

1 Per cent lateral contraction at a point $1/32$ in. below the base of the notch (measured by micrometer caliper before and after testing).

2 Total (maximum) angle of bend. Obtained from deflection-angle curve.

3 Total energy absorbed. Obtained by planimetering load-deflection curve.

4 Fracture mode expressed as per cent shear. Obtained by visible observation of fracture.

The specimens, in sets of about twenty, were broken at various temperatures. In general, three specimens were tested at each temperature.

The data obtained were plotted on the basis of testing temperature, and envelopes were drawn around the plotted points to indicate the amount of scatter. The curves for $1/2$ -in. unwelded plate are shown in Figs. 10, 11, and 12.

To determine ductility transition temperatures the arbitrary lateral contraction level of 1 per cent is chosen, regardless of specimen thickness. This level has been used also by investigators at

the Union Carbide and Carbon Research Laboratory.^{4,5} It may be noted from a comparison of Figs. 10, 11, and 12 for $1/2$ -in.-thick material that the transition temperature at 18 deg angle of bend and the transition temperature at 7500 in.-lb of absorbed energy are approximately the same as that obtained at 1 per cent lateral contraction (-132 F). This is as should be expected, because all three sets of data are measurements of different manifestations of the same phenomenon, namely, the ductility transition of the base metal.

Lateral-contraction data for $1/2$ -in. welded plate and 1-in. unwelded and welded plates are presented graphically in Figs. 13 through 15. Similar curves based upon angle of bend and total energy were plotted, but are not shown. For 1-in.-thick material, the transition temperature at 11 deg angle of bend and the transition temperature at about 13,500 in.-lb of absorbed energy are approximately the same as that obtained at 1 per cent lateral contraction (-78 F). Fig. 16 shows a typical $1/2$ -in. welded notch-bend specimen, before and after testing.

The fracture mode transition temperature was also determined for each thickness of plate in the welded and unwelded conditions. This transition temperature is defined arbitrarily as the temperature at which 50 per cent of the fracture occurs in the shear mode. The results for $1/2$ -in. plate are shown graphically in Fig. 17.

The ductility and fracture transition temperatures for $1/2$ -in. and 1-in. steel, based on the notch-bend test, are summarized in Table 3. It may be noted that welding, in all cases, raised the transition temperatures. However, the significant fact is that even after welding, the ductility transition temperature is still low.

The concepts of ductility and fracture transition temperatures may be somewhat new to many, and accordingly, the following brief discussion will attempt to explain their significance.

A schematic diagram showing the ductility and fracture transitions as obtained in the notch-bend test is shown in Fig. 18. Over a certain temperature range, the middle of which is designated T_F in Fig. 18, the fracture appearance changes from fibrous (shear mode) to predominantly granular (cleavage mode), exhibiting the chevron-type markings that point to the origin of failure. A drop also occurs in ductility, as measured by angle of

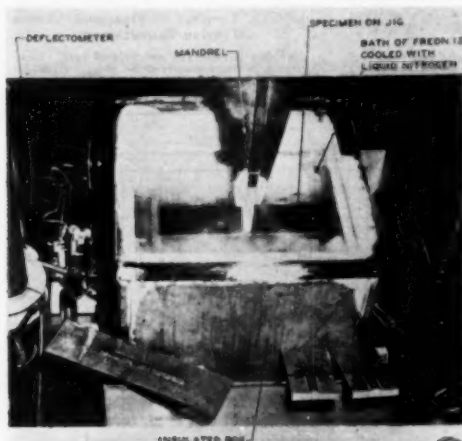


FIG. 9 DETAIL VIEW OF INSULATED BOX AND DEFLECTOMETER FOR LOW-TEMPERATURE BEND TESTING

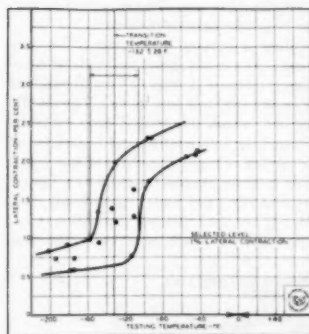


FIG. 10 LATERAL CONTRACTION VERSUS TESTING TEMPERATURE (Unwelded Kinzel-type notch-bend test; $1/2$ -in. quenched-and-tempered T-1 steel.)

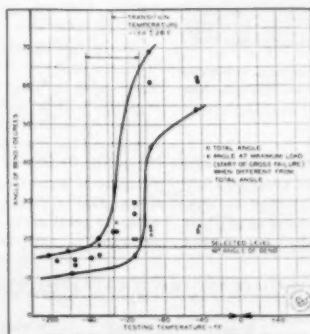


FIG. 11 ANGLE OF BEND VERSUS TESTING TEMPERATURE (Unwelded Kinzel-type notch-bend test; $1/2$ -in. quenched-and-tempered T-1 steel.)

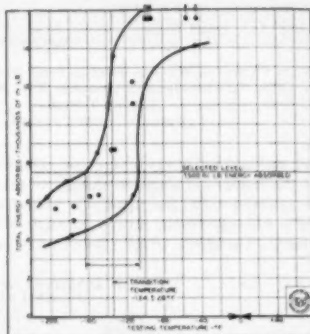


FIG. 12 ENERGY ABSORBED VERSUS TESTING TEMPERATURE (Unwelded Kinzel-type notch-bend test; $1/2$ -in. quenched-and-tempered T-1 steel.)

⁴ "Factors Affecting the Weldability of Carbon and Alloy Steels—Development of Test Procedure and Effect of Composition, Part I," by C. M. Offenbauer and K. H. Koopman, *The Welding Journal*, vol. 27, 1948, pp. 234-S-252-S.

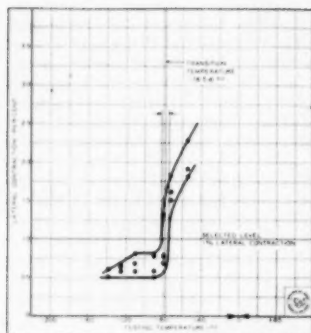


FIG. 13 LATERAL CONTRACTION VERSUS TESTING TEMPERATURE
(Welded Kinsel-type notch-bend test; 1/2-in. quenched-and-tempered T-1 steel. E12015 electrode.)

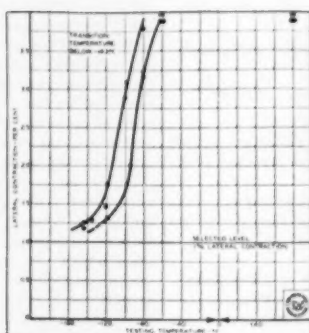


FIG. 14 LATERAL CONTRACTION VERSUS TESTING TEMPERATURE
(Unwelded Kinsel-type notch-bend test; 1-in. quenched-and-tempered T-1 steel.)

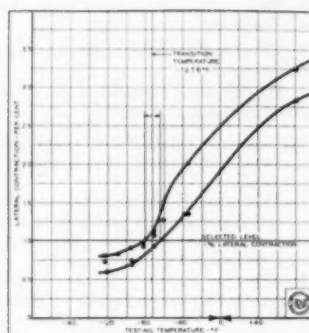


FIG. 15 LATERAL CONTRACTION VERSUS TESTING TEMPERATURE
(Welded Kinsel-type notch-bend test; 1-in. quenched-and-tempered T-1 steel. E12015 electrode.)

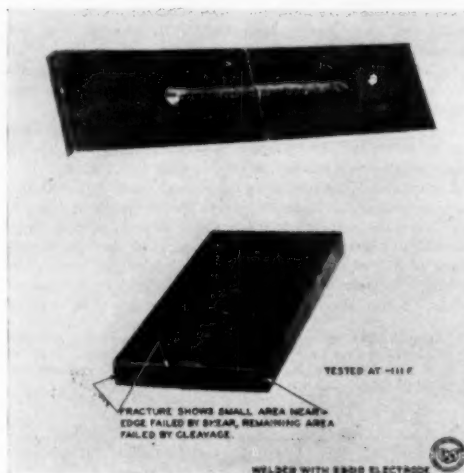


FIG. 16 TYPICAL WELDED KINSEL-TYPE NOTCH-BEND SPECIMEN OF 1/2-IN. QUENCHED-AND-TEMPERED T-1 STEEL BEFORE AND AFTER TESTING
(Welded with E6010 electrode.)

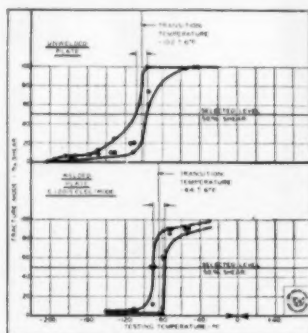


FIG. 17 FRACTURE MODE VERSUS TESTING TEMPERATURE
(Unwelded and E12015 welded Kinsel-type notch-bend tests. 1/2-in. quenched-and-tempered T-1 steel.)

bend, and in total energy absorption. However, despite the fact that the fracture appearance changes to that of predominantly cleavage failure, and the ductility is reduced somewhat, the ductility is still appreciable; in fact, an angle of bend of as much as 40 deg is often found. Such a failure could hardly be considered

brittle. Cleavage-type failures have also been observed in tension test specimens after large elongations obtained.

As the testing temperature is lowered still further, the ductility continues to decrease. For some specimens and for some steels, a temperature range is reached at which all manifestations of ductility drop rapidly to an extremely low value. The middle of the temperature range over which this second drop occurs is considered the ductility transition temperature and is designated T_D in Fig. 18. From the testing of many hundreds of specimens it has been found that this drop occurs most rapidly at a lateral contraction level of approximately 1 per cent. Accordingly, this value is arbitrarily selected as the ductility transition temperature, i.e., the temperature at which practically the last

TABLE 3 SUMMARY OF DUCTILITY AND FRACTURE TRANSITION TEMPERATURES FOR 1/2-IN. AND 1-IN. QUENCHED AND TEMPERED CARLLOY T-1 STEEL

Plate thickness, in.	Kinsel-type notch-bend test—			Tee-bend test—	
	Unwelded	Welded with E12015	Welded with E6010	Welded with E12015	Welded with E6010
	Ductility transition temperature, deg F (1 per cent lateral contraction)				
1/2	—132 ± 26	—78 ± 4	—84 ± 4	—128 ± 28	—124 ± 10
1	below —143	—72 ± 8	—78 ± 16	—144 (approx)	—124 ± 10
	Fracture transition temperature, deg F (50 per cent shear)				
1/2	—102 ± 8	—84 ± 8	—92 ± 10	—62 (approx)	—100 ± 26
1	—76 ± 8	—44 ± 8	—64 ± 12	—40 ± 6	—72 ± 8

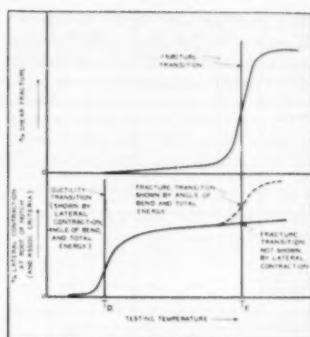
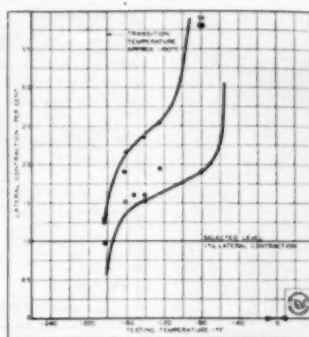
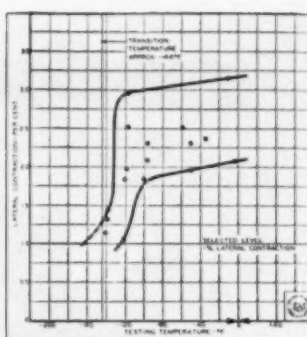
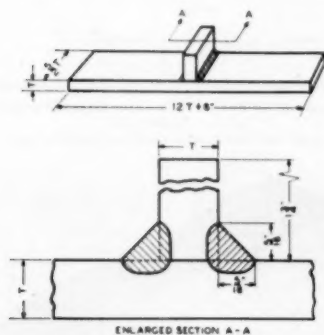


FIG. 18 SCHEMATIC DIAGRAM SHOWING DUCTILITY AND FRACTURE TRANSITIONS

FIG. 20 LATERAL CONTRACTION VERSUS TESTING TEMPERATURE—TEE-BEND TEST
(1/2-in. quenched-and-tempered T-1 steel.
E12015 electrode.)FIG. 21 LATERAL CONTRACTION VERSUS TESTING TEMPERATURE—TEE-BEND TEST
(1-in. quenched-and-tempered T-1 steel.
E12015 electrode.)

WELDING CONDITIONS	
ELECTRODE DIAMETER	5/32"
CURRENT (AMPS)	145
VOLTAGE	27
SPEED OF TRAVEL (IN / MIN)	3.0
HEAT INPUT (WATT SEC. / IN.)	78,300

FIG. 19 DETAILS OF TEE-BEND SPECIMEN

vestige of ductility departs and completely brittle failure is imminent. The authors feel that the ductility transition temperature, which occurs at a low level of performance, is of far more significance than the fracture transition temperature, because

practically all service failures have occurred with almost no manifestations of ductility. In the failures of many ships it was noted that along the fracture path a very slight contraction in the thickness of the plates obtained. These contractions were measured with a micrometer caliper and the value was found to be in the vicinity of 1 per cent.

It should always be borne in mind that at the present time there is no absolute correlation between transition temperature as obtained experimentally with the various types of specimens, and service performance; the numerical values given in this paper are those of test specimens only. It may be that there will never be as complete a correlation as could be desired, because of the many variables involved, such as thickness, design, strain rate, chemical composition, degree of cold work, heat-treatment, temperature, and degree of restraint. However, the relative values obtained from the same types of tests on different materials are very helpful. In Table 4 are shown the transition temperatures of T-1 steel and mild steel. These hitherto unpublished data on mild steel were taken from other researches by the authors' company. It will be seen that normalizing the killed steel lowered its transition temperatures considerably.

Tee-Bend Tests. This test is also a notch-bend test. Details of the specimen are shown in Fig. 19. In it the notch effect of the intersection between the face of a fillet weld and the base metal is used. This notch is an actual one which occurs in many places throughout welded structures. Most structural failures were associated with fillet welds. In a properly made fillet weld (and the welds used on the test specimens were carefully made), the concentration of stress at the 45-deg angle is less than that ob-

TABLE 4 SUMMARY OF DUCTILITY AND FRACTURE TRANSITION TEMPERATURES FOR VARIOUS STEELS; KINZEL-TYPE NOTCH-BEND TEST

Type of steel	Plate thickness, in.	Condition	Ductility transition temperature, deg F (1 per cent lateral contraction)			Fracture transition temperature, deg F (50 per cent shear)		
			Unwelded	Welded with E6010	Welded with E12015	Unwelded	Welded with E6010	Welded with E12015
USS Carillon T-1	1/2	Quenched and tempered	-132 ± 26	-84 ± 4	-78 ± 4	-102 ± 6	-92 ± 10	-84 ± 6
	1	Quenched and tempered	Below -143	-78 ± 16	-72 ± 8	-76 ± 8	-64 ± 12	-44 ± 8
Semikilled C—0.17 per cent Mn—0.45 per cent	1/2	As-rolled	-160 ± 7	-6 ± 10	...	+55 ± 8	+75 ± 9	...
Fully killed Fine-grained C—0.21 per cent Mn—0.84 per cent Si—0.19 per cent	1/2	As-rolled	Below -94	+24 ± 24	...	+48 ± 16	+60 ± 12	...
	1 1/2	Normalized	Below -94	0 ± 8	...	-48 ± 10	+4 ± 3	...

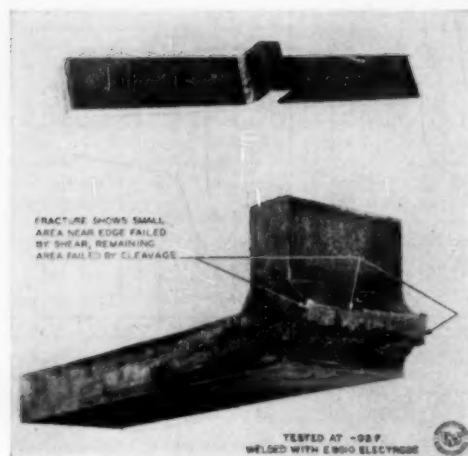


FIG. 22 TYPICAL TEE-BEND SPECIMEN OF 1-IN. QUENCHED-AND-TEMPERED T-1 STEEL, BEFORE AND AFTER TESTING (Welded with E6010 electrode; tested at -98°F .)

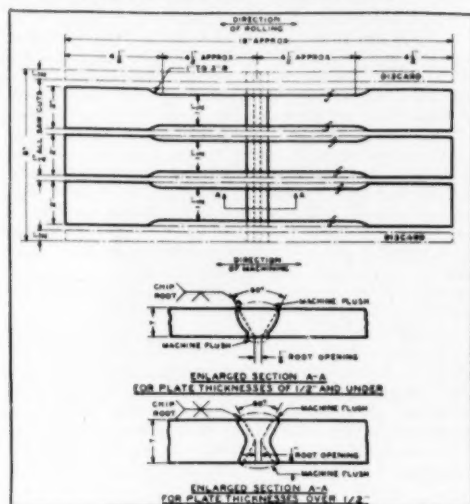


FIG. 23 DETAILS OF STANDARD TRANSVERSELY BUTT-WELDED TENSILE SPECIMENS

taining at the root of the artificially milled notch in the notch-bend specimens. In practice, however, if undercutting or ill-formed welds obtain, much more severe notches will result than those brought about by the theoretically perfectly formed fillet.

The procedure followed in testing the tee-bend specimens was the same as that used for the notch-bend specimens, except that the percent lateral contraction was determined at a point $1/3$ in. below the toe of the fillet nearest the failure. The bending conditions are shown in Fig. 7.

Lateral contraction test data for $1/2$ -in. and 1-in. tee-bend speci-

TYPE OF TEST	MECHANICAL PROPERTY DETERMINED (1)	1/2" PLATE WELDED WITH			1" PLATE WELDED WITH		
		E6010 (LOW N)	E1300 (LOW N)	E1300 (LOW N)	E6010 (LOW N)	E1300 (LOW N)	E1300 (LOW N)
LONGITUDINALLY BUTT-WELDED TENSILE	YIELD STRENGTH (0.2% OFF-SET) (PSI)	92,000	104,000	103,000	92,000	104,000	100,000
	TENSILE STRENGTH (PSI)	111,000	119,000	122,000	111,000	121,500	125,400
	ELONGATION IN 2 IN. (PERCENT)	29.3	30.0	35.0	34.0	33.2	37.0
	ELONGATION IN 8 IN. (PERCENT)	12.9	14.0	15.9	13.1	13.0	12.0
TRANSVERSELY BUTT-WELDED TENSILE	REDUCTION IN AREA (PERCENT)	37.8	40.0	39.0	44.0	41.1	38.0
	TENSILE STRENGTH (PSI)	VALUE	87,500	118,400	117,800	92,000	119,800
	LOCATION OF FAILURE	WELD METAL	BASE METAL	BASE METAL	WELD METAL	WELD METAL	BASE METAL
	JOINT EFFICIENCY BASED ON ACTUAL TENSILE STRENGTH (PERCENT)	73	100	100	74	99	100
DOUBLE FILLET-WELDED TENSILE	TENSILE STRENGTH (PSI)	VALUE	118,800	—	109,100	—	—
	LOCATION OF FAILURE	BASE METAL	—	—	BASE METAL	—	—
	REDUCTION IN AREA (PERCENT)	—	—	—	—	—	—
	JOINT EFFICIENCY BASED ON SPECIFIED TENSILE STRENGTH (PERCENT)	78	100	100	80	100	100

(1) AVERAGE OF THREE TESTS. ALL TESTING DONE AT ROOM TEMP.

FIG. 24 RESULTS OF BUTT-WELDED AND FILLET-WELDED TENSILE TESTS ($1/2$ -in. and 1-in. quenched-and-tempered T-1 steel.)

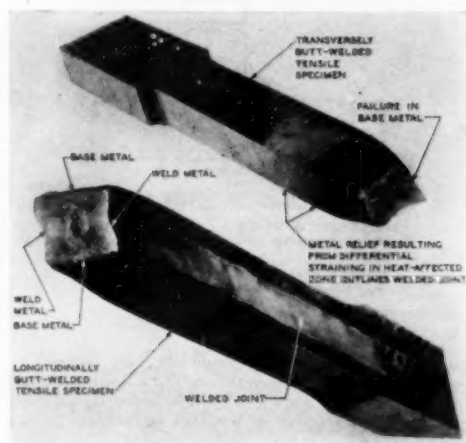


FIG. 25 TYPICAL FRACTURES IN BUTT-WELDED TENSILE SPECIMENS OF 1-IN. QUENCHED-AND-TEMPERED T-1 STEEL (E12015 electrodes.)

mens are presented graphically in Figs. 20 and 21. Similar curves based on angle of bend and total energy were plotted but are not shown. A typical tee-bend specimen of 1-in. plate is shown in Fig. 22.

The ductility and fracture transition temperatures for $1/2$ -in. and 1-in. tee-bend tests are summarized in Table 3. As anticipated for a specimen having a much less severe notch, the ductility transition temperatures were decidedly lower than those obtained with the welded notch-bend specimen.

In view of the fact that the fillets deposited on the test specimens are better formed than those obtaining in practice, it would probably be better to use the results obtained from notch-bend specimens in estimating the minimum safe operating temperature of welded structures rather than the results obtained from tee-bend specimens.

Tensile Tests of Transversely Butt-Welded Specimens. The transversely butt-welded specimen shown in Fig. 23 serves one

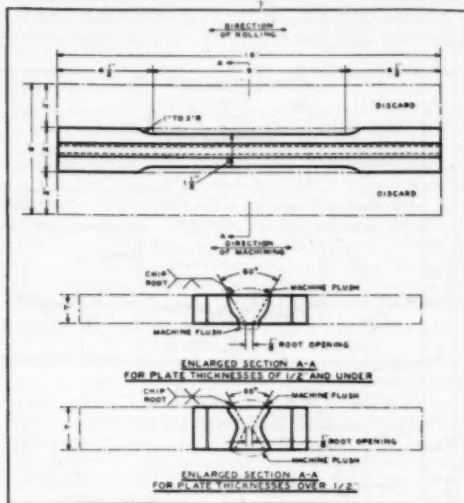


FIG. 26 DETAILS OF STANDARD LONGITUDINALLY BUTT-WELDED TENSILE SPECIMENS

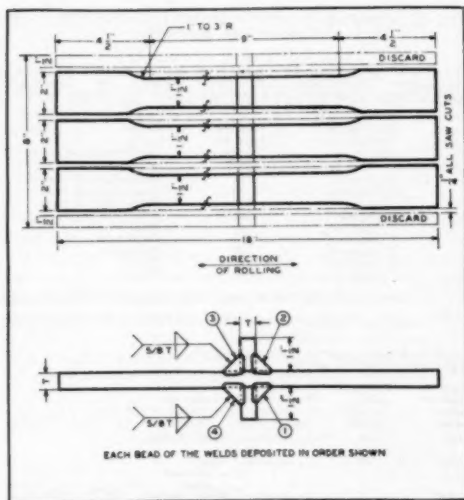


FIG. 27 DETAILS OF STANDARD DOUBLE-FILLET-WELDED TENSILE SPECIMENS

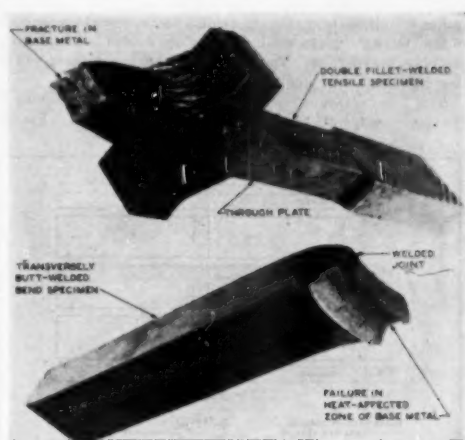


FIG. 28 TYPICAL FRACTURES IN FILLET-WELDED TENSILE AND BUTT-WELDED BEND SPECIMENS OF 1-IN. QUENCHED-AND-TEMPERED T-1 STEEL (E12015 electrode.)

purpose only, namely, it shows whether or not the deposited weld metal is stronger than the base metal. The measurement of elongations between gage points across the joint is meaningless, because the materials between the gage points are of many different characteristics. The results of the tests of the transversely butt-welded specimens are shown in Fig. 24. It will be seen that the joints, with the reinforcements machined off, broke in the base metal, and 100 per cent joint efficiency was developed. A typical fracture is shown in Fig. 25.

Tensile Tests of Longitudinally Butt-Welded Specimens. The longitudinally welded specimen, as shown in Fig. 26, is used to determine the ductility of the welded joint as a whole. The weld metal, the heat-affected zones, and the unaffected base metal are all stretched together. If one is deficient in ductility, that one will cause the others to fail. A comparison between the data in Fig. 24 and the data in Table 2 shows that the per cent elongations in the welded specimens are, in general, somewhat lower than those of the comparable base-metal specimens, but the values are still good considering the high strength developed. A typical fracture is shown in Fig. 25.

Tensile Tests of Double-Fillet-Welded Specimens. This type of specimen shown in Fig. 27 consists of a "through" plate, to which are attached on both sides transverse plates double-fillet-welded to the through member. The specimen simulates the situation in structures wherein a continuous main stress member has stiffeners or other parts welded to both sides. The properties of T-1 steel are those imparted to it by heat-treatment, and the question naturally arises as to whether or not the heat of welding impairs those properties. The effect of welding on toughness has already been discussed. The double-fillet-welded specimens are intended to show the effect of the heat of welding on ultimate tensile strength. To this end the fillet welds were deposited with a high heat input and in rapid succession. The accumulation of heat in the joint as welding progressed raised the peak temperature of the through plate at mid-thickness to a value that would be attained only under the most adverse fabricating conditions.

In Fig. 24 it will be seen that the double-fillet-welded tensile specimens failed in the base metal. A typical fracture is shown

in Fig. 28. If the heat effect of welding had impaired the strength of the "through" plate, see Fig. 28, failure would have occurred in the plate near a fillet. The effect of the heat of welding will be discussed further in a subsequent section on hardness.

Bend Tests of Transversely Welded Specimens. The details of the transversely butt-welded bend specimens are shown in Fig. 29.

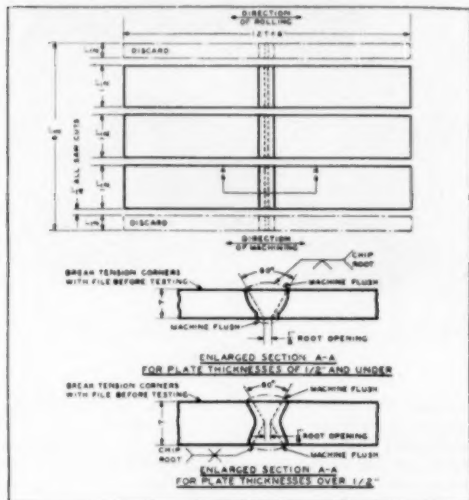


FIG. 29 DETAILS OF STANDARD TRANSVERSELY BUTT-WELDED BEND SPECIMENS

These specimens were tested in two ways, by static bending, with a continuously applied load at mid-length, and by "treading," a progressive bending technique used by pressure-vessel fabricators. The results of the static bend tests are given in Table 5.

The angles of bend for specimens tested at +70 are particularly good, considering the small radius of mandrel used in the bending. A typical fracture is shown in Fig. 28. Because of the fact that the bending is largely concentrated in the weld metal, base-metal failures did not occur. The low-temperature bend results show that the E12015 welds are capable of considerable deformation at -96 F.

The results of treading bend tests of 1-in. specimens welded with E12015 electrodes, as given in Table 6, show that Carilloy T-1 is capable of enduring a considerable degree of progressive bending in fabrication.

Hardness. Vickers hardness surveys to determine the weld metal, heat-affected zone, and base-metal hardnesses were made on sections cut from a butt-welded joint in 1-in. plate. All im-

pressions were made with a 2 1/2-lb. load. It will be seen in Fig. 30 that the peak hardness obtained in the coarsened zone was about 420 VHN. In the weld metal, very much lower hardnesses were found owing to the tempering of subsequent passes. The absolute value of this peak hardness is considerably greater than that obtaining in ordinary mild-carbon steels. The excellent bend-test results for butt-welded joints of this type, as shown in Tables 5 and 6, demonstrate the fact that high hardness resulting from welding on T-1 steel does not preclude good performance.

It will be noted in Fig. 30 that the unaffected base metal has a hardness of approximately 300 VHN. At a point just outside the

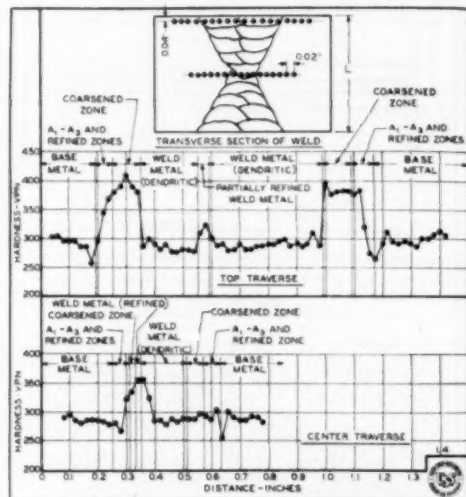


FIG. 30 TYPICAL HARDNESS SURVEYS FOR AN E12015 BUTT-WELDED JOINT IN 1-IN. T-1 STEEL

TABLE 6 RESULTS OF TREADING BEND TESTS OF TRANSVERSELY BUTT-WELDED SPECIMENS OF 1-IN.-THICK QUENCHED AND TEMPERED CARILLOY T-1 STEEL WELDED WITH E12015 ELECTRODES

Min. inside radius of specimen, in.	Angle of bend to failure, deg ^a	Location of failure
1/4 (approx)	81	Heat-affected zone
1/4 (approx)	98	Heat-affected zone
1/4 (approx)	133	Heat-affected zone
1/4 (approx)	166	Weld
1 (approx)	147	Heat-affected zone
1 (approx)	165	Bond zone
2 (approx)	146	No failure
2 (approx)	79 ^b	Weld ^b
3 (approx)	49 ^b	Weld ^b

^a All values are for individual tests. All testing done at room temperature.

^b Premature failure attributed to a void observed near the extreme fiber.

TABLE 5 RESULTS OF TRANSVERSE BUTT-WELD BEND TESTS OF 1/2-IN. AND 1-IN. QUENCHED AND TEMPERED CARILLOY T-1 STEEL

Plate thickness, in.	Type of electrode used	Testing temp., deg F	Mandrel radius, in.	Angle of bend to failure, deg ^a	Fracture mode, per cent shear	Final min. inside radius, in.	Location of failure
1/2	E12015 (low H)	+70	1/4	130	100	1/4 (approx)	Weld metal
1	E12015 (low H)	+70	1/4	101	100	1/4 (approx)	Heat-affected zone
1	E12015 (low H)	-96	1/4	28 ^b	2	1/4 (approx)	Weld metal

^a Average of three tests unless otherwise specified.

^b Average of four tests.

A₁-A₂ zone, the hardness has decreased to a value of about 255 to 260 VHN; in other words, an actual softening has taken place. It is well known that the hardness and tensile strength of a steel are directly proportional. The minimum hardness corresponds to an ultimate tensile strength of about 120,000 psi; in other words, the weakest spot to be found in the vicinity of the weld is considerably stronger than the specified tensile strength of the base material. However, as has been shown previously, the various types of tension specimens fail completely outside of the heat-affected zones of the base metal. This is due to the fact that only one or two small areas of any cross section of the joint have been decreased in strength slightly. It should also be borne in mind that this survey was made on a relatively large multiple-pass welded joint.

Electrodes and Weld Metal. The problem of developing electrodes to weld such a high-strength steel is a difficult one indeed. The high strength and great toughness of the base metal are imparted to it by quenching and tempering. Obviously, quenching is not possible on any but the simplest of welded structures. Accordingly, the weld metal must, in its as-welded condition, have comparable properties. Remarkable progress has been made in the development of such weld metal. Electrodes to develop the strength of T-1 steel should be those of the ASTM-AWS Classifications E12015 and E12016. These designations are applied to electrodes developing an ultimate tensile strength of 120,000 psi or more and having a coating which evolves very little hydrogen. Many joints in welded structures are called upon to develop merely a nominal strength, such as certain joints in longitudinal shear. In those cases electrodes of a lesser strength, such as the E10015 or E10016, or even E8015 and E8016 could be used, but always the electrodes should be of the low-hydrogen type. One E12015 electrode used in the testing described herein deposited weld metal (undiluted) having the composition and tensile properties given in Table 7.

TABLE 7 WELD-METAL COMPOSITION AND TENSILE PROPERTIES

C	Mn	P	S	Si	Ni	Cr	Mo	V	Cu	Ti
0.06	1.12	0.014	0.018	0.40	2.11	0.11	0.95	0.21	0.11	0.005
0.06	1.11	0.011	0.018	0.46	1.96	0.11	0.90	0.27	0.10	0.013

Condition	Yield strength, psi	Ultimate tensile strength, psi	Elongation in 2 in., per cent	Reduction of area, per cent
As deposited	109000	126500	20.0	59.0
	117600	131900	21.0	58.3
Stress-relief-annealed at 1100 F	115800	127700	18.0	59.3
	116300	129700	19.5	59.6

This metal was capable of developing the full tensile strength of the base metal, even in plates 4 in. thick.

In order to determine the effect of stress-relief annealing on weld metal, a number of tests were conducted on all-weld-metal specimens which had been stress-relief-annealed at 1100 F. The tensile properties of the weld metal in that condition are as shown in Table 7. It can be seen that stress-relief annealing made but little change in the ductility as determined by tensile testing.

To ascertain the effect of such treatment on the toughness of

TABLE 8 DUCTILITY TRANSITION TEMPERATURES FOR E12015 WELD METAL AND CARILLOY T-1 STEEL; CHARPY KEYHOLE IMPACT TEST

Material	Condition	Ductility transition temperature, deg F
E12015 weld metal	As deposited	-60
E12015 weld metal	Stress-relief-annealed at 1100 F	Above +130
Carilloy T-1 steel	Quenched and tempered	-240

weld metal a series of Charpy (keyhole) impact specimens were tested. The ductility transition temperatures of the weld metal are given in Table 8.

It will be noted that a considerable rise in the transition temperature of the weld metal was brought about by the stress-relief-annealing treatment. A typical value of the transition temperature for T-1 base metal has been added for comparison. In other tests it has been found that in the case of the base metal,

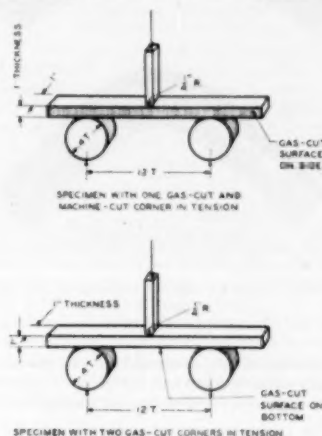


FIG. 31 GAS-CUT BEND TESTS

stress-relief annealing at a temperature below the 1200 F tempering temperature of the plate has little or no effect on the transition temperature of the base metal. In general, it is definitely recommended for the present that structures of T-1 steel, welded with electrodes depositing weld metal of a composition similar to that shown, should not be stress-relief-annealed. The omission of this expensive and time-consuming process should be most welcome. Further discussion of stress-relief annealing in general will be found under Residual Stresses.

Automatic submerged-arc welding, i.e., welding under a blanket of flux, has thus far been little used for the welding of T-1 steel. The two leading manufacturers of submerged-arc welding equipment are working on the problem of developing suitable electrode material, but some time may elapse before submerged-arc weld metal, having properties comparable to those of the base metal, will be available. The principal manufacturer of inert-gas shielded semiautomatic metal-arc welding is also working on the problem, and here again some time may elapse before such weld metal can be used.

Gas Cutting. With many types of alloy steels it is necessary to resort to preheating before gas cutting. Preheating is always a nuisance and is always difficult to enforce. To ascertain the effect of gas cutting on a quenched and tempered steel, two new types of bend tests were developed. The specimens for these tests are shown in Fig. 31. They are prepared by first making two automatic gas cuts at 70 F sufficiently far apart that the heat of the second cut does not affect the material adjacent to the first. Then a mechanical cut is made midway between the two gas-cut edges, providing a specimen with one gas-cut edge which has not been affected by any subsequent thermal operation. One of the specimens is bent with one gas-cut corner and one machine-cut corner in tension, as shown in the upper half of Fig. 31. This type of bending is applied to plates when they are shaped in fabrica-

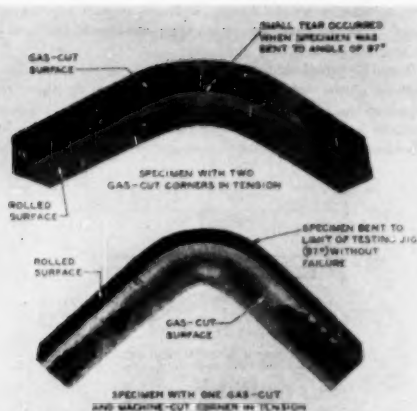


FIG. 32 TYPICAL GAS-CUT BEND SPECIMENS OF 1-IN. QUENCHED-AND-TEMPERED T-1 STEEL (Tested at -98°F .)

tion. The other specimen is bent with the two gas-cut corners in tension, as shown in the lower half of Fig. 31. This latter type of bending, although seldom encountered in fabrication, is the more severe.

The results of the gas-cut bend tests of 1-in. steel are shown in Table 9.

TABLE 9 RESULTS OF GAS-CUT BEND TESTS OF 1-IN. QUENCHED AND TEMPERED CARBLOY T-1 STEEL

Orientation of gas cut	Temperature of testing, deg F	Angle of bend to failure, deg*	Remarks
Two gas-cut corners in tension	-98	97	Small tear
One gas-cut corner and one machine-cut corner in tension	-98	Over 97 (jig capacity)	

* Average of two tests.

Typical specimens tested at -98°F are shown in Fig. 32. From the results it may be seen that gas cutting does not affect the bend performance of the steel adversely at even very low temperatures.

ENGINEERING CONSIDERATIONS

In order to take full advantage of the excellent mechanical properties available in T-1 steel and yet not use this more expensive material where it is not economical, there are several considerations which the engineer must bear in mind.

Tension. The major use of the new plate steel will be in applications in which tension is the main consideration. Here the full potentialities of the steel can be developed.

In some cases tensile deflection may prevent full utilization of a yield strength of 100,000 psi and more. With a fixed design, the factor governing deflection is modulus of elasticity. The modulus of elasticity of T-1 steel, as with all structural steels, is about 30,000,000 psi. If this strong steel is stressed to 15,000 psi, it will elongate the same amount as would ordinary carbon structural steel. If both were stressed to 33,000 psi, they would both elongate to the same degree. Upon release of the load, the T-1 steel would return to its original shape; the mild steel might or might not, depending upon whether or not its yield point had been exceeded.

One type of structure wherein tension is the paramount stress is the pressure vessel. In such vessels, generally speaking, deflection is of little consequence. Let us assume that a factor of safety on the yield point of 1.83 is to be used. This would result in a working stress of 18,000 psi, based on a yield point of 33,000 psi. If the same factor of safety based on yield strength were to be used with T-1 steel, a working stress of 54,500 psi could be permitted. In both cases the factor of safety would be 1.83; in the former the margin of safety on the yield point would be 15,000 psi; with the T-1 steel, the margin of safety would be 45,500 psi. This would be a far greater margin than has heretofore obtained in practice, and yet the working stresses would be on the order of 3 times those normally used. This brings up the very interesting question as to whether or not the designer is interested in factors of safety or margins of safety. If the latter be the case, it might be that even higher working stresses would be permissible.

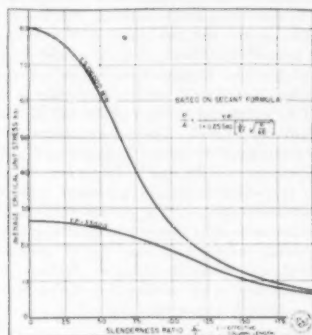


FIG. 33 CRITICAL STRENGTH FOR STEEL COLUMNS

Compression. In Fig. 33 are shown curves giving the ultimate permissible compressive stresses in columns. These graphs are calculated from the secant formula. Data for ordinary carbon structural steel and T-1 steel are shown. When the L/r ratio is 125, often used as the maximum permissible ratio for main members, the allowable stress is about 20 per cent greater for T-1 steel than for mild-carbon steel. For a ratio of 60, a relatively small value, the permissible stress in T-1 steel would be about 2.4 times that allowable with carbon steel. The stresses shown in Fig. 33 are calculated, but experimental verification exists for the 33,000-psi yield-point material. No experimental proof of the values for T-1 steel is at hand because such a steel has never before been available for test. However, it is felt that the curves provide a reasonable guide for the use of this steel in compression. Also, it should be noted that no factor of safety has been applied to the average critical stress.

Shear. Precise torsional tests to determine the yield and ultimate shear strength of T-1 steel have not yet been made. However, transverse shear tests of $1/8$ -in.-diam pins in double shear have been conducted. The results were as follows:

	Load, lb	Load, psi 2 X area
Specimen A.....	31800	81000
Specimen B.....	34300	87500
Specimen C.....	32200	82200

The ultimate shear strength as determined by this method is about 70 per cent of the ultimate tensile strength. This ratio is about the same as that for ordinary structural steel.

Fatigue. A series of $\frac{1}{2}$ -in. and 1-in.-thick plate specimens were tested in a Rayflex resonant-frequency fatigue testing machine, as shown in Fig. 34. It will be seen that the specimens are of appreciable size; they retain the original rolled surfaces complete with mill and heat-treating scale. The results of these tests are shown in Fig. 35. The endurance limit for 2,000,000 cycles of alternating stress was about 35,000 psi, or only about 31 per cent of the ultimate tensile strength. This ratio is low compared to

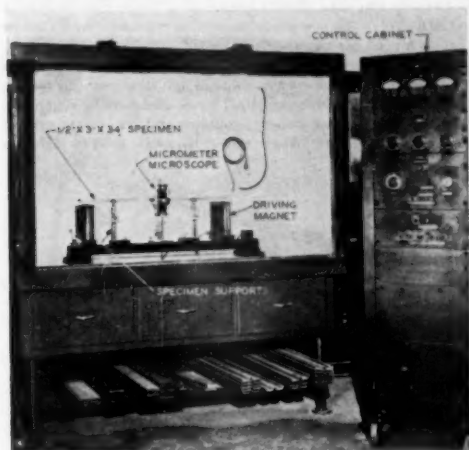


FIG. 34 GENERAL VIEW OF RAYFLEX TUNED-RESONANCE FATIGUE TESTING MACHINE

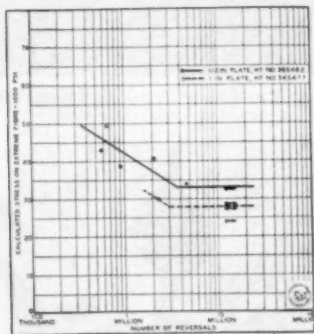


FIG. 35 RESULTS OF FATIGUE TESTS ON T-1 STEEL, SPECIMENS WITH ORIGINAL PLATE SURFACES

those obtained from fatigue tests conducted on polished specimens. An endurance limit of 67,000 psi has been gotten from polished rotating-beam specimens.

It is obvious that in an application subjected to severe alternating stresses, scale should be removed. However, in structural applications where fillet welds are involved, and reinforcements are left on welds, square corners are tolerated, and stressed material is stopped abruptly, surface discontinuities caused by scale would be but a minor factor.

Bending. Since bending is a combination of tension and com-

pression, it follows that the principal consideration in beams in bending is the resistance to buckling. In designing members to resist bending, careful study should be given to unsupported flange width, to local buckling between stiffeners, to side buckling, and to all other aspects of compression.

Concentrated Stresses. The previous discussion on the different stresses pertains to those which are determinate, but what about concentrations of stresses? The intensity of concentrated stresses is a function of the configuration of the part and is often expressed as a multiple of the design stress. The numerical value of these concentrated stresses is calculated on the assumption that the stresses do not exceed the yield strength of the material. If, however, the yield strength of the material is exceeded and a certain amount of local plastic deformation takes place, the stresses are reduced to the yield-strength value at that location. If, on the other hand, the material is of such a nature that under the existing conditions of stress and temperature, a minute amount of plastic deformation cannot take place, then brittle failure will result, possibly catastrophically. In the case of T-1 steel the transition temperature is so low, even after welding, forming, gas cutting, and all the other fabricating operations that the material at any atmospheric temperatures will behave in a ductile manner and will permit the necessary small local plastic deformation to redistribute stress.

Residual Stresses. The fact that the material will remain ductile at atmospheric temperatures encountered anywhere in the world, brings up some very interesting questions as to the necessity of postheating. Stress-relief annealing, as ordinarily practiced, serves a number of purposes, as follows:

- 1 It reduces the hardness of the base metal and the heat-affected zones therein.
- 2 It improves the ductility of the heat-affected base metal.
- 3 It reduces residual stresses to a low value.
- 4 It restores the transition temperatures of the various base-metal elements of the structure to the original transition temperature of the base metal, or nearly so.

The thinking in the past has been concentrated largely on items (1), (2), and (3); it may be that item (4), namely, restoration of the original transition temperature, is the important one, and the others are by-products. If this be true, then the use of T-1 steel should render stress-relief annealing unnecessary for weldments to operate at atmospheric temperatures. If at first glance this appears startling, let us reconsider the various points enumerated in the foregoing.

The hardnesses resulting from welding on T-1 steel, as shown in Fig. 30, are high relative to those obtaining in mild steel, but all of the various bending and tension tests show that this hardness per se has not harmfully affected the ability of the steel to endure distortion.

Tests of longitudinally welded tension specimens show that the weld metal and the heat-affected zones in the base metal as-welded have nearly as great ductility as has the base metal.

No direct correlation between residual stress and service failure has ever been established. Considerable evidence exists to show that for all practical purposes residual stress is not a factor in brittle failure. Theoretically, however, residual stress can contribute to brittle failure when the state of residual stress is such that brittle failure is imminent and a small imposed stress is added. In the case of T-1 steel, the transition temperature after having been welded has been shown to be so low that a structure operating at any atmospheric temperature would remain ductile and be able to endure the necessary local redistribution of stress.

So far as restoring the original transition temperature is concerned, if the transition temperature raised by welding, torch

cutting, forming, or any other fabricating operation is still lower than the operating temperature, then what would be the necessity of restoring the original?

The foregoing discussion is at present the product of pure reasoning. However, arrangements are being made to build and test several pressure vessels of T-1 steel. These as-welded vessels will be subjected to various kinds of destructive tests at low temperatures to demonstrate that stress-relief annealing is not necessary with T-1 steel, and that this steel is a suitable material for pressure vessels.

Resistance to Abrasion. No data are available on the resistance of the new steel to abrasion. Tests are under way in the coke chutes of one of the large coking plants of the United States Steel Company. Comparative materials are placed in these chutes and subjected to the scouring action of thousands of tons of coke. It is felt that the performance of T-1 steel under these conditions will be considerably better than that of softer steels, and it is hoped in the not too distant future to be able to verify this assumption.

Some thought has also been given to the manufacture of T-1 steel with a higher hardness. Laboratory tests of steel heat-treated to 341 Bhn have demonstrated that the steel maintains an adequate degree of toughness even at this high level of hardness.

Resistance to Corrosion. At the present time no actual data are available on this aspect of service. However, based on the known effect of composition, the copper content, together with the nickel and chromium, should provide the steel with an atmospheric corrosion resistance of at least 2 to 3 times that of a plain carbon steel. Specimens are in place on atmospheric testing racks at Vandergrift, Pa., Kearny, N. J., Kure Beach, N. C., and elsewhere to obtain data on this point. However, it will be some years before results of such tests are available.

Machining. Machining appears to offer no problem. This steel is harder than the usual structural grades of material; however, the hardness is not at a high enough level to cause unusual difficulties.

Hot-Forming. Hot-forming above the tempering temperature of the steel (about 1200 F) will destroy the mechanical properties imparted by the original heat-treatment. Therefore such forming must be avoided unless facilities are available for water-quenching and tempering the hot-formed part. Simple members have been hot-formed successfully and subsequently re-treated by quenching and tempering. It was then necessary to make certain corrections to bring the parts to the desired contours because of distortion encountered in the water-quenching operation. Hot-forming and water-quenching of complex parts is extremely difficult, owing to the danger of cracking, and the distortion problems encountered are severe.

Cold-Forming. The steel itself is sufficiently ductile to undergo bending to reasonable radii. However, in contemplating a cold-forming operation, serious consideration should be given to the strength of the bending equipment. Fig. 36 shows a typical cold-formed component for a large power shovel. This piece was made of 3 1/2-in.-thick plate bent to a 16-in. radius. Plates of T-1 steel as thick as 5 in. have been bent to generous radii. Possibilities of furnishing annealed rather than quenched and tempered plate, to be cold-formed into difficult objects and subsequently heat-treated, have not yet been fully explored.

Punching. Very little punching of T-1 steel has been done to date. It is believed advisable to drill rather than punch holes in this steel. However, if anyone contemplates punching this hard material, consideration should be given to the strength of equipment, and the safety of operating personnel.

Shearing. The thickness which can be cold-sheared is largely dependent upon the strength of the available equipment. Plates

as thick as 1 in. are regularly sheared in the plants of the authors' company.

Rolled Shapes. One of the limitations of this new material is that rolled shapes, for example, I-beams, channels, and angles cannot now be manufactured satisfactorily. These shapes can be rolled readily, but in the subsequent quenching and tempering, it is feared that they will twist and distort to such an extent that it will not be practicable to straighten them. At first glance the lack of rolled sections might appear to be a very serious drawback to the utility of the new steel, but further consideration will show that such need not necessarily be so.

There are three principal uses for rolled shapes, namely, as compression members, such as columns and struts, etc., as beams, and as stiffeners holding principal stress members in alignment. In two of these cases, namely, columns and beams, the critical stress is compression. Where rolled shapes are used to maintain

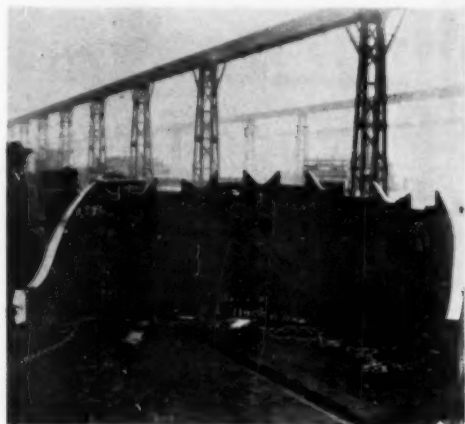


FIG. 36 COLD-FORMED LIP FOR A 45-CU-YD BUCKET
(3 1/2-in.-thick Carlinoy T-1 steel.)



FIG. 37 45-CU-YD BUCKET USED IN STRIP MINING
(Bucket lip of 3 1/2-in.-thick T-1 steel.)

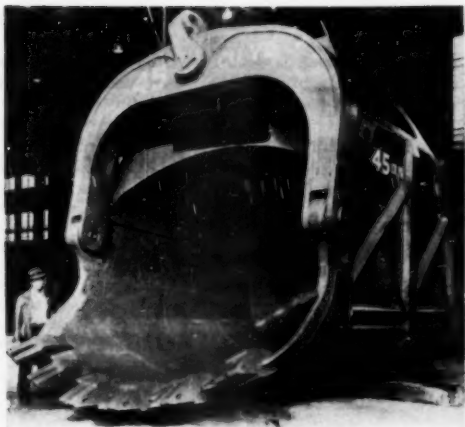


FIG. 38 45-CU-YD BUCKET OF T-1 STEEL

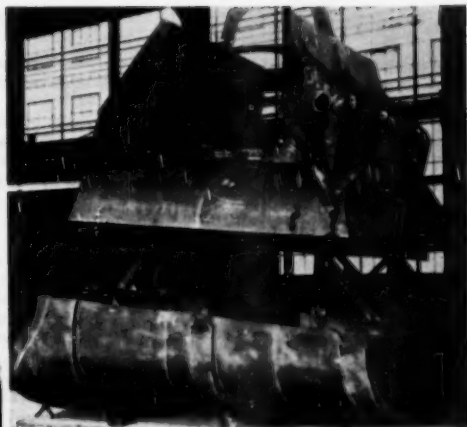


FIG. 39 45-CU-YD BUCKET DURING ASSEMBLY



FIG. 40 SIDE VIEW OF DIPPER STICK FOR 45-CU-YD BUCKET



FIG. 41 CABLE EQUALIZER FOR POWER SHOVEL USED IN STRIP MINING
(61/2-in.-thick T-1 steel.)



FIG. 42 SAND AND GRAVEL BUCKETS FOR LADDER DREDGE
(3/4-in. and 1-in. T-1 steel.)

the alignment of plates, the latter generally carry the principal stresses, and the stiffening shapes could be made of almost any material.

It is, of course, possible to fabricate shapes from plates. There are many advantages to such a procedure, particularly in the case of curved members. In some instances it may be advantageous to use the exact proportions needed for a certain part and by so doing utilize T-1 most economically.

APPLICATIONS

Actual Applications. The outstanding application to date of this new steel has been the lips of the buckets of the enormous power shovels used for stripping the overburden in coal-mining operations. Such a lip, as shown in Fig. 36, was cold-formed and gas-cut into this intricate shape. The lip in operation digging rock is shown in Fig. 37.

Under these very adverse conditions, lips of T-1 steel have performed satisfactorily for a much longer time than have lips of any other material. This application makes use of the ability of T-1 steel to endure most abusive treatment.

A large electrical-products manufacturer has used T-1 steel in generator components where high strength was required for parts whose contours necessitated considerable gas-cutting. It had been the manufacturer's practice to machine the desired contours from a high-carbon, quenched-and-tempered steel. By substituting T-1 steel it was possible to gas-cut the desired contours and maintain the necessary strength level and eliminate many costly machining operations. This application makes use of the excellent welding and gas-cutting characteristics of T-1 steel.

Prospective Applications. In this category are included parts which may or may not have been fabricated, but as yet have not been in service.

In Fig. 38 is shown a large bucket made of T-1 steel. The teeth bases, which have not yet been welded in place, are made of a much harder and less weldable heat-treated alloy steel. Fig. 39 shows the jiggling for welding the front and back to the side sheets.

A side view of the dipper stick for this large bucket is shown in Fig. 40.

In Fig. 41 is depicted a cable equalizer which connects to the structural frame of the stripping shovel.

In Fig. 42 are shown a number of buckets for a ladder dredge. These will be used for digging sand and gravel.

A number of smaller buckets and dipper sticks for power shovels have been made for service in the iron mines in northern Minnesota. Many failures of shovel parts have occurred in this area owing to the extremely low winter temperatures. These applications make use of all of the characteristics of T-1 steel, including its excellent toughness at extremely low atmospheric temperatures.

Tension rods in dam gates and other structures, in fact, tension members in general, offer a good field for the application of T-1 steel.

Another application under consideration is the use of this tough, high-yield-strength steel for shipbuilding. Plates with these characteristics might be particularly suitable for critical locations in large ships.

The use of T-1 steel plates as a substitute for forgings is being studied. It is quite probable that certain parts now made from forgings could be fabricated to the desired contours by gas-cutting, thus eliminating forging and heat-treating costs.

In general, any application requiring a structural steel of great strength, excellent toughness, good weldability, and the capacity to be gas-cut and cold-formed is a potential application for T-1 steel. The foregoing qualities will be manifested in ability to resist abuse, toughness at low atmospheric temperatures, reduc-

tion in weight and inertia, reduction in freight and handling costs, possible elimination of shop and field stress-relief annealing, and increased pay loads in mobile structures.

AVAILABILITY

Under existing circumstances, the quantities of this steel available for commercial experiment and trial applications must necessarily be very limited. However, changes from normal working stresses to values many times higher than those ever used before are not to be contemplated lightly, and considerable time must be spent in study and design before these potentialities can be translated into reality. It is hoped that this paper will serve to stimulate thinking among engineers and users of steels so that when the time comes that unrestricted use of materials is again permissible, much preliminary work will have been done toward the utilization of this revolutionary new structural steel.

Discussion

ADRIEN F. BUSICK, JR.* In the past two years our company has processed approximately 435 tons of USS Carilloy T-1 steel in the fabrication of dippers and dipper handles for power shovels. Prior to the development of T-1 steel, we had been using a nickel-copper-moly alloy plate, quenched and tempered to a yield strength level of 80,000 psi. Over a period of five years we used approximately 1800 tons of the latter type of steel and we regard our experience with it as a good indicator of the possibilities in the use of T-1 steel.

Our use of the high-yield-strength steels can be divided into two separate categories as follows:

1 To reduce the dead weight of front-end equipment in order to increase the load-carrying capacity of a given machine. This was the original incentive to adopt this type of material.

2 To replace mild steel in dipper handles which were giving trouble when operating at subzero temperatures. In this case the sections and weight were not reduced as it was desired to obtain increased strength and take advantage of the low-temperature characteristics of this type of steel when subjected to impact loads.

In the commercial use of these steels we made certain tests and adopted shop practices which have worked out quite satisfactorily as far as our product is concerned.

Our early testing program indicated that welding electrodes conforming to the AWS/ASTM, Type E-9015, (Arcos Manganese 1-M) were entirely satisfactory for the nickel-copper-moly steel, forerunner of the Carilloy T-1 steel, and this was confirmed by production and field experience over a five-year period. With the introduction of Carilloy T-1 steel, we initiated another testing program to determine proper welding electrodes and procedures for it. In view of the higher strength of the T-1 steel over the nickel-copper-moly, we considered a welding electrode of the AWS/ASTM, Type 10016, (Arcos Tensile 100) in addition to the E-9015 rod. Tensile, side-bend, and face-bend specimens were prepared and tested, using both type rods and various pre-heat temperatures. After welding, half of the bars were furnace stress-relieved, and half were not.

All tensile bars made with E-9015 or E-10016 rod, tested in the stress-relieved condition, failed in the parent metal entirely away from the weld, developing the full strength of the plate. In the as-welded condition, one bar with the E-9015 and one with E-10016 failed in the weld, but in both cases slight weld defects were noted.

All face and side bend specimens tested in the stress-relieved

* Chief Engineer, Marion Power Shovel Company, Marion, Ohio.

condition, except one, passed the test without flaws. The bar that failed did not have complete root fusion.

All face and side bend specimens tested in the as-welded condition failed after a very small bend angle.

As a result of these tests, and in view of our field experience with nickel-copper-moly steel, we adopted the AWS/ASTM-E-9015 rod as standard and called for a minor preheat with a furnace stress-relief operation after welding wherever possible. We were, no doubt, influenced by the fact that it has been our standard practice for some years to stress-relieve practically all of our weldments which are subjected to heavy impact loads and also by our feeling that ductility of the metal in the welded joint is of prime importance in our class of service.

We understand that there is considerable doubt regarding the feasibility of stress-relieving 12015 rod because of embrittlement so we would be very cautious in considering the use of this rod for our type of service. Many weldments using 9015 rod have gone through our stress-relieving ovens and into successful field service.

Our shop problems in processing this type of material are more or less confined to the difficulty of forming because of the high yield strength of the steel and the heavy sections which we use. Shop equipment which has proved adequate for mild steel and low-alloy high-strength steel, often does not have the reserve power required for handling Carilloy T-1 steel.

The results obtained by the use of nickel-copper-moly and Carilloy T-1 steels have been highly gratifying and we expect to expand our use of the material in our standard products as soon as restrictions on its use will permit.

AUTHORS' CLOSURE

The authors are grateful to Mr. Busick for his discussion. It is especially pleasing to have supporting evidence from one so closely associated with the fabrication of Carilloy T-1 steel. The additional tension and bend test data for joints of Carilloy T-1 steel welded with E-10016 (Arcos Tensilend 100) and E-9015

(Arcos Manganend 1-M) electrodes are a welcome contribution to the fund of information on the welding of this new steel.

Since preparing the paper, tests have been conducted by the United States Steel Company to determine the Charpy-keyhole-impact properties of E-10015 (Arcos Manganend 2-M) weld metal joining T-1 steel. The chemical composition of undiluted weld metal deposited by the electrode is as follows:

C	Mn	P	S	Si	Ni
0.16	1.97	0.023	0.017	0.41	0.22
Cr	Mo	V		Cu	Ti
0.16	0.43	0.002		0.14	0.018

The ductility-transition temperatures of the weld metal in the as-deposited and stress-relieved conditions are as follows:

Condition	Ductility-transition temperature, F
As-deposited	-172
Stress-relief annealed at 1100 F.	-99

It will be recalled that the transition temperature of as-deposited E-12015 weld metal (Arcos Tensilend 120) is -60 F (Table 8 of the paper), whereas the transition temperature of the as-deposited E-10015 weld metal, as indicated above, is much lower. The transition temperature of the E-10015 weld metal was raised approximately 75 F by stress-relief annealing, but this impairment is much less than that for the E-12015 weld metal described in Table 8. It will be noted that, either as-deposited or as-stress-relief annealed, the transition temperature of the E-10015 weld metal is considerably superior to that of E-12015, as-deposited. In applications requiring maximum notch toughness, the as-deposited E-10015 weld metal would be preferable despite a slightly lower tensile strength, compared with that for E-12015 weld metal. The transition temperature of stress-relieved E-10015 weld metal is sufficiently low that such weld metal would be suitable for structures fabricated by those persons who choose to employ a stress-relief treatment.



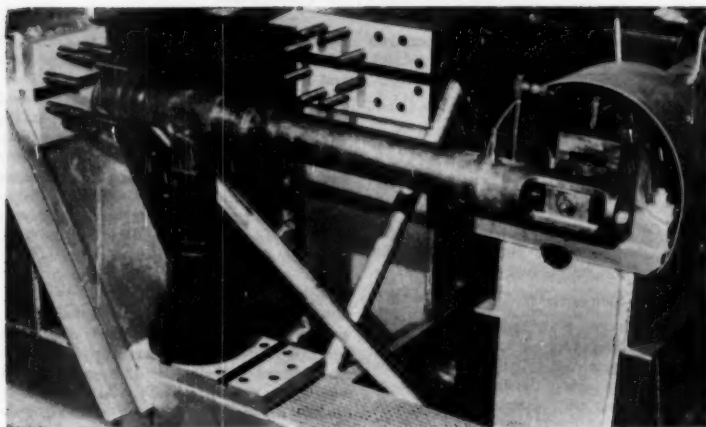


FIG. 1 VIEW OF END BANK OF FATIGUE-TEST MACHINE SHOWING A FABRICATED TEE MOUNTED FOR IN-PLANE BENDING TEST

Fatigue Tests of Piping Components

By A. R. C. MARKL,¹ LOUISVILLE, KY.

This paper presents a compilation of available fatigue-test data on piping components and derives therefrom stress-intensification factors relative to straight pipe. These factors are strictly applicable only to the limited range of sizes for which fatigue tests were made. In view of the importance of proper consideration of stress intensifications in cyclically stressed piping and the lack of theoretical developments which would serve to evaluate their magnitude for all shapes involved, the author has taken it upon himself to suggest empirical correlations by which the application of the available data can be expanded to a wider range of sizes and conditions.

INTRODUCTION

ABOUT five years ago the Product Engineering and Research Department of the author's company initiated a program of fatigue-testing full-scale piping components to provide design data urgently needed by piping engineers for an intelligent appraisal of the safety of piping systems subjected to cyclically varying bending moments resulting from thermal expansion and contraction, from pressure pulsations, or from vibrations.

To date two partial reports on the results of this investigation have been published (1, 2),² one dealing with fatigue of welding

elbows and double-miter bends of specific proportions, and a second with flanged assemblies.

The present paper is intended to round out available knowledge on the bending fatigue of piping components by presenting new results obtained on plain and welded straight pipe, reducers, welding elbows and long-radius bends, forged welding tees, miter bends, and fabricated intersections of various types. A study of the effect of length of arc of welding elbows and angle and spacing of joints of miter bends is also included.

TEST EQUIPMENT

The test equipment for the full-scale tests, a machine of the specific-strain reversed-bending type, was described in an earlier paper (1); it will be sufficient for the present purposes to recall its design by means of Fig. 1.

The isometric diagram, Fig. 2, shows the three alternative

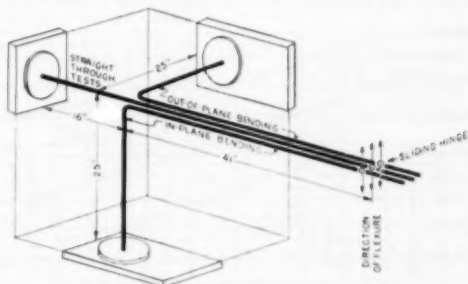


FIG. 2 BASIC TYPES OF ASSEMBLY AND LOADING

¹ Chief Research Engineer, Tube Turns, Inc.

² Numbers in parentheses refer to the Bibliography at the end of the paper.

Contributed by the Petroleum Division and presented at the Petroleum Mechanical Engineering Conference, Tulsa, Okla., September 24, 1926, of THE AMERICAN SOCIETY OF MECHANICAL ENGINEERS.

NOTE: Statements and opinions advanced in papers are to be understood as individual expressions of their authors and not those of the Society. Manuscript received at ASME Headquarters, May 28, 1951. Paper No. 51-PET-21.

anchor locations available in each bay of the machine, and the manner of loading the two basic types of assembly, which follows:

1 Straight assemblies with no directional properties (plain and welded straight pipe, reducers).

2 Essentially ell-shaped assemblies (welding elbows, curved and mitered bends, forged tees, and fabricated intersections), which behave differently under bending in and out of the plane described by the pipe axes.

In all tests, one end of the assembly is anchored rigidly and the other, a hinged end, is constrained to deflect cyclically through a given amplitude maintained by a cam setting.

TEST SPECIMENS

Detailed dimensional descriptions of the test specimens will be given later under separate headings applying to each type.

The material in all cases conformed to ASTM Specification A106, Grade B. The carbon contents of the diverse components used ranged from 0.15 to 0.29 per cent, manganese from 0.50 to 0.90 per cent, and silicon from 0.12 to 0.22 per cent. The tensile strength ran between 62,400 and 86,300 psi, the yield strength between 38,900 and 56,200 psi, and the elongation in 2 in. between 32 and 55 per cent.

In addition, fatigue tests were carried out on an R. R. Moore fatigue machine of the rotating-beam constant-load type using polished bars machined from two heats of pipe selected to bracket the extremes of physical properties encountered in Grade B pipe in the as-received condition. The results of these tests are shown in Fig. 3 together with *S-N* data for an average heat communicated by the National Tube Company and one for a low-strength material taken from R. L. Dennison's paper (3). All tests were made in air and, while different machines and speeds were used, the results are roughly comparable.

It is interesting to note that despite the relatively wide spread in physical properties, the endurance strengths of the two materials tested by the author's company closely parallel each other. The mathematical expression for the *S-N* curve shown, which was derived using 29 individual test points for each of the two steels, following a procedure suggested by M. G. Corson (4, 5), is

$$\frac{S - 35,900}{1000} = 1.0741 \frac{S - 35,900}{1000} = \frac{1,242,900}{N} \dots \dots [1]$$

where *N* is the number of cycles of stress reversal to failure and *S* (psi) is the corresponding stress amplitude known as the "endurance strength" for a given number of cycles.

The "endurance limit," i.e., the stress amplitude which can be supported indefinitely, is found by setting $N = \infty$, reducing the

right side of the equation to zero; its average value is 35,900 psi, whereas individual evaluations for each of the heats gave 34,200 and 37,300 psi, respectively.

For the opposite limit, i.e., the strength available for a single load application, insertion of $N = 1$ in Equation [1] gives 182,000 psi. It is interesting to note that this value corresponds to the average of the true ultimate strengths² computed for the two heats, which are 165,000 and 199,500 psi, respectively.

Attention is directed to the consistency of the test data, considering that part of the tests were carried out in a range of pronounced yielding, at elastically calculated extreme fiber stresses approaching double the yield strength.

PROCEDURE AND EVALUATION

As in the earlier tests, the assemblies were mounted in the machine, subjected to individual load-deflection calibrations, filled with water to provide a ready means for detecting failure, and finally flexed cyclically through a predetermined amplitude maintained by a cam setting until a leak signaled a crack through the entire wall.

The results are recorded as points on *S-N* plots. The number *N* of cycles of full stress reversal withstood by the specimen was read directly on a revolution counter. The corresponding nominal stress *S* (psi) is computed from the ordinary beam formula:

$$S = \frac{PL}{Z} \dots \dots \dots [2]$$

The load *P* (lb) herein is taken from the load-deflection calibration curve of the individual assembly or, for loads causing plastic flow, from a straight-line extrapolation of the elastic portion of the curve. In effect, this defines the computed stresses strictly as products of the applied strains and Young's modulus; wherever they exceed the yield point, they are obviously fictitious.

The lever arm *L* (in.) is directly measured from the point of load attack (center of hinge) to the point of initial failure.

The section modulus *Z* (cu in.) used in Equation [2] is that of pipe of the size and schedule or weight with which the fitting is intended to be used, which is not necessarily that of the fitting itself; the difference may be considerable, as in the case of forged tees where excess metal is distributed variously to provide reinforcement for the branch opening. This procedure recognizes the practical application; since straight pipe composes the major part of piping and hence is the dominant factor in piping stress

² The true ultimate strength is obtained by dividing the applied load to failure in a standard tensile test by the necked-down area, rather than by the original cross section as is done in obtaining the conventional ultimate strength.

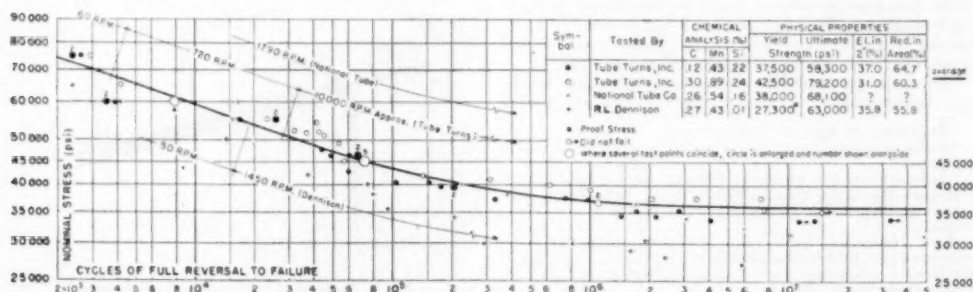


FIG. 3 S-N DATA FROM POLISHED-BAR FATIGUE TESTS

analysis, it furnishes the most practical reference for the evaluation of the effects of other components, which are of local influence only.

The stresses thus computed are plotted against the number of loading cycles sustained in Figs. 4 to 17, inclusive; the results obtained in laboratories of the author's company are indicated by circles, those transcribed from a paper by D. B. Rosheim and the author (7) by squares, and those obtained by J. S. Blair (8) in England by diamonds. Where specimens did not fail, this is shown by an arrow pointing to the right; for specimens which were tested under internal pressure, an arrow pointing up is shown, the tip of the arrow indicating the equivalent endurance strength for complete reversal in accordance with a relation suggested by H. F. Moore and J. D. Kommers (9). The different groups of tests will be discussed in detail in the following sections.

In order to make this test information useful to the practicing engineer, the individual data preferably should be correlated and expressed in the form of equations or design constants which can be used directly in calculations. A first step in such an endeavor is to search for a mathematical formula which will fit the individual test data. Ideally, this should be valid over a range embracing the practical limits, which in the present case are $N = 1/4$, corresponding to a single load application, and $N = \infty$, corresponding to an unlimited number of cycles. A formula of the type of Equation [1] derived for the polished-bar tests was studied for application also to the full-scale fatigue tests, but the available data were considered insufficient in number, too limited in range, and too divergent to warrant advocating a more refined formula than the one adopted in the earlier paper (1) which is

$$S = mN^{-a} \quad [3]$$

This formula has a limited range of application only, roughly from $N = 10^1$ to $N = 10^6$. S and N are endurance strength and number of reversals, respectively, and m and a are constants which will be discussed more in detail later.

By the method of least squares, the most probable values for these constants can be derived to fit any given group of test points, but, in general, both the factor m and the exponent a will differ from group to group. For design use, on the other hand, it would be desirable if the exponent could be assumed to be identical for straight pipe and all types of fittings, since this would permit expressing the endurance strength of any component in terms of that of straight pipe, by the application of a so-called stress-intensification factor i . A study of the data has indicated that a selection of $a = 0.2$ serves all types of fittings investigated⁴

⁴ Evaluation of individual test series gave values of a ranging between extremes of about 0.1 to 0.3, but most values were within 20 per cent of 0.2, which represents a fair average; it is interesting to note that C. E. Strohmeier (6) in 1914 advocated an exponent $a = 0.25$ in a slightly different formula for correlating endurance strength and cycles to failure.

reasonably well, and that the base factor can be taken as $m = 245,000$ for straight pipe,⁵ leading to the following generally applicable formula

$$iS = 245,000 N^{-0.2} \quad [4]$$

To the extent that direct test data are available, this formula may be looked upon as a satisfactory means of correlating endurance strengths of different fittings or fabricated connections over the range from about 100 to 1,000,000 cycles. However, to date only the 4-in. size in standard weight has been explored to any major extent. Even this has taken many years of concentrated effort, and if its fruits are to be made available today to the practicing engineer, who has to work with a wide range of sizes and thicknesses, some vehicle for extrapolation to other sizes and proportions has to be established. For curved pipe, several theoretical analyses (10, 11, 12, 13) are available which will serve the purpose; for all other shapes, no relevant theories are yet available. It is thought, however, that the effects of variations in significant proportions of forged tees, miter bends, and fabricated intersections might be predicted by analogy with curved pipe, and an attempt at such a correlation is discussed later.

PLAIN AND WELDED STRAIGHT PIPE

The $S-N$ curve for straight pipe provides the most logical reference line for the correlation of the fatigue properties of other piping components, and hence it becomes important that it be established properly.

In Fig. 4 all the available test data on plain unwelded pipe have been compiled. The squares are points from tests by Wallstrom and Slesak (7) which were used in the author's prior papers (1, 2) to establish a base line for straight pipe, for which the formula is given by introducing $i = 1$ in Equation [4] of the present paper. Failure in these cantilever tests, which were carried out in a lathe, occurred at the chucked end, as was to be expected, this being the point of maximum moment. However, clamping stresses apparently contributed to failure in these tests, as was proved by check tests run by the author's company (recorded as open circles); by substituting a collet-type holder to distribute and moderate the clamping action, an improvement in endurance strength of the order of 20 per cent was effected. For a final test series, a special shape of test specimen was devised and secured in the form of upset forgings. Significant dimensions of the test section proper of this smooth-transition type of specimen are shown in Fig. 18; no machining was done at or near the test section, only light grinding to remove flaws and die gripping marks. Endurance strengths over 50 per cent higher than in

⁵ The factor $m = 245,000$, originally established in reference (1), was confirmed by the present tests as a reasonable base value for welded or clamped straight pipe.

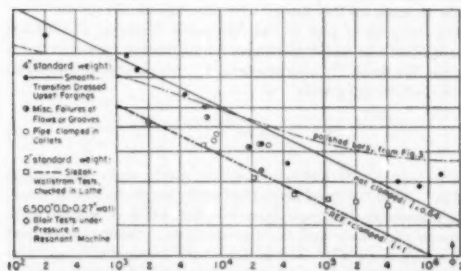


FIG. 4 PLAIN STRAIGHT PIPE

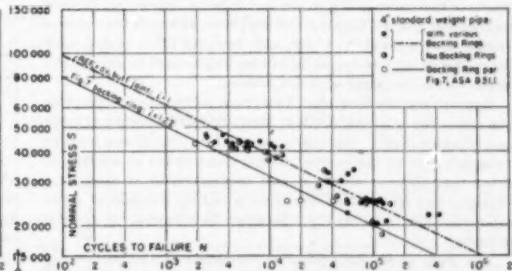


FIG. 5 BUTT-WELDED JOINTS IN STRAIGHT PIPE

the Slezak-Wallstrom tests were obtained. Specimens in which minor defects were left (half-filled circles) gave intermediate strengths. Finally, two points from J. S. Blair's tests (8) under pressure on a resonant type of testing machine are plotted (diamonds with arrows); it is suspected that these results were influenced by the clamping action of the actuator.

Fig. 5 shows the results of tests on pipe with a circumferential butt weld. The welding groove in all cases was a standard V-groove (see Fig. 12 of Code for Pressure Piping, ASA B31.1-1951), but the welding procedure was varied by using different gap widths ($1/16$ in. to $1/8$ in.), different electrode sizes for the first pass ($1/16$ in. and $3/16$ in.), different finished external weld contours (varying from flush grind to $1/4$ in. overlay) and different postweld heat-treatments (furnace and torch stress relief versus as-welded); also a variety of backing rings were used for comparison of joint performance with that for welds made without backing rings. While procedural differences appeared to affect the endurance strength, the effect was not pronounced; in fact, more variation was observed between the strength of welds produced by different qualified welders using supposedly identical procedures.

Specifically, welds made with and without backing rings gave nearly the same results; the unbacked joints were a little weaker on the average and slightly more erratic in performance, probably as a result of lack of penetration. This bears out the general experience that welds of equal quality can be made with and without backing rings, but that backing rings give a better assurance of consistent penetration. Attention is directed to the test points obtained with recessed backing rings of 10-deg taper made in accordance with Fig. 7 of the Code for Pressure Piping, which have been segregated because they showed a consistently lower endurance strength than any of the other backing rings. This could be interpreted to reflect no more than the effect of the reduction in the wall thickness of the pipe at the weld peculiar to this construction.

Failures invariably occurred as circumferential cracks, in both the plain and the welded pipe. In the latter, cracks predominantly were located at the edge of the weld when stresses in excess of the yield strength were applied, and at the center of the weld when stresses below the yield point were applied or the weld overlay had been ground off.

This summarizes the test data. The question now arises what particular set of data should be established as the point of departure for purposes of correlation; to make a happy decision on this crucial point, it appears proper to look ahead at the other test data, i.e., to consider all the graphs in Figs. 6 to 17, inclusive.

Since polished-bar fatigue tests are easily run, the curve for polished bars given in Fig. 3 would be ideal as giving the basic material information, to which all other data could be correlated through a shape factor. Unfortunately, as is evident from the replot of this curve in Fig. 4, the test data for commercial straight pipe do not parallel those for polished bars, although they show a similar knee around $N = 10^6$, and those for other piping components give no evidence at all of trending toward an asymptotic value within the range of cycles covered.

Renouncing this basis, one would next incline toward adopting the endurance strength of plain (unwelded and unclamped) pipe as a reference basis. But this is not practical; maximum bending moments in a piping system always occur either at anchors or other restraints, at points of load application or at directional changes, and all of these introduce a certain measure of stress intensification; even in the laboratory they cannot be avoided entirely.

The least stress intensification encountered in practice apparently is that introduced by clamping pipe or by a butt-welded joint; and this accordingly furnishes the most practical basis to

which to correlate new data. Graphically, this basis is represented by the heavy dash-dot line repeated on all charts; it can be expressed mathematically by setting $i = 1$ in Equation [4].

REDUCERS

On the basis of reasoning, as also from what was learned in testing welding neck flanges (2), it was anticipated that smoothly contoured commercial reducers made to the dimensions of ASA Standard B16.9 would show similar fatigue behavior as butt-welded joints of the smaller size. This was verified by tests on three 4-in. \times 2-in. standard weight reducers. If the test points were plotted in Fig. 5 they would practically fall on the dash-dot base line, indicating that $i = 1$. The type of failure likewise was identical, being circumferential, with the crack appearing at the edge of the attachment weld to the 2-in. pipe in the one specimen stressed beyond the yield point, and through the center of the weld in the other two lower-stressed specimens.

CURVED PIPE

Since the discovery, over 40 years ago, that curved pipe is more flexible than straight pipe, a number of explanatory mathematical theories have been advanced. Most piping stress analysts are familiar with the parallel developments by Th. von Kármán (10) and Wm. Hovgaard (11) for in-plane bending, and that of I. Vigness (12) for out-of-plane bending. On the other hand, L. Beskin's (13) refinement and extension of von Kármán's analysis, which applies to both types of loading, has been little used, probably because his findings were expressed in an unfamiliar form. Since his is the most accurate practical theory, as the tests communicated herein confirm, it is thought desirable to include, as Table 1, values from which curves for Beskin's stress-

TABLE 1 BESKIN'S FLEXIBILITY AND STRESS-INTENSIFICATION FACTORS

Flexibility characteristic $IR/r^3 = k$	Flexibility factor, k	Transverse stress (intensif. factor for)		Longitudinal stress (intensif. factor for)	
		In-plane bending, γ	Out-of-plane bending, β	In-plane bending, β	Out-of-plane bending, β
0.033	30	18.091	14.727	8.12	10.22
0.046	35.4	14.247	11.739	6.43	8.10
0.066	25.0	11.273	9.273	5.09	6.46
0.092	17.7	8.967	7.433	4.08	5.19
0.132	12.50	7.000	5.795	3.26	4.17
0.185	8.85	5.362	4.673	2.54	3.28
0.264	6.17	4.318	3.682	1.99	2.60
0.330	4.91	3.682	3.182	1.68	2.23
0.462	3.36	2.851	2.538	1.277	1.76
0.660	2.34	2.109	1.973	1.010	1.439
0.924	1.720	1.558	1.500	0.881	1.238
1.330	1.375	1.114	1.091	0.889	1.123
1.848	1.190	0.804	0.794	0.937	1.063
2.640	1.096	0.565	0.562	0.968	1.032
3.360	1.048	0.453	0.451	0.979	1.021
∞	1	0	0	1	1

intensification and flexibility factors can be constructed. Also it was thought to be helpful toward an understanding of its significance to compare this theory with the older theories.

Fig. 19 gives a plot of the Hovgaard, Vigness, and Beskin longitudinal and transverse stress-intensification factors β and γ against the flexibility characteristic k ; this parameter is defined by the following formula

$$k = \frac{IR}{r^3} \quad [5]$$

where t is pipe-wall thickness, R is bend radius, and r is mean pipe radius. Note the good accord between the predictions of alternate theories in the range above $k = 0.3$, which covers the more common pipe sizes and bend proportions. Similar agreement exists with respect to the location of the maximum stress; also for the flexibility factor k which expresses how many times greater the deflection of curved pipe is as compared with straight

pipe under comparable loading. All this is no longer true for lower values of h where the accord rapidly deteriorates. The older theories are no longer adequate, and Beskin's is the only valid approach, as will become evident from the experimental evidence to be adduced.

Before going on to the tests, it may be worth while briefly to indicate what Beskin's theory would lead us to expect. It will be noted that his transverse factor γ is much higher than his longitudinal factor β over the entire range of flexibility characteristics over which significant stress intensifications exist, particularly for in-plane bending; this leads to an expectation of failure by longitudinal cracks. As a detailed study of Beskin's paper (13) will reveal, these cracks should occur directly at the side of the curved pipe, irrespective of the bend proportions in the case of in-plane bending. For out-of-plane bending, the location of maximum transverse stress depends upon the flexibility characteristic; for $h = 0.03$ it is located about 15 deg from the side of face toward the inner arc (as measured around the pipe circumference) for $h = 0.25$ about 30 deg from the inner arc, for $h = 0.6$ about 40 deg from the inner arc, and for larger values it asymptotically approaches 45 deg, i.e., the mid-meridian between the crotch and the side of the bend. As concerns the flexibility factor, Beskin shows that this varies approximately as the inverse of the flexibility characteristic (at least up to $h = 1$) and thus can exceed greatly the limit of $k = 10$ given by the earlier theories.

With a basis for comparison established by these introductory notes, the test results will now be discussed. Table 2 lists the significant dimensions of the variants investigated by the author's company and others, and presents condensed test results in the form of experimentally derived stress-intensification factors i .

Figs. 6 and 7 show all the $S-N$ data available on short-radius 90-deg welding elbows, for in-plane and out-of-plane bending,

respectively. Two test variants are included in each graph, standard weight ($h = 0.210$) and special lightweight ($h = 0.062$) elbows, the latter made from tubing machined and dressed externally before processing to give a fitting of minimum practicable flexibility characteristic. It will be noted that the test points of both variants roughly parallel the dash-dot curve labeled "REF." carried over from Fig. 4.

In a similar manner, Figs. 8 and 9 summarize the results obtained for long-radius elbows, except that six tests under pressure, treated in a prior paper (1), are omitted for the sake of clarity, since they leave conclusions unchanged. Two thicknesses were tested, standard weight ($h = 0.316$) and 0.101 in. ($h = 0.129$), the former through a wide range of arc lengths, the latter in the form of 90-deg elbows only. Averages for the 90-deg arcs are shown by solid and dash lines; those for the different arcs are plotted separately against arc in Fig. 20.

Additionally, tests of 4-in. IPS standard weight, 20-in. bend radius ($h = 1.057$) hot-formed shop bends were run in both in-plane and out-of-plane bending. This test series was beset by troubles due to repeated weld failures and, while actually three specimens were tested in each direction, only one of each group was considered sufficiently reliable for use in establishing the stress-intensification factors shown in Table 2. No plot is included for this series, nor for the results abstracted from reference (7) relating to 2-in. IPS standard weight, 12-in. radius ($h = 1.500$) bends tested essentially in the plane of curvature.

Type and location of the failures in our tests in general agreed surprisingly well with predictions from Beskin's theory, considering that tests were made using standard commercial products without any effort to select perfect specimens. Fig. 21 shows a selection of failed specimens, not only of elbows, but also of other types of fittings which were found to be related by their behavior, as will be discussed later.

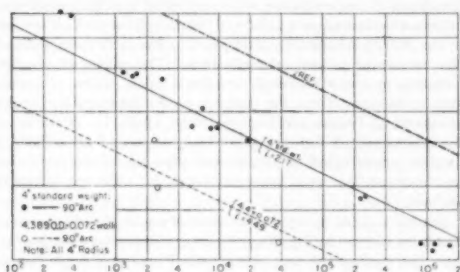


FIG. 6 SHORT-RADIUS ELBOWS, IN PLANE

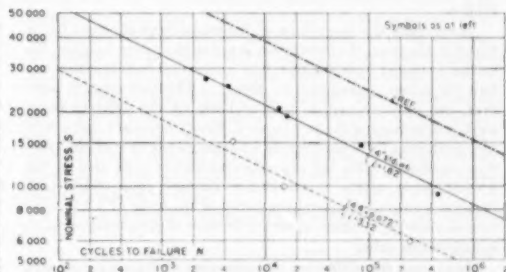


FIG. 7 SHORT-RADIUS ELBOWS, OUT OF PLANE

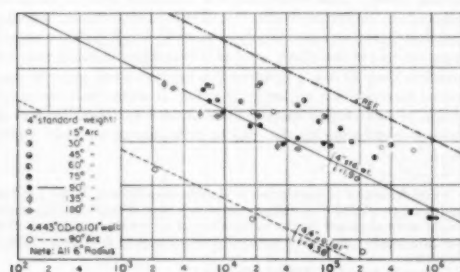


FIG. 8 LONG-RADIUS ELBOWS, IN PLANE

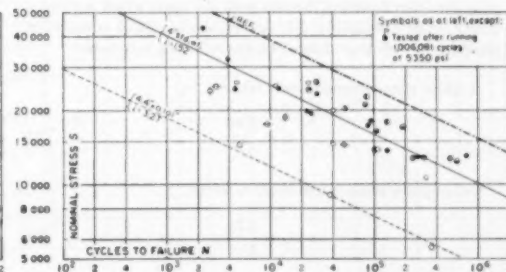


FIG. 9 LONG-RADIUS ELBOWS, OUT OF PLANE

TABLE 2 DIMENSIONS AND EXPERIMENTALLY DERIVED STRESS-INTENSIFICATION FACTORS FOR ELBOWS AND BENDS

Average measured dimensions				Derived data		Experimentally determined stress-intensification factors	
Outside diam. OD	Wall thickness, t	Bend radius, R	Arc, α	Mean pipe radius, r	Flex. characteristic, k	In plane, i_i	Out of plane, i_o
4.399	0.072	4	90	2.158	0.062	4.49	3.32
4.530	0.241	4	90	2.144	0.210	2.17	1.82
4.443	0.101	6	90	2.171	0.129	4.38	3.27
4.534	0.245	6	180	2.144	0.320	2.02	2.07
4.548	0.340	6	135	2.151	0.319	2.10	1.95
4.511	0.240	6	90	2.135	0.316	1.90	1.52
4.548	0.252	6	75	2.148	0.328	1.70	1.43
4.537	0.253	6	60	2.142	0.331	1.53	1.32
4.541	0.249	6	45	2.146	0.324	1.36	1.29
4.552	0.255	6	30	2.148	0.332	1.28	1.39
4.536	0.261	6	15	2.142	0.328	1.46	1.63
4.542	0.244	20	243	2.149	1.057	0.87	0.94
2.373*	0.164	12	135	1.110	1.590	1.21	-

* This test series from reference (7); all other tests by author's company.

Under in-plane bending, all elbows of 45 deg or more (with one anomalous exception) failed by the formation of a regular longitudinal crack along one or both sides, where theory predicts the maximum stress; this was located in the body of the fitting in all cases, except for three of the 45-deg arcs which cracked across the weld. Arcs of 30 deg or less, on the other hand, always failed by circumferential cracking, either in the attachment weld or alongside it, or, in one instance, in the crotch midway between welds.

Under out-of-plane bending, two alternate types of failure were encountered; the lightweight fittings, both short- and long-radius types, showed regular longitudinal cracks within 15 deg or less of the circumferential location predicted by theory. Most of the standard-weight fittings, including all tests of arcs shorter than 90 deg, failed by circumferential cracking at the weld or through the body of the fitting, but a few cracked longitudinally in the middle third zone between the inside arc and the side of the fitting, again roughly where theory would lead one to expect failure.

As concerns the magnitude of the stress-intensification factor found in the tests, the correlation is not as clear cut; roughly, the values i derived from the test data correspond to only about one half the values γ predicted by theory. This discrepancy, however, can be explained, in part at least, by the different bases used in determining the two factors; theory considers shape only and predicates its deductions on a homogeneous tube of ideal surface condition, while the experimental factors i , as used in the present paper, relate to a welded or clamped pipe, which itself involves a proved stress-raising factor of the order of 1.5 in relation to plain pipe, which in turn falls short of presenting an ideal homogeneous tube.

Apart from this difference in basic point of departure, the test results correlate rather well with the Beskin theory. This will be apparent from an examination of Fig. 22 wherein the stress-intensification factors i , derived from the tests, which covered a broad range of flexibility characteristics, are plotted as circles in comparison with lines defined by the following equations:

In-plane stress-intensification factor

$$i_i = \frac{0.90}{k^{1/2}} \quad [6]$$

Out-of-plane stress-intensification factor

$$i_o = \frac{0.75}{k^{1/2}} \quad [7]$$

These equations give values i_i and i_o roughly equal to one half the

values γ_i and γ_o read from Fig. 19; $i_i = i_o = 1$ should be used as a minimum.

For the flexibility factor k , i.e., the ratio of the actual deflection of a curved tube to that predicted for it by the ordinary beam theory, Beskin has proposed a similar approximation, as follows:

Flexibility factor (for either plane)

$$k = \frac{1.65}{\gamma} \quad [8]$$

An evaluation of the load-deflection calibrations preceding our fatigue tests served as a rough confirmation of Beskin's prediction, but no detailed data are given here because the type of assembly used for the fatigue tests was poorly suited to a precise determination of flexibility factors; moreover, Pardue and Vigness' paper (14)* has already established the adequacy of Beskin's theory in this respect.

The latter source also presents a rather thorough exploration of the effects of end restraints, which indicated that flanges directly attached to the ends of an elbow or return bend cancel a large part of the latter's inherent flexibility and at the same time diminish the associated stress intensification. The effect of straight tangents, on the other hand, was found to be minor. It would appear, however, from the author's earlier investigation⁷ and a discussion of Pardue and Vigness' paper by D. R. Zeno⁸ that if the inherent flexibility of a curved tube is to be fully utilized, a tangent length equal to at least two pipe diameters, preferably greater, must be present between its ends and adjoining flanges or anchors.

Our tests, made to explore the effect of arc length, the results of which are plotted in Fig. 20, gave lower stress-intensification factors, the smaller the arc; for practical purposes, these factors could be approximated by simple interpolation between unity, corresponding to zero angle, and the value of i determined for a 90-deg elbow. This would indicate that there is a tendency for tangents to inhibit the ovalization of curved tubes under bending, but that this effect extends only a relatively small distance inward from the end of the elbow, so that it becomes noticeable only for arcs less than 90 deg. Incidentally, for very small arcs the suggested interpolation no longer is valid; it seems that the interaction of two closely spaced welds creates an intensification of stresses overshadowing that due to curvature under these conditions.

* The flexibility factors given in the last two lines of Table 2 of the reference straddled the values computed from Equation [8]; these values were obtained by the application of moments to bends involving tangents of moderate length, of a wide range of flexibility characteristics.

⁷ Refer to fig. 15, p. 879 of reference (1).

⁸ See fig. 20, p. 87 of reference (14).

WELDING TEES

While drawn tees must and do conform to certain dimensional and strength requirements set forth in ASA Standard B16.9, commercial products differ considerably in external contour and metal distribution. To explore the effect of shape on fatigue strength, three sets of 4-in. standard-weight tees were tested, for which the significant dimensions are given in Table 3; this also lists stress-intensification factors obtained by an empirical correlation in comparison with averages from the tests.

TABLE 3 DATA FOR ASA WELDING TEES

Contour	Barrel-shape	Cylindrical	Conical
External crotch radius, in.	1 1/8	1	5/8
Average run thickness, in.	0.336	0.293	0.348
Average crotch thickness, in.	0.436	0.406	0.395
Stress-intensification factors:			
As computed	1.30	1.58	1.50
From In-plane tests	1.13	1.34	1.49
Out-of-plane tests	1.27	1.63	1.91
Computed			
Ratio: Avg from tests	1.08	1.06	0.88

Tests were conducted in bending in and out of the plane, in three positions: 1, moment carried through branch into one end of run and thence to anchor; 2, moment carried through one end of run into branch and thence to anchor; and 3, moment carried straight through run. Fig. 1 represents the second position, and also shows the pipe extension, of a length equal to two pipe diameters, which was attached to the unused outlet to simulate the presence of another unstressed pipe run.

The results are recorded in Figs. 10 and 11. For any one style of tee, the first and second loading positions gave practically identical results, so that there appeared to be no need for making a distinction in plotting the data. The third position as a rule gave higher endurance strengths; data for it have been disregarded in arriving at the average stress-intensification factors shown, since it would complicate unduly application to piping stress analyses if separate values were to be specified.

The specimens tested through the branch (first or second positions) in most instances cracked in the same way as a similarly situated elbow would, as is evident from a study of Fig. 21. Under in-plane bending, the main cracks occurred along an arc paralleling the crotch, although magnetic-powder inspection revealed additional circumferential fissuring at the crotch, which, however, did not cause failure. For out-of-plane bending, cracks were directed more or less radially, corresponding to the transverse cracks found in elbows under this loading. In distinction from elbows, however, tees revealed a higher stress intensification in out-of-plane bending than in in-plane bending. For the straight-through tests (third position), failure occurred by

cracking along the center or edge, or across the apex, of the weld attaching the branch to the run.

The three types of tee selected for this study exhibited pronounced differences in endurance strength. In light of what was observed relative to location and nature of failures, the metal thickness available in the crotch zone and the crotch radius were thought to be the controlling factors. It was reasoned that a satisfactory correlation should be obtainable by considering the tees as if they had been elbows of an effective thickness t_e equal to the average of the crotch and side-wall thicknesses, and an effective bend radius R_e equal to the sum of the pipe radius r and the crotch radius r_c . This led to the assumption of the following effective flexibility characteristic h_e for use in Equation [6]⁹ giving the stress-intensification factor

$$h_e = c \frac{t_e R_e}{r^3} = \left(\frac{t_e}{t} \right)^{1.5} \frac{t_e (r + r_c)}{r^3} = \left(\frac{t_e}{t} \right)^{1.5} \frac{t}{r} \left(1 + \frac{r_c}{r} \right) \dots [9]$$

The coefficient c takes account of the increased section modulus of the tee, as compared with straight pipe; while the increase in section modulus is given directly by the ratio of the effective thickness t_e of the tee to the thickness t of the matching pipe, this ratio has to be raised to the three-halves power in view of h_e entering the formula for the stress-intensification factor in the two-thirds power.

By reference to the last line in Table 3 it will be noted that the procedure suggested produces a reasonably satisfactory correlation, considering the complex shape involved, at least for the three variants tested.

MITER BENDS

Bends produced by welding miter-cut pieces of pipe together may be expected to involve higher local stresses than smoothly curved bends of the same over-all radius. Factors which may influence the magnitude of the stress intensifications under bending are miter angle and miter spacing, in addition to the common variables of pipe radius and thickness. The test program undertaken was designed to explore the effects of these variables.

Fig. 12 gives the significant dimensions of the variants tested, and, together with Fig. 13, serves as a record of the individual test results. From these data average stress-intensification factors have been computed, but in order to avoid confusion on the charts, only those applying to a crotch spacing $s = 4 1/2$ in. have been represented by lines.

A plot covering the stress-intensification factors for all the

⁹ Use of Equation [6] applicable to elbows under in-plane bending is suggested to provide a conservative correlation for both in-plane and out-of-plane bending.

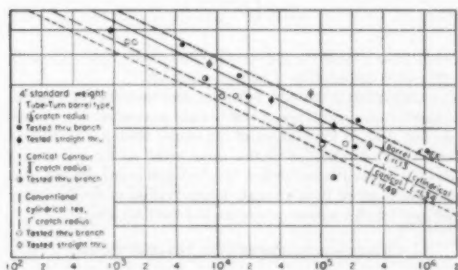


FIG. 10 FORGED WELDING TEES, IN PLANE

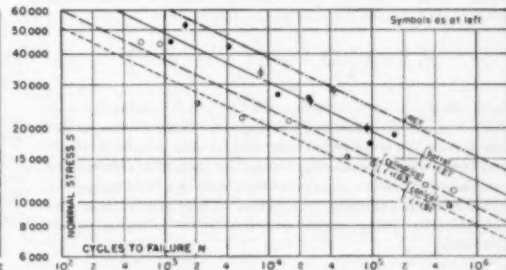


FIG. 11 FORGED WELDING TEES, OUT OF PLANE

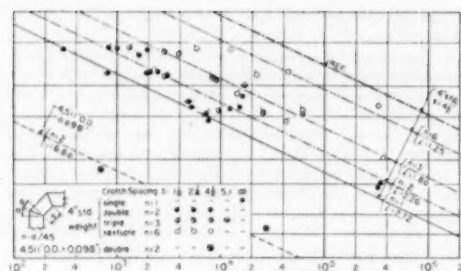


FIG. 12 FABRICATED MITER BENDS, IN PLANE

variants of 4-in. standard weight is given in Fig. 23, using the miter angle α as abscissa. A marked increase in stress-intensification factor is evidenced as the miter angle is increased from $7\frac{1}{2}$ deg, corresponding to six miters per 90-deg arc, to 45 deg for a single-miter bend. A second plot, Fig. 24, against the miter spacing at the crotch or inner arc, reveals that this has a modifying influence which is particularly pronounced in the case of the smaller miter angles. Earlier in this paper, attention was directed to a similar effect in the case of small-arc smooth elbows, and points for the latter have been included in this plot to illustrate the similarity in trend.

Attention is directed to the fact that, as contrasted with smooth bends, the stress-intensification factor for out-of-plane bending is generally higher than that for in-plane bending, an observation which has been made already for forged tees and will later be shown to apply equally to fabricated intersections.

Representative illustrations of failed test specimens are included in the top row of Fig. 21. Under in-plane bending, the cracks causing failure were about evenly divided between longitudinal cracks at the side of the elbow, where they ordinarily occur in smooth bends, and circumferential cracks, either in or alongside the welds, these being oriented further toward the inner arc than one would expect from the curved-pipe analogy. Under out-of-plane bending, only a few failures occurred in the form of longitudinal cracks, these being located about 30 deg inward from the side, roughly where they would be expected for curved bends; the majority of the cracks were circumferential through the center or alongside the welding bend, directly at the side of the bend, or displaced up to 30 deg toward the inner arc.

The observed similarities in character and location of failure suggest that a correlation of the stress-intensification factors with those for smooth elbows should prove possible, as was found to be the case for forged tees. As a first assumption for the effective bend radius R_e , the center-line radius of the inscribed elbow might be used; from geometry, this is

$$R_e = r + \frac{s}{2} \cot \alpha = r \left(1 + 0.5 \frac{s}{r} \cot \alpha \right) \dots [10a]$$

where r is the mean pipe radius, s is the crotch spacing between miters, and α is the miter angle in degrees. A correlation on this basis is found to serve reasonably well for 4-in. standard-weight miter bends with close spacing, but not for such with wide spacing or single-miter bends. It appears that there is a limiting spacing beyond which the effective bend radius remains substantially constant, the latter being roughly described by the following empirical formula

$$R_e = r \frac{1 + \cot \alpha}{2} \dots [10b]$$

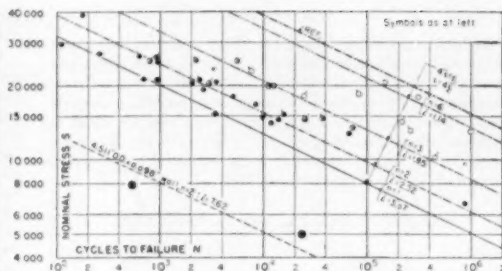


FIG. 13 FABRICATED MITER BENDS, OUT OF PLANE

It will be noted that this second formula gives a limiting bend radius equal to the pipe radius for a single-miter bend ($\alpha = 45$), as would appear reasonable; also that it operates less and less as a limitation as the miter angle α approaches zero, or, what is the same, the contour of the miter bend approaches that of an elbow, as is illustrated in Fig. 25.

Using the foregoing values of R_e in place of R in Equation [5], the following expression for the effective flexibility characteristic h_e for miter bends is obtained

$$h_e \leq \left(1 + 0.5 \frac{s}{r} \cot \alpha \right), \leq \frac{1}{2} \left(1 + \cot \alpha \right) \dots [11]$$

In Fig. 22 the experimentally determined stress-intensification factors i are plotted against values h_e so computed. It will be noted that the test points, indicated by squares, roughly fall within the band defined by Equations [6] and [7], except for those applying to thin-wall miter bends which fall considerably above the top line. This would indicate that the correlation obtained is adequate for proportions represented by the 4-in. standard-weight specimens, but that a strong modifying influence of the thickness-to-diameter ratio is present which is not accounted for.

Fig. 25 has been prepared to illustrate the effect of the number of miters used in making a 90-deg elbow, as evaluated by the procedure suggested. It will be noted that the stress-intensification factor is sharply reduced in going from a single- to a double-miter bend, and for a larger number of miters progressively approaches the value applicable to an elbow of the same radius. This study also serves to point out how differences between alternate designs are magnified if they are considered not in terms of the controlling stress iS , but in terms of fatigue life N ; this becomes readily apparent by rewriting Equation [4] in the following form

$$N = \left(\frac{245,000}{iS} \right)^b \dots [4a]$$

This served as a basis for the computation of the figures given in Fig. 25 under the heading "Corresponding Life."

An examination of the load-deflection data indicates that single- and double-miter bends are not as flexible as comparable smooth bends, but that, as the number of miters per 90-deg arc increases beyond three, flexibilities of the same order as for elbows are attained. As mentioned earlier, the test specimens did not lend themselves to more than a rough determination of the flexibility factor, and for this reason no specific data will be given.

UNREINFORCED FABRICATED INTERSECTIONS

Tests to be reported upon under this heading refer to assemblies made by cutting an opening in straight pipe and welding onto it a

branch cut from the same size and weight of pipe so as to produce a full-size tee. Significant dimensions are given in Fig. 14, and this together with Fig. 15, serves to record the direct test results.

The *S-N* data for tees fabricated from 4 1/2-in-OD pipe of 0.237 in. and 0.203 in. thickness, specifically the former for which a large number of individual tests were run, show trends closely paralleling that of the reference line representing straight pipe. The exploratory pairs of tests carried out with fittings of only 0.100 in. and 0.053 in. wall, on the other hand, do not fit too well, which might reflect the effect of the actual size of the intersection weld which could assume importance in view of the light wall. The data taken from Blair's paper (8) fall well in line and also serve to indicate that it makes little difference, if any, whether the branch is set onto the run or into it.

The failure pattern for bending through the branch again bore resemblance to that encountered in curved pipe, as is evident from the second and fourth illustrations in the bottom row of Fig. 21. Under in-plane bending, the cracks invariably crossed the attachment weld in the same position in which they would be found in the body of an elbow. Under out-of-plane bending, the cracks occurred along the weld on the side, about where they occurred in miter bends, but fine cracks across the weld, corresponding to longitudinal cracks in elbows, were also observed. For bending straight through, with the unloaded branch up, the cracks were located at the side bisecting the angle formed there by the attachment weld.

In attempting a correlation with curved pipe, it was found that the same type of formula as was found applicable for single-miter bends could be used with good success. Introducing $\alpha = 45$ in Equation [10b], the bend radius is found to equal the pipe radius, and the effective flexibility characteristic k_s simply becomes

$$k_s = \frac{tR_s}{r^2} = \frac{t}{r} \quad [12]$$

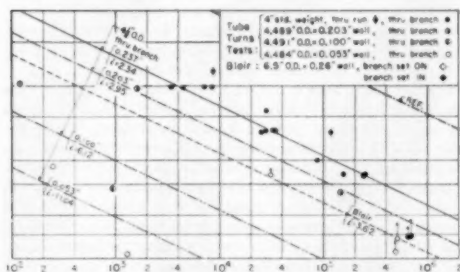


FIG. 14 UNREINFORCED INTERSECTIONS, IN PLANE

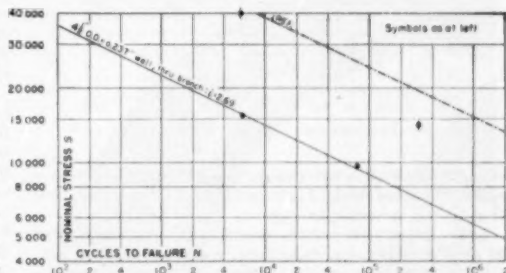


FIG. 15 UNREINFORCED INTERSECTIONS, OUT OF PLANE

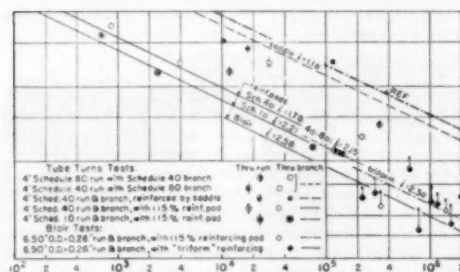


FIG. 16 REINFORCED INTERSECTIONS, IN PLANE

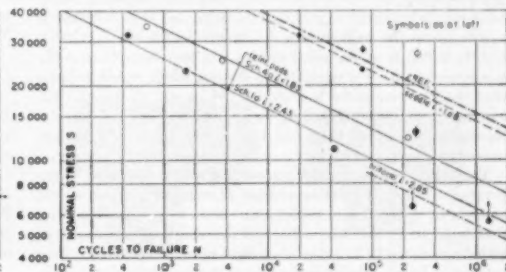


FIG. 17 REINFORCED INTERSECTIONS, OUT OF PLANE

In Fig. 22 the stress-intensification factors, obtained from tests on fabricated tees of widely varying *t/r*-ratio, are plotted as diamonds against values of k_s computed from this formula. The test points are reasonably well aligned with the heavy line corresponding to Equation [6], but, as in the case of miter bends, the correlation tends to give unconservative results for low values of k_s , particularly if it is considered that bending out of plane (for which condition test data are available only for standard weight) may be expected to produce higher stress intensifications.

REINFORCED FABRICATED INTERSECTIONS

All the available *S-N* data on reinforced fabricated intersections are compiled in Figs. 16 and 17. Sketches and essential data on the test assemblies are given in Fig. 26; it will be noted that the variants tested differed both in the way the reinforcement was provided and in the amount of reinforcement included. The percentage of reinforcing is shown computed on two different bases: in the first, which is designated as the ASA basis, the available reinforcing area per par. 634(c) of the Code for Pressure Piping, ASA B31.1-1951 is given as a percentage of the required area, this being defined as the product of the diameter of the finished opening times the wall thickness of the pipe which the fitting is to match; in the second basis, the excess weight of the reinforced fitting over that of an unreinforced fitting of the thickness and diameter of the matching pipe is given as a percentage of the weight of metal removed from the run at the opening.

The variants will be discussed in the order in which they appear in Fig. 26. In-plane bending will be considered primarily, since this is the only loading condition under which all the variants were tested. Where out-of-plane bending tests were made, stress-intensification factors of approximately the same magnitude as for in-plane bending were obtained, so that comparisons drawn for the condition of in-plane bending may be considered equally applicable to cases of out-of-plane bending. The endurance

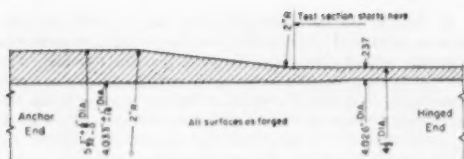


FIG. 18 DETAILS OF UPSET PIPE

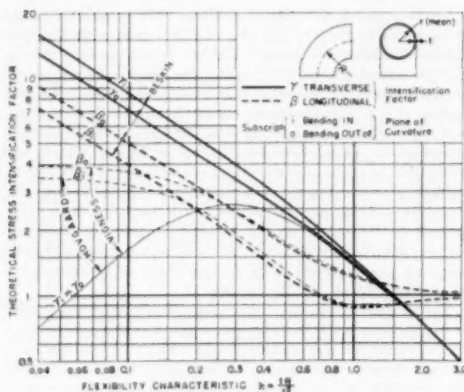


FIG. 19 THEORETICAL FACTORS FOR CURVED PIPE

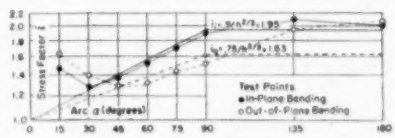


FIG. 20 EXPERIMENTAL FACTORS FOR ODD-ARC ELBOWS

strengths, obtained in tests straight through the run, were always higher than those obtained in tests through the branch and have been ignored in forming averages.

In the first two alternatives investigated, no more than 80 or 50 per cent reinforcing, respectively, was provided by the substitution of Schedule 80 pipe for Schedule 40 pipe in either the run or the branch. These variants were tested only under in-plane bending, and the failures were found to be located similarly as in unreinforced fabricated intersections, i.e., they initiated as cracks across the weld joining the branch to the run. In addition to failing in an identical fashion, the two variants gave the same average stress-intensification factors, which would indicate that the thickness at the intersection (which was identical for the two variants) is the controlling factor, and the distance the reinforcement is carried along the run or branch is of secondary importance only.

The third variant, in which a welding saddle was used, incorporated the largest relative amount of reinforcement of all the assemblies tested. The replacement area was well over twice that required by the ASA rules, and the weight of reinforcement added amounted to 11 times the weight of metal removed. This extremely heavy reinforcing explains the low stress-intensification factor found. It would be improper to expect similar values

for larger sizes where the reinforcement in many instances is barely adequate to meet the rules of par. 634(c) of the Code for Pressure Piping. Subsequent tests conducted on two pairs of different assemblies with saddles proportioned more nearly to the requirements of this paragraph gave average stress-intensification factors of 1.38 and 1.57, respectively, and indicated that saddles have approximately the same reinforcing value against cyclic bending as pad-reinforced intersections of equivalent diameter, wall and pad thickness.

Typical failures of both pad- and saddle-reinforced assemblies, are shown in Fig. 27. Failure in both types predominantly occurred in the branch along the toe of the weld, but a number of failures alongside the attachment weld to the run were also encountered.

An attempt to provide a correlation for all the types of reinforced intersections covered to this point follows; this is obviously more difficult than for unreinforced intersections owing to the additional variables introduced by the way in which the reinforcement is distributed around the opening. On the assumption that the average thickness of the run and branch at the intersection is controlling and that reinforced tees of the type discussed otherwise behave like unreinforced ones, the following effective flexibility characteristic k_e can be established

$$k_e = c \frac{t_e R_s}{r^3} = \left(\frac{t_e}{l} \right)^{1.5} \frac{l_e r}{r^3} = \left(\frac{t_e}{l} \right)^{2.5} \frac{l}{r} \quad [13]$$

As in the case of the welding tees (see Equation [9]) the coefficient c takes account of the increased section modulus. For full-size tees, i.e., such of equal run and branch size, it is suggested that the effective thickness t_e be taken as the thickness of the matching pipe wall increased by one half the excess thickness provided in either run or branch by the use of thicker pipe, a reinforcing pad, or a welding saddle. How stress-intensification factors, computed by this procedure, compare with those obtained as averages from the tests can be seen by referring to the last line in Fig. 26; it will be noted that for the test variants, the error resulting from the use of the proposed correlation ranges from an underestimate of 16 per cent to an overestimate of 37 per cent.

The last design shown in Fig. 26, for which J. S. Blair (8) has coined the descriptive term "triform," differs radically from all the others and hence requires separate treatment. While the basic design, without shoes or gussets, is soundly conceived from the standpoint of absorbing intersection stresses introduced by internal pressure, the presence of sharp discontinuities in the form of ribs would, by all known standards of judgment, be expected to result in poor performance under fatigue conditions. Actually, Blair's tests gave comparable stress-intensification factors for the "triform" and a one-third-lighter pad-reinforced construction. Failure occurred in the branch alongside one of the crotch stiffeners under both in-plane and out-of-plane bending, the cracks being located at the crotch for the former and at the face or side for the latter condition.

SUMMARY

The results of over 400 individual fatigue tests on full-scale 4-in. IPS assemblies, involving piping components of various shapes and proportions, conducted in the laboratories of the author's company over the past 5 years, are summarized in this paper. Similar information published by other investigators here and abroad has been used to supplement the findings of this research. Finally, the combined data have been analyzed in an effort to develop correlations intended to enlarge the scope of application of the test results to a wider range of sizes and proportions.

The primary use of the data is to provide design constants for the analysis of stresses caused in piping systems by thermal expan-

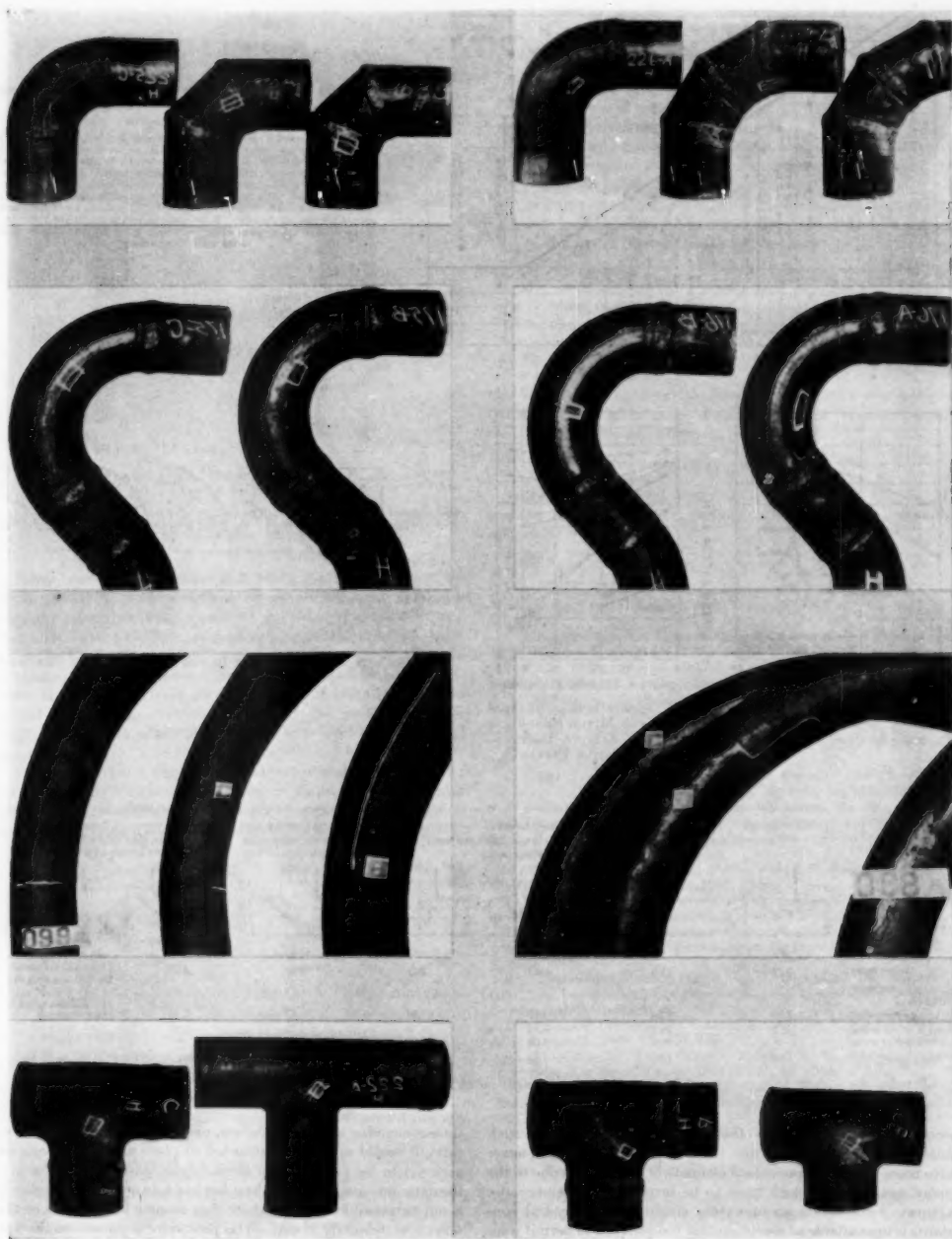


FIG. 21 VIEW OF FAILURES IN UNREINFORCED COMPONENTS

(At left, failures under in-plane bending; at right, failures under out-of-plane bending. Top, short-radius elbows and miter bends; second from top, 135-deg long-radius elbows; third from top, 5-diam radius bends; bottom, welding tees and unreinforced fabricated tees.)

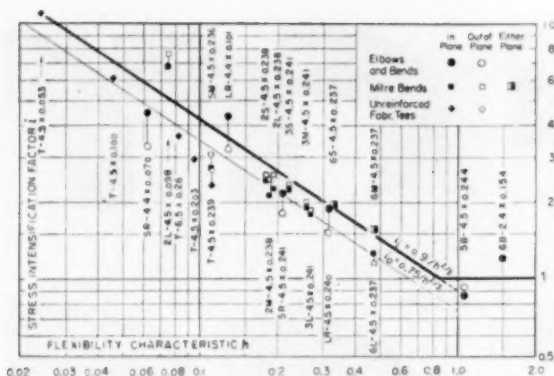


FIG. 22 (left) CORRELATION OF MITER BENDS AND UNREINFORCED FABRICATED INTERSECTIONS WITH CURVED ELBOWS

(Symbols used: SR = short-radius welding elbow; LR = long-radius welding elbow; 6B = smooth bends of 6 nominal diameter radius; 6M = single-miter bend; 2M = double-miter bend with short [1 1/4 in.] crotch spacing; 3L = same, with medium (2 1/4 in.) spacing; 3M = same, with long (4 1/4 in.) spacing; 3L, 6M, 6L similar for triple and sextuple miter bends; T = unreinforced fabricated tee intersections. Figures after bytchen give approximate OD and wall thickness.)

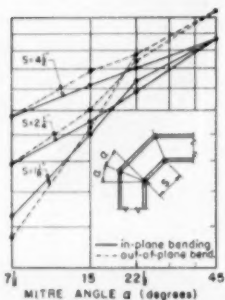


FIG. 23 STRESS-INTENSIFICATION FACTORS FOR MITER BENDS PLOTTED AGAINST MITER ANGLE

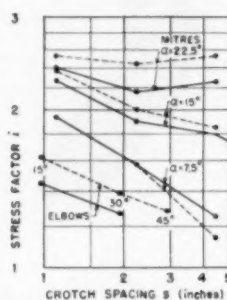


FIG. 24 STRESS-INTENSIFICATION FACTORS FOR MITER BENDS AND SMALL-ARC ELBOWS PLOTTED AGAINST CROTCH DISTANCE

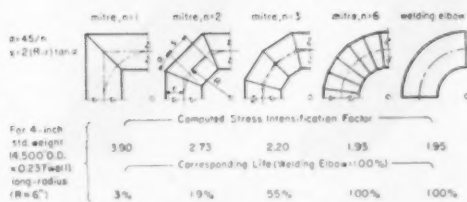


FIG. 25 COMPARISON OF MITER BENDS WITH WELDING ELBOWS

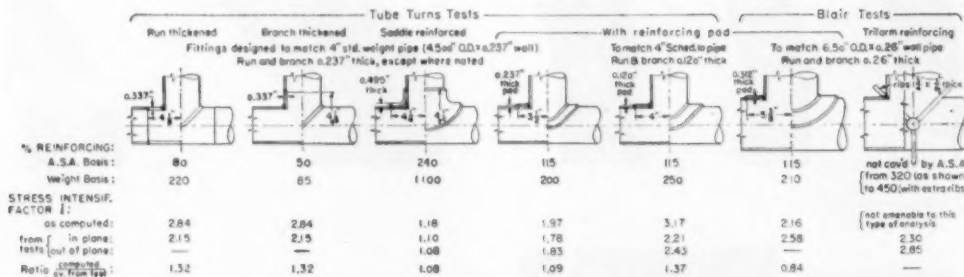


FIG. 26 DATA FOR REINFORCED FABRICATED INTERSECTIONS

sion. Those familiar with this problem will agree that such analyses, however precise from a mathematical standpoint, never give more than an approximate estimate of the stresses due to the many assumptions which have to be introduced either because accurate information on operating conditions or physical constants is unavailable or conditions are too complex to permit solution within a reasonable time.

Considering that flexibility calculations are burdensome and

time-consuming and, nevertheless, produce only approximate results, it would appear unwarranted to place undue emphasis on accuracy in the evaluation of stress-intensification factors, even if the data were available; on the other hand, to ignore them entirely is not permissible, at least where they assume large values or the service is definitely cyclic. The procedure proposed in the following presents an attempt to achieve balance between these opposing considerations.

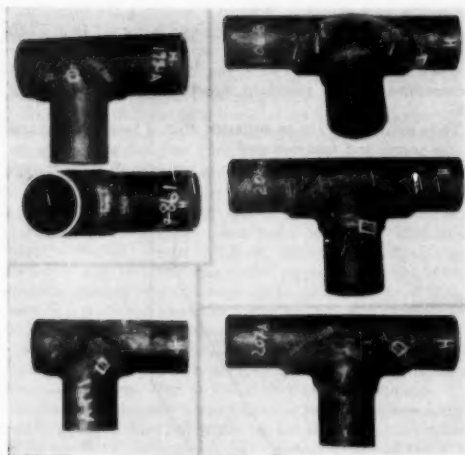


FIG. 27 VIEWS OF FAILURES IN REINFORCED FABRICATED INTERSECTIONS

[At left, pad-reinforced intersection; at right, saddle-reinforced intersection. In each column, top and middle views show failures under in-plane bending; bottom view shows failure under out-of-plane bending.]

It has been indicated earlier that Beskin's theory offers a satisfactory basis for the evaluation of stress-intensification factors in curved pipe, and that Equations [6] and [7], applying to in-plane and out-of-plane bending, respectively, give values of adequate accuracy for engineering use. Piping stress calculations could be simplified if one and the same factor could be used for both conditions, and the author suggests the adoption of Equation [6] since it will produce conservative results for curved pipe and, with a slight modification, also affords a fair correlation for other related shapes.¹⁰

If this approach is accepted, the stress-intensification factors i for welding elbows, smooth bends, miter bends, welding tees, and plain and reinforced fabricated 90-deg branch intersections could be estimated from the following formula, for bending in any plane

$$i = \frac{0.9}{h_e/t} \geq 1 \dots \dots \dots [14]$$

where

- $h_e = c (t_e R_e / r^2) =$ effective flexibility characteristic (dimensionless)
- $c = (t_e / t)^{1.4} =$ section-modulus correction factor (dimensionless)
- $= 1$ wherever fitting has same thickness as matching pipe
- $t_e =$ effective fitting thickness, in.
- $=$ average of crotch and side-wall thickness,¹¹ for welding tees conforming to ASA Standard B16.9
- $=$ pipe-wall thickness increased by one-half excess thickness

¹⁰ Caution is advised in applying this correlation to miter bends and fabricated intersections with t/r -ratios much below 0.1, where it may lead to an appreciable underestimate of the stress-intensification factor.

¹¹ Measurements of representative tees taken from stock gave averages ranging from 1.6 to 1.9 times the wall thickness of the pipe; the fittings were designed to match, and, accordingly, it appears conservative to assume $t_e = 1.6 t$ in the absence of direct measurements.

provided in either run or branch, by use of thicker piping or pad or saddle, for reinforced fabricated intersections

- $= t$ for welding elbows, curved or miter bends, or unreinforced fabricated intersections of a thickness equal to that of matching pipe

$t =$ thickness of matching pipe, in.

$r =$ mean radius of matching pipe, in.

$R_e =$ effective bend radius, in.

$= R =$ radius to center line of curvature for elbows or smooth bends

$= r + r_c$ for welding tees, where r_c designates crotch radius

$= r$ for single-miter bends and unreinforced and reinforced fabricated 90-deg branch intersections

$\leq r + 0.5 s \cot \alpha, \leq r \frac{1 + \cot \alpha}{2}$ for multiple-miter bends,

where s designates miter crotch spacing or minimum distance between centers of miter welds (in.), and α is miter angle, deg

For straight pipe, whether plain or welded, for reducers, and also for butt welding or welding neck flanges, the stress-intensification factor can be taken as unity. For other types of flanged connections, reference (2) should be consulted.

ACKNOWLEDGMENT

Tests were conducted under the supervision of Mr. H. H. George, whose assistance in the evaluation is herewith gratefully acknowledged.

BIBLIOGRAPHY

- 1 "Fatigue Tests of Welding Elbows and Comparable Double-Miter Bends," by A. R. C. Markl, Trans. ASME, vol. 69, 1947, pp. 869-879.
- 2 "Fatigue Tests on Flanged Assemblies," by A. R. C. Markl and H. H. George, Trans. ASME, vol. 72, 1950, pp. 77-87.
- 3 "The Strength and Flexibility of Corrugated and Creased-Bend Piping," by R. L. Dennison, *Journal of the American Society of Naval Engineers*, vol. 48, 1935, pp. 343-433.
- 4 "The N-S Relationship in Endurance Testing," by M. G. Corson, *The Iron Age*, vol. 166, March 10, 1949, pp. 103-105.
- 5 "Economy in Fatigue Testing," by M. G. Corson, *Metal Progress*, vol. 56, October, 1949, pp. 518-519.
- 6 "The Elasticity and Endurance of Steam Pipes," by C. E. Strommeyer, *Engineering*, vol. 135, June 19, 1914, pp. 856-858.
- 7 "The Significance of, and Suggested Limits for, the Stress in Pipe Lines Due to the Combined Effects of Pressure and Expansion," by D. B. Rossheim and A. R. C. Markl, Trans. ASME, vol. 62, 1940, pp. 443-464.
- 8 "Reinforcement of Branch Pieces," by J. S. Blair, reprint from *Engineering*, London, England, 1947, 31 pp.
- 9 "Textbook of the Materials of Engineering," by H. F. Moore, McGraw-Hill Book Company, Inc., New York, N. Y., 1941, p. 57.
- 10 "Über die Formänderung dünnwandiger Rohre," by Th. von Kármán, *Zeitschrift des Vereines deutscher Ingenieure*, vol. 55, 1911, p. 1889.
- 11 "Bending of Curved Pipes," by W. Hovgaard, Proceedings of the Third International Congress for Applied Mechanics, Stockholm, Sweden, vol. 2, 1930, pp. 331-341.
- 12 "Elastic Properties of Curved Tubes," by I. Vigness, Trans. ASME, vol. 65, 1943, pp. 105-120.
- 13 "Bending of Thin Curved Tubes," by L. Beskin, *Journal of Applied Mechanics*, Trans. ASME, vol. 67, 1945, p. A-1.
- 14 "Properties of Thin-Walled Curved Tubes of Short Bend Radius," by T. E. Pardue and I. Vigness, Trans. ASME, vol. 73, 1951, pp. 77-87.

Discussion

J. S. BLAIR.¹² While the paper gives a lot of useful information, it is perhaps worth drawing attention to the fact that the author

¹² Manager, Engineering Research, Stewarts and Lloyds, Limited, Corby, Northants, England. Mem. ASME.

states that the tests which the writer carried out showed that the compensating ring gave about the same stress-raising factor as the "triform" reinforcement. It is true that one of the compensating rings tested gave a result about equal to the average of the triform reinforcements, but the other gave a very much higher stress-concentration value than any of the triform types. Admittedly, there were rather few tests carried out on the compensating ring, so that it is difficult to know whether the good one or the bad one was more representative of the usual results. It certainly looks, however, as though the compensating rings would never give as good results as the best triforms and in many cases might give results worse than the worst triforms. This, of course, applies to vibration tests. In so far as internal pressure tests are concerned, we have never found that the compensating rings give as satisfactory results as the triforms.

W. M. JACKSON.¹³ Although this paper understandably does not cover branch welding fittings, one of the increasingly major phases of branch construction, it is most significant to note the manner in which the correlations from the test data pertain to this type of fitting. The design basis of the branch welding fitting is such as to compensate in the most efficient manner for the bending moment as shown in Fig. 28 of this discussion. The correlations resulting from the author's fatigue tests as they are applied to the branch fitting both qualitatively and quantitatively would seem to bear out the soundness of this principle.

The qualitative results of the three different types of branch construction tested are quoted as follows:

Welding tees: "... the metal thickness available in the crotch zone and the crotch radius were thought to be the controlling factors."

Intersections reinforced by thickening the run and branch pipes respectively: "... the thickness at the intersection is the controlling factor and the distance the reinforcement is carried along the run or branch is of secondary importance only."

All the types of reinforced intersections covered: "... the average thickness of the run and branch at the intersection is controlling."

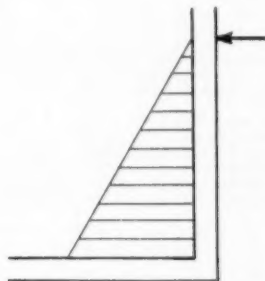


FIG. 28

In whichever of the three categories mentioned the author wishes to place the branch welding fitting, it can be seen that the thickness at the intersection and the funnel shape are most desirable for fatigue conditions, Fig. 29 herewith.

The quantitative effect of these factors can be appreciated readily by applying to the branch fitting the author's method of determining stress-intensification factor. Since several of the methods outlined for determining R_c of the funnel would apply,

the results vary slightly. Without considering the funnel feature of the fitting, the stress-intensification factor is 1.19. When acknowledging the presence of the funnel feature, the computation of a standard weight 4 in. \times 4 in. branch fitting by the most conservative method reveals a stress-intensification factor of 1.03.

These results show the quantitative effect of both the thickness at the crotch and funnel-shaped inlet and indicate definite inclusion of this type of construction in the over-all consideration of fatigue in branch connections.



FIG. 29

H. F. MOORE.¹⁴ During the past decade it has become increasingly evident that the resistance of structural and machine parts to repeated stress (fatigue strength) cannot be determined directly from results of fatigue tests of small polished specimens of the metal used. Such tests do give a fairly good measure of the strength of the metal tested, but they do not measure the effect of size of the specimen, of the effect of stress raisers, of the effect of the surface of the part, or of the effect of the volume of metal subjected to stress as great (or nearly as great) as the fatigue strength of the metal.

The ideal method of making fatigue tests of structural or machine parts is to test a considerable number of full-size specimens of the structural or machine part. In some cases this is feasible, for example, for coil springs. However, in cases of large parts or in cases where only a few parts are available full-size tests are not feasible.

The paper gives results of repeated-bending tests of full-size specimens of piping components, mainly for 4-in. pipe and corresponding pipe fittings, and presents suggestions and examples of estimating the fatigue strength for other sizes of pipe. This paper is worthy of study by all students of fatigue of metals.

The writer wishes to present a brief study of the differences between the $S-N$ diagrams for tests of small polished specimens tested on an R. R. Moore rotating-beam testing machine and the $S-N$ diagrams for full-size pipe as shown in Fig. 4 of the paper. The difference between the test results for full-size pipe held in a collet show, as is noted by the author, an increase of approximately 50 per cent in the fatigue strength for a given number of cycles of stress (fatigue strength) over the value for specimens held in a lathe chuck. The $S-N$ diagrams for the full-size pipe specimens show no evidence of an endurance limit (stress for an indefinitely large number of cycles of stress) up to 1,000,000 cycles of stress, while the test results for the small polished specimens show an endurance limit at approximately 56,000 psi. It may be noted that, for reversed stress above about 56,000 psi, the full-size pipe specimens show higher fa-

¹³ Development Engineer, Welding Fittings Division, Bonney Forge & Tool Works, Allentown, Pa.

¹⁴ Research Professor Emeritus, Engineering Materials, University of Illinois, Urbana, Ill. Mem. ASME.

tigue strength (stress for a given number of cycles at failure) than do the small polished specimens.

Three other factors (and perhaps many more) may be considered in comparing the fatigue strength of the full-size pipe specimens and that of the small polished specimens:

Size Effect. Fatigue tests made at several laboratories show that endurance limit (stress for an indefinitely large number of cycles of stress) is somewhat smaller for large specimens than for smaller specimens. The volume of metal in the thin surface layer in which fatigue failures start is greater for the large specimens, and the probability of a weak spot in which a fatigue crack may start and spread is greater in a larger specimen. This effect might be studied by tests of different sizes of pipe. In this connection it may be noted that recent experiments at the Massachusetts Institute of Technology and at the University of Illinois show that a number of cracks may start, but stop their growth without spreading to fracture.

Vibratory Tests Versus Rotating-Beam Tests. The R. R. Moore specimens as they revolve are subjected to maximum stress at every longitudinal fiber at the surface of the specimen. The vibrated pipe specimens are subjected to maximum stress at only two longitudinal fibers, one at the top and the other at the bottom of the specimen. This means that a greater number of the R. R. Moore specimens are subjected to the maximum stress than is the case for a vibrated specimen of the same cross section, and that the probability of starting a fatigue crack under a given stress pattern is greater than in the vibrated specimen. Tests reported by the Fatigue of Metals Committee of the American Society for Testing Materials some years ago, showed slightly higher endurance limit for vibrated specimens than for rotating-beam specimens. This factor might be checked by tests of small pipe specimens in a rotating-beam machine, and tests from similar specimens in a vibratory machine.

Effect of Surface Finish. The effect of surface polish might be studied by tests in a vibratory fatigue testing machine of longitudinal specimens cut from pipe. Half of these specimens could be tested with the upper surface as produced by rolling or extruding, and the other half tested with that curved surface polished. A considerable amount of test data give indication that the surface condition is very important. In the longitudinal test specimens the surfaces other than the rounded top surface should be polished.

T. E. PARDUE¹⁵ AND IRWIN VIGNESS.¹⁶ Three factors are considered in this discussion as follows:

1 The maximum stress-intensification factors, as determined by methods involving fatigue fracture, are not generally equivalent to those determined by calculations, or by static measure-

ments involving elastic strains. The measurements made by the author are of great importance in indicating the endurance of piping under conditions of fatigue, but are of lesser significance for checking theoretical results of stress-concentration factors.

2 In his discussion of theoretical analyses of stresses in curved tubes, the author gives data taken from von Kármán for in-plane bending, from Vigness for transverse bending, and from Beskin for both types of bending. The author correctly points out that results from all available theories agree for λ greater than 0.3. This is to be expected because the basic assumptions in all the theories are identical. For λ less than 0.3, values taken from von Kármán and from Vigness do not agree with those taken from Beskin. This is because the data quoted from von Kármán and Vigness are for the lowest order of approximation of their assumed Fourier-series solution. If sufficient terms are taken for the solution, the results of all theories are very nearly identical. This was illustrated in a discussion of Beskin's paper given by Symonds and Vigness.¹⁷ The upper limit of 10, for the flexibility factor, does not occur in any of the theories when a sufficient degree of approximation is used. This important point apparently has been generally overlooked; in particular, it was overlooked by Beskin. It would be expected that the general neglect of the term involving the ratio of the tube radius to the bend radius would become a serious source of error as the bend radius becomes small; however, Symonds¹⁷ has shown that this error is small.

3 The writers recently completed measurements of flexibility and stress-intensification factors on a large number of curved tubes (obtained from author's company), similar to those used by the author. The maximum stress-intensification factors, obtained by measuring strains on the outside surface of the tube by means of wire-resistance strain gages, are given in Table 4, herewith. The data are for bends with straight tangents, of length greater than 5 pipe diameters, attached to the ends of the tube turns. The table shows the following:

(a) For out-of-plane bending the transverse stress-intensification factors are in all cases less than the longitudinal stress factors. This is contrary to theoretical predictions.

(b) For tube turns with a bend radius 2 times the tube radius, the transverse stress-intensification factors are less than the longitudinal stress factors for both in-plane and out-of-plane bending.

(c) For in-plane bending, tube turns with a bend radius 3 times the tube radius have transverse stress factors larger than the longitudinal stress factors, as predicted by theory. However, in the case of a 180-deg bend, where agreement between theory and experiment should be best, the measured longitudinal stress fac-

¹⁵ Discussion of Beskin's paper by P. S. Symonds and Irwin Vigness, *Journal of Applied Mechanics*, Trans. ASME, vol. 68, 1946, p. A-66.

¹⁷ See appendix to "Properties of Thin-Walled Curved Tubes of Short-Bend Radius," by T. E. Pardue and Irwin Vigness, Trans. ASME, vol. 73, 1951, p. 83.

TABLE 4 STRESS-INTENSIFICATION FACTORS OBTAINED FROM STRAIN MEASUREMENTS

Length of arc, deg	Actual $\lambda = \frac{tR}{r^2}$	Nominal $\frac{R}{r}$	Nominal diam, in.	Nominal wall thickness, in.	Stress-intensification factors—			
					In-plane bending		Out-of-plane bending	
					K_t	%	K_b	%
45	0.467	3	4	0.337	2.10	1.93	2.06	1.80
45	0.406	3	6	0.432	2.11	2.17	2.50	2.00
45	0.313	3	4	0.237	2.08	2.13	2.52	2.25
45	0.250	3	6	0.280	2.17	2.33	3.15	3.13
90	0.467	3	4	0.337	1.98	2.31	2.51	2.25
90	0.406	3	6	0.432	2.14	2.37	2.71	2.52
90	0.313	3	4	0.237	2.48	2.75	3.31	3.00
90	0.250	3	6	0.280	2.62	3.25	3.33	3.22
90	0.321	2	4	0.337	2.73	2.40	2.96	2.24
90	0.250	2	6	0.432	2.84	2.45	3.20	2.55
90	0.215	2	4	0.237	2.73	2.40	2.96	2.24
90	0.137	2	6	0.280	3.89	3.08	4.81	4.27
180	0.467	3	4	0.337	2.13	2.23	2.65	2.20
180	0.406	3	6	0.432	2.08	2.26	2.52	2.31
180	0.313	3	4	0.237	2.67	3.00	3.12	2.92
180	0.250	3	6	0.280	3.01	3.88	3.53	3.48

¹⁶ Naval Research Laboratory, Washington, D. C.

tors are larger than the theoretical values, while measured transverse factors are smaller than predicted by theory.

In the writers' opinion, such factors as (a) effects of end constraints at the end of a curved tube of bend length in the order of, or less than, the diameter of the tube, and (b) neglecting values of stress which tend to cause different stress on the inside and outside wall of the tube surface,¹⁸ are the major causes of difference between theory and experiment.

The results of this paper clearly support the author's contention that stress concentrations are an important factor in determining the life of piping components subjected to cyclic loads. The author points out the importance of stress concentrations arising from end clamps and other end constraints, surface defects, and cross-sectional deformation of straight tubes.

It is interesting to consider the author's results on curved tubes in the light of the stress factors obtained from strain measurements. Cracks which occur along the tube axis, under cyclic load, even though the transverse stresses are smaller than longitudinal values, can be explained by local material weaknesses or stress raisers which are elongated in the axial direction in the process of fabrication. This consideration emphasizes the importance of using the author's experimental data properly and at the same time cautions against extending the results to new shapes or materials without experimental verification.

AUTHOR'S CLOSURE

Welding fittings and fabricated connections employed for directional changes and branch take-offs in piping systems generally have shapes and proportions which do not lend themselves to precise stress analysis; for most of them any form of mathematical evaluation is lacking, even for the simplest loadings. This leaves experimentation as the only alternative for obtaining information useful in design. If the variants could be tested in sufficient number to permit application of statistical principles, a properly conducted test program should lead to reliable empirical formulas. Unfortunately, every individual full-scale fatigue test reported by the author involved considerable expenditure for labor and parts, and economic considerations hence necessitated limitation to the more basic and generally applied shapes and proportions; peculiar or proprietary constructions could not be included in the test program. Even for the types tested, the number of specimens had to be limited; only the pressing need for design information in the field of piping stress analysis induced the author to attempt to translate the imperfectly defined patterns of results obtained into working constants. As a corollary, extrapolation of the data given to shapes or proportions

radically departing from those tested is liable to appreciable error; also, it would be improper to draw fine distinctions between different types of construction on the basis of these values.

The foregoing remarks should make it clear to Messrs. Blair and Jackson that no slight was intended in omitting their constructions from the test program. The test results obtained by Mr. Blair with the "triform" construction were included for their general interest; the author questions its alleged superiority from a fatigue standpoint and believes that putting this construction on a par with pad reinforcements represents a fair evaluation in view of the paucity of test data; a discussion of relative merits as pressure containers is irrelevant. The author cannot affirm or disprove the favorable values computed by Mr. Jackson for his particular design of branch connection; the author would again warn against applying conclusions derived from tests on specific shapes to others which bear only a remote resemblance, and would suggest that Mr. Jackson substantiate his claims by tests.

How important it is, however, to make such tests on a properly comparable basis, is very clearly brought out in Professor Moore's discussion: the size of the specimen has a very definite effect, the surface condition is very important, and even the type of testing machine used has an influence on the results. The author wishes to emphasize that all the fittings used in his tests were taken at random from stock, that fabrication where required accorded with common practice, and that all variants were tested under similar conditions so that results may be considered to fairly represent typical installations.

Incidentally, all welding was done with Fleetweld No. 5 electrodes. Mr. M. A. Scheil¹⁹ has called attention to the omission of this statement in a private communication, in which he also expressed a desire for more information of a metallurgical nature on the series of tests of welded joints in straight pipe. Information of this type would have been included but for the fact, fortunate from the piping stress analyst's viewpoint, that differences in results between variants in welding procedure were minor, avoiding the need for establishing distinctions.

Messrs. Pardue and Vigness deserve particular credit for the valuable information they have so generously contributed from their own research. The author is in full accord with the statements contained in the second part of their discussion; the more precise analysis has been associated with Beskin's name largely for simplicity of reference, since Kármán's and Vigness' developments are generally known only in the more approximate form.

As far as the first and third parts of their discussion are con-

¹⁸ Discussion to footnote 17, by Nicol Gross and Hugh Ford, Trans. ASME, vol. 73, 1951, p. 84.

¹⁹ Director, Metallurgical Research, A. O. Smith Corporation, Milwaukee, Wis.

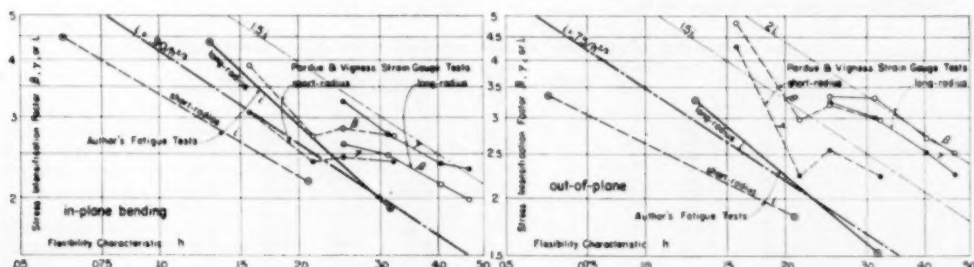
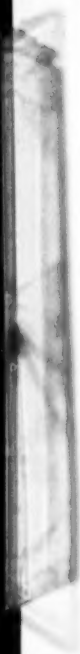


FIG. 30 COMPARISON OF STRESS-INTENSIFICATION FACTORS OBTAINED FROM STRAIN GAGE AND FATIGUE TESTS FOR LONG AND SHORT-RADIUS WELDING ELBOWS

cerned, the author's primary purpose was not to prove or disprove existing theoretical developments, to which the discussers' strain-gage determinations no doubt lend themselves better, but rather to establish reasonably reliable design constants; he believes that Messrs. Pardue and Vigness would be the first ones to concede that the author's fatigue tests are probably the more significant from the standpoint of evaluating the safety of a piping system.

The author was very much interested in the data shown in Table 4 on stress-intensification factors derived from strain measurements. The factors applicable to 90 deg arcs are plotted in Fig. 30 for comparison with similar data abstracted from Table 2; plots of Equations [6] and [7], representing one half of the

stress-intensification factors computed by Beskin's theory, have been included for comparison. It will be noted that the data obtained from strain-gage tests are up to 50 per cent higher for in-plane bending, and up to 100 per cent higher for out-of-plane bending, than the average values obtained from fatigue tests. That the longitudinal strains should have been found to dominate for in-plane bending of short-radius elbows is puzzling; the direction of the cracks in the author's tests left no doubt that the transverse stresses definitely controlled under in-plane bending. The author has no adequate explanation for the differences in results obtained by the two approaches, but would venture the opinion that work-hardening and stress relief as a result of cyclic bending may be significant factors.



Analysis of Some Corrosion Problems in Petroleum Refineries

By J. F. MASON, JR.,¹ NEW YORK, N. Y.

Over the past 25 years the Corrosion Engineering Section of the Development and Research Department of the author's company has co-operated with the petroleum industry in analyzing corrosion problems encountered in refineries and in running spool tests to determine the most suitable and economical materials that might be used in specific applications. It is the purpose of this paper to present 15 actual corrosion problems that have been submitted for consideration and to show the steps taken to analyze them in the light of our practical experience and available test data obtained under the same or similar conditions. In some cases, where the problems were not readily solvable, based on available information, it was necessary to resort to the installation of spool-type specimen holders in the operating equipment to determine the relative suitability of various metals and alloys under actual service conditions. From the nature of the problems, it is indicated that Type 302 stainless steel is a highly acceptable and reasonably economical material as a replacement for mild steel except in instances where mineral acids or chlorides may be present as well as highly alkaline solutions at elevated temperatures. Under the latter conditions, the trend is toward the use of more highly alloyed materials such as Monel and nickel together with the copper-base alloys like 70-30 cupronickel, Admiralty metal, and Muntz metal.

CORROSION of equipment in petroleum refineries for many years has represented a major portion of operating costs, and oftentimes this condition has been aggravated by the misapplication of available metals and alloys. Over the past 25 years the Corrosion Engineering Section of the author's company has been active in investigating corrosion problems in the petroleum industry, and considerable quantitative information has been obtained on the behavior of different materials of construction under varying conditions of service. It is the purpose of this paper, therefore, to present an analysis of 15 actual problems concerning corrosion of refinery equipment that were submitted for our consideration. The solutions to the problems are based on the accumulated practical experience of the staff of the Corrosion Engineering Section, as well as on such quantitative test data as we have developed in refinery services through the use of our spool-type specimen holders.

The spool holders referred to are shown in Fig. 1. Briefly, the assembly consists of previously cleaned and weighed specimens of the several metals and alloys to be tested, mounted on the spool-type holder with nonmetallic parts of bakelite or porcelain to separate and insulate the specimens from each other and from the

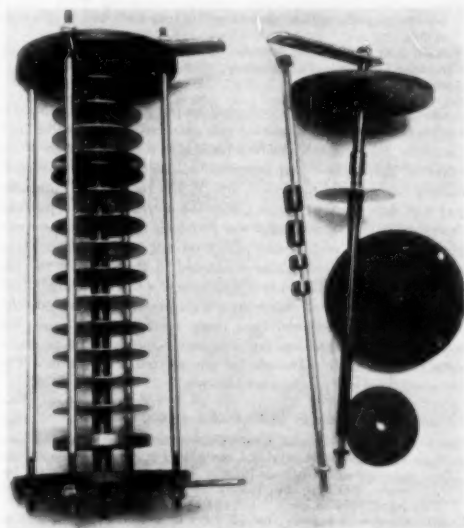


FIG. 1 TYPE OF SPOOL HOLDER

metallic parts of the holder. Two similar specimens of each material were included on each spool. The completed test assemblies were fastened firmly in place in the desired test locations in operating plant equipment and allowed to remain for sufficient periods of time to give reliable indications of corrosion behavior. Each of the test specimens used had an exposed area of 0.5 square decimeter.

Upon completion of tests, the spools were removed, dismantled, and the specimens examined, cleaned of all scale and corrosion product, and reweighed. From the weight losses, areas of specimens, and duration of exposure, the corrosion rates were calculated in terms of milligrams per square decimeter per day (mdd), and these rates transposed to inch penetration per year (ipy), the unit used in the accompanying tables. This unit is based on the assumption of uniform corrosion in practice from one side of the metal only. The rate shown for each material is the average of the two specimens included in each test. In addition, each specimen was examined for cracking, pitting, and other forms of local attack. Where pitting or local attack occurred, depth of the five or ten deepest pits was measured microscopically or with a depth gage. This method of test was substantially in accord with ASTM Recommended Practice for Conducting Plant Corrosion Tests, A224-41.²

The problems submitted for analysis are as follows:

¹ Corrosion Engineering Section, Development and Research Department, International Nickel Company.

Presented at the Petroleum Mechanical Engineering Conference, Tulsa, Okla., September 24-26, 1951, of THE AMERICAN SOCIETY OF MECHANICAL ENGINEERS.

NOTE: Statements and opinions advanced in papers are to be understood as individual expressions of their authors and not those of the Society. Manuscript received at ASME Headquarters, July 6, 1951. Paper No. 51-PET-4.

² ASTM Standards. Part I, 1944, p. 522.

PROBLEM 1

Materials Used. Steel tubes with an 0.095-in. wall in a heat exchanger used in combined straight run and cracking distillation service gave a life of only 9 months when failure occurred due to pitting and general corrosion, particularly where the tubes passed through the steel baffle plates. Muntz-metal tubes were used as replacement and the life was increased from 3 to 5 months.

Service Conditions.

Tube interior: Gas oil having 0.6 to 0.8 per cent organic-sulphur compounds.

Tube exterior: Depropanized naphtha containing 0.035 to 0.10 per cent organic sulphur, including 4-40 mg RSH/100 cc plus trace of H₂S.

Temperature: 350-650 F (average 450 F)

Operating pressure: 225 psi inside tubes and 40 psi outside.

Aeration: None.

Discussion. Depropanized naphtha per se is not considered to be particularly corrosive even at elevated temperatures and, therefore, the problem resolves itself into a consideration of the effect of the organic and inorganic sulphur compounds in promoting corrosion of mild steel and Muntz metal. No quantitative test data were available under the actual service conditions described but an opportunity was provided to expose some specimens of various metals and alloys on our standard spool-type specimen holders in naphtha contained in the sump of the top tray of a topping unit and in the bottom of a fractionating bubble tower wherein sulphur compounds were present at elevated temperatures. It is believed that these conditions are somewhat analogous to the problem application to indicate the probable suitability of other materials for the service in question. The test conditions and results are as follows:

TABLE 1 TEST DATA, PROBLEM 1

- Test 1 Specimens exposed for 538 days in sump of the top tray of a topping unit to naphtha containing 0.008 per cent sulphur plus traces of H₂O and H₂S. The temperature varied between 290 and 360 F with an average of 320 F, and the velocity was 6 ips.
- Test 2 Specimens exposed for 75 days in bottom of fractionating bubble tower handling oil with a sulphur content of 0.751 per cent and a boiling range of 164 F to 600 F at normal pressure. The temperature varied between 675 F and 700 F with an average of 690 F. Aeration was nil and agitation was turbulent.

Material	Indicated corrosion rate, in. penetration per year		
	Test 1	Max pitting during test, in.	Test 2
Monel	0.0003	None	"
Nickel	<0.0001	None	"
Inconel	0.0001	0.003	0.0022
Types 302 and 304 SS	0.0001	0.008	0.0003
Type 316 SS	<0.0001	0.006	"
Mild steel	0.0031	0.021	0.144
Type 502 SS	"	"	0.017
Type 410 SS	"	"	0.0015
Red brass	"	"	"
Admiralty metal	"	"	0.0039

" Specimens, originally 0.031 in. thick, were completely destroyed during test period.

The data from Test 1 (Table 1) indicate that while the general corrosion resistance of mild steel is of a satisfactorily low order, it has a strong tendency to suffer severe localized attack in the form of pitting. The chromium-containing materials such as Inconel and the austenitic stainless steels also showed the same tendency but to a much lesser degree. Monel and nickel were free of this type of attack, and, in addition, showed negligibly low over-all corrosion rates based upon weight loss at this temperature.

In Test 2 none of the specimens showed any evidence of pitting attack but it will be observed that mild steel was subject to a high rate of corrosion. Monel and nickel cannot be considered for the application because as shown by the data in this test they are susceptible to severe general and intergranular attack by sulphur compounds at temperatures much in excess of 500 F.

It was mentioned that Muntz-metal tubes were substituted for mild steel and that an additional 3 to 5 months' life was obtained. It was not reported how these tubes failed, but if it was caused by dezincification, there is a good possibility that inhibited Admiralty metal will give greatly superior performance since its general corrosion rate in Test 2 was only 0.0059 in. per year. Another material worth while considering is Type 502 stainless steel, which showed a superiority over mild steel of about 10 to 1. By increasing the chromium content to 13 per cent (Type 410 stainless), the ratio is extended to approximately 100 to 1. It seems that the latter materials would probably represent the more economical investment.

The accelerated corrosion that occurred on the steel tubes where they passed through the baffle plates was in all probability caused by concentration cell corrosion of the metal-ion type. In practice, these cells are usually set up by differences in the rate of movement of the corroding solution, or, more effectively, by movement of one part of the solution while another part remains practically stationary. In this way the stagnant portion in the crevice between the tubes and baffle plates becomes saturated with products of corrosion, or metallic ions, while the moving portion sweeps them away leaving the solution low in concentration of corrosion products. This condition sets up a flow of electric current which causes galvanic or accelerated corrosion of the metal in the region where a relatively low ion concentration is maintained, that is, at the edge of the juncture of the tubes and baffle plates.

PROBLEM 2

Material Used. Steel tubes with an 0.095-in. wall in a heat exchanger used in combined distillation and cracking service gave a life of 12 months when pitting occurred on the outside surface and accelerated corrosion where the tubes passed through the steel baffle plates.

Service Conditions.

Tube interior: Crude petroleum with 0.3 to 0.5 per cent organic sulphur.

Tube exterior: Gas oil having 0.6 to 0.8 per cent organic sulphur compounds.

Temperature: -10 to 650 F (average 450 F).

Operating pressure: 225 psi inside tubes and 300 psi outside.

Aeration: None.

Discussion. This case of pitting and corrosion of the outside of the tubes by gas oil containing organic sulphur compounds is similar to Problem 1 and the same comments would seem to apply. In other words, there is every indication that Types 410 and 502 stainless steel as well as inhibited Admiralty metal will provide much better performance in the service in question than mild steel.

PROBLEM 3

Material Used: Steel tubes with a 0.095-in. wall in a heat exchanger used in conjunction with a sulphuric-acid alkylation unit gave a life of 3 to 4 months when failure occurred at junction of tubes and steel tube sheet on acid side.

Service Conditions.

Tube interior: Steam at 140 psi.

Tube exterior: Black alkylation spent acid 89.91 per cent H₂SO₄, 98 per cent fresh acid added to bring concentration to 92 per cent.

Temperature: 300 F max, 200 F average.

Operating pressure: 140 psi inside tubes and 65 psi outside.

Discussion. The point of failure is typical of concentration cell corrosion of the metal-ion type as discussed in Problem 1. High concentrations of sulphuric acid over about 80 per cent and low or moderate temperatures are favorable for the satisfactory performance of mild steel, except where conditions of high velocity or turbulence are encountered. The effect of the latter forces is to remove the protective ferrous-sulphate coating that forms. How-

ever, it generally is not practical to use mild steel with concentrated sulphuric-acid solutions at elevated temperatures up to 300 F even under quiet or stagnant conditions, because of excessive corrosion attack. Usually its application is confined to temperatures under about 120 F.

Type 316 stainless steel and Carpenter 20 while also resistant to concentrated sulphuric-acid solutions even under velocity conditions cannot be used safely at temperatures in excess of about 180 F. Under the circumstances, it seems apparent that the only material that might be considered worth while for the application in question is Hastelloy B, which is reported to have fair resistance to corrosion by concentrated solutions of sulphuric acid at temperatures up to 300 F. The silicon irons, such as Duriron and Durichlor, as well as Hastelloy D, would also demonstrate adequate resistance to attack, but these materials are available only in cast form and would not readily lend themselves to use as heat-exchanger tubing.

Another possibility is the use of Karbate tubing but this material is somewhat brittle and care must be exercised in handling it. Apparently, since the corrosive conditions are so severe and the availability of materials in wrought form is rather limited for tubular elements in a heat exchanger, it might be considered practical to redesign the unit along the lines of the standard sulphuric-acid concentrators in refineries where the evaporator bodies usually are of steel, lined with lead and this covered with acid-resistant brick. The heater tubes or thimbles commonly are of Hastelloy D, and other parts of Duriron, Corrosiron, and carbon are used.

PROBLEM 4

Material Used. Carbon-steel lye-regeneration tower with cast-iron trays and bubble caps. The steel distributor pipe on the un-regenerated-lye inlet was completely corroded away and was replaced with a splash plate located 4 ft from the nozzle or 1 ft from the opposite side of the tower. A hole $\frac{1}{2}$ in. diam developed in the tower shell directly opposite the inlet nozzle. This hole was in the upper part of a badly corroded area 6.5 in. \times 10-in. with lesser corrosion over a large area. The splash plate had been corroded through over an area 8 in. in diam. At present this tower has been in service over 2 years.

Service Conditions. Regeneration of lye or caustic soda of 20 deg Bé (15 per cent) containing mercaptans and hydrogen sulphide. Temperature: At bottom of tower 270 F. At top of tower 240 F. Operating pressure: 20 psi. Aeration: Moderate.

Discussion. Carbon steel as well as cast iron is generally subject to severe corrosive attack in contact with caustic-soda solutions at elevated temperatures. The presence of velocity or turbulence in such equipment tends to accelerate corrosion. It seems evident that the latter effects caused premature failure of the distributor pipe, and impingement attack shortened the life of the area in the tower shell opposite the inlet nozzle as well as the splash plate.

The results of some plant corrosion tests in caustic regeneration units are given in Table 2.

It will be noted that in one test mild-steel specimens, originally 0.062 in. thick, were completely destroyed in 140 days, while in the other three tests the corrosion rates of the material were of a relatively high order. Monel and Inconel gave outstanding performance and as a matter of fact Monel is being rather widely used in the petroleum industry for caustic-soda regenerator reboilers and tubes, for lining the bottom sections of regenerator towers, and for pumps, piping, and preheaters handling the hot solutions.

Inconel has also proved to be a useful material for evaporator tubes or other parts of regenerator systems and should be

TABLE 2 PLANT CORROSION TESTS IN CAUSTIC REGENERATION UNITS

- Test A** In reboiler of caustic-soda regenerator unit. Solution entering contained 1-2 per cent sodium hydroxide, 3 per cent sodium phenolate and 0.07 mg per 100 cc of solution as sodium mercaptides. Test specimens were located directly above Monel heating tubes. Temperature 255 F. Duration of test 131 days.
- Test B** In vapor section of caustic-soda regenerator unit. Solution entering contained 13.2 per cent sodium hydroxide, 0.37 per cent sulphide sulphur, and 0.80 per cent mercaptide sulphur. The average temperature was 300 F. The duration of test was 55 days.
- Test C** In reboiler of caustic-potash regenerator unit. Solution entering contained 25.5 per cent potassium hydroxide, 37.8 potassium isobutyrate, 5.5 per cent potassium sulphide, 1.9 per cent potassium mercaptides, and 2.1 per cent potassium carbonate. Test specimens were located in boiling liquor at upstream side of overflow weir. Average temperature 286 F. Duration of test 140 days.
- Test D** Same as Test C, except test specimens were exposed in vapor at downstream side of overflow weir. Average temperature 286 F. Duration of test 140 days.

Material	Corrosion rate, in. per year			
	Test A	Test B	Test C	Test D
Monel	0.001	0.002	0.003	0.002
Nickel	0.024	0.002	0.022	0.016
Inconel	0.001	0.003	0.001	0.002
Mild steel	0.020	0.033	a	0.012
Ni-Resist (Type 1)	0.023	0.013	0.046	0.019
Cast iron	0.017	..	0.040	0.014

a Specimens completely destroyed during test, original thickness of specimens 0.062 in.

used rather than Monel in this service where metal temperatures in excess of 500 F are encountered, since Monel is subject to sulphur embrittlement at higher temperatures.

In view of the difficulties described with mild steel and the proved outstanding performance of Monel under such conditions, it was suggested that the affected parts of the tower be replaced or lined with Monel.

PROBLEM 5

Material Used. Carbon steel piping, 10-in. diam \times $\frac{1}{2}$ in. wall in a crude flash tower handling Quiriquire crude suffered a loss of $\frac{1}{2}$ in. in a year accompanied by severe pitting and a gouging effect.

Service Conditions. Crude is charged to flash tower at rate of 25,000 WG per hr and at a viscosity of 400 sec at 100 F Saybolt. The crude is reported to contain organic acids (naphthenic acids), chlorides, and sulphides. Temperature: 580-630 F (average 600 F). Operating pressure: 15 psi. Aeration: None.

Discussion. Naphthenic-base crudes such as Quiriquire and Monaca, have proved to be highly corrosive at elevated temperatures. Some plant corrosion tests have been made in the processing of these crudes and the data obtained are given in Table 3.

The temperature conditions of the tests are somewhat higher than in the problem application but the data might serve to indicate the relative behavior of the various materials investigated. It will be observed that in Test 1 mild steel showed a corrosion rate of 0.095 in. per year which is almost identical with the $\frac{1}{2}$ -in. loss per year reported for the 10-in. piping in the service in question. Apparently, some improvement of the order of 3 to 1 would be provided by the substitution of Type 502 stainless steel and, of course, the higher-chromium-content alloy, Type 430, as well as the austenitic stainless steels and Inconel would give superior performance.

It should be noted the powerful effect sulphur compounds at elevated temperatures above 500 F have on Monel and nickel in causing accelerated corrosion.

TABLE 3 PLANT CORROSION TEST DATA, PROBLEM 5

- Test 1 Specimens exposed for 17.5 days in a second-stage separator of a combination unit handling cracked petroleum gas oil from Monaca crude containing combined sulphur up to 1.27 per cent as H_2S , mercaptans, and organic sulphides. The temperature was 750-780 F with an average of 760 F, and the flow varied between 17,000 to 21,500 WG/hr through a 6-in. ipse line.
- Test 2 Specimens exposed for 196 days in a first-stage intercondenser of a combination unit handling cracked petroleum reduced crude containing up to 1.1 per cent sulphur as H_2S , mercaptans, plus organic sulphides. For 131 days Monaca crude was being processed during the test and for 65 days Quiriquine crude. The temperature was 790-820 F with an average of 800 F, and the flow varied between 16,000 to 18,000 WG/hr through a 12-in. extra-heavy pipe.

Material	Indicated corrosion rate, in. penetration per year	
	Test 1	Test 2
Monel	0.238*
Nickel	0.232*
Inconel	0.0074	0.0092
Type 302 SS	0.0042	0.0023
Type 316 SS	0.0037	0.0022
Type 430 SS	0.0060	0.0033
Type 502 SS	0.030	0.071
Cast iron	0.043	0.034
Mild steel	0.095	0.027

* Specimens, originally 0.031 in. thick, were completely destroyed during test period.

PROBLEM 6

Material Used. 10 lb lead on walls and 14-lb lead on cones of steel shell light fuel-oil agitators. The lead lining on the walls is replaced every 5 to 6 years, and the lining on the cone-shaped bottoms every 3 to 5 years. The agitator roofs are replaced approximately every 3 years. Considerable patching is required during the life of the linings and corrosion of the underlying steel shell occurs through holidays in the linings.

Service Conditions. Treating light fuel oils with one of the following: 93-98 per cent H_2SO_4 , 2-10 per cent sodium hydroxide, and 19-25 per cent sodium plumbite solution. In addition, the oils contain mercaptan sulphur, elemental sulphur, and polysulphides. During acid treating the batch is agitated with air for 15 min, and during lye treating the batch is agitated with air for 6 to 12 hr. It was also reported that the batches contained small quantities of elemental sulphur and lead sulphides as suspended solids, and that a maximum copper pickup from the equipment of 0.5 ppm copper can only be tolerated. The temperature of the acid batch varies between 65 and 95 F with an average of 75 F, and of the lye batch between 120 and 130 F with an average of 125 F.

Discussion. In these batch operations the same vessel was used for acid washing, neutralization, and "doctoring" for removal of traces of mercaptans. A plant corrosion test was made in a batch vessel in which the acid treatment, water washing, and caustic treatment were all carried out in the same unit, and agitation was done with air. Table 4 gives the test conditions and the results obtained, together with some data from a sodium plumbite solution.

The data from Test 1 (Table 4) indicate that Hastelloy A was the best of the materials tested, followed by Worthite, Inconel, and Monel. It should be mentioned that Monel is being widely used in this service particularly where mechanical agitation is employed. Air agitation increases somewhat the corrosion rate of Monel during the acid-treating cycle, although it is not excessive because of the relatively short time of contact of only 15 min with the media during the cycle. While Inconel showed comparable corrosion resistance with Monel in the test we would prefer to see the latter material used in such service because of its better reliability in contact with dilute solutions of sulphuric acid. In practice, while concentrated sulphuric acid is added to the oil batch, it is readily diluted down by picking up water from the oil and usually must be further diluted with water to accomplish good separation of the acid sludge after treatment, so that water

TABLE 4 TEST DATA AND RESULTS, PROBLEM 6

- Test 1 Specimens immersed 3 ft above bottom of cone in fuel-oil treating tank during treatment with 4 lb/bbl of 66 Bé sulphuric acid followed by water washing and treatment with 10 Bé caustic soda. Agitated with air. Temperature 80-105 F. Duration of test 56 days.
- Test 2 Specimens installed in an agitator and immersed in sour gasoline, mixed with a sodium plumbite solution for the removal of mercaptans and H_2S . Moderate aeration and high agitation. Temperature 60-80 F (average 70 F). Duration of test 150 hours actual operation but spool was installed for 125 days.

Material	Test 1	Indicated corrosion rate, in. penetration per year	
		Test 2	
		Based on 150 hr	Based on 125 days
Monel	0.019	0.0002	<0.0001
Nickel	0.037	0.0002	<0.0001
Inconel	0.016	0.0001	<0.0001
Worthite	0.012
Hastelloy A	0.003	0.003	0.0037
Chemical lead	0.038	0.073	<0.0001
Type 1 Ni-Resist	0.036	0.0008	0.0006
Cast iron	0.056	0.612	0.0005
Mild steel	0.021	0.010	0.0005

solutions of acid concentration down to 5 or 10 per cent may be encountered in the separation systems. Monel is not resistant to attack by sulphuric-acid solutions in excess of about 80 per cent concentration at atmospheric temperature and, when 66 Bé acid is added to an oil batch, care is exercised to avoid any contact of it with the side walls of the Monel vessel until it has had a chance to mix with the oil.

The Hastelloy alloys are rather expensive and in the event this might eliminate them from consideration, the next most logical replacement material for chemical lead is Monel, which, based on the test results, should give better than twice the life of the present equipment without the necessity of continual patching. The ultimate performance of Monel could be considerably improved by providing mechanical agitation instead of air agitation during the acid-washing cycle, thereby also reducing the amount of copper pickup to a minimum.

In referring to Test 2 wherein the corrosive was sour gasoline mixed with a sodium-plumbite solution, it will be noted that lead was the poorest of the materials tested, and it is this metal of which the equipment was constructed. Here again, the indications are that Monel would probably represent the most practical and economical material to use in this particular service. For cast equipment such as pump bodies and valves, Ni-Resist would seem to be an excellent choice as it showed up to be more than 10 times better than cast iron as well as mild steel.

PROBLEM 7

Materials Used. 12-in. extra-heavy carbon-steel pipe with a 1/8-in. wall used as a tube and tank cracking coil failed in 1 1/2 to 2 years due to general corrosion by vapors in bends leading from top of separator to high-pressure exchangers.

Service Conditions. Pipe handles reduced crude vapor containing mercaptans, H_2S , free sulphur, SO_2 , and chlorides. Temperature: 730-740 F (average 735 F). Operating pressure: 70 psi. Aeration: None.

Discussion. The change in flow of the vapors in the pipe at bends evidently sets up a more or less turbulent condition at these locations which causes accelerated corrosion of steel through the mechanism of removing or preventing the formation of protective corrosion-product films. No data were available to illustrate the effect of velocity on steel in the service in question, but the plant test data given in Table 5 were obtained under turbulent conditions and they will give some ideas as to what materials might be used to better advantage by providing additional corrosion-resistant insurance.

TABLE 5 TEST DATA AND RESULTS, PROBLEM 7

- Test 1 Specimens exposed in cracking-coil fractionator for 197 days to reduced crude oil having an average sulphur content of 0.21 per cent and an average API gravity of 29.
Temperature: 700-720 F (average 715 F).
Aeration: None.
Agitation: Turbulent.
- Test 2 Specimens exposed in cracking-coil fractionator for 122 days to reduced crude-oil vapors having an average sulphur content of 0.6 per cent.
Temperature: 575-600 F (average 590 F).
Aeration: None.
Agitation: Turbulent.

Material	Indicated corrosion rate, in. penetration per year	
	Test 1	Test 2
Monel
Nickel
Inconel	0.0008	0.0015
Type 302 SS	0.0001	0.0004
Type 410 SS	0.0006	0.0015
Type 502 SS	0.0033	0.0031
Hastelloy A	0.0002	0.0004
Mild steel	0.018
Type 1 Ni-Resist	0.058	0.025
Cast iron	0.052	0.024

* Specimens, originally 0.031 in. thick, were completely destroyed during test period.

† Specimens, originally 0.062 in. thick, were completely destroyed during test period.

The data indicate that under some conditions mild steel can suffer exceedingly high rates of attack and if the reader will refer to Test 1 it will be noted that specimens of this material, originally 0.062 in. thick, were completely destroyed during the exposure period of 197 days. Under the same conditions Type 502 stainless steel gave very satisfactory performance and would seem to be the most practical and economical material to use to replace the present steel piping. There does not appear to be any necessity in going to the more highly alloyed and more expensive materials for the service in question.

PROBLEM 8

Material Used. Carbon-steel propane (cracked distillate) accumulator with an acid-proof cement lining (Vitic No. 10). It is reported that general corrosion and severe pitting occur with a loss of about 1/8 in. per year.

Service Conditions. Two phases in accumulator as follows:
Liquid phase: small percentages of sulphides and chlorides having an acidity of 1.0 mg of KOH per gram with an average pH of the water settlement 4.4.

Gas phase: petroleum gas containing methane, ethane, propane, butane, and a small percentage of H₂S.

Temperature: 75-90 F (average 80 F).

Operating pressure: 60 psi.

Aeration: None.

Agitation: 8000 WG of distillate charge per hr.

Discussion. We presumed that corrosion of the steel beneath the coating occurred through porosity or bare spots that were not covered initially. The corrosion was evidently caused by hydrolysis of the chlorides to form small amounts of hydrochloric acid. While no data were available from a propane accumulator, some were developed in a rerun gasoline-condensate accumulator and in a reflux water separator where the water layers contained some HCl and H₂S. The test conditions and results are given in Table 6.

The rate of corrosion exhibited by mild steel in Test 1 is much higher than the rate reported of about 0.015 in. per year which, incidentally, does not appear to be intolerable. The results from Test 2 appear to be more in line with the problem conditions, and it should be pointed out that if something better than mild steel is required for the 10-ft X 30-ft accumulator in question that Monel or nickel in the form of lining or clad on steel be used. While the chromium-containing materials, including Inconel and Types 302, 410, and 502 stainless steel also showed usefully low corrosion rates, they were subject to pitting attack and in view of

TABLE 6 TEST DATA AND RESULTS, PROBLEM 8

- Test 1 Specimens exposed for 59 days in a rerun gasoline-condensate accumulator where water layer contained some HCl and H₂S. The pH of water varied from 2.1 to 6.5 and temperature 70-95 F with an average of 88 F. There was no aeration, but velocity was 0.67 fps.
- Test 2 Specimens exposed for 414 days in reflux water separator where water layer contained some HCl and H₂S. Average temperature was 120 F.

Material	Indicated corrosion rate, in. penetration per year	
	Test 1	Test 2
Monel	0.0015	0.0019
Nickel	0.0023	0.0023
Inconel	0.0004	0.0002*
Type 302 SS	0.0005	0.0001*
70/30 Cu-Ni	0.011
Mild steel	0.056	0.018
Type 410 SS	0.0006*
Type 502 SS	0.0061†

* Fitted to a maximum depth of 0.003 in. during test period.

† Fitted to a maximum depth of 0.015 in. during test period.

‡ Fitted to a maximum depth of 0.010 in. during test period.

§ Fitted to a maximum depth of 0.018 in. during test period.

their known tendency in this respect, when used in contact with halogen salts or solutions, we would hesitate to suggest their use in the problem application.

PROBLEM 9

Material Used. Carbon steel for tower top, 70-30 for condenser tubes, Monel for condensate drum lining, carbon steel for transfer lines and for run-down tank. It is reported that general corrosion and pitting of some of the materials is occurring but life seems to be indefinite.

Service Conditions. Mixture of light naphtha and water bearing H₂S and some HCl with pH controlled to 6.5 to 7.5 by addition of anhydrous ammonia.

Temperature: 80-110 F (average 95 F).

Operating pressure: 10 psi.

Aeration: Moderate.

Agitation: Turbulent in lines—quiet in drums.

Discussion. While some slight general corrosion and pitting are being encountered with the various materials in this service, it does not appear, based on plant corrosion tests, that their lives will be premature. As an example, tests made in the water-settling section at the bottom of a gas separator, taking the overhead from a rerun tower handling gasoline and water from crude naphtha from Oficina (50 per cent), Loudon (38.3 per cent) and Mid-Continent (11.7 per cent) crude oils, show negligible corrosion rates for the materials in question. The test was run for 194 days at a temperature varying between 70-112 F with an average of 98 F. The results are given in Table 7.

TABLE 7 TEST DATA AND RESULTS, PROBLEM 9

Material	Indicated corrosion rate, in. penetration per year	
	Test 1	Test 2
Monel	0.0008	0.0007
Nickel	0.0007	0.0001*
Inconel	0.0031	0.0031
70/30 Cu-Ni	<0.0001	<0.0001
Type 302 and 304 SS	<0.0001	<0.0001
Type 316 SS	<0.0001	<0.0001
Type 410 SS	0.0005*	0.0005*
Type 502 SS	0.0043	0.0020
Type 1 Ni-Resist	0.0020	0.0020
Mild steel	0.0090	0.0078
Cast iron	0.0078	0.0078

* Fitted to a maximum depth of 0.004 in. during test period.

† Fitted to a maximum depth of 0.006 in. during test period.

It is evident that mild steel has a reasonably useful corrosion rate, while Monel and 70/30 Cu-Ni are highly resistant to corrosion. It was indicated in the report of the problem that steel has a life of 10 years, while that of Monel and 70/30 is indefinite. The data would seem to bear this out and what little pitting has been observed in practice is probably not of the serious and penetrating type that leads to untimely failure.

PROBLEM 10

Materials Used. Carbon steel, 1/2 in. thick, used for stack on process furnace employed in fractional distillation of naphtha. In 10 months corrosion had destroyed metal at one point near base completely around stack. Repairs were made to stack by welding 6-in. I beams as stiffeners around base plus an interior lining over corroded area. In another 12 months repairs were again made as corrosion had attacked weld metal on interior of stack.

Service Conditions. Flue gas containing high content of SO_2 and SO_3 .
Temperature: 60 F at base of stack to 500 F.
Operating pressure: Atmospheric.
Aeration: Complete.
Agitation: Turbulent.

Discussion. The temperature at the base of the stack is below the dew point of the gas, and as a result some sulphurous acid is formed which is oxidizing in nature and highly corrosive to carbon steel. The results of a corrosion test made under sulphurous-acid conditions at atmospheric temperature are given in Table 8.

TABLE 8 RESULT OF CORROSION TEST, PROBLEM 10

Material	Indicated corrosion rate, in. penetration per year
Monel	0.006*
Nickel	0.007*
Inconel	0.0025*
Type 302 SS	<0.0001 ^b
Type 304 SS	0.0002 ^b
Type 316 SS	<0.0001
Mild steel	0.011

* Specimens, originally 0.031 in. thick, were perforated during test period.
^b Specimens of these materials were pitted to a maximum depth of 0.012 in. during test period.

While in this test the corrosion rate of mild steel is not very high, nevertheless it has been observed to corrode at a more rapid rate under similar circumstances. Type 316 stainless steel proved to be the best of the materials tested, and from a practical standpoint it has worked out to be one of the most suitable alloys that may be used in contact with dilute sulphurous-acid solutions. Almost without exception Monel, nickel, Inconel, and the straight 18-8 types of stainless steel suffer localized attack in the form of pitting in this type of service.

PROBLEM 11

Material Used. Carbon-steel tower, lines and pump used in fractional distillation of naphtha. General corrosion and pitting of steel occurs particularly at liquid level in tower and in pump casings. It is reported that bottom of tower was lined with stainless steel about a year ago and impeller in one pump was replaced with 4-6 per cent chrome steel.

Service Conditions. Hot cracked naphtha containing H_2S with traces of water.
Temperature: 600-625 F.
Operating pressure: 100 psi.
Aeration: None.
Agitation: Turbulent.

Discussion. Here again, the corrosive conditions must be considered to be similar to Problem 1. As mentioned previously, cracked naphtha has not proved to be active in promoting corrosion of metal and alloys and therefore our concern lies with the effect of sulphur or sulphur compounds at elevated temperatures on materials of construction. It was shown in the tests listed under Problem 1 that mild steel can be subject to high rates of general attack as well as severe pitting in contact with naphtha and/or gas oil containing organic sulphides and traces of water at temperatures between 290 and 690 F.

The available data indicate that the use of 18-8 stainless steel was a wise choice for the lining of the bottom section of the tower where maximum corrosion was encountered with mild steel. It is further indicated that the substitution of Type 302 stainless steel for the impeller is a move in the right direction and it would

seem practical to consider using this material for the pump casings as well. Of course, if somewhat better service life is desired over the expected performance of the Type 502 alloy, without going all the way to the use of the austenitic stainless steels, Type 410 should be considered since the corrosion-test results indicate a definite superiority of about 10 to 1.

PROBLEM 12

Material Used. Carbon steel used for vacuum tower, overhead vapor line, and vacuum condensate transfer line in fractional distillation of crude oil. Steel suffers general corrosion and pitting. Vitric-acid-proof cement is used as lining in tower but it breaks up exposing underlying steel to corrosion. Shell from tray 7 to 16 is very close to limiting thickness, and Type 347 stainless steel has been applied as a lining at trays 10 and 11. About five of the remaining sections will be in need of relining either with vitric-acid-proof cement or with stainless steel in the near future.

Service Conditions. Gas oil mixed with water containing H_2S plus some chlorides at a pH of 2.0 to 5.0.
Temperature: 70-100 F (average 80 F).
Operating pressure: Atmospheric.
Aeration: Moderate.
Agitation: Turbulent.

Discussion. The acidity of the gas oil-water mixture is in all probability due to hydrolysis of the chlorides that are present with the formation of small amounts of hydrochloric acid. Corrosion by such conditions was discussed under Problem 8 and data were presented to show the effects of this mineral acid on the performance of various metals and alloys in a rerun gasoline-condensate accumulator where the pH of the water layer varied between 2.1 and 6.5, and in a reflux water separator where acid conditions also prevailed.

It was shown in these tests that steel can suffer relatively high rates of attack, and that there are other materials available that are better suited for the application, namely, Monel and nickel. These materials have proved to be outstanding in their resistance to corrosion by dilute solutions of hydrochloric acid, and the best practical example that may be cited of the use of Monel, in particular, in petroleum refineries is for the lining of the top sections of crude-oil fractionating towers where temperatures below 500 F are encountered and corrosion by hydrochloric-acid conditions must be provided against.

Neither the austenitic stainless steels nor the straight chromium varieties are employed in this service because of their generally known and proved susceptibility toward pitting attack. The test data from the reflux water separator bear this out quantitatively by the pitting measurements that have been made on specimens of these materials after an exposure of 414 days.

Based on the evidence at hand and practical experience, it would seem more logical to consider the use of Monel or nickel instead of Type 347 stainless steel for relining the remaining five sections of the tower, and also for overhead vapor lines and vacuum condensate-transfer lines.

PROBLEM 13

Material Used. Carbon steel used for debutanizing tower top, overhead lines, fittings, and reflux condensate drum. In 1949 corrosion in top head of tower caused metal loss of 1/32 in. per year and in shell from 1/16 to 1/8 in. per year. More recently there appears to be a considerable increase of corrosion over that of previous years. Metal loss in top head of reflux drum was 1/32 in. per year and in shell and bottom head 1/16 in. per year. It was also reported that debutanizer tower overhead and reflux lines both show a corrosion rate of 1/16 in. per year.

Service Conditions. Light naphtha mixed with water containing H_2S and some HCl at a pH of 2.0 to 5.0.
Temperature: 250 F at top of tower—70 F in reflux drum.
Operating pressure: 60 psi.
Aeration: None.
Agitation: Turbulent.

Discussion. This problem should be considered along with Problems 8 and 12 wherein corrosion by hydrochloric acid, the most active constituent in the mixture, is the principal cause of the deterioration of the steel equipment. As mentioned previously, it is not generally good practice to use the austenitic stainless steels or the straight chromium types under such conditions because of pitting tendencies, and especially at the top of the debutanizer tower where the maximum temperature is 250 F, since it would be expected that the localized attack would be increased seriously. Under the circumstances, therefore, it would be suggested that Monel or nickel be considered for the service in question, especially since they have proved over the years to be the most suitable and practical materials to use in somewhat similar or comparable applications.

PROBLEM 14

Materials Used. Steel regenerating tower used in a furfural-recovery system.

Service Conditions. Furfural and water at 360 F. Severe corrosion of mild steel above vapor line at each tray level in less than a year's time rendered tower useless and required installation of a lining.

Discussion. Under some conditions it has been found that the decomposition products of furfural at elevated temperatures can be highly corrosive to steel, and the data given in Table 9 obtained in a furfural extract separation tower tend to verify this experience. Specimens were exposed for 122 days in the down-pour between the bubble trays in the tower where the temperature of the furfural averaged 450 F. There was no aeration, but some agitation was reported due to flow of the extract.

TABLE 9 RESULTS OF TEST, PROBLEM 14

Material	Indicated corrosion rate, in. penetration per year	Maximum pitting during test, in.
Monel	<0.0001	None
Nickel	<0.0001	None
Inconel	<0.0001	None
Type 302 stainless steel	<0.0001	None
Type 316 stainless steel	<0.0001	None
Chemical lead	0.0026	Perf*
Type 410 stainless steel	0.0014	0.012
Aluminum 2S	0.0002	None
Type 502 stainless steel	<0.0001	None
Mild steel	<0.0112	Perf*
Ni-Resist	<0.0001	None
Cast iron	0.0001	None

* Specimens of these materials were originally 0.062 in. thick.

The data indicate that chemical lead, mild steel, and Type 410 stainless steel are apparently unsuitable for use under the particular test conditions because of their tendency to suffer severe localized corrosion. All of the other materials investigated showed an absence of this form of corrosion and at the same time showed negligibly low rates of general attack. Under the circumstances, therefore, it would appear practical to select one of these as a lining material to protect the steel tower in question which is doomed to premature failure.

The author has had some firsthand experience with a Monel-lined furfural treating tower equipped with Monel internals and a recent checkup on this installation indicates that it is still in satisfactory condition after better than 12 years' service.

PROBLEM 15

Material Used. Steel straight-run fractionating tower and trays. Trays were $\frac{1}{4}$ in. thick and lasted only a year, and shell was severely pitted after 2 years. Severe condition occurred in uppermost section of tower.

Service Conditions. Crude oil being processed with a gravity of 20 to 26. Sulphur content varied from 1.3 to 2.5, and salt content from 15 to 30 lb per 1000 bbl. Total sulphur in gasoline varied from 0.12 to 0.40 per cent. Temperature at top of tower was maintained at 300 to 340 F, and 18 per cent gasoline was being produced.

Discussion. Corrosion in the top sections of atmospheric crude distillation units arises chiefly from hydrochloric acid either formed by hydrolysis of chloride salts, especially calcium and magnesium chloride, entrained in the crudes, or added by the acidizing of wells. Despite the customary practice of settling the salt water from crudes, and in some cases the use of special desalting processes, there still appears to be enough salt water dispersed in such crudes to result in the formation of an acid condition. Corrosion is mitigated in some cases by injection of ammonia into the distillation system to neutralize part of the acid, but experience would indicate that this frequently is not an adequate solution to the problem.

It is probable that with salty charging stocks, maximum hydrolysis of magnesium and calcium chlorides occurs in the hot-test region at the bottom of distillation towers; however, maximum acid corrosion occurs in the top portion of such towers, in reflux and distillate condensers, coolers and accumulators, and in reflux and run-down lines, where temperatures are low enough for an aqueous acid phase to condense. Maximum corrosion by sulphur compounds will, on the other hand, occur in the higher temperature ranges in the bottom portions of distillation towers and in crude heaters. As the alloys most resistant to acid corrosion frequently are not resistant to high-temperature sulphur attack, it is common practice to line the top and bottom portions of distillation towers with different materials to obtain most favorable performance.

Numerous corrosion tests have been made on or above the top plate of atmospheric crude distillation towers in a number of refineries in different geographical locations and the results, given in Table 10, are typical of those representing probably some of the worst conditions involving the processing of West Texas crude. The specimens were exposed for 60 days to the straight run gasoline vapor at the top of the tower maintained at an average temperature of 250 F.

TABLE 10 TEST RESULTS, PROBLEM 15

Material	Indicated corrosion rate, in. penetration per year	Maximum pitting during test, in.
Monel	0.0031	None
Nickel	0.0037	0.013
Inconel	0.017	0.016
Type 302 stainless steel	"	"
Type 304 stainless steel	"	"
Type 316 stainless steel	0.053	0.001
5 per cent nickel steel (SAE 2512)	"	"
Mild steel	"	"
Ni-Resist	0.051	None
Cast iron	0.181	Graphitized

* Specimens of Types 302 and 304 stainless steel and 5 per cent nickel steel, originally 0.031 in. thick, and mild steel, 0.062 in. thick, were completely destroyed during test period.

The test data indicate that mild steel as well as the 18-8 types of stainless steel, 5 per cent nickel steel, and cast iron are definitely unsuitable under these conditions. It is apparent also that nickel and Inconel are not adequate because of their susceptibility to severe pitting attack. The Type 316 stainless steel showed a reasonable corrosion rate and while the depth of local attack was rather insignificant, this tendency nevertheless exists, and it has been noted to be much more serious under similar circumstances. Of the remaining materials, Monel proved to be outstanding from the standpoint of resistance to both general corrosion and pitting. Because of this fact, it has been adopted to a considerable extent as a lining or as a Monel-clad steel shell for upper tower sections, reflux and distillate accumulators and condenser shells, and in some cases for reflux and run-down lines. It is also used for fabricated bubble caps, plates, and fittings in upper tower sections.

The foregoing problems are typical of many that have been encountered with corrosion of refinery-processing equipment and, as demonstrated, they often can be solved by referring to available

information and data obtained by an experienced corrosion engineer under the same or similar conditions.

On occasion a situation is involved whereby no clear-cut answer to the problem is evident because of the lack of either practical experience and/or available data and, under these circumstances, it is necessary to resort to the use of spool-type specimen holders for such information as may be obtained. The advantageous use of these assemblies should be encouraged once the details of the problem are established, and a check on the sources of existing data discloses no pertinent information under the particular set of corrosive conditions that might be used as a basis for selecting suitable metals and alloys for the environment in question.

Discussion

THOMAS N. GRISWOLD.¹ This is the type of paper which refiners welcome, as it touches on typical refinery corrosion problems, with good discussions of the various alloys' capabilities. Many of Mr. Mason's discussions of the problems presented have a broad applicability.

Most of the problems are viewed from the standpoint of alloy change rather than from the other possible methods of corrosion retarding such as design changes, addition of inhibitors and neutralizers, or protective nonmetallic or sacrificial coatings. Although these other measures go beyond the scope of the paper, they are usually carefully weighed in practice, particularly during periods of scarcities of certain metals.

In Problem 1 the information provided was somewhat meager; hence all possibilities could not be accurately considered. A design change such as putting two exchangers in series in place of one, using conventional countercurrent flow, would allow the safe use of a chrome alloy for tubes in the warmer bundle and a copper alloy for the cooler bundle. Another type of test which seems appropriate in this situation is direct testing of sample tubes in the exchanger, providing the metals tested are reasonably expected to last as long as the tube metal in preponderance. As an example, when the bundle was retubed with Muntz, some of the chrome alloys could be tested also. Such a test would give

a more accurate answer than test spools exposed anywhere else since pitting under baffles is involved in this case.

The regular-size ASTM spools have disadvantages when selection of exchanger-tube metals is involved because the velocities, temperatures, corrosive concentrations, and so on, are not exactly reproduced in locations where large spools can be accommodated. In some cases a specially designed coupon rack installed inside of the exchanger itself will give valuable information. These can be located in an inlet or outlet nozzle or in a small space within the bundle and in many cases in the most corrosive environment in the hottest fluid. There are, however, many special cases where this method cannot be used, the outstanding example being where the cooler side of the tube metal is being corroded. In the case where a fluid being cooled on the shell side of an exchanger is corrosive at a critical temperature, such as the point of initial water condensation, the area of maximum difficulty is pin-pointed with a coupon rack of special dimensions. Another advantage to these nonstandard-sized coupons and test racks is their adaptability to special immersion devices with which they can be inserted and removed in many kinds of equipment while the unit is on stream.

In Problem 2, although inhibited Admiralty is suggested as a more economical tube-metal choice, the tube metal near the 650 F gas-oil inlet will be close to this upper temperature limit, assuming countercurrent flow, and therefore would be above the generally recommended limits of copper alloys.

AUTHOR'S CLOSURE

Mr. Griswold's comments are well taken and, as pointed out, the scope of the paper was dedicated to a review of some typical refinery corrosion problems in the light of a possible selection of a more suitable metal or alloy for the particular services, rather than to a consideration of other methods of corrosion mitigation such as design changes, addition of inhibitors and neutralizers, or protective nonmetallic or sacrificial coatings.

With reference to the disadvantages of the regular-size ASTM spools, it is well recognized that these are not readily adaptable for use in heat exchangers to determine the relative suitability of various tubular materials where hot-wall effects have to be taken into consideration. However, we have designed special assemblies which can be accommodated in inlet or outlet nozzles or in

¹ Metallurgist, Manufacturing Department, Continental Oil Company, Ponca City, Okla.

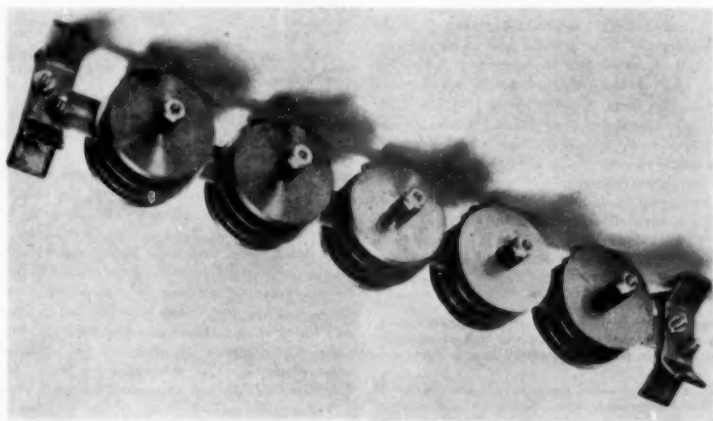


FIG. 2

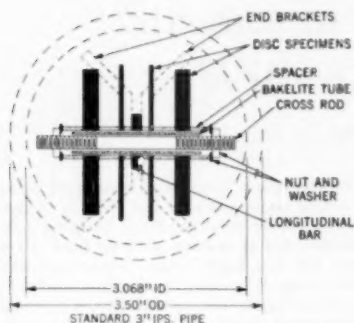


FIG. 3

a small space within the heat-exchanger bundle and in this way we have been able to approximate somewhat the actual corrosive conditions existing on the tube wall. Illustrations of these devices are shown in Figs. 2, 3, and 4. As an alternative to this method and on special occasions, use is also made of several full-size tubes of different alloys in a bundle consisting mainly of steel or some similar material which has proved to be unsatisfactory in the particular service. The tubes can be weighed carefully before and after exposure and a corrosion rate developed on this basis, or micrometer measurements might be made on the tube

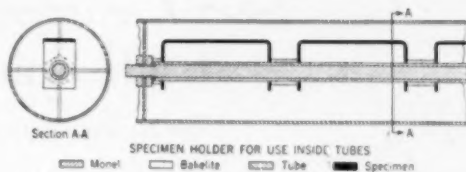


FIG. 4

wall to determine the loss in thickness. Under some conditions, where corrosion of the internal surfaces of the tubes has occurred, it will be necessary to slit the tubes longitudinally for visual examination and in order to measure the depth of any localized corrosion that might have developed in the form of pitting.

The device shown in Figs. 2 and 3 is designed for conducting tests in pipe lines of 3 in. diam or larger. It may be placed in a pipe line in any position without permitting the disk specimens to touch the wall of the pipe and it does not materially interfere with the fluid flow through the pipe.

The specimen holder illustrated in Fig. 4 is designed for conducting tests in pipe lines or tubes $1\frac{1}{2}$ in. inside diameter or larger. The specimen is a strip, $\frac{1}{2}$ wide \times 3 in long, bent at each end, and provided with $\frac{11}{64}$ in. diam holes in the bent portions. Twisted wire spiders attached to each end of the holder locate the specimens in the center of the tube and prevent galvanic contact.



Stresses in a Pressure Vessel With a Conical Head¹

By G. W. WATTS² AND H. A. LANG,³ CHICAGO, ILL.

This paper presents the results of computations for determining the stresses in a pressure vessel with a conical head. The accurate bending theory of shells is used to evaluate the local bending stresses in the neighborhood of the junction of the conical head and the cylindrical body. Tables show the magnitudes of the shear stress, the circumferential stress, and the axial stress at the junction as multiples of $pd/2t$. For the axial and circumferential stresses, the tables show the magnitude and sense of the stress on both the internal and external surfaces of the vessel. Additional results show the magnitude and location of the maximum stress (of each of the three types) in the cylinder. Curves are given showing the maximum stresses for values of cone apex angle, ratio of conical head thickness to cylinder thickness, and ratio of cylinder diameter to cylinder thickness which will include most of the vessels encountered in practice.

Tables of influence numbers for the conical head are presented. These can be utilized in many problems which require attaching a conical shell to some other elastic structure. A discussion of the mathematical procedure is contained in an Appendix.

NOMENCLATURE

The following nomenclature is used in the paper:

- δ = radial deflection of middle surface at junction, positive outward, in.
- δ' = rotation of middle surface at junction, positive as indicated in Fig. 1
- T = thickness of cone, in.
- t = thickness of cylinder, in.
- E = modulus of elasticity, psi
- p = internal pressure, psi
- μ = Poisson ratio = 0.3 for steel
- α = half vertex angle of cone
- ξ = cone parameter = $2m \sqrt{(y/T) \cot \alpha}$
- ξ_0 = cone parameter at base = $m \sqrt{2(d/T) \cot \alpha \csc \alpha}$
- d = diameter of cone base, diameter of cylinder, in.
- $m^2 = 12(1 - \mu^2)$
- $\beta = m/\sqrt{dt}$
- $\lambda = \beta M_0/Q_0$

- y = distance of point from apex of cone measured along middle surface, in.
- Q_0 = shear force per unit length, lb per in.
- M_y, M_θ = bending moments per unit length, lb
- N_y, N_θ = tensile forces per unit length, lb per in.
- x_1 = location of maximum shear stress in cylinder
- x_2 = location of maximum axial stress in cylinder
- c_1 = location of maximum circumferential stress in cylinder
- I = stress index = $\frac{\text{stress}}{pd/2t}$
- a_1, a_2, \dots, a_5
 b_1, b_2, \dots, b_5 = influence numbers

INTRODUCTION

This paper, dealing with the stresses in a pressure vessel with a conical head, is part of a continuing program instituted by the Design Division of the Pressure Vessel Research Committee of the Welding Research Council of the Engineering Foundation. This program, which consists of both analytic and experimental investigations, is intended to benefit engineers engaged in the design and manufacture of pressure vessels.

The paper is the first of a series which ultimately will cover the kinds of vessel heads in common use. Two additional papers dealing with flat and hemispherical heads will be published later. Each design paper consists of tables and curves for determining the maximum stress in a pressure vessel under the specified end closure.

The elements of the theory (which are well known)⁴ are not repeated here and the report limits itself to a description of the computational procedure together with a discussion of the results. The problem logically consists of two parts: (1) The shear force Q_0 and axial bending moment M_0 at the cone-cylinder junction (see Fig. 1), must be determined from the continuity of the radial displacement and rotation at the junction. (2) When these are known we may determine the shear, circumferential and axial stresses at the junction in the cylinder and in the cone. The maximum stresses in the cylinder other than at the junction also can be found. Details are given in the Appendix. Each stress is divided by $pd/2t$, the circumferential stress in a thin unrestrained cylinder under uniform pressure, to form the stress index denoted by I . The values at the junction are distinguished from the cylinder maxima by subscripts j and m , respectively. The subscripts s, a, c denote shear, axial, and circumferential, respectively. There are thus nine stress indexes, denoted by I_{sm}, I_{am}, I_{cm} and I_{sj}, I_{aj}, I_{cj} . It will be clear from the context whether the last three of these refer to the cylinder or the cone. The stress index in the cone I_{aj} will be called axial though properly it has the direction of y , Fig. 1. The stresses in the cone other than at the junction have not been computed.

The stress ratio I has two distinct advantages. It reduces the magnitude of the results and enables one to tell immediately

¹ This work is part of a continuing program instituted in 1946 by the Design Division of the Pressure Vessel Research Committee of the Welding Research Council of the Engineering Foundation, New York, N. Y.

² Director of Engineering, Standard Oil Company (Indiana). Fellow ASME.

³ Project Engineer, Engineering Research Department, Standard Oil Company (Indiana). Mem. ASME.

Contributed by the Petroleum Division and presented at the Petroleum Mechanical Engineering Conference, Tulsa, Okla., September 24-26, 1951, of THE AMERICAN SOCIETY OF MECHANICAL ENGINEERS.

NOTE: Statements and opinions advanced in papers are to be understood as individual expressions of their authors and not those of the Society. Manuscript received at ASME Headquarters, July 6, 1951. Paper No. 51-PET-8.

⁴ The theory of shells is discussed in "Theory of Plates and Shells," by S. Timoshenko, first edition, McGraw-Hill Book Company, Inc., New York, N. Y., 1940, Chapt. XII. A general mathematical treatment of pressure vessels will be found in "The Basic Elastic Theory of Vessel Heads Under Internal Pressure," by G. W. Watts and W. R. Burrows, Trans. ASME, vol. 71, 1949, pp. 85-73.

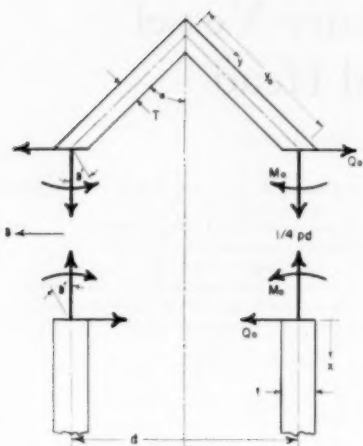


FIG. 1 LOADS AT JUNCTION OF HEAD AND SHELL

whether a stress is greater or less than the hoop stress in a thin cylinder. It frequently is substantially linear when plotted against the diameter-thickness ratio, d/t , of the cylinder. By contrast, a curve of stress divided by pressure is more nearly parabolic.

Since the theory of the shell is concerned with middle surface displacements, conditions at the junction of a physical shell do not correspond precisely with the junction conditions formulated here. This is indicated in Fig. 2 where it is apparent that

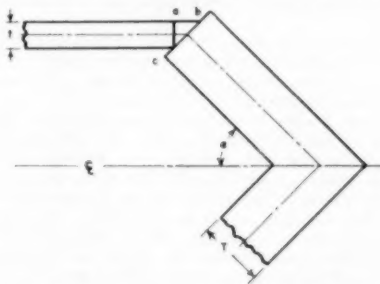


FIG. 2 DETAIL AT JUNCTION OF HEAD AND SHELL

the cylinder and head overlap. To state this differently, we have a cylinder, cone, and a transition element of triangular cross section ($a b c$). Some discrepancy, even in the absence of yielding, is to be expected between the computed results and any results obtained experimentally because of the effect of this transition element. Questions of this sort constitute a problem in local stresses and lie outside the scope of shell theory.

The determination of a correction for this local state of stress is being investigated by a PVRC Design Division Subcommittee. Their findings, which will be published, can be used to extend the results tabulated in the present paper.

ANALYSIS

The deflection and rotation at the junction can be expressed in the forms

$$\frac{Et\delta}{pd^3} = \frac{M_0}{pd^3} a_1 + \frac{Q_0}{pd} a_2 + a_3 = \frac{M_0}{pd^3} a_4 + \frac{Q_0}{pd} a_5 + a_6 \quad [1]$$

$$\frac{ET\delta'}{m^2pd^2} = \frac{M_0}{pd^2} b_1 + \frac{Q_0}{pd} b_2 + b_3 = \frac{M_0}{pd^2} b_4 + \frac{Q_0}{pd} b_5 + b_6 \quad [2]$$

(for cone) (for cylinder)

The quantities a_1, a_2, a_3, b_1, b_2 , and b_3 are dimensionless "influence numbers" for the conical head. Thus a_2 represents the effect of unit pressure in producing a deflection $ET\delta/d^3$ at the base of the cone. Similarly, a_4, a_5, a_6, b_4, b_5 , and b_6 are dimensionless influence numbers for the cylinder. The definition of all influence numbers is given in the Appendix.

The dimensionless ratios M_0/pd^3 and Q_0/pd , computed from Equations [1] and [2], are sufficient to determine the stress indexes listed in Table 1.

RANGE OF CALCULATIONS

The values of T/t used are

For $\alpha = 0$ deg $T/t = 0.8, 1, 1.25$

For $\alpha = 15$ deg $T/t = 0.8, 1$, sec 15° (1.0353)

For $\alpha = 30$ deg $T/t = 0.8, 1$, sec 30° (1.1547)

For $\alpha = 45$ deg $T/t = 0.8, 1, 1.2$, sec 45° (1.4142)

For $\alpha = 60$ deg $T/t = 0.8, 1, 1.2, 1.6$, sec 60° (2.0)

For each half cone angle, values of ξ_0 are selected which will lead to seven to nine values of d/T extending from 3 to 500. The values of d/T are not evenly spaced but fall mostly between 5 and 100, which is the range occurring frequently in practice. Non-integer initial values of ξ_0 were selected so that $d/T = 4, 10, 40, 80, 100, 300, 500$ at $\alpha = 45$ deg. A few additional values of ξ_0 are required at other angles. The 16 values of ξ_0 chosen yield 121 values of d/t in the range 3 to 500. Table 2 shows the ξ_0 chosen and the values of T/t and α for which each ξ_0 is used.

The numerical results are sufficiently complete to allow the designer to interpolate for most values of α , T/t , and d/t encountered in practical problems.

DISCUSSION OF RESULTS

(a) *Two Cylinders.* If the thickness T refers to a cylinder which replaces the conical head in Fig. 1, the stress indexes for $T/t = 0.8$ are shown in Table 8.² Only the shear stress varies with change in diameter-thickness ratio, d/T or d/t . The maximum circumferential stress in the thinner cylinder is the largest stress. It is 26 per cent greater than the hoop stress $pd/2t$. For equal thicknesses the moment M_0 and a shear force Q_0 vanish and the circumferential index is 1 everywhere, while the axial index is $1/2$ everywhere. There is no shear stress.

We should expect the stresses to be greater in the thinner cylinder. The only exception to this conclusion is the maximum shear-stress index. Since stresses in a cylinder decay exponentially with distance from the junction, the greater shear-stress index in the thicker cylinder results from its closer proximity to the junction.

All stress indexes are either unchanged or decrease with increase in d/t . This corresponds to an increase in the common diameter of the cylinders while the thicknesses remain fixed. Such an increase leads to larger values of the influence coefficients and a corresponding decrease in M_0/pd^3 and Q_0/pd .

That the signs of M_0/pd^3 and Q_0/pd are negative can be seen physically. Under uniform pressure, the thinner cylinder expands more. A negative shear force is necessary to enforce continuity of deflection. The angle turned through by a line element at the junction when unit negative shear force $Q_0/pd = 1$

² Interchanging cylinders, the results also apply when $T/t = 1.25$.

TABLE 1
STRESS INDEXES IN CONICAL HEAD AT JUNCTION

$$\begin{aligned}
 I_{si} &= 3 \frac{t}{T} \left[\frac{Q_0}{pd} \right]_0 = 3 \frac{t}{T} \left[\frac{Q_0}{pd} \cos \alpha - \frac{1}{4} \sin \alpha \right] \\
 I_{si} &= 2 \frac{t}{T} \left[\frac{N_0}{pd} \right]_0 + 12 \frac{d}{T} \left[\frac{M_0}{pd^2} \right]_0 \\
 &= 2 \frac{t}{T} \left[\frac{1}{4} \cos \alpha + \frac{Q_0}{pd} \sin \alpha \right] + 12 \frac{d}{T} \left[\frac{M_0}{pd^2} \right]_0 \\
 I_{ci} &= 2 \frac{t}{T} \left[\frac{N_0}{pd} \right]_0 + 12 \frac{d}{T} \left[\frac{M_0}{pd^2} \right]_0 \\
 &= 2 \frac{t}{T} \left\{ m^2 \sin \alpha \left[\frac{M_0}{pd^2} \left(b_1 + \frac{3\mu \xi^2 \tan \alpha}{m^4} \right) + \frac{Q_0}{pd} b_2 + b_1 \right] \right. \\
 &\quad \left. + \left[\frac{M_0}{pd^2} 2a_1 + \frac{Q_0}{pd} (2a_2 + \mu \sin \alpha) + 2a_2 + \frac{\mu \cos \alpha}{4} \right] \right\}
 \end{aligned}$$

STRESS INDEXES IN CYLINDER AT JUNCTION

$$\begin{aligned}
 I_{si} &= 3 \left[\frac{Q_0}{pd} \right] \\
 I_{si} &= \frac{1}{2} + 12 \frac{d}{t} \left[\frac{M_0}{pd^2} \right] \\
 I_{ci} &= \left[1 - 2m \sqrt{\frac{d}{t}} \frac{Q_0}{pd} (1 + \lambda) \right] + 12 \mu \frac{d}{t} \left[\frac{M_0}{pd^2} \right]
 \end{aligned}$$

MAXIMUM STRESS INDEXES IN CYLINDER

$$\begin{aligned}
 I_{sm} &= \frac{I_{si} \sqrt{1 + 2\lambda + 2\lambda^2}}{e^{\tan^{-1} \frac{1 + \lambda}{\lambda}}} \quad \frac{x_1}{d} = \frac{\tan^{-1} \frac{1 + \lambda}{\lambda}}{m \sqrt{\frac{d}{t}}} \\
 I_{sm} &= \frac{1}{2} + 3.4126 \sqrt{\frac{d}{t}} I_{si} \quad \frac{x_2}{d} = \frac{x_1}{d} - \frac{\pi}{4} \frac{1}{m \sqrt{\frac{d}{t}}}
 \end{aligned}$$

where

$$\lambda = m \sqrt{\frac{d}{t}} \frac{M_0/pd^2}{Q_0/pd}$$

TABLE 2 VALUES OF ξ_2

Angle $\xi_2 \sqrt{t/d}$	15° All	30° All	45° All	0.8	1.0	1.2	1.6	2.0
6.1145								
9.6678								
16.0000								
19.3356								
27.3447								
30.5723								
36.0000								
42.0000								
52.9528								
68.3817								
84.0000								
100.0000								
107.0000								
136.0000								
172.0000								
218.0000								

acts is represented by b_2 in the left cylinder and b_1 in the right. But $b_2 = -1/2$ and $b_1 = -(1/2) (T/t)^2 = -0.32$. This means that the left cylinder rotates in a positive sense by an amount $0.18(Q_0/pd)$ more than the right cylinder rotates. A negative bending moment is required to reconcile this difference and maintain continuity of deflection.

(b) *Stress Indexes.* 1 All nine stress indexes tend to increase with angle α except for the two circumferential stress indexes I_{ci} at the junction which decrease at sufficiently small values of d/T but increase at larger values of d/T . This exception is apparently caused by the decrease in a_1 and b_1 which outweighs increases in a_1 , b_1 , a_2 , and b_2 in the cone at the junction. In the cylinder at the junction the shear force reduces the circumferential stress arising from pressure and this reduction is greater than the increase in circumferential stress arising from the bending.

2 As d/T increases, the stress indexes I_{sm} (in cylinder), I_{sm} (in cylinder), and I_{si} (in both cone and cylinder) increase. The remaining stress indexes may decrease or increase depending on the values of α and T/t . These changes are caused primarily by the relative effect of changes in the influence numbers.

3 As T/t increases, the stress indexes I_{si} and I_{si} in the cone decrease while I_{ci} in the cylinder increases. The index I_{ci} (in the cone) decreases except at $\alpha = 15$ deg and large d/T when it increases, the remaining indexes tend to increase at low d/T and decrease at large d/T for each value of α . The reasoning here follows the argument given in the preceding discussion.

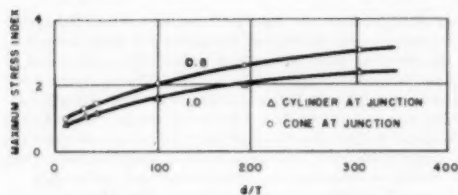
4 The ratios x_1/d , x_2/d , and x_3/d , specifying the location of maximum stresses in the cylinder, tend generally to decrease with increasing d/T , increasing T/t , and decreasing angle α . As the angle decreases we approach more nearly two cylinders and the corresponding decrease in λ leads to maximum cylinder stresses nearer the junction. The increase in d/T or T/t results in a thicker cone or cylinder. The strain energy induced by the moment and shear force is confined, on the average, to the same volume since M_0/pd^2 and Q_0/pd change relatively slowly. The increase in thickness then requires a decreasing length x/d in which the stress is high. Consequently, the maximum stresses should approach the junction.

5 The type of stress index which is the greatest of the nine indexes is shown in Table 3. Generally the axial stress in the cone at the junction is greatest for $T/t = 0.8$, or alternatively for $T/t = 1.0$ and d/T sufficiently large. The axial stress in the cylinder at the junction is greatest for $T/t > 1$, or alternatively for $T/t = 1.0$ and d/T sufficiently small. At angles $\alpha = 45$ deg or less and small d/T , the circumferential stress may be greatest. The greatest computed stress index is in the cone at the junction when $\alpha = 60$ deg and $T/t = 0.8$. The value of this index is 19.825. At $\alpha = 15$ deg and $T/t = 1.0$, the discontinuity in axial stress at the junction is extremely small. Thus two symbols are inserted in this column of Table 3.

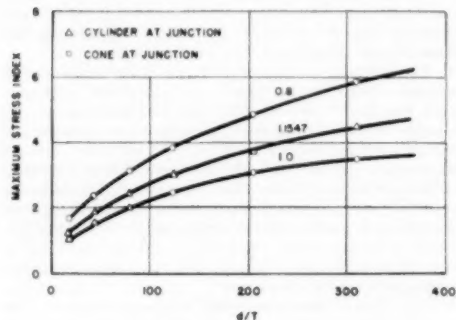
Where the axial stress at the junction does not govern, the values of d/T are small and the conical head is not a thin shell as the theory contemplates. Using the legend of Table 3, Figs. 3, 4, 5, and 6 show the variation of maximum stress index with d/T where d/T extends from approximately 5 to 400.

Figs. 3 to 6 show immediately that it is desirable to make the vertex half angle α and d/T as small as possible, that is, the more nearly the cone becomes a cylinder the lower the maximum stress. Also, increasing the thickness of the cone relative to its diameter decreases the maximum stress. The curves suggest that the most favorable thickness ratio is $T/t = 1.0$. When $T/t < 1.0$, the cone is thinner than the cylinder and there is a large axial stress at the junction in the cone. When $T/t > 1.0$, the cone is thicker than the cylinder and there is a large axial stress at the junction in the cylinder. Where it is not possible to have the thickness the same in both cone and cylinder, it is more desirable to make the cone thicker. This is indicated by the fact that curve $T/t = 1.2$, Figs. 5 and 6, leads to lower stress than the curve $T/t = 0.8$. A slight increase in cone thickness at small values of angle α affects this maximum stress very little.

For sufficiently large angle α , variations in T/t not too much in excess of 1.0 produce very small changes in maximum stress.



Axial stress index = axial stress $\div \frac{pd}{2t}$;
 $\frac{d}{T}$ = diameter of cylinder \div thickness of cone
 FIG. 3 AXIAL-STRESS INDEX VERSUS d/T FOR CONICAL HEAD
 ($\alpha = 15$ deg; $T/t = 0.8$ and 1.0 .)



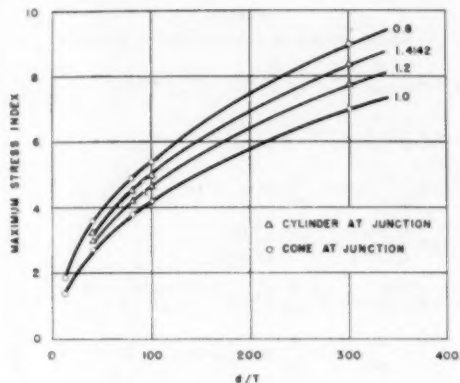
Axial stress index = axial stress $\div \frac{pd}{2t}$;
 $\frac{d}{T}$ = diameter of cylinder \div thickness of cone
 FIG. 4 AXIAL-STRESS INDEX VERSUS d/T FOR CONICAL HEAD
 ($\alpha = 30$ deg; $T/t = 0.8, 1.0, 1.1547$ = sec 30 deg.)

In conclusion, it is well to note that the possibility of selecting a cone which yields no discontinuities at the junction requires that (1) $a_3 = a_4$ and (2) $b_2 = 0$. The quantities a_3 and a_4 are of opposite sign so that this possibility is precluded.

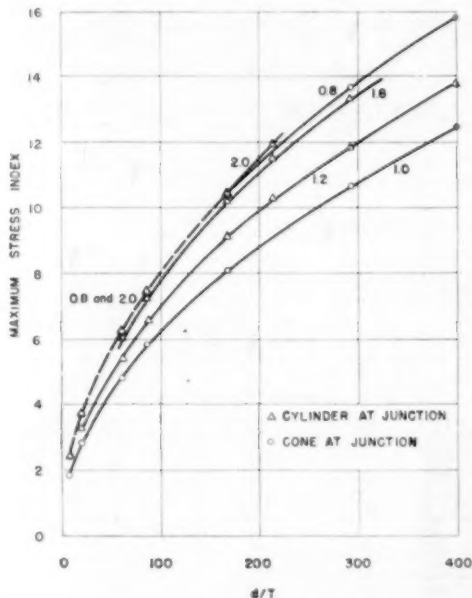
CONCLUSIONS

The general conclusions of interest to designers and engineers engaged in shell problems are summarized as follows:

- 1 Under uniform pressure p alone and no edge constraints but the axial tension $(\frac{1}{2})pd$, required for equilibrium, a cone deflects inwardly (toward its axis) at its base circle.
- 2 It is impossible to design a conical head to eliminate moment and shear at the junction since the cylinder always deflects outward and the head inward when an internal pressure is applied to each.
- 3 In a cylindrical pressure vessel with a conical head, the greatest stress is the axial stress at the junction. It may be located in the cylinder or the cone. To minimize the stress, it is desirable to make the cone and cylinder equally thick if the angle α does not exceed 45 deg. Where this is not possible, the cone should possess the greater thickness. Angles greater than 45 deg require a thicker head. Reducing the cone vertex angle or the diameter-thickness ratio of the vessels also reduces the stress.
- 4 The usual theory of shells shows that the maximum axial



Axial stress index = axial stress $\div \frac{pd}{2t}$;
 $\frac{d}{T}$ = diameter of cylinder \div thickness of cone
 FIG. 5 AXIAL-STRESS INDEX VERSUS d/T FOR CONICAL HEAD
 ($\alpha = 45$ deg; $T/t = 0.8, 1.0, 1.2, 1.4142$ = sec 45 deg.)



Axial stress index = axial stress $\div \frac{pd}{2t}$;
 $\frac{d}{T}$ = diameter of cylinder \div thickness of cone
 FIG. 6 AXIAL-STRESS INDEX VERSUS d/T FOR CONICAL HEAD
 ($\alpha = 60$ deg; $T/t = 0.8, 1.0, 1.2, 1.6, 2.0$ = sec 60 deg.)

stress may reach values of 10 or more times the circumferential stress $pd/2t$ in the unrestrained thin cylinder. The greatest com-

TABLE 3 MAXIMUM STRESS INDEXES FOR CONICAL HEADS

Angle α ($^\circ$, T/t)	15°			30°			45°				60°				
	0.8	1.0	1.0353 (sec 15°)	0.8	1.0	1.1547 (sec 30°)	0.8	1.0	1.2	1.4142 (sec 45°)	0.8	1.0	1.2	1.6	2.0
6.1145							0	—	—	—	0	0	—	—	—
9.6678				—	—	—	0	—	—	—	0	0	—	—	—
16.0000							0	0	—	—	0	0	—	—	—
19.3356	+	□	□	0	—	—	0	0	—	—	0	0	—	—	—
27.3447							0	0	—	—	0	0	—	—	—
30.5723	+	□	□	0	—	—	0	0	—	—	0	0	—	—	—
36.0000											0	0	—	—	—
42.0000				0	—	—					0	0	—	—	—
52.9528	0	—	—	0	0	—	0	0	—	—	0	0	—	—	—
68.3817	0	—	—	0	0	—	0	0	—	—	0	0	—	—	—
84.0000				0	0	—									
100.0000	0	—	—												
107.0000				0	0	—									
136.0000	0	—	—												
172.0000	0	—	—												
218.0000	0	—	—												

LEGEND:

- Axial-stress index in cylinder at junction
 0 Axial-stress index in cone at junction
 + Circumferential-stress index in cone at junction
 □ Maximum circumferential-stress index in cylinder

TABLE 4 INFLUENCE COEFFICIENTS FOR CONE, $\alpha = 15$ DEG

d/T	a ₁	a ₂	a ₃	b ₁	b ₂	b ₃
3.9231	- 6.3685	+ 1.6034	+ 0.1080	+ 3.6189	- 0.4913	- 0.0199
9.8076	- 18.0642	+ 2.7141	+ 0.0360	+ 5.7543	- 0.4987	- 0.0218
29.4229	- 48.4194	+ 7.7846	- 0.0889	+ 9.9995	- 0.4960	- 0.0314
49.0382	- 80.7915	+ 6.1783	- 0.1941	+ 12.9205	- 0.4986	- 0.0323
104.9339	- 173.0857	+ 6.0713	- 0.3679	+ 18.9165	- 0.4991	- 0.0329
194.0819	- 320.2775	+ 12.3660	- 0.6085	+ 25.7384	- 0.4994	- 0.0331
310.4304	- 512.4286	+ 15.8604	- 0.8391	+ 32.5590	- 0.4995	- 0.0333
498.4761	- 822.3524	+ 19.8700	- 1.1111	+ 41.3758	- 0.4996	- 0.0333

TABLE 6 INFLUENCE COEFFICIENTS FOR CONE, $\alpha = 45$ DEG

d/T	a ₁	a ₂	a ₃	b ₁	b ₂	b ₃
4.0000	- 5.7796	+ 1.2340	- 0.0725	+ 4.0325	- 0.4372	- 0.0741
10.0000	- 15.5974	+ 2.1521	- 0.2854	+ 6.0971	- 0.4739	- 0.0877
40.0000	- 64.9345	+ 4.5965	- 0.9558	+ 13.5059	- 0.4913	- 0.1163
80.0000	- 130.8284	+ 6.8964	- 1.3547	+ 19.1883	- 0.4949	- 0.1202
100.0000	- 163.7829	+ 7.4152	- 1.5562	+ 21.4784	- 0.4967	- 0.1211
300.0000	- 483.8916	+ 13.0171	- 2.9847	+ 37.3106	- 0.4980	- 0.1235
500.0000	- 822.7623	+ 16.8714	- 3.9179	+ 48.2200	- 0.4986	- 0.1249

puted stress index is 19.825 for a cone having $\alpha = 60$ deg, $T/t = 0.8$, $d/T = 509.1167$. This stress occurs in the cone at the junction. The high values of stress index suggest early yielding at and near the junction.

SAMPLE PROBLEM

To illustrate the use of the curves for determining the secondary bending stresses, assume a 6-ft-diam vessel with a wall thickness of 0.3 in. The internal pressure is 100 psi and the conical head has an apex angle of 120 deg. Therefore $d/t = 72/0.3 = 240$ and $\alpha = 60$ deg, $pd/2t = 12,000$ psi. Using Fig. 6, the following table can be constructed:

$T/t =$	0.8	1.0	1.2	1.6	2.0
$d/T =$	300	240	200	150	120
$I = \frac{s}{pd/2t} =$	13.8	9.6	9.8	9.6	8.9
$s =$	163000	115000	118000	115000	107000

The magnitude of these stresses indicates, of course, that some yielding and stress relief has occurred in the neighborhood of the junction between the body and head.

CONVENTION USED IN TABLES 8 THROUGH 23

In this paper the problem of determining the magnitude of the maximum stress has been primarily emphasized. A few additional calculations make it possible to indicate not only the stress

TABLE 5 INFLUENCE COEFFICIENTS FOR CONE, $\alpha = 30$ DEG

d/T	a ₁	a ₂	a ₃	b ₁	b ₂	b ₃
4.0025	- 6.3678	+ 1.5230	+ 0.0030	+ 3.6148	- 0.4730	- 0.0447
16.3299	- 28.5094	+ 3.1620	- 0.2207	+ 7.7977	- 0.4913	- 0.0634
40.6248	- 68.8652	+ 5.2493	- 0.5138	+ 12.5984	- 0.4997	- 0.0863
77.0489	- 128.6227	+ 7.2665	- 0.9047	+ 17.0707	- 0.4972	- 0.0760
122.4743	- 201.5480	+ 9.3045	- 1.0940	+ 21.5459	- 0.4980	- 0.0707
204.1239	- 336.2996	+ 11.9299	- 1.4770	+ 27.8396	- 0.4986	- 0.0713
308.1959	- 506.0946	+ 14.6953	- 1.8760	+ 34.2261	- 0.4989	- 0.0718
500.0751	- 824.8978	+ 18.7620	- 2.4829	+ 42.6180	- 0.4992	- 0.0719

TABLE 7 INFLUENCE COEFFICIENTS FOR CONE, $\alpha = 60$ DEG

d/T	a ₁	a ₂	a ₃	b ₁	b ₂	b ₃
8.4853	- 12.2804	+ 1.5114	- 0.3207	+ 6.9846	- 0.4372	- 0.1486
21.2132	- 33.0871	+ 2.6361	- 0.7589	+ 11.4443	- 0.4720	- 0.1609
50.1018	- 82.7159	+ 4.6512	- 1.5623	+ 19.2642	- 0.4861	- 0.2008
84.8529	- 137.7489	+ 6.6295	- 2.0339	+ 23.3530	- 0.4913	- 0.2063
169.7086	- 277.5290	+ 8.0911	- 3.0837	+ 28.2351	- 0.4949	- 0.2103
212.1320	- 347.4572	+ 9.0817	- 3.5116	+ 37.1965	- 0.4957	- 0.2114
294.1496	- 482.6726	+ 10.7465	- 4.2314	+ 45.9550	- 0.4966	- 0.2126
400.3580	- 657.8465	+ 12.5860	- 5.0371	+ 51.2120	- 0.4973	- 0.2135
636.3950	- 1047.2780	+ 15.9438	- 6.4797	+ 64.6377	- 0.4980	- 0.2145

magnitude but its sense (whether tension or compression) and its location (whether on the internal or external surface of the vessel). In Tables 8 through 23 the following convention is adhered to:

1 For every circumferential or axial-stress index, two figures are listed for each diameter-thickness ratio. The upper figure represents the value of the stress index at the external surface of the vessel. The lower figure represents the value of the stress index at the internal surface of the vessel. A plus sign denotes tension and a minus sign denotes compression.

2 Every shear-stress index refers to a shear stress at the middle surface of the vessel. The shear stress acting on the cylinder at the junction is positive when it has the direction of Q_s in Fig. 1. The shear stress acting on the cone at the junction is positive when its component parallel to the axis of the shell is to the left in Fig. 1. The maximum shear stress in the cylinder is positive when it has the direction of Q_s in Fig. 1. The shell wall, to which the stress refers, is to the left.

Appendix

INFLUENCE NUMBERS FOR THE CYLINDER

The deflection and rotation produced by loads p , Q_s , M_s are:

* See "Theory of Plates and Shells," S. Timoshenko, first edition, McGraw-Hill Book Company, Inc., New York, N. Y., 1940, pp. 393, 407.

TABLE 8* STRESS INDEX IN TWO CYLINDERS, $\alpha = 0$, $T/t = 0.8$
(Upper values refer to stress at external surface; lower values refer to stress at internal surface. + = tension; - = compression.)
Left Cylinder, Thickness t

d/t	d/T	Cone at Junction			Cylinder at Junction		
		Shear I_{sj}	Max. Stress Index I_{sj}	Max. Stress Index I_{cj}	Shear I_{sm}	Max. Stress Index I_{sm}	Max. Stress Index I_{cm}
3.2	-0.0419	-0.4831	-1.0963	-0.0106	-0.4354	-0.9929	0.4546 0.2110 0.6495
		-0.5169	-1.1064		-0.5646	-0.9949	
8.0	-0.0285	-0.4831	-1.0963	-0.0067	-0.4354	-0.9929	0.3875 0.1347 0.5373
		-0.5169	-1.1064		-0.5646	-0.9949	
32.0	-0.0132	-0.4831	-1.0963	-0.0033	-0.4354	-0.9929	0.1437 0.0674 0.3886
		-0.5169	-1.1064		-0.5646	-0.9949	
64.0	-0.0094	-0.4831	-1.0963	-0.0024	-0.4354	-0.9929	0.1016 0.0476 0.1899
		-0.5169	-1.1064		-0.5646	-0.9949	
80.0	-0.0084	-0.4831	-1.0963	-0.0021	-0.4354	-0.9929	0.0609 0.0438 0.1699
		-0.5169	-1.1064		-0.5646	-0.9949	
240.0	-0.0048	-0.4831	-1.0963	-0.0012	-0.4354	-0.9929	0.0525 0.0248 0.0981
		-0.5169	-1.1064		-0.5646	-0.9949	
400.0	-0.0037	-0.4831	-1.0963	-0.0008	-0.4354	-0.9929	0.0407 0.0191 0.0760
		-0.5169	-1.1064		-0.5646	-0.9949	

Right Cylinder, Thickness T

d/t	d/T	Cone at Junction			Cylinder at Junction		
		Shear I_{sj}	Max. Stress Index I_{sj}	Max. Stress Index I_{cj}	Shear I_{sm}	Max. Stress Index I_{sm}	Max. Stress Index I_{cm}
4.0	-0.0624	-0.3486	-1.0906	-0.0085	-0.6333	-1.2624	0.4674 0.2514 0.5462
		-0.6514	-1.1455		-0.3167	-0.9218	
10.0	-0.0331	-0.3486	-1.0906	-0.0054	-0.6333	-1.2624	0.2056 0.1590 0.3455
		-0.6514	-1.1455		-0.3167	-0.9218	
40.0	-0.0166	-0.3486	-1.0906	-0.0027	-0.6333	-1.2624	0.1470 0.0795 0.1727
		-0.6514	-1.1455		-0.3167	-0.9218	
80.0	-0.0117	-0.3486	-1.0906	-0.0019	-0.6333	-1.2624	0.1045 0.0562 0.1221
		-0.6514	-1.1455		-0.3167	-0.9218	
100.0	-0.0105	-0.3486	-1.0906	-0.0017	-0.6333	-1.2624	0.0835 0.0503 0.1062
		-0.6514	-1.1455		-0.3167	-0.9218	
300.0	-0.0060	-0.3486	-1.0906	-0.0010	-0.6333	-1.2624	0.0540 0.0390 0.0631
		-0.6514	-1.1455		-0.3167	-0.9218	
500.0	-0.0047	-0.3486	-1.0906	-0.0008	-0.6333	-1.2624	0.0418 0.0355 0.0489
		-0.6514	-1.1455		-0.3167	-0.9218	

* Correction to Table 8. For d/t of 240.0, under Junction Stress Index, I_{cj} of 1.1964 should be 1.1064.

TABLE 10 STRESS INDEXES IN A CYLINDRICAL PRESSURE VESSEL WITH CONICAL HEAD, $\alpha = 15$ DEG, $T/t = 1.0$
(Upper values refer to stress at external surface; lower values refer to stress at internal surface. + = tension; - = compression.)

d/t	d/T	Cone at Junction			Cylinder at Junction		
		Shear I_{sj}	Max. Stress Index I_{sj}	Max. Stress Index I_{cj}	Shear I_{sm}	Max. Stress Index I_{sm}	Max. Stress Index I_{cm}
3.9231	3.9231	+0.1019	+0.3860	+0.7936	+0.0955	-0.3486	+0.8038
			+0.6306	+0.8925		+0.8314	+0.8826
9.9076	9.9076	+0.1020	+0.3148	+0.7056	+0.0954	-0.3153	+0.7094
			+0.7941	+0.8636		+0.7847	+0.8603
29.4228	29.4228	+0.1006	+0.0882	+0.5001	+0.0968	-0.0588	+0.5040
			+1.0549	+0.8491		+1.0688	+0.8393
49.0361	49.0361	+0.1001	+0.2396	+0.3588	+0.0973	+0.2394	+0.3593
			+1.2392	+0.8053		+1.2394	+0.8059
104.9316	104.9316	+0.0994	+0.6032	+0.0590	+0.0960	+0.6030	+0.0597
			+1.6029	+0.7215		+1.6030	+0.7215
194.0610	194.0610	+0.0999	+0.0133	+0.2827	+0.0984	+0.0133	+0.2827
			+2.0122	+0.6245		+2.0122	+0.6246
310.4304	310.4304	+0.0988	+1.4192	+0.6257	+0.0967	+1.4192	+0.5012
			+2.4192	+0.5257		+2.4192	+0.4581
498.6781	498.6781	+0.0980	+1.8379	+1.0644	+0.0969	+1.8379	+0.9321
			+2.9360	+0.3944		+2.9370	+0.2638

d/t	d/T	Maxima in Cylinder			Location of Maxima in Cylinder		
		Shear I_{sm}	Max. Stress Index I_{sm}	Max. Stress Index I_{cm}	Shear I_{sj}	Max. Stress Index I_{sj}	Max. Stress Index I_{cj}
3.9231	3.9231	-0.0097	+0.5486	+1.0140	0.5864	0.3363	0.6360
			+0.4344	-0.9958			
9.9076	9.9076	-0.0074	+0.5767	+1.0189	0.3905	0.2526	0.4409
			+0.4213	-0.9950			
29.4228	29.4228	-0.0067	+0.6240	+1.0266	0.3397	0.1960	0.3647
			+0.3760	-0.9951			
49.0361	49.0361	-0.0068	+0.8361	+1.0339	0.1843	0.1223	0.2065
			+0.3419	-0.9899			
104.9316	104.9316	-0.0068	+0.7300	+1.0494	0.1265	0.0843	0.1415
			+0.2700	-0.9852			
194.0610	194.0610	-0.0068	+0.8129	+1.0672	0.0831	0.0621	0.1044
			+0.1871	-0.9800			
310.4304	310.4304	-0.0066	+0.8963	+1.0850	0.0737	0.0491	0.0926
			+0.1037	-0.9747			
498.6781	498.6781	-0.0068	+1.0031	+1.1080	0.0581	0.0392	0.0632
			+0.0001	-0.9678			

TABLE 9 STRESS INDEXES IN A CYLINDRICAL PRESSURE VESSEL WITH CONICAL HEAD, $\alpha = 15$ DEG, $T/t = 0.8$
(Upper values refer to stress at external surface; lower values refer to stress at internal surface. + = tension; - = compression.)

d/t	d/T	Cone at Junction			Cylinder at Junction		
		Shear I_{sj}	Max. Stress Index I_{sj}	Max. Stress Index I_{cj}	Shear I_{sm}	Max. Stress Index I_{sm}	Max. Stress Index I_{cm}
3.1384	3.9231	+0.1875	+0.4480	+0.9089	+0.0622	-0.3818	+0.9584
			+0.7862	+1.0134		-0.5082	+0.4035
7.8461	9.9076	+0.1517	+0.2423	+0.8097	+0.0754	-0.2583	+0.9496
			+0.9976	+1.0259		-0.7417	+0.8048
23.5383	29.4228	+0.1374	-0.1108	-0.5835	+0.0872	-0.0270	+0.4909
			+1.3616	+1.0083		-0.9730	+0.6062
39.3305	49.0361	+0.1327	-0.3508	-0.3961	+0.0911	-0.1234	+0.3390
			+1.5975	+0.9813		-1.1234	+0.4649
83.9455	104.9316	+0.1273	-0.8208	-0.9519	+0.0955	-0.4348	+0.7264
			+2.0804	+0.9206		-1.4246	+0.1715
155.2656	194.0610	+0.1242	-1.3464	-0.3414	+0.0981	-0.7829	+0.5933
			+2.5081	+0.8452		-1.7629	+0.1644
248.3443	310.4304	+0.1234	-1.8730	-0.7351	+0.0996	-1.0968	+0.5012
			+3.1224	+0.7872		-2.0848	+0.4581
398.9425	498.6781	+0.1209	-2.5469	-1.2384	+0.1008	-1.5265	+0.9321
			+3.7918	+0.6553		-2.5265	+0.2638

d/t	d/T	Maxima in Cylinder			Location of Maxima in Cylinder		
		Shear I_{sm}	Max. Stress Index I_{sm}	Max. Stress Index I_{cm}	Shear I_{sj}	Max. Stress Index I_{sj}	Max. Stress Index I_{cj}
3.1384	3.9231	-0.0047	+0.5282	+1.0081	0.6962	0.4522	0.7873
			+0.4718	-0.9982			
7.8461	9.9076	-0.0049	+0.5464	+1.0100	0.4707	0.3165	0.3270
			+0.4536	-0.9970			
23.5383	29.4228	-0.0057	+0.5961	+1.0204	0.2891	0.1800	0.3016
			+0.4048	-0.9939			
39.3305	49.0361	-0.0061	+0.8314	+1.0202	0.2083	0.1374	0.2315
			+0.3686	-0.9916			
83.9455	104.9316	-0.0067	+0.7083	+1.0447	0.1391	0.0920	0.1563
			+0.2817	-0.9867			
155.2656	194.0610	-0.0070	+0.7971	+1.0639	0.1013	0.0667	0.1140
			+0.2025	-0.9810			
248.3443	310.4304	-0.0072	+0.8878	+1.0832	0.0797	0.0522	0.0907
			+0.1134	-0.9753			
398.9425	498.6781	-0.0074	+1.0032	+1.1080	0.0636	0.0409	0.0704
			+0.0032	-0.9688			

TABLE 11 STRESS INDEXES IN A CYLINDRICAL PRESSURE VESSEL WITH CONICAL HEAD, $\alpha = 15$ DEG, $T/t = 1.0353$
(Upper values refer to stress at external surface; lower values refer to stress at internal surface. + = tension; - = compression.)

d/t	d/T	Cone at Junction			Cylinder at Junction		
		Shear I_{sj}	Max. Stress Index I_{sj}	Max. Stress Index I_{cj}	Shear I_{sm}	Max. Stress Index I_{sm}	Max. Stress Index I_{cm}
4.0614	3.9231	+0.0639	+0.3545	+0.7762	+0.1003	-0.6380	+0.7887
			+0.6120	+0.8759		-0.9620	+0.8725
10.1536	9.9076	+0.0958	+0.3066	+0.6908	+0.0993	-0.7940	+0.6943
			+0.7572	+0.8639		-0.2060	+0.8797
30.4608	29.4228	+0.0960	+0.0530	+0.4531	+0.0961	-1.0743	+0.4678
			+1.0187	+0.8167		-0.0743	+0.5234
50.7680	49.0361	+0.0959	+0.2355	+0.3531	+0.0962	-1.2583	+0.3424
			+1.1913	+0.7779		-0.2583	+0.7979
108.6334	104.9316	+0.0957	+0.5733	+0.0592	+0.0954	-1.6320	+0.0415
			+1.5391	+0.6928		-0.6320	+0.7208
200.9384	194.0610	+0.0956	+0.9647	-0.2758	+0.0965	-2.0616	+0.3022
			+1.9306	+0.5921		-1.0616	+0.6388
321.3812	310.4304	+0.0956	+1.3543	-0.4901	+0.0985	-2.4692	+0.6486
			+2.3202	+0.6115		-1.4692	+0.5349
516.2696	498.6781	+0.0955	+1.8505	-1.0412	+0.0986	-3.0010	+1.0867
			+2.8164	+0.3543		-2.0010	+0.4139

d/t	d/T	Maxima in Cylinder			Location of Maxima in Cylinder		
		Shear I_{sm}	Max. Stress Index I_{sm}	Max. Stress Index I_{cm}	Shear I_{sj}	Max. Stress Index I_{sj}	Max. Stress Index I_{cj}
4.0614	3.9231	-0.0103	+0.5711	+1.0153	0.5442	0.3296	0.6224
			+0.4289	-0.9955			
10.1536	9.9076	-0.0077	+0.5637	+1.0180	0.3617	0.2461	0.4312
			+0.4163	-0.9946			
30.4608	29.4228	-0.0068	+0.6285	+1.0276	0.2313	0.1530	0.2596
			+0.3715	-0.9918			
50.7680	49.0361	-0.0067	+0.8633	+1.0349	0.1808	0.1302	0.2090
			+0.3377	-0.9896			
108.6334	104.9316	-0.0066	+0.7336	+1.0501	0.1246	0.0831	0.1397
			+0.2684	-0.9831			
200.9384	194.0610	-0.0065	+0.8138				

TABLE 12 STRESS INDEXES IN A CYLINDRICAL PRESSURE VESSEL WITH CONICAL HEAD, $\alpha = 30$ DEG, $T/t = 0.8$

(Upper values refer to stress at external surface; lower values refer to stress at internal surface. + = tension; - = compression.)

d/t	d/T	Cone at Junction			Cylinder at Junction		
		Shear I_{sj}	Axial I_{aj}	Circum. I_{cj}	Shear I_{sj}	Axial I_{aj}	Circum. I_{cj}
3.2060	4.0875	+0.2918	-0.2325	-0.6763	+0.1634	-0.2589	-0.7027
			+0.9662	-0.9394		+0.7412	-0.8474
13.0639	16.3299	+0.3705	-0.4625	-0.2855	+0.1832	-0.1912	-0.3710
			-1.6977	-0.9420		-1.1912	-0.7857
32.6399	40.8248	+0.2569	-1.2059	-0.2291	+0.1957	-0.6691	-0.9632
			-2.4485	-0.8628		-1.6691	-0.6392
61.6391	77.0489	+0.2486	-1.9337	-0.7523	+0.2022	-1.1379	-0.4690
			-3.1848	-0.8163		-3.1379	-0.5137
97.9795	122.4743	+0.2457	-2.6237	-1.2699	+0.2069	-1.5805	-0.9499
			-3.8779	-0.6907		-2.5805	-0.2962
163.2391	204.1239	+0.2421	-3.5868	-1.9910	+0.2094	-2.1980	-1.5063
			-4.8441	-0.5510		-3.1980	-0.0524
246.5564	306.1955	+0.2397	-4.5604	-2.7235	+0.2116	-2.8211	-2.1932
			-5.8187	-0.4056		-3.8211	-0.2006
400.0601	500.0751	+0.2375	-5.9957	-3.8015	+0.2136	-3.7247	-3.1186
			-7.2470	-0.1863		-4.7247	-0.5758

d/t	d/T	Maxima in Cylinder			Location of Maxima in Cylinder		
		Shear I_{sm}	Axial I_{am}	Circum. I_{cm}	x_1/d	x_2/d	x_3/d
3.2060	4.0875	-0.0145	-0.5397	+1.0193	0.6405	0.4914	0.7218
			-0.4100	-0.9945			
13.0639	16.3299	-0.0129	-0.3943	+1.0345	0.3508	0.3313	0.3945
			-0.3405	-0.9099			
32.6399	40.8248	-0.0138	-0.7692	+1.0578	0.2220	0.1484	0.2496
			-0.2506	-0.9638			
61.6391	77.0489	-0.0145	-0.9673	+1.0633	0.1607	0.1097	0.1809
			-0.1127	-0.9752			
97.9795	122.4743	-0.0149	-1.0029	+1.1089	0.1269	0.0623	0.1426
			-0.0029	-0.9678			
163.2391	204.1239	-0.0153	-1.1073	+1.1433	0.0978	0.0649	0.1102
			-0.1073	-0.9673			
246.5564	306.1955	-0.0158	-1.3357	+1.1794	0.0794	0.0618	0.0994
			-0.3357	-0.9466			
400.0601	500.0751	-0.0159	-1.5842	+1.2328	0.0631	0.0495	0.0790
			-0.5842	-0.9307			

TABLE 14 STRESS INDEXES IN A CYLINDRICAL PRESSURE VESSEL WITH CONICAL HEAD, $\alpha = 30$ DEG, $T/t = 1.1347$

(Upper values refer to stress at external surface; lower values refer to stress at internal surface. + = tension; - = compression.)

d/t	d/T	Cone at Junction			Cylinder at Junction		
		Shear I_{sj}	Axial I_{aj}	Circum. I_{cj}	Shear I_{sj}	Axial I_{aj}	Circum. I_{cj}
4.7140	4.0625	+0.1713	-0.1631	+0.5356	+0.2046	-0.1588	-0.5523
			-0.7050	-0.7561		-0.8812	-0.7890
18.9362	16.3299	+0.1767	-0.2620	+0.2390	+0.1974	-0.4253	-0.1832
			-1.1259	-0.9609		-1.4253	-0.7483
47.1404	40.8248	+0.1761	-0.7304	-0.1350	+0.1962	-1.0501	-0.3804
			-1.5840	-0.3267		-2.0501	-0.9897
68.9484	77.0489	+0.1756	-1.1959	-0.5795	+0.1969	-1.6711	-0.7288
			-2.0607	-0.3843		-2.6711	-0.5741
141.4212	122.4743	+0.1753	-1.6378	-0.9855	+0.1993	-2.3804	-1.1799
			-2.5608	-0.2418		-3.3804	-0.4768
235.7020	204.1239	+0.1750	-2.2150	-1.5589	+0.1996	-3.0847	-1.8153
			-3.1212	-0.0362		-4.0847	-0.3355
355.8735	306.1955	+0.1749	-2.8810	-2.1422	+0.1999	-3.9182	-2.4616
			-2.7464	-0.1705		-4.9182	-0.1894
577.4370	500.0751	+0.1747	-3.7879	-3.0013	+0.2001	-5.1411	-3.4125
			-4.6836	-0.4797		-6.1411	-0.0279

d/t	d/T	Maxima in Cylinder			Location of Maxima in Cylinder		
		Shear I_{sm}	Axial I_{am}	Circum. I_{cm}	x_1/d	x_2/d	x_3/d
4.7140	4.0625	-0.0163	-0.6355	+1.0291	0.5331	0.3333	0.6050
			-0.3645	-0.9912			
18.9362	16.3299	-0.0135	-0.4906	+1.0420	0.2961	0.1966	0.3324
			-0.3502	-0.9872			
47.1404	40.8248	-0.0138	-0.8006	+1.0645	0.1916	0.1387	0.2146
			-0.1894	-0.9808			
68.9484	77.0489	-0.0127	-0.9078	+1.0875	0.1495	0.0946	0.1572
			-0.0622	-0.9738			
141.4212	122.4743	-0.0126	-1.0119	+1.1090	0.1117	0.0754	0.1250
			-0.0119	-0.9873			
235.7020	204.1239	-0.0126	-1.1595	+1.1416	0.0887	0.0585	0.0970
			-0.1595	-0.9878			
355.8735	306.1955	-0.0126	-1.3088	+1.1739	0.0706	0.0477	0.0790
			-0.3088	-0.9482			
577.4370	500.0751	-0.0126	-1.5315	+1.2214	0.0555	0.0375	0.0620
			-0.5315	-0.9341			

TABLE 13 STRESS INDEXES IN A CYLINDRICAL PRESSURE VESSEL WITH CONICAL HEAD, $\alpha = 30$ DEG, $T/t = 1.0$

(Upper values refer to stress at external surface; lower values refer to stress at internal surface. + = tension; - = compression.)

d/t	d/T	Cone at Junction			Cylinder at Junction		
		Shear I_{sj}	Axial I_{aj}	Circum. I_{cj}	Shear I_{sj}	Axial I_{aj}	Circum. I_{cj}
4.0825	4.0825	+0.2111	-0.1922	-0.5026	+0.1893	-0.1961	-0.6138
			+0.9000	-0.9229		+0.9009	-0.7961
16.3299	16.3299	+0.2063	-0.3303	-0.2606	+0.1925	-0.3274	-0.2849
			-1.3246	-0.7640		-1.3274	-0.7614
40.8248	40.8248	+0.2030	-0.8999	-0.1793	+0.1979	-0.8998	-0.1796
			-1.8979	-0.9386		-1.8988	-0.9397
77.0489	77.0489	+0.2014	-1.4844	-0.6385	+0.2009	-1.4842	-0.6400
			-2.4844	-0.5369		-2.4842	-0.5369
122.4743	122.4743	+0.2000	-1.9994	-1.0821	+0.2001	-1.9990	-1.0841
			-3.0000	-0.4143		-3.9990	-0.4459
204.1239	204.1239	+0.1997	-2.7474	-1.7085	+0.2026	-2.7482	-1.7105
			-3.7481	-0.3271		-3.7483	-0.3293
306.1955	306.1955	+0.1979	-3.5024	-2.3484	+0.2045	-3.5046	-2.3473
			-4.5053	-0.0543		-4.5045	-0.0834
500.0751	500.0751	+0.1971	-4.6125	-3.2891	+0.2054	-4.6149	-3.2949
			-5.6189	-0.2174		-5.6160	-0.2193

d/t	d/T	Maxima in Cylinder			Location of Maxima in Cylinder		
		Shear I_{sm}	Axial I_{am}	Circum. I_{cm}	x_1/d	x_2/d	x_3/d
4.0825	4.0825	-0.0173	-0.6100	+1.0895	0.5878	0.3539	0.6458
			-0.5810	-0.9934			
16.3299	16.3299	-0.0123	-0.4540	+1.0395	0.3162	0.2093	0.3553
			-0.3169	-0.9032			
40.8248	40.8248	-0.0132	-0.7668	+1.0616	0.2034	0.1258	0.2381
			-0.2132	-0.9617			
77.0489	77.0489	-0.0132	-0.9897	+1.0632	0.1486	0.0694	0.1665
			-0.1033	-0.9746			
122.4743	122.4743	-0.0133	-1.0037	+1.1061	0.1179	0.0789	0.1322
			-0.0037	-0.9678			
204.1239	204.1239	-0.0134	-1.1554	+1.1497	0.0913	0.0611	0.1023
			-0.1551	-0.9561			
306.1955	306.1955	-0.0135	-1.3101	+1.1739	0.0743	0.0497	0.0832
			-0.3101	-0.9483			
500.0751	500.0751	-0.0136	-1.5394	+1.2229	0.0583	0.0389	0.0653
			-0.5394	-0.9335			

TABLE 15 STRESS INDEXES IN A CYLINDRICAL PRESSURE VESSEL WITH CONICAL HEAD, $\alpha = 45$ DEG, $T/t = 0.8$

(Upper values refer to stress at external surface; lower values refer to stress at internal surface. + = tension; - = compression.)

d/t	d/T	Cone at Junction			Cylinder at Junction		
		Shear I_{sj}	Axial I_{aj}	Circum. I_{cj}	Shear I_{sj}	Axial I_{aj}	Circum. I_{cj}
3.2000	4.0000	+0.4261	-0.3965	-0.6414	+0.2679	-0.1005	-0.5194
			-1.2340	-0.8969		-0.8969	-0.7391
8.0000	10.0000	+0.4183	-0.8725	-0.1259	+0.2801	-0.3089	-0.2422
			-1.6725	-0.9009		-1.3089	-0.7288
32.0000	40.0000	+0.3943	-2.0472	-0.9766	+0.3182	-1.2783	-0.6095
			-3.5640	-0.8017		-2.3793	-0.4580
64.0000	80.0000	+0.3725	-2.9680	-1.9334	+0.2888	-2.3245	-1.5025
			-4.8927	-0.6445		-3.2245	-0.1322
80.0000	100.0000	+0.3693	-3.3543	-2.3214	+0.3322	-2.5806	-1.8331
			-5.4197	-0.5743		-3.5606	-0.0032
240.0000	300.0000	+0.3575	-5.6435	-5.0224	+0.3455	-4.8603	-4.1421
			-9.0209	-0.0415		-5.8603	-0.9259
400.0000	500.0000	+0.3538	-7.5568	-6.8650	+0.3497	-6.4307	-7.7884
			-11.4773	-0.4079		-7.4307	-1.5609

d/t	d/T	Maxima in Cylinder			Location of Maxima in Cylinder		
		Shear I_{sm}	Axial I_{am}	Circum. I_{cm}	x_1/d	x_2/d	x_3/d
3.2000	4.0000	-0.0234	-0.6431	+1.0307	0.6515	0.4099	0.7396
			-0.3569	-0.9909			
8.0000	10.0000	-0.0202	-0.6980	+1.0419	0.4445	0.3917	0.5903
			-0.3050	-0.9875			
32.0000	40.0000	-0.0220	-0.9236	+1.0814	0.2350	0.1487	0.2529
			-0.0744	-0.9729			
64.0000	80.0000	-0.0234	-1.1380	+1.1379	0.1580	0.1040	0.1778
			-0.1380	-0.9882			
80.0000	100.0000	-0.0239	-1.2256	+1.1858	0.1410	0.0927	0.1396
			-0.2256	-0.9638			
240.0000	300.0000	-0.0254	-1.8440	+1.2085	0.0805	0.0528	0.0907
			-0.8440	-0.9141			
400.0000	500.0000	-0.0280	-2.2749	+1.3810	0.0631	0.0405	0.0700
			-1.2749	-0.8885			

TABLE 16* STRESS INDEXES IN A CYLINDRICAL PRESSURE VESSEL WITH CONICAL HEAD, $\alpha = 45$ DEG, $T/t = 1.0$

(Upper values refer to stress at external surface; lower values refer to stress at internal surface. + = tension; - = compression.)

d/t	d/T	Cone at Junction			Cylinder at Junction		
		Shear $I_{\theta j}$	Axial $I_{\theta j}$	Circum. $I_{\theta j}$	Shear $I_{\theta j}$	Axial $I_{\theta j}$	Circum. $I_{\theta j}$
4.0000	4.0000	+0.3263	-0.0119	-0.3750	+0.2887	-0.0015	-0.5278
			-0.9911	-0.7712		-1.0015	-0.7270
10.0000	10.0000	+0.3255	-0.4850	-0.1259	+0.2997	-0.4781	-0.5144
			+1.4853	-0.7527		+1.4751	-0.7193
40.0000	40.0000	+0.3101	-1.7497	-0.8130	+0.3114	-1.7500	-0.8225
			+2.7504	-0.5183		+2.7500	-0.5278
80.0000	80.0000	+0.3041	-2.7669	-1.8373	+0.3200	-2.7713	-1.8443
			+3.7757	-0.5061		+3.7713	-0.5144
100.0000	100.0000	+0.3024	-3.1730	-1.9724	+0.3223	-3.1785	-1.9839
			+4.1840	-0.2159		+4.1785	-0.2236
300.0000	300.0000	+0.2965	-5.9640	-4.3908	+0.3308	-5.9735	-4.3194
			+8.9830	-0.4954		+8.9735	-0.4953
500.0000	500.0000	+0.2948	-7.8743	-5.9223	+0.3334	-7.8850	-5.9223
			+8.8957	-0.9526		+8.8850	-0.9013

d/t	d/T	Maxima in Cylinder			Location of Maxima in Cylinder		
		Shear $I_{\theta m}$	Axial $I_{\theta m}$	Circum. $I_{\theta m}$	Shear x_1/d	Axial x_2/d	Circum. x_3/d
4.0000	4.0000	-0.0243	-0.6860	-1.0356	0.5910	0.3750	0.6896
			-0.3340	-0.9894			
10.0000	10.0000	-0.0201	-0.7166	-1.0465	0.4042	0.2078	0.4541
			-0.2834	-0.9862			
40.0000	40.0000	-0.0201	-0.9338	-1.0631	0.2083	0.1400	0.2332
			-0.0662	-0.9733			
80.0000	80.0000	-0.0206	-1.1202	-1.1353	0.1473	0.0990	0.1649
			-0.1302	-0.9597			
100.0000	100.0000	-0.0206	-1.2106	-1.1528	0.1317	0.0885	0.1474
			-0.2106	-0.9546			
300.0000	300.0000	-0.0216	-1.7757	-1.2739	0.0757	0.0507	0.0848
			-0.7757	-0.9164			
500.0000	500.0000	-0.0219	-2.1879	-1.3881	0.0565	0.0392	0.0856
			-1.1679	-0.8534			

* Correction to Table 16. Under Cone at Junction, last entry for $I_{\theta j}$ should be minus.TABLE 16** STRESS INDEXES IN A CYLINDRICAL PRESSURE VESSEL WITH CONICAL HEAD, $\alpha = 45$ DEG, $T/t = 1.4142$

(Upper values refer to stress at external surface; lower values refer to stress at internal surface. + = tension; - = compression.)

d/t	d/T	Cone at Junction			Cylinder at Junction		
		Shear $I_{\theta j}$	Axial $I_{\theta j}$	Circum. $I_{\theta j}$	Shear $I_{\theta j}$	Axial $I_{\theta j}$	Circum. $I_{\theta j}$
5.0589	4.0000	-0.3173	-0.0015	+0.2961	+0.3154	-0.2133	-0.2697
			-0.7119	-0.9394		-1.2133	-0.8977
19.1421	10.0000	-0.2257	-0.2791	-0.4898	+0.2985	-0.7573	-0.0453
			-0.9871	-0.1041		-1.7573	-0.7091
56.5685	40.0000	-0.2244	-1.0408	-0.6307	+0.3011	-2.2911	-1.9475
			+1.7400	-0.1106		-3.3911	-0.6212
113.1371	80.0000	-0.2233	-1.8589	-1.2999	+0.3034	-3.5200	-1.9025
			-2.3811	-0.1824		-4.5200	-0.5095
141.4214	100.0000	-0.2230	-1.9085	-1.5704	+0.3040	-4.0157	-2.2485
			-2.6091	-0.3064		-5.0157	-0.4610
424.2841	300.0000	-0.2219	-3.8122	-3.4810	+0.3061	-7.4285	-6.8540
			+4.3163	-1.4692		-8.4285	-0.1031
707.1068	500.0000	-0.2216	-4.7609	-4.7682	+0.3068	-9.7683	-6.3124
			+5.4654	-1.5173		-10.7683	-0.1528

d/t	d/T	Maxima in Cylinder			Location of Maxima in Cylinder		
		Shear $I_{\theta m}$	Axial $I_{\theta m}$	Circum. $I_{\theta m}$	Shear x_1/d	Axial x_2/d	Circum. x_3/d
5.0589	4.0000	-0.0244	-0.6862	-1.0425	0.5138	0.3321	0.5691
			-0.3016	-0.9873			
19.1421	10.0000	-0.0197	-0.7523	-1.0542	0.3473	0.2324	0.3692
			-0.2477	-0.9639			
56.5685	40.0000	-0.0181	-0.9646	-1.0997	0.1806	0.1234	0.2056
			-0.0354	-0.9703			
113.1371	80.0000	-0.0180	-1.1327	-1.1401	0.1397	0.0860	0.1470
			-0.1327	-0.9583			
141.4214	100.0000	-0.0180	-1.2282	-1.1568	0.1152	0.0789	0.1285
			-0.2282	-0.9534			
424.2841	300.0000	-0.0189	-1.7643	-1.2714	0.0687	0.0487	0.0744
			-0.7642	-0.9192			
707.1068	500.0000	-0.0180	-2.1341	-1.3808	0.0517	0.0355	0.0756
			-1.1341	-0.8955			

** Table 18. For d/t of 19.1421, under Cone at Junction, $I_{\theta j}$ of 0.9871 should be 0.9872.TABLE 17 STRESS INDEXES IN A CYLINDRICAL PRESSURE VESSEL WITH CONICAL HEAD, $\alpha = 45$ DEG, $T/t = 1.2$

(Upper values refer to stress at external surface; lower values refer to stress at internal surface. + = tension; - = compression.)

d/t	d/T	Cone at Junction			Cylinder at Junction		
		Shear $I_{\theta j}$	Axial $I_{\theta j}$	Circum. $I_{\theta j}$	Shear $I_{\theta j}$	Axial $I_{\theta j}$	Circum. $I_{\theta j}$
4.8000	4.0000	+0.3630	-0.0068	-0.2353	+0.3037	-0.1096	-0.2108
			-0.8345	-0.6706		-1.1096	-0.7090
12.0000	10.0000	+0.3678	-0.3884	-0.1155	+0.2956	-0.8220	-0.0406
			+1.1099	-0.5853		-1.8220	-0.7138
48.0000	40.0000	+0.3600	-1.3509	-0.7060	+0.3072	-2.0424	-0.9413
			+2.1815	-0.3014		+2.0424	-0.5847
96.0000	80.0000	+0.2579	-2.1484	-1.4412	+0.3123	-3.1917	-1.7830
			+2.9610	-0.0406		+4.1917	-0.4339
120.0000	100.0000	+0.2971	-2.4950	-1.7396	+0.3137	-3.4806	-2.1241
			+3.3002	-0.0875		+4.4806	-0.3683
360.0000	300.0000	+0.2541	-4.6332	-3.8229	+0.3168	-8.8051	-4.4978
			-4.4938	-0.8423		-7.8051	-0.2848
600.0000	500.0000	+0.2532	-6.1520	-5.2825	+0.3203	-9.9644	-6.1350
			-6.9503	-1.4158		-9.9644	-0.4563

d/t	d/T	Maxima in Cylinder			Location of Maxima in Cylinder		
		Shear $I_{\theta m}$	Axial $I_{\theta m}$	Circum. $I_{\theta m}$	Shear x_1/d	Axial x_2/d	Circum. x_3/d
4.8000	4.0000	-0.0245	-0.6832	-1.0393	0.5487	0.3515	0.6297
			-0.3188	-0.9883			
12.0000	10.0000	-0.0199	-0.7261	-1.0506	0.3735	0.2488	0.4191
			-0.2649	-0.9850			
48.0000	40.0000	-0.0190	-0.9483	-1.0943	0.1939	0.1316	0.2187
			-0.0817	-0.9713			
96.0000	80.0000	-0.0191	-1.1387	-1.1371	0.1377	0.0936	0.1539
			-0.1387	-0.9692			
120.0000	100.0000	-0.0192	-1.2104	-1.1538	0.1232	0.0838	0.1378
			-0.2104	-0.9542			
360.0000	300.0000	-0.0195	-1.7607	-1.2706	0.0711	0.0484	0.0796
			-0.7607	-0.9194			
600.0000	500.0000	-0.0196	-2.1575	-1.3515	0.0551	0.0374	0.0815
			-1.1575	-0.8953			

TABLE 18 STRESS INDEXES IN A CYLINDRICAL PRESSURE VESSEL WITH CONICAL HEAD, $\alpha = 60$ DEG, $T/t = 0.8$

(Upper values refer to stress at external surface; lower values refer to stress at internal surface. + = tension; - = compression.)

d/t	d/T	Cone at Junction			Cylinder at Junction		
		Shear $I_{\theta j}$	Axial $I_{\theta j}$	Circum. $I_{\theta j}$	Shear $I_{\theta j}$	Axial $I_{\theta j}$	Circum. $I_{\theta j}$
6.7882	8.4053	-0.5659	-1.0960	-0.1270	+0.3397	-0.5338	-0.0288
			+2.3901	-0.9029		-1.3838	-0.6791
16.9708	21.3132	-0.5363	-2.4839	-0.8822	+0.4377	-1.4912	-0.6558
			+3.7397	-0.8211		-2.4912	-0.5088
46.4815	58.1018	-0.5006	-4.8992	-2.6772	+0.4853	-2.0596	-2.1173
			+6.2247	-0.6783		+4.0596	-0.0186
87.8822	84.8528	-0.4996	-6.1454	-2.5836	+0.4997	-2.8638	-2.8952
			+7.4916	-0.5221		+4.8638	-0.2769
135.7844	169.7086	-0.4863	-9.0680	-5.8117	+0.5210	-5.7638	-4.7864
			+10.4750	-0.1101		+6.7638	-1.0287
235.3125	294.1406	-0.4782	-12.2583	-8.2178	+0.5339	-7.7825	-6.8453
			+12.6540	-0.2706		+8.7825	-1.8696
320.2864	400.3580	-0.4745	-14.4405	-9.8877	+0.5386	-9.1912	-8.2787
			+15.8446	-0.7295		+10.1912	-2.4620
509.1167	638.3959	-0.4699	-18.4103	-12.9377	+0.5472	-11.7353	-10.8838
			+19.8249	-1.3843		+12.7353	-3.5528

d/t	d/T	Maxima in Cylinder			Location of Maxima in Cylinder		
		Shear $I_{\theta m}$	Axial $I_{\theta m}$	Circum. $I_{\theta m}$	Shear x_1/d	Axial x_2/d	Circum. x_3/d
6.7882	8.4053	-0.0275	-0.7442	-1.0524	0.4891	0.2333	0.5497
			-0.2559	-0.9644			
16.9708	21.3132	-0.0292	-0.9109	-1.0862	0.3151	0.2103	0.3534
			-0.0891	-0.9737			
46.4815	58.1018	-0.0333	-1.2539	-1.1681	0.1883	0.1250	0.2113
			-0.2739	-0.9506			
87.8822	84.8528	-0.0348	-1.4774	-1.2099	0.1549	0.1024	0.1740
			-0.4774	-0.9375			
135.7844	169.7086	-0.0372	-1.9603	-1.3178	0.1083	0.0713	0.1216
			-0.9603	-0.9054			
235.3125	294.1406	-0.0389	-2.5343	-1.4387	0.0816	0.0535	0.0919
			-1.5343	-0.8700			
320.2864	400.3580	-0.0397	-2.9217	-1.5199	0.0697	0.0456	0.0785
			-1.9217	-0.8452			
509.1167	638.3959	-0.0407	-3.5324	-1.8723	0.0550	0.0359	0.0820
			-2.8324	-0.7998			

TABLE 20 STRESS INDEXES IN A CYLINDRICAL PRESSURE VESSEL WITH CONICAL HEAD, $\alpha = 60$ DEG, $T/t = 1.0$

(Upper values refer to stress at external surface; lower values refer to stress at internal surface. + = tension; - = compression.)

d/t	d/T	Cone at Junction			Cylinder at Junction		
		Shear $I_{\theta j}$	Axial $I_{\theta j}$	Circum. $I_{\theta j}$	Shear $I_{\theta j}$	Axial $I_{\theta j}$	Circum. $I_{\theta j}$
8.4853	8.4853	+0.4491	-0.8307	-0.0888	+0.4000	+0.8031	-0.0884
			+1.7835	-0.6820		+1.8021	-0.6923
21.2132	21.2132	+0.4336	-1.8750	-0.7923	+0.4339	+1.8763	-0.8259
			+2.8768	-0.8466		+2.8783	-0.8597
58.1018	58.1018	+0.4142	-5.7437	-2.2353	+0.4706	+5.7655	-2.2772
			+4.7872	-0.2615		+4.7888	-0.2615
84.8528	84.8528	+0.4087	-4.7120	-3.0202	+0.4616	+4.7410	-3.0825
			+5.7601	-0.0565		+5.7410	-0.0822
169.7056	169.7056	+0.4007	-7.0167	-4.9245	+0.4877	+7.0641	-4.9637
			+6.0914	-0.4489		+6.0541	-0.4312
294.1406	294.1406	+0.3959	-9.4807	-6.9633	+0.5073	+9.5393	-7.0292
			-10.9721	-1.0280		+10.5383	-1.0118
400.3580	400.3580	+0.3937	-11.8244	-8.4399	+0.5117	+11.2379	-8.4641
			-12.2823	-1.4283		-12.2379	-1.4314

d/t	d/T	Maxima in Cylinder			Location of Maxima in Cylinder		
		Shear $I_{\theta m}$	Axial $I_{\theta m}$	Circum. $I_{\theta m}$	Shear x_1/d	Axial x_2/d	Circum. x_3/d
8.4853	8.4853	-0.0268	+0.7634	+1.0568	0.4475	0.2992	0.5017
			+0.2386	+0.8432			
21.2132	21.2132	-0.0269	-0.9230	+1.0908	0.2911	0.1973	0.3253
			+0.0770	+0.9730			
58.1018	58.1018	-0.0292	-1.2395	+1.1630	0.1759	0.1193	0.1965
			-0.2595	+0.9514			
84.8528	84.8528	-0.0301	-1.4453	+1.2650	0.1451	0.0962	0.1632
			-0.4453	+0.9395			
169.7056	169.7056	-0.0315	-1.9006	+1.3007	0.1020	0.0628	0.1141
			-0.9006	+0.9105			
294.1406	294.1406	-0.0325	-2.3984	+1.4078	0.0771	0.0519	0.0863
			-1.3984	+0.8766			
400.3580	400.3580	-0.0328	-2.7471	+1.4624	0.0650	0.0443	0.0738
			-1.7471	+0.8564			

TABLE 21* STRESS INDEXES IN A CYLINDRICAL PRESSURE VESSEL WITH CONICAL HEAD, $\alpha = 60$ DEG, $T/t = 1.2$

(Upper values refer to stress at external surface; lower values refer to stress at internal surface. + = tension; - = compression.)

d/t	d/T	Cone at Junction			Cylinder at Junction		
		Shear $I_{\theta j}$	Axial $I_{\theta j}$	Circum. $I_{\theta j}$	Shear $I_{\theta j}$	Axial $I_{\theta j}$	Circum. $I_{\theta j}$
10.1823	8.4853	+0.3729	-0.8302	-0.0865	+0.4040	+0.8075	-0.1892
			+1.4337	-0.5152		+1.8075	-0.7033
25.4558	21.2132	+0.3626	-1.4475	-0.6675	+0.4288	+2.1814	-0.9497
			+2.2768	-0.3256		+3.1814	-0.8297
58.1222	58.1018	+0.3504	-2.9362	-1.9365	+0.4580	+4.3051	-2.4300
			+3.7656	-0.0833		+5.3051	-0.4974
101.8233	84.8528	+0.3468	-3.6732	-2.6299	+0.4667	+5.4067	-3.2359
			+4.5347	-0.3170		+6.4067	-0.3181
203.6467	169.7056	+0.3416	-5.5308	-4.2149	+0.4783	+8.0243	-5.1508
			+6.3598	-0.0088		+9.0243	-0.0062
354.5583	212.1320	+0.3408	-6.2071	-4.9974	+0.4825	+9.0725	-5.5289
			+7.0881	-1.1527		+10.0725	-1.1834
552.9687	294.1406	+0.3395	-7.4336	-6.1473	+0.4866	+10.8203	-7.2391
			+8.3107	-1.3671		+11.8203	-1.4409
480.4206	400.3580	+0.3371	-8.7600	-7.4308	+0.4900	+12.7679	-8.6886
			+9.6579	-2.0297		+13.7679	-2.7281

d/t	d/T	Maxima in Cylinder			Location of Maxima in Cylinder		
		Shear $I_{\theta m}$	Axial $I_{\theta m}$	Circum. $I_{\theta m}$	Shear x_1/d	Axial x_2/d	Circum. x_3/d
10.1823	8.4853	-0.0256	+0.7811	+1.0604	0.4146	0.2792	0.4640
			+0.2199	+0.9820			
25.4558	21.2132	-0.0258	-0.9358	+1.0944	0.2166	0.1850	0.3019
			+0.0602	+0.9719			
58.1222	58.1018	-0.0269	-1.2673	+1.1647	0.1645	0.1128	0.1834
			-0.2673	+0.9510			
101.8233	84.8528	-0.0275	-1.4463	+1.2332	0.1360	0.0832	0.1517
			-0.4463	+0.9386			
203.6467	169.7056	-0.0284	-1.8827	+1.2968	0.0959	0.0636	0.1070
			-0.8827	+0.9116			
354.5583	212.1320	-0.0286	-2.3856	+1.3349	0.0857	0.0586	0.0896
			-1.0690	+0.9093			
552.9687	294.1406	-0.0290	-2.7587	+1.3990	0.0737	0.0497	0.0811
			-1.3587	+0.8812			
480.4206	400.3580	-0.0293	-3.6801	+1.4702	0.0623	0.0425	0.0804
			-1.6801	+0.9630			

* Correction to Table 21. For d/t of 254.5583, under Cylinder at Junction, $I_{\theta j}$ of 5.5289 should be 5.9289.TABLE 22 STRESS INDEXES IN A CYLINDRICAL PRESSURE VESSEL WITH CONICAL HEAD, $\alpha = 60$ DEG, $T/t = 1.6$

(Upper values refer to stress at external surface; lower values refer to stress at internal surface. + = tension; - = compression.)

d/t	d/T	Cone at Junction			Cylinder at Junction		
		Shear $I_{\theta j}$	Axial $I_{\theta j}$	Circum. $I_{\theta j}$	Shear $I_{\theta j}$	Axial $I_{\theta j}$	Circum. $I_{\theta j}$
13.9764	8.4853	+0.3308	-0.3878	-0.0396	+0.4601	+1.3634	-0.3448
			+0.9991	-0.2773		+2.3634	-0.7126
33.9411	21.2132	+0.2773	-0.8994	-0.5332	+0.4117	+2.5628	-1.1339
			+1.5091	-0.0120		+3.5628	-0.7158
92.9630	58.1018	+0.2517	-1.6238	-1.9769	+0.4297	+4.8652	-2.8500
			+2.4461	-0.5872		+5.8652	-0.8281
125.7644	84.8528	+0.2700	-2.5069	-2.1653	+0.4350	+6.5070	-2.4607
			+2.9334	-0.8533		+7.5070	-0.9638
271.5389	169.7056	+0.2678	-3.4804	-3.5658	+0.4427	+10.1675	-5.4161
			+4.0824	-1.5748		+10.1675	-0.3844
339.4111	212.1320	+0.2670	-5.9234	-4.1199	+0.4445	+12.3452	-6.3594
			+4.5587	-1.8708		+11.3544	-0.3073
470.6249	294.1406	+0.2682	-4.7001	-5.1000	+0.4471	+12.3452	-7.5334
			+5.3553	-2.2683		+12.3452	-0.1737

d/t	d/T	Maxima in Cylinder			Location of Maxima in Cylinder		
		Shear $I_{\theta m}$	Axial $I_{\theta m}$	Circum. $I_{\theta m}$	Shear x_1/d	Axial x_2/d	Circum. x_3/d
13.9764	8.4853	-0.0247	+0.8106	+1.0667	0.3647	0.2474	0.4074
			+0.1895	+0.9802			
33.9411	21.2132	-0.0237	-0.9708	+1.1011	0.2383	0.1641	0.2853
			+0.0291	+0.9699			
92.9630	58.1018	-0.0241	-1.2837	+1.1704	0.1496	0.1008	0.1620
			-0.2897	+0.9483			
125.7644	84.8528	-0.0244	-1.4884	+1.2079	0.1207	0.0828	0.1342
			-0.4884	+0.9381			
271.5389	169.7056	-0.0247	-1.8917	+1.2988	0.0854	0.0582	0.0950
			-0.8917	+0.9110			
339.4111	212.1320	-0.0248	-2.0831	+1.3356	0.0764	0.0529	0.0849
			-1.0831	+0.9001			
470.6249	294.1406	-0.0250	-2.3517	+1.3973	0.0648	0.0449	0.0721
			-1.3517	+0.8816			

TABLE 23 STRESS INDEXES IN A CYLINDRICAL PRESSURE VESSEL WITH CONICAL HEAD, $\alpha = 60$ DEG, $T/t = 2.0$

(Upper values refer to stress at external surface; lower values refer to stress at internal surface. + = tension; - = compression.)

d/t	d/T	Cone at Junction			Cylinder at Junction		
		Shear $I_{\theta j}$	Axial $I_{\theta j}$	Circum. $I_{\theta j}$	Shear $I_{\theta j}$	Axial $I_{\theta j}$	Circum. $I_{\theta j}$
16.9706	8.4853	+0.2380	-0.2480	-0.0182	+0.3271	+1.4210	-0.4481
			+0.7195	-0.1226		+2.4210	-0.7106
42.4284	21.2132	+0.2379	-0.5620	-0.4469	+0.3073	+3.7752	-1.2376
			+1.0607	-0.2310		+3.7752	-0.7276
116.2037	58.1018	+0.2358	-1.1909	-1.7728	+0.3963	+5.2213	-2.7436
			+1.6996	-0.8421		+6.2213	-0.6873
169.7055	84.8528	+0.2349	-1.5099	-1.8826	+0.3994	+6.9008	-3.5499
			+1.9008	-1.1728		+7.9008	-0.6506
339.4111	169.7056	+0.2329	-2.2718	-2.1281	+0.4035	+9.5532	-5.4070
			+2.7549	-1.9712		+10.5532	-0.6799
424.2839	212.1320	+0.2326	-2.5778	-2.6301	+0.4045	+10.7785	-6.2682
			+3.0614	-2.2943		+11.7785	-0.4986

d/t	d/T	Maxima in Cylinder			Location of Maxima in Cylinder		
		Shear $I_{\theta m}$	Axial $I_{\theta m}$	Circum. $I_{\theta m}$	Shear x_1/d	Axial x_2/d	Circum. x_3/d
16.9706	8.4853	-0.0258	+0.8215	+1.0712	0.3390	0.2322	0.3663
			+0.1685	+0.9788			
42.4284	21.2132	-0.0221	-0.9911	+1.1054	0.2146	0.1777	0.2382
			+0.0689	+0.9886			
116.2037	58.1018	-0.0230	-1.3083	+1.1735	0.1311	0.0810	0.1497
			-0.3083	+0.9483			
169.7055	84.8528	-0.0220	-1.4790	+1.2102	0.1088	0.0706	0.1209
			-0.4780	+0.9374			
339.4111	169.7056	-0.0221	-1.7821	+1.2989	0.0771	0.0538	0.0854
			-0.7821	+0.9110			
424.2839	212.1320	-0.0222	-2.0991	+1.3247	0.0690	0.0480	0.0786
			-1.0991	+0.9003			

$$\delta = -\frac{1}{2\beta^2 D} (\beta M_0 + Q_0) - \frac{pd^2}{8Et} (2 - \mu)$$

$$\delta' = -\frac{1}{2\beta^2 D} (2\beta M_0 + Q_0)$$

These equations may be rearranged⁷ to

$$\frac{ET\delta}{pd^2} = \left[-\frac{m^2}{2} \frac{d}{t} \frac{M_0}{pd^2} - \frac{m}{2} \sqrt{\frac{d}{t}} \frac{Q_0}{pd} + \left(\frac{2-\mu}{8} \right) \right] \frac{T}{t}$$

$$\frac{ET\delta'}{m^2 pd^2} = - \left[m \sqrt{\frac{d}{t}} \frac{M_0}{pd^2} + \frac{1}{2} \frac{Q_0}{pd} \right] \left(\frac{T}{t} \right)^2$$

Comparing with Equations [1] and [2]

$$a_4 = -\frac{m^2}{2} \frac{d}{t} \frac{T}{t} \quad b_4 = -m \sqrt{\frac{d}{t}} \left(\frac{T}{t} \right)^2$$

$$a_5 = -\frac{m}{2} \frac{T}{t} \sqrt{\frac{d}{t}} \quad b_5 = -\frac{1}{2} \left(\frac{T}{t} \right)^2$$

$$a_6 = \left(\frac{2-\mu}{8} \right) \frac{T}{t} \quad b_6 = 0$$

INFLUENCE NUMBERS FOR THE CONICAL HEAD

Influence numbers for the conical head are determined by a procedure identical to that just illustrated. The final results are

$$a_1 = \frac{b_1 \xi_0^3 \tan \alpha \sin \alpha}{2}$$

$$a_2 = \frac{\xi_0^3 B}{4} - \mu^2 G \sin \alpha$$

$$a_3 = \frac{2-\mu}{8} \sec \alpha - \frac{a_1}{4} \tan \alpha + \frac{3b_1(1+\mu)}{8\xi_0^3} \sec \alpha$$

$$b_1 = \frac{2G}{C+2\mu G} \frac{\xi_0^3 \tan \alpha}{4}$$

$$b_2 = \frac{A/2}{C+2\mu G}$$

$$b_3 = \frac{6(1+\mu)}{\xi_0^4} b_1 \csc^2 \alpha - \frac{b_1 \tan \alpha}{4} - \frac{3 \sec \alpha \csc \alpha}{2 \xi_0^3}$$

where

$$A = \xi_0 (ber_1' \xi_0 ber_2 \xi_0 - bei_1' \xi_0 ber_2 \xi_0)$$

$$B = (ber_1' \xi_0)^2 + (bei_1' \xi_0)^2$$

$$C = \xi_0 (ber_2 \xi_0 ber_1' \xi_0 + bei_2 \xi_0 bei_1' \xi_0)$$

$$G = (ber_2 \xi_0)^2 + (bei_2 \xi_0)^2$$

The formulas for the *ber* and *bei* functions are given by N. W. MacLachlan.⁸ Asymptotic expressions for these functions and their derivatives are accurate to four or more significant figures whenever ξ_0 exceeds 8.

The calculations are based on the relations

$$ber_2 \xi_0 = M_0 \cos \theta_0 \quad bei_2 \xi_0 = M_0 \sin \theta_0$$

$$ber_1 \xi_0 = M_1 \cos \theta_1 \quad bei_1 \xi_0 = M_1 \sin \theta_1$$

⁷ The sign of quantities δ , M_0 , Q_0 are changed, β is replaced by m/\sqrt{dt} , D by Et^3/m^2 , h by t , a by $d/2$.

⁸ "Bessel Functions for Engineers," by N. W. MacLachlan, Oxford University Press, London, England, 1934.

The asymptotic formulas for M_0 , M_1 , θ_0 , θ_1 are given by MacLachlan.⁹ The functions *ber*, ξ_0 and *bei*, ξ_0 and their derivatives can be found from the same reference.¹⁰

The exponential factor common to the asymptotic expressions for M_0 and M_1 can be omitted in the calculations because the quantities A , B , C , and G appear only as ratios in the definitions of a_1 , b_1 , and b_2 .

MAXIMUM STRESSES IN CYLINDER

The ordinary theory of maxima and minima can be applied to determine the maximum stress index (of any type) in the cylinder away from the junction. The expressions of Table I imply that the location and magnitude of the shear-stress index and axial-stress index are determined by the value of the shear-stress index at the junction and by the ratio $\lambda = \beta M_0/Q_0$. The remark also applies to the circumferential-stress index. This index is omitted from Table I because its complete specification has many possible forms depending upon the sign and magnitude of both Q_0 and M_0 .¹¹

MAXIMUM STRESSES IN CONICAL HEAD

Analogous to the maximum stresses in the cylinder, there are maximum stresses in the conical head away from the junction. These could be determined by further computations. However, in contrast to the cylinder, it is not possible to establish simple expressions for the three stress indexes since it is quite tedious to compute the values of ξ which establish the location of these indexes.

Discussion

H. C. BOARDMAN.¹² This paper is just what it purports to be, namely, an analysis based on the theory of elasticity, giving the reader a clear mental picture of the elastic behavior of the cylinder-cone junction regions of originally ideal, isotropic, stress-free, and seamless pressure vessels, each consisting of a perfect cylindrical shell and two perfect conical heads directly joined thereto. This analysis indicates that for many—perhaps for most—commercial pressure vessels, each made of one cylinder and two conical heads, the elastic action covered by the paper occurs only during the first part of the ordinary hydrostatic test to $1\frac{1}{2}$ times the design pressure, and is followed in the later stages of the test by some plastic deformation which gives the cylinder-head region a new form and sets up a system of residual stresses such that the subsequent behavior of the vessel in service, although wholly elastic, is not calculable from the theory of elasticity because the vessel shape and the pattern and intensity of the locked-up stresses are unknown.

For example, the sample problem presented by the authors records computed stresses varying from 107,000 psi to 163,000 psi depending upon the T/t ratio, and explains them by stating that "the magnitude of these stresses indicates, of course, that some yielding and stress relief has occurred in the neighborhood of the junction between the body and head." From one point of view the term "stress relief" is a misnomer in this case since it implies that the calculated stress intensities were reached and then reduced; actually, plastic deformation prevents stresses of the calculated intensities and leaves residual stresses when the test pressure is reduced to zero.

⁹ See footnote 8, equations [59] to [62], p. 133.

¹⁰ See footnote 8, equations [159] and [160], p. 168, equations [15] to [19], p. 158.

¹¹ Details of the results and procedure can be obtained from the second author.³

¹² Director of Research, Chicago Bridge and Iron Company, Chicago, Ill. Mem. ASME.

The sample problem and the foregoing quoted comment thereon constitute an acknowledgment by the authors that the theory of elasticity is unable to solve fully the basic problem of the cylinder-cone junction. If, perforce, wholly fictitious and really impossible calculated stresses must be involved as one link in a chain leading to the solution of this problem, then, eventually, they must in some usable way be related to the actual change of shape and residual-stress system and evaluated in terms of service performance and safety.

The writer has a growing conviction that the Pressure Vessel Research Committee (PVRC) of the Welding Research Council should and must assume the task of and responsibility for interpreting such papers as the authors' in terms which will throw light on the major job of deciding how to arrive at safe but economical designs, taking into account the plastic deformation occurring during the hydrostatic test and the residual-stress system established thereby. This, the writer believes, is what the financial sponsors of the PVRC want, not only with reference to conical heads, without knuckles and compression rings, with compression rings but without knuckles, and with knuckles without compression rings; but also with reference to the shallower torispherical and ellipsoidal heads.

The authors have done a splendid analytical job and their paper in conjunction with others of its kind and the results of the work of the PVRC Design Division at Purdue University, provides a foundation upon which, by an exercise of combined experience, experiment, analysis, and judgment, the PVRC must, if it attains its avowed objective, reach specific workable conclusions which, in effect, will confirm the ASME Code rules of design as they are, or recommend revisions thereof, or advocate entirely new rules.

The authors deserve commendation for preparing a very thought-provoking paper. Following are some of the questions which it raises in the writer's mind:

1 Are not conclusions 1 and 2 self-evident? It appears axiomatic that a cylinder under internal gas pressure expands; that the base of a cone suspended on a vertical canvas cylinder and under internal gas pressure contracts since the canvas cannot resist the components perpendicular to the axis, of the along-the-element stresses; and that the tendency of the cylinder to expand and of the cone base to contract must cause discontinuities at their junction.

2 Are localized working stresses of high intensity just as dangerous to the vessel as general stresses of the same intensity would be? Put in another way, would a streamlined vessel with a general working stress intensity equal to the localized working stress intensity of a conventional vessel (such as that of the sample problem) be just as safe as the latter?

If the answer is "yes," then industry should simultaneously streamline its pressure vessels and raise the design stress, thus promoting both safety and economy in materials.

3 What is the optimum test pressure in terms of the working pressure and nominal working stress? Otherwise expressed, what test pressure will establish the optimum residual stresses and how can it be determined?

4 Should there be any design limit, short of that which will produce buckling, on the ring compressive stress at a cylinder-cone junction? Put in another way, are all of the stress factors of Table 3 of equal significance? Should they all be held to the same numerical value?

5 The authors state, "Where it is not possible to have the thickness the same in both cone and cylinder, it is more desirable to make the cone thicker." Under what conditions would it be "not possible" to have the cone and cylinder the same thickness?

Do the words "not possible" imply an excessive ring stress in the cone when the apex angle is large?

6 How does a weld at the cylinder-cone junction affect the strains and stresses in the junction regions?

Such queries haunt and hound the thoughtful reader of this paper; perhaps its greatest value lies in this fact.

AUTHORS' CLOSURE

The authors wish to thank Mr. Boardman for his careful and thought-provoking review of the paper. They wish to offer a number of comments in answer to his points.

Mr. Boardman's first paragraph indicates that plastic flow will probably occur at some points of a pressure vessel during the hydrostatic test but that the subsequent behavior in service will be wholly elastic. Since the volume of material involved in plastic flow may be extremely small, it seems entirely possible that some plastic deformation may occur each time the vessel is loaded or unloaded due to elastic stress in the other parts of the vessel. Such a wringing action could eventually result in a crack. Thus the high stresses indicated by elastic analysis are valuable since they point out locations where trouble may be expected.

In locations where it is possible for plastic flow to occur, the maximum stress will be limited to the flow stress and the high peaks indicated by elastic analysis will be redistributed by increasing the stress to the flow value at nearby points. The authors agree that the term "stress relief" for this effect is a misnomer and "stress redistribution" might be preferable.

Continuing his discussion, Mr. Boardman points out that because of the plastic flow which intervenes at points of stress concentration, the results of elastic analysis must be "evaluated" or "interpreted" before being applied to practical vessels. The authors believe that this is an oversimplified view of the situation. Having made an elastic analysis, as in this paper, it then becomes necessary to analyze those small areas of the vessel where plastic flow is indicated. To compute the plastic stresses and strains in such areas is another problem of considerable difficulty in itself. Although these phases of the over-all design problem are only beginning to be investigated by rational methods it will be necessary to have such solutions before conclusions on the safety of practical vessels can be drawn.

Mr. Boardman concluded by asking six questions. The authors' comments on these are as follows:

1 The "obvious" conclusions 1 and 2 were drawn to call attention to a basic defect in any design having sharp corners. It has been shown that severe stress concentrations are set up at such points. In many practical cases plastic flow permits a vessel to resist the loads without damage. However, there are also circumstances where plastic flow is impossible so that such a design is unsafe. Two examples may be mentioned: (a) Ordinary structural steel at low temperatures; (b) low-alloy steels which have a high yield point obtained at the expense of reduced ductility.

2 The authors believe that a design with stresses of high intensity throughout the vessel would be much more likely to fail than one where high stresses are confined to small areas. The following comments may be made: (a) When the high stress is localized, the surrounding elastic region exerts restraint on the region of high stress and makes the vessel stronger than if the high stress were general. (b) If a single local crack developed in either case, the localized stress is safer because the surrounding elastic region has, at least potentially, strain energy available up to rupture to absorb the energy released by the crack. (c) A general high stress is likely to produce cracks at some weak point of a structure. On grounds of probability a localized high stress may not occur at a weak point.

3 The answer to this question requires analysis of the plastic regions as discussed above. Both the elastic and plastic analyses are essential for a complete solution to these problems. The elastic analysis is needed to define the areas where plastic flow may occur. If residual stresses are set up by plastic flow, the elastic analysis is still needed to compute the total stress at a point during cycles of loading and unloading. It seems obvious that approximate elastic theories would be of little use since precise values of stress at all points must be known if a combined elastic and plastic case is to be correctly analyzed.

4 The authors agree that, in general, the significance of positive and negative stresses will be different. The importance of ring compressive stresses was emphasized in the recent paper by Messrs. Wilkin and Wetterstrom.¹³

¹³ "Lateral Buckling of Circular Stiffening Rings in Compression," by L. A. Wilkin and Edwin Wetterstrom. Presented at the Annual Meeting of THE AMERICAN SOCIETY OF MECHANICAL ENGINEERS, Atlantic City, N. J., Nov 25-30, 1951.

It is mainly in recent years that rational methods have been applied in studying the flow of metals under biaxial or triaxial stresses. Considerable progress has been made on problems of forming, drawing, rolling, etc., but much less attention has been given to the conditions under which failure of the material will occur. This is certainly an area where future research work should make a concentrated attack.

5 The authors had in mind the occasional assembly of small vessels from salvaged components, as might be necessary for emergency repairs or experimental work. It is also conceivable that it might be necessary to use a thicker head to provide sufficient metal for reinforcement around openings which might be necessary after the vessel is erected and which might be difficult to otherwise reinforce.

6 A large amount of current research is devoted to welding. Several years will probably elapse before firm conclusions can be drawn regarding the behavior of welds under structural loads.

Recommended Practices for the Cleaning of Turbine Lubricating Systems After Service

Section I on Oil Systems of Turbines of Technical Committee C of ASTM Committee D-2 on Petroleum Products and Lubricants sponsored the paper on "Recommended Practices for the Cleaning of Turbine Lubricating Systems Before Service" presented at the 1947 ASME Annual Meeting (ASME Trans. 1948, vol. 70, pp. 363-367). In 1950 it was agreed that Section I of Technical Committee C of ASTM Committee D-2 would function as a Joint ASTM-ASME Committee on Turbine Lubrication. The Joint Committee sponsored the paper on "Recommended Practices for the Cleaning of Turbine Lubricating Systems After Service" presented at the 1950 ASME Annual Meeting. Appendix I to this paper, prepared in March, 1951, by the Joint Committee, covers "Recommended Practice for the Purification of Turbine Oils."

IT SHOULD be emphasized that the procedure for cleaning lubricating systems of turbines after service should be accomplished through the co-operative efforts of the turbine builder, the operator, and the oil supplier. No phase of this work should be undertaken without a thorough understanding of the possible effects on subsequent operation of the unit, nor should it be entrusted to persons lacking in experience without adequate supervision.

WHY CLEANING MAY BE NECESSARY

Trouble-free operation of steam turbines depends to a large extent upon the cleanliness of the lubricating-oil system. After use, there may accumulate in such systems deposits as a result of contamination by impurities such as dust, dirt, lint, pulverized coal, fly ash, rust, welding beads, scale, water, emulsions, insoluble oil degradation products, and combinations of these. In addition, there is always the possibility of other materials in the surrounding atmosphere getting into the oil system such as cement dust, chemicals, and so forth, as well as the possibility of other foreign materials such as rustproof or pipe-thread compounds, gasket or lagging materials, or cutting oil being left in the system after repairs or changes are made. These foreign materials may cause clogging of the oil lines with resultant bearing damage or failures, fouling of governors, deposit on coolers, and the like. In addition, they may cause foaming, emulsification of the oil with water, and accelerate oil degradation. Blistering or flaking of permanent-type protective coatings in tanks may occur, and the loosened material may clog the lubricating system. It should be emphasized that mere draining of the oil from the system may remove only a small portion of the deposits described in the foregoing.

Adequate oil purification during circulation, through the use of oil-purifying equipment of proper size and design, will go far to prevent build-up of insoluble foreign matter in the system. Periodic inspections of the lubricating system will indicate

Contributed by the Joint ASTM-ASME Committee on Turbine Lubrication in co-operation with the Petroleum, Power, and Production Engineering Divisions and presented at the Annual Meeting, November 26-December 1, 1950, New York, N. Y., of THE AMERICAN SOCIETY OF MECHANICAL ENGINEERS.

NOTE: Statements and opinions advanced in papers are to be understood as individual expressions of their authors and not those of the Society. Manuscript received at ASME Headquarters October 30, 1950.

whether proper maintenance practices are being followed and should be supplemented by other inspections when serious variations in operating data are observed. The following recommended practices cover normal procedures for checking on the extent of accumulation of deposits and for removing them from the system.

WHEN CLEANING MAY BE NECESSARY

Turbine manufacturers usually recommend that within the first year of operation, a new turbine be taken down for complete general inspection. This offers an excellent opportunity also for inspecting the oil system for evidences of deposits, corrosion, and abnormal wear.

When a turbine is placed in service, a close watch should be kept until operating conditions have stabilized. By this means, normal oil outlet and inlet temperatures to bearings, coolers, and other parts can be established. It is common practice to keep as a part of the log the temperature differentials across bearings and coolers. When this temperature differential at the coolers departs from the established norm, deposits may be accumulating on either the oil or water side of the cooler. It is also common practice to take frequent samples of the oil for visual inspection for the presence of water, emulsions, or suspended matter. Laboratory tests made upon periodic samples will indicate whether any significant change in the oil is occurring which might lead to the accumulation of deposits. Frequent inspections of the oil-sump drain, and of the oil-purifying equipment also will help to indicate the rate of deposit accumulation.

Any unusual conditions noted (increase in rate of deposit removal by the oil-purifying equipment, departure from normal oil pressure at any point in the system or oil-purifying equipment, presence of water in the oil, change in temperature differential, change in oil tests) will be a warning that some abnormal condition is present in the turbine system. Through inspection, the source of the difficulty must be determined and any deposits which have accumulated must be removed. It is, of course, desirable to eliminate the causes as soon as possible, to hold formation of deposits to a minimum, and possibly avoid necessity for extensive cleaning of the lubricating system.

CLEANING OF TURBINE SYSTEMS

Inspection of the turbine-lubricating system may show deposits ranging from a viscous oil film to solids which completely choke oil passages. When an appreciable quantity of deposit is found in a turbine system, it must be removed. The method of cleaning will depend, of course, on the amount and the nature of the insoluble material present. Laboratory examination of a representative sample of the deposit will assist in determining the best means of removal. Obviously, it is impractical to make any all-inclusive statement on what should be considered an appreciable amount of deposit; only experience will serve as a guide to the evaluation of conditions.

Final decision as to the means of removing the insoluble material should be reached only after consultation with all parties concerned, including the turbine manufacturer and oil supplier.

OIL COOLERS—STATIONARY AND MARINE

A marked change in the oil temperature differential across the cooler with no change in water flow or water temperature may

indicate an excessive build-up of deposits on the oil or water side of the cooler, or of both. On larger units, twin coolers are usually installed so that one of them can be removed from service for cleaning without interruption of turbine operation. Where the cooler tube bundle can be removed from the system, cleaning methods may be employed which would not be considered practical for the turbine lubricating system proper. Hot water or steam washing, or petroleum flushing oil usually are employed for cleaning the oil side of the coolers.

If other cleaning agents are employed, they should be used only with full appreciation of the following:

Regardless of the materials used, all traces of the cleaner should be removed thoroughly to prevent subsequent oil contamination. The cleaner employed should not attack the finish of the tubes, since such attack may lead to the formation of metallic soaps which can stabilize oil-water emulsions. In addition, cases have been reported where cleaners have activated cooler tube surfaces making them extremely effective catalysts for turbine-oil oxidation. After cleaning, hydrostatic tests should be made on coolers to check for leaks.

OIL SYSTEMS OF STATIONARY UNITS

The following methods have been used with success for the cleaning of stationary units of varying sizes. The particular method selected will depend to a large extent upon laboratory examination of the deposit and cleaning materials, facilities and time available. Regardless of the method selected, when appreciable quantities of deposit are present and accessible, the bulk of the deposit, of course, should be removed manually.

STEAM AND HOT-WATER CLEANING—STATIONARY UNITS

Tarry matter from oil-degradation products and oil-water emulsions often can be removed from turbine parts by steam or hot-water washing. Individual cleaning of parts is desirable when using these methods. Care must be taken not to blow steam or hot water into bearings or governor mechanisms which usually are cleaned manually. Steam is preferable to hot water owing to the possibility of scalding.

When using hot water, boiler feedwater at a temperature above 180 F usually is employed and is blown through the piping at high velocity. If the piping can be dismantled, this may be done to insure more thorough cleaning. Bearing pedestals and oil reservoirs are cleaned by directing a stream of hot water against the surface of the parts. Clean dry air should be used immediately after the hot water to dry the parts.

Steam at high velocity has been used with good success under a variety of conditions. A flexible steam hose is used with the end covered with a cap tapped for the insertion of a short nipple with an opening approximately $\frac{1}{4}$ in. diam. Pedestals, reservoirs, and pipe are steamed out and dried with clean dry compressed air.

Since steam or hot-water washing will remove protective oil films from metal surfaces making them prone to rusting, the lubricating system should be protected as quickly as possible with a rust-inhibited turbine or flushing oil. Governor parts should be dipped in the rust-inhibited oil immediately after cleaning, and the unit should be assembled and a rust-inhibited turbine or flushing oil circulated through it, as soon as possible.

CLEANING WITH FLUSHING OIL—STATIONARY UNITS

The oiling system should be arranged so as to obtain maximum oil flow and velocity. The exact steps to be taken depend entirely upon the turbine construction. In some instances, maximum flow is secured by removing the upper halves of the bearings and any external orifices, if used; or by rolling the lower halves of the bearings about the shaft sufficiently to uncover the

oil-supply passages. The bearing-pedestal covers are then replaced to prevent unnecessary oil leakage. In other cases, maximum oil flow is obtained easily by removing the internal connection pieces between the oil-supply-line and each bearing. The connection pieces are within the bearing housings and are accessible by removing inspection-opening covers placed there for that purpose.

A sufficient charge for flushing (50-75 per cent normal oil charge) of rust-inhibited turbine or flushing oil is then placed in the turbine. The oil is heated in any convenient manner to between 150 and 180 F, and maintained at this temperature while being circulated by the turbine auxiliary oil pump for from 4 to 24 hr or more, depending on the size of the turbine, or nature and amount of deposits. The oil may be heated by passing hot water through the water section of the cooler or by installing a temporary low-pressure (5 psi maximum) steam coil in the oil reservoir. Venting devices and continuous by-pass oil purifiers, available as part of the oiling system, should remain in operation during the entire flushing period.

Oil piping, passages and parts in the governing system which come in contact with oil need to be cleaned. This should be done without danger of scoring the working parts of the governing mechanisms. During the flushing operation the pilot valves can be removed and the pistons either removed or blocked in their open position.

In some instances the high-pressure oil passages to the governor and their control mechanisms are blanked off during the early stages of flushing so as to have relatively clean oil for flushing the governor system. Toward the end of the flushing period, the blanks should be removed so the flushing oil can clean the oil piping and passages of the governing system.

After flushing, the governor parts, passages, and so forth should be cleaned manually with lintless cloths.

A clue to the required duration of flushing may be obtained from a periodic check of the strainers and other oil-purifying equipment. When successive inspections reveal no noticeable increase in deposits, it is reasonably certain that all contaminants have been removed from the system. Clean lintless cloth bags are often placed inside the strainers, their appearance during flushing giving a ready check on the progress of cleaning.

As soon as the flushing is completed, the oil should be drained from the tanks, coolers, and oil-purifying equipment while they are still hot, but venting should continue until the system returns approximately to room temperature. This will assure more complete drainage, as well as the removal of any impurities that may be oil-soluble at flushing temperatures, and will minimize condensation that could cause rusting. All low spots that could serve as traps must be drained and the accessible parts of the lubrication system inspected as thoroughly as possible, any remaining deposits being removed manually with lint-free cloths.

Then bearings and piping may be returned to their original locations, and assembly of the turbine completed. The turbine is then charged with a supply of clean lubricating oil of the grade to be used for regular operation, and given the customary operational checks accorded every unit before it is placed in regular service. At the conclusion of this step, many operators consider it good practice to make a final investigation of the cleanliness of the oiling system. When conditions permit, the oil may be removed temporarily from the system so that the latter can be given a thorough inspection. If this is impossible, or inadvisable, at least the strainers and oil-purifying equipment should be checked for the presence of excessive or unusual deposits.

CLEANING DURING SERVICE—STATIONARY UNITS

In some instances, where a lightly sludged unit cannot be taken out of service for a sufficient time for thorough cleaning

prior to an oil change, continuous by-pass circulation of the oil in the system, through a clay filter, has been used to remove from the system solids and partially soluble oil degradation products. It should, of course, be appreciated that passing an inhibited oil through clay will remove the inhibitors—hence it is suggested that the oil supplier be consulted before employing this procedure.

Because the unit is in operation when such a process is followed, governor operation and bearing temperatures should be watched carefully, since solid particles may be loosened which would be large enough to restrict oil flow and interfere with operation.

CLEANING MARINE PROPULSION UNITS

It is not practical to use the same methods in cleaning dirty marine units that can be employed for stationary units because of the more extensive piping and the presence of gear sets with their lubricating devices, which make the marine oil system more complicated than those of stationary units. The inaccessibility of the oil piping in marine units makes it impractical to clean by flushing with hot water or steam. The complex oiling systems of marine units may permit greater build-up of deposits in inaccessible locations. For such systems deposits can be removed most effectively by consecutive flushings with a rust-inhibited flushing oil, followed by turbine oil of the grade recommended for regular operation. The following procedure has been used in a number of cases:

The used oil is drained from the system, which is then arranged so as to secure maximum oil flow and velocity to all parts of the assembly. This is done by removing the upper halves of the bearings and any restricting orifices, if used; or, if necessary, by rolling the lower halves of the bearings about the shaft sufficiently to uncover the oil-supply passages. The bearing pedestal covers must be replaced to prevent leakage. At the same time, all tanks and sumps should be cleaned manually to remove as much of the deposits as possible, to avoid unnecessary circulation of such material while the actual flushing operation is under way.

The flushing oil (50 to 75 per cent of normal oil charge) is then placed in the system and heated to a temperature of 150 to 180 F by any of the means suggested previously. This improves the solvency of the oil and expands the piping and other parts, both of which contribute to the removal of the maximum amount of deposits.

During flushing, the dehumidifier system (if used), oil-purifying equipment, and strainers should be kept in continuous operation. Near the end of the flushing operation, the turbine should be rotated by the turning gear a number of revolutions equivalent to about one revolution of the ship's propeller, in order to facilitate complete flushing. In some cases, auxiliary filters, pumps and lines have been employed to assist in the removal of contaminants.

It is recommended that the hot flushing oil be circulated through the system for 2 hr, then stopped for 1 hr; and that this cycle then be repeated two more times. Following this three-cycle schedule, the oil coolers, bearing oil header, and oil strainers should be cleaned, since this will permit later inspection of their condition to serve as an indication of the progress in cleaning. Circulation now should be resumed and continued until the system is clean. This will be determined by inspection each 6 hr of the oil coolers, bearing oil header, and strainers. At more frequent intervals the pressure drop across the strainer should be observed, as a ready clue to the rate at which deposits are accumulating. When deposits no longer accumulate on the inspected parts, the system can be considered clean. Approximately 48 hr over-all is usually sufficient for a thorough cleaning, even under extremely dirty conditions. The use of a lance has

been found effective for washing down interior parts of the gear casing and sides of the gears. Temporary fine-mesh strainers or lintless cloth bags may be inserted in lines during preliminary flushing.

When the system is clean, the flushing oil should be drained immediately while still hot, to promote complete drainage and to prevent oil-soluble contaminants from again becoming insoluble and precipitating out of the oil on the cleaned metal surfaces.

Immediately after draining, new rust-inhibited turbine oil of the grade to be used for regular operation should be put in the system and circulated for about 2 hr for displacement purposes. During this period, either the turbine should be rotated again by the turning gear as already described, or turned continuously by the turning gear during the flushing period. This will establish on all lubricated surfaces a film of the same oil which will be used normally. The turbine oil used for displacement must be drained completely, even from the low pockets that can serve as traps.

During flushing with turbine oil or with flushing oil and the displacement oil, as the case may be, the governing assembly should be cleaned in a similar manner to that recommended for stationary installations. Following the final flushing operation, the governor assembly should be cleaned manually with lintless cloths.

Any flexible-shaft couplings should be inspected carefully for cleanliness.

After completion of flushing, an inspection of tanks, sump, and accessible piping should be made. Remaining oil and deposits should be removed manually with lint-free wiping cloths. All parts previously altered to secure maximum oil flow should be returned to their proper condition, and the system charged with the correct grade of turbine oil.

In exceptionally dirty marine turbine systems, it has been the practice of certain commercial turbine-cleaning companies to employ the use of powerful cleaning agents such as organic solvents or chemical solutions. In some instances certain of these materials are mixed with petroleum flushing oils prior to use. Such materials, while they may not dissolve the deposits, are often used since they will dissolve the materials which act as binders for the other solids such as rust, scale, dirt, and the like. The successful application of such materials requires highly specialized knowledge and equipment and should not be attempted by those not fully aware of the hazards involved. In the past, where suitable precautions have not been followed, serious damage has resulted owing to corrosion of certain component parts of the system or because of the fact that it was impossible to remove completely from the system all of the cleaning agents used or the compounds formed by their use, and these had a serious effect on the performance and life of the equipment and/or the turbine oil subsequently placed in the system.

Appendix

RECOMMENDED PRACTICE FOR PURIFICATION OF TURBINE OILS

In order to insure continuity of operation in the modern turbine station there are always provided duplicate auxiliaries such as pumps, coolers, motors, and even spare boiler and generating capacity. These are purchased and installed to keep the station running so that there will be no unexpected shutdown and the resultant loss of income. An oil-purification system is in this same category in that it is insurance against lubrication failures.

The purpose of an oil-purification system is to keep the oil free from contamination by water, solid materials, and deterioration

products. Such contaminants may interfere with the continuous and satisfactory operation of the turbine and/or shorten the useful life of the oil.

Since it is difficult to determine when contamination is likely to occur and since it is desirable to remove it as quickly as possible, it is recommended that the purification system be operated continuously while the turbine is running. In fact, it also might be advisable to operate the system when the turbine is not in operation, although this is not usually necessary.

In current practice 10 to 20 per cent of the volume of oil in the turbine system is put through the purifying equipment every hour. This applies both to inhibited and noninhibited oils. This practice may be altered up or down as local conditions might indicate as being necessary.

There are four types of turbine-oil purification systems, i.e., gravity separation, centrifugal separation, pressure filtration, and vacuum vaporization. Currently available equipment may employ a single system or may combine two of these systems, the most common combination consisting of a pressure filter plus one of the other systems. The pressure filtration may follow gravity, or centrifugal separation to provide a polishing action, that is, the removal of colloidal particles of fly ash, dust, and so forth, to below 5 microns in size; and to provide for the removal of moisture haze. Pressure filtration may be with inert filtering media for either straight mineral or inhibited oils. Adsorbent earth may be preferred for straight mineral oil.

The purification system usually includes its own pump or pumps for the recirculation of the oil, independent of the turbine circulation system. The purification system should not remove rust or oxidation inhibitors or other additives.

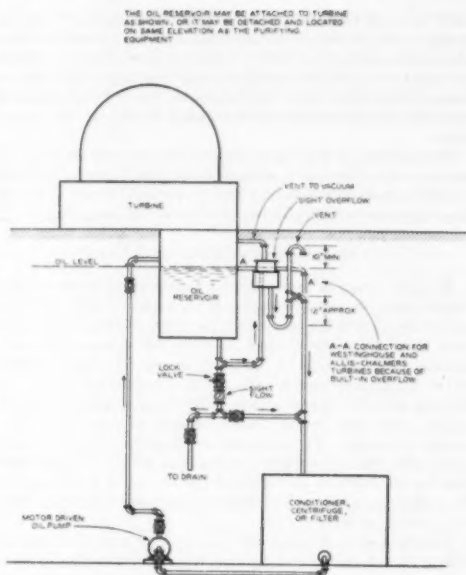
The take-off point at which the oil that is thus by-passed for conditioning should be the lowest part of the turbine oil reservoir. On some turbines a built-in internally vented overflow is provided. On those not so constructed by the turbine manufacturer, an external overflow should be provided to maintain the normal operating level of oil in the turbine. In the case of small turbines where there is no vacuum above the oil in the reservoir, this overflow may be vented to the atmosphere. Where the turbine is equipped with a vapor extractor for maintaining a vacuum above the oil in the turbine reservoir, this external overflow must be vented back into the vacuum.

After passing through the oil-conditioning equipment the re-entry of the clean oil should be at a point in the turbine oil reservoir as remote from the take-off as possible. This re-entry point should be above the normal operating level of the oil in order to prevent flow-back to the filtering equipment, when the turbine is shut down and filtering equipment is below the oil reservoir. As a precautionary measure a check valve also should be placed in this line.

It is considered desirable to install a by-pass with lock valve in the drain line around the overflow from the bottom of the reservoir direct to the purifying equipment. The purpose of this is to remove any water that may possibly have "pocketed" in the reservoir, and preferably should be done when the turbine is not running, or if necessary during operation, suitable (watching) precaution should be taken not to drain any oil.

As several types of oil-purifying or conditioning equipment, such as filters and conditioners, operate on either a low or a high pressure, the level gage or the pressure gage would be the signal for inspecting the filtering or conditioning equipment. In other words, when a predetermined high head or pressure has been reached in the filter or conditioner, or the bowl-cleaning schedule of a centrifugal purifier calls for it, the equipment should be cleaned or filter elements renewed, as called for by the supplier of this equipment.

The factors which affect the life and lubrication qualities of



FLOW DIAGRAM OF TURBINE OIL PURIFICATION

turbine oils are, in general, heat, moisture, contact with some metals, oxidation products, sludge, and solid particles. Effective removal of water, sludge, and solid particles of contamination are important. The oil is often warm enough coming from the turbine oil reservoir for satisfactory conditioning, but sometimes it is necessary to increase the temperature. The heaters used for this purpose should be so designed that spot overheating will not occur. In the case of gravity filters, the oil should not be left in contact with the water that has been separated and all interior parts should be coated with a satisfactory corrosion-preventive sealer.

As in the case of the oil reservoir in the turbine itself, it is also desirable to remove moisture above the oil surfaces in some types of filtering or conditioning equipment by means of a small vapor extractor. If insurance regulations demand it, this blower should exhaust to the outside of the building. Any tanks, special equipment, or piping used in connection with the oil-conditioning system should be cleaned thoroughly by approved methods in such cases where it is not possible to coat them with a sealer as described in the foregoing.

As part of this report the committee at large requested that we include the following excerpts in regard to water washing and clay filters which were endorsed by the committee at its June 24, 1946, meeting as follows:

WATER WASHING

"The committee went on record against water-washing oils containing rust and oxidation inhibitors since experience indicates such practice may cause some reduction in inhibitor content. The only exception to the recommendation might be in the case of contamination of the rust and oxidation-inhibited turbine oil with corrosive materials which are water soluble. The committee sees no objection to water-washing straight mineral turbine oils

if such practice is desirable to remove corrosive materials, oil deterioration products, or potentially corrosive contaminants. It is recommended that, where water washing is employed, the water have a pH of 6.5-8, and a conductivity of 2-5 micromhos."

CLAY FILTERS

"The committee went on record against the use of clay filters

with rust and oxidation-inhibited turbine oils since experience indicates such filters will remove the rust inhibitor and some types of oxidation inhibitor from present-day rust and oxidation-inhibited turbine oils."

Where straight mineral oil is used it is sometimes desirable to remove products of oxidation, corrosive materials, and so forth by the use of clay-type filters.



Line-Reversal Techniques in the Determination of Temperature of Gun Flash or Other Rapid Transient Phenomena¹

By J. T. AGNEW,² LAFAYETTE, IND.

A modification of the conventional line-reversal technique has been utilized for the determination of the temperature of an exploding gas mixture. A monochromator, employing either a photomultiplier or lead-sulphide photoconductive cell as the detector, has been used to isolate characteristic sodium, potassium, and water-vapor radiation at 0.589, 0.77, and 0.942 microns, respectively. Peak temperature values were determined for the external gaseous explosion commonly known as secondary flash, associated with the firing of a gun. Values obtained by reversal of the characteristic radiation just mentioned did not agree even when corrected for the possible error due to the variation in emissivity of the tungsten comparison source. This result was not unexpected and is discussed in terms of the reaction kinetics involved. A general discussion of the significance of temperature of gaseous explosions is also presented. It is believed that techniques such as those presented should be useful in combustion research.

INTRODUCTION

RECENT developments in the field of combustion research have led to the desirability of a technique for the determination of the temperature of the reaction as a function of time. Many of these reactions are of relatively short time duration of the order of 1 millisecond or less. Conventional techniques such as the use of thermocouples, or other temperature-indicating devices having an appreciable mass, have proved inadequate for measurements of this type. The line-reversal method of determining flame temperature, as postulated by Féry (1)³ in 1903, represents a favorable possibility for the determination of the temperature of transient flames. Briefly the theory behind Féry's method is as follows: As seen in Fig. 1, an image of an incandescent filament is focused in the position at which the temperature of a mass of gas is to be determined. The image is in turn focused on the entrance slit of a conventional spectroscope, and the combination spectra produced by the hot incandescent filament and the flame in the optical path are observed in the focal plane of the spectroscope. With no flame present in the optical path, the observed intensity at a particular wave length, usually that of sodium D-line radiation, can be expressed as

$$I_{obs} = CT^4 E_{\lambda,T} \dots \dots \dots [1]$$

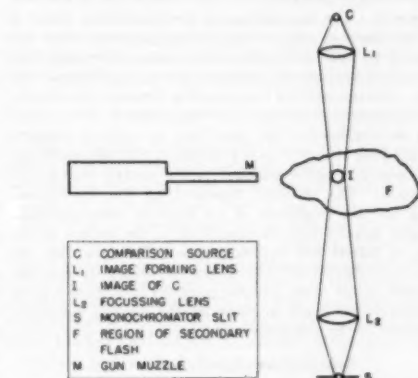


FIG. 1 SCHEMATIC DIAGRAM OF EXPERIMENTAL ARRANGEMENT

where C is a constant depending largely upon the apertures of the instrument, and $E_{\lambda,T}$ is the emissivity of the source (assumed a black body) at the wave length λ , and the temperature T . With a flame containing dispersed sodium atoms (assumed for purpose of discussion to be a steady flame) the observed intensity can be expressed as

$$I_{obs} = CT^4 \left[E_{\lambda,T} (1 - \alpha_{\lambda,T}) + \left(\frac{T'}{T} \right)^4 \epsilon_{\lambda,T} \right] \dots \dots [2]$$

where C and $E_{\lambda,T}$ are the same as before, $\alpha_{\lambda,T}$ is the absorptivity of the sodium flame at wave length λ , and temperature T' , and $\epsilon_{\lambda,T}$ is the corresponding emissivity of the sodium flame. By Kirchhoff's law

$$E_{\lambda,T} = \alpha_{\lambda,T} \dots \dots \dots [3]$$

and since

$$T^4 E_{\lambda,T} = T_a^4 \dots \dots \dots [4]$$

Equation [2] can be written

$$I_{obs} = CT^4 E_{\lambda,T} \left[1 - \alpha_{\lambda,T} \left\{ 1 - \left(\frac{T'}{T_a} \right)^4 \right\} \right] \dots \dots [5]$$

where T_a is the apparent temperature of the image of the source.

We can now consider the three cases for which the flame is either (a) at a higher temperature than, (b) at a lower temperature than, or (c) at the same temperature as the comparison source. For case (a), T' is greater than T_a ; therefore $1 - (T'/T_a)^4$ is negative, and the observed intensity of the sodium D-line radiation will be greater than the intensity of radiation at this frequency from the comparison source, and the sodium lines will appear brighter than the background.

¹ Based on research performed for the Army Ordnance Corps.
² Professor of Mechanical Engineering, Purdue University. Mem. ASME.

³ Numbers in parentheses refer to the Bibliography at the end of the paper.

Contributed by the Heat Transfer Division and presented at the Fall Meeting, Minneapolis, Minn., September 26-28, 1951, of THE AMERICAN SOCIETY OF MECHANICAL ENGINEERS.

NOTE: Statements and opinions advanced in papers are to be understood as individual expressions of their authors and not those of the Society. Manuscript received at ASME Headquarters, June 6, 1951. Paper No. 51-F-6.

For case (b) T' is less than T_a and $1 - (T'/T_a)^4$ is positive. In this case the intensity of the sodium-line radiation will be less than that of the background radiation and the sodium D-lines will appear as dark lines. Absorption is taking place in this case due to the flame being at a lower temperature than the comparison source.

For case (c) $T_a = T'$ and therefore $\left(\frac{T'}{T_a}\right)^4 = 1$. The observed intensity at the sodium D-line frequency will then be the same as if there were no flame present so that the sodium D-lines are indistinguishable from the background. In this case the temperature of the flame is considered to be the same as that of the comparison source. The temperature of the comparison source is usually determined by means of an optical pyrometer which has previously been calibrated with a black-body source and some other secondary temperature standard, such as a calibrated thermocouple. The operation of the pyrometer depends upon matching the brightness of the comparison source used in these experiments to the brightness of the black body at a known temperature. A red filter is used in most pyrometers with the result that the brightness is actually matched in the spectral region near 0.665 micron. The quantity measured by the line-reversal method is also the brightness of the flame at some particular wave length, usually that corresponding to the sodium D-line radiation at 0.5890 and 0.5896 micron. The fact that the pyrometer is calibrated at 0.665 micron and the line-reversal determinations are at other spectral positions is discussed later, and corrections are made to allow for the spectral emissivity characteristics of the comparison source.

STEADY FLAME APPLICATIONS

In steady flame applications of the method, the detector utilized is the human eye which, of course, has a limited frequency response which is not rapid enough for determinations of transient phenomena such as described in this paper. In the present application, two types of detectors were used, depending upon the spectral region in which the determinations were made. For observations of the reversal of the sodium-line radiation, a 1P21 photomultiplier tube was used, and for observations of reversal of potassium-line radiation near 0.77 micron and the water-vapor band at 0.942 micron, a lead-sulphide photoconductive cell was used. The experimental setup for the rapid temperature determinations, which will be discussed, was essentially the same as is conventionally used in steady-state line-reversal experiments, with the exception that an exit slit was used to isolate the particular spectral range being observed, and the detectors just mentioned were used in place of the human eye. The signals generated by the detectors were amplified through conventional electronic amplifiers and presented by a single sweep arrangement on an oscilloscope screen. The resulting trace was photographed as a simple time exposure with a 35-mm camera.

The data presented in this paper are relative to a particular transient flame which is developed by the firing of a gun and is usually referred to as secondary flash. The muzzle gases which are released as the projectile leaves the barrel contain a large percentage of two principal combustibles, carbon monoxide and hydrogen. The burning process which is in progress inside the barrel up to the time of projectile emergence, is extinguished as the muzzle gases expand by a practically adiabatic process. However, the mixing of atmospheric oxygen with the muzzle gases produces a combustible mixture which can be ignited, and the result is a secondary explosion which is initiated some distance ahead of the muzzle of the gun. As shown in Fig. 1, the image of the comparison source is focused some distance ahead of the muzzle at a position where it has been determined previously

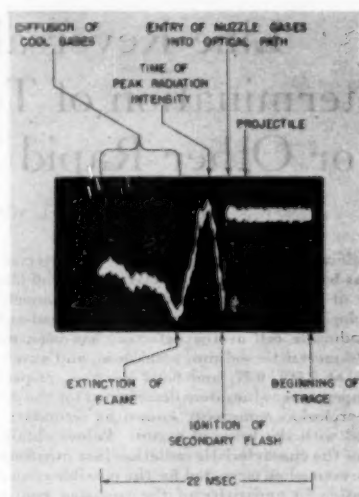


Fig. 2 SEQUENCE OF EVENTS ON TYPICAL OSCILLOSCOPE TRACE

that ignition of this secondary explosion is likely to occur.

Fig. 2 is a typical oscilloscope trace produced by the absorption of the sodium-line radiation which has occurred during the time of the secondary explosion. All subsequent traces will have this same general appearance so that a description of the events shown in Fig. 2 will serve as an introduction to the type of information which has been obtained. The beginning of the trace corresponds to the instant at which the firing pin makes contact with the primer. A time scale is indicated progressing from right to left, and the first event recorded is the passage of the projectile through the optical path. This results in an absorption of radiation from the comparison source which has been energized previously and its temperature determined by means of the optical pyrometer. Approximately 2 millisecond later the muzzle gases which have emerged from the barrel and have cooled adiabatically due to the sudden expansion, enter the region intercepted by the optical path. Since they are at that time much cooler than the comparison source, absorption of the radiation from the comparison source by the cold sodium atoms present as impurities in the muzzle gases results in a downward deflection of the oscilloscope trace.

Ignition of the secondary explosion then occurs, a flame is established, and its temperature begins to increase. A maximum temperature is reached approximately 4 millisecond after projectile emergence, following which the temperature of the flame decreases, reaching a minimum in about 4 millisecond after the maximum. The cold sodium atoms present in the optical path are then dispersed, and the trace gradually rises back to the original level corresponding to no absorption. Thus we have represented in the entire trace a somewhat more complicated series of events than is ordinarily encountered with steady-state applications of the line-reversal technique.

Initially, it was intended to obtain an indication of the peak temperature of the secondary-flash reaction according to the following reasoning: The initial absorption process is due to the fact that the comparison source is at a temperature considerably higher than the temperature of the cooled muzzle gases which

initially enter the optical path. The subsequent rise in temperature due to the secondary-explosion results in the peak emission being at a level near the original base line. The peak of the emission curve would be on an extension of the original base line if the peak temperature generated by the secondary flash were just that of the comparison source. If the peak flash temperature were higher than that of the comparison source, the trace would rise above the initial base line, and, if the peak flash temperature were below that of the comparison source, the maximum would be below the initial base line. Traces of this type will be discussed later in connection with Figs. 4, 5, and 6.

Fig. 3 is a plot of the relationship between the current passing through the incandescent tungsten filament being used as a comparison source, and the temperature of this source as indicated by a Leeds & Northrup optical pyrometer. Actually, the temperature indicated in Fig. 3 is the temperature of the image of the comparison source as it was formed ahead of the muzzle as shown in Fig. 1. This technique was used in order to avoid errors due to absorption by the lens used to form the image of the comparison source.

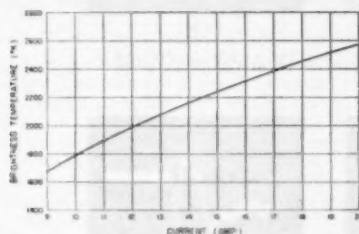


FIG. 3 TEMPERATURE-CURRENT RELATIONSHIP FOR TUNGSTEN COMPARISON SOURCE

DISCUSSION OF RESULTS

In general, it can be stated that the validity of the line-reversal method of determining temperature depends upon the establishment of the following types of equilibrium in the reaction zone (2):

- Translational degrees of freedom.
- Internal degrees of freedom.
- Chemical equilibrium.

The theoretical flame temperature corresponds to the state of complete statistical equilibrium of items (a), (b), and (c), and, according to Lewis and von Elbe (3) "can be calculated for a given content of total energy of the gas from heat capacities and dissociation equilibria obtained by statistical-mechanical methods from band-spectroscopic and other data." Experimental flame temperature, on the other hand, corresponds to equilibrium of the translational degrees of freedom obtained by determining the parameters of the gas law, pressure, and molar volume.

Concerning item (b), Lewis and von Elbe (3) found that "with monatomic gases argon and helium as diluents the experimental and theoretical temperatures are identical within narrow limits of error, but that with diatomic gases like excess oxygen or nitrogen the experimental temperatures are appreciably higher than the theoretical. This indicates that the latter gases are slow to absorb energy in the internal degrees of freedom which they possess in distinction to the monatomic gases, and that equilibrium (b) is not established in the burned gas behind the flame front. The phenomenon has been referred to as excitation lag (3), implying that the collisional excitation of the internal degrees of freedom,

particularly those of vibration, is lagging behind the chemical reaction."

Lewis and von Elbe made the following comment (2) concerning Bauer's (4) work relative to the determination of the temperature of Mekker-burner flames by reversal of sodium and other characteristic lines in the visible spectrum, wherein identical temperatures were found in every case: "It does not seem possible to interpret this result in any other way than that statistical equilibrium is established in all cases, either completely or at least between the electronic degrees of freedom of the metal atoms and the translational degrees of freedom of the gas."

The phenomenon of excitation lag and the question of whether or not complete equilibrium has been established are pertinent to the present experiments since the atomic "thermometers," sodium and potassium atoms are used as well as the molecular thermometer H_2O for the temperature determinations.

REVERSAL OF SODIUM-LINE RADIATION

Fig. 4 is a series of traces similar to the one shown in Fig. 2 for comparison source temperatures as indicated, and for reversal of sodium-line radiation. The technique used to obtain this series of traces and those shown in Figs. 5 and 6 was as follows: The monochromator was adjusted so that radiation of the desired frequency passed through the exit slit. The image of the comparison source was adjusted for a particular temperature, according to the curve shown in Fig. 3, and formed ahead of the muzzle of the gun in the position indicated in Fig. 1. This image of the comparison source was then focused on the entrance slit of the monochromator. The gun was fired and the sequence of the events previously discussed, and shown in Fig. 2, took place.

The comparison source was then adjusted for a different temperature and the process repeated until a temperature was found for which the position of peak emission would lie on an extension of the initial base line. In Fig. 4 curve (a) is an oscilloscope trace showing the time variation of intensity from the secondary explosion with no current flowing through the comparison source. The passage of time proceeds from right to left at a rate indicated by the calibration shown in (b). Trace (c) was obtained with 10 amperes flowing through the comparison source, giving a brightness temperature of 1785 K. The peak temperature of the flash is obviously greater than 1785 K, since very little initial absorption has taken place, and the peak intensity from the explosion lies considerably above the initial base line. In traces (d) and (e) the temperature of the comparison source was increased to 1890 K and 1990 K, respectively, with the indication that the peak temperature was still higher than 1990 K.

Traces (f), (g), and (h) are repeat runs at 2065 K, showing that the maximum temperature is being approached. It will be noticed that the peak intensity for these three traces is consistently slightly above the original base line. With a comparison temperature of 2120 K as indicated by traces (i), (j), and (k), the peak intensity is very close to the level of the original base line and, finally, in traces (l) and (m), a comparison temperature has been reached which is definitely higher than the temperature corresponding to the maximum intensity from the reaction zone. A consideration of all the traces shown in this figure would indicate that the peak temperature of the reaction was approximately 2130 K.

The sharp downward spike due to the passage of the projectile through the optical path is readily seen in traces (c), (d), and (e). The variation in depth of this initial sharp spike is due to the change in intensity of radiation from the comparison source. It will also be noticed that the "grass" on the base line increases in magnitude as the current through the comparison source is increased. This is due to the increased intensity of the random

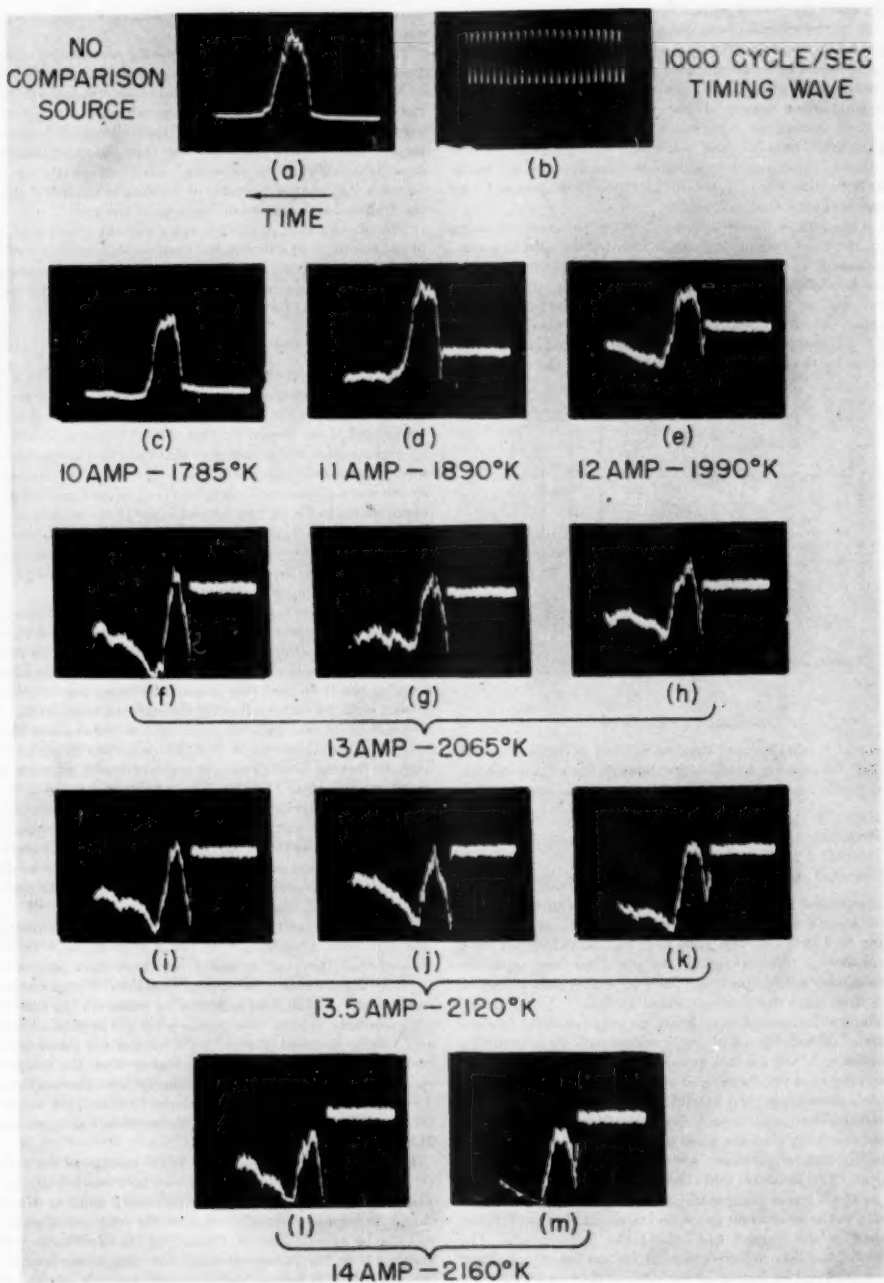


FIG. 4 TEMPERATURE DETERMINATION BY MEANS OF REVERSAL OF Na-LINE RADIATION AT 0.589 MICRON

fluctuations inherent in the photomultiplier tube at the higher light levels.

It is known that potassium is effective in the suppression of the secondary explosion when added in sufficient quantity as some salt such as potassium sulphate. This would indicate that potassium takes part in a chemical reaction, either as the atom or as the oxide, probably in connection with intermediate products formed during the secondary reaction.

If no potassium salts are added intentionally, the potassium atoms present as impurities but not in sufficient quantity to suppress the secondary reaction, might still take part in the reaction and thus perhaps not be in chemical equilibrium with the system. This could, of course, result in obtaining a value of temperature different from that indicated by sodium-line reversal, since establishment of chemical equilibrium was one of the necessary postulates for the validity of the line-reversal technique. Therefore the experiment was repeated with the spectroscopy adjusted to pass the strong potassium doublet near 0.77 micron through the exit slit. A lead-sulphide photoconductive cell was used as the detector in this case since the photomultiplier does not have sufficient sensitivity in this region of the spectrum.

TEMPERATURE DETERMINATION BY POTASSIUM-LINE REVERSAL

Fig. 5 is a group of traces showing the results of temperature determination by potassium-line reversal, and the following comments are relative to this figure: Traces (a) and (b) have the same significance as in Fig. 4. The remaining traces shown [(c) to (k) inclusive] cover a relatively narrow temperature region since it was indicated by the sodium line-reversal experiments that the temperature was probably above 2000 K. Traces (c), (d), and (e), with the comparison source at 2160 K, indicate that the peak temperature is somewhat higher than this value. Traces (f), (g), and (h) at 2200 K indicate that this value is near but just slightly below the correct value. Traces (i), (j), and (k) indicate that the value is somewhat less than 2240 K. An averaging technique based upon the distance of the peak intensity for each trace above or below an extension of the base line results in a value of 2215 K for the peak temperature of the flash as determined by potassium-line reversal. It is believed that this value is significantly higher than the value of 2130 K determined by sodium-line reversal. This is discussed in more detail later.

REVERSAL OF WATER-VAPOR BAND

In order to compare temperature values as determined by a polyatomic thermometer, reversal of the water-vapor band at 0.942 micron was studied. The results are shown in Fig. 6 and the following comments are relative to this figure:

Traces (a) and (b) have the same significance as previously, with the exception that increasing time is from left to right. A wide range of temperatures is shown because of the fact that considerably more variation in results at any particular temperature was found with this series of determinations. Traces (c), (d), and (e) at 2065 K indicate that the peak temperature is greater than this value. All three of these traces are consistently above the base line at the peak intensity. With the comparison source at 2160 K [traces (f), (g), and (h)], the temperature at the peak-intensity position is consistently above the base line except on trace (f). However, the shape of this trace at the peak is flat, a condition which was not usually encountered. The flat top on trace (f) is not felt to be due to an electronic difficulty but to a peculiarity in the emission of the characteristic radiation from the radiating water-vapor molecules.

Traces (i), (j), and (k) are a good illustration of the degree of inconsistency encountered in the determination of temperature with the water-vapor molecule, the value of 2240 K being ap-

parently too high in trace (i), and too low in traces (j) and (k). The inconsistency is also apparent, relative to the value of 2320 K, as shown in traces (l), (m), and (n). Only at a temperature of 2390 K was the position of peak intensity consistently below the initial base line.

The same averaging process used in connection with Fig. 5 was used for the water-vapor determination with the resulting value for the peak temperature of the flash being 2230 K. It will be noted that this figure is close to the value of 2215 K determined by potassium-line reversal but still considerably higher than the value of 2130 K as determined by sodium-line reversal. It will be noticed in most of the traces shown in Figs. 5 and 6 that the initial downward deflection caused by the passage of the projectile through the optical path is very sharp on the downward portion but rises slowly toward the initial base line, in most cases just reaching the initial base line before the second rapid downward deflection due to absorption by the cold muzzle gases. This is particularly noticeable in frame (f), Fig. 5. The spreading out of the deflection due to the projectile in Figs. 5 and 6, as compared to the very sharp spike in the traces in Fig. 4, is due to the poor frequency response of the lead-sulphide photoconductive cell.

POSSIBLE SOURCE OF ERROR

One possible source of error in the present determinations is that due to the variation of emissivity of the comparison source as a function of wave length. The emissivity of tungsten decreases at longer wave lengths and, therefore, the spectral brightness is lower. A lower brightness means that the temperature of the filament must be raised to give a reversal temperature equivalent to that obtained in a wave-length region of greater brightness. Thus consider reversal at the wave lengths used in the present determinations, that is, at 0.589, 0.77, and 0.942 microns. The pyrometer is calibrated at 0.665 micron with reference to a black body whose emissivity is unity at all wave lengths. The emissivity of tungsten at the wave lengths being considered is given in Table 1.

TABLE 1 SPECTRAL EMISSIVITY OF TUNGSTEN AT 2200 K

Wave length, microns	Emissivity
0.589	0.446
0.665	0.433
0.77	0.416
0.942	0.387

For example, if the peak temperature of the flash were actually 2200 K, as determined by the reversal of a hypothetical spectral line at 0.665 micron (the wave length for which the pyrometer is calibrated) the height of the oscilloscope trace at a peak flash intensity would just reach the level of the original base line, if the image of the comparison source was adjusted for a temperature of 2200 K. If now the temperature were determined by reversal of the sodium line at 0.589 micron, since the brightness of the comparison source is greater at this wave length, the intensity of the flash would not match the comparison radiation and the false conclusion would be that the flash temperature was below 2200 K.

If the potassium line at 0.77 micron were used, the reverse would be true due to the lower value of emissivity of tungsten at this wave length, and an excessively high value of temperature would be obtained. The magnitude of the error to be expected due to this phenomenon can be calculated readily. It can be seen in Table 1 that the percentage change in emissivity from 0.589 micron to 0.77 micron is

$$\frac{0.446 - 0.416}{0.431} = \text{approximately 7 per cent}$$

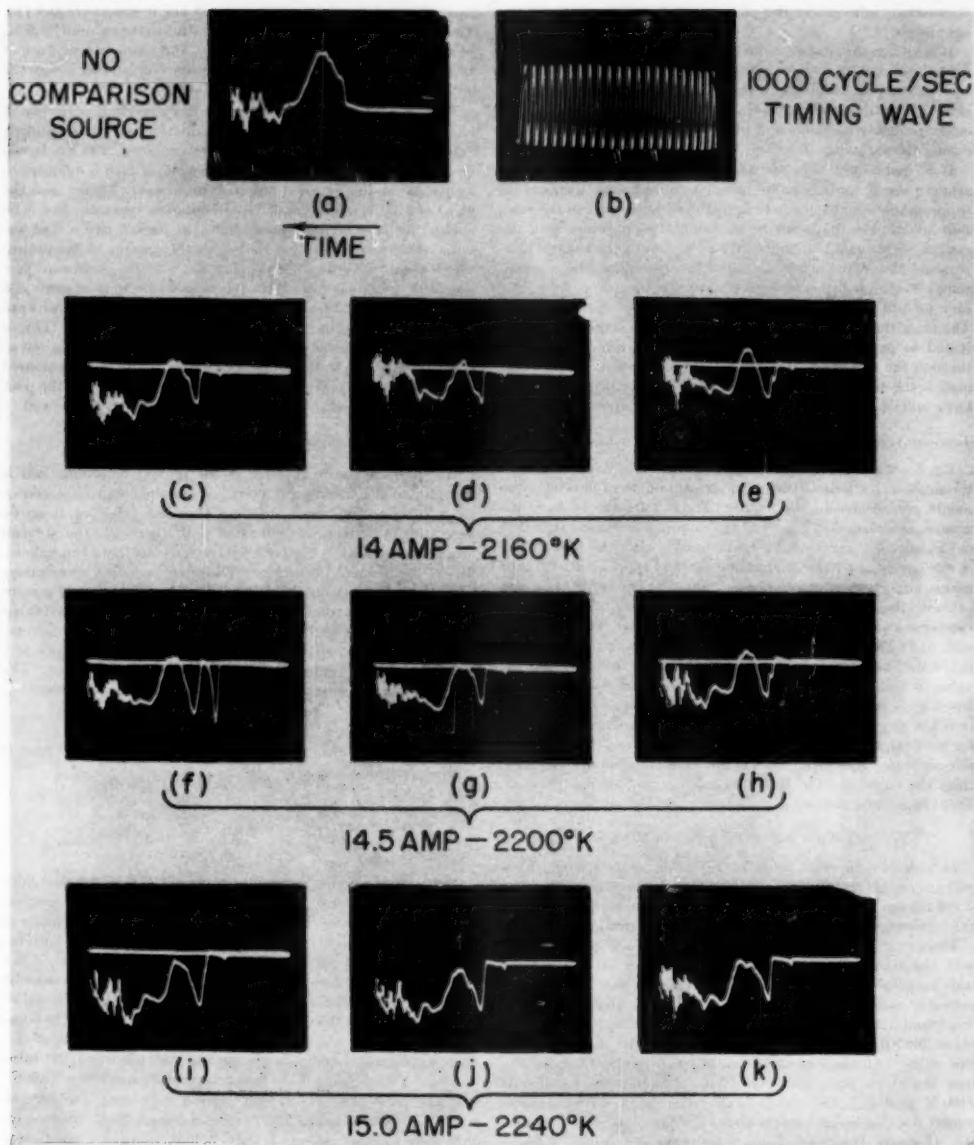


FIG. 5 TEMPERATURE DETERMINATION BY MEANS OF REVERSAL OF K-LINE RADIATION AT 0.77 MICRON

In order to evaluate the error in temperature introduced by a change in emissivity of 7 per cent, consider the expression for the monochromatic brightness in the visible spectrum of a nonblack body

$$B_{\lambda(\text{nb})} = \epsilon_{\lambda} \frac{C_1}{\lambda^5} \frac{1}{e^{C_2/\lambda T}} \quad (6)$$

The problem is: How much of a temperature change corresponds to a 7 per cent change in ϵ_{λ} for a constant $B_{\lambda(\text{nb})}$? Thus

$$\frac{d\epsilon_{\lambda}}{\epsilon_{\lambda}} = \frac{d/dT(e^{C_2/\lambda T})}{e^{C_2/\lambda T}} = 0.07$$

or

$$\frac{C_2 dT}{\lambda T^2} = 0.07$$

Consider the temperature range near 2200 K and a wave length of 0.77 micron

$$dT = \frac{0.07 \times 0.77 \times (2200)^2}{14,320} = 20 \text{ deg (approx)}$$

and

$$T = 2200 - 20 = 2180 \text{ K}$$

This would be the value of temperature obtained by reversal of the sodium line at 0.589 micron as compared to the value of 2200 K determined at the wave length of 0.77 micron by potassium-line reversal.

The actual values of temperature determined were 2130 K with sodium-line reversal and 2215 K with potassium-line reversal, a difference of 85 deg. This is, of course, considerably greater than the possible error just calculated, owing to the change in emissivity of the comparison source. The situation with regard to reversal of the water-vapor band is somewhat more serious. As shown in Table 1, the change in emissivity from 0.589 micron to 0.942 micron is

$$\frac{0.446 - 0.387}{0.416} = 14 \text{ per cent (approx)}$$

A calculation similar to the previous calculation would indicate that a value of 2200 K, as determined by reversal of the water-vapor band at 0.942 micron, would correspond to a value of 2160 K, as indicated by sodium-line reversal, a difference of 40 deg. The experimental values found were 2130 K with sodium-line reversal and 2230 K by water-vapor reversal, a difference of 100 deg. From these calculations the peak temperature of gun flash as determined by the three different methods and corrected for the change in emissivity of the comparison source is as follows:

By sodium-line reversal.....	2130 K
By potassium-line reversal.....	2215 — 20 = 2195 K
By H ₂ O band reversal.....	2230 — 40 = 2190 K

The temperature as determined by sodium-line reversal was left uncorrected.

CONSISTENCY OF SODIUM-LINE-REVERSAL RESULTS

Attention is again called to the consistency of the results obtained with sodium-line reversal, as shown in Fig. 4. This is taken as an indication of the establishment of equilibrium between the electronic degrees of freedom of the metal sodium atoms and the translational degrees of freedom of the gas. Also, it is believed

that these results would indicate the establishment of chemical equilibrium between the sodium atoms and the remainder of the system.

The higher values of temperature indicated by potassium-line and water-vapor-band reversal are believed to be due to the following: In the case of potassium, since it is believed that the potassium atoms take part in the chemical reactions, they are probably not in chemical equilibrium with the system and are probably excited to a level corresponding to a temperature greater than the equilibrium temperature for the system. The less consistent results with potassium-line reversal could be due to variations in the extent to which the potassium atoms have taken part in the reaction.

The situation with respect to water vapor is somewhat different for two principal reasons, as follows:

(a) The thermometer in this case is a polyatomic molecule, and the establishment of temperature equilibrium with respect to this molecule might be much more complex than is the case with the metal atoms.

(b) Water vapor is an actual end product of the chemical reaction, and the phenomenon of self-absorption due to cooler layers of water vapor near the outside of the reaction zone could be present in various degrees.

It is known that the use of totally colored flames in line-reversal determinations leads to values of temperature which are probably intermediate between the maximum temperature at the center of the reaction zone and the minimum temperature in the outer layers. However, in connection with secondary gun flash it is not necessarily true that a large degree of temperature inhomogeneity exists.

Because of the nature of the occurrence of the flame, it is possible that the entire zone being observed is essentially homogeneous in temperature.

COMPARISON WITH WORK OF OTHER INVESTIGATORS

Assuming that the value of 2130 K, as determined by sodium-line reversal, is the most nearly correct value of the three values obtained, it is of interest to compare this value with the values found by other investigators for other fast combustion flames. For example, Rasweiler and Withrow (5) determined a temperature of 2333 K at the firing end of an Otto-cycle engine using line-reversal method. Later, Hottel and Eberhardt (6) calculated this temperature to be 2344 K on the basis of adiabatic combustion. El Wakil, et al. (7), using a technique similar to that described in this paper, obtained a value of 2900 K for the flame temperature in an internal-combustion engine. The lower values reported in this paper could be due to a number of possibilities, the most pertinent of which are probably as follows:

(a) The use of totally colored flames, possibly not serious as mentioned previously.

(b) A high degree of excitation lag due to the speed of the reaction.

(c) An actual difference in the maximum flame temperature for the flames referred to in references (5, 6, and 7), and the flames studied in the present investigation.

CONCLUSION

In conclusion it should be noted that with proper regard for the phenomenon of excitation lag, the method should prove useful for the determination of the variation of temperature with time for rapid transient flames. The technique described should prove useful in reaction-kinetics studies, since components, which have

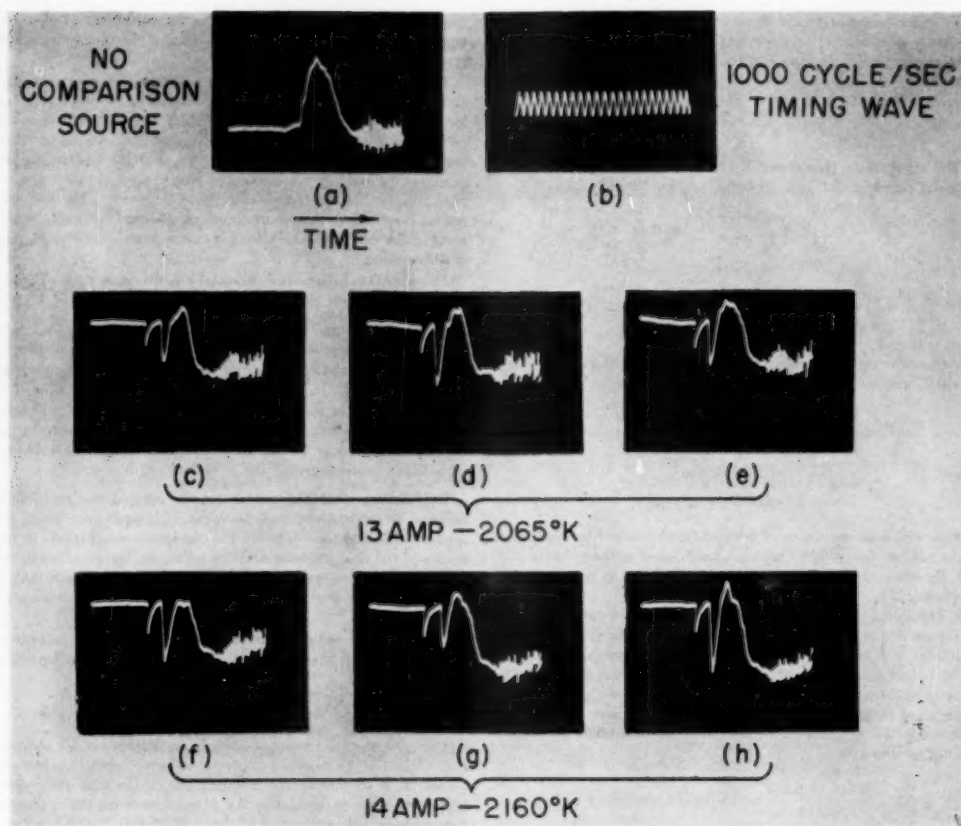


FIG. 6 (Above and right on facing page) TEMPERATURE DETERMINATION BY MEANS OF REVERSAL OF H_2O BAND RADIATION AT 0.942 MICRON

characteristic emission lines and which take part in the reaction, should give varying temperature values, and these values should be capable of interpretation in terms of the particular system of reactions being studied.

BIBLIOGRAPHY

- 1 "Sur la Température des flammes," by Ch. Féry, *Compte Rendus*, vol. 137, 1903, pp. 909-912.
- 2 "Flame Temperature," in "Temperature, Its Measurement and Control in Science and Industry," by B. Lewis and G. von Elbe, Reinhold Publishing Corporation, New York, N. Y., 1941.
- 3 "Combustion, Flames and Explosions of Gases," by B. Lewis and G. von Elbe, Cambridge University Press, London, Eng., 1938.
- 4 "Recherches sur le rayonnement," by E. Bauer, thesis, Gauthier-Villars, Paris, France, 1912.
- 5 "Flame Temperatures Vary With Knock and Combustion-Chamber Position," by G. M. Haasweiler and L. Withrow, *SAE Journal*, vol. 36, 1935, pp. 125-133.
- 6 "A Mollier Diagram for the Internal-Combustion Engine," by H. C. Hottel and J. E. Eberhardt, *Chemical Reviews*, vol. 21, 1937, pp. 438-460.
- 7 "An Instantaneous and Continuous Sodium-Line-Reversal Pyrometer," by M. M. El Wakil, P. S. Myers, and O. A. Uyehara, *Trans. ASME*, vol. 74, February, 1952, pp. 255-267.

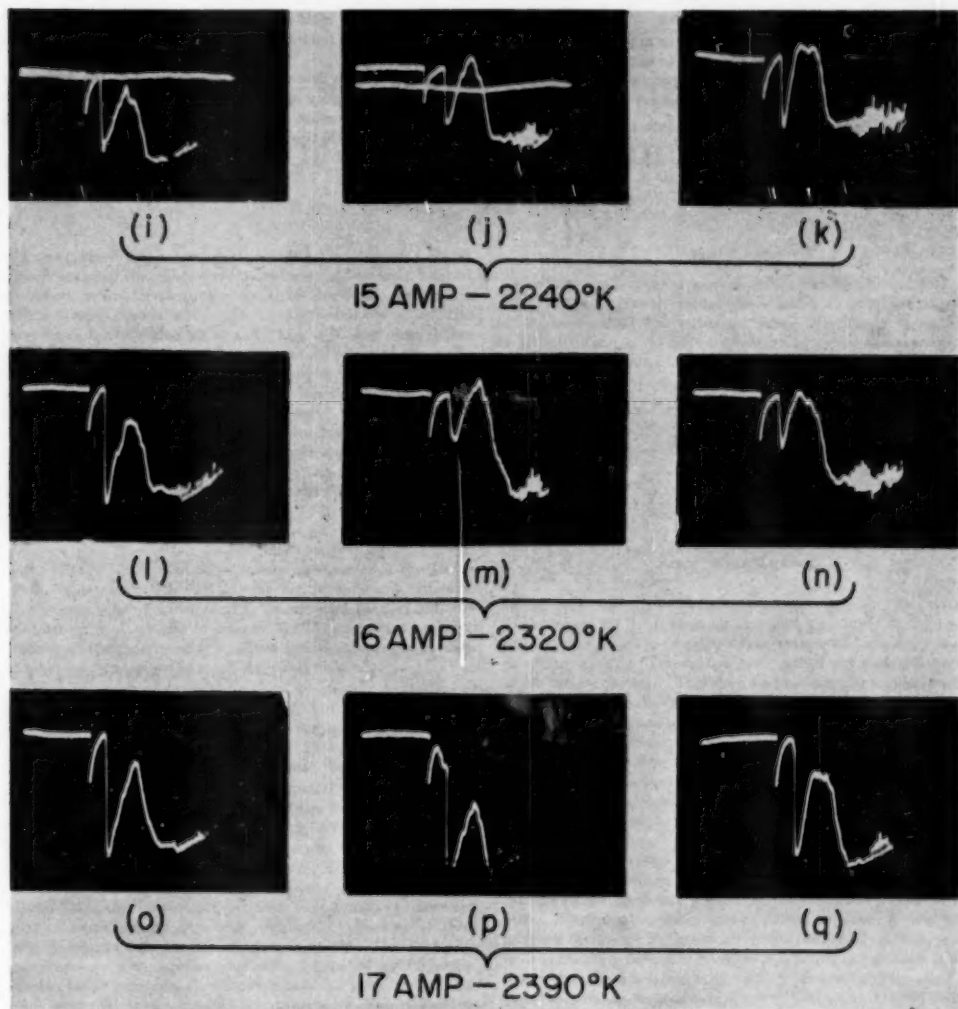
Discussion

J. H. POTTER.⁴ The photocell technique, initiated by Graff,⁵ has been used in a number of internal-combustion-engine tests with apparently satisfactory results. At the present time the writer is working on an application of the Graff method, using sodium-line reversal as a temperature-calibrating device.

It is unfortunate that the author gave so brief an account of his experimental apparatus. The data in such a test could be accumulated in a relatively short time, but the details of the instrumentation and the methods for mounting the test equipment would have been a most welcome addition. Experience has shown that the tungsten lamp and the method for injecting the alkali salt may constitute auxiliary research problems in themselves. The author has indicated to the writer that the sodium and potassium salts, which produced the characteristic oscillo-

⁴Professor of Mechanical Engineering, University of Illinois, Urbana, Ill. Mem. ASME.

⁵"Messung des Gastemperaturverlaufs in Verbrennungskraftmaschinen," by H. Graff, *Zeitschrift des Vereines deutscher Ingenieure*, vol. 86, 1942, pp. 461-465.



scope patterns, were present as impurities in the propellant charge.

With both sodium and potassium salts present in each explosion, it occurs to the writer that it might have been possible to use a spectroscope with two photocells set for the two respective wave lengths, as used by Uyehara, et al.⁶ This would have established an average value of the flame temperature by two simultaneous line reversals on the identical gun flash. It is possible that some of the spread of the flame-temperature values could have been reduced in such a method. In fact, it is not clear as to the exact

⁶ "Flame-Temperature Measurements in Internal-Combustion Engines," by O. A. Uyehara, P. S. Myers, K. M. Watson, and L. A. Wilson, *Trans. ASME*, vol. 68, 1946, pp. 17-30.

method by which the flame temperatures were established from the oscillograms.

Although it is perhaps a trivial matter, it might be well to shift the line following Equation [5] of the paper so that it follows immediately after Equation [4] in the final printed version of the paper. This would make the development of the equation read more smoothly.

In the section comparing the present work with that of other investigators, there is no need for concern over a lack of agreement. It is probable that the present work dealt with a more nearly homogeneous flame temperature than any of the tests run on internal-combustion engines.

AUTHOR'S CLOSURE

The comments of Professor Potter are appreciated and, due to the fact that several other people have expressed a desire for a more complete description of the experimental methods, the author has communicated with Mr. Robert Benn,⁷ one of his

⁷ Research Engineer, The Franklin Institute Laboratories for Research and Development, Philadelphia, Pa.

former associates, relative to the preparation of an additional paper which will contain details of the experimental techniques.

Professor Potter is correct in assuming that the apparatus could be rather easily adapted to the method of simultaneous intensity determination at two or more wave lengths. The author intends to do this in the near future.

Distribution of Heat-Transfer Coefficients Around Circular Cylinders in Crossflow at Reynolds Numbers From 20 to 500

By E. R. G. ECKERT¹ AND E. SOEHNGEN²

An experimental investigation using the Zehnder Mach interferometer reveals the temperature field around heated cylinders in an air stream normal to the axis. From the temperature distribution the local distribution of the heat-transfer coefficient around the cylinder circumference is obtained. The thermal boundary layers are quite thick, especially for the lower Reynolds numbers investigated and the separation occurs farther downstream than at high Reynolds numbers. Accordingly, the contribution of the stagnant region at the downstream side of the cylinder to the over-all heat transfer is low (approximately 15 per cent), and the heat flow into the upstream side is much larger than into the downstream side.

INTRODUCTION

KNOWLEDGE of heat-transfer coefficients at low Reynolds numbers is valuable for the development of instruments using wires, such as thermocouples and hot-wire anemometers. It is also of interest for investigations on heat-transfer at low pressures (1).³ These investigations are by their nature usually confined to small Reynolds numbers.

There exists considerable literature on average heat-transfer coefficients of cylinders in crossflow (2, 3). Investigations are also known on the local distribution of the heat-transfer coefficients at high Reynolds numbers (3, 4, 5). This paper deals with an experimental determination of the local Nusselt numbers on cylinders in the low Reynolds-number range.

The investigations were carried out at the Power Plant Laboratory of the Air Materiel Command, Wright Patterson Air Force Base, Dayton, Ohio, using an interferometer which was built at this laboratory (6). The experiments were not very extensive in nature and some basic difficulties which are connected with low Reynolds-number investigations and which will be discussed later on could not be overcome completely. Because of these facts the results were not published immediately. There seems to exist, however, a widespread interest in data in the low Reynolds-number range justifying that the results of our investigations are made available to the public. Permission by Wright Field to publish the results of the investigation is gratefully acknowledged.

¹ Both authors worked on the investigations covered in this paper when affiliated with the Power Plant Laboratory, AMC Wright Patterson Air Force Base, Dayton, Ohio. The senior author is now with the National Advisory Committee for Aeronautics, Lewis Flight Propulsion Laboratory, Cleveland, Ohio. Mem. ASME.

² U. S. Air Force, Office of Air Research, Dayton, Ohio.

³ Numbers in parentheses refer to the Bibliography at the end of the paper.

Contributed by the Heat Transfer Division and presented at the Fall Meeting, Minneapolis, Minn., September 26-28, 1951, of THE AMERICAN SOCIETY OF MECHANICAL ENGINEERS.

NOTE: Statements and opinions advanced in papers are to be understood as individual expressions of their authors and not those of the Society. Manuscript received at ASME Headquarters, June 6, 1951. Paper No. 51-F-9.

TEST SETUP

The investigations were carried out in a rectangular tunnel as shown in Fig. 1. The tunnel consists of an inlet nozzle, a rectangular channel, a duct which changes the rectangular cross section to a circular one, a cylindrical piece with by-pass louvers, and a conical duct at the end of which a fan is arranged. The fan sucks

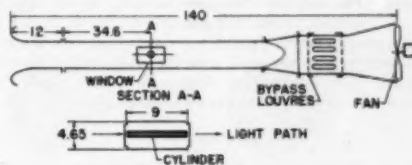


FIG. 1 FLOW TUNNEL

air with velocities up to 25 fps through the channel. The tunnel was designed by T. J. Keating and used for a study on the transition from laminar to turbulent flow within the boundary layer on a flat plate (7). The studies were carried out with a Zehnder Mach interferometer. Therefore two rectangular windows were arranged in the walls of the rectangular channel consisting of optically ground glass plates with a thickness of 0.1 in.⁴

During the experiments it was found that the air flow continued for a considerable time after the electric power was cut off from the fan. It decelerated only gradually. This, together with the fact that the interferometer obtains the whole field in one photograph, made it possible to conduct with the duct investigations at very low velocities. By arranging cylinders with different diameters in the cross section A-A of the duct, the experiments at low Reynolds numbers to be described were carried out. The cylinders were made out of solid copper and heated prior to the tests. Their heat capacity was sufficient to assure a slow temperature decrease. Three cylinders with 0.5, 1, 1.5 in. diam and 9 in. lengths were used. By order-of-magnitude calculations it was found that the deceleration of the flow was sufficiently small to cause only minor deviations of the flow field around the cylinders from a steady-flow condition.

There is an inherent difficulty connected with low Reynolds-number investigations in a duct. The boundary layers along the walls of the duct build up so fast that they have already met in the center when the air leaves the entrance nozzle. Therefore it seems impossible to obtain in any cross section a field with practically uniform velocity. Therefore it was thought more favorable to have at least a well-defined velocity field. Such a field exists in cross sections where the flow is already fully developed. The shape of this field is identical with the shape which a thin membrane assumes when it is stretched over the cross section considered and when a constant pressure is supplied to one side of the membrane. The velocity field determined in this way along

⁴ Manufactured by the Optron Laboratory, Dayton, Ohio.

the two center lines of the rectangular cross section is shown in Fig. 2. Also indicated in the figure is the size of the largest cylinder used in the investigations.

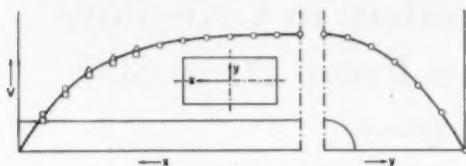


FIG. 2 VELOCITY FIELD IN CROSS SECTION A-A OF TUNNEL

At the time the investigations were made, no instrument was available to the authors with which the low air velocities of some inches per second could be measured. In addition there exists a basic difficulty in measuring velocities at very low Reynolds numbers. The ordinary Pitot-tube formulas do not apply at very low velocities, as was first pointed out by M. Barker (8). Therefore the Reynolds number was determined from the average Nusselt number obtained from the evaluation of the interferograms. The temperature field around the cylinder was obtained from the same interference photographs.

EVALUATION

The interferometer was adjusted in such a way that the interference lines are lines of constant density. At the low velocities the pressure variation in the flow field around the cylinders can be neglected as compared to the temperature variation. Therefore the interference lines are at the same time lines of constant temperature (isotherms). The evaluation of the interferograms was handled in the same way as in reference (9).

Fig. 2 shows that the air velocity decreases toward the ends of the cylinder which spans the whole tunnel. No attempt was made to correct the interferogram which integrates the air density along the light path for the thermal end effects caused by this deviation from the two-dimensional flow. The small boundary-layer thickness obtained, however, made a correction necessary which takes into account the refraction of the light rays in traveling through the test section. As indicated in Fig. 3, a light ray *A* is bent in traveling through a region where a density gradient exists normal to the light-ray direction.



FIG. 3 LIGHT-RAY REFRACTION IN HEATED BOUNDARY LAYER

In the case under consideration, the density gradient is caused by the temperature gradients through the heated boundary layer around the cylinders. In the tests the variation of the temperature throughout the boundary layer was small as compared to the absolute temperature *T*. As a consequence, the angle β under which the light ray leaves the heated boundary layer along the object with the length *l* is small. With this assumption and neglecting temperature variations in the direction parallel to the cylinder axis, the angle β is expressed by the following equation

$$\beta = \frac{dy}{dx} = \int_0^l \frac{1}{n} \frac{dn}{dy} dx \quad [1]$$

in which *n* is the refraction coefficient, and *x* and *y* are the co-

ordinates along and normal to the investigated object. Assuming the gradient of the refraction coefficient dn/dy to be constant along the light ray the expression simplifies to

$$\beta = \frac{1}{n} \frac{dn}{dy} l \quad [2]$$

For the small displacement *b* occurring in the experiments the foregoing assumption is justified. The refraction coefficient *n* is for gases determined by the expression

$$\frac{n-1}{\rho} = C \quad [3]$$

in which ρ is the density and *C* a constant. From this equation the gradient of the refraction coefficient is found

$$\frac{dn}{dt} = C \frac{d\rho}{dt} \quad [4]$$

Expressing the density ρ by the equation of state of an ideal gas with the pressure *p* and the gas constant *R*, the angle β finally becomes

$$\beta = \frac{Cl}{n} \frac{p}{RT^2} \frac{dT}{dy} \quad [5]$$

Since the shape of the light path as determined from Equation (2) is a parabola, the transverse displacement *b* of the light path on the side where the light ray leaves the boundary layer is

$$b = \frac{\beta l^2}{2} = \frac{Cl^3}{2n} \frac{p}{RT^2} \frac{dT}{dy} \quad [6]$$

At this place the temperature is lower by the amount $(dT/dy)b$ than on the spot where the light ray enters the test section. The average amount by which the temperature along the bent light-ray path is lower than at the spot where the light ray enters can be found easily by an integration to be $(dT/dy)b/3$. The screen on which the interference lines appeared was focused on the center plane of the channel. At this adjustment the optical system compensates to a first approximation half the above value (10). Therefore the temperature correction is

$$\Delta t = \frac{Cl^3}{12n} \frac{p}{RT^2} \left(\frac{dT}{dy} \right)^2 \quad [7]$$

In the experiments described here the maximum amount of the temperature correction determined from Equation (7) was 2 deg F or 10 per cent of the temperature variation throughout the boundary layer.

The local Nusselt number *Nu* for the heated cylinder based on the diameter *D* of the cylinder is (9)

$$Nu = \frac{D}{\delta_t'} \quad [8]$$

when δ_t' is the subtangent on the temperature profile as shown in

Fig. 4. This temperature profile along a normal to the surface is found for any position around the cylinder from the evaluation of the interferograms.

The Reynolds number for the tests was determined from the average Nusselt number \bar{Nu} which was found by an integration of the local Nusselt number around the cylinder circumference. For such a procedure a relationship between the average Nusselt number and the Reynolds number is

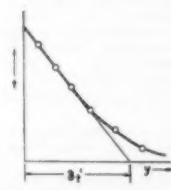


FIG. 4 DETERMINATION OF SUBTANGENT

necessary. The Reynolds number as used in this paper is the product of the cylinder diameter and the onstream velocity, divided by the kinematic viscosity of the air. McAdams (2) gives for the Reynolds-number range under consideration the empirical expression

$$\bar{Nu} = 0.32 + 0.43 Re^{0.52} \dots [9]$$

A similar expression which contains the square root of the Reynolds number instead of the power 0.52 was derived theoretically in reference (1). It is known generally that the Nusselt number for any two-dimensional laminar boundary-layer region is proportional to the square root of the Reynolds number as long as the boundary-layer thickness may be regarded as small. Therefore the constant term in Equation [9] takes care of the fact that at low Reynolds numbers, the boundary-layer thickness becomes considerable as compared to the cylinder diameter. A qualitative understanding of this mechanism may be obtained from a very simple calculation introduced by I. Langmuir and applied to the heat-transfer on cylinders.³ Replacing the boundary layer by a stationary film of uniform thickness and calculating the heat transfer by the heat conduction through this film leads to the expression

$$\bar{Nu} = \frac{2}{\ln(1 + 2B/D)} \dots [10]$$

in which B is the thickness of this film, and D the cylinder diameter. The thickness B is now determined in such a way that Equation [10] changes to a relationship

$$\bar{Nu} = C \sqrt{Re} \dots [11]$$

when the ratio of the film thickness to the cylinder diameter goes toward zero. In this way the equation

$$\bar{Nu} = \frac{2}{\ln\left(1 + \frac{2}{C\sqrt{Re}}\right)} \dots [12]$$

is obtained. In order to simplify this unhandy expression, it is developed in a series in \sqrt{Re} around $Re = 10$. Retaining only the first two terms of the series and introducing the value 0.451, determined from test results at higher Re number for the constant C , results in the expression

$$\bar{Nu} = 0.765 + 0.480 \sqrt{Re} \dots [13]$$

A better agreement with the existing experimental values is obtained by a correction of the first constant in the equation. The formula

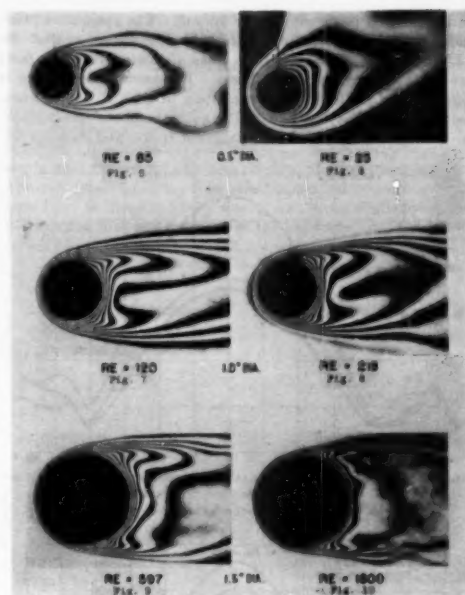
$$\bar{Nu} = 0.43 + 0.48 \sqrt{Re} \dots [14]$$

represents in the Reynolds-number range from 1 to 4000 within 4 per cent Hilpert's experimental values (11) which seem to be especially reliable. This formula was used for the determination of the Reynolds number from the measured average Nusselt number. The calculation in reference (1) gave values for the constants which are only slightly different.

RESULTS

Figs. 5 to 10, inclusive, show interference illustrations on cylinders at low Reynolds numbers. Three cylinder diameters were used in the investigations. From the figures it can be seen that a thermal boundary layer develops around the cylinder.

³ Reference (2), p. 222.



FIGS. 5-10 INTERFERENCE PHOTOGRAPHS SHOWING ISOTHERMS AROUND CYLINDERS

Its thickness decreases with increasing Reynolds number. The point on the cylinder where the flow separates from the surface is considerably farther downstream than at high Reynolds numbers. The region behind the place of separation is fairly steady at low Reynolds numbers and starts to become turbulent at the highest Reynolds number shown in Fig. 10. Some asymmetry toward the flow direction which is from left to right may be observed, especially at the smaller Reynolds numbers. This asymmetry is caused by free convection effects. These temperature fields have to be compared with the corresponding flow field.

Fig. 11 shows the flow field around cylinders in the interesting Reynolds-number range, as observed by Homann (12) by flow visualization. It is seen that for Reynolds numbers smaller than 1, no separated region exists on the downstream side of the cylinder. However, because of the viscous forces the flow lines close in more slowly behind the cylinder than they departed ahead of the cylinder. At a Reynolds number around 20, a stagnant region with a slow internal circulation can be observed. At Reynolds numbers larger than 100, vortices separate alternately on the upper and lower sides of the cylinder and are carried downstream forming von Kármán's vortex street.

Evaluations of the interferograms are presented in Figs. 12 and 13 in a rectangular co-ordinate system, and

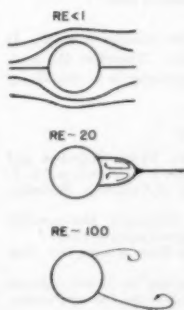


FIG. 11 FLOW AROUND CYLINDERS

in Fig. 14 in a polar co-ordinate system. The stagnation point indicated by $\alpha = 0$ in the figures was determined so that the curves are symmetrical on both sides of this point. Two facts are again obvious in these figures. The point of separation is considerably farther downstream than at high Reynolds numbers, especially at the lowest Reynolds numbers investigated. Accordingly, the range of the stagnant region and its contribu-

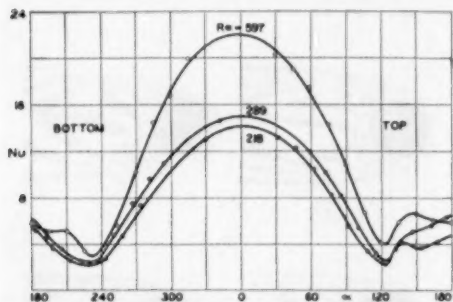


FIG. 12 DISTRIBUTION OF LOCAL NU NUMBER AROUND CIRCUMFERENCE OF CIRCULAR CYLINDERS
(α = angular distance from stagnation point.)

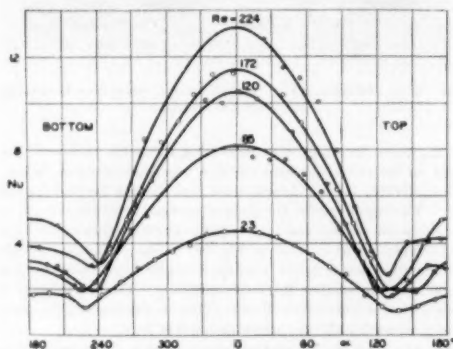


FIG. 13 DISTRIBUTION OF LOCAL NU NUMBER AROUND CIRCUMFERENCE OF CIRCULAR CYLINDERS
(α = angular distance from stagnation point.)

tion to the over-all heat transfer to the cylinder is small. It was found to be smaller than 15 per cent. Therefore the cooling effect of an air stream on a heated cylinder is in this Reynolds-number range quite ununiform.

BIBLIOGRAPHY

- 1 "Forced Convection Heat-Transfer From Cylinders and Spheres in Rarefied Gases," by R. M. Drake, F. M. Sauer, and S. A. Schaaf, Report No. HE-150-74, University of California, Berkeley, Calif., 1950.
- 2 "Heat Transmission," by W. H. McAdams, McGraw-Hill Book Company, Inc., New York, N. Y., second edition, 1942.
- 3 "Heat Transfer," by M. Jakob, John Wiley & Sons, Inc., New York, N. Y., 1949.
- 4 "Wärmeabgabe eines geheizten Zylinders," by E. Schmidt and K. Wenner, *Forschungsarbeiten auf dem Gebiete des Ingenieurwesens*, vol. 12, 1941, pp. 651-673.
- 5 "A Study of Local Heat Transfer and Skin Friction on a Circular Cylinder in the Critical Flow Region," by W. H. Giedt, Dissertation, University of California, Berkeley, Calif., 1950.

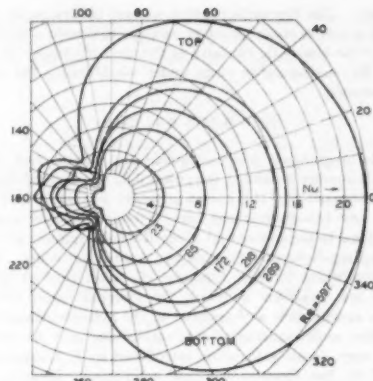


FIG. 14 DISTRIBUTION OF LOCAL NU NUMBER AROUND CIRCUMFERENCE OF CIRCULAR CYLINDERS
(α = angular distance from stagnation point.)

6 "Manufacture of a Zehnder-Mach Interferometer," by E. R. G. Eckert, R. M. Drake, and E. Soehngen, AF Technical Report No. 5721, 1948.

7 "Interferometric Studies of Beginning Turbulence in Free and Forced Convection Boundary Layers on a Heated Plate," by E. R. G. Eckert, Heat Transfer and Fluid Mechanics Institute, Berkeley, Calif., 1949.

8 "On the Use of Very Small Pitot Tubes for Measuring Wind Velocities," by M. Barker, *Proceedings of the Royal Society of London*, vol. 101, 1922, p. 435.

9 "Studies on Heat Transfer in Laminar Free Convection With the Zehnder-Mach Interferometer," by E. R. G. Eckert and E. Soehngen, AF Technical Report No. 5747, 1948.

10 "Refraction Effect in Interferometer of Boundary Layer of Supersonic Flow Along Flat Plate," by P. Wachtell, *Physical Review*, vol. 78, 1950, p. 333.

11 "Wärmeabgabe von geheizten Drähten und Rohren im Luftstrom," by R. Hilpert, *Forschungsarbeiten auf dem Gebiete des Ingenieurwesens*, vol. 4, 1933, pp. 215-224.

12 "Einfluss grosser Zähigkeit bei Strömung um Zylinder," by F. Homann, *Forschungsarbeiten auf dem Gebiete des Ingenieurwesens*, vol. 7, 1936, p. 1.

Discussion

R. M. DRAKE, JR.⁶ The paper presents for the first time some experimental evidence of the distribution of the local heat-transfer coefficients around horizontal circular cylinders in flows at low Reynolds numbers. The value of the experimental data would have been enhanced if an independent determination of the Reynolds number could have been made rather than relying upon the experimental correlation given by Hilpert for its determination. Such an independently determined Reynolds number together with the Nusselt number as determined optically would have given a check on the validity of the Hilpert and King data in the low Reynolds-numbers range as well as upon the optical method for determining the Nusselt number. The writer appreciates the fact that these omissions are easier to point out than to rectify.

The analysis referred to in reference (1) of the paper, which was based on the idea of pure radial conduction from the cylinder to an infinite medium, predicts a local heat-transfer coefficient distribution of the form

$$Nu = \frac{4}{\pi^2} \int_0^\infty \frac{e^{-k u \sqrt{r_1}}}{J_0^2(u \sqrt{r_1}) + Y_0^2(u \sqrt{r_1})} \frac{du}{u}$$

⁶ Assistant Professor of Mechanical Engineering, University of California, College of Engineering, Berkeley, Calif.

where θ is the angle from stagnation, and r_1 the radius of the cylinder, which when integrated around the cylinder for an average Nusselt number for Reynolds numbers greater than 300, yields

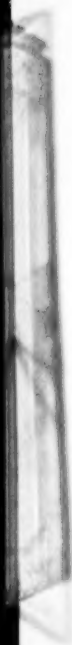
$$\overline{Nu} = 0.50 + 0.44 \sqrt{Re}$$

This result compares well with Equation [14] of the paper which the author used, as he has indicated. Local values of Nusselt number as predicted by the analysis in reference (1) do not correspond with the local experimental values as determined optically. This is not surprising as pointed out by the assumptions made in the analysis, and on such bases it is probably fortuitous that the integrated average values indicate the demonstrated

correspondence. The experimental local values are considered to be more representative than the analytical values.

AUTHORS' CLOSURE

The authors are aware of the fact that additional measurements would have been required in order to make the paper a complete study of the problem of heat transfer at low Reynolds numbers. Unfortunately this was not possible since the experiments were carried out only as a side line of other investigations. A way of determining the Reynolds number independently would have been to measure under steady conditions the volume flow through the duct and to calculate the velocities from the known velocity distribution field, Fig. 2.



Peculiar Behavior of Steel Beams Under Dead Loads That Produce Inelastic Strains

By H. T. CORTEN,¹ M. E. CLARK,² AND O. M. SIDEBOTTOM,³ URBANA, ILL.

Inelastic deformation in metals is known to be a time-dependent phenomenon; however, the theoretical relations between load and deformation do not, in general, include the effect of time. Most of the experimental data, confirming these theoretical relations, have been obtained using screw-powered or hydraulic testing machines in which the load "falls off" as inelastic deformation occurs. Furthermore, these tests have been made without regard to the length of time necessary for inelastic deformation to cease at any given load. This investigation was undertaken to determine the effect of testing members under dead load where each increment of load could be maintained on the member a sufficient length of time until equilibrium was attained. Five statically determinate beams, four mild-steel beams of various cross sections, and one rail-steel rectangular beam were tested in a dead-load testing machine. The load-deformation diagrams were found to have a staircase appearance, unlike the smooth continuous curves usually reported. The ultimate load-carrying capacity of the mild-steel beams was found to be considerably below that predicted by theory, and time delays of appreciable magnitude were observed for the initiation of inelastic deformation at a given load. A more stable behavior was observed for the rail-steel beam under dead load, and the experimental results were found to correlate well with theory.

INTRODUCTION

THE literature of today contains much experimental and theoretical work on the nature of inelastic deformation in steel members and its influence on the load-carrying capacity. The theoretical relations, in general, are based upon the stress-strain diagram of the material as obtained from the standard tension test and a suitable assumption as regards the stress distribution in the member. These theoretical relations have been confirmed by sufficient test data (at least for the bending of beams) so that they have become accepted as valid. Attention must be called, however, to the fact that most of the confirming test data have been obtained using screw-powered or hydraulic testing machines. This type of testing machine is not well suited to investigate the time-sensitive inelastic behavior of load-carrying members since it is a deformation-producing machine, not a load-producing one. When the machine applies a given deformation to a member (and presumably a given load) and the inelastic deformation proceeds with time, the actual load on the member decreases or "falls off." Therefore data obtained using such a machine give an inaccurate representation of the inelastic load-

carrying capacity of the member. Since in many applications it is required that a load must be carried for long periods of time, it was deemed advisable to conduct a series of tests in which the load was applied and maintained constant until deformation ceased for each load during the test.

The dead-load machine, shown in Fig. 1, was built so that the loads could be applied directly to the test member. Such loads were applied by adding dead weights to the weight rack connected to the main loading rod. Any increment of load could be

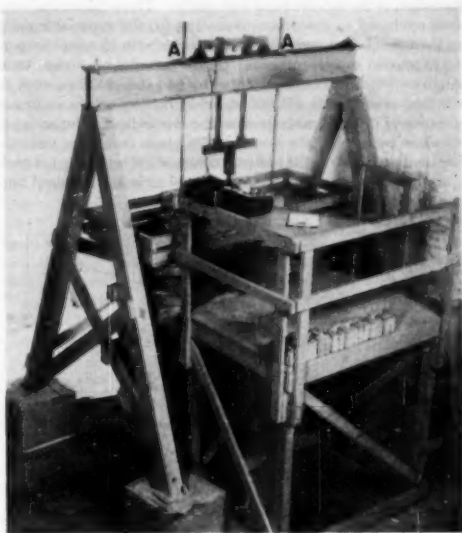


FIG. 1 25,000-POUND-CAPACITY DEAD-LOAD TESTING MACHINE

applied up to a total capacity of about 25,000 lb. Use of this dead-load type of testing machine eliminated the disadvantage of the deformation type of machine since any load that was applied remained constant in magnitude regardless of the deformation which took place at that load.

Tests were run at room temperature on straight annealed mild-steel beams of rectangular, circular, and I cross sections and on a straight annealed rail-steel beam of rectangular cross section. Each load which produced inelastic deformation was maintained until such deformation ceased. The initiation of this inelastic deformation or yielding was found to have an appreciable time delay in the mild-steel-beam tests, and its duration was found to be several hours in most instances. The resulting moment-strain relation was found to resemble a stair-step diagram. Furthermore the "fully plastic" resisting moment or the ultimate load-carrying capacity for all mild-steel beams was appreciably below that predicted by theory.

¹ Instructors in Theoretical and Applied Mechanics, University of Illinois.

² Assistant Professor of Theoretical and Applied Mechanics, University of Illinois. Jun. ASME.

³ Contributed by the Metals Engineering Division and presented at the Fall Meeting, Minneapolis, Minn., September 26-28, 1951, of THE AMERICAN SOCIETY OF MECHANICAL ENGINEERS.

NOTE: Statements and opinions advanced in papers are to be understood as individual expressions of their authors and not those of the Society. Manuscript received at ASME Headquarters, June 14, 1951. Paper No. 51-F-4.

This behavior was typical of three different mild steels that were investigated and may be expected to occur in service applications where the load is essentially constant and large enough to produce inelastic deformation. The phenomenon may explain the loosening of shrink fits and other peculiarities which occur in steel members and should be considered in the formulation of more rational procedures for the design of structural elements.

Since all the tests were performed at room temperature, the variable of temperature was not considered in this investigation. Undoubtedly, in some service applications, the temperature may vary considerably from ordinary room temperature; this may cause the behavior of a member to be significantly different from that herein reported. Additional work is contemplated to study further the effect of this important variable.

THEORY

The theoretical moment-strain relations as they appear in the literature will now be presented in order to have a basis for the discussion of the experimental test results. These theoretical relations are based on the assumptions that (a) the material making up the beam is homogeneous and isotropic with identical properties in tension and compression; (b) the material has stress-strain diagrams which can be represented by two straight lines, such as is indicated in Fig. 2; (c) inelastic deformations which occur are of the same order of magnitude as the elastic-limit deformations; (d) plane sections of the beam remain plane even after inelastic deformation; and (e) the inelastic deformation is initiated in each fiber of the beam at the same stress level as in the standard tension specimen.

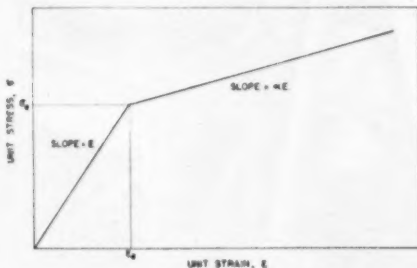


FIG. 2 IDEALIZED TENSILE OR COMPRESSIVE STRESS-STRAIN DIAGRAM FOR MATERIAL

The moment-strain diagram for a beam is a function of the shape of the cross section, and since experimental results were obtained for beams having three different shapes, the corresponding relations for these cross sections will be given. For a straight beam of rectangular cross section, the theoretical moment-strain relation (1)¹ in dimensionless form is

$$\frac{M}{M_e} = (1 - \alpha) \frac{3}{2} - \frac{1 - \alpha}{2} \left(\frac{\epsilon}{\epsilon_y} \right)^3 + \alpha \frac{\epsilon}{\epsilon_y} \dots [1]$$

where M is the resisting moment corresponding to a strain ϵ in the most strained fibers, M_e is the maximum elastic resisting moment (computed by the ordinary flexure formula $M_e = \sigma_y I/c$, where σ_y is the yield stress corresponding to the yield strain ϵ_y), and α is a factor (see Fig. 2) which gives a measure of the strain-hardening of the material. Equation [1], if α is set equal to zero, gives the

¹ Numbers in parentheses refer to the Bibliography at the end of the paper.

relation for a beam of rectangular cross section made of a mild steel having a definite yield point.

The theoretical relations for the circular (1) and I cross sections (2) will be presented for mild-steel beams, that is, for α equal to zero. The relation for the circular cross section is

$$\frac{M}{M_e} = \frac{1}{\pi} \left[\frac{4}{3} \left(1 - \frac{\epsilon^3}{\epsilon_y^3} \right)^{3/2} + 2 \left(1 - \frac{\epsilon^3}{\epsilon_y^3} \right)^{1/2} + 2 \frac{\epsilon}{\epsilon_y} \arcsin \frac{\epsilon_y}{\epsilon} \right] \dots [2]$$

Two expressions are required for the I cross section, the first being

$$\frac{M}{M_e} = \frac{1}{1 - B^2 + AB^3} \left[\frac{3}{2} - \frac{1}{2} \frac{\epsilon^2}{\epsilon_y^2} + B^2 (A - 1) \frac{\epsilon}{\epsilon_y} \right] \dots [3]$$

which is valid for inelastic deformation or yielding confined to the flanges of the I beam. The second expression is

$$\frac{M}{M_e} = \frac{1}{1 - B^2 + AB^3} \left[\frac{3}{2} (1 - B^2 + AB^3) - \frac{A}{2} \frac{\epsilon^2}{\epsilon_y^2} \right] \dots [4]$$

which applies when yielding penetrates through the flanges into the web. In Equations [3] and [4], A is the ratio of web thickness to flange width, and B is the ratio of depth of the beam to distance between the inner surfaces of the flanges.

Equations [1] through [4] are plotted in Fig. 3 where it can be seen that the theoretical load-carrying capacity, that is, the extent

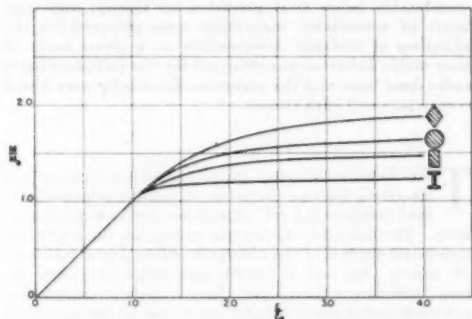


FIG. 3 THEORETICAL DIMENSIONLESS MOMENT-STRAIN DIAGRAMS SHOWING EFFECT OF BEAM CROSS SECTION

to which the load must be increased in order to produce a given deformation, is greatly affected by the shape of the cross section. To illustrate this effect further, the dimensionless moment-strain relation for a diamond cross section is also shown. It should be noted that the theoretical moment-deflection relation for a straight beam can be obtained by replacing the ratio ϵ/ϵ_y in Equations [1], [2], [3], [4] by the ratio Δ/Δ_y , if the deflection Δ is measured over a length of the beam which is subjected to a constant bending moment.

DESCRIPTION OF TEST BEAMS AND METHODS OF TESTING

Tests were made on four mild-steel straight beams with rectangular, circular, and I cross sections (two I-beams were tested) and on one rail-steel beam with rectangular cross section. Mild steels from three different sources were used in the beam tests; one source was used for the rectangular beam, another for the circular beam, and still another for the two I beams. The rail-steel ma-

terial had a carbon content of approximately 0.8 per cent. All of the steels were tested in the annealed condition.

All five beams were tested in the dead-load testing machine shown in Fig. 1. The beams were loaded by four-point loading as shown in Figs. 4, 5, 6, and 7, so as to have the center length subjected to a constant bending moment. Each beam is listed in Table 1 where the dimensions of the cross section, the span length

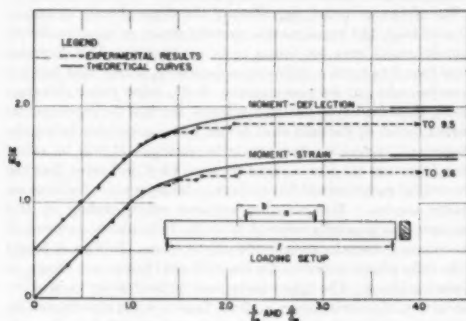


FIG. 4 DIMENSIONLESS MOMENT-DEFLECTION DIAGRAMS FOR A MILD-STEEL BEAM WITH RECTANGULAR CROSS SECTION

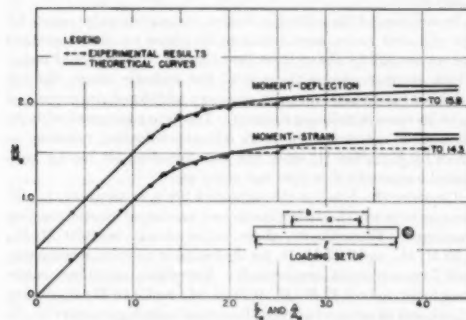


FIG. 5 DIMENSIONLESS MOMENT-DEFLECTION DIAGRAMS FOR A MILD-STEEL BEAM WITH CIRCULAR CROSS SECTION

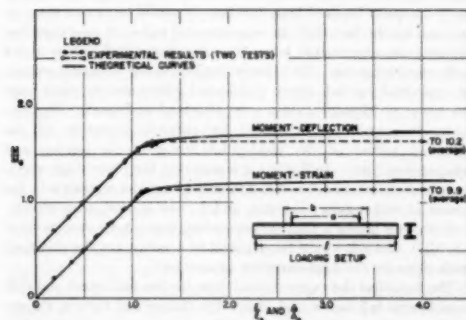


FIG. 6 DIMENSIONLESS MOMENT-DEFLECTION DIAGRAMS FOR A MILD-STEEL BEAM WITH I CROSS SECTION

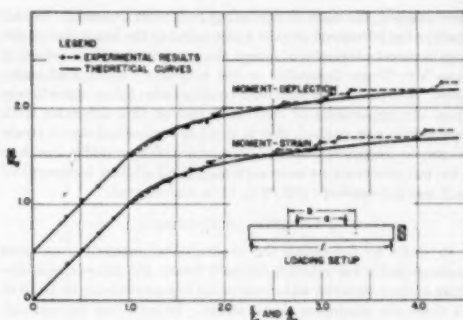

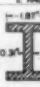




FIG. 7 DIMENSIONLESS MOMENT-DEFLECTION DIAGRAMS FOR A RAIL-STEEL BEAM WITH RECTANGULAR CROSS SECTION

l , and the length a , subjected to constant moment, are given along with other pertinent data which will be discussed subsequently.

Yielding in mild-steel beams is known to be heterogeneous (1, 4), but the average strain is known to have a linear distribution across the depth of the beam (1). Since the theoretical relations were based on a linear strain distribution, the average strains in the most strained fibers of each of the mild-steel beams were measured by SR-4 type A-9 electrical-resistance gages having 6-in. gage lengths. The strain in the rail steel was known to be reasonably homogeneous so the strains were measured by type A-11 SR-4 gages having 1-in. gage lengths. The deflection of each beam was measured by a pair of 0.0001-in. dial gages, one mounted on each side of the beam to obtain an average reading as well as to check for unsymmetrical bending. As indicated in Figs. 4 through 7, or in Table 1, the length b over which the deflection was

TABLE 1 DIMENSIONS OF BEAMS AND PROPERTIES OF MATERIALS

BEAM NUMBER	1	2 AND 3	4	5
CROSS-SECTION DIMENSIONS				
LENGTH DIMENSIONS*	l - in. 36.3 a - in. 0.31 b - in. 15.3	23.60 11.00 13.50	23.00 11.00 13.50	23.60 8.00 10.75
MATERIAL	SAE 1020	MILD STEEL	MILD STEEL	RAIL STEEL
PROPERTIES OF THE MATERIALS	E , lb./sq. in. 28,000 σ_y , lb./sq. in. 0.00094 σ_u , lb./sq. in. 0 ANF, % 2.50	28,400 0.00095 0 2.50	30,000 0.00090 0 2.50	38,400 0.00137 0.086 3.50

* l IS THE LENGTH OF SPAN, a IS THE LENGTH OF CONSTANT MOMENT SECTION, AND b IS THE LENGTH OVER WHICH THE DEFLECTION WAS MEASURED.
† n IS THE NUMBER OF TENSION AND COMPRESSION SPECIMENS TESTED.

measured was slightly longer than the constant-moment section. A comparison of the measured SR-4 strains with those computed from the deflection measurements indicated that SR-4 cement-bonded gages are reliable for measuring strains 10 to 15 times the elastic-limit strains that are held for extended periods of time.

In the beam tests in the dead-load machine, the loads were applied in increments. At the beginning of each test several loads were applied which resulted in elastic response, and from the data recorded, the elastic behavior of each beam was obtained. In adding increments of load in the inelastic range, the nuts on the safety rods (labeled A in Fig. 1) were first tightened so that the increment of load was carried by these safety rods. This procedure reduced the inertial effect in the specimen of applying the sudden increment of load. After the proper load increment had

been applied, the nuts on the safety rods were loosened. In this manner the increment of load was applied to the beam during the time interval necessary to loosen the safety-rod nuts, a period of some 5 to 30 sec depending on the magnitude of the load increment. The strain and deflection readings were taken immediately upon the application of each load and at time intervals until equilibrium was reached, that is, until no further increase in strain occurred. In general, the inelastic deformation ceased in less than 6 hr, but observations were continued, and another increment of load was not applied until 12 to 72 hr had elapsed.

PROPERTIES OF MATERIALS

In order to determine the experimental moment-strain and moment-deflection relation for each beam, the stress-strain diagram of each material was required for inelastic strains up to 10 or 15 times the maximum elastic strain. In each case tension and compression specimens were machined from the same bar of material as was the beam specimen. The tension specimens were standard $1/2$ -in.-diam round specimens with a 2-in. gage length, and the compression specimens were standard $3/4$ -in.-diam round specimens with a 1-in. gage length. The strains were measured by mechanical gages and standard testing procedures were followed throughout.

Appreciable variation was observed in the properties of the materials as found from these tension and compression tests. Therefore, in order to obtain additional stress-strain diagrams for the material near the test section of each beam, the sections near the ends of the beam which had not been inelastically deformed were cut up into tension and compression specimens after the beam had been tested. Since standard specimens could not be machined from the I-beams, two plate tension specimens having a cross section of $1/4$ in. \times $3/4$ in. were machined from the flanges at each end of the beam. In Table 1 the quantities σ_y , ϵ_y , and α (strain-hardening factor, see Fig. 2), are listed for the material in each beam along with the number of specimens tested. An indication of the scatter of the material properties is given by the quantity $\Delta\sigma_y$, which is the range of variation of the yield stress obtained from all specimens in each group.

DISCUSSION OF RESULTS

The theoretical dimensionless moment-strain curves, which are shown as solid lines in Figs. 4 through 7, were obtained using the equations previously presented. The curve, as plotted in Fig. 4 for the mild-steel beam, having a rectangular cross section, was obtained using Equation [1] with α set equal to zero. In Fig. 5 Equation [2] was used to obtain the curve for the mild-steel beam with the circular cross section. The theoretical curve, see Fig. 6, for the mild-steel I beam was obtained by using Equations [3] and [4] with constants A and B having values of 0.166 and 1.336, respectively. Equation [1] with a value of α equal to 0.081 was used to obtain the theoretical curve for the rectangular rail-steel beam as plotted in Fig. 7. In obtaining the theoretical dimensionless moment-deflection curves, the assumption was made that Δ/Δ_y was equal to ϵ/ϵ_y , so that the curves are identical to the theoretical moment-strain curves. This assumption is valid only in case the deflection is computed for a length of the beam subjected to constant bending moment. Although in the test beams the deflection was measured over a length slightly longer than the constant-moment section, the maximum error involved was calculated to be approximately 1 per cent. It will be noted that the moment-deflection diagram in each of Figs. 4 through 7 is shifted upward a distance of 0.5 (M/M_y) above the moment-strain diagram.

Readings of deflection and strain were taken at each of the various increments of load in all of the beam tests. For loads which produced inelastic deformation, these readings were taken

immediately after the load was applied and at various time intervals until the deformation ceased. For each load the bending moment was calculated and divided by the maximum elastic moment M_y , and the average strain and deflection for the beginning and end of each deformation period were divided by ϵ_y and Δ_y , respectively, the maximum elastic strain and deflection. These test points are plotted in Figs. 4 through 7 for the various beams and are connected by dashed lines.

For all beams tested, regardless of the shape of cross section or type of steel, the experimental moment-strain or moment-deflection diagrams were not found to be continuous. The diagrams were found to have a stair-step appearance, a fact that has not been brought out by investigators (5, 6), using either deformation-type or load-type testing machines. Each of the experimental curves for all of the mild-steel beams fell considerably below the theoretical curves for large inelastic strains. It will be noted that Equation [1] (for α equal to zero) (2, 4) indicates that the theoretical curves would have a horizontal asymptote for large inelastic strains. The resisting moment corresponding to this asymptote is generally referred to as the fully plastic moment or the moment corresponding to the plastic hinge. In Figs. 4, 5, and 6 the fully plastic moments for the mild-steel beams are shown as horizontal lines. The upper horizontal dashed line for each of the experimental curves shown in these figures is the experimentally determined fully plastic moment, the numbers listed at the ends of these lines gives the magnitude of the strain ratio ϵ/ϵ_y , and the deflection-ratio Δ/Δ_y when yielding ceased at the fully plastic moment.

In contrast to the mild-steel beams, the experimental points for the rail-steel beam were found to lie either on the theoretical curves or slightly above them (see Fig. 7). The rail-steel beam, which strain-hardened throughout the inelastic range, did not exhibit a fully plastic moment since any additional strain resulted in an increase in resisting moment. This is in agreement with the theoretical moment-strain and moment-deflection relations as given by Equation [1] since this equation does not have a horizontal asymptote if α does not equal zero.

Consider the data for the mild-steel beam in terms of the difference between the fully plastic and maximum elastic resisting moments. Theoretically, these values should be $0.70 M/M_y$, $0.50 M/M_y$, and $0.23 M/M_y$ for the beams of circular, rectangular, and I cross sections, respectively. Experimentally, these values were found to be $0.52 M/M_y$, $0.33 M/M_y$, and $0.16 M/M_y$, or only 77, 65, and 58 per cent of their theoretical values, respectively. As stated in the Introduction, the theoretical values can be substantiated by experimental tests if the tests are conducted without regard to the effect of time. Since many service applications involve constant loads of long duration, it would seem necessary to account for the fact that the experimental values of load-carrying capacity are appreciably lower than the theoretical values under such circumstances. This lower load-carrying capacity cannot be explained by the upper yield-point phenomenon, since only the lower yield-point values were obtained and used. Furthermore, it cannot be explained by possible variation in the observed values of the yield-point stress in the tension and compression tests. In Table 1 it is seen that the percentage variations in yield stress σ_y are 5.8, 3.0, and 4.0 for the materials in the beams of rectangular, circular, and I cross section, respectively. Calculations indicate that corresponding percentage variations of 8.8, 12.0, and 8.2 would be required to account for the observed reductions in the load-carrying capacities.

The fact that the experimental data for the mild-steel and rail-steel beams fall below and above the theoretical curves, respectively, can be attributed to the different types of inelastic deformation exhibited by the two steels. As is well known, the inelastic deformation in mild-steel members is very nonhomogeneous (1,

3, 4). On polished surfaces this nonhomogeneity can be seen in the form of the well-known Lüders' bands. The material within the boundaries of the Lüders' bands may be strained to a value several times the yield strain of the material while the surrounding material will be strained to approximately the yield strain of the material. In mild-steel beams the Lüders' bands appear as wedges extending from the most strained fibers inward toward the neutral surface. Since the point of the wedge forms a discontinuity in the material, it can be thought of as a stress raiser. Therefore, if given a sufficient amount of time, yielding will penetrate to a depth greater than that predicted by the theoretical relations which are based on the assumption of homogeneous yielding. Once the yield wedges have penetrated to a point near the neutral surface, the yielding spreads longitudinally along the beam from each of the wedges. Since the fully plastic moment is less than its theoretical value, it would seem logical that discontinuities similar to that existing at the point of the wedge are present in or along the boundary of the Lüders' bands which act as stress raisers to initiate wedges which branch from the original ones. Thus, if given sufficient time, the yielding at these stress raisers proceeds and spreads along the length of the beam under an applied moment less than the theoretical fully plastic one.

Whereas the mild steel deforms heterogeneously, the rail-steel material strain-hardens even for small inelastic strains so that the deformation is reasonably homogeneous. In view of this, Lüders' bands were not observed to occur in the rail-steel-beam test. The load-deformation characteristics of the beam were found to be more stable than the mild-steel beam for inelastic strains 10 to 15 times ϵ_y and the moment-strain and moment-deflection curves were not lowered by testing under dead loads.

It is interesting to note that the I beam is very efficient in resisting forces in the elastic range, if laterally supported, because of the effectual distribution of the material; however, it is practically useless in offering additional load-carrying capacity by allowing small inelastic strains to occur. The reason for this fact is that yielding progresses rather rapidly through the flanges of the beam and then only the small amount of material in the web is left to add any increase in the load-carrying capacity. Theoretically, yielding had penetrated only to one half the depth of the flanges in the two I beam tests when actually the strain readings indicated that the whole cross section was fully plastic.

Another of the peculiarities of dead-load testing is the time delay (7) required for the initiation of inelastic deformation at a given load. This was observed particularly in the mild-steel-beam tests. If the beam was allowed to reach a state of static equilibrium at any load which had produced inelastic deformation, a small increment of load was not found to initiate inelastic deformation until after an appreciable time delay. Typical time-deformation diagrams are shown in Fig. 8 for the mild and rail-steel beams of rectangular cross section. The two curves for the mild-steel beam were obtained for the last two load increments corresponding to the last two stair levels shown in Fig. 4. Although the load represented in Fig. 4 by an M/M_y ratio of 1.33 was the fully plastic load, inelastic deformation did not begin at this load until after 30 min had elapsed. The time delay for yielding at the lower load was approximately 15 min, the shorter delay being attributed to the fact that the previous load had been maintained on the beam for only a period of 4 hr. This time was probably not long enough for the beam to reach a position of static equilibrium, since, in general, this condition was not reached until at least a period of 6 hr had elapsed. The time delay of inelastic deformation in mild-steel beams also depends upon the magnitude of the increase in stress caused by the increment of load. The time delay has been observed for increases in stress of 1000 to 1800 psi, while other tests indicate that the time delay was eliminated when the increase in stress was 3000 psi. The curves

for the rail-steel beam in Fig. 8 do not indicate any measurable time delay for initiation of yielding. However, the time required to reach static equilibrium was approximately the same as for the mild-steel beams.

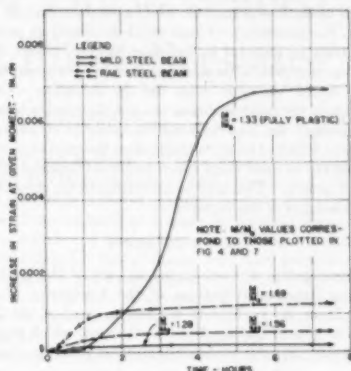


FIG. 8 TYPICAL CONSTANT-LOAD TIME-DEFORMATION DIAGRAMS FOR MILD-STEEL AND RAIL-STEEL RECTANGULAR BEAMS

SUMMARY AND CONCLUSIONS

The theoretical load-deformation relations which have been developed for members made of ductile materials, in general, do not include the effect of time on the inelastic behavior. The experimental tests performed in view of checking these relations have usually disregarded time effects since the applied loads were not maintained long enough for the member to reach a state of static equilibrium at each load. The express purpose of this investigation was to study the behavior of steel members subjected to dead loads which were maintained constant until inelastic deformation ceased before additional increments of load were applied. Four mild-steel beams with various cross sections and one rail-steel rectangular beam were tested in a dead-load testing machine. The results of the investigation are believed to be sufficient to justify the following conclusions:

1 The moment-strain and moment-deflection diagrams, Figs. 4 through 7, were found to be discontinuous and not smooth curves such as those usually reported. The diagrams were found to have a staircase form.

2 For the mild-steel beams, the experimental moment-strain and moment-deflection diagrams were found to lie below the theoretical curves that were based upon the conventional tension and compression stress-strain diagrams. This phenomenon is attributed to nonhomogeneous yielding as is exhibited by Lüders' bands. The experimental moment-deformation diagrams for the rail-steel beam were found to be located on or above the theoretical curves; this was attributed to the fact that rail steel yields in a more homogeneous manner and does not exhibit Lüders' bands.

3 For the mild-steel beams of circular, rectangular, and I cross sections reported herein the difference between theoretical values of the fully plastic and maximum elastic moments are $0.70 M/M_y$, $0.50 M/M_y$, and $0.23 M/M_y$, respectively. Experimentally, these values were found to be $0.52 M/M_y$, $0.33 M/M_y$, and $0.16 M/M_y$, or only 77, 65, and 58 per cent, respectively, of their theoretical values. These results clearly indicate that the so-called fully plastic moment, based on the assumption of homogeneous yield-

ing, gives an unsafe estimate of the ultimate load-carrying capacity of a beam.

4 When a load which has produced inelastic deformation is maintained on a mild-steel beam until a condition of static equilibrium is reached, the material builds up a resistance to immediate inelastic deformation when a small increment of load is added. For increments of load which produced an increase of stress of 1000 to 1800 psi in the most strained fibers, inelastic deformation was delayed as much as 30 min. In contrast to the mild-steel beam, the time delay for the initiation of inelastic deformation in the rail-steel beam was not observed in these tests.

5 In general, the load-deformation behavior of the rail-steel material was found to be more stable than the mild-steel material when subjected to dead loads which produced inelastic strains up to 10 to 15 times ϵ_u . This may be attributed to the strain-hardening characteristics of the material.

ACKNOWLEDGMENTS

This investigation was conducted as part of the work of the Engineering Experiment Station of the University of Illinois of which Dean W. L. Everitt is Director, and of the Department of Theoretical and Applied Mechanics of which Prof. F. B. Seely is Head. Special acknowledgment is made to Prof. J. O.

Smith, under whose supervision the project was carried out, for his continued interest and many helpful suggestions.

BIBLIOGRAPHY

- 1 "The Effect of Non-Uniform Distribution of Stress on the Yield Strength of Steel," by D. Morkovin and O. Sidebottom, Bulletin No. 372, Engineering Experiment Station, University of Illinois, December, 1947.
- 2 "An Investigation of the Inelastic Deflection of Beams," by W. J. G. Cameron, master's thesis, University of Illinois, 1948.
- 3 "Theory of Flow and Fracture of Solids," by A. L. Nadai, McGraw-Hill Book Company, Inc., New York, N. Y., second edition, vol. 1, 1950, pp. 367-368 and 512-526.
- 4 "The Initiation and Propagation of the Plastic Zone in a Tension Bar of Mild Steel Under Eccentric Loading," by J. Miklowitz, Trans. ASME, vol. 69, 1947, pp. 21-30.
- 5 "Carrying Capacity of Simply Supported Mild Steel Beams," by J. W. Roderick and I. H. Phillippe, Engineering Structures, Butterworths Scientific Publications, London, England, 1949, pp. 9-48.
- 6 "The Yield Point of Mild Steel With Particular Reference to the Effect of Size of Specimen," by J. L. M. Morrison, Journal and Proceedings of The Institution of Mechanical Engineers, vol. 142, 1943, pp. 192-223.
- 7 "The Time Delay for Initiation of Plastic Deformation at Rapidly Applied Constant Stress," by D. S. Clark and D. S. Wood, Proceedings of the American Society of Testing Materials, vol. 49, 1949, pp. 717-735.

An Experimental Investigation of Over-Straining in Mild-Steel Thick-Walled Cylinders by Internal Fluid Pressure

By M. C. STEELE¹ AND JOHN YOUNG,² URBANA, ILL.

The purpose of this paper is to study the mechanism of yielding and to compare with plastic theories strains observed at the bore and outside surfaces of mild-steel cylinders of 2:1 diameter ratio under internal fluid pressure. Observations disagree with theoretical assumptions concerning the progression of yielding; wedge regions of overstrained material, occupying a small fraction of the total volume, characterize the yielding process. Discrepancies with theory are observed in the measured strains. The fully plastic³ load-carrying capacities predicted from theory are higher than those observed in the experiments. Stability of deformation (creep) under maintained constant loads is discussed.

INTRODUCTION

THEORETICAL analyses of thick-walled cylinders subjected to internal uniform pressure have been presented by several prominent investigators (1 to 5).⁴ Accurate solutions for the all-elastic, elastic-plastic, and fully plastic cylinders are well known. Differences in treatment lie in the assumptions regarding the plastic stress-strain relations and flow condition of the plastic material. In all cases the elastic-plastic boundary is taken to be circular and the cylinder to be comprised of two regions, an inner plastic and an outer elastic one, both of homogeneous material. The yielding of mild steel is characterized by the formation of wedge-shaped veins of overstrained material, and it is doubtful whether the theories, so far presented, can describe adequately the stresses and deformations in a mild-steel cylinder.

The purpose of this paper is twofold: (a) To investigate by experiment the mechanism of yielding in mild-steel cylinders and to compare it with the conventional assumptions of the theories of plasticity; (b) to measure strains at the bore and outside surfaces and estimate the nature and extent of deviations from theoretical values. In addition, the highly important problem to the engineer, of stability of deformations (creep) under maintained loads, is brought to the fore.

WORK OF PREVIOUS EXPERIMENTAL INVESTIGATIONS

Prof. G. Cook (4) of the University of Glasgow, has contributed

¹ Research Assistant Professor, Department of Theoretical and Applied Mechanics, University of Illinois.

² Research Assistant, Department of Theoretical and Applied Mechanics, University of Illinois.

³ "Fully plastic" pressure for a mild-steel cylinder is defined as that pressure causing one or two wedge regions to reach the outside surface. At this value, the pressure versus circumferential strain curves become parallel to the strain axis.

⁴ Numbers in parentheses refer to the Bibliography at the end of the paper.

Contributed by the Metals Engineering Division and presented at the Fall Meeting, Minneapolis, Minn., September 25-28, 1951, of THE AMERICAN SOCIETY OF MECHANICAL ENGINEERS.

NOTE: Statements and opinions advanced in papers are to be understood as individual expressions of their authors and not those of the Society. Manuscript received at ASME Headquarters, June 14, 1951. Paper No. 51-F-3.

outstanding work in this field. He subjected mild-steel cylinders of varying wall ratios to internal fluid pressure and observed the changes in outside diameter, circumferentially and axially. Tensile tests of the material were made on carefully prepared specimens and tested on a special machine which recorded upper and lower yield points. His cylinders were also prepared carefully and the results showed the counterpart of upper and lower yield stress in a tension test. Discrepancies from theory were noted, and their cause was attributed to the existence of this latter phenomenon.

The existence of an upper and lower yield point for mild-steel material is well established. It is unreasonable, however, to expect close correlation to occur between a tension test and a thick-walled cylinder. The magnitude of the upper yield point in a tension test is dependent upon many factors (e.g., testing machine, surface finish, specimen shape), and such conditions are difficult to reproduce in the testing of a cylinder. In addition, the stress distributions are different, and these must have a bearing on the stability of the sudden deformation. The authors feel that, by the careful preparation of Cook's specimens, the true nature of the mechanism of yielding was masked. Muir (6) pointed out, and the authors believe quite rightly, that an overstrained cylinder of mild steel is composed mostly of elastic material with only a small volume of plastic material in the form of wedges. His argument was qualitative at the time, as the extent and number of wedges were not known. Thus one would expect that the records of changes at the outside diameter, a position remote from the yielded material, would disagree with a theory based upon homogeneous yielding. The measurement of changes at the bore surface, where yielding initiates, would help to clarify the situation, and such observations are recorded in the experimental work of this paper.

EXPERIMENTAL EQUIPMENT

Pressure Apparatus. The apparatus is designed to apply internal fluid pressures to open-ended thick-walled cylinders. In principle, a fluid is confined inside the test cylinder and compressed by means of a plunger and loading machine.

Fig. 1 shows the assembled arrangement in section. It consists of a central core *A* which fits inside the test cylinder. The core is built in two parts which enable it to be fitted without interference to electrical strain gages on the bore surface of the cylinder. Synthetic rubber O-ring seals *B* prevent leakage at the ends. A plunger *C* operates in a fitted hole, and connecting holes *D* allow the system to be filled with fluid. A load on the plunger compresses the fluid which transmits a pressure to the inside of the test cylinder. An O-ring seal on the plunger and a neoprene washer *E* at the screw thread insure a leakage-free system. *F* is a pressure-gage pipe connection of the Bridgman "unsupported-area" type. At *G*, two of eight units are shown (two per flat). They are set in the core to convey electrical leads out of the pressure area, and are shown in an adjoining detail. The load is transmitted from a compression machine to the plunger via a spherical head *H*.

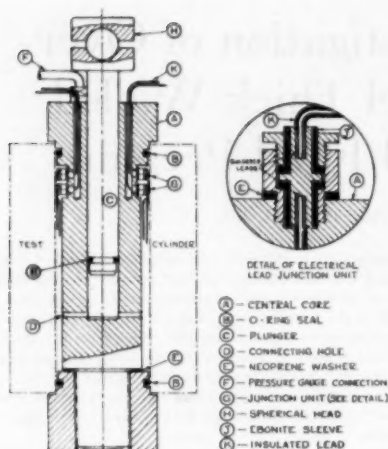


FIG. 1 SECTIONAL ARRANGEMENT OF PRESSURE APPARATUS

The test cylinder moves axially against a small amount of friction at the O-rings; nevertheless, the open-ended condition of testing is closely assimilated. The ratio of cylinder length under pressure to total cylinder length is 0.9375. The system is leakage-free, and sensitive control of the application of pressure is a feature of the apparatus.

Measuring Devices. A 25,000-psi Bourdon gage measures pressure. Its smallest division reads 100 psi, and an estimation correct to 20 psi is obtainable. The gage is calibrated against a dead-weight calibrator before and after each test.

Electrical resistance gages were used in the measurement of strain. Records were made on a standard Young bridge unit. Paper-backed gages of 1-in. gage length were used on the outside diameter of the test cylinder. Preliminary work on paper gages under fluid pressure gave unreliable results, hence bakelite gages of $1/4$ -in. gage length were used on the bore surface. Standard procedures were adopted for the mounting of all gages.

It was found that no protection was necessary for the internal gages from the fluid pressure. The effect of pressure on them was studied in preliminary work and is given in the Appendix. This work consisted of mounting gages on a rectangular strip and immersing it in the fluid under pressure. The effect of pressure was found to be small and may be allowed for by assuming Lamé's theory for the elastic strains to be correct.

Mounting of the bakelite gages requires a curing sequence consisting of a temperature treatment under a normal pressure of from 100 to 200 psi. This pressure was effected by the spring-loaded device shown in Fig. 2. Neoprene pads fastened to metal shoes containing a spring insure the necessary uniform normal pressure. This device assisted also in the accurate positioning of the gages in the cylinder.

In three of the cylinders the end faces were polished for the observation of Lüders' lines.

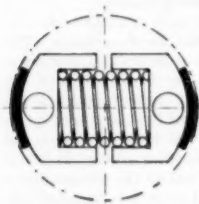


FIG. 2 SYMMETRICAL SECTION—PERPENDICULAR TO CYLINDER AXIS—OF SPRING-LOADED DEVICE FOR MOUNTING AND CURING BAKELITE GAGES

One of the cylinders was polished on the outside surface also.

Specimens. Tests were performed on four cylinders, Fig. 3. The material was mild steel and specimens were rough-machined from a hot-rolled billet, annealed at 1630 F, and cooled in the furnace. They were finish-machined to size by a sharp tool and adequate lubricant.

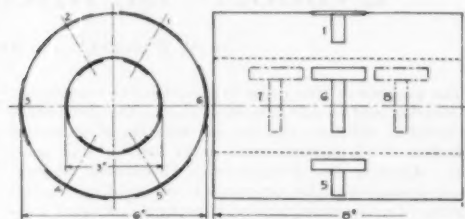


FIG. 3 TEST CYLINDER SHOWING GAGE LOCATIONS

Fig. 4(a) shows the position of cylinders taken from the billet and the material for tension tests. Tensile specimens were taken from positions, Fig. 4(b), corresponding to the bore layers in the test cylinders. They were given the same annealing treatment. Average material characteristics are shown in Table 1 for four positions in the billet. The stress-strain diagrams in tension have a sharply defined yield point as shown in Fig. 4(c).

Polishing of the cylinders for the observation of Lüders' lines consisted of grinding, followed by finishing with 00 emery cloth.

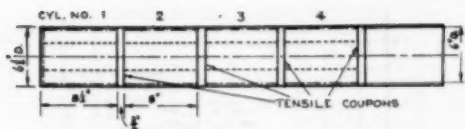
TEST PROCEDURES

Readings of strain were recorded every 500 psi in the early part of elastic straining, and 200 psi close to the initiation of yield, and in the subsequent progression of yield wedges to the outside surface. Each pressure was held for at least 15 min and longer in some cases when creep was found to be operative. For example, in cylinder No. 4 the maximum pressure was held for 100 min to study more fully the effect of creep.

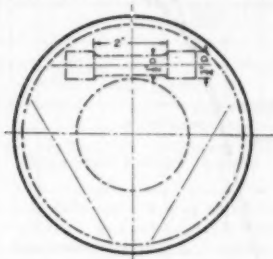
Cylinder No. 1. Four circumferential gages were placed symmetrically around the central surface of the bore. Four pairs of circumferential and axial gages were placed in corresponding positions on the outside. This cylinder was the first to be tested and the end faces were not polished for the observation of Lüders' lines. The fully plastic value of pressure was reached in one loading cycle.

Cylinders Nos. 2, 3, and 4. Gages were affixed at six symmetrical positions as shown in Fig. 3. The end faces were polished and, in the case of cylinder No. 4, the outside surface also. Cylinder No. 2 was loaded, unloaded, and then reloaded three times, each loading reaching a higher pressure and causing more yielding before the wedges reach the outside. No. 3 was taken to the fully plastic value in one cycle of loading. No. 4 cylinder was loaded to give a theoretical depth of yield corresponding to slightly more than one half the wall thickness. The apparatus was then disassembled and the Lüders' lines observed. Subsequently, the cylinder was reloaded to cause the yield wedges to penetrate to the outside and the Lüders' lines again observed.

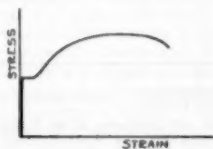
Cylinder No. 3 had additional gages placed at the quarter points, see Fig. 3. This was to decide if the cylinder length-to-diameter ratio was large enough to eliminate end effects at the measuring sections.



(a) POSITION OF TENSILE SPECIMENS RELATIVE TO LENGTH OF BILLET



(b) POSITION OF TENSILE SPECIMENS RELATIVE TO CROSS SECTION


 (c) TYPICAL TENSILE STRESS STRAIN DIAGRAM FOR MATERIAL
FIG. 4 MATERIAL TEST DETAILS

RESULTS

Fig. 5 presents the results for all the gages on cylinder No. 2. Similar variations in strain were recorded but are not shown for the remaining cylinders. Bore gage No. 5 failed near the end of the test. Outside axial gage No. 4 was found to be faulty.

In Fig. 6 the wedges observed on the polished surfaces are shown. The corresponding positions of gages marked on cylinder No. 2, apply to cylinders Nos. 3 and 4 also.

Fig. 7 is designed to show the variation in circumferential strains corresponding to the wedge regions. The dotted lines in cylinder No. 4 refer to the increase in observations made on the second loading.

Figs. 8, 9, and 10 show nondimensional plots of the averages for the bore, outside circumferential and axial strains, respectively. The bore gages for cylinders Nos. 3 and 4 failed at comparatively low pressures. This is attributed to a loosening of the bond due to using a faulty cement. The bakelite cement deteriorates with age.

Fig. 11 illustrates the effect of creep at maintained constant pressures.

DISCUSSION OF RESULTS

Measurement Techniques. A technique was developed for the measurement of bore strains in thick-walled cylinders. The effect of pressure on the gages was deduced by assuming Lamé's theory to be correct. This effect is found to be so small that it may be ignored. Consequently, all the graphs are plotted without any correction for pressure. The technique is further verified by the consistent behavior of gages on subsequent reloadings. In general, the gages fail at large strains at the bore surface in a decisive

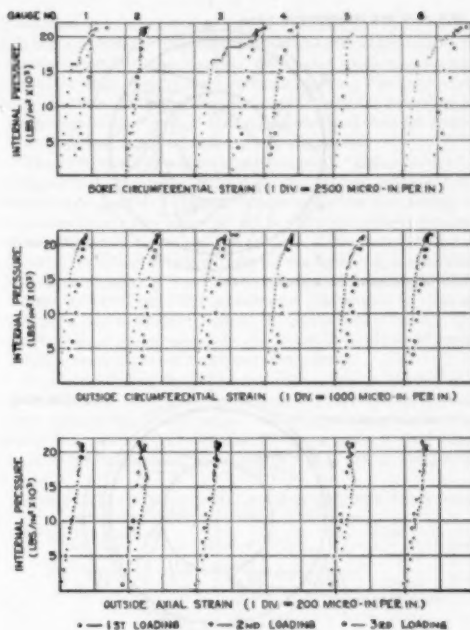


FIG. 5 STRAINS MEASURED ON CYLINDER NO. 2

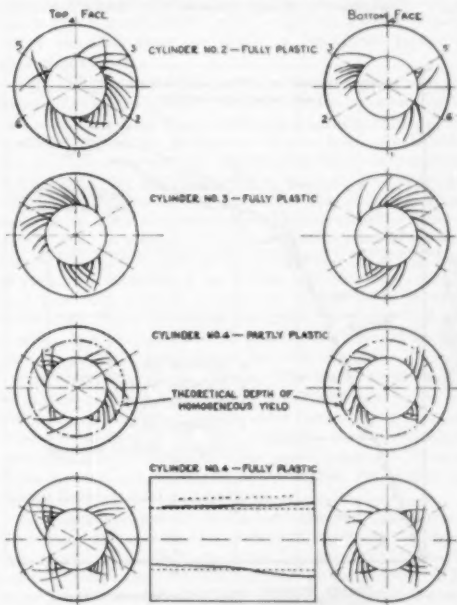


FIG. 6 LOCATION OF WEDGE REGIONS OF OVERSTRAIN

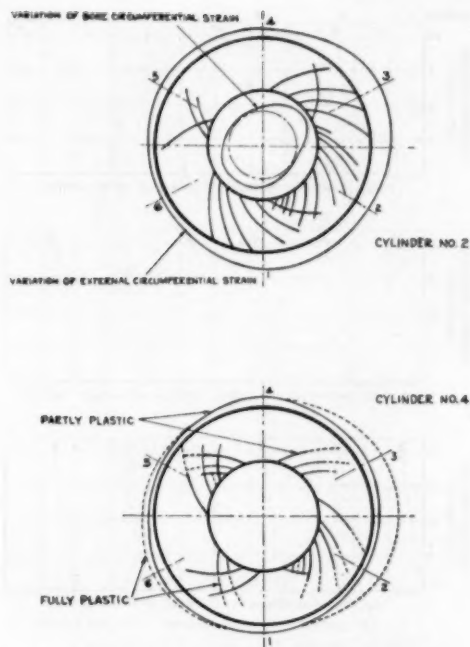


FIG. 7 COMPARISON OF WEDGE REGIONS WITH STRAIN VARIATIONS

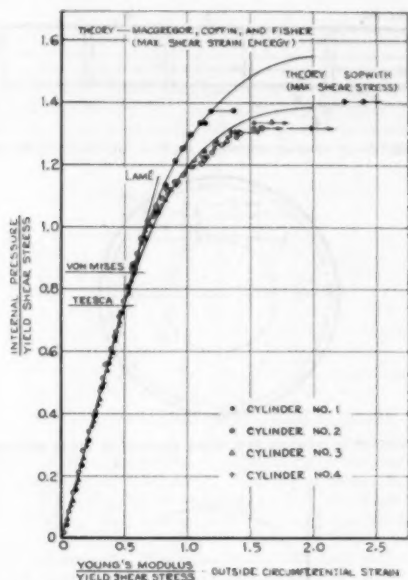


FIG. 9 COMPARISON OF AVERAGE TEST RESULTS OF OUTSIDE CIRCUMFERENTIAL STRAINS WITH PLASTIC THEORIES

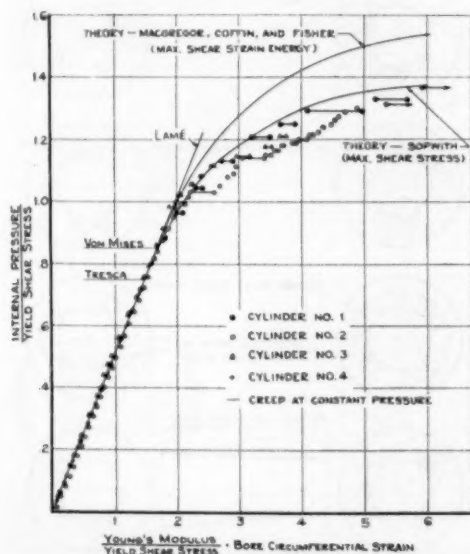


FIG. 8 COMPARISON OF AVERAGE TEST RESULTS OF BORE CIRCUMFERENTIAL STRAINS WITH PLASTIC THEORIES

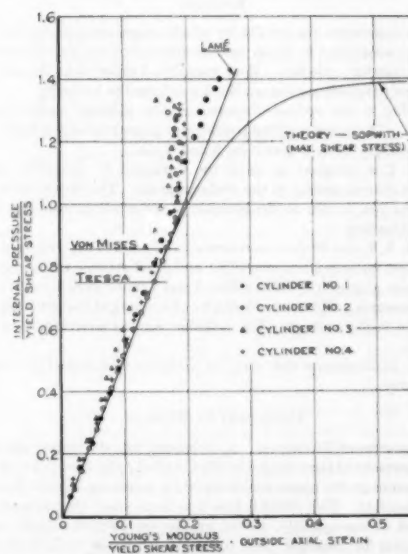


FIG. 10 COMPARISON OF AVERAGE TEST RESULTS OF OUTSIDE AXIAL STRAINS WITH PLASTIC THEORIES

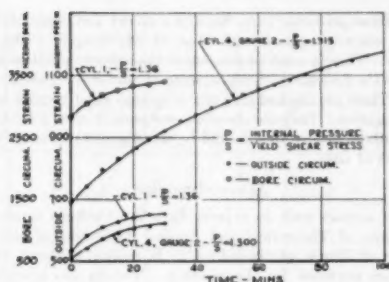


FIG. 11 EFFECT OF CREEP ON CIRCUMFERENTIAL STRAINS FOR MAINTAINED CONSTANT PRESSURE

manner at a value of pressure causing approximately the full yielding of the cylinder. As is pointed out in a previous section, however, this failure was premature for cylinders Nos. 3 and 4 owing to the use of a deteriorated cement.

The nondimensional theoretical plot for the theories assumes the cylinder boundaries to remain circular and, consequently, provide a pressure versus change-in-length relationship. The question arises, therefore, whether the average of the several strain recordings adequately describes the average change in a length dimension. This is pertinent only for a material such as mild steel where adjacent regions carry widely different strains due to the occurrence of Lüders' bands. Load-deformation tests have been performed in the Department of Theoretical and Applied Mechanics, University of Illinois, on mild-steel beams (7) with gages of different gage lengths, yet covering the same overall dimension. It has been shown that the average of several gages of small length agree with observations made over the overall dimension, even though wide variations exist among the smaller gages. It is desirable, of course, to obtain a true statistical mean, to place as many gages as possible around the circumference of the test cylinder. Space limitations allow six ($\frac{1}{4}$ -in. gage length) at the most for the size of cylinders used. It is considered that four gages are on the lower limit for obtaining a true statistical mean but six are adequate. Cook (4) measured outside-diameter changes in two positions at right angles and considered this to be satisfactory. One of the authors in some previous work (8) compared the average results from four electrical gages on the outside with mechanical measurements made at two positions at right angles. Good agreement was found and hence the measurement of average strains by four electrical gages placed equidistantly around the circumference was assumed to be sound.

In cylinder No. 3 gages were located at the quarter sections along the length, Fig. 3. The results for these gages are not presented, but they showed exactly the same strain readings (within the limits of experimental error) as the corresponding ones at the central section. It is deduced therefore that the cylinder length-to-diameter ratios are large enough to eliminate end effects at the measured sections.

The Mechanism of Yielding. It is seen from Fig. 5 that large variations in strains occur circumferentially. This is due, undoubtedly, to the existence of an asymmetrical distribution of wedge regions of overstrain. They may be studied from Fig. 6 and several important features are recognizable.

It is of practical and theoretical interest that a fully plastic condition for the cylinders is obtained with only a small volume of the material actually in the overstressed condition. This is considered important because it would be unreasonable to suggest that conventional plastic theories, based on isotropic material

properties, can describe adequately the stresses and strains existing in the cylinders. It is customary in theoretical treatments to assume a Prandtl-Reuss material (flat-topped tensile stress-strain curve) for mild steel, at least for small strains. The very existence, however, of the flat-topped curve leads to the formation of wedge regions of overstrain (Lüders' bands), and then the stress-strain relations based on isotropy become invalid.

The distribution of wedges is asymmetrical. Hence it may be deduced that the onset of yielding at the weakest point will destroy the symmetry of the arrangement and effect the yielding at other positions. If symmetry of shape and material were possible then initial yield would commence at all places round the inner boundary, and the wedges would take the form of a symmetrical orthogonal family of logarithmic spirals. It is seen that the wedges do form logarithmic spirals since the tangent to them at any point is at a constant angle to the radius to that point. The constant angle is approximately 45 deg and the wedges obviously progress along planes of maximum shear stress.

It is noticed that the position of the wedges on the top and bottom faces of the cylinders correspond. This is not too obvious from cylinder No. 2 since, as can be seen from the position from which it is taken in the billet, Fig. 4(a), a variation in yield stress must be presumed along its length. Table 1. In general, how-

TABLE 1 AVERAGE MATERIAL PROPERTIES FOR FOUR POSITIONS IN THE BILLET

Billet position numbers from left (see Fig. 4a)	Young's modulus ($\times 10^6$ psi)	Yield stress (= 2 X yield shear stress) (psi)
1	28.97	23000
2	29.6	22500
3	28.9	22000
4	30	22500

ever, the wedges extend along the length of the test cylinder from face to face. In cylinder No. 4 the wedges can actually be seen, Fig. 6, extending along the length on the outside surface in three places.

Fig. 7 illustrates the comparison of wedge regions with the measured strains. It is seen that the inner and outer boundaries take on a complex shape due to the asymmetrical nature of the straining. In addition, an important feature is shown in cylinder No. 4. There is preference for the straining due to additional load to be taken up by the propagation of originally formed wedges rather than the formation of new ones. This would not necessarily be the case if a constant pressure is maintained for hours or days on end. It is reasoned that an increase in pressure is necessary to cause further propagation of the wedges once they have stopped. The formation of new wedges, however, under constant load have been observed in mild-steel beams by Sidebottom, Corten, and Clark (9) several hours after the steady load was applied. It is concluded that the important problem of stability under a maintained load requires further investigation.

Comparison With Plastic Theories. The plastic theories shown by full lines in Figs. 8, 9, and 10 are due to MacGregor, Coffin, and Fisher (2), based upon maximum shear-strain energy flow condition and to Sopwith (3), using maximum shear stress. Both assume rotationally symmetric elastic-plastic boundaries, Prandtl-Reuss material, and isotropy in the two regions. In plotting the curves, Poisson's ratio of 0.3 is used.

Good agreement is shown for the bore circumferential strains in the elastic region and the early regions of overstrain. Cylinders Nos. 1 and 2 yield initially at a value of pressure computed on the basis of Tresca's theory of failure (maximum shear stress). This is not the case for cylinder No. 3. It is reasoned that the very nature of the yielding mechanism precludes the accurate determination of the pressure at which yield commences. The over-all

results, however, seem to favor a yield condition based on Tresca. However, if reference is made to the outside circumferential observations, Fig. 9, one is misled by an apparent linearity up to pressures even exceeding the yield condition proposed by von Mises (maximum shear - strain energy). This is especially true of cylinder No. 1 where the strains continue to lie on the curve of MacGregor, Coffin, and Fisher until the wedge regions predominate and, finally, on reaching the outside of the cylinder, conform more to the theoretical stiffness given by Sopwith.

The maximum values of pressure fall short of those predicted in Sopwith's theory and considerably more so when compared with the theory of MacGregor, Coffin, and Fisher. Thus it must be concluded that invalid theoretical assumptions do not describe adequately the behavior of mild-steel cylinders. It is of practical importance that deviations from theory are on the unsafe side.

It is seen from Fig. 10 that axial strains show large discrepancies with theory. This is to be expected in a cylinder composed largely of elastic material with only a small volume plastic in the form of wedges. The elastic strains lie to the left of the Lamé line and this may be attributed to a small amount of friction at the O-ring seals. The magnitude of the axial strains is small and the maximum deviation from Lamé is of the order of 14 microinches per in.

Time Effects. Creep of the strains under constant pressure is an important feature of the tests. After each pressure increment the load was maintained constant until creep was not apparent. The time on the average was 15 min but in some cases, especially near the fully plastic value, this time was longer. Once the wedges reach the outside surface of the cylinder, the creep persists over comparatively large periods of time. This is exemplified in Fig. 11 where it is seen that at the largest pressure ($P/S = 1.315$) in cylinder No. 4, the outside strains were still increasing after 100 min. Plots are also shown for a cylinder No. 1 gage ($P/S = 1.36$), indicating increases with time of 20 per cent and 23 per cent for bore and outside circumferential strains, respectively. In so far as can be gathered from this observation over a period of 30 min, the deformations are stabilized, but additional tests are an urgent necessity to estimate these effects over larger periods of time, even days or weeks. It may also be observed from the strain figures that at the lower pressures small creeps occur at the bore with little effect on the outside measurements. This is important in an interference-fit assembly in which the interference pressure is dependent upon the deformations of the scantling.

CONCLUSIONS

1 Techniques have been developed in this investigation to measure strains at the bore surface of thick-walled cylinders and to observe the formation and propagation of Lüders' lines on the end faces and outside surfaces. They are applied to an experimental investigation of mild-steel cylinders of 2:1 wall ratio.

2 The mechanism of yielding in mild steel is characterized by the formation of wedge regions of overstrain. The plastic material occupies a very small volume of the total. This conflicts with the conventional theoretical assumptions which predict regions of elastic and plastic isotropic material connected by a rotationally symmetric boundary. As a consequence, measured bore, outside circumferential and axial strains show discrepancies with theory.

3 Bore strain measurements predict initial yield to commence at a pressure calculated using Tresca's maximum shear-stress theory of failure. This is not observed on the outside-diameter circumferential measurements because of the afore-mentioned mechanism of yielding in mild steel.

Fully plastic (i.e., where the pressure versus strain curves become parallel to the strain axis, which corresponds to one or two wedges reaching the outside surface) values of pressure are lower

than those predicted from Sopwith's theory and considerably in error when compared with that of MacGregor, Coffin, and Fisher. Thus it must be concluded that theory predicts unsafe values for the load-carrying capacity of mild-steel cylinders.

4 There are marked time effects (creep) which require further investigation. They are observed over periods up to 100 min, but the authors believe they should be investigated over much longer periods of time.

ACKNOWLEDGMENTS

The authors wish to express their indebtedness to the Department of Theoretical and Applied Mechanics of the University of Illinois, of which Prof. F. B. Seely is the head, for the facilities provided for the research. Thanks are extended to Prof. J. O. Smith for his active interest in the work, and to Dr. C. K. Liu and Mr. T. M. Ellessor for their generous assistance.

The work was performed as part of a contract sponsored by the Wright-Patterson Air Force Base, Dayton, Ohio, Contract AF 33(038)-15677.

BIBLIOGRAPHY

- 1 "The Theory of Combined Plastic and Elastic Deformation With Particular Reference to a Thick Tube Under Pressure," by R. Hill, E. H. Lee, and S. J. Tupper, *Proceedings of the Royal Society of London, series A*, vol. 191, 1947, p. 278.
- 2 "Partially-Plastic Thick-Walled Tubes," by C. W. MacGregor, L. F. Coffin, Jr., and J. C. Fisher, *Journal of the Franklin Institute*, vol. 245, 1948, p. 135.
- 3 "The Stresses and Strains in a Partly-Plastic Thick Tube Under Internal Pressure and End Load," by D. G. Sopwith, presented at the seventh International Congress of Applied Mechanics, England, 1948.
- 4 "The Stresses in Thick-Walled Cylinders of Mild Steel Overstrained by Internal Pressure," by G. Cook, *Proceedings of The Institution of Mechanical Engineers*, vol. 126, 1934, p. 407.
- 5 "Theory of Flow and Fracture of Solids, vol. 1," by A. Nadai, McGraw-Hill Book Company, Inc., New York, N. Y., second edition, 1950, pp. 458-472.
- 6 J. Muir, see discussion in reference (4).
- 7 Unpublished work by H. T. Corten and M. E. Clark, Department of Theoretical and Applied Mechanics, University of Illinois.
- 8 "On the Overstraining of Thick-Walled Cylinders Under Internal Fluid Pressure and Under Interference Fit Pressure," by M. C. Steele, Dissertation, University of Glasgow, Scotland, 1951.
- 9 Unpublished work by O. M. Sidebottom, H. T. Corten, and M. E. Clark, Department of Theoretical and Applied Mechanics, University of Illinois, Urbana, Ill.

Appendix

Preliminary tests were performed to estimate the effect of fluid pressure on the bakelite gages used to measure bore strains. They consisted of cementing three gages onto a rectangular strip and

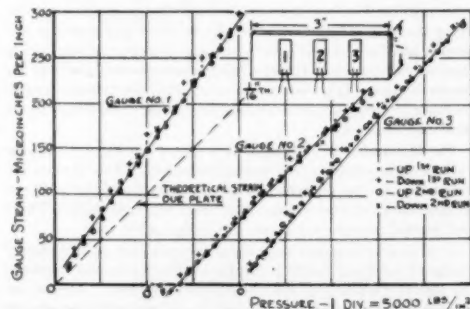


FIG. 12 EFFECT OF PRESSURE ON 3 BAKELITE STRAIN GAGES

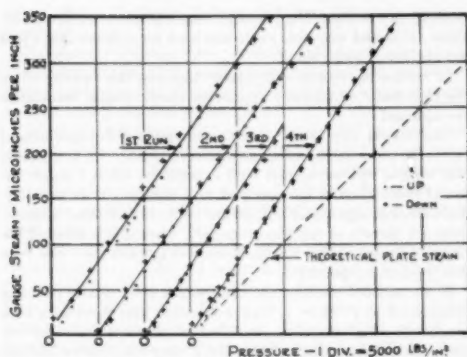


FIG. 13 REPEAT PRESSURE TESTS ON NO. 1 GAGE

subjecting the whole to pressures up to 25,000 psi (maximum cylinder pressure used was 21,350 psi).

Results are presented in Figs. 12 and 13. Fig. 12 shows comparative results from two test runs for the three gages. Fig. 13 shows results from several test runs for one gage, in order to investigate the effect of repeating the pressure cycle. Four factors emerge as follows:

- 1 There is a small pressure effect causing a compressive strain from 2 to 5 microinches per in. per 1000 psi.
- 2 Small variations in pressure effect exist among gages. These differences and also the total pressure effects are small compared to the circumferential bore strains in a cylinder of 2:1 wall ratio.
- 3 In all cases the gages show linear response over most of the pressure range. This factor enables the pressure effect to be deduced accurately in the elastic range of the straining of a cylinder and by extrapolation for pressures causing overstraining.
- 4 There is a marked consistency for any one gage which is subjected several times to the pressure cycle. No permanent set or creep was noticed and it may be concluded that a gage behaves in a stable and consistent fashion under the fluid pressure.

Discussion

A. M. FREUDENTHAL.⁶ This paper represents an important contribution to the theory of plasticity and merits the attention particularly of those workers in the field who tend to confuse the inelastic behavior of metals, in particular of mild steel, with that of the isotropic, homogeneous, ideal plastic body. Its results support the engineering point of view that the progress being made in developing the incremental mathematical theories of the ideal plastic body (flow theories) has relatively little bearing on problems of elastically contained plastic deformation, as exemplified by the thick-walled cylinder. It is fairly obvious that the sharp break in the stress-strain diagram characteristic of the ideal elastic-plastic body is, in reality, closely associated with a pronounced anisotropy of the insetting plastic deformation (glide wedges). Hence, instead of the theoretically assumed radially spreading plastically deformed isotropic regions, the deformation proceeds along spiral-shaped wedges, a number of which reach the surface far in advance of any quasi-isotropic region that might be formed by the coalescence of a large number of short wedges. Therefore it is not surprising that the limiting pressures at

which the elastically contained plastic deformation is transformed into plastic flow is, in all cases, lower than the pressure values predicted by the theories of the isotropic plastic body. It is also characteristic that the discrepancies are much higher along the bore where the strains are essentially plastic, than along the outside circumference where deformations are averages of elastic and plastic components, and the discrepancies become significant only when the plastic wedges have almost reached the surface.

The conclusions reached in the paper support the view that the design of mild-steel parts and structures on the basis of the so-called "theory of limit design," based on the ideal plastic body, results in an overestimate of the total carrying capacity. This carrying capacity represents one extreme (maximum), while the carrying capacity, based on the conventional elastic theory, represents the other (minimum). The actual carrying capacity will be somewhere between the extremes; previous investigations,⁶ as well as the results of this paper suggest that the mid-point between the extremes might be a reasonable engineering value.

A. S. T. THOMSON.⁷ The writer has read this paper with very particular interest since Mr. Steele is a member of the staff of this department on two years' leave of absence in the United States, and Mr. Young is a former member of staff. The experimental work described in the paper is an important contribution to the subject of plastic flow, and the authors are to be congratulated on their fine achievement.

It may be of interest to record how this advance in quite fundamental knowledge has developed from what was essentially a very practical problem. Some years ago the British Shipbuilding Research Association asked this department to carry out an investigation into the causes of failure in the shrink fits of built-up marine-engine crankshafts. Before facing the task of dealing with full-scale shafts, various series of small-scale experiments with simple fitted rings and plugs were undertaken. These covered a wide range of fit allowances and it was assumed that the grip could be related to the fit—other factors constant—through the medium of the usual theoretical relations, such as those of Sopwith, which the authors use for comparison with their results. But correlation on these lines proved quite impossible and it was soon realized that these shrink-fit experiments were either producing new evidence or involved new factors.

Assemblies of this type form a self-straining arrangement and neither internal pressure nor internal strain can be measured directly. It was obvious that the system had to be broken down into less complex elements. The departmental research team, under the leadership of Prof. A. W. Scott and Dr. C. M. Moir, decided, therefore, to investigate bore strains in cylinders subjected to internal fluid pressure. This problem was delegated to Mr. Steele who was then a member of the team, and an apparatus similar to the one described in the paper was designed and constructed. Mr. Steele continued the work in the United States and it is gratifying to note that the early difficulties have been overcome so successfully.

There are many aspects of these results that will doubtless arouse interest and discussion. The divergences from accepted theory are rather surprising in nature and extent and the demonstrations of measurable creep effects in yield are both new and significant. But the features of most interest to the authors' previous associates in this department lie in the observation of Lüders' lines and the discussion of their characteristics. This

⁶ "The Inelastic Behavior of Engineering Materials," by A. M. Freudenthal, John Wiley & Sons, Inc., New York, N. Y., 1950, pp. 496-500.

⁷ Professor and Head of the Department of Civil and Mechanical Engineering, The Royal Technical College, Glasgow, C. I., Scotland.

⁶ Professor of Civil Engineering, Columbia University, New York, N. Y.

immediately brings into the forefront of this subject the conception of the mechanism of yield originally propounded by the late Professor Muir who occupied the Chair of Natural Philosophy in this college until 1938. As a consequence of close study of progressive yield in bending he advanced the explanation of yield in fine wedge formations with the main body of the material behaving elastically.³ On the appearance of Professor Cook's paper, authors' bibliography (4), he extended this conception to the case of the cylinder, without having specific experimental evidence to quote in support. It was then he made three statements that may now be considered prophetic although then classed as opinionative. In effect, these statements amounted to (a) the assertion that plasticity was initiated by the formation, and progressed by the extension, of fine wedges of fully yielded material; (b) that the amount so affected was very small and so the cylinder was mainly composed of elastic material; (c) that the chance that decided the wedge positions implied nonsymmetrical straining of the wall. These may require qualification or modification but in the light of the authors' observations they would appear to be fundamentally sound. The theory of the partially overstrained thick cylinder will require that some attention be given to these ideas. As it stands at present, it is incapable of incorporating any one of them. But it is not the least of the authors' achievements that they have by their new experimental work justified and substantiated the ideas of one whose knowledge in this field was impressive and whose physical insight was always sound.

C. M. MOIR.³ The relationship between bore strain and internal fluid pressure has never been obtained experimentally. The production of such evidence is an achievement of supreme importance. The authors are to be congratulated in presenting these results.

In addition to the gage records, diagrammatic sketches of Lüders' lines on the ends of the cylinders are shown. The appearance of these lines is perhaps surprising, especially on a plane where there is neither bore pressure nor axial pressure. It is doubtful whether these observed effects at this section are representative of what is occurring at the center where there are both axial and radial pressures on a plane section.

The phenomenon is not, of course, new. It is referred to both by Cook and Muir in the former's paper (4). The fact is, however, that it has not received the degree of attention which it demands. The formation of these wedges, together with the idea of elastic behavior incorporating a shear-stress condition for the body of the material in which flow has taken place, are the particular assumptions required in developing a theory.

The authors appear unwilling to accept the upper yield in steel against the evidence of their own results. The suggestion that it is more difficult to obtain the upper yield in steel in the testing of a cylinder than it is in testing a simple tensile specimen is definitely not correct. One cannot agree that the careful preparation given to his specimens by the late Professor Cook of Glasgow University masked the mechanism of yielding.

If the authors study their bore-gage results carefully, they will notice that the break in the initial linear variation comes on at a ratio of internal pressure/initial yield stress = unity. This is 1.33 times greater than that given by Tresca, which the authors appear to favor. The break is also reproduced faintly in the external gage readings.

Professor Cook obtained similar results in all his six tests of carefully prepared specimens. Perhaps the authors might com-

ment on the fact that No. 1 tensile coupon gives such a low-yield-stress value and why this value was used for cylinder No. 1 and not also for cylinder No. 2.

In comparing results with plastic theories, the authors stress the fact that "rotationally symmetric elastic-plastic boundaries are assumed."

The reasons why theory fails to correspond with experimental values lie more in the other assumptions made. It is expected that results will correspond with experiment when a single rational assumption is incorporated in a theory. It is most improbable that agreement will obtain when two or three assumptions are thrown in together, especially when one is selected because of its suitability for mathematical gymnastics. See Sopwith's paper, reference (3).

If the authors consider the axial strain after plastic flow has commenced at $P/sy = 1$, they will notice that it remains at a practically constant value—an effect of plasticity. If they examine the axial gages in cylinder No. 2, they will observe that the second and third loadings give smaller readings than those during the first loading, due, of course, to the elastic reversion obtained from the first unloading. All this is due to the fact that after plastic flow is initiated at $P/sy = 1$, the axial strain remains unchanged, an experimental fact on which the authors make no comment. The corresponding feature is shown in Professor Cook's experiments in which the cylinders had closed ends.

The use of the term "slow yielding" is preferable to that of creep, and "slip planes in elastic material" gives a better picture of what is taking place in the material which is not strictly in plastic condition.

It is surely not permissible to use the word "creep" except to bodies which are completely plastic. In a partly plastic cylinder, where the outer material is elastic, there can be no creep and the "time" effect is simply the slow yielding of the inner plastic material which will continue until conditions of equilibrium are attained.

The outstanding merit of this paper lies in its suggestion that all established analytical developments, which are based on uncertain premises, cannot be readily applied to mild steel. This is a very important challenge to make and may perhaps be the first step in giving a physical explanation of plastic flow with the possibility of the theory being presented to engineers stripped of elaborate mathematical symbolism.

AUTHORS' CLOSURE

The authors are grateful to Professors Freudenthal and Thomson for their interesting comments. The main feature emerging from the paper and the discussion lies in the discrepancies existing between the ideally plastic theories and experiment, resulting from the mechanism of yielding in mild steel. The authors do not claim this as being a new discovery, but rather an old phenomenon brought to the fore.

The question arises as to the steps which should be taken to provide the practicing engineer with a theory, which, by taking account of the physical aspects of wedge initiation and propagation in a nonuniform stress field, more closely represents the behavior of an overstrained part. Presumably this could be attacked in two ways. First, by including in the theory the observed mechanism of yielding. Thus an analysis for wedge regions of overstrain embedded in an elastic medium would have to be considered, and, so far, this problem has proved exceedingly difficult. Second, by a modification of existing theories to correct for the false assumptions concerning the mechanism of flow. The latter approach would be, of course, empirical but may be successful for problems in "limit design," since the methods employed are usually independent of the "limiting force actions," the values of which could easily be corrected to agree more closely with ob-

³ "Overstraining of Steel by Bending," by J. Muir and D. Binnie, *Engineering*, Dec. 19, 1926, p. 743.

³ The Royal Technical College, Glasgow, Scotland.

served fact. Professor Freudenthal has indicated such an approach.

The authors welcome most cordially Professor Thomson's remarks on the origin of the work, since mention of the preliminary studies, carried out at the Royal Technical College in Glasgow, was regrettably omitted in the paper.

Dr. Moir's comments are greatly appreciated in view of his close association with the problem of thick-walled cylinders over the last few years. Several controversial issues have been raised and although space does not permit a complete discussion of all the points, an attempt will be made to support the interpretations given in the paper.

With regard to the query raised concerning the wedges on the two ends of the cylinder not being representative of conditions at the center, Dr. Moir is referred to the lower diagram of Fig. 6. Here it is seen that three Lüders' lines appear on the polished outside surface of cylinder No. 4. Two of them extend the length of the cylinder to match up with wedges appearing on the end faces. The third extends (shown dotted in Fig. 6) slightly over three quarters of the cylinder length, and it too is seen to agree with a wedge appearing on each of the end faces. If Lüders' lines on the two ends were not representative of conditions at the center of the cylinder, it would be expected to find many more axial lines of varying length near the center on the outside surface. Fig. 6 shows that this is not the case. It is recalled that 94 per cent of the cylinder length was under pressure and this undoubtedly has a bearing on the question under discussion. It is agreed that the end planes may not show exactly what happens at the center, but they certainly are representative.

The authors regret that Dr. Moir misread their remarks concerning the upper yield point of mild steel. They merely stated that it was considered unreasonable to expect close correlation to obtain between the upper yield point in a tension test and its counterpart in a thick-walled cylinder. It is well-known¹⁰ that the upper yield point in a tension test is dependent on certain factors (e.g., testing machine, surface finish, specimen shape, speed of loading) and these factors are not likely to be reproduced closely in the testing of a cylinder. The authors maintain that the careful preparation of Cook's specimens threw emphasis on the upper-yield-point phenomenon rather than the mechanism of flow and in this respect they either "masked the mechanism of yielding" or the investigator chose to ignore it.

The bore gage results, when plotted out to a larger scale, indicate deviation from linearity at a value of P/S (ratio internal pressure to yield shear stress) less than unity, the figure Dr. Moir

has selected. However, the very nature of yielding in a cylinder which has a commercial finish (i.e., chance distribution of stress raisers—see Professor Thomson's discussion) is such that the initial deviation from the elastic line is slight. At some stage (constant pressure, following an increment of load), which the authors believe is dependent on the chance formation of previous wedges, a minor "chain reaction" occurs which is defined by the formation of new wedges (and possibly extension of old ones) and is due to the highly unsymmetrical stress distribution within the cylinder. The chain reaction ceases when the redistribution of stress is sufficient to produce equilibrium. This is noticed at various values of P/S , Fig. 8, and it should be emphasized that attainment of the equilibrium condition requires at least fifteen minutes and that no sudden process is envisaged. The argument is a consequence of the observed mechanism of flow, and the effects of wedges in a nonuniform elastic stress field would have to be taken into account if any correspondence to upper yield in a tension test were sought.

Tensile coupons removed from the billet, Fig. 4, showed a variation of yield stress to exist near the ends of the billet. Consequently, the yield stress varied along the lengths of the first two cylinders as observed by the authors, and tensile coupon No. 1 does not give a representative yield stress for all the material in cylinder No. 2.

Dr. Moir's remarks on the various theoretical assumptions are not fully understood. The mathematical theory of plasticity predicts closely, observations made on specimens with uniform stress fields (e.g., thin-wall cylinder under combined stress). The observed discrepancies between theory and experiment for non-uniform stress fields must be attributed to an invalid extension of one or more of the assumptions used for members, which have no stress gradient. In view of the completely different conception, between theory and experiment, of the mechanism of flow for the ideally plastic material, it seems reasonable to conclude that this may be an important factor in the interpretation of discrepancies.

The authors believe that the important conclusion regarding the axial-strain results is that straining in the axial direction is essentially elastic and does not resemble even closely the plastic theory. It is agreed that the observed axial strains remain approximately constant after the wedges have penetrated the cylinder wall so far, but the experimental evidence was considered insufficient to draw any general conclusions.

Dr. Moir's exception to the term "creep" is understandable in that it is not used in accordance with its usual technical meaning. It is not agreed, however, that the term creep can be used only for bodies that are completely plastic. Clearly, creep within wedges is a plastic phenomenon even though the outer restraining material is elastic.

¹⁰ See Bibliography (5), chap. 19.

Dynamic Properties of Nodular Cast Iron¹— Part I

By HARRY MAJORS, JR.,² UNIVERSITY, ALA.

This paper presents the experimental results of an investigation on the mechanical properties of magnesium-treated nodular cast iron in the annealed and as-cast condition. The dynamic stress-concentration factors are compared with Neuber's theoretical factors for hyperbolic notches, with Peterson's results on steel, with Frocht's photoelastic results, and with Grant's data on flake cast iron and cerium-treated nodular iron. Fatigue results are shown for square and 45-deg V-shaped notches at speeds of 200 and 6000 rpm, as well as for various notch depths. The trend in size effect is indicated. Static damping capacities obtained from hysteresis loops in tension and compression are compared with torsional damping capacities and static damping capacities from bending.

INTRODUCTION

WHEN any new engineering material enters into widespread application, a number of properties are necessary for use in design, as well as being of scientific interest. In all probability (1)³ nodular iron will be produced at a rate of 2,000,000 to 5,000,000 tons annually within the next few years, taking an important place in the industrial economy. Among the many physical properties that must be obtained for a material in order to ascertain its engineering usefulness, the dynamic properties are the most difficult. Even though there has been much work on the effect of notches on the endurance limit of steels, very little systematic information is available on the effect of notch depth, notch radius, and notch angle on the dynamic stress-concentration factor. Peterson (2) was one of the earliest to present some of this information for steels. Of course, none of these are known for nodular iron, although Grant (3) reported some results for flake and acicular cast iron; and cerium-treated nodular iron for a 45-deg-notched fatigue specimen with a 0.03-in. root radius, and for a grooved fatigue specimen with a 0.05-in. radius, both notches having the same depth and shank diameter. No results were tabulated for notched magnesium-treated nodular iron. In the several conclusions that were stated by Grant, the following are of interest for comparison:

(a) The endurance ratio of unnotched flake-graphite irons decreased from 0.46 to 0.34 as the nominal tensile strength increased from 36,000 to 68,000 psi.

(b) The endurance ratios of cerium-treated nodular irons

varied from 0.59 to 0.46 for tensile strengths of 48,000 to 80,000 psi.

(c) The endurance ratios of magnesium-treated irons varied from 0.45 to 0.38 for tensile strengths of 54,000 to 90,000 psi.

(d) There was almost no notch sensitivity in the 36,000-psi tensile flake-graphite iron, but the notch-sensitivity factor increased with the higher-strength irons. The dynamic stress-concentration factor for the 68,000-psi tensile acicular iron with a 45-deg V-notch, 0.03-in. root radius was 1.35.

(e) Nodular irons were much more notch-sensitive than flake-graphite irons.

Similar ratios of endurance limit at 10,000,000 cycles to the nominal tensile strength were reported by other investigators, Table 1, for untreated cast irons having diameters about 0.35 in.

TABLE 1 RATIOS OF ENDURANCE LIMIT TO TENSILE STRENGTH

Investigator	Ratio, Endurance limit Tensile strength
Moore and Lyon (4).....	0.35 to 0.46
Thum and Ude (5).....	0.35 to 0.45
Kommers (6).....	0.38 to 0.57
Dasech (7).....	0.41
Lorig and Schnee (8).....	0.41 to 0.47
Collins and Smith (9).....	0.38 to 0.44

Kommers (10) presents the trend in the stress-concentration factor with increasing tensile strength as indicated in Table 2 for flake cast iron having square notches.

TABLE 2 STRESS-CONCENTRATION FACTORS

Nominal tensile strength, psi	Endurance limit, plain specimens, psi	Dynamic stress- concentration factor, K_f
20000	9300	1.00
23200	11800	1.05
30300	15000	1.10
33600	22000	1.40
37100	19500	1.20
42500	24100	1.26

The size effect of the endurance limit of magnesium-treated nodular iron was reported by Eagen and James (11), who obtained low endurance ratios of 0.32 to 0.34 for 1-in.-diam test pieces machined from 2-in.-thick walls. There is no size effect on the endurance limit of ordinary cast iron as reported by Peterson (25).

Recently, attention has been directed to low-speed effects upon the fracture line of laboratory fatigue tests (12), namely, speeds under 200 rpm. Smith, Brueggeman, and Harwell conducted axial fatigue tests on 0.032-in.-thick flat-sheet specimens of bare and Alclad 24S-T3 aluminum alloy where the frequency was 12 and 1000 cycles per min (cpm). The tests showed that the fatigue strengths were slightly less when tested at 12 cpm, the data tending to fall to the left edge of the scatter of those made at 1000 cpm.

When tests are conducted in the range 1000 to 10,000 cpm, only a negligible difference is observed (13). Freudenthal and Dolan (14) point out that on metals possessing a low melting point some

¹ This investigation was started in December, 1949, under the sponsorship of the University of Alabama Research Committee.

² Director, Research Experiment Station, University of Alabama. Mem. ASME.

³ Numbers in parentheses refer to the Bibliography at the end of the paper.

Contributed by the Metals Engineering Division and presented at the Fall Meeting, Minneapolis, Minn., September 25-28, 1951, of THE AMERICAN SOCIETY OF MECHANICAL ENGINEERS.

NOTE: Statements and opinions advanced in papers are to be understood as individual expressions of their authors and not those of the Society. Manuscript received at ASME Headquarters, May 3, 1951. Paper No. 51-F-5.

observations show an appreciable reduction in endurance limit under very slow repetition of load.

No data showing the speed effect have been reported for magnesium-treated iron.

Damping capacity first acquired prominence in German literature a little over 25 years ago, when the term "Dämpfungsfähigkeit" in reference to metals was made popular by O. Föppl (15), and correlations of this property with fatigue endurance were attempted. American technical literature contains no reference to damping capacity until about 1928 (16), and the bibliography furnished in Brophy's (18) paper shows a limited research activity. Several investigators (17) have shown that the damping characteristics for a material do not become stable until it has been subjected to a cyclic stress of several million stress reversals. The author (19) has subjected low-carbon-steel torsion rods to cycles of plastic torsion and found that the loops rapidly stabilized after four cycles into a constant area and shape.

All new engineering materials should be tested for damping capacity at high and low stresses, as well as for the static properties and dynamic properties of notch sensitivity. Damping-capacity values are a direct measure of the ability of a material to dissipate vibrational energy (20). Evidence is beginning to accumulate on the relation of damping capacity to other well-known physical properties, and many workers are aware that damping capacity is structure-sensitive (21, 22, 23, 24).

TEST PROGRAM

In the light of this literature review, a series of tests were planned to determine the following effects on magnesium-treated iron:

- Comparison of static tensile properties in the as-cast condition with the annealed condition.
- The effect of rotating fatigue specimens at 200 and 6000 rpm upon the fracture line of stress versus cycles of stress reversal.
- Effect of notch depth with constant notch angle and radius upon the endurance limit for a square notch and 45-deg notch angle.
- Effect of size of test specimen upon the endurance limit.
- Comparison of specific damping capacity by various methods.

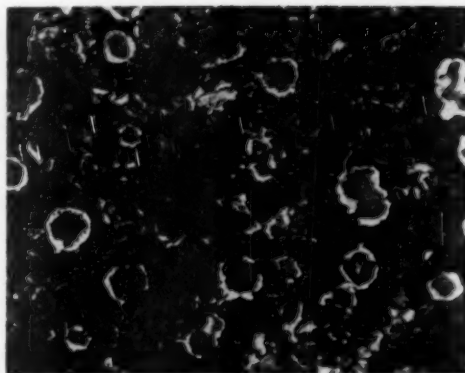
TYPE OF CAST IRON TESTED

The magnesium-treated iron used in these experiments was provided by the American Cast Iron Pipe Company. It was cast on 4-21-49 (ladle 2) in the form of plates 5 in. \times 10 in. \times $\frac{1}{4}$ in., having the following analysis:

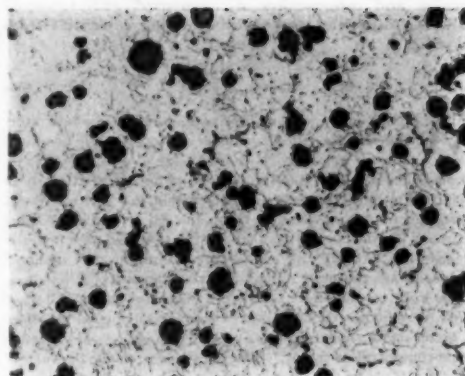
	Per cent
Total carbon	3.80
Silicon	2.79
Manganese	0.37
Sulphur	0.022
Phosphorus	0.07
Magnesium	0.039
1.33 per cent Cu-Mg (70-30) added to ladle	

Fig. 1 shows the structure of the magnesium-treated iron in the as-cast condition and annealed condition. The following heat-treatment was used to obtain the annealed condition with a Brinell hardness of 170 yielding a ferritic structure:

15 hr at 1400 F
Cooled from 1400 F to 1000 F in 3 hr
Air cooled



(a)



(b)

FIG. 1 MAGNESIUM-TREATED-IRON PLATES, 6 IN. \times 10 IN. \times $\frac{1}{4}$ IN.

(a, graphite nodules in an almost entirely pearlitic matrix; as-cast. b, matrix entirely ferritic; annealed. Nital etch; \times 100.)

TESTING PROCEDURE FOR FATIGUE

The fatigue tests were carried out on a 140-in.-lb Krouse, rotating cantilever fatigue testing machine at zero mean stress per cycle. Two speeds of testing were used: 6000 rpm for the majority of the tests, and 200 rpm to determine the speed effect on the fracture line for specimens having 0.25 in. shank diameter. Specimens having shank diameters of $\frac{1}{4}$ in. and $\frac{1}{2}$ in. were used only to note the size-effect trend. Part 2 will consider further the effect of size on the plane and notched specimens.

Figs. 2 and 3 show the general shape of specimens used in determining the physical properties and size effects. Figs. 4 and 5 show the static stress-strain curves in tension and torsion, respectively.

TEST RESULTS ON FATIGUE

Speed effects are shown for plane and square notched specimens ($d/D = 0.60$) in the annealed and as-cast condition in Figs. 6 and

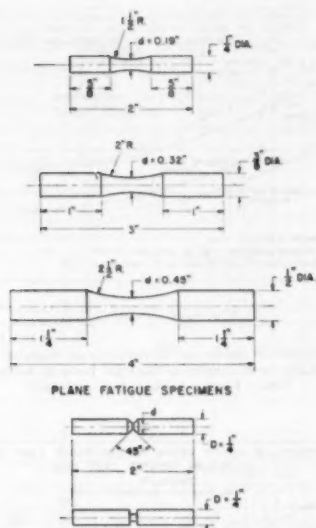


FIG. 2 PLANE AND NOTCHED FATIGUE-TEST SPECIMENS

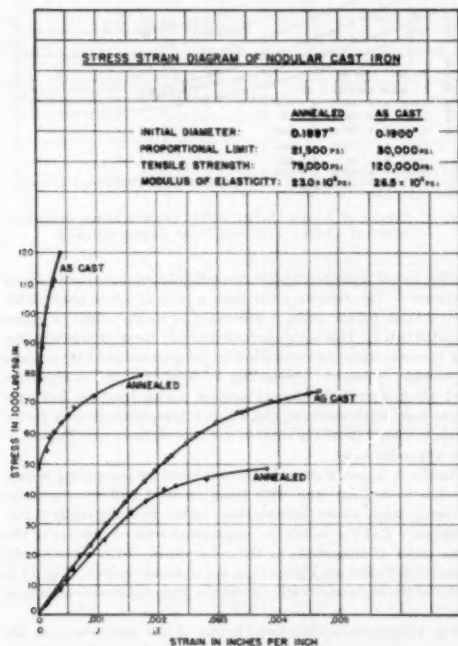


FIG. 4 TRUE STRESS-STRAIN DIAGRAM IN STATIC TENSION OF NODULAR CAST IRON IN THE AS-CAST CONDITION AND ANNEALED CONDITION

[As-cast condition specimen was obtained from keel block No. 2804 (AC1PO). Annealed specimen obtained from plate material (see page 366 and Fig. 35 of author's closure on page 380 of this issue).]

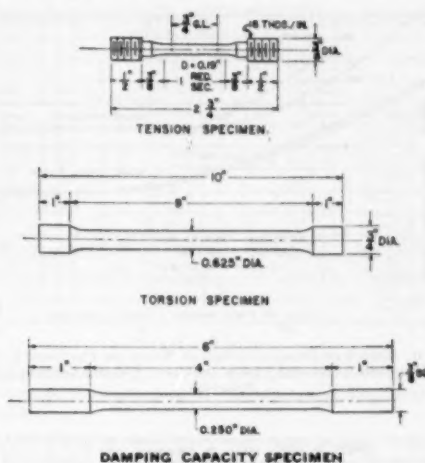


FIG. 3 SPECIMENS USED FOR STATIC TENSION AND TORSION PROPERTIES—DIMENSIONS OF TORSIONAL DAMPING-CAPACITY SPECIMEN

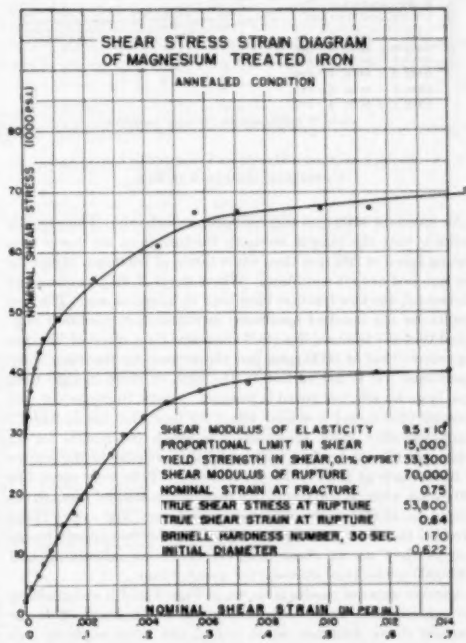


FIG. 5 STATIC SHEAR-STRESS DIAGRAM OF ANNEALED MAGNESIUM-TREATED IRON

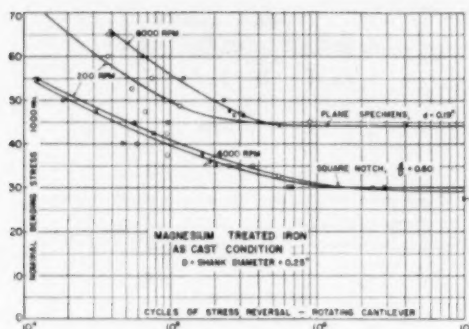


FIG. 6 EFFECT OF SPEED AND SQUARE NOTCH ON FRACTURE LINE OF MAGNESIUM-TREATED IRON AS-CAST UNDER ALTERNATING STRESSES

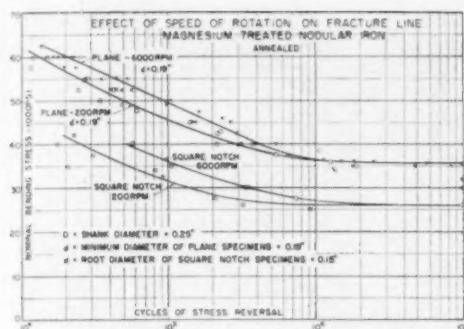


FIG. 7 EFFECT OF SPEED OF ROTATION AND SQUARE NOTCH ON FRACTURE LINE OF MAGNESIUM-TREATED IRON IN ANNEALED CONDITION UNDER ALTERNATING STRESSES

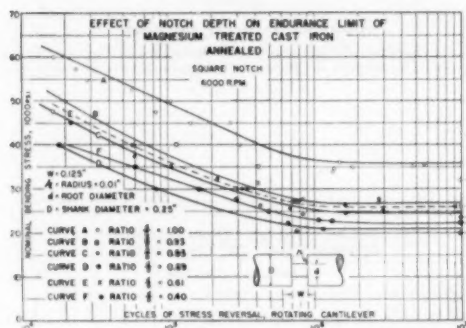


FIG. 8 EFFECT OF NOTCH DEPTH ON ENDURANCE LIMIT, ANNEALED CONDITION, SQUARE NOTCHES

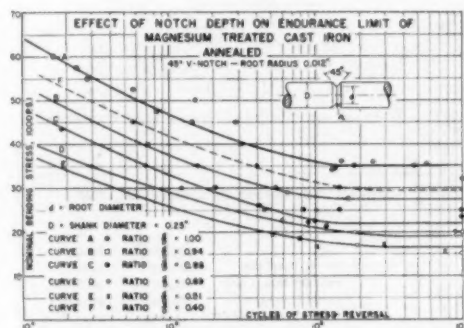


FIG. 9 EFFECT OF NOTCH DEPTH ON ENDURANCE LIMIT, ANNEALED CONDITION 45-DEG V-NOTCH, ROOT RADIUS 0.012 IN.

7, for speeds of 6000 rpm and 200 rpm, respectively. These results indicate that the fatigue strength fracture lines are lower at a testing speed of 200 rpm than when tested at 6000 rpm except for the notched as-cast condition. Where the S-N diagram becomes horizontal, the two fracture lines tend to merge as one. The test results for the notched specimens in the as-cast condition indicated that the fracture line (S-N diagram) for a speed of 200 rpm was above that at 6000 rpm, just the reverse for the other three conditions. It is not certain in the light of these meager tests how large an effect of speed is present. Smith, Brueggeman, and Harwell (25) found a similar effect for bare and Alclad 24S-T3 aluminum-alloy sheet specimens "in which the results for 12 cycles per minute tend to fall toward the left edge of the scatter of those made at 1000 cycles per minute." Tests were carried to 100 cycles whereas the results for magnesium-treated iron are extended to 10,000 cycles. It appears at very low cycles (high stresses) to failure, the fracture lines for the two speeds merge just as they do at about 200,000 cycles for aluminum and 2,000,000 cycles (low stresses) for nodular iron.

Another series of results is shown in Figs. 8 and 9 summarizing the experimental work to determine the notch-depth effect for constant shank diameter, notch radius, and notch angle for two different types of notches at 6000 rpm. Fig. 10 is a concise summary of the fatigue testing in which the dynamic stress-con-

centration factor is plotted against the ratio of root diameter to shank diameter. The trend is clear from a ratio of 1.0 to about 0.65. Two scatter points make it uncertain as to the effect of ratios from 0.5 to 0.2. It is not clear for extremely deep notches whether the dynamic stress-concentration factor goes toward 1.00 or tends to become constant. According to Neuber's (26) analysis for deep circumferential external notches under bending, having a hyperbolic notch contour, the static stress-concentration factor tends toward 1.00 as the ratio of d/r approaches 1 (see Table 6 in the Appendix also).

Tables 3, 4, and 5 provide another basis for comparing square notches in nodular iron with those in steel and a comparison of the dynamic stress-concentration factor with the static value. It appears that the values for magnesium-treated iron are of the same order of magnitude as those for steels. In every case the theoretical values are higher than the dynamic values. Fig. 11 is a plot of the endurance ratio versus the dynamic stress-concentration factor.

Fig. 12 summarizes the trend in size of test specimen upon the endurance limit for sizes from 0.19 in. to 0.45 in. diam which is similar to that observed for steels. A further comparison with other types of cast iron is made in Fig. 13. In Part 2 of the paper the size effect will be explored further for the magnitude of its effect.

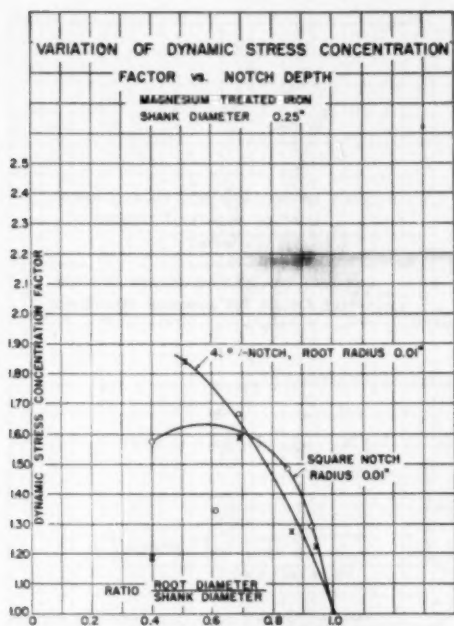


FIG. 10 VARIATION OF DYNAMIC STRESS-CONCENTRATION FACTOR VERSUS NOTCH DEPTH

TABLE 5 COMPARISON OF NOTCH SENSITIVITY OF MAGNESIUM-TREATED IRON WITH STEEL, NOTCH RADIUS APPROXIMATELY 0.01 IN. (30)

Shank diam., in.	Notch diam., in.	Ratio, Notch diam. to shank diam.	Kind of notch	Endurance limit as notched, psi	Dynamic stress-concentration factor	Material
0.40	0.275	0.69	Square	23000	2.08	0.40 per cent C steel
0.40	0.275	0.69	Square	14000	1.86	Ingot iron
0.25	0.175	0.69	Square	21000	1.70	Magnesium-treated iron, annealed
0.25	0.150	0.60	Square	30000	1.47	Magnesium-treated iron, as-cast
0.40	0.275	0.69	90-deg V-notch	18000	2.67	0.40 per cent C steel
0.25	0.175	0.69	45-deg V-notch	19000	1.94	Magnesium-treated iron, annealed

DAMPING CAPACITY

The purpose of this phase of the investigation was to determine the variation of damping capacity with stress, using the following methods:

- By obtaining static stress-strain curves in direct tension and compression with a closed loop.
- By obtaining static stress-strain curves in bending with a closed loop.
- By obtaining dynamic stress-strain curves in bending.
- By performing the torsional damping test.

(a) *Static Stress-Strain Curves in Direct Tension and Compression.* Fig. 14 shows the tension-compression specimen made from annealed magnesium-treated iron to which were attached four SR-4 type A-S wire strain gages in the longitudinal direction. These gages were connected in series and used in conjunction with an SR-4 strain indicator. Suitable increments of load were chosen in advancing from zero load to some maximum in tension,

TABLE 3 COMPARISON OF DYNAMIC STRESS-CONCENTRATION FACTOR FOR MAGNESIUM-TREATED IRONS WITH STATIC FACTORS AND WITH DYNAMIC FACTORS FOR STEEL—SQUARE NOTCHES OR SHOULDERS

Root diam., in.	Ratio, root to shank diam. $\frac{d}{D}$	Ratio, notch depth to notch radius $\frac{h}{r}$	Ratio, notch radius to root diam. $\frac{r}{d}$	Static stress-concentration factor from photoelasticity, Frocht (27)	Dynamic stress-concentration factor on steel, Peterson (28)	Dynamic stress-concentration factor, nodular iron, square notch, annealed
d				K_s	K_f	K_f
0.231	0.93	0.95	0.043	2.30	1.41	1.32
0.214	0.85	1.8	0.047	2.28	1.40	1.45
0.172	0.69	3.9	0.058	2.15	1.31	1.69
0.153	0.61	4.9	0.065	2.00	1.27	1.37
0.100	0.40	7.5	0.100	1.90	1.16	1.60

TABLE 4 COMPARISON OF DYNAMIC STRESS-CONCENTRATION FACTOR FOR MAGNESIUM-TREATED IRONS WITH OTHER MATERIALS AND STATIC FACTORS—V-SHAPED NOTCHES

Root diam., in.	Ratio, root to shank diam. $\frac{d}{D}$	Ratio, notch depth to notch radius $\frac{h}{r}$	Ratio, notch radius to root diam. $\frac{r}{d}$	Theoretical stress-concentration factor, hyperbolic notch contour circumferential external, Neuber (26)	Dynamic stress-concentration factor, 60 deg V-notch, steels (29)	Dynamic stress-concentration factor, 45 deg V-notch, Grant (3)	Dynamic stress-concentration factor, cast iron 45 deg V-notch, Grant (3)	Dynamic stress-concentration factor, magnesium-treated iron, 45 deg V-notch, annealed
d				K_s	K_f	K_f	K_f	K_f
0.235	0.94	0.625	0.051	2.14	1.44			1.25
0.215	0.86	1.46	0.0558	2.24	1.96			1.59
0.173	0.69	3.17	0.0695	2.30	2.30			1.84
0.128	0.51	5.08	0.0938	2.00	2.30			2.15
0.331	0.552	13.5	0.03	3.40	2.50	1.00	1.72	
0.331	0.552	13.5	0.03	3.40	2.50	1.12	2.19	
0.331	0.552	13.5	0.03	3.40	2.50	1.35	2.22	

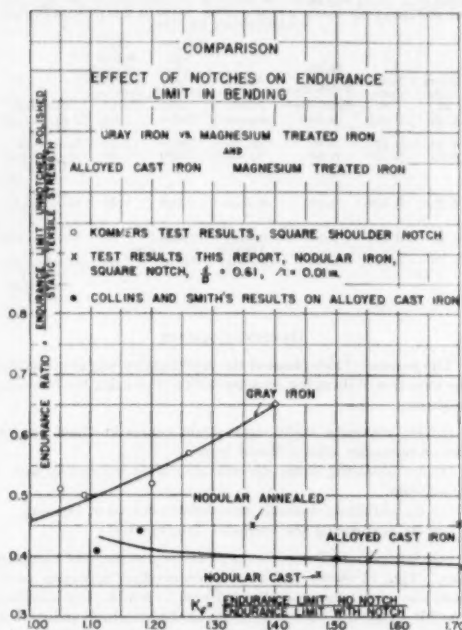


FIG. 11 COMPARISON OF EFFECT OF NOTCHES ON ENDURANCE LIMIT WITH GRAY IRON AND ALLOYED CAST IRON

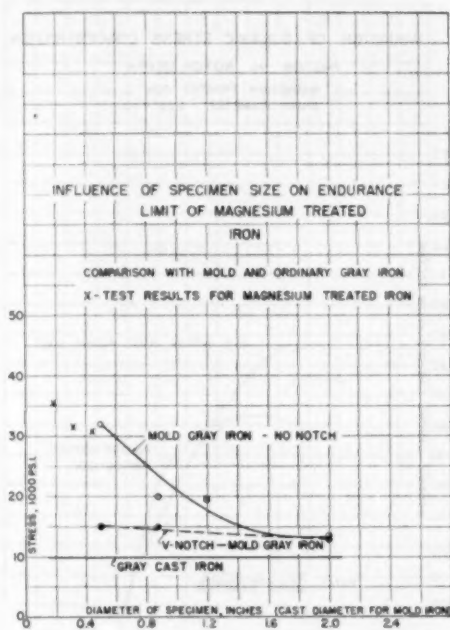


FIG. 13 COMPARISON OF SIZE OF TEST SPECIMEN OF MAGNESIUM-TREATED WITH MOLD GRAY IRON AND GRAY CAST IRON [Data from mold iron from Reference (33).]

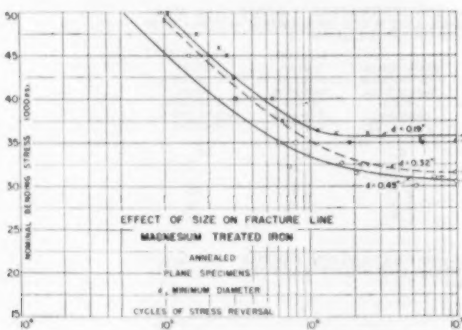


FIG. 12 EFFECT OF SIZE ON FRACTURE LINE IN ENDURANCE TEST OF MAGNESIUM-TREATED CAST IRON

from the maximum tension back to zero, from zero load to some maximum in compression and finally, from a maximum in compression back to zero load. Thus a closed-loop stress-strain curve was determined for a stress level. All tests were conducted at succeeding higher stress levels.

A typical static stress-strain plot at a stress level of 50,000 psi in direct tension and compression appears in Fig. 15. The method of computing the specific damping ratio is indicated in Fig. 16, where the area A is called the work of deformation at maximum

strain per unit volume for a particular cycle, and the area d is the area of the hysteresis loop. If units are used, then

$$\begin{aligned} A &= \text{in-lb per cu in.} \\ d &= \text{in-lb per cu in.} \\ p &= \text{specific damping ratio} \\ p &= d/A, \text{ dimensionless} \end{aligned}$$

Potter (20) in a review of the seven methods for determining the damping capacity of materials, comments that the use of static stress-strain curves is applicable only to high stresses where sizable loops can be planimeted and is unsatisfactory on a low damping material. The test results appear in Fig. 17 and it is seen that the lower limit is about 20,000 psi.

(b) *Static Stress-Strain Curves in Bending.* A Krouse cantilever fatigue specimen was mounted in the fatigue machine, Fig. 18, and one type A-8 strain gage was mounted longitudinally on the surface. With the fatigue specimen rotated to a position where the

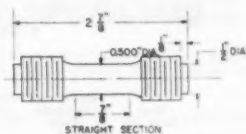


FIG. 14 DIRECT TENSION-COMPRESSION DAMPING-CAPACITY SPECIMEN STATIC

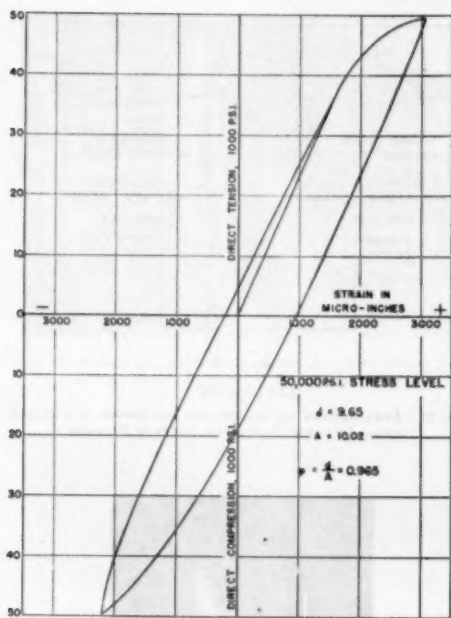


FIG. 15 HYSTERESIS LOOP IN DIRECT TENSION-COMPRESSION AT 50,000-PSI STRESS LEVEL

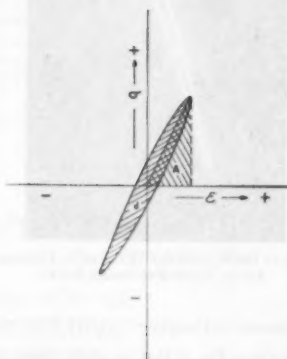


FIG. 16 DIAGRAM ILLUSTRATING HOW SPECIFIC DAMPING CAPACITY IS DEFINED AS RATIO OF AREA d TO AREA A

wire strain gage was on top measuring maximum static strains, increasing static loads were applied and corresponding strains measured up to some maximum load and down to zero load. Then the specimen was rotated 180 deg with the strain gage on the bottom side to measure maximum compression strains up to the same stress level as before and back to zero again. Fig. 19 shows a typical stress-strain loop obtained under static bending conditions

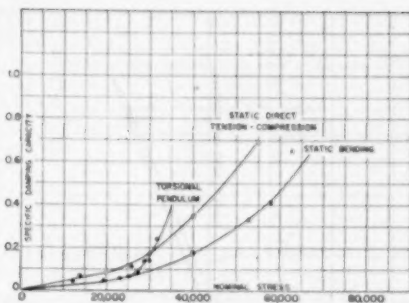


FIG. 17 COMPARISON OF DAMPING CAPACITY DETERMINED BY THREE METHODS

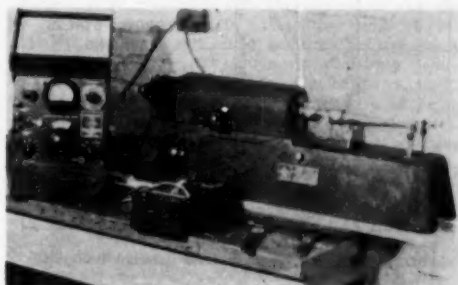


FIG. 18 EQUIPMENT USED TO DETERMINE STATIC DAMPING CAPACITY IN BENDING

for a stress level of 40,000 psi. The damping capacity results for this test appear in Fig. 17.

(c) *Dynamic Hysteresis Loops in Bending.* No quantitative results were obtained using this method, but the oscillographic record gave a visual pattern that offers some promise. It was not sure whether the equipment in Fig. 20, as represented in Fig. 21, with the resulting typical hysteresis loop shown in Fig. 22, gave specific damping capacities for the system or the test specimen. Fig. 20 shows a Sonntag fatigue-testing machine type SF-2 with the cantilever beam of annealed magnesium iron upon which were mounted two type A-8 strain gages; one gage was used to measure dynamic strain and the other gage was used to measure dynamic load. The resulting signals were amplified in the strain circuit through a Baldwin type BA-1 amplifier and through a Packard-Hewlett amplifier in the stress circuit. Resulting signals were connected to the y and z axes of an oscilloscope. A 35-mm camera attached to the oscilloscope gave a permanent record as shown in Fig. 22.

(d) *Torsional Damping Test.* Fig. 23 shows the arrangement of the equipment and electronic apparatus for obtaining a permanent record of the torsional damped vibrations of a test specimen. A type A-19 wire strain gage ($\frac{1}{16}$ -in. gage length) was mounted at 45 deg to the longitudinal axis of the damping specimen in Fig. 3. The strain-gage signals were amplified through a Brush amplifier before feeding into a Brush recording-pen machine. A sector mounted on the upper fixed frame permitted the angle of twist to be measured. A typical record appears in Fig. 24. To the

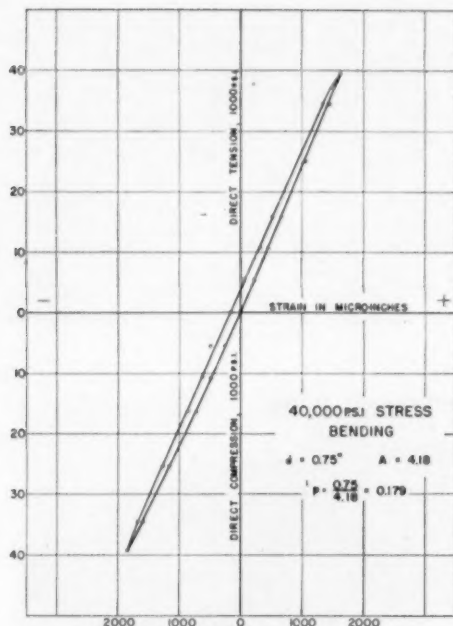


FIG. 19 TYPICAL HYSTERESIS LOOP IN STATIC BENDING

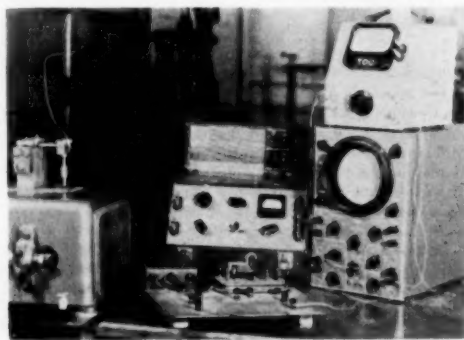


FIG. 20 EQUIPMENT USED TO EXPLORE POSSIBILITY OF DETERMINING DYNAMIC DAMPING CAPACITY IN BENDING

knowledge of the author, this is the first time that wire strain gages have been used for determining damping capacities from a torsional pendulum. The usual method is to follow the path of reflected light from mirrors mounted on the torsional crossarm. Fig. 24 shows a uniform decay record. A close examination of other records reveals that there is not precisely a uniform decrease in height of each succeeding cycle. The torsional damping-capacity ratio is plotted against the shear stress in Fig. 17 which enables one to form a comparison with the other methods.

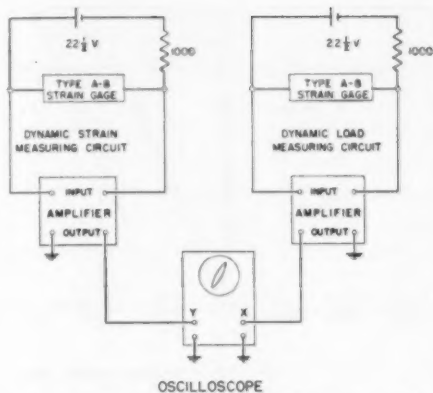


FIG. 21 ARRANGEMENT OF ELECTRONIC EQUIPMENT FOR DETERMINING DYNAMIC HYSTERESIS LOOPS IN BENDING



FIG. 22 TYPICAL OSCILLOGRAPHIC RECORD IN DYNAMIC BENDING, ABOUT 20,000-PSI STRESS LEVEL

SUMMARY OF DAMPING-CAPACITY RESULTS

It can be seen from Fig. 17 that the static direct tension-compression method produces hysteresis loops that are too small to planimeter below 20,000 psi normal stress; thus no values of specific damping capacity were determined below this stress. This was found true for the static bending tests, but the lower stress value is about 40,000 psi. The torsional-pendulum method, using the described electronic instruments, permits the determination of damping capacity from plastic strains to very small elastic strains with a slight disadvantage in measuring successive heights of the decay curve. Dynamic-bending tests gave higher values of specific damping than the static bending.

Higher damping values were found for static direct tension-

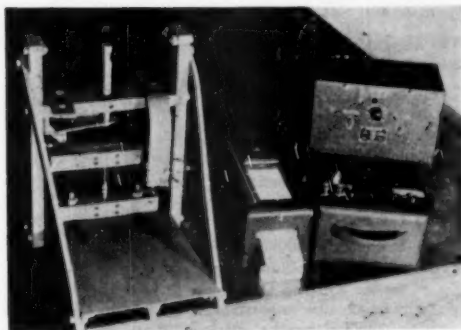


FIG. 23 TORSIONAL DAMPING-CAPACITY MACHINE WITH BRUSH RECORDER AND ELECTRICAL RELEASE EQUIPMENT

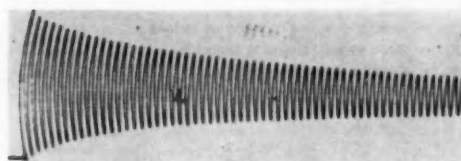


FIG. 24 TYPICAL TORSIONAL-DECAY CURVE USING WIRE STRAIN GAGES

compression than for static-bending tests because all of the fibers are stressed in the former method whereas there is a distribution of stress in bending. Damping capacity is defined in terms of energy ratios. In the torsional-pendulum test, the fibers are under a state of combined stress as well as varying from zero stress at the center to some value at the outside fiber. If stress intensity is defined as follows

$$\text{Stress intensity} = \frac{1}{\sqrt{2}} \sqrt{(\sigma_1 - \sigma_2)^2 + (\sigma_2 - \sigma_3)^2 + (\sigma_3 - \sigma_1)^2}$$

$$\sigma_1, \sigma_2, \sigma_3 = \text{principal stresses}$$

$$\tau = \text{shear stress in torsion test}$$

then for a tension test

$$\sigma_1 = \text{direct normal stress}$$

$$\sigma_2 = \sigma_3 = 0$$

$$\text{stress intensity} = \sigma_1$$

whereas for a torsion test

$$\sigma_1 = \tau = -\sigma_3 \text{ and } \sigma_2 = 0$$

then the stress intensity is $1.73 \sigma_1$ or 1.73τ .

The results from the torsional-pendulum test in Fig. 17 have been replotted for comparison with SAE 1020 steel annealed and cast iron melted in a cupola as shown in Fig. 25. Magnesium-treated iron has lower damping values than cast iron or annealed SAE 1020 steel.

ACKNOWLEDGMENT

The author wishes to acknowledge the work of Mr. Charles

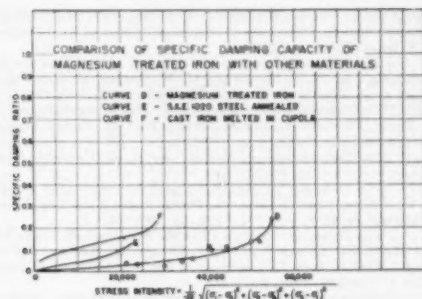


FIG. 25 COMPARISON OF SPECIFIC DAMPING CAPACITY OF MAGNESIUM-TREATED IRON WITH SAE 1020 STEEL AND CAST IRON

Hoffman in the preparation of the drawings and the photography of the experimental equipment. The author thanks Mr. Adams and Mr. Allender for very careful preparation of test specimens. The author appreciates the encouragement of Dean Cudworth. The University of Alabama Research Committee was very generous in providing funds and sponsoring the program, for which the author is grateful. Mr. Stephen Moxley, vice-president, American Cast Iron Pipe Company, was instrumental in providing the magnesium-treated iron. Dr. James T. MacKenzie and Mr. Charles Donoho provided invaluable comments on the manuscript.

BIBLIOGRAPHY

- 1 "The Industrial Status of Ductile Iron," by A. P. Gagnebin, *Mechanical Engineering*, vol. 73, February, 1951, pp. 101-108.
- 2 "Two- and Three-Dimensional Cases of Stress Concentration, and Comparison With Fatigue Tests," by R. E. Peterson and A. M. Wahl, *Journal of Applied Mechanics*, Trans. ASME, vol. 58, 1936, pp. A-15-22.
- 3 "Notched and Unnotched Fatigue Tests on Flake and Nodular Cast Irons," by J. W. Grant, Research Report No. 251, *Journal of Research and Development*, BCIRA, vol. 3, April, 1950, pp. 333-354.
- 4 "Fatigue Tests of Cast Iron," by H. T. Moore and S. W. Lyon, *Transactions of the American Foundrymen's Association*, vol. 35, 1927, pp. 410-425.
- 5 "Die Elastizität und die Schwingungsfestigkeit des Gusseisens," by A. Thum and H. Ude, *Die Gusserei*, vol. 16, 1920, pp. 501-513.
- 6 "The Static and Fatigue Properties of Some Cast Irons," by J. B. Koppers, *ASTM Proceedings*, vol. 28, 1928, Part 2, pp. 174-197.
- 7 "Notes on Fatigue Properties of Cast Iron," by H. L. Daasch, *Transactions of the American Foundrymen's Association*, vol. 44, 1936, pp. 528-541.
- 8 "Damping Capacity, Endurance, Electrical and Thermal Conductivities of Some Gray Cast Irons," by C. H. Lorig and V. H. Schnee, *Transactions of the American Foundrymen's Society*, vol. 48, 1940, pp. 425-446.
- 9 "The Notch Sensitivity of Alloyed Cast Irons Subjected to Repeated and Static Loads," by W. L. Collins and J. O. Smith, *ASTM Proceedings*, vol. 42, 1942, pp. 639-656.
- 10 "Understressing and Notch Sensitiveness in Fatigue," by J. B. Koppers, *Engineering News Record*, vol. 109, 1932, pp. 353-355; also *Cast Metals Handbook*, third edition, 1949, p. 402.
- 11 "A Practical Evaluation of Ductile Cast Iron," by J. E. Eagen and J. D. James, *Iron Age*, vol. 164, December 15, 1940, pp. 77-82.
- 12 "Comparison of Fatigue Strengths of Bars and Alclad 245-T3 Aluminum-Alloy Sheet Specimens Tested at 12 and 1000 Cycles Per Minute," by F. C. Smith, W. C. Bruggeman, and R. H. Harwell, *NACA Technical Note 2231*, December, 1950.
- 13 "Über Einflüsse auf die Schwingungsfestigkeit von Aluminium-Legierungen," by E. Von Rajakovic, *Metallwirtschaft*, vol. 22, April 20, 1943, pp. 225-229.
- 14 "The Character of Fatigue of Metals," Fourth Progress Report on an Investigation of the Behavior of Materials Under Re-

peated Stress, Contract N69ri-71, Task Order IV, Engineering Experiment Station, University of Illinois, and Office of Naval Research, U. S. Navy, February, 1948.

"Fracture and Ductility of Lead and Lead Alloys for Cable Sheathing," by H. F. Moore and C. W. Dollins, Bulletin No. 347, Engineering Experiment Station, University of Illinois, 1943.

15 "Drehachwingungsfestigkeit und Dämpfungsfähigkeit," by O. Föppl, Werkstoffaushuss Bericht No. 36, Verein Deutscher Eisenhüttenleute, 1923.

16 "Internal Friction in Metals," by R. H. Canfield, *Physical Review*, vol. 32, 1928, pp. 520-530.

17 "The Behavior of Metals Subjected to Repeated Stresses," by H. J. Gough and D. Hanson, Proceedings of the Royal Society of London, series A, vol. 104, 1923, pp. 538-565.

"The Behavior of Single Crystals of Aluminum Under Static and Repeated Stresses," by H. J. Gough, D. Hanson, and S. J. Wright, Philosophical Transactions of the Royal Society of London, series A, vol. 226, 1926, pp. 1-30.

"The Importance of the Capacity for Damping in the Valuation of Materials of Construction," by O. Föppl, *Metallwirtschaft*, vol. 8, 1929, pp. 419-422.

"Über die Materialdämpfung bei Dauerbeanspruchung durch Torsionsschwingungen," by H. Kortum, *Technische Mechanik und Thermodynamik*, vol. 1, 1930, pp. 297-307.

"Nachwirkung und Hysteresis," by H. Fromm, *Handbuch D. Phys. und Tech. Mechanik*, vol. 4, 1931, p. 436.

18 "Damping Capacity of Steels and Correlation With Other Properties," by G. R. Brophy, *Iron Age*, vol. 130, November 24, 1932, pp. 800-802.

19 Unpublished Report on Torsional Fatigue Under a Low Number of Stress Reversals, by Harry Majors, Jr., Engineering Experiment Station, University of Alabama, University, Ala.

20 "Damping Capacity of Metals," by E. V. Potter, U. S. Bureau of Mines, Report of Investigations, No. 4194, March, 1948.

21 "The Practical Importance of the Damping Capacity of Metals, Especially Steels," by O. Föppl, *Journal of the Iron and Steel Institute*, vol. 134, 1936, pp. 393-423.

22 "Die Dauerprüfung der Werkstoffe," by O. Föppl, E. Becker, and G. S. Von Heydekampf, Julius Springer, Berlin, 1931.

23 "Damping Capacity at Low Stresses in Light Alloys and Carbon Steel With Some Examples of Nondestructive Testing," by Leopold Frommer and A. Murray, *Journal of the Institute of Metals*, vol. 70, 1944, pp. 1-50.

24 "Changes in Damping Capacity During Annealing of Alpha Brass," by J. T. Norton, Trans. American Institute of Mining and Metallurgical Engineers, Inst. Metals Division, vol. 137, 1940, pp. 49-58.

25 See reference (12).

26 "Theory of Notch Stresses," by H. Neuber, J. W. Edwards, Ann Arbor, Mich.

27 "Factors of Stress Concentration Photoelastically Determined," by M. M. Frocht, Trans. ASME, vol. 57, 1935, pp. 67-68.

28 See reference (2).

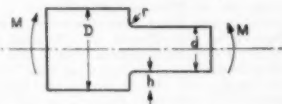
29 "Formulas for Stress and Strain," by R. J. Roark, McGraw-Hill Book Company, Inc., New York, N. Y., 1943, pp. 339 and 344.

30 "The Fatigue of Metals," by H. F. Moore and J. B. Komers, McGraw-Hill Book Company, Inc., New York, N. Y., 1927.

Appendix

Tables 6, 7, 8, 9, and 10 provide additional material for comparison of the static and dynamic stress concentrations of steels with those for nodular cast iron.

TABLE 6 FORMULAS FOR STRESS AND STRAIN,* ELASTIC STATIC BENDING (27)



$\frac{A}{r}$	$\frac{r}{d}$	0.05	0.10	0.20	0.27	0.50	1.0
0.5	1.61	1.49	1.39	1.34	1.22	1.07	
1.0	1.91	1.70	1.48	1.38	1.22	1.08	
1.5	2.00	1.73	1.50	1.39	1.23	1.08	
2.0	2.07	1.74	1.52	1.39	1.23	1.09	
3.5	2.11	1.76	1.54	1.40	1.23	1.10	

* See reference (29) p. 334.

DAMPING CAPACITY

The amplitude of the oscillations produced in this torsional damping test is given by the equation

$$A = A_0 \cos \omega t e^{-\delta t}$$

A = amplitude at time t

A_0 = initial amplitude at time t_0

t = time, sec

f = frequency of oscillations

$\omega = 2\pi f$

δ = logarithmic decrement

A_m = maximum amplitude of cycle

A_{m+n} = maximum amplitude, n cycles after m

p = specific damping capacity, or P as defined by Föppl which is the ratio of the energy loss per cycle to the potential energy at maximum stress

$$p = \frac{\text{Energy loss per cycle}}{\text{Potential energy at maximum stress}}$$

$$p = \frac{\text{area } d}{\text{area } A} \quad (\text{see Fig. 16 in text})$$

p_0 = specific damping capacity at surface

p_m = mean specific damping capacity

τ_0 = shearing stress at surface

$$p = 2\delta$$

$$p = \frac{\delta}{A} = 2\delta$$

where $\cos \omega t = 1$

$$\frac{A_m}{A_{m+n}} = \frac{A_0 \cos \omega t e^{-\delta/m}}{A_0 \cos \omega t e^{-\delta/(m+n)}}$$

$$\frac{A_m}{A_{m+n}} = e^{\delta n}$$

$$\delta = \frac{1}{n} \ln_0 \frac{A_m}{A_{m+n}} \quad \text{logarithmic decrement}$$

Approximate equation

$$\delta = \frac{2}{n} \frac{A_m - A_{m+n}}{A_m + A_{m+n}}$$

error is less than 1 per cent if A/A_{m+n} is less than 1.40.

A more correct expression is

$$\delta = \frac{1}{n} \ln_0 \frac{(A_m - A_{m+n})}{A_m + A_{m+n}}$$

error less than 1 per cent for values of A_m/A_{m+n} up to 1.65.

For the case that values of decrement change rapidly, another method is used

$$A_{\max} = A_0 e^{-\delta t}$$

$$\frac{dA_{\max}}{dt} = A_0 e^{-\delta t} (-\delta f) \ln_0 (e)$$

$$\frac{dA_{\max}}{dt} = A_{\max} (-\delta f)$$

$$\delta = \frac{1}{f A_{\max}} \frac{dA_{\max}}{dt}$$

TABLE 7 NOTCHED AND UNNOTCHED FATIGUE TESTS ON FLAKE AND NODULAR CAST IRONS*

$\frac{A}{r}$	Iron	D	d	r	$\frac{A}{D}$	$\frac{r}{d}$	Notch angle	K_f	
2.7	A	0.600	0.331	0.95	0.552	0.151	0	1.06	Flake pearlitic
2.7	B	0.600	0.331	0.95	0.552	0.151	0	1.27	Flake pearlitic
2.7	V636	0.600	0.331	0.95	0.552	0.151	0	1.23	Flake acicular
13.5	A	0.600	0.331	0.91	0.552	0.03	45°	1.06	Flake pearlitic
13.5	B	0.600	0.331	0.91	0.552	0.03	45°	1.12	Flake pearlitic
13.5	V636	0.600	0.331	0.91	0.552	0.03	45°	1.35	Flake acicular
13.5	NOD67	0.600	0.331	0.93	0.552	0.151	0	1.41	Nodular cerium treated
13.5	W16	0.600	0.331	0.95	0.552	0.151	0	1.59	Nodular cerium treated
13.5	W105	0.600	0.331	0.95	0.552	0.151	0	1.48	Nodular cerium treated
13.5	NOD67	0.600	0.331	0.91	0.552	0.03	45°	1.72	Nodular cerium treated
13.5	W16	0.600	0.331	0.91	0.552	0.03	45°	2.19	Nodular cerium treated
13.5	W105	0.600	0.331	0.91	0.552	0.03	45°	2.22	Nodular cerium treated

* See Bibliography (3), by J. W. Grant, *Journal of Research on Development*, vol. 3, British Cast Iron Research Association April, 1950.

TABLE 8 TWO- AND THREE-DIMENSIONAL CASES OF STRESS CONCENTRATION, AND COMPARISON WITH FATIGUE TESTS (2)

Material	d	D	A	r	$\frac{A}{r}$	K_f
0.45 per cent C steel	0.25	0.50	0.125	2.0	0.250	1.16
0.45 per cent C steel	0.41	0.82	0.205	2.0	0.250	1.19
0.45 per cent C steel	1.50	3.00	0.750	2.0	0.350	1.22
0.45 per cent C steel	0.25	0.50	0.125	7.45	0.067	1.44
0.45 per cent C steel	0.41	0.82	0.205	7.45	0.067	1.525
0.45 per cent C steel	1.60	3.20	0.80	7.45	0.067	1.845
Ni-Mo steel	0.25	0.50	0.125	2.94	0.170	1.330
Ni-Mo steel	0.41	0.82	0.205	3.33	0.150	1.44
Ni-Mo steel	2.13	3.19	0.53	1.66	0.150	1.51
Ni-Cr steel	0.4	0.8	0.20	7.13	0.070	1.71
Ni-Cr steel	1.0	2.0	0.50	6.25	0.080	1.74
Ni-Cr steel	0.3	0.085	2.16
0.33 per cent C, 1.07 Mn	0.6	0.095	1.78

Material	d	D	r	K_f	Endurance limit
0.45 per cent C steel	0.47	0.94	...	1.00	32300
0.45 per cent C steel	0.25	0.50	0.25	1.16	27600
0.45 per cent C steel	0.41	0.82	0.25	1.19	27200
0.45 per cent C steel	1.50	3.00	0.25	1.22	26500
0.45 per cent C steel	0.25	0.50	0.067	1.44	22500
0.45 per cent C steel	0.41	0.82	0.067	1.525	21200
0.45 per cent C steel	1.60	3.20	0.067	1.845	17500
Ni-Mo Steel	0.47	0.94	...	1.00	52800
Ni-Mo Steel	0.25	0.50	0.17	1.32	40000
Ni-Mo Steel	0.41	0.82	0.15	1.44	36700
Ni-Mo Steel	2.13	3.19	0.15	1.51	35000
Ni-Cr Steel	1.0	2.00	...	1.00	59900
Ni-Cr Steel	0.4	0.8	0.07	1.71	35000
Ni-Cr Steel	1.0	2.0	0.08	1.74	34500
Cr-Ni-W	0.38	...	0.05	2.3	...
Cr-Ni-W	0.30	...	0.17	1.40	...
Cr-Ni-W	1.18	...	0.1	2.1	...

TABLE 10 FORMULAS FOR STRESS AND STRAIN*—REPEATED STRESS BENDING

Material	D	d	$\frac{A}{r}$	r	K_f
0.45 per cent C Steel (ht)	0.40	0.275	0.063	...	2.04
0.45 per cent C Steel (ht)	2.00	1.050	0.500	2.66	0.185
Steel A, low alloy to 78400 psi	0.80	0.25	0.125	6.25	0.08
Steel B, low alloy to 70800 psi	0.50	0.25	0.125	6.25	0.08
Steel C, low alloy to 91300 psi	0.50	0.25	0.125	6.25	0.08
Steel, 1.42 per cent C to 73400 psi	3.50	1.00	0.950	...	2.30
Steel, 1.42 per cent C to 73800 psi	1.94	1.60	0.170	...	1.90
Steel 1.44 per cent C to 87000 psi	...	0.35	2.10

* See reference (29), p. 338.

TABLE 9 DYNAMIC STRESS-CONCENTRATION FACTORS; V-NOTCH IN CIRCULAR SHAFT

Formulas for Stress and Strain*						
Material	d	D	$\frac{d}{D}$	$\frac{A}{r}$	r	K_f
0.33 per cent C steel	0.445	0.45	0.990	1.00	0.6	72°
0.33 per cent C steel	0.445	0.45	0.990	4.00	0.001	72°
0.33 per cent C steel	0.445	0.45	0.990	7.00	0.0007	72°
0.33 per cent C steel	0.440	0.45	0.990	1.00	0.011	63 1/2°
0.33 per cent C steel	0.400	0.45	0.890	4.00	0.014	63 1/2°
0.33 per cent C steel	0.360	0.45	0.800	7.00	0.018	63 1/2°
Formulas for Stress and Strain*						
SAE 2330 ht, 128700 ts	0.25	0.3	0.833	2.50	0.40	60
SAE 4130 normal 76200 ts	0.25	0.3	0.833	2.50	0.40	60
SAE 4130 ht, 136500 ts	0.25	0.3	0.833	2.50	0.40	60
Alcoa 27 st ht, to 60000	0.25	0.3	0.833	2.50	0.40	60
Steel 0.84C ht, 360 Bhn	0.25	0.3	0.833	0.45	0.003	55
Steel 0.84C	0.343	0.38	0.982	5.83	0	75
Steel 0.10C	0.343	0.35	0.982	0.83	0	75
Steel 0.91 per cent C, 225000 ts	0.20	0.25	0.800	8.33	0.015	60
Steel 1.04 per cent C, 23700 ts	0.20	0.25	0.800	8.33	0.015	60
Cr-Van steel, 237000 ts	0.20	0.25	0.800	8.33	0.015	60
Steel 0.84C, ht 360 Bhn	0.25	0.30	0.833	3.20	0.003	55
Steel 0.84C, ht 360 Bhn	0.25	0.30	0.833	6.40	0.003	55

* See reference (29), p. 339.

† Ibid., p. 344.

Discussion

B. J. LAZAN.⁴ The author indicates that in low-carbon steel under torsion hysteresis "loops rapidly stabilized after four cycles (of stress) into constant area and shape." Furthermore, he diagrammed his damping-capacity data as a function of stress magnitude only, implying that "stress history" is not a significant variable. Work now in progress at the University of Minnesota shows that stress history is a very significant variable for most materials as will be discussed for mild steel.

With recently developed equipment now in use at the University, it is possible to measure damping capacity continuously under rotating cantilever stress during the course of a reversed-bending fatigue test.⁵ Fig. 26, herewith, shows the variation in

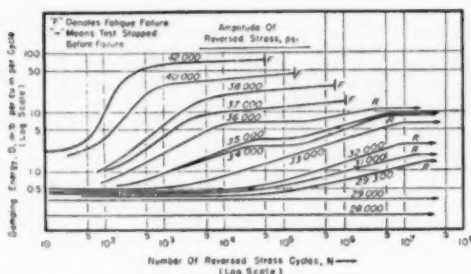


Fig. 26 D-N-S DIAGRAM SHOWING EFFECT OF SUSTAINED REVERSED STRESS OF SEVERAL MAGNITUDES ON DAMPING ENERGY OF STRESS-RELIEVED MILD STEEL

damping energy during a reversed constant-bending stress-fatigue test. The relationship between the damping energy shown in this curve and the author's specific damping ratio has been given by the writer.⁶ The uppermost curve, for example, shows that at the above-fatigue-limit stress of $\pm 42,000$ psi, the virgin specimen (or more accurately, a specimen with only 10 cycles of stress) has a damping energy of 2 in-lb per cu in. per cycle; after 100 cycles of $\pm 42,000$ psi fatigue stress, the damping is 10, after 1000 cycles the damping is 60, and, finally, after 50,000 cycles the damping attains an ultimate value of 80 as the specimen fails in fatigue. The below-fatigue-limit stress of $\pm 32,000$ psi may be considered as a second example. Here the damping does not increase significantly until after 10,000 cycles of stress, then changes from approximately 0.5 to 3.0 at 107 cycles (point R), beyond which the damping does not change under additional reversed stress. This point, R, at which the damping becomes stable with respect to additional cyclic stress shall be defined as the "stabilized damping point." At the relatively low stresses of 28,000 and 29,000 psi, the damping capacity is not affected by sustained reversed stress. For the particular series of specimens diagrammed in Fig. 26 it may be observed that either a specimen fails in fatigue (see points F) or it attains a condition of stabilized damping (see points R) after which fatigue failure appears to be extremely unlikely.

The significance of the stabilized damping point and the gen-

erality of its occurrence in other materials is not completely clear at present. Early investigators have implied that stabilized damping is attained in a fatigue test. Bairstow⁷ reported that for axle steel (55,000-psi yield strength and 85,000-psi tensile strength) the "cyclical permanent set" (which corresponds to the width of the hysteresis loop) attains a definite constant value after approximately 10,000 stress cycles at stresses both below and above the fatigue limit. However, in Bairstow's experiments, the stress on each specimen was increased stepwise (virgin specimens not used at each different stress level). Furthermore relatively few cycles of stress were used and, although the linear plots may indicate impending stabilization at 10,000 cycles, logarithmic plots such as Fig. 26 of this discussion may indicate an entirely different situation. Gough⁸ has observed a similar stabilized damping behavior during cyclic stress tests in Arco iron, which he identifies by the controversial term "elastic hysteresis." However, none of the early investigators apparently covered a wide range of stress on virgin specimens subjected to a large number of cycles.

Therefore it appears unlikely that long-term tests with sufficiently sensitive instruments would reveal a stabilized damping region beyond 4 cycles as reported in the paper. The author refers to torsional stress, whereas the data reported in this discussion are for bending stress. However, in earlier work by the writer,⁶ hollow tubes in torsion displayed gradually changing damping under sustained cyclic stress even after thousands of cycles.

At low stress, usually significantly below the fatigue strength, many materials display stabilized damping properties, that is, damping which is independent of stress history. In the case of the mild steel shown in Fig. 26, the stress, which may be defined as "cyclic stress sensitivity limit," above which damping is sensitive to stress history is about 29,000 psi, approximately 20 per cent below the fatigue limit.

The effect of both stress magnitude and stress history on damping may be diagrammed in two ways, as shown in Figs. 27 and 28, herewith. In Fig. 27 the damping is represented as the height to the surface above the S-N base plane. The slope of this surface indicates the rate of change of damping, either with respect to changing stress magnitude S, or changing stress history N. This surface ends abruptly, of course, at the S-N fatigue-failure abyss, defined by fracture line A'-D'. In the below-fatigue limit tests, damping becomes constant beyond the stabilized damping line D'-F', and the surface becomes a surface having zero slope in the horizontal N-direction, but one that goes uphill with increasing stress. Below the cyclic-stress sensitivity limit G'-F', the surface is also level in the horizontal N-direction, and it slopes downward toward zero stress.

The S-N-D surface in Fig. 27 of this discussion may be shown in a form involving use of iso-damping contour lines, or lines of equal damping, as illustrated in Fig. 28. These iso-damping lines, which are similar in nature to contour lines on a map for showing points of equal elevation, indicate trends and rapidity of change (uphill and downhill) in damping. The horizontal contour lines to the right of the stabilized damping line and below the cyclic stress sensitivity limit indicate the insensitivity of damping to additional cyclic stress in these regions. This diagram also permits quantitative determination of damping as a function of stress and number of cycles and, consequently, can be considered useful as a design chart.

The type of data shown in Figs. 26, 27, and 28 has been pro-

⁴ Professor of Materials Engineering, University of Minnesota, Minneapolis, Minn.

⁵ "Damping, Elasticity and Dynamic Stress-Strain Properties of Mild Steel," by B. J. Lazan and T. Wu, Proceedings of the American Society for Testing Materials, vol. 51, 1951.

⁶ "Some Mechanical Properties of Plastics and Metals Under Sustained Vibration," by B. J. Lazan, Trans. ASME, vol. 65, 1943, pp. 87-98.

⁷ "The Elastic Limits of Iron and Steel Under Cyclical Variation in Stress," by L. Bairstow, Philosophical Transactions of the Royal Society of London, vol. A, 1910, p. 210.

⁸ "The Fatigue of Metals," by H. J. Gough, D. Van Nostrand Company, Inc., New York, N. Y., 1926.

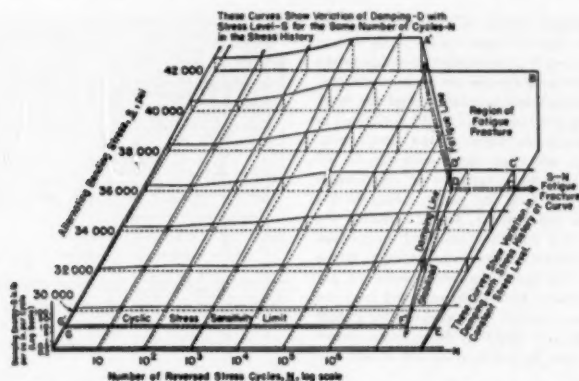


FIG. 27 S-N-D DIAGRAM INDICATING RELATIONSHIPS AMONG DAMPING ENERGY, STRESS MAGNITUDES, NUMBER OF REVERSED-STRESS CYCLES, AND FATIGUE FAILURE FOR STRESS-RELIEVED MILD STEEL

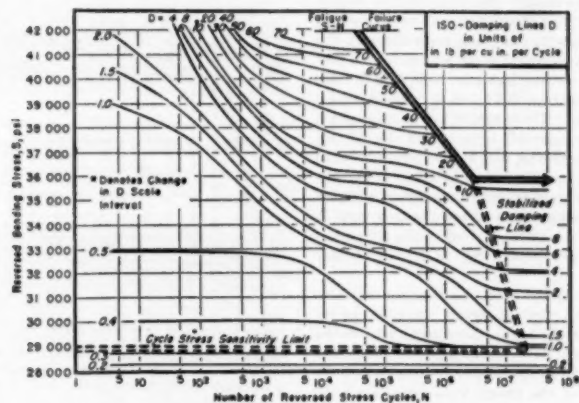


FIG. 28 S-N-D DIAGRAM RELATING STRESS, NUMBER OF CYCLES, AND ISO-DAMPING LINES FOR STRESS-RELIEVED MILD STEEL

cured for a wide variety of materials,⁹ and recently, studies have been completed on nodular iron and cast iron of the general type discussed in the paper. To date, cast iron is the only material which does not display significant stress-history effects. So far it has been impossible to generalize the stress-history patterns; some materials display increasing damping under sustained cyclic stress like mild steel, others decrease, others decrease and then increase, and still others increase and then decrease. In one case,⁹ a decrease of 99 per cent has been observed.

Comments by the author on any indication of the foregoing changes in damping under sustained cyclic stress that he has observed in his work would be appreciated.

A comparison of his damping data, as shown in Fig. 25 of the paper, with data recently procured at the University of Minnesota, reveals the following: There is reasonably good agreement for nodular iron whereas the Minnesota measurements indicate

⁹ "Damping, Elasticity and Fatigue Properties of Temperature Resistant Materials," by B. J. Lazan and L. Demer, Proceedings of the American Society for Testing Materials, vol. 51, 1951.

significantly lower damping for mild steel (even for a wide range of stress histories) and substantially higher damping for cast iron.

In fatigue-notch-sensitivity work now in progress at the University of Minnesota, specimen-preparation techniques were found to exert a pronounced influence on fatigue properties. It would be appreciated if the author would indicate how his notched and unnotched fatigue specimens were machined and polished.

J. W. GRANT.¹⁰ It is most interesting to study the results of notch-sensitivity tests on what the author describes as "a new engineering material." One must realize, however, that nodular cast iron represents a family of materials varying in strengths from 55,000-110,000 psi, with elongations from 1 to 30 per cent, according to composition and heat-treatment. Damping properties and the response to notches in fatigue likewise vary appreciably according to the type of iron.

¹⁰ British Cast Iron Research Association, Birmingham, England.

While the stress-concentration factors of magnesium-treated nodular irons are of the same order as those of steel, these factors can vary over a wide range, and it is misleading to compare the materials unless they are both tested under the same conditions, i.e., same test-piece size and surface-finish limits, and the same machine and care in carrying out the tests. Small variations in any of these factors can affect the value of the comparison. Accordingly, it is difficult to see what importance can be attached to the comparison of notch sensitivity of magnesium-treated iron and steel in Table 5 of the paper, owing to the variation in notch diameters, notch shape, and presumably the type of machine used. In this table the annealed magnesium nodular iron has a higher dynamic stress-concentration factor than the as-cast material. The notch diameters, however, are different. If the figures for the 0.15-in.-diam annealed bars are substituted, Fig. 8 of the paper, so that the test pieces for as-cast and annealed iron are identical, we find that the dynamic stress-concentration factor is 1.38, that is, less than for the as-cast material.

The nodular iron used in these tests has an exceptionally high tensile strength for the stated chemical composition. Is this an average figure, and to what extent is the high value due to the smallness of the tensile specimens? Based upon the fatigue strength of the 0.19-in.-diam test pieces, the endurance ratio of the as-cast material is only 0.37. In tests carried out at the British Cast Iron Research Association so far, we have found that endurance ratios on as-cast nodular iron vary from 0.38 to 0.42, and on annealed nodular iron from 0.43 to 0.51, using 0.301-in.- and 0.331-in.-diam test pieces. These results are on magnesium nodular irons having carbon contents between 2.9 and 3.3 per cent. On as-cast cerium nodular iron, with 3.6 to 3.9 per cent total carbon, the endurance ratios vary from 0.46 to 0.59. It appears that higher endurance ratios are obtained, in general, with higher carbon contents. For the composition of nodular iron used in the author's tests a lower tensile strength would bring the endurance ratio more in line with previously reported data on nodular iron.^{11,12}

The increase in fatigue strength as specimen diameter decreases is most enlightening, and the effect of section size could be investigated to advantage for static tests. No doubt Part 2 of the paper will produce some useful data on this aspect. The writer would be most interested to know the conditions under which the "mold gray iron," Fig. 13 of the paper, were tested, and the source of information from which the points were plotted.

AUTHOR'S CLOSURE

It was gratifying, indeed, to receive the kind comments of Professor Lazan and Mr. Grant which have contributed to the paper.

Mr. LAZAN's discussion as reflected in Figs. 26, 27, and 28 contributes far more information than the author could have obtained in the time allotted. Figs. 29 and 30 are submitted in support of the statement that in testing low-carbon steel under reversed torsion "hysteresis loops rapidly stabilized after four cycles into a constant area and shape." Mr. Lazan has added in parenthesis (stress) which does not appear in the original manuscript! The tests were conducted under constant reversed torsional strain, isothermally. Mr. Lazan implies that his test results are obtained from constant reverse-stress-fatigue cycles, adiabatically. There may be a difference. The curves of Figs. 29 and 30 were obtained on rods of mild steel fully annealed,

¹¹ "Notched and Unnotched Fatigue Tests on Flake and Nodular Cast Irons," by J. W. Grant, Research Report No. 251, Journal of Research and Development, British Cast Iron Research Association, vol. 3, April, 1950, pp. 333-354.

¹² "Ductile Cast Iron," by A. P. Gagnebin, K. D. Millis, and N. B. Pilling, *Iron Age*, vol. 163, February 17, 1949, pp. 76-84.

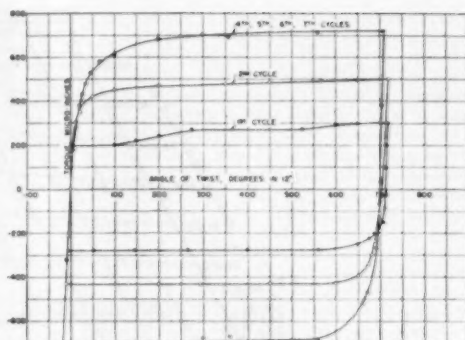


FIG. 29 HYSTERESIS LOOPS OF MILD STEEL IN REVERSED TORSION, ISOTHERMAL CONDITION
(1 Microinch = 2 in. lb. Maximum strain of each cycle, 720 deg per 12 in.)

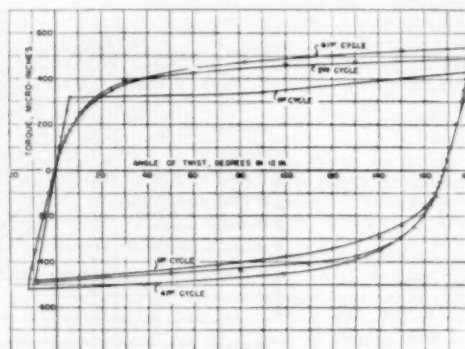


FIG. 30 HYSTERESIS LOOPS OF MILD STEEL IN REVERSED TORSION, ISOTHERMAL CONDITION
(1 Microinch = 2 in. lb. Maximum strain of each cycle, 180 deg per 12 in.)

21 3/4 in. long with a straight section of 12 in. and a diam of 0.505 in. (19). Torque in inch pounds versus angle of twist in degrees in 12 in. was plotted until an angle of twist of 720 deg in 12 in. was obtained for Fig. 29, and 180 deg in 12 in. for Fig. 30. Then, the data was observed for decreasing torques to zero torque. Now, data was observed for reversed torque up to an angle of twist of 720 deg in 12 in. and then for torques decreasing to zero, which completed one cycle at constant reversed shear strain. The total time to obtain the data for any cycle (strain) was ten minutes, so that the test is essentially an isothermal one at room temperature as indicated in Fig. 29. There was hardly any change during the fourth, fifth, sixth, or seventh cycles. Rupture occurred during the eighth cycle.

Fig. 30 is for another torsion specimen (mild steel annealed) twisted in one direction, then another 180 deg per 12 in. Note that the second cycle (strain) approaches very closely the shape of the 41st cycle. This was an isothermal test at room temperature, using 5 min per cycle. Plots were made about every fourth cycle after the tenth, and all were about the same shape and area.

A third series of reversed torsion cycles on the same material were made to twists of 23 deg per 12 in. under isothermal conditions at room temperature. There were 332 cycles of reversed

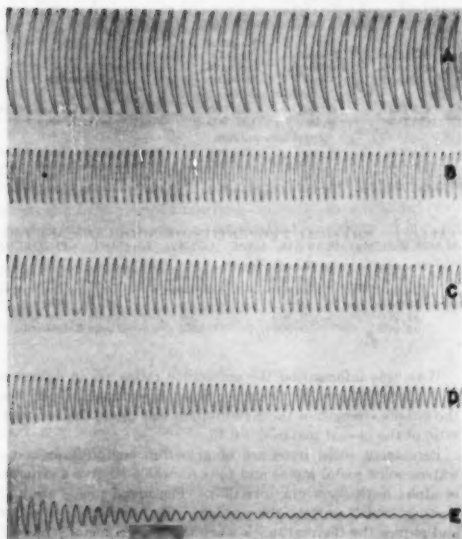


FIG. 31 COMPARISON OF TORSIONAL DECAY CURVES FOR VARIOUS MATERIALS, INITIAL STRESS FOR ALL MATERIALS ABOUT 5500 LB PER SQ IN.

(Curve A, 14S-T aluminum alloy; curve B, SAE 4140 alloy steel, curve C, annealed magnesium nodular iron; curve D, SAE 1020 steel annealed; curve E, gray cast iron.)

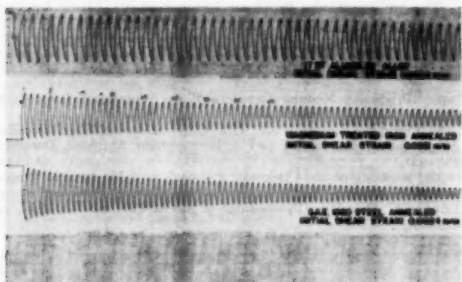


FIG. 32 COMPARISON OF TORSIONAL DECAY CURVES FOR VARIOUS MATERIALS, INITIAL STRAIN ABOUT THE SAME AS INDICATED

torison. Stabilization was obtained after the seventh cycle. A machine should be built to reverse specimens automatically at different rates of straining to obtain results beyond 400 cycles.

Professor Lahan is quite right in indicating that damping capacity is affected by "stress history", which the author did not stress clearly. Nevertheless, if one wishes to compare the damping capacity of materials before and after a change in the material, he would obtain a series of curves as indicated in Figs. 31 and 32 and the static torsion curves, Fig. 33. Thus Fig. 34 was produced which is an improvement upon Fig. 25 of the text. The author did not obtain experimentally curves E and F of Fig. 25. Curves E and F were obtained from reference (21).

All unnotched fatigue specimens were polished with emery cloth No. 1, 0, 00, and 000 to remove the radial tool scratches.

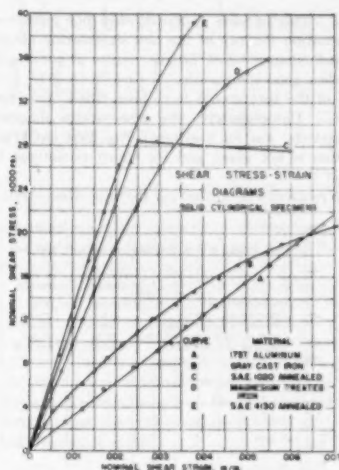


FIG. 33 STATIC SHEAR STRESS-STRAIN DIAGRAMS

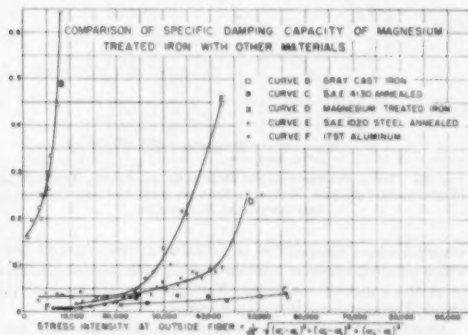


FIG. 34 TORSIONAL DAMPING CAPACITY VERSUS STRESS LEVEL

The same tool was used for all specimens for the last few finishing cuts. A series of tests were performed on specimens in which one group was polished longitudinally while another group was polished on the lathe. No difference was observed in the endurance curves. The normal scatter of test results obscured any effect.

The notched fatigue specimens were not polished after machining. All specimens were measured in the optical comparator.

An examination of the fatigue-specimen surface with the Brinell hardness microscope reveals a surface potted with semispherical cavities filled with graphite. The specimen has stress raisers that polishing cannot eliminate.

Mr. Grant has made excellent comments. These remarks are to justify certain procedures. Magnesium nodular iron was used in this investigation of the composition indicated because that chemical analysis gave optimum properties (31). The values indicated in Table 5 were not satisfactory but they were the best that could be obtained. This indicates the paucity of our knowledge on the effect of notch depth, angle, notch radius, size, and possibly grain size upon the dynamic properties of

materials. This is more apparent when one endeavors to find the information for any of the new engineering alloys. If the author had time, notched fatigue results of some steels would have made a good comparison.

Fig. 4 of the text should have been titled "true stress-strain diagrams." Unfortunately, the stress-strain diagram of the as-cast material was for keel block No. 2804 (ACIPCO) whose composition is not given and for which no fatigue tests were conducted.

Fig. 35 replaces Fig. 4, showing the true stress-strain curve for

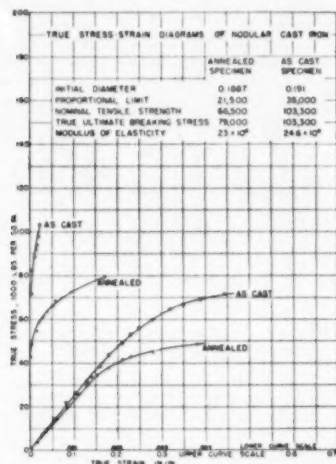


FIG. 35 TRUE STRESS-STRAIN DIAGRAMS IN STATIC TENSION OF MAGNESIUM-TREATED NODULAR IRON IN THE AS-CAST CONDITION AND ANNEALED CONDITION

material whose composition is indicated in the text and from which all specimens were machined, either in the as-cast condition or in the annealed condition. Table 11 is a summary of the physical properties for this plate material.

Also, from the same cast of 4-21-49, 1-in.-diam bars were cast, from which 0.505-in.-diam tensiles were made. The physical properties are shown in Table 12 (32).

TABLE 11 PHYSICAL PROPERTIES OF THE PLATE MATERIAL—MAGNESIUM-TREATED NODULAR IRON

Tension specimen, No.	Tension specimen, diam	Nominal tensile strength, lb/sq. in.	Remarks
<i>As-cast condition</i>			
CAT-3	0.188	93,500	Plate 1, ladle 2, cast 4-21-49
CAT-4	0.191	103,500	Plate 1, ladle 2, cast 4-21-49
<i>Annealed condition</i>			
CAT-5	0.188	70,200	Plate 2, ladle 2, cast 4-21-49
CAT-6	0.188	69,200	Plate 2, ladle 2, cast 4-21-49
CAT-7	0.189	66,500	Plate 3, ladle 2, cast 4-21-49
CAT-8	0.197	67,200	Plate 3, ladle 2, cast 4-21-49

TABLE 12 PHYSICAL PROPERTIES OF NODULAR CAST IRON, MAGNESIUM-TREATED, CAST 4-21-49, AS-CAST CONDITION

Nominal tensile strength, lb/sq. in.	Tension specimen diameter, in.	Brinell hardness, No.	Remarks
94,200	0.505	269	Ladle 2, first iron
94,000	0.505	262	Ladle 2, last iron

With this information the endurance ratios are in agreement with those obtained by Grant for this composition. Based upon the fatigue strength of the 0.19-in.-diam test piece, the endurance ratio of the as-cast material is 0.45.

Permanent mold irons are of gray-iron composition cast in water-cooled metal molds and fully annealed to give a structure of alpha ferrite and graphite (33). The metal molds are given coatings which prevent the castings from adhering to the mold and reduce the thermal shock when the molten metal strikes the mold. Fig. 13 of the paper represents the results obtained from the paper by Schneidewind and Hoenicke (33) in which Fig. 3 of that article was reproduced. Fig. 13 shows the influence of cast section and notches on the endurance limit of permanent iron. Standard fatigue specimens were prepared but the notch angle, notch radius, and depth are not reported.

The author thanks Professor Lazan and Mr. Grant for their interest and comments.

BIBLIOGRAPHY

- 31 "Producing Nodular Graphite With Magnesium," by C. K. Donoho, *American Foundryman*, February, 1949.
- 32 Private communication with C. K. Donoho, chief metallurgist, American Cast Iron Pipe Co., Birmingham, Alabama, December 28, 1951.
- 33 "A Study of the Chemical, Physical, and Mechanical Properties of Permanent Mold Gray Iron," by Richard Schneidewind and Edward C. Hoenicke, *Proceedings of the ASTM*, vol. 42, 1942, pp. 622-634.

Relaxation of Stress in a Heat-Exchanger Tube of Ideal Material

By E. A. DAVIS,¹ EAST PITTSBURGH, PA.

Since relaxation tests are usually run on tensile specimens, the behavior of members under a state of combined stress is not well known. Analytical solutions of the relaxation of an elasticoviscous tube in a rigid tube sheet in both plane stress and a modified plane strain are worked out. The effect of reloading tensile specimens in relaxation is discussed and results of tests on an aluminum alloy are presented to illustrate these effects.

NOMENCLATURE

The following nomenclature is used in the paper:

- r, θ, z = radial, tangential, and axial directions
- σ = normal stress
- τ = shearing stress
- $\epsilon, \epsilon', \epsilon''$ = total, elastic, and plastic normal strain
- E = modulus of elasticity
- ν = Poisson ratio
- σ^*, ϵ^* = initial stress and strain in relaxation tests
- t = time
- p = pressure on outside surface of tube
- a, b = inside and outside radii of tube
- u, v = stress variables

$$u = \sigma\theta + \sigma_r, v = \sigma\theta - \sigma_r$$

$\psi = 3\phi$ = coefficient of viscosity

INTRODUCTION

Relaxation is the redistribution and decay of the stress in a body in which a constant total strain is maintained. Under such circumstances any increase in plastic strain must be counterbalanced by an equivalent reduction in the elastic strain. Probably the most familiar example of relaxation is the decay of the stress in the bolts of turbine-cylinder or steam-piping joints. However, the redistribution and the decay of the shrink-fit stresses in turbine disks and the rolled-in stresses in heat-exchanger tubes are also examples of relaxation. Actually, these examples represent true relaxation problems only if the flanges or the shafts or the tube sheet can be considered as rigid. In most cases the stresses in these parts are much lower than in the parts under consideration and hence the assumption of relaxation conditions is made. In the heat-exchanger tube sheet, for example, the minimum spacing between holes is usually about 4 times the tube-wall thickness. This makes the average hoop stress in the tube at least twice that part of the tube-sheet stress that is due to the tube rolling. Furthermore, the tube-sheet material is usually much stronger than that used in the tubes.

¹ Advisory Engineering, Westinghouse Electric Corporation, Mem. ASME.

Contributed by the Heat Transfer and Applied Mechanics Divisions and presented at the Annual Meeting, New York, N. Y., November 26-December 1, 1950, of THE AMERICAN SOCIETY OF MECHANICAL ENGINEERS.

NOTE: Statements and opinions advanced in papers are to be understood as individual expressions of their authors and not those of the Society. Manuscript received at ASME Headquarters, October 9, 1950. Paper No. 50-A-122.

Practically all relaxation tests are carried out on tensile specimens. Therefore very little is known about the effect of a state of combined stress upon the relaxation of materials. The present paper is concerned with the relaxation of a very simple ideal material in which the behavior under combined stress can be determined. It was the plan of the author at the beginning of this investigation to treat the problem more generally and to attempt to determine the behavior of actual materials, but the difficulties of integration were too great and the only material that could be treated analytically was the ideal elasticoviscous material. This is a material that has two independent sets of properties. It has elastic properties determined by two elastic constants E and ν , and also plastic properties which are determined by a constant coefficient of viscosity $\psi = 3\phi$.

RELAXATION OF ELASTICOVISCOUS MATERIAL

The elastic strains are

$$\epsilon_i' = \frac{1}{E} (\sigma_i - \nu\sigma_2 - \nu\sigma_3), \text{ etc.} \quad [1]$$

and the plastic strain rates are

$$\frac{d\epsilon_i''}{dt} = \frac{1}{\phi} \left(\sigma_i - \frac{\sigma_2}{2} - \frac{\sigma_3}{2} \right), \text{ etc.} \quad [2]$$

The relaxation under pure axial tension ($\sigma_2 = \sigma_3 = 0$) is determined from the condition of constant total strain

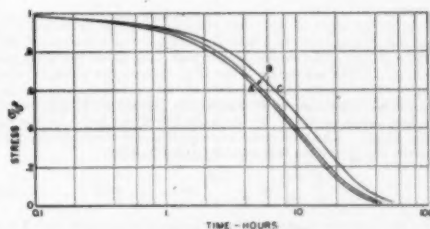
$$\epsilon = \epsilon' + \epsilon'' = \epsilon^* \quad [3]$$

The components of strain will vary with the time in the following manner

$$\frac{d\epsilon'}{dt} + \frac{d\epsilon''}{dt} = 0 \quad [4]$$

By substituting Equations [1] and [2] in Equation [4] we get

$$\frac{1}{E} \frac{d\sigma}{dt} + \frac{1}{\phi} \sigma = 0 \quad [5]$$



A, Tensile specimen—Equation [6]
B, Tube under plane stress—Equation [33] or [34]
C, Tube under plane strain—Equation [45] or [46]

FIG. 1 RELAXATION OF ELASTICOVISCOUS MATERIAL, $E/\phi = 0.1 \frac{1}{H_2}$

The solution of this equation is the well-known relaxation expression of Maxwell

$$\sigma = \sigma^* e^{-Et/\phi} \quad [6]$$

where σ^* is the initial stress in the specimen at $t = 0$. This is the stress corresponding to the strain ϵ^* when it is totally elastic

$$\sigma^* = E\epsilon^* \quad [7]$$

Equation [6] with a value of E/ϕ equal to 0.1 is plotted as curve A in Fig. 1.

In the following we shall deal with a thick-walled tube that has been rolled into a rigid tube sheet. The elasticity of the tube sheet could be taken into account by reducing the elastic modulus of the tube material by an appropriate amount,² but in this example we will discuss the simple problem of the rigid tube sheet. The outside diameter of the tube is $2b$ while the inside diameter is $2a$. The subscripts θ , r , and z are used to designate the tangential, the radial, and the axial directions, respectively. The stress distribution at $t = 0$ with an external pressure p will be the elastic distribution and hence we can write that at $t = 0$

$$\sigma_r = -\frac{pb^2}{b^2 - a^2} \left(1 - \frac{a^2}{r^2}\right) = -c_1 \left(1 - \frac{a^2}{r^2}\right) \quad [10]$$

$$\sigma_\theta = -\frac{pb^2}{b^2 - a^2} \left(1 + \frac{a^2}{r^2}\right) = -c_1 \left(1 + \frac{a^2}{r^2}\right) \quad [11]$$

These equations will be used as part of the boundary conditions for the relaxation problem.

In dealing with problems of rotational symmetry, it is sometimes more convenient to introduce two new variables u and v which are defined as

$$u = \sigma_\theta + \sigma_r, \quad v = \sigma_\theta - \sigma_r \quad [12]$$

In terms of these new variables Equations [10] and [11] can be written

$$u = -2c_1 \quad [13]$$

$$v = -2c_1 \frac{a^2}{r^2} \quad [14]$$

The equilibrium of forces on an element of material in a body is not affected by the presence of small plastic strains and, therefore, the equilibrium equation from the elastic problem can be used

$$r \frac{\partial \sigma_r}{\partial r} + \sigma_r - \sigma_\theta = 0 \quad [15]$$

In terms of u and v this is

² As an example of how this reduced modulus is obtained, consider the uniaxial case of a bolt in a flange. For relaxation of the assembly of bolt and flange it is now necessary to set the total tensile strain rate in the bolt equal to the total compressive strain rate in the flange. This means that the sum of the two strain rates must be zero. The expression corresponding to Equation [5] will now contain two terms for the stress in the bolt and two terms for the stress in the flange. The two terms representing the elastic strain rates in both the flange and the bolt must be added together

$$\frac{1}{E_b} \frac{d\sigma_b}{dt} + \frac{1}{E_f} \frac{d\sigma_f}{dt} + \dots = 0 \quad [8]$$

If the stress in the flange is k times the stress in the bolt $\sigma_f = k\sigma_b$ the term $d\sigma_b/dt$ can be factored out of the sum just obtained. The remaining factor $(1/E_b) + (k/E_f)$ is the reciprocal of the reduced modulus E_{bf}

$$\frac{1}{E_{bf}} = \frac{1}{E_b} + \frac{k}{E_f} \quad [9]$$

$$r \frac{\partial u}{\partial r} = r \frac{\partial v}{\partial r} + 2v \quad [16]$$

For the development of the compatibility equation, it will be necessary to take into account the total strain $\epsilon = \epsilon' + \epsilon''$. When the radial displacement is eliminated from the expressions for the strains for the symmetrical case considered here, the compatibility equation is

$$r \frac{\partial \epsilon_\theta}{\partial r} + \epsilon_\theta - \epsilon_r = 0 \quad [17]$$

In order to express this in terms of the stresses it is necessary to break it up into its elastic and plastic components and to differentiate with respect to the time t

$$r \frac{\partial^2 \epsilon_\theta'}{\partial r \partial t} + r \frac{\partial^2 \epsilon_\theta''}{\partial r \partial t} + \frac{\partial \epsilon_\theta'}{\partial t} + \frac{\partial \epsilon_\theta''}{\partial t} - \frac{\partial \epsilon_r'}{\partial t} - \frac{\partial \epsilon_r''}{\partial t} = 0 \quad [18]$$

It is also necessary to define the nature of the stress in the axial direction.

PLANE STRESS

For the case of plane stress, $\sigma_z = 0$, the strain-rate relations are

$$\left. \begin{aligned} \frac{\partial \epsilon_\theta'}{\partial t} &= \frac{1}{E} \left(\frac{\partial \sigma_\theta}{\partial t} - \nu \frac{\partial \sigma_r}{\partial t} \right), \text{ etc.} \\ \frac{\partial \epsilon_r''}{\partial t} &= \frac{1}{\phi} \left(\sigma_\theta - \frac{\sigma_r}{2} \right), \text{ etc.} \end{aligned} \right\} \quad [19]$$

When these relationships and Equation [15] are substituted in Equation [18], the compatibility equation can be expressed in terms of u as

$$\frac{\partial^2 u}{\partial r \partial t} = -\frac{E}{\phi} \frac{\partial u}{\partial r} \quad [20]$$

If this is integrated with respect to the time t , we get

$$\frac{\partial u}{\partial r} = A_1 e^{-Et/\phi} \quad [21]$$

but at $t = 0$ the boundary conditions, as given in Equation [13], require that u will not vary along the radius. Therefore we must set A_1 equal to zero. The solution of Equation [21] then becomes

$$u = -2c_1 f_1(t) \quad [22]$$

where $f_1(t)$ must have the value of unity at $t = 0$.

Since $\partial u/\partial r = 0$ from Equation [22] it is evident that the right side of Equation [16] can also be set equal to zero

$$r \frac{\partial v}{\partial r} + 2v = 0 \quad [23]$$

The solution of this equation is

$$v = \frac{A_2 f_2(t)}{r^2} \quad [24]$$

If u is to be equal to v at $r = a$ for all values of t , then

$$v = -2c_1 \frac{a^2}{r^2} f_1(t) \quad [25]$$

The function of time $f_1(t)$ must be evaluated now from the boundary conditions imposed by the rigid tube sheet upon the relaxation of the tube. At the outside radius of the tube $r = b$, there will be no radial displacement. This is equivalent to stat-

ing that at $r = b$ the tangential strain ϵ_θ will not vary with the time t

$$\frac{\partial \epsilon_\theta}{\partial t} = \frac{\partial \epsilon_\theta^e}{\partial t} + \frac{\partial \epsilon_\theta^p}{\partial t} = \frac{1}{E} \left(\frac{\partial \sigma_\theta}{\partial t} - \nu \frac{\partial \sigma_r}{\partial t} \right) + \frac{1}{\phi} \left(\sigma_\theta - \frac{\sigma_r}{2} \right) = 0 \quad [26]$$

In terms of u and v this becomes

$$(1 - \nu) \frac{\partial u}{\partial t} + (1 + \nu) \frac{\partial v}{\partial t} = - \frac{E}{2\phi} (u + 3v) \dots [27]$$

and when Equations [22] and [25] for $r = b$ are substituted, it reduces to

$$[b^2(1 - \nu) + a^2(1 + \nu)] \frac{df_1}{dt} = - \frac{E}{2\phi} [b^2 + 3a^2] f_1 \dots [28]$$

* The time function then is

$$f_1 = e^{-EBt/\phi} \dots [29]$$

where

$$B_1 = \frac{b^2 + 3a^2}{2[b^2(1 - \nu) + a^2(1 + \nu)]} \dots [30]$$

The quantities u and v then become

$$u = -2c_1 e^{-EBt/\phi} \dots [31]$$

$$v = -2c_1 \frac{a^2}{r^2} e^{-EBt/\phi} \dots [32]$$

and the stresses are

$$\sigma_r = - \frac{pb^2}{b^2 - a^2} \left(1 - \frac{a^2}{r^2} \right) e^{-EBt/\phi} = \sigma_r^* e^{-EBt/\phi} \dots [33]$$

$$\sigma_\theta = - \frac{pb^2}{b^2 - a^2} \left(1 + \frac{a^2}{r^2} \right) e^{-EBt/\phi} = \sigma_\theta^* e^{-EBt/\phi} \dots [34]$$

These equations are identical with the elastic equations at $t = 0$. The stress distribution remains the same as in the elastic case as the relaxation takes place. A comparison of the relaxation of a tube under plane stress with that of a tensile specimen is shown in Fig. 1. Curve B represents either Equation [33] or [34] with the same value of E/ϕ as was used in Equation [6] for curve A. For the tube represented by curve B the inside diameter has been taken as 0.75 times the outside diameter and the Poisson ratio has been taken as 0.3. The value of the constant B_1 in Equations [33] and [34] under these circumstances is 0.94 as compared to unity for pure tension.

The constant B_1 depends upon the dimensions of the tube and upon the Poisson ratio. For a very thin-walled tube the stress in the tube approaches pure circumferential compression, and it can be seen that B_1 approaches unity as a approaches b . Another interesting case is noted when $\nu = 0.5$. This corresponds to an incompressible material, and with this value of ν the constant B_1 again is unity. The incompressible tube relaxes in the same manner as the tensile specimen.

PLANE STRAIN

The cases of plane strain and plane stress were introduced into elasticity problems in order to simplify the three-dimensional equations. When total strains composed of both elastic and plastic components are considered, however, the usual condition of plane strain, $\epsilon_z = 0$, does not correspond to a simplified case. Hence in this paper a modified plane strain in which the axial stress is the average of the other two stresses, is considered.

$$\sigma_z = \frac{\sigma_\theta + \sigma_r}{2} \dots [35]$$

This is what σ_z would be for a purely viscous material under plane strain. It also would be correct for an incompressible elastic body where $\nu = 0.5$. For all other values of ν it does not quite meet the conditions of plane strain.

The strain rates for this modified plane strain are

$$\left. \begin{aligned} \frac{\partial \epsilon_\theta^e}{\partial t} &= \frac{1}{E} \left[\left(1 - \frac{\nu}{2} \right) \frac{\partial \sigma_\theta}{\partial t} - \frac{3\nu}{2} \frac{\partial \sigma_r}{\partial t} \right] \\ \frac{\partial \epsilon_r^e}{\partial t} &= \frac{1}{E} \left[\left(1 - \frac{\nu}{2} \right) \frac{\partial \sigma_r}{\partial t} - \frac{3\nu}{2} \frac{\partial \sigma_\theta}{\partial t} \right] \\ \frac{\partial \epsilon_\theta^p}{\partial t} &= \frac{3}{4\phi} (\sigma_\theta - \sigma_r) \\ \frac{\partial \epsilon_r^p}{\partial t} &= \frac{3}{4\phi} (\sigma_r - \sigma_\theta) \end{aligned} \right\} \dots [36]$$

The equilibrium and compatibility equations are the same as for the previous case. Therefore Equations [15], [16], and [18] are applicable to this case. By combining Equations [15], [18], and [36] and making use of the variables u and v as defined in Equation [12], the compatibility equation reduces to

$$\frac{2 - \nu}{E} \frac{\partial}{\partial t} \left(r \frac{\partial v}{\partial r} + 2v \right) + \frac{3}{2\phi} \left(r \frac{\partial v}{\partial r} + 2v \right) = 0 \dots [37]$$

which may be transformed by making use of Equation [16] to

$$\frac{2 - \nu}{E} \frac{\partial^2 u}{\partial r^2} + \frac{3}{2\phi} \frac{\partial u}{\partial r} = 0 \dots [38]$$

This equation is the same in form as Equation [20] and we can write

$$u = -2c_1 f_2(t) \dots [39]$$

$$v = -2c_1 \frac{a^2}{r^2} f_2(t) \dots [40]$$

where the time function $f_2(t)$ must be established as before by considering the relaxation of a given tube just as was done in Equation [26]. In the present case the equivalent of Equation [26] is

$$\frac{\partial \epsilon_\theta}{\partial t} = \frac{\partial \epsilon_\theta^e}{\partial t} + \frac{\partial \epsilon_\theta^p}{\partial t} = \frac{2 - \nu}{2E} \frac{\partial \sigma_\theta}{\partial t} - \frac{3\nu}{2E} \frac{\partial \sigma_r}{\partial t} + \frac{3}{4\phi} (\sigma_\theta - \sigma_r) = 0 \dots [41]$$

In terms of u and v this becomes

$$(1 - 2\nu) \frac{\partial u}{\partial t} + (1 + \nu) \frac{\partial v}{\partial t} = - \frac{3E}{2\phi} v \dots [42]$$

By substituting Equations [39] and [40] in this equation and integrating, we get for the time function

$$f_2(t) = e^{-EBt/\phi} \dots [43]$$

where

$$B_2 = \frac{3a^2}{2[(1 - 2\nu)b^2 + (1 + \nu)a^2]} \dots [44]$$

The stresses are then given by

$$\sigma_r = \sigma_r^* e^{-EBt/\phi} \dots [45]$$

$$\sigma_0 = \sigma_0^* e^{-EBd/\phi} \dots \dots \dots [46]$$

Curve C in Fig. 1 is a plot of these equations with the same values of ν , a , and b as was used for curve B. The curves in Fig. 1 show that the tube under plane stress relaxes at a slightly lower rate than the pure-tension specimen, and that the tube under plane strain relaxes more slowly than the tube under plane stress. The increase in relaxation properties of the tube under plane stress over that of the tensile specimen is due mainly to the stress distribution in the tube wall. In the tube the highest stresses and therefore the most rapid relaxation is at the inside surface of the tube. The stresses are lower at the surface where the rolled-in fit occurs. In an elasticoviscous disk shrunk on a shaft it can be shown that the rate of relaxation is greater than in a tensile specimen. The relative increase in relaxation properties for the plane-strain condition is due to the added restraint of the axial stress. Since both σ_r and σ_θ are compressive stresses, an intermediate compressive stress σ_z would tend to lower the magnitude of the shearing stresses in the tube wall.

It must be remembered that the expressions just developed are for an ideal material in which the plastic-strain rates are proportional to the stress. In order to approximate the behavior of actual materials it would be necessary to replace the constant ϕ in Equations [19] and [36] with some function of the state of stress and possibly also of the plastic strain.³ Several attempts at such an approximation have been tried, but the integrations involved have been too difficult for analytical solutions. The simple cases that have been worked out show that the data from relaxation tests in pure tension provide a safe estimate of the relaxation of stress in heat-exchanger tubes.

For actual materials it might be argued that since the plastic-strain rates are proportional to higher powers of the stress, the stress distribution would change in a manner that would spread the stress out more evenly along the radius and thus work the material more advantageously. Such an argument would show that tubes of actual materials would relax much more slowly than specimens in pure tension. It is difficult, however, to picture all the factors that affect the relaxation of stress in a tube or a disk and hence such arguments should be pursued with caution.

EFFECT OF RELOADING ON RELAXATION

The data to be presented here were obtained from tests on an aluminum alloy. Although this is not a commonly used heat-exchanger-tube material, its behavior should be quite typical of such alloys. The actual quantitative values of stress will not be of importance, but the general shape of the relaxation curves and the behavior of the material when reloaded will be quite similar to that of heat-exchanger tubes.

In Fig. 2 is shown a set of relaxation curves. Each curve represents a separate relaxation test. The initial stress or the stress to which the specimen was loaded initially is denoted by an asterisk. For practical purposes relaxation tests are not run for extremely long times. The test curves must be extrapolated to longer times. To facilitate this extrapolation the curves are plotted on semilog paper. An occasional long-time test is run to be used as a guide in the extrapolation.

There are two ways in which the effect of reloading can be studied. One way is to allow a specimen to relax for a certain time and then to raise the stress back up to the initial stress. This is the type of reloading that occurs when bolts are retightened. The other way is to unload the specimen and to let it stand at temperature for some time and then to reload to the strain that

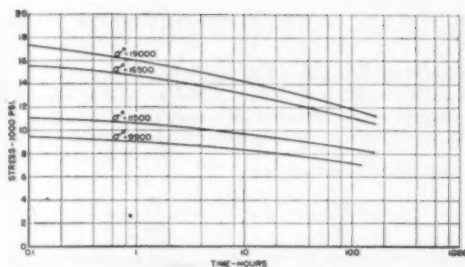
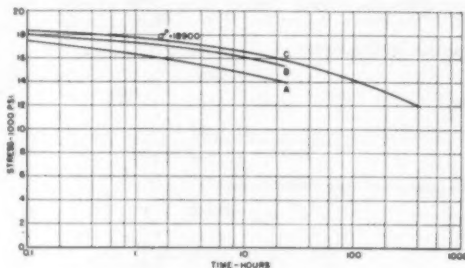


FIG. 2 RELAXATION OF ALUMINUM ALLOY



A. Original relaxation
B. After first reloading
C. After second reloading

FIG. 3 RELOADING AFTER ONE DAY OF RELAXATION

existed just before the unloading. Presumably a period at no load and at normal temperature could be added to this unloaded time without affecting the over-all results. In the reloading the specification of the previous strain rather than the previous stress has been deliberate. This is to take into account the recovery or shortening of a tensile specimen that takes place while the specimen is unloaded.

In a rolled-in heat-exchanger tube there are stresses due to several factors, and it may be quite difficult to determine how or when a heat-exchanger tube is reloaded. When the tubes are first rolled in, there is a compressive stress in the tube wall due to the rolling process. This stress is increased as the temperature is raised if the thermal expansion of the tube material is greater than that of the tube sheet. In so far as the author knows, the only way this tube can be unloaded and reloaded is by changing the temperature. Decreasing the temperature will have the effect of unloading the tube partially, but this also will slow down any recovery that might take place. The actual case, then, is somewhat different from the two ways of unloading that are to be described, but it is felt that test results illustrating the two previously mentioned ways of reloading will be of interest.

In Fig. 3 is shown the effect of reloading a specimen after 24 hr of relaxation. In Figs. 4 and 5 is shown the effect of reloading after 1 week of relaxation. In all of these tests the reloading has been done according to the first-mentioned way of reloading. It will be noted that in every instance the curve obtained after the first reloading is considerably better than the original curve. This is mainly due to the strain hardening that occurred during the original test. The relaxation is again improved by a second reloading in all cases, except that shown in Fig. 4 where the improvement is very slight.

³ For a discussion of this topic, see the author's paper "Increase of Stress With Permanent Strain and Stress-Strain Relations in the Plastic State for Copper Under Combined Stresses," *Journal of Applied Mechanics*, Trans. ASME, vol. 65, 1943, p. A-187.

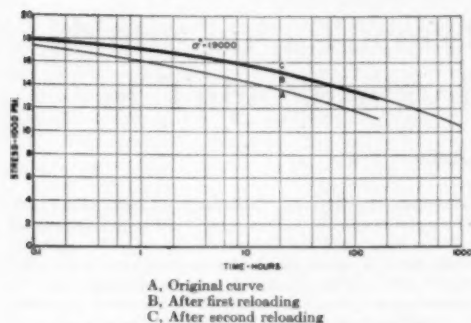


FIG. 4 RELOADING AFTER ONE WEEK OF RELAXATION

The effect of reloading according to the second type of reloading is shown in Fig. 6. Here the specimen was unloaded and then reloaded to the previous strain. In the first and third unloadings the specimen was reloaded immediately after unloading. There was very little time for recovery to take place. For this reason the stress after reloading was only slightly higher than that existing just before unloading. In the second and fourth unloading about 3 hours elapsed before the specimen was reloaded. This lapse gave greater time for recovery, and the recovery caused the stress to be noticeably higher after reloading. This increase in stress, however, quickly dies out, and the relaxation curve continues as though no unloading had taken place.

CONCLUSIONS

For the ideal elasticoviscous material a rolled-in condenser tube will relax at a slower rate than a tensile specimen. For actual materials it would seem that the tube would relax still more slowly. In any event the tensile-relaxation data will offer a safe guide to the relaxation of the tube. Based upon the results of these calculations this same comment cannot be made for the relaxation of a disk on a shaft.

For the type of unloading and reloading present in heat-exchanger tubes, the relaxation is not much affected by reloading.

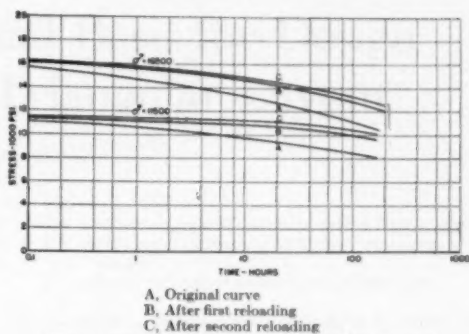


FIG. 5 RELOADING AFTER ONE WEEK OF RELAXATION

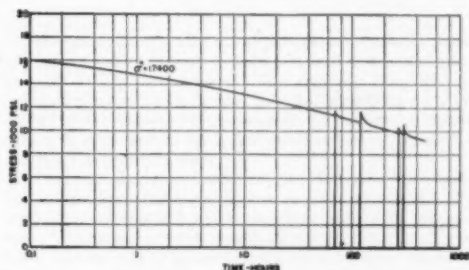


FIG. 6 UNLOADING AND RELOADING OF RELAXATION SPECIMEN

ACKNOWLEDGMENTS

The author wishes to acknowledge the assistance of D. D. Frederick and R. T. Jones in the running of the reloading tests and to thank the Westinghouse Electric Corporation for permission to publish these results.



The following table shows the results of the experiments conducted by the author. The data is presented in a tabular format with columns for various parameters and rows for different experimental conditions.

Parameter	Condition 1	Condition 2	Condition 3
Value 1	1.2	1.5	1.8
Value 2	2.5	3.0	3.5
Value 3	4.0	4.5	5.0
Value 4	6.0	6.5	7.0
Value 5	8.0	8.5	9.0

The results of the experiments show that the curve rises and then levels off, indicating a maximum value. The shaded area represents the total area under the curve, which is proportional to the total value of the function.

The following table shows the results of the experiments conducted by the author. The data is presented in a tabular format with columns for various parameters and rows for different experimental conditions.

Parameter	Condition 1	Condition 2	Condition 3
Value 1	1.2	1.5	1.8
Value 2	2.5	3.0	3.5
Value 3	4.0	4.5	5.0
Value 4	6.0	6.5	7.0
Value 5	8.0	8.5	9.0

The results of the experiments show that the curve rises and then levels off, indicating a maximum value. The shaded area represents the total area under the curve, which is proportional to the total value of the function.

The following table shows the results of the experiments conducted by the author. The data is presented in a tabular format with columns for various parameters and rows for different experimental conditions.

Parameter	Condition 1	Condition 2	Condition 3
Value 1	1.2	1.5	1.8
Value 2	2.5	3.0	3.5
Value 3	4.0	4.5	5.0
Value 4	6.0	6.5	7.0
Value 5	8.0	8.5	9.0

Notes on a Theoretical Basis for Design of Tube Sheets of Triangular Layout

By I. MALKIN,¹ NEW YORK, N. Y.

This paper offers an approximate analytical procedure for determination of the elastic surface of tube sheets under bending. The procedure derived has been used successfully for several years as a basis for design of tube sheets of the frequently applied triangular pitch. The design formulas developed in the paper underwent experimental tests recently with satisfactory results. A description and detailed discussion of the experimental work are given also.

NOMENCLATURE

The following nomenclature is used in the paper:

- a } = outer and inner radii, respectively, of a cylindrical shell
- b } = side lengths of a rectangular plate
- c } = one of the two side lengths of a rectangular cross section
- C } = $1/3\beta h^3 E/(1+\nu)$
- d } = diameter of a circular hole
- e_{xx} } = the three important strain components in problem of plate in bending
- e_{yy} }
- e_{xy} }
- E = Young's modulus of elasticity
- E' = same for "equivalent" plate to be defined later
- h = thickness of plate or tube sheet; also, one of two side lengths of a rectangular cross section
- I = moment of inertia of cross-sectional area of a bar
- $K = C/EI$
- L = length of a bar
- m = reciprocal of the Poisson ratio
- p = uniformly distributed load
- $r_0 = 1/2(a+b)$
- s = spacing of holes in tube sheet
- U = strain energy
- w = deflection of plate or tube sheet
- x } = Cartesian rectangular co-ordinates
- y }
- z }
- β = numerical coefficient occurring in theory of torsion of bars of rectangular cross section (see following)
- Γ = a constant defined by Equation [28]
- Δ = Laplacean differential operator in plane
- η = one of three co-ordinates of a Cartesian rectangular system $\xi\eta z$
- θ = angle of rotation
- $\mu = 4\sqrt{3}Lc/s^3$

- ν = Poisson ratio
- ν' = same for "equivalent" plate to be defined later in paper
- ξ = one of three co-ordinates of a Cartesian rectangular system $\xi\eta z$
- ρ = radius of curvature of middle surface of tube sheet
- σ_x } = the three important stress components in problem of plate in bending
- σ_y }
- τ_{xy} }
- φ = azimuth angle

INTRODUCTION

There are a variety of heat exchangers, which function by means of a great number of tubes, enclosed in a shell or in a casing and properly fixed in tube sheets. A tube sheet is a plane plate of constant thickness with circular holes for connection with the tubes. For a better understanding of the subsequent discussion it is important to say a few words about the connection between tubes and tube sheet.

In the case of pressure vessels a tight attachment of the tubes to the tube sheet is necessary in order to prevent leakages. The methods of realizing such a tight connection will not be discussed here; contributions to this question will be found in the literature.² In the case of an air heater there is no great danger of leakages, and the question of a tight connection between tubes and tube sheet is of less importance. It must be emphasized, however, that in consequence of its complicated connection with the tubes, a tube sheet is generally the object of particular care in the design of heat exchangers. If one realizes that tube sheets of, say, 10 ft diam and 4 or 5 in. thick for a system of several thousand tubes are not impossible in the design of modern pressure vessels, it is not difficult to understand why the engineer values so highly any information able to throw some light on the problem of satisfactory tube-sheet design. The questions involved are not only those concerning high material costs of a plate of dimensions of the order indicated and not only those of drilling several thousand holes of quite considerable length—there is still another question of great importance; if such a tube sheet fails, its repair or replacement will cause a long interruption in the functioning of the heat exchanger owing to the complicated work of separating the tube sheet from a bundle of such a great number of tubes.

As to the arrangement of the holes in a tube sheet,³ we will be concerned here with tube sheets of triangular layout only (see Fig. 1); tube sheets with holes arranged in square pitch seem to be less frequent. Fig. 1 is drawn to scale and it conveys, therefore, a correct idea of the relative dimensions of the holes and ligaments, as far as certain groups of air heaters and pres-

¹ Standards and Design Engineer, Foster Wheeler Corporation. Mem. ASME.

Contributed by the Heat Transfer and Applied Mechanics Divisions and presented at the Annual Meeting, New York, N. Y., November 26-December 1, 1950, of THE AMERICAN SOCIETY OF MECHANICAL ENGINEERS.

NOTE: Statements and opinions advanced in papers are to be understood as individual expressions of their authors and not those of the Society. Manuscript received at ASME Headquarters, October 30, 1950. Paper No. 50-A-120.

² "Theory of the Expanding of Boiler and Condenser Tube Joints Through Rolling," by A. Nadai, Trans. ASME, vol. 65, 1943, pp. 865-880.

"The Holding Power and Hydraulic Tightness of Expanded Tube Joints," by J. N. Goodier and G. J. Schoenow, Trans. ASME, vol. 65, 1943, pp. 489-496.

"Notes on the Tightness of Expanded Tube Joints," by G. Sachs, *Journal of Applied Mechanics*, Trans. ASME, vol. 69, 1947, pp. A-285-286.

³ "Heat Transmission," by W. H. McAdams, McGraw-Hill Book Company, Inc., New York, N. Y., 1942, p. 350.

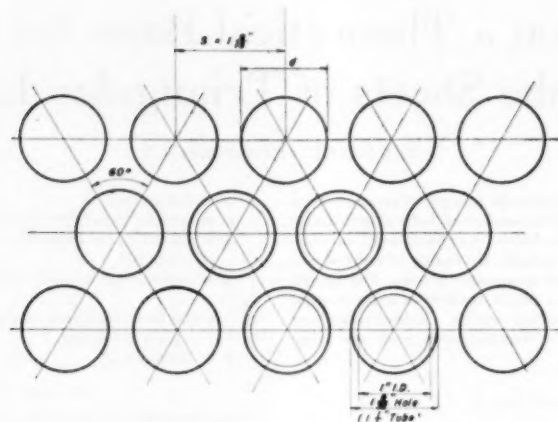


FIG. 1 PART OF A TUBE SHEET FOR TUBE BUNDLES OF TRIANGULAR PITCH

sure vessels are concerned. The thickness of a tube sheet is, of course, a function of pressure or load acting on the tube sheet. In pressure vessels it reaches proportions indicated, while in air heaters the thickness of a tube sheet may be a fraction of the hole diameter. The outside diameter of the tubes may be anywhere from 1 to 3 in.

In attempting to deal with the elastic problem of the tube sheet analytically, we shall start with the simpler type of problem, and this is the case of the air heater. This case is simpler, because the expansion of the tube ends into the holes of the tube sheet does not affect materially the state of stresses in the tube sheet.

The problem of the elastic tube sheet can be idealized as a special case of the problem of the plane plate with an arbitrary number of holes. This problem was recently treated by K. J. Schulz.⁴ Starting from the well-known stress function of Airy, used in the treatment of two-dimensional problems of elasticity, Schulz developed a solution of the problem of the plate with an arbitrary number of holes by introducing a number of stress functions assigned to the holes and adjusted to each other in such a way that the shear and normal stresses vanish along the boundary of each hole. The fulfillment of the latter boundary conditions requires the solution of an infinite number of linear equations for the indeterminate constants, which is being achieved by means of the method of iteration—a gigantic amount of work, which has been carried out successfully by Schulz for a great number of combinations of holes in the plate. His publications thus represent a powerful and practically productive generalization of the method of Airy in the problem of the plate. It applies primarily to the problem of a perforated plate under tension; an extension to the problem of a perforated plate under bending, which Schulz already effectively started, was cut short by his death under tragic circumstances.

It appears then that theoretical foundations for the design of tube sheets under bending with formulas ready for immediate

application to practical problems do not exist at the present time. The approximate analysis given in this paper is intended to fill the gap to an extent satisfying practical requirements.

Resuming the case of a tube sheet in an air heater, the following method of attack will be used.

Considering a tube sheet without tubes, we replace its circular holes by holes in the form of regular hexagons of the same area (Fig. 2), which reduce the perforated part of the tube sheet to a system of short elastic beam elements under bending and torsion. The beam elements are, in other words, in stress conditions similar to those of the elemental beams in a rectangular grid work discussed in the literature;⁵ they are connected into a hexagonal grid, in which each of them will be treated as a bar in bending and torsion.

It must be admitted at the outset that the small length of the elemental beams (as compared with the dimensions of the concentrations of material at the intersections of those beam elements) in our hexagonal grid work will more or less impair the accuracy of the results, but at the same time attention must be called to the fact that the mathematical analogy developed in the paper is entirely correct in the case of a hexagonal grid work in which the length of the beam elements is sufficiently large. As we diminish the length of the beam elements, we introduce deteriorating factors, but it is plausible to expect that even in the case of the hexagonal grid work with the short beam elements there still remains a fairly close affinity between the actual state of stresses and the one which follows from the application of the mathematical analogy just mentioned. In so far as the reliability of this analogy can be established, it leads to the determination of the elastic constants of an equivalent plate and thus to the solution of the elastic problem of the tube sheet. Knowing the elastic constants of the equivalent plate, we can find the components of curvature in the beam elements of the tube sheet for given loading conditions and thus the stresses in them as well. As to the question of reliability, the reader is referred to the concluding sections of the paper, which give a detailed account of the experimental verification of the formulas derived theoretically in the first part of the paper.

⁴ "Over den Spanningstoestand in Doorboorde Platen," by K. J. Schulz, Doctor Thesis, Delft, Holland, 1941, 112 pp., followed by many additional contributions published in the *Bulletins of the Netherlands Akad. Wetenschap*. An abstract of the work carried out by the late Dr. Schulz will be found in "Advances in Applied Mechanics," the report by Prof. C. B. Bieseno, in *Academic Press*, New York, N. Y., vol. 1, 1948, pp. 121-128.

⁵ "Theory of Plates and Shells," by S. Timoshenko, McGraw-Hill Book Company, Inc., New York, N. Y., and London, England, 1940, p. 190.

APPROXIMATE REDUCTION OF TUBE-SHEET PROBLEM TO PROBLEM OF A PLATE OF CERTAIN ELASTIC CONSTANTS

The starting point of our derivation of an approximate solution of the problem of a tube sheet under bending is the Hamiltonian "principle of least action,"¹ which reduces here simply to the "principle of minimum of potential energy" due to absence of motion. Thus, to give the problem of the tube sheet under bending an analytical expression, we shall approximate the perforated plate by an elastic solid of a form which permits a convenient way of computing the potential energy of deformation. The expression of the strain energy of the modified tube sheet allows us to reduce the tube-sheet problem to that of an equivalent plate. This reduction makes ultimately possible a determination of the stress distribution in the tube sheet. The paper deals only with the derivation of the formulas for the reduction just mentioned and with their experimental check.

We replace the actual tube sheet, as already indicated, by a nearly equivalent "idealized" tube sheet, characterized by a system of holes shown in Fig. 2. The circular holes are approximated by regular hexagons of the same area. To determine the deformation energy of the entire idealized tube sheet, we subdivide it into elements of the form *ABCDEF* (Fig. 2). All ele-

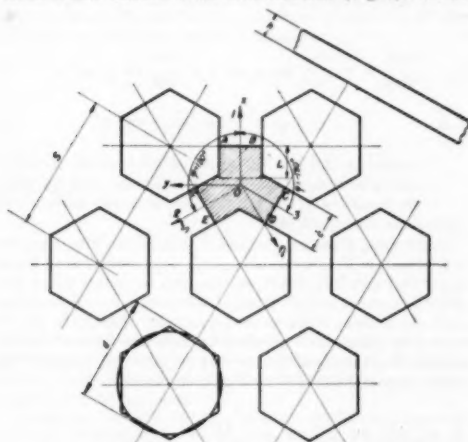


FIG. 2 IDEALIZED TUBE SHEET OF TRIANGULAR LAYOUT

ments are in essence equally oriented with respect to the three directions 01, 02, 03. (More accurately expressed, the integrand of Equation [16] does not change its sign, if x and y are replaced by $-x$ and $-y$, respectively.) We begin with computing the deformation energy of one of the beam elements. The deformation energy of the entire system will be determined by integration over the entire idealized tube sheet.

The deformation energy of any of the elements consists substantially (1) in bending of the beam elements 1-1, 2-2, 3-3 (Fig. 3), in the three respective planes passing through 1-1, 2-2, 3-3 perpendicularly to the middle plane of the tube sheet, and (2) in torsion of those elemental beams around axes parallel to the lines 1-1, 2-2, 3-3, respectively, as known to the reader, for example, from the treatment of the grid-work problem,² and more

generally from the treatment of the plate problem. Indeed, the formulas for the computation of the energy amounts for the tube-sheet problem can be derived easily from Kirchhoff's theory of plates in bending as follows:

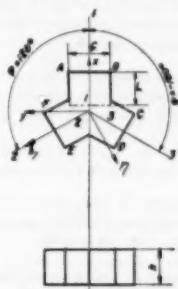


FIG. 3 ELEMENT OF IDEALIZED TUBE SHEET

Referring to a rectangular xyz -system of co-ordinates, with the middle surface of the plate in the xy -plane, the deformation energy of a plate under bending is given by the integral

$$U = \frac{1}{2} \iint \iint (\sigma_x \epsilon_{xx} + \sigma_y \epsilon_{yy} + \tau_{xy} \epsilon_{xy}) dx dy dz \dots [1]$$

where $\sigma_x, \sigma_y, \tau_{xy}$ are the three important stress components and $\epsilon_{xx}, \epsilon_{yy}, \epsilon_{xy}$ the three corresponding strain components, the integration being extended over the entire plate. Designating by w the deflection of the plate, by E and ν the modulus of elasticity and Poisson's ratio, respectively, we have, with w_{xx}, w_{yy}, w_{xy} representing the second derivatives of w with respect to x and y , the formulas

$$\left. \begin{aligned} E^{-1}(\sigma_x - \nu \sigma_y) &= \epsilon_{xx} = -zw_{xx} \\ E^{-1}(\sigma_y - \nu \sigma_x) &= \epsilon_{yy} = -zw_{yy} \\ 2E^{-1}(1 + \nu)\tau_{xy} &= \epsilon_{xy} = -2zw_{xy} \end{aligned} \right\} \dots \dots \dots [2]$$

Solving these equations for $\sigma_x, \sigma_y, \tau_{xy}$ and substituting the resulting expressions for the stress components, as well as those for the components $\epsilon_{xx}, \epsilon_{yy}, \epsilon_{xy}$ of strain, in terms of the derivatives of w into Equation [1], we obtain the expression for the potential energy of the plate under bending in terms of the derivatives of w , namely

$$U = \frac{Eh^3}{24(1 - \nu^2)} \iint_{\Phi} [(\Delta w)^2 - 2(1 - \nu)(w_{xx}w_{yy} - w_{xy}^2)] dx dy \dots \dots [3]$$

where h = thickness of plate, Φ = integration domain of plate in middle plane (xy -plane), and

$$\Delta w = w_{xx} + w_{yy} \dots \dots \dots [4]$$

(Δ = Laplacean differential operator in the plane.) Now let us resume the problem of the tube sheet proper.

In the case of the tube sheet the set of formulas just given undergoes the following modification. We have reduced the tube sheet to a system of elements *ABCDEF* (Fig. 2); each of these elements consists of three "beams" extending in the directions 01, 02, 03, respectively, and subjected, as already indicated, to bending and torsion. Consider the element 01 with the system xy of co-ordinates shown in Fig. 3. Since we have here to deal with a one-dimensional system under combined bending and torsion, we obviously have to use the formulas

¹ "Methoden der Mathematischen Physik," by R. Courant, Berlin, Germany, vol. 1, 1924, p. 207 (recently reprinted in this country by the Dover Publications, New York, N. Y.).

² "Treatise on the Mathematical Theory of Elasticity," by A. E. H. Love, Dover Publications, New York, N. Y., 1927, p. 166.

$$\frac{1}{2} \iiint \sigma_{xz} = -zw_{xx}, \sigma_{yz} = -Ezw_{xy} \left\{ \dots \dots [5] \right.$$

where, with the designations in Fig. 3

$$I = \frac{1}{12} c h^3 \dots \dots [6]$$

represents the moment of inertia of the cross section of the beam with respect to the neutral axis, parallel to the y -direction, of the cross section, while L = length of the beam element, and^{5,6}

$$\frac{1}{2} \iiint \tau_{xy} \epsilon_{xy} dx dy dz = \frac{1}{2} CL w_{xy}^2 \dots \dots [7]$$

where

$$C = \frac{\beta h c^3}{2(1 + \nu)} E \dots \dots [8]$$

is the torsional rigidity of the elemental beam; the numerical values of the coefficient β are given in Fig. 4.⁹ It must be em-



FIG. 4 COEFFICIENTS α AND β
(According to S. Timoshenko, "Strength of Materials," reference 5.)

phasized that in Equation [8] c always designates the shorter side of the rectangular cross section. Substituting the Equations [5] and [7] into Equation [1] we obtain the following expression for the strain energy U_1 of the elemental beam 01

$$U = \frac{1}{2} EIL \left(w_{xx}^2 + \frac{C}{EI} w_{xy}^2 \right) \dots \dots [9]$$

It should be noted that w_{xx} and w_{xy} are assumed to be constant in deriving Equations [5] and [7]; hence they represent mean values of w_{xx}, w_{xy} for the element $ABCDEF$.

We turn now to the beam elements extending in the two remaining directions 02 and 03, respectively.

Considering the element 02 with its system $\xi\eta$ of co-ordinates as shown in Fig. 3, we see at once from analogy with Equation [9] that the deformation energy of the beam element 02 can be written in the form

$$U_2 = \frac{1}{2} EIL \left(w_{\xi\xi}^2 + \frac{C}{EI} w_{\xi\eta}^2 \right) \dots \dots [10]$$

and it is now only necessary to express the derivatives $w_{\xi\xi}$ and $w_{\xi\eta}$ in terms of the derivatives of w with respect to one system of co-ordinates, and we choose our xzy -system for this purpose.

The $\xi\eta$ -system can be obtained from the xzy -system by a clock-

wise rotation through an angle $\varphi = 120$ deg. Consequently we have (see Fig. 5)

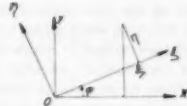


FIG. 5 TRANSFORMATION OF CO-ORDINATES

$$x = \xi \cos \varphi - \eta \sin \varphi, y = \xi \sin \varphi + \eta \cos \varphi$$

from which

$$\frac{\partial w}{\partial \xi} = \frac{\partial w}{\partial x} \frac{\partial x}{\partial \xi} + \frac{\partial w}{\partial y} \frac{\partial y}{\partial \xi} = \frac{\partial w}{\partial x} \cos \varphi + \frac{\partial w}{\partial y} \sin \varphi$$

$$\frac{\partial w}{\partial \eta} = \frac{\partial w}{\partial x} \frac{\partial x}{\partial \eta} + \frac{\partial w}{\partial y} \frac{\partial y}{\partial \eta} = -\frac{\partial w}{\partial x} \sin \varphi + \frac{\partial w}{\partial y} \cos \varphi$$

and by further differentiation we obtain

$$\frac{\partial^2 w}{\partial \xi^2} = \frac{\partial^2 w}{\partial x^2} \cos^2 \varphi + 2 \frac{\partial^2 w}{\partial x \partial y} \sin \varphi \cos \varphi + \frac{\partial^2 w}{\partial y^2} \sin^2 \varphi \dots \dots [11]$$

$$\frac{\partial^2 w}{\partial \xi \partial \eta} = -\frac{\partial^2 w}{\partial x^2} \sin \varphi \cos \varphi + \frac{\partial^2 w}{\partial y^2} \sin \varphi \cos \varphi$$

$$+ \frac{\partial^2 w}{\partial x \partial y} (\cos^2 \varphi - \sin^2 \varphi) \dots \dots [12]$$

Equations [11] and [12] apply to the beam 03 as well, if only φ be replaced by $-\varphi$. We thus obtain for the beam 03 Equations [11a], [12a], which it is not necessary to write down here explicitly.

Substituting Equation [11] and Equation [12] into Equation [10] we obtain U_2 in terms of w_{xx}, w_{xy}, w_{yy} . Substituting Equations [11a] and [12a] into Equation [10], we obtain the expression U_3 for the potential energy of deformation for the beam element 03 in terms of the same derivatives. Taking the sum of the energy amounts U_1 as given by Equation [9], and U_2, U_3 , computed as just explained, we find the potential energy of the entire element $ABCDEF$ to be given by the formula

$$U = \frac{1}{2} EIL \left\{ (1 + 2 \cos^2 \varphi + 2K \sin^2 \varphi \cos^2 \varphi) w_{xx}^2 \right. \\ \left. + (2 \sin^2 \varphi + 2K \sin^2 \varphi \cos^2 \varphi) w_{yy}^2 \right. \\ \left. + [8 \sin^2 \varphi \cos^2 \varphi + 2K(\cos^2 \varphi - \sin^2 \varphi)^2 + K] w_{xy}^2 \right. \\ \left. + 4 \sin^2 \varphi \cos^2 \varphi (1 - K) w_{xx} w_{yy} \right\} \dots [13]$$

where

$$K = C/EI \dots \dots [14]$$

Introducing into Equation [13]

$$\varphi = 120 \text{ deg, } \sin \varphi = \frac{1}{2} \sqrt{3}, \cos \varphi = -\frac{1}{2}$$

we find by simple computation

$$U = \frac{3}{16} (3 + K) EIL \left[(\Delta w)^2 - 4 \frac{1 + K}{3 + K} (w_{xx} w_{yy} - w_{xy}^2) \right] \dots \dots [15]$$

To find the density of energy distribution of bending over the

⁵ "Strength of Materials," by S. Timoshenko, D. Van Nostrand Company, Inc., New York, N. Y., vol. 1, 1940, p. 270.

⁶ "Theory of Elasticity," by S. Timoshenko, McGraw-Hill Book Company, Inc., New York, N. Y., 1934, pp. 245-249.

⁹ For practical purposes it is necessary to draw Fig. 4, on fine cross-section paper very accurately to a larger scale; the numerical values of β are given in a quantity, sufficient to plot the curve, in the books mentioned in the preceding two footnotes.

middle plane of the tube sheet, we divide the amount by the area

$$\frac{s^2 \sqrt{3}}{4}$$

the dimension s being given in Fig. 2. Multiplying the result by $dx dy$ and integrating over the middle plane of the tube sheet, we obtain, after substitution of Equation [6], the total deformation energy of the tube sheet to be given by the formula

$$U^* = \frac{(3+K)ELch^3}{16\sqrt{3}s^2} \iint \left[(\Delta w)^2 - 4 \frac{1+K}{3+K} \times (w_{xx}w_{yy} - w_{xy}^2) \right] dx dy \dots [16]$$

Comparison of the result, Equation [16], obtained for the tube sheet, with Equation [3], valid for a uniform elastic plate, yields an important conclusion. Since the Hamiltonian principle determines the entire behavior of the system considered, we see from this comparison at once that the deformation of the middle plane of the tube sheet can be determined exactly in the same way as that of a plate, if only we attribute to this fictitious plate, replacing the tube sheet, a modulus of elasticity E' and a Poisson ratio ν' satisfying the two relations

$$2(1-\nu') = 4 \frac{1+K}{3+K} \dots [17]$$

$$\frac{(3+K)ELch^3}{16\sqrt{3}s^2} = \frac{E'h^3}{24(1-\nu'^2)} \dots [18]$$

from which

$$E' = 4\sqrt{3} \frac{1+K}{3+K} \frac{Lc}{s^2} E \dots [19]$$

$$\nu' = \frac{1-K}{3+K} \dots [20]$$

Attention must be paid to the fact that in the case of a tube sheet of triangular layout, the equivalent fictitious plate is still a plate of isotropic material, which simplifies the computing work in the applications very considerably.

Equations [19] and [20] are accurate (within the limits of accuracy of the theory of bending and torsion of beams), if the ratio Lc is sufficiently large, i.e., if the ligaments are thin enough as compared with the diameter of the hexagonal holes. Of course, a hexagonal grid work of such characteristics cannot be obtained by replacing the circular holes by hexagonal ones, because the equivalent circular holes would overlap each other. In the case of a large (Lc) let us designate by μ the ratio of the area, occupied by the ligaments in the plane of the plate, to the total area of the fictitious full plate, so that (Fig. 2)

$$3Lc : \frac{\sqrt{3}}{4}s^2 = \mu \dots [21]$$

Then Equation [19] for E' assumes the simpler form

$$E' = \frac{1+K}{3+K} \mu E \dots [22]$$

a formula which may be used, with the same justification as Equation [19], in the case of the actual tube sheet as well. Designating by d the diameter of the circular holes we have then, with reference to Fig. 1, the following expression for μ

$$\mu = \left(\frac{1}{2} \sqrt{3}s^2 - \frac{1}{4}\pi d^2 \right) : \frac{1}{2} \sqrt{3}s^2 \dots [23]$$

This formula makes the computation of L , occurring in Equation [21], unnecessary. As to the width c of the elemental beams, a quantity which we will have to use, the equality of the area of a circular hole and that of the replacing hexagon yields the formula

$$c = s - 0.952d \dots [24]$$

Before discussing the question of an experimental check of Equations [19], [20], we shall apply an approximate analytical check.

APPROXIMATE VERIFICATION

Assume a tube sheet of triangular layout and of any boundary line, formed by the external lateral faces of the limiting hexagonal elements (Fig. 6), to be subjected to the action of bending moments $M = \text{const}$, uniformly distributed along that boundary line, and imagine the tube sheet subdivided into equal prismatic elements of regular hexagonal cross section just mentioned and illustrated by Fig. 6 in plan and elevation. On the basis of the analogy just developed, all of the hexagonal elements are in

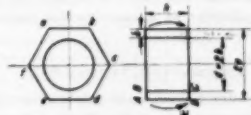


FIG. 6. TUBE-SHEET ELEMENT

identical conditions (as in the case of a full plate), characterized by the moment M acting on each of the six plane lateral faces of the element. Owing to this complete uniformity of distribution of moments, the tube sheet will assume a spherical shape, like a full plate, and the problem of the tube sheet is reduced to the problem of one of these hexagonal elements. The generatrices of the latter remain straight after deformation as well by reasons of symmetry. This means that the deformation of such an element will consist in a rotation of the rectangle $ABCD$ (Fig. 6), as a rigid area, in its own plane. Under these conditions the angle θ of rotation can be estimated and thus the radius ρ of curvature of the tube sheet as well. This value of ρ should be approximately equal to that derived for the equivalent uniform plate. The computation is to be carried out as follows:

Replace first the hexagon in Fig. 6 by an approximately equivalent circle leading to a circular cylinder of the radii a and b . The angle θ of rotation due to the moments M is given by¹⁰

$$\theta = \frac{12Mr_0}{EA^3 \log_e(a/b)}$$

and the radius of curvature is

$$\rho = \frac{r_0}{\theta} = \frac{EA^3}{M} \frac{1}{12} \log_e \left(\frac{a}{b} \right) \dots [25]$$

For the fictitious plate we obtain¹¹

$$\rho = \frac{1}{12(1-\nu')} \frac{EA^3}{M} \dots [26]$$

Referring to the designations in Figs. 1, 6, we consider the following example

¹⁰ Reference (7), vol. 2, p. 179.

¹¹ Reference (5), p. 46.

$$s = 3.125 \text{ in.}, d = 2s = 2.50 \text{ in.}, h = 0.875 \text{ in.}$$

From Equations [23] and [24] we get now

$$\mu = 0.42, c = 0.745 \text{ in.}$$

Referring to Fig. 6, we find that the side length ab of a hexagonal element $abcdef$ of the tube sheet is $s/\sqrt{3}$; the circle of equal area has a diameter $d_0 = 2a = 3.28 \text{ in.}$; $a = 1.64 \text{ in.}$ For $h/c = 0.875/0.745 = 1.174$, Fig. 4 gives $\beta = 0.165$, so that, according to Equations [14], [6], [8]

$$K = \frac{6\beta}{1 + \nu} \left(\frac{c}{h} \right)^2 = 0.553 \dots \dots \dots [27]$$

From Equations [20] and [22] we get

$$\nu' = 0.126, E' = 0.183E$$

With these numerical values Equations [25] and [26] give

$$\rho = 0.0225 (Eh^3/M) \text{ and } \rho = 0.0175 (Eh^3/M)$$

respectively. The approximation is, of course, quite rough; however, a better result was hardly to be expected from a primitive check. Possibilities of a more careful examination must be studied now.

EXPERIMENTAL VERIFICATION

Equations [19], [20] have been in practical use for design purposes since the beginning of 1946. Their field of application, as already mentioned, is in the design of tubular air heaters and of pressure vessels with tube chambers for chemical processes of certain special kinds. The latter field of application is the much more important one. In problems of this second group, slight modifications have been introduced into the fundamental formulas, modifications intended to take care of the stiffening influence of the tightly rolled-in tubes (see Introduction). A considerable number of pressure vessels with tube chambers for high pressure have been designed and fabricated on the basis of the tube-sheet formulas derived in the second section of the paper. These pressure vessels have been subjected to the test procedures prescribed by the pressure-vessel codes. In these tests as well as in operation the design has proved to be entirely satisfactory. This is, of course, a strong argument in favor of the tube-sheet design Equations [19], [20]; it is, however, no complete substitute for an experimental verification.

A convenient experimental test of the Equations [19], [20] can be derived from formulas for deflection of plates in bending. The subject of bending experiments with plates has been thoroughly discussed by A. Nadai.¹² A relatively simple check is afforded by the bending test of a circular plate on three point supports 120 deg apart along its circumference; an exact solution for this problem has been given by A. Nadai.¹³ As to the application of Nadai's solution to experiments with tube sheets, we shall return to this question later. Another promising check is provided by the bending test of a rectangular plate under uniformly distributed load and resting on four-point supports at its corners. An approximate formula for the maximum deflection in this case has been developed by A. and L. Foepl.¹⁴ This

formula was chosen to check Equations [19], [20]. The advantages and drawbacks of experimentation with rectangular plates on four-point supports will be briefly discussed.

The formula derived by A. and L. Foepl can be written in the form¹⁵

$$w = \Gamma \left[a_1^4 \left(1 - \frac{8}{m\pi^2} \frac{b_1^2}{a_1^2} \right) + b_1^4 \left(1 - \frac{8}{m\pi^2} \frac{a_1^2}{b_1^2} \right) \right] \dots [28]$$

where

w = center deflection of rectangular plate simply supported at its four corners and acted upon by uniformly distributed load

a_1, b_1 = side lengths of rectangular plate

m = reciprocal of the Poisson ratio

$$\Gamma = \frac{768 (m^2 - 1)}{\pi [(m\pi^2)^2 - 64]} \frac{p}{Eh^3} \dots \dots \dots [29]$$

where

p = intensity of uniformly distributed load, psi

E = modulus of elasticity, psi

h = plate thickness, in.

The constants E and m have to be figured out from the dimensions of a tube sheet under consideration in accordance with the derivations given in the second section of the paper.

EXPERIMENTAL CHECK OF EQUATIONS [19] AND [20]

The tube sheets used for an experimental check of Equations [19] and [20] are shown in Figs. 7 and 8. The original dimensions of tube sheet No. 1 (Fig. 7), were 42.125 in. \times 42.875 in. as shown; later the tube sheet was reduced as indicated in the following. The deflection was measured both with the original and with the reduced tube sheets for reasons which will be given. All tests described subsequently have been carried out by L. Nilsen.¹⁶

The holes in the tube sheets were punched, after which the tube sheets were straightened out "by putting them between two parallel plates with a weight on top and heating them in a furnace to 1200 F for 1 1/2 hr. In this treating, the specific stress-relieving was also accomplished," and "the resulting plates were considered sufficiently level to compare favorably with commercial plates used in the tube-sheet construction."

"The procedure in obtaining the deflection was as follows:

"1 The center of the plate was located by the intersection of two carefully drawn diagonal lines on both sides of the plate and the center was marked. In the case of plate No. 2, the center happened to be located in one of the punched holes. Therefore the deflection had to be taken about 1/4 in. from the actual center of the plate.

"2 The 'zero' point (the point at no deflection) was determined by mounting two bolts of precisely the same length at diagonally opposite corners of the plate. The plate was then placed in a vertical position on a perfectly level layout table and its weight was supported by a wire suspended at a point above the plate. A straight edge was placed on the two bolts and the distance measured from the straight edge down to the center of

¹² "Elastische Platten," by A. Nadai, J. Springer, Berlin, Germany, 1925, pp. 39-45, 198-201, and 301-308.

¹³ "Die Verbiegungen in einzelnen Punkten unterstützter Kreisförmiger Platten," by A. Nadai, *Physikalische Zeitschrift*, vol. 23, 1922, pp. 366-376. An abstract of Nadai's paper will be found in reference (5), pp. 270-272; also reference (12), pp. 193-197.

¹⁴ "Drang und Zwang," by A. and L. Foepl, Muenchen and Berlin, Germany, vol. 1, 1920, pp. 147-149.

¹⁵ Attention must be called to an error in equations [44], reference (14), p. 149. The factor (b^2/a^2) in the second of the two equations [44] must be replaced by (a^2/b^2) . The error invalidates other formulas on the same page of the source.

¹⁶ Research Engineer, Foster Wheeler Corporation, Research Laboratory, Carteret Works, Carteret, N. J. The parts, given in quotation marks, of the following text are reproduced from Mr. Nilsen's report.

the plate. This procedure was followed on both sides of the plate.

¹³ The plates were placed in a horizontal position supported on four vertically mounted bolts of equal height, fastened to the afore-mentioned layout table. These bolts were placed in such a manner that the plates resting on them would be supported an equal distance from the center. The four bolts had been ground to a truncated point and the support point on the plates was about $\frac{1}{4}$ in. from each corner. Again the straight edge was

placed on the two bolts mounted on the plate and the distance from the straight edge to the center of the plate was recorded. The difference between the reading at the zero point and the latter reading was taken as the deflection due to the weight of the plate. Deflections were read to the nearest 0.005 in. using a micrometer."

The deflection measurements were taken on each side of a tube sheet and the average was registered as resulting deflection. This led to

$$w = 0.0460 \text{ in.} \quad [30]$$

at the center of tube sheet No. 1, and

$$w = 0.1495 \text{ in.} \quad [31]$$

at the center of tube sheet No. 2.

In both cases the tube sheets were acted upon by their own weight only. An additional experiment, in which tube sheet No. 2 carried an additional load uniformly distributed along its shorter center line, will be discussed a little later on.

Much more important, however, is another additional experiment which must be reported and discussed here before turning to the computation of the deflections by means of Equations [19], [20], [28], and [29].

In order to compare the measured deflections with the corresponding theoretical results to be obtained in the following section it is necessary to reduce the former to the same basis, on which the analytical determination takes place. The actual tube sheet is provided with a rim of much greater rigidity than the tube sheet proper, a rim which is not represented in the Equations [28] and [29]. Before the results, Equations [30] and [31], can be compared with the theoretical results, it is necessary to eliminate from the measurements Equations [30] and [31] the influence of the rim. For this purpose the following additional experiment was made on tube sheet No. 1:

The original weight of this tube sheet was $126\frac{1}{2}$ lb. After removal of $7\frac{1}{2}$ lb of rim material taken off all along the boundary

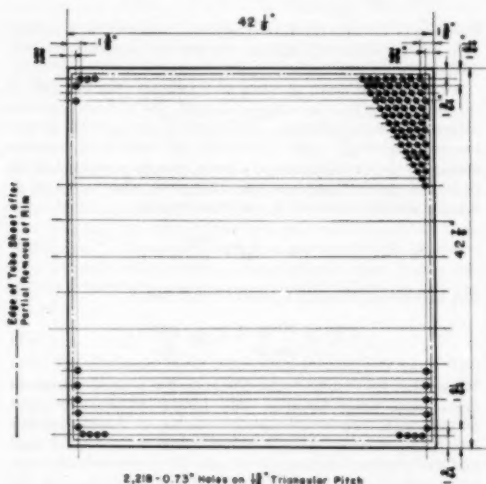


FIG. 7 TUBE SHEET NO. 1, 42 1/8 IN. X 14 1/2 IN. X 0.510 IN. FOR EXPERIMENTAL TESTS

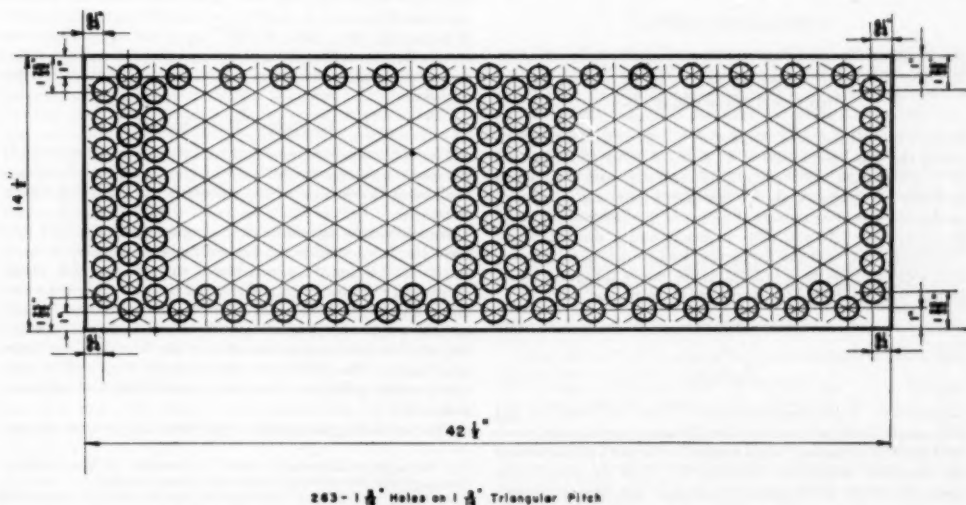


FIG. 8 TUBE SHEET NO. 2, 42 1/8 IN. X 14 1/2 IN. X 0.246 IN., FOR EXPERIMENTAL TESTS

of the tube sheet, the deflection at the center of the latter was measured again and the result was 0.0505 in. as compared with 0.0460 in. in Equation [30].

Now let us determine the weight of the tube sheet proper. This is the sum of the weights of all regular ligaments surrounding the 2218 holes of the tube sheet. The weight of each ligament (Fig. 6) was estimated as 0.0491 lb from the dimensions of the tube sheet and the density of the material (0.2833 pci). The weight of the entire tube sheet proper is, accordingly, $0.0491 \times 2218 = 109$ lb. In other words, after the removal of $7\frac{1}{2}$ lb from the boundary of the tube sheet, there is still a weight of 10 lb accumulated around the outer holes of the tube sheet, a weight which does not belong to the tube sheet proper.

We see from this that linear extrapolation leads to the following deflection after removal of all rim material

$$w = 0.0460 + \frac{0.0505 - 0.0460}{7.5} (126.5 - 109) = 0.0565 \text{ in.} \quad [32]$$

This is to be considered as the measured deflection of the tube sheet No. 1 proper, to be compared with the deflection computed from the system, Equations [19], [20], [28], and [29].

As to tube sheet No. 2, experiments of rim elimination have not been applied to it. Its rim is relatively much smaller than that of the first one.

COMPUTATION OF THE DEFLECTIONS FROM EQUATIONS [19], [20], [28], [29]

The fundamental data of tube sheets Nos. 1 and 2 are given in the first three lines of Table 1. Starting from these data and following the computing procedure given in the second section of the paper and illustrated in the third section, we arrive at the results in the lines 4 to 11 of the table. The weight of the tube sheet proper per 1 sq. in. of its total area is, with $\mu = 0.449$ (line 4 of table)

$$0.1445 \times 0.449 = 0.0648 \text{ lb}$$

in the case of tube sheet No. 1. The weight of 1 sq. in. of steel plate of 0.246 in. thickness is

$$0.2833 \times 0.246 = 0.070 \text{ psi}$$

the weight of the tube sheet proper per 1 sq. in. of its total area is, with $\mu = 0.360$

$$0.070 \times 0.360 = 0.0252 \text{ psi}$$

in the case of tube sheet No. 2 (see line 11 of table). Substituting the numerical values of $E' = 0.172 \times 30 \times 10^6$ psi and $E'' = 0.154 \times 30 \times 10^6$ psi, respectively, and those of m' , given in Table 1 correspondingly for the quantities E and m , as well as the corresponding numerical values of the distributed load p , into Equations [28] and [29], we finally obtain the deflections. The results are, with the supporting lengths (see preceding section, point 3) $2a = 2b = 41.50$ in. in the case of tube sheet No. 1, and $2a = 42$ in., $2b = 14$ in. in the case of tube sheet No. 2

$$w = 0.0699 \text{ in.} \quad [33]$$

and

$$w = 0.1750 \text{ in.} \quad [34]$$

respectively. Comparing Equations [31] and [32] with [34] and [33], respectively, we see that the differences between the measured and the computed values amount to 19 and 14.5 per cent of the computed deflections, respectively. If, in the second tube sheet, the effects of the (relatively smaller) rim were eliminated, the error would be smaller. Taking into consideration that an error in terms of deflection is much larger than in terms of the

TABLE 1 TUBE SHEET DATA

Tube sheet no.	Funda-mental	Thickness... h in.	1	2
1		Spacing... s in.	0.510	0.246
2		Hole diam., d in.	15/16	21/16
3	data		0.73	21/16
4	Equation [23]	a	0.449	0.280
5	Equation [24]	c	0.243	0.312
6	Fig. 4	b	0.233	0.175
7	Equation [27]	A'	0.244	0.5
8	Equation [20]	E'	0.233	0.143
9	Equation [22]	E''	0.172	0.154
10		$m' = 1/\nu'$	4.29	6.99
11		p , psi	0.0648	0.0252

thickness of the tube sheet, because of the factor h^{-2} in Equation [29], we may consider Equations [19] and [20] as satisfactory for design purposes.

An interesting detail in favor of Equations [19] and [20] is the following: The system Equations [28], [29] is an approximate expression for the deflection. It is easy to see that this system becomes practically quite accurate as the ratio b/a becomes small; in the limiting case of a beam, simply supported at its ends, the system Equations [28], [29] gives, with $\nu = 1/m = 0.3$, and after division by $17(1 - \nu^2)$ the formula

$$w = 0.222 \frac{pa^4}{EI} \quad [35]$$

The well-known accurate formula for this case is

$$w = \frac{80a^4p}{384EI} = 0.208 \frac{pa^4}{EI} \quad [36]$$

We see that the accurate value Equation [36] is smaller than the approximate result Equation [35], with a difference of about 6 1/2 per cent. There are plausible reasons to believe that this relationship between the approximate result of A. and L. Foepl and the accurate solution will be valid for a considerable range of the ratio b/a . Tube sheet No. 2 is in the vicinity of this range. In other words, there is reason to believe that the introduction of constants Equations [19], [20] into Equations [28], [29] must yield, in the case of tube sheet No. 2, a good test for the validity of Equations [19], [20]. The favorable result obtained with this tube sheet is, therefore, a valuable argument in favor of Equations [19], [20]. In the case of the square plate the system Equations [28], [29] is obviously less accurate, which would explain the less satisfactory results obtained with the larger tube sheet.

ADDITIONAL EXPERIMENTS

The additional experiments, one of which is to be reported in this section, were intended only to give some complementary qualitative illustrations of the subject of the foregoing discussions.

We relate here an additional experiment carried out on tube sheet No. 2. A steel bar of 9 lb weight, approximately 1 in. \times 1 1/2 in. \times 14 1/2 in. long, was placed with its 1-in. side on the short center line of the tube sheet, and the deflection was measured; then the bar was cut into 7 pieces of roughly equal weight and the weight was distributed uniformly along the same center line, and the deflection at the center of the tube sheet was measured again. The result was approximately the same in both cases, namely 0.098 in. Now let us calculate the deflection just measured.

The concluding paragraph of the preceding section implies

¹⁷ "Strength of Materials," by S. Timoshenko, D. Van Nostrand Company, Inc., New York, N. Y., vol. 2, 1941, p. 120.

¹⁸ "Plates and Shells" (reference 5), fig. 135, p. 348, where the straight branches of the diagram, referring to plates of a widely varying ratio of width to length, differ from each other only slightly.

that the deflection of tube sheet No. 2 can be approximated fairly well by that of a beam on two supports at its ends. Indeed, if we apply Equation [36] to a strip 1 in. wide and 42 in. long, of tube sheet No. 2, loaded by its own weight of the amount $p = 0.0252$ lb per linear in. (see Table 1) then we obtain, with $I = (1/12) \times 0.246^3 = 0.00124$ cu in.

$$w = 0.208 \frac{0.0252 \times 194,500}{0.154 \times 30 \times 10^6 \times 0.00124} = 0.177 \text{ in.}$$

as compared with $w = 0.175$ in. in Equation [34]. This suggests the possibility of using for the tube sheet the theory of beam deflections in the case of a concentrated load as well. Designating the latter by P , which is in the case considered here $9.14 = 0.643$ lb, we have

$$w = \frac{0.643 \times 74,088}{0.154 \times 30 \times 10^6 \times 0.00124 \times 48} = 0.173 \text{ in.} \quad [37]$$

as compared with the measured value 0.098 in. The explanation of this discrepancy is obtained by attentive reading of the section, Experimental Check of Equations [19] and [20], point 3: "... the four (supporting) bolts had been ground to a truncated point." Such supports cause quite considerable friction as soon as the deflection becomes comparatively large. In our case the total calculated deflection according to Equations [34] and [35] is

$$0.175 \text{ in.} + 0.173 \text{ in.} = 0.348 \text{ in.}$$

while the thickness of the tube sheet is only 0.246 in. This means that the tube sheet is in a condition similar to that of a plate with large deflections, while its edges are clamped.¹⁹ The diagram referred to in the preceding footnote shows that in problems of this kind large discrepancies between calculated and measured deflections can be expected, if the theory of small deflections is used in the computations, which is exactly the basis of our tube-sheet formulas. Summarizing, we may say that the experiment just reported yields only a qualitative testimony, namely, an inequality $(0.348 \text{ in.} > 0.1495 \text{ in.} + 0.098 \text{ in.} = 0.2475 \text{ in.})$ in favor of our Equations [19], [20].

SUMMARY

The results of the study presented can be summarized now as follows: The experimental tests have been carried out with rectangular tube sheets on four-point supports. A circular tube sheet on three-point supports 120 deg apart, of course, has not less than three great advantages, namely, the problem has an exact solution (see section, Experimental Verification); the boundary conditions can be realized very easily and accurately (statically determined problem); the solution is known both for the uniformly distributed and centrally applied concentrated load. However, the circular tube sheet has a drawback indicated in the following. Returning to the rectangular tube sheets, actually used in the experiments, it must be admitted that the experiments with them are open to some objections, directed both at the approximate nature of the Föppl system, Equations [28] and [29], and at the difficulty to realize equal distribution of load among the four supports. As to the first objection, there are reasons to believe that the inaccuracy of Equations [28] and [29] does not assume serious proportions in the case of a ratio of the sides of the rectangle, say, not larger than $1/2$; as to the difficulties of the four-point support, they must be

considerably smaller in the case of a tube sheet than in the case of a full plate. On the other hand, attention must be called to the fact that in the case of a rectangular tube sheet the holes approach any of the four rectilinear edges uniformly; this is an advantage for carrying out the experimental test, because it permits one to eliminate conveniently the influence of the rim on the deflection (see section, Experimental Check of Equations [19] and [20]). The latter condition is not fulfilled in the case of a circular tube sheet, so that in this case the additional problem of estimating the rim effects must be solved satisfactorily before this otherwise ideal solution can be applied to tube-sheet experiments. Resuming again the tests with the rectangular tube sheets we may say that notwithstanding certain shortcomings these experiments produce a respectable measure of confidence. In the light of the very satisfactory results which have been achieved with Equations [19] and [20] as a basis for practical design the approximate analytical solution of the tube-sheet problem, as developed in the second section, together with the presentation of the experimental tests for its verification, and the discussion of further possibilities of its experimental check may be of sufficient practical value so as to deserve attention and interest of the engineers of the pressure-vessel industry.

ACKNOWLEDGMENT

The author welcomes the opportunity of expressing once more his gratitude to the Foster Wheeler Corporation for having granted him the possibility to carry out a study in a problem of great practical importance and theoretical interest. In particular, the author deeply appreciates the encouragement which he received from the interest of Messrs. Martin Frisch and A. H. Egnieker of the Foster Wheeler Corporation, in such problems, from a theoretical treatment of which clarification of design questions can be expected. The author wishes also to thank Mr. John Blizard, Research Director, for all possible assistance in the materialization of the experimental tests, and to Mr. L. Nilsson, who carried out the testing work in the research laboratory, finally also to Mr. John Kupstas for valuable information in many matters covering practices of fabrication and operation.

Discussion

G. HORVAY.²⁰ This method of determining the deflections of laterally loaded tube sheets by replacing them, for purposes of calculations, by homogeneous sheets of such elastic constants E and ν that they deform in the same manner as the originally perforated sheets, is of great practical importance. H. Poritsky and the writer have employed a three-dimensional analog of the method for the analysis of stresses and strains in a welded tube bundle.²¹ The plane stress problem of a tube sheet is considered in another paper.²²

K. A. GARDNER.²³ All those interested in the development of rational methods of tube-sheet design will be greatly indebted to the author for his valuable paper. The writer is primarily interested because the author's results not only prove (in part) one assumption made in his own paper²⁴ but also may be used to

¹⁹ Engineering Division, Knolls Atomic Power Laboratory, General Electric Company, Schenectady, N. Y.

²⁰ "Stresses in Pipe Bundles," by H. Poritsky and G. Horvay, *Journal of Applied Mechanics*, Trans. ASME, vol. 73, 1951, pp. 241-250.

²¹ "Thermal Stresses in Perforated Plates," by G. Horvay, Proceedings of the First U. S. National Congress of Applied Mechanics.

²² Assistant Chief Engineer, The Gracem-Russell Company, Massillon, Ohio. Mem. ASME.

²³ "Heat-Exchanger Tube-Sheet Design," by K. A. Gardner, *Journal of Applied Mechanics*, Trans. ASME, vol. 70, 1948, pp. 377-385.

¹⁹ The problem of plates with large deflections, including the case of plates with simply supported edges, is elaborately discussed and illustrated by many graphs both in S. Timoshenko's "Plates and Shells," reference (5), pp. 329-350, and in Nadai's "Elastische Platten," reference (12), pp. 284-308.

evaluate quantitatively a constant which was considered empirical. The assumption was that any uniformly perforated plate may be considered to deflect exactly like some identically loaded solid plate of lesser thickness. The constant is the "deflection efficiency," in the flexural rigidity equation

$$D = \frac{Eh^3\eta_w}{12(1-\nu^2)}$$

From the author's Equations [22] and [23] the same value must be given by

$$D = \frac{\mu Eh^3}{12 \left[1 - \left(\frac{1-K}{3+K} \right)^2 \right]} \left(\frac{1+K}{3+K} \right) \\ = \frac{Eh^3(3+K)}{96} \left[1 - \frac{\pi\sqrt{3}}{6} \left(\frac{d}{s} \right)^2 \right]$$

where the nomenclature is that of the paper. Solving for η_w

$$\eta_w = \frac{(3+K)}{8} (1-\nu^2) \left[1 - \frac{\pi\sqrt{3}}{6} \left(\frac{d}{s} \right)^2 \right]$$

for tubes on triangular pitch only.

This deflection efficiency involves the tube-sheet thickness h , through the term K , although the writer had assumed in his paper that it would be the same regardless of thickness. The TEMA standards (3) set the minimum value of h for good tube-expanding practice as equal to d and, in effect, set the value of c at $(1.25 \pm 0.952d) = 0.298d$ for tube sheets of shell-and-tube exchangers. This value of c is seldom exceeded except in finned tube exchangers where the tube pitch is set by the fin diameter rather than by the minimum ligament for tube expanding. Therefore the minimum value of (h/c) is about 3.35 which, by the author's Equation [27], corresponds to a maximum K value of approximately 0.12. The effect on the foregoing equation for deflection efficiency is thus seen to be small, varying only about 2.5 per cent from a mean value of

$$\eta_w = 0.35 \left[1 - \frac{\pi\sqrt{3}}{6} \left(\frac{d}{s} \right)^2 \right]$$

over the entire normal range of tube-sheet thicknesses. Similarly, the variation of the effective value of ν from the commonly used 0.3 is also small; the maximum possible value is, of course, 0.333 and the minimum (for $K = 0.12$) is 0.281.

Thus, for the normal run of heat-exchanger tube sheets, no great error is introduced if the effect of tube-sheet thickness on η_w is neglected and if ν is assumed to have its usual value for solid isotropic plates. These remarks are not valid, however, for tube sheets in which the ligament aspect ratio (h/c) is appreciably less than 3.

Although the author states explicitly in his title that his analysis applies only to tube sheets with the perforations on a triangular pitch, it perhaps should be emphasized that the same methods applied to square-pitch layouts do not yield similar results. The writer learned this to his embarrassment upon investigating his own naive suggestion that the author's paper be expanded to cover square layouts. The equation corresponding to the author's Equation [16] is, for square pitch

$$U^* = \frac{ELch^3}{12s^2} \iint \left[(\Delta w)^2 - 2(w_{xx}w_{yy} - Kw_{xy}^2) \right] dx dy$$

which, by comparison with Equation [3], does not yield simple fictitious values E^* and ν^* ; it is, in fact, the expression for an anisotropic plate.

The fact remains, however, that some method of estimating a value of η_w for square layouts is required. If by a stretch of engineering conscience (which can become quite elastic when a matter of either an approximate answer or no answer at all is involved) the integrals in the foregoing equation and Equation [3] could be considered approximately equal, and

$$\mu = \frac{4Lc}{s^2} = \left[1 - \frac{\pi}{4} \left(\frac{d}{s} \right)^2 \right]$$

then

$$\eta_w \cong 0.23 \left[1 - \frac{\pi}{4} \left(\frac{d}{s} \right)^2 \right]$$

for square-pitch tube sheets. Bearing in mind the assumptions involved, it is interesting to observe that, on this basis, there is less impairment of the resistance of a plate to bending if it is uniformly perforated with holes of a given diameter and pitch on a triangular layout than on a square layout, even though more metal is removed in the former case. Further confirmation of this conclusion can be obtained by comparison of the foregoing equation for U^* and Equation [16] of the paper for the case where $K = 1$, under which conditions the integrals in both become identical. It will be found that the effective flexural rigidity of the triangular pitch plate is $\sqrt{3}$ times as great as that of the square-pitch plate.

AUTHOR'S CLOSURE

The author acknowledges gratefully the appreciation expressed in each of the two preceding contributions to the discussion. As to the statement of Mr. Horvay's, however, concerning analogy of methods, the author is sorry to say that, notwithstanding repeated previous admonitions by the author, both oral, in the public discussion at the 1950 Annual Meeting of the ASME in New York City, and even some stronger ones in written form in reply to Mr. Horvay's contentions in his preprinted publication,²² Mr. Horvay insistently continues to claim a relationship between the author's approximate method given on the preceding pages of this paper, and his own analysis worked out together with H. Poritsky. Actually, there is no possibility of deriving any of the two solutions in question from the other, there is no possibility of applying the results of one of them to the treatment of the other, there is no mathematical relationship whatsoever between the respective methods of attack and procedures of solution.

In his publication,²⁴ Mr. Gardner recommends experimental determination of deflection coefficients for the use in tube-sheet design computations. He concedes, in the concluding part of his paper, that a great number of such experiments with tube sheets of various design characteristics and dimensions will be necessary to obtain those coefficients, without which no stress analysis will be possible. Mr. Gardner uses the author's approximate solution, given above, for figuring out those coefficients (see also the second part of his paper, presented at the 1951 Annual Meeting of the ASME in Atlantic City, N. J., Paper No. 51-A-38), but this is, of course, an emergency step, because there is no logical reason for switching to Mr. Gardner's coefficients, if the author's procedure of solution is being used. On the other hand, it must be admitted that, if and when the experimental program advocated by Mr. Gardner is actually carried out, it will be very desirable to compare its results with the author's formulas.

Analysis of Stresses and Displacements in Heat-Exchanger Expansion Joints

By GLENN MURPHY,¹ AMES, IOWA

This paper presents a procedure for the analysis of stresses and displacements in an expansion joint, when the latter is assumed to be a surface of revolution. The analysis as presented employs a method of successive approximations, but, in general, the solution will be rapidly convergent. Possible thermal gradients in the joint are not included in the analysis as given, but may be introduced in the solution.

NOMENCLATURE

The following nomenclature is used in the paper:

- x = longitudinal or axial co-ordinate
- y = radial co-ordinate
- s = co-ordinate along joint, usually inclined to x
- r = radius of shell
- t = thickness of shell
- ϕ = direction tangent to shell in transverse plane
- w = radial deflection of shell
- θ = angle between longitudinal planes
- N_x = longitudinal force
- V = cross-shearing force
- σ = unit normal stress, with subscript to denote direction
- τ = unit shearing stress
- M = bending moment in shell
- M_1 = bending moment in beam equation
- E = modulus of elasticity of shell material
- μ = Poisson's ratio
- I = moment of inertia of strip cut from shell
- P = unit internal pressure
- ϵ = unit strain
- c = $t/2$
- X = $r\sigma_x$
- Y = $r\tau_{xy}$
- Z = Mr/t

INTRODUCTION

In the design and investigation of heat exchangers the evaluation of the stresses and displacements that occur in expansion joints presents some difficulties because the joint is normally part of a closed and, therefore, statically indeterminate system, and because of the variety of shapes utilized for expansion joints.

Since the joint is part of a statically indeterminate system, the analysis for stresses and displacements must be based on the equations of equilibrium, and considerations of the changes in the geometry of the joint and assumed properties of the material. It is shown that the equations of equilibrium for a longitudinal strip through the joint may be reduced to the same form as the

differential equation for a planar frame with a variable load. The conjugate frame² analysis is then applied to evaluate displacements. Once the displacements are known, stresses may be evaluated.

ANALYSIS

The inside and outside surfaces of the joint are assumed to be coaxial surfaces of revolution, and the joint is assumed to be subjected to axial load and internal pressure. The conventional assumptions of homogeneous elastic material not stressed above the proportional limit are made.

The first step is to establish a planar member, the displacements of which will represent the displacements of the surface of revolution. This is done by considering the characteristics of a strip cut from the joint by two longitudinal planes containing the axis of revolution. The angle between the planes is taken as θ , as shown in Fig. 1(a). The resulting strip has a width at any point proportional to the radius r , at that point, and is subjected to a longitudinal force N_x , a normal pressure p , and a distributed circumferential force on each of the sides. Because of symmetry, all strips cut by a pair of planes with an internal angle θ will be identical. A representative strip is shown in Fig. 1(a).

In Fig. 1(b) is shown a free-body diagram of an element of the strip between two planes normal to the longitudinal axis and a distance dx apart. Unless the surface has a constant radius the length of element is greater than dx , and is designated as ds . The ends of the element are subjected to a normal force, shear, and bending, while the sides are subjected to normal force only. Shear and bending are absent on the sides because of symmetry.

The force equation of equilibrium, written in the horizontal (axial, or X) direction, gives

$$\sigma_x t \theta + p r \theta ds \frac{dr}{ds} = \left(\sigma_x + \frac{d\sigma_x}{ds} ds \right) \left(t + \frac{dt}{ds} ds \right) \times \left(r + \frac{dr}{ds} ds \right) \theta \dots [1]$$

which reduces to

$$p \frac{r}{t} \frac{dr}{ds} = \sigma_x \frac{dr}{ds} + r \frac{d\sigma_x}{ds} \dots [1a]$$

if differentials of higher order are dropped, and if the thickness t , of the element is constant.

Equation [1a] may be simplified to

$$p \frac{r}{t} \frac{dr}{ds} = \frac{dX}{ds} \dots [1b]$$

by letting

$$X = r\sigma_x \dots [1c]$$

Equation [1b] may be integrated directly to give

² "The Conjugate Frame as a Tool for Evaluating Deflections," by Glenn Murphy, Proceedings of the Seventh International Congress of Applied Mechanics, London, England, Section 1, Paper I.12, vol. 1, 1948, pp. 131-138.

¹ Professor of Theoretical and Applied Mechanics, Iowa State College. Mem. ASME.

Contributed by the Heat Transfer and Applied Mechanics Divisions and presented at the Annual Meeting, New York, N. Y., November 26-December 1, 1950, of THE AMERICAN SOCIETY OF MECHANICAL ENGINEERS.

NOTE: Statements and opinions advanced in papers are to be understood as individual expressions of their authors and not those of the Society. Manuscript received at ASME Headquarters, October 30, 1950. Paper No. 50-A-133.

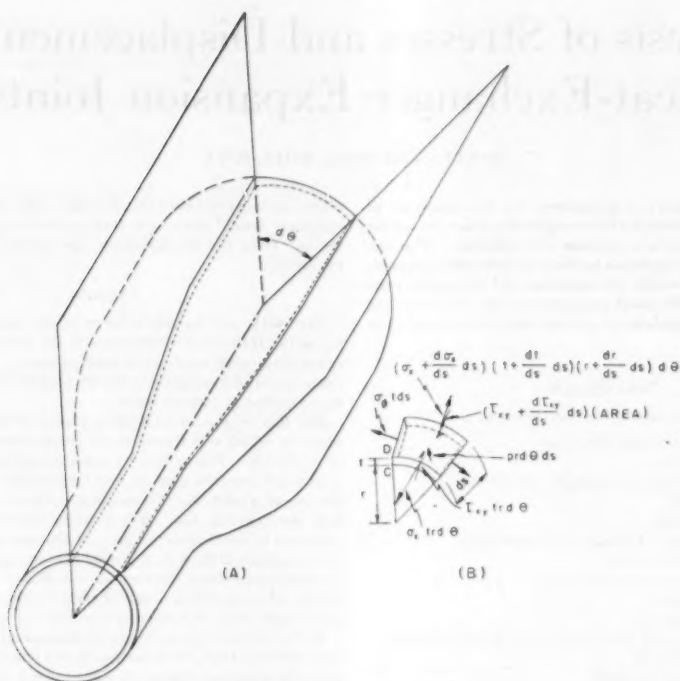


FIG. 1 ELEMENT OF EXPANSION JOINT

$$X = X_0 + \frac{p}{2t} (r^2 - r_0^2) \quad [1d]$$

in which X_0 is the value of $r\sigma_r$ at any arbitrary reference point and r_0 is the radius of the surface at the arbitrary point. The force equation of equilibrium, written in the vertical (radial) direction, gives

$$\tau_{xy} t r \theta + p r \theta ds \frac{dx}{ds} = \left(\tau_{xy} + \frac{d\tau_{xy}}{ds} ds \right) \times t \left(r + \frac{dr}{ds} ds \right) \theta + \sigma_\phi ds \theta \quad [2]$$

if the thickness of the element is constant. This reduces to

$$\sigma_\phi = p \frac{r}{t} \frac{dx}{ds} - \frac{dY}{ds} \quad [2a]$$

in which

$$Y = r\tau_{xy} \quad [2b]$$

Similarly, the moment equation of equilibrium yields

$$X \frac{dr}{ds} + Y \frac{dx}{ds} = \frac{dZ}{ds} \quad [3]$$

in which

$$Z = \frac{M}{t} r \quad [3a]$$

If it is assumed that a straight line normal to the neutral surface such as CD in Fig. 1(b), remains straight during the loading process and remains in the original longitudinal plane, the unit strain ϵ_r at a distance c from the neutral surface and in the longitudinal direction may be expressed in terms of the radial deflection w as (approximately)

$$\epsilon_r = c \frac{d^2 w}{ds^2} \quad [4]$$

The strain in the circumferential direction at the same point is

$$\epsilon_\phi = \frac{w}{r} \frac{dx}{ds} \quad [4a]$$

From the standard stress-strain relationships, it follows that

$$\frac{\sigma_r}{E} - \mu \frac{\sigma_\phi}{E} = c \frac{d^2 w}{ds^2} \quad [4b]$$

$$\frac{\sigma_\phi}{E} - \mu \frac{\sigma_r}{E} = \frac{w}{r} \frac{dx}{ds} \quad [4c]$$

The circumferential stress may be eliminated, giving

$$\frac{\sigma_r(1 - \mu^2)}{E} = c \frac{d^2 w}{ds^2} + \mu \frac{w}{r} \frac{dx}{ds} \quad [5]$$

If the effect of the axial stress upon σ_r is neglected, Equation [5] reduces to

$$\frac{d^3 w}{ds^3} = \frac{M(1-\mu^2)}{EI} - \frac{\mu w}{cr} \frac{dx}{ds} \quad [5a]$$

This is the differential equation of a representative strip cut from the joint subject to the assumptions listed.

The standard differential equation for the deflection of a planar structure subjected to bending is of the form

$$\frac{d^2 w}{ds^2} = \frac{M_1}{EI} \quad [6]$$

From the conjugate-frame theory it is known that if the bending moments divided by EI in a planar structure are assumed to be applied as loads to the conjugate frame, which is geometrically similar to the original structure, the bending moments in the conjugate frame are proportional to the bending deflections in the original structure.

It will be noted that Equation [5a] is of the form of Equation [6] if

$$\frac{M_1}{EI} = \frac{M(1-\mu^2)}{EI} - \frac{\mu w}{cr} \frac{dx}{ds} \quad [6a]$$

Hence, if values of M_1/EI of the magnitudes given by Equation [6a] are applied to the conjugate frame in the standard manner as loads, the deflections of the original strip will be obtained as the moments at the corresponding points in the conjugate frame. By equating the computed deflections to known deflections at certain control points, the unknowns involved in M may be found and from them the stresses evaluated.

SOLUTION

As developed, the solution requires the evaluation of the moment M_1 . Since M_1 involves w , as shown in Equation [6a], and since r is a function of s , the suggested procedure is to determine an approximate value for w by neglecting the second term of Equation [6a], and then correct M_1 by the value of w so obtained. The primary solution, then, requires the evaluation of M .

The moment M_s at some point B , a distance x from an arbitrary origin may be evaluated from a free-body diagram of the strip between the origin and point B . The moment at B is a function of the moment at the origin, the shear, the axial force, the pressure, and σ_θ . If the effect of the deflection on the major geometry of the system is neglected

$$M_s = M_0 + Vx + \sigma_s t r_0(r - r_0) \theta + \int_0^x p r \theta ds - \int_0^x \sigma_\theta t \theta ds \quad [7]$$

$$\frac{M_s}{\theta} = \frac{M_0}{\theta} + \frac{Vx}{\theta} + \sigma_s t r_0(r - r_0) + p \int_0^x r ds - t \int_0^x \sigma_\theta ds \quad [7a]$$

in which x denotes the moment arm of the element of length ds with respect to the point at which the moment is being evaluated.

It is evident that

$$\begin{aligned} \frac{M_s}{EI} &= \frac{12 M_0}{E r \theta^3} \quad [7b] \\ &= \frac{M_0}{EI} + \frac{Vx}{EI} + \frac{N y}{EI} + \frac{12}{E} \left(\frac{p}{r^3} \int_0^x r ds - \frac{1}{r^3} \int_0^x \sigma_\theta ds \right) \quad [7c] \end{aligned}$$

At this point in the solution of a specific problem, the factors M_0 , V , σ_s , and σ_θ , are usually unknown. Since usually only three of them may be determined from geometrical conditions, a trial solution must be made. In general, for the first approximation σ_θ may best be taken equal to zero.

The M/EI values, which form the load on the conjugate structure, may be obtained (with M_0 , V , and σ_s as unknowns) from the first four terms in Equation [7c] and the shape of the original strip. With these as loads, the moment with respect to an x -axis at point B , for example, will give the x -component of the deflection at point B with respect to the origin. Similarly, the deflection of the strip at point B in the y -direction (with respect to the origin) is given by the moment (with respect to a y -axis at B) of the M/EI diagram, between the origin and B . The rotation of point B with respect to the origin is equal to the area of the M/EI diagram between the origin and B .

Hence an approximate value of M_0 , V , and σ_s may be obtained from the constraints and properties of the rest of the tube and supports.

As the next step, the influence of σ_θ may be taken into account. Since approximate values of X and Z are now known, the shearing factor Y may be evaluated from Equation [3].

From a knowledge of the variation of Y , σ_θ may be determined using Equation [2a].

All of the factors have now been introduced into the analysis, and the remainder of the solution consists in making a sufficient number of trials to satisfy Equations [2a], [3], and [7c] simultaneously with the displacement conditions that may be stipulated by the rest of the shell.

The solution for the deflections may be carried out algebraically or graphically.

Appendix

EXAMPLE

To illustrate the general procedure involved in the calculations, an academic "design" is investigated. The shell is assumed to be 36 in. diam, and the expansion joint varies linearly from 36 in. to 48 in. diam as shown in Fig. 2(a). The material is assumed to be steel, with a constant thickness of 0.25 in. The internal pressure is taken to be 150 psi. Finally, the joint is assumed to be attached to the shell by a rigid flange.

In Fig. 2(b), is shown a longitudinal section of a representative strip included between two longitudinal planes with an internal angle θ of 0.1 radian. In addition to the forces and couples indicated there will be a distributed force due to σ_θ on the front and back sides.

To facilitate calculations a tabular form is employed, with the joint divided into 12 sections, each having a projected length on the x -axis of 1 in. Table 1 contains the calculations for the loading on the conjugate frame due to the internal pressure on the strip, the end moment M , the shear V at the left end, and the axial force $N_s = N$. The values for the moment developed by the pressure are calculated from

$$\begin{aligned} M &= 5x^3 (54 + x) \text{ for } 0 \leq x \leq 6 \\ M &= 30 \left[360 + \frac{1}{6} (x - 6)^3 (78 - x) \right] \text{ for } 6 \leq x \leq 12 \\ &= 30 \left(360 + \frac{x^3}{6} \right) \end{aligned}$$

which may be developed directly from the statics of the strip of variable width.

The conjugate frame is L -shaped, to conform to the geometry

TABLE 1 CALCULATIONS FOR ORDINATES OF LOADING DIAGRAM FOR CONJUGATE FRAME

Station	r	r^2	EI	For moment		For shear		For thrust		For internal pressure					
				M	$M \times 10^{-4}$	V	$V \times 10^{-4}$	N	$N \times 10^{-4}$	$5x^2$	$5x + z$	M	a	b	ab
0	18	1.8	70500	M	14.21	0	0	0	0	0	54	0	0	0	0
1	19	1.9	74300	M	13.49	V	13.5	N	13.5	5	55	275	0	0	0
2	20	2.0	78300	M	12.80	2V	25.6	2N	25.6	20	56	1120	0	0	0
3	21	2.1	82100	M	12.20	3V	36.6	3N	36.6	45	57	2565	0	0	0
4	22	2.2	86000	M	11.61	4V	46.5	4N	46.5	80	58	4640	0	0	0
5	23	2.3	90000	M	11.11	5V	55.6	5N	55.6	125	59	7375	0	0	0
6	24	2.4	93900	M	10.68	6V	64.0	6N	64.0	180	60	10800	0	72	0
7	25	2.5	98000	M	11.11	7V	78.0	7N	78.0	245	61	15125	71	71	5041
8	26	2.6	102000	M	11.61	8V	92.0	8N	92.0	320	62	20320	142	72	10224
9	27	2.7	106000	M	12.20	9V	109.6	9N	109.6	405	63	26445	213	73	15621
10	28	2.8	110000	M	12.80	10V	128.0	10N	128.0	500	64	33500	284	74	21016
11	29	2.9	114000	M	13.49	11V	148.1	11N	148.1	605	65	41505	355	75	26625
12	30	3.0	118000	M	14.21	12V	170.9	12N	170.9	720	66	50400	426	76	32376

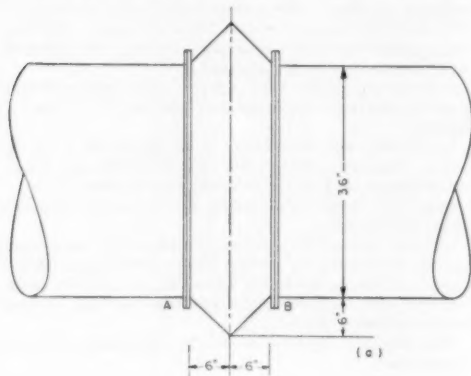


FIG. 2 ELEMENTS OF JOINT IN EXAMPLE

of the original strip, and the loading q on it as a result of the M/EI values due to the internal pressure is indicated in Fig. 3. The other q , or M/EI values are plotted in Fig. 4 as a function of x .

The three necessary conditions for evaluating the three unknowns M , V , and N come from the geometry of the joint. In the solution presented here it is assumed that the joint is clamped at the ends so that no deflection or rotation occurs at A and B . It is further assumed that the two ends remain the same distance apart. From these assumptions several equations for boundary conditions may be written. The three independent conditions selected are the following

- 1 No rotation of B relative to A

$$\int_A^B q ds = 0 \quad [8]$$

- 2 No horizontal translation of B relative to A

$$\int_A^B q y ds = 0 \quad [8a]$$

- 3 No vertical translation of B relative to A

$$\int_A^B q x ds = 0 \quad [8b]$$

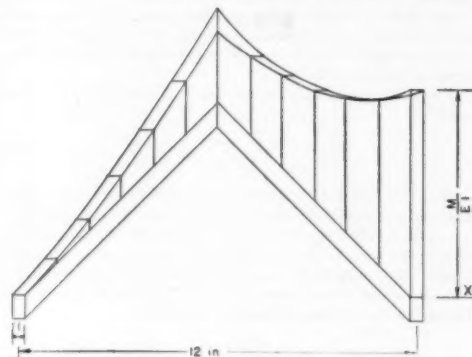
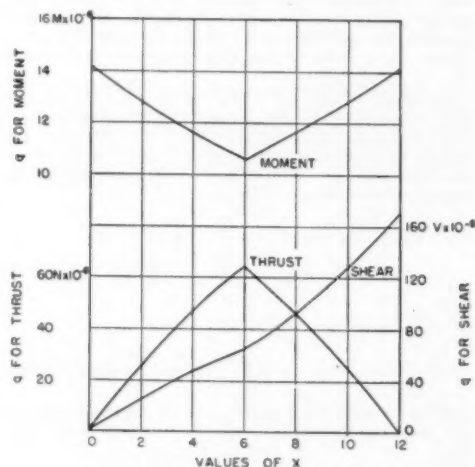


FIG. 3 CONJUGATE FRAME WITH COMPONENT OF LOAD FROM INTERNAL PRESSURE

FIG. 4 VALUES OF M/EI

For these particular conditions it will be noted that the conjugate frame is comparable to the analogous column for the strip. The next step is to calculate the quantities indicated by the left-hand side of Equations [8]. This may be done conveniently in tabular form, replacing the integrals by summations and using the same increments ($\Delta s = \sqrt{2}$ in.) as before. The areas under the curves may be approximated as rectangles and tri-

angles. A condensation of these calculations is given in Table 2.

When the appropriate values from Table 2 are substituted in Equation [8] the following equations result

$$208 M + 1180 V + 594 N + 1,783,800 = 0 \dots [9]$$

$$1249.7 M + 4809.4 V + 3560.8 N + 6,473,500 = 0 \dots [10]$$

$$594.5 M + 3568.2 V + 2317.8 N + 5,404,000 = 0 \dots [11]$$

From which

$$M = 1424 \text{ in-lb}$$

$$V = 1870 \text{ lb}$$

$$N = 181 \text{ lb}$$

Side-rule calculations were used throughout.

A partial check on the calculations may be obtained from the condition that V should equal the vertical component of the pressure integrated over the strip from x equals zero to x equals 6. This value of V is 1890 lb, and was used in subsequent calculations instead of 1870 lb.

The next step is to calculate the values of M_1/EI as given in Equation [6a]. This involves incorporating the influence of σ_0 into the expression for M and making the corrections for Poisson's ratio and the deflection w .

In order to evaluate σ_0 from Equation [2a], values of V must be found from Equation [3]. The quantity X is determined from Equation [1d], and Z is determined from Equation [3a]. These calculations for this example lead to corrections which are for the most part small compared with the values of q determined from the pressure, and the values obtained from the solution of Equations [9], [10], and [11] will be altered by less than 3 per cent.

To this point, no correction has been made for Poisson's ratio of the material as the effect would cancel out of the calculations, but it should be included in the calculations for the determination of the deflection.

The deflections are evaluated from the moments on the conjugate frame of the final M_1/EI values treated as loads.

The stresses may be evaluated from the values of M , H , and V .

EFFECTS OF ASSUMPTIONS

In the analysis several assumptions were made as follows:

1 The material is homogeneous and isotropic. This is a conventional assumption.

2 The stresses are below the proportional limit of the material. This assumption is also conventional.

3 The joint is a figure of revolution of constant thickness. Deviation from this assumption would complicate the analysis considerably.

4 The joint is in equilibrium. Another conventional assumption.

5 A straight normal line remains straight after loading. This is a conventional assumption in shell theory and is reasonable for small strains. It corresponds to the plane-section assumption for beams.

6 Axial strains are negligible in comparison with flexural strains in the joint (Equation [4]). The validity of this assumption depends on the geometry of the joint. However, joints are built for the purpose of obtaining flexibility, and that results primarily from bending.

7 Thermal gradients are neglected for simplicity. If the thermal gradient is radially symmetrical, its effect in bending the joint may be incorporated readily into the analysis by adding a term to Equations [4] and [6a], which will carry through to appear as an added term in Equations [5a] and [6a]. Hence the effect of a thermal gradient may be included by making an additional correction to the solution as outlined.

8 Other assumptions made in the example, such as the joint being attached to a rigid flange, are not inherent in the method. If the end of the expansion joint is able to move longitudinally,

TABLE 2 CALCULATIONS FOR MOMENTS ON CONJUGATE FRAME

Section	For moment—Coefficients of $M \times 10^{-4}$								For shear—Coefficients of $V \times 10^{-4}$							
	q^*	q^*	q^*	q^*	q^*	q^*	q^*	q^*	q^*	q^*	q^*	q^*	q^*	q^*	q^*	q^*
0-1	13.49	0.72	11.5	11.67	0.5	0.33	219	5.9	9.6	0.17	0	13.5	0	108.2	0	6.4
1-2	12.80	0.60	10.5	10.67	1.5	1.33	190	5.2	27.1	0.65	13.5	12.1	201	98.5	28.6	14.2
2-3	12.20	0.60	9.5	9.67	2.5	2.33	164	4.1	45.2	0.99	25.6	11.0	244	72.5	90.4	20.8
3-4	11.61	0.50	8.5	8.67	3.5	3.33	140	3.6	57.4	1.39	36.6	9.9	440	58.3	181	25.7
4-5	11.11	0.50	7.5	7.67	4.5	4.33	118	2.7	70.6	1.82	46.5	9.1	492	47.1	298	30.1
5-6	10.68	0.43	6.5	6.67	5.5	5.33	97.9	2.0	83.0	1.62	45.6	8.4	511	37.5	432	33.7
6-7	10.68	0.43	5.5	5.67	6.5	6.33	85.0	1.8	83.0	1.62	44.0	14.0	498	52.9	498	32.8
7-8	11.11	0.50	4.5	4.67	7.5	7.33	70.6	1.5	70.6	1.52	78.0	13.0	496	45.9	496	45.9
8-9	11.61	0.59	3.5	3.63	8.5	8.33	57.4	1.4	57.4	1.39	93.0	16.6	480	39.1	480	39.1
9-10	12.20	0.60	2.5	2.63	9.5	9.33	43.2	1.0	43.2	0.99	109.6	18.4	386	30.3	386	30.3
10-11	12.80	0.69	1.5	1.67	10.5	10.33	27.1	0.7	27.1	0.65	128.0	20.1	272	18.9	272	18.9
11-12	13.49	0.72	0.5	0.67	11.5	11.33	9.6	0.2	9.6	0.17	148.1	22.7	105	5.3	105	5.3
	143.78	7.06					1219.8	22.9	581.8	12.68	798.5	170.8	4205	604.4	3245	323.2
	203						22.9		12.7		85.4		604.4		323.2	
	208						1249.7		594.5		883.9		4809.4		3568.2	

Section	For thrust—Coefficients of $N \times 10^{-4}$								For internal pressure $\times 10^{-4}$							
	q^*	q^*	q^*	q^*	q^*	q^*	q^*	q^*	q^*	q^*	q^*	q^*	q^*	q^*	q^*	q^*
0-1	0	13.5	11.5	11.33	0.5	0.67	0	108.2	0	6.4	0	3700	0	20100	0	1305
1-2	13.5	12.1	10.5	10.33	1.5	1.67	201	88.5	28.6	14.2	3700	10000	54900	77400	7840	11230
2-3	25.6	11.0	9.5	9.33	2.5	2.67	344	72.5	90.4	20.8	14300	16900	192000	111400	50500	31900
3-4	36.6	9.9	8.5	8.33	3.5	3.67	440	58.3	181	25.7	31200	22700	275000	133900	104200	58000
4-5	46.5	9.1	7.5	7.33	4.5	4.67	492	47.1	298	30.1	53800	28100	370000	145000	142500	92800
5-6	55.6	8.4	6.5	6.33	5.5	5.67	511	37.5	432	33.7	62900	33000	473000	147800	137000	132000
6-7	55.6	8.4	5.5	5.67	6.5	6.33	434	33.7	432	33.7	115000	8000	805000	33500	805000	33500
7-8	48.5	9.1	4.5	4.67	5.5	5.67	295	30.0	298	30.1	123000	18100	788000	55500	788000	55500
8-9	36.6	9.9	3.5	3.67	6.5	6.33	181	25.7	181	25.7	142000	27000	703000	63500	703000	63500
9-10	25.6	11.0	2.5	2.67	7.5	7.33	91	20.8	90.4	20.8	169000	38500	597000	63400	597000	63400
10-11	13.5	12.1	1.5	1.67	8.5	8.33	29	14.3	28.6	14.2	207500	50500	440000	47800	440000	47800
11-12	0	13.5	0.5	0.67	9.5	9.33	9.6	6.4	0	6.4	258000	64000	182000	15100	182000	15100
	355.6	128.0					3018	542.8	2056	261.8	1100500	322000	5549900	923800	4797040	606935
	64						542.8		261.8		161000		923800		606935	
	419.6						3560.8		2317.8		1261500		6473500		5403975	
	594										1783761					

* For rectangular portion of diagram.

† For triangular portion of diagram.

as normally will be the case, the relative displacement of the two ends must be equated to the x -displacement of the rest of the structure (shell and tubes). This will necessitate determining the relationship between the forces on the rest of the structure and its displacements, which is a similar problem.

CONCLUSIONS

The method outlined presents a feasible approach to the prob-

lem of evaluating the stresses and displacements in expansion joints which possess axial symmetry and constant thickness.

The conventional assumptions of elastic theory are involved, and it is assumed that the distortion results from bending.

The procedure outlined involves successive approximations but it is not an approximate method, granting the assumptions. It is adaptable to any shape of joint, provided that radial symmetry is preserved.

Strain-Hardening and Softening With Time in Reference to Creep and Relaxation in Metals

By A. NADAI,¹ PITTSBURGH, PA.

Analytical expressions are formulated for describing the influence of strain-hardening, of the time rate of change of the flow resistance, and of recovery strains on the creep and relaxation of metals under uniaxial stress.

INTRODUCTION

THE problems of the slow deformation or creep of metals under stress at high temperatures raise many questions of a metallurgical, a physical, and a mechanical nature. Leaving aside a discussion of the involved phenomena occurring in the lattice structure of the polycrystalline metals, causing creep and fracture in metals after long exposure to stress at elevated temperatures, the interest of engineers has not subsided in a mechanical interpretation and treatment of these questions. Such a treatment is still required to correlate the results of the numerous long-time creep tests which have been made during the last 20 to 25 years under varying conditions in industrial laboratories for supplying much needed information to machine designers.

The mechanical theory of creep is concerned with the relation between stress, the elastic and permanent parts of the strains, the rates of the permanent strains, and the time at given temperatures.

In this paper, cases of flow under uniaxial stress will only be considered with a view toward improving the correlation between tensile tests of various types. Term σ denotes the normal stress, τ a shearing stress, $\epsilon' = \sigma/E$ (E Young's modulus) the elastic, ϵ'' the permanent part of the strain $\epsilon = \epsilon' + \epsilon''$, t the time, $u' = d\epsilon'/dt$, $u'' = d\epsilon''/dt$, and $u = d\epsilon/dt = u' + u''$ the elastic, permanent, and total rate of strain, respectively, and ϵ''' a recovery strain.

EQUATION OF STATE

From the experimental evidence derived from the stress-strain diagrams in tensile tests of the ductile metals, it is known that the stress σ depends on the permanent strains ϵ'' or on the rates of strain $u'' = d\epsilon''/dt$ or on both. With a few exceptions, σ increases monotonically with the previous permanent strain ϵ'' and with the rate of strain u'' . Two important cases² can be distinguished. In one case the resistance to permanent deformation as measured by σ in a state of uniaxial stress and the octahedral shearing

stress³ τ_{\max} in states of triaxial stress does not depend upon the time t ; in the other it does. At comparatively low temperatures, within the strain-hardening range of metals, the former case, and at elevated temperatures the latter case predominates.

In the strain-hardening range existence of an equation of state either in finite form

$$F(\sigma, \epsilon'', u'') = 0 \quad \dots\dots\dots [1]$$

or in differential form, for example, if the permanent strains ϵ'' and rates u'' are assumed as the independent variables and the flow stress σ as the dependent variable

$$d\sigma = \frac{\partial \sigma}{\partial \epsilon''} d\epsilon'' + \frac{\partial \sigma}{\partial u''} du'' = \psi d\epsilon'' + \phi du'' \dots\dots\dots [2]$$

is postulated in which the time t does not appear explicitly as a variable. $\psi = \partial \sigma / \partial \epsilon''$ may be interpreted as the rate of strain-hardening, and $\phi = \partial \sigma / \partial u''$ as a variable coefficient of viscosity of the metal. Equation [1] may be interpreted geometrically as the equation of a surface in a space having the rectangular coordinates ϵ'' , $u'' = d\epsilon''/dt$ and σ which may be called also "a stress surface." Such a surface exists if Equation [2] is a complete differential.

In practice one desires to determine the dependence of the variables ϵ'' , u'' , or σ on the time t for each one of several fundamental tests. These include the tensile long-time creep test under a constant stress or a constant load, the tensile test at a constant rate of permanent strain $u'' = \text{const}$, at a constant rate of stress $d\sigma/dt = \text{const}$, and the tensile relaxation test for which $\epsilon = \epsilon' + \epsilon'' = \text{const}$. If a stress surface exists these fundamental tests may be described by constructing their paths as curves situated on the stress surface, Equation [1].

If σ_0 denotes the stress referred to the original cross section of a tensile bar or the load per unit of area, for incompressible material

$$\sigma_0 = \frac{\sigma}{1 + \epsilon''} \dots\dots\dots [3]$$

a second surface $\sigma_0 = g(\epsilon'', u'')$ may be constructed representing the load in function of ϵ'' and u'' . The time t appears as a variable only implicitly in Equations [1], [2], and [3] for a state of flow in the metals.

This is adequate for the simpler types of creep in the lower range of temperature. It is no longer adequate in the so-called intermediate range of temperatures when strain-hardening is combined with softening with time. The time t appears now explicitly in the equation of state; the Equations [1] and [2] must be assumed in the form

$$F(\sigma, \epsilon'', u'', t) = 0 \dots\dots\dots [4]$$

² "On the Creep of Solids at Elevated Temperature," *Journal of Applied Physics*, vol. 8, 1937, pp. 418-432.

¹ Pittsburgh, Pa. Fellow ASME.

² "The Creep of Metals," *Trans. ASME*, vol. 55, 1933, paper APM-55-10; also *Journal of Applied Mechanics*, *Trans. ASME*, vol. 58, 1936, p. A-7.

Contributed by the Heat Transfer and Applied Mechanics Divisions and presented at the Annual Meeting, New York, N. Y., November 26-December 1, 1950, of THE AMERICAN SOCIETY OF MECHANICAL ENGINEERS.

NOTE: Statements and opinions advanced in papers are to be understood as individual expressions of their authors and not those of the Society. Manuscript received at ASME Headquarters, October 10, 1950. Paper No. 50-A-21.

and

$$d\sigma = \frac{\partial\sigma}{\partial\epsilon''} d\epsilon'' + \frac{\partial\sigma}{\partial u''} du'' + \frac{\partial\sigma}{\partial t} dt = \psi d\epsilon'' + \phi du'' + \chi dt \quad [5]$$

$\chi = \partial\sigma/\partial t$ expresses a rate of softening (annealing) with the time t in the metal when $\chi < 0$, or of hardening (aging, age-hardening) when $\chi > 0$. The fundamental tests may be discussed under the latter conditions, but if $d\sigma$ in Equation [5] is not a complete differential two tests originating at the same initial values of ϵ'' , u'' , σ , and t , but following different pathways ending at the same values of, say, ϵ'' , u'' , and t will not terminate at the same values of the stress σ . The various fundamental tests can now be described geometrically by the pathways or orbits of a mathematical point P having the co-ordinates ϵ'' , u'' , σ in space moving on a surface $F(\sigma, \epsilon'', u'') = 0$ which is being displaced itself as a whole or which is distorted continuously in time t .

In a long-time creep test under a constant stress σ $d\sigma = 0$ and from Equation [5], after solving for the increment du''

$$du'' = -\frac{\psi}{\phi} d\epsilon'' - \frac{\chi}{\phi} dt \quad [6]$$

we see that in the softening range of temperature when the effect of χ becomes more pronounced, since $\psi > 0$, $\chi < 0$, the creep rate u'' will decrease due to strain-hardening and increase due to softening of the metal. Thus a balance of the two right-hand terms in Equation [6] will determine the sign of du'' or of the rate du''/dt at which the creep rate u'' changes with time. This is in accordance with the ideas expressed by R. W. Bailey⁴ and P. G. McVetty⁵ on the gradual decrease of the creep rates during the primary creep period toward a minimum rate u_{\min}'' .

A minimum rate u_{\min}'' is reached when $du''/dt = 0$ and

$$u_{\min}'' = \left(\frac{d\epsilon''}{dt}\right)_{\min} = -\frac{\chi}{\psi} \quad [7]$$

assuming that $\psi > 0$, $\chi < 0$, i.e., when the decrease of creep rate due to strain-hardening just becomes equal to the increase due to softening.

It should be noted that other causes besides softening or age-hardening of a metal (depending on whether $\chi < 0$ or $\chi > 0$) may be responsible for decreasing the creep rates during the primary creep period in a metal.⁶ We may quote four possible causes for primary creep:

(a) If the metal flows according to a time-independent equation of state (Equations [1], [2], and [3]) under a constant load $\sigma_0 = \text{const}$ (most long-time creep tests are run in this manner in the conventional type of creep machines with dead-weight loading devices) a primary period of creep under decreasing rates $u'' = d\epsilon''/dt$ is observable. When $\sigma_0 = \text{const}$, from Equation [3]

$$\sigma_0 = \frac{\sigma}{1 + \epsilon''} = \text{const} \quad [8]$$

Since

$$d\sigma_0 = \frac{\partial\sigma_0}{\partial\epsilon''} d\epsilon'' + \frac{\partial\sigma_0}{\partial u''} du'' = 0 \quad [9]$$

after dividing by dt

⁴ "Note on the Softening of Strain-Hardened Metals and Its Relation to Creep," by R. W. Bailey, *Journal of the Institute of Metals*, vol. 35, 1926, p. 27.

⁵ "Interpretation of Creep Tests," by P. G. McVetty, *Proceedings of the ASTM*, vol. 34, 1934, part 2, pp. 16-116.

⁶ In the latter case ($\chi > 0$, aging) creep proceeds under a constant stress σ as long as new points P may be found on the stress surface in which the passive resistance to flow is equal to σ . In fact, at the instant $t = t_1$ when the diminishing creep rate vanishes, when $u'' = 0$, the stress surface $F = 0$, Equation [4] moves away from the point $P(\epsilon'', u'' = 0, \sigma)$ leaving P at this position at rest.

$$\frac{du''}{dt} = -\frac{u''}{\frac{\partial\sigma_0}{\partial u''}} \quad [10]$$

A minimum condition $du''/dt = 0$ may be satisfied by letting

$$\frac{\partial\sigma_0}{\partial u''} = \frac{\partial}{\partial u''} \left(\frac{\sigma}{1 + \epsilon''} \right) = 0 \quad [11]$$

This is the same condition as the one determining the maximum of the load $\sigma_{0 \max}$ (the "tensile strength") in a constant-rate tensile test $u'' = \text{const}$, defining the instant at which a cylindrical bar starts to contract locally and necking begins to develop. At high temperatures this may occur at small permanent strains ϵ'' for metals having high melting points.

(b) On the other hand, if the time t appears explicitly in the Equations of state (Equation [4] or [5]), as a variable, as we have seen, du''/dt vanishes under a constant stress σ when the creep rate u'' reaches its minimum value according to Equation [7] equal to

$$u_{\min}'' = -\frac{\chi}{\psi} \quad [12]$$

(c) A generally viscous solid having no strain-hardening property ($\psi = 0$) for which the coefficient of viscosity ϕ increases first with time t to a maximum value and then decreases while the strains ϵ'' remain small, may show under a stress $\sigma = \text{const}$ a primary creep period during which the creep rates u'' decrease toward a minimum value. Taking $\psi = 0$ and $d\sigma = 0$, from Equation [5]

$$\frac{du''}{dt} = -\frac{\chi}{\phi} \quad [13]$$

du''/dt will vanish and an inflection point in the creep-time curve may be observable at a time $t = t_m$ if

$$\chi(t_m) = \left(\frac{\partial\sigma}{\partial t} \right)_{t=t_m} = 0 \quad [14]$$

A perfectly viscous substance having a viscosity ϕ which changes according to the curve in Fig. 1 with the time t would be an example. For such a substance

$$\sigma = \phi(t)u'' \quad [15]$$

so that for it

$$\chi = \frac{\partial\sigma}{\partial t} = \phi'(t)u''$$

and du''/dt , according to Equation [13] becomes

$$\frac{du''}{dt} = -\frac{\phi'(t)u''}{\phi(t)} \quad [15a]$$

du''/dt vanishes when the viscosity ϕ reaches its analytic maximum at which the time derivative $\phi'(t) = 0$. A primary creep period would be observed during the interval of time $0 \leq t \leq t_m$ in which ϕ increases and $\chi > 0$ and after which χ changes its sign. Such a solid substance would be said to harden first (so long as $\chi > 0$) and to soften thereafter.

For example, if the viscosity should vary according to the function of the time t

$$\phi = \frac{\phi_0}{1 + \alpha(t - t_1)^2} \quad [16]$$

FIG. 1 TIME-DEPENDENT VISCOSITY ϕ

(α , ϕ_1 , t_1 are constants) ϕ would increase from the initial value equal to

$$\phi_0 = \frac{\phi_1}{1 + \alpha t_1^2}$$

at time $t = 0$ to the maximum value ϕ_1 reached at time t_1 , so that the constant α also is equal to

$$\alpha = \left(\frac{\phi_1}{\phi_0} - 1 \right) : t_1^2$$

(Fig. 1). After solving Equation [15] for u^* the differential equation of the creep curves, assuming $\sigma = \text{const}$

$$u^* = \frac{d\epsilon^*}{dt} = \frac{\sigma}{\phi} = \frac{\sigma}{\phi_1} [1 + \alpha(t - t_1)^2] \quad [17]$$

would be obtained, furnishing in its integral (satisfying the initial condition $t = 0$, $\epsilon^* = 0$) the corresponding long-time creep curves

$$\epsilon^* = \frac{\sigma}{3\phi_1} [\alpha t^3 - 3\alpha t t_1^2 + 3(1 + \alpha t_1^2)t] \quad [18]$$

representing a family of affine curves (Fig. 2) having inflection points at the same time t_1 and at the creep strains

$$\epsilon_{\text{inf}}^* = \frac{\sigma}{3\phi_1} (3 + \alpha t_1^2) t_1 \quad [19]$$

and the minimum creep rates

$$u_{\text{min}}^* = \frac{\sigma}{\phi_1} \quad [20]$$

The coefficient χ , expressing the time rate of change of the inner resistance of the material to deformation, is found to be equal to

$$\chi = \frac{\partial \sigma}{\partial t} = u^* \frac{d\phi}{dt} = - \frac{2\alpha\sigma(t - t_1)}{1 + \alpha(t - t_1)^2} \quad [21]$$

When $0 < t < t_1$, $\chi > 0$, the substance may be said to harden.⁷

(d) A fourth case in which a primary creep period may be observable may occur under more complex conditions of flow in which also recovery strains are at work.

⁷ If the constant t_1 does not depend upon the stress σ as was just assumed, all inflection points occur along a vertical line in Fig. 2 at time $t = t_1$. However, if t_1 should be assumed to depend on σ and, for example, would be inversely proportional to σ , the inflection points would occur along a horizontal line $\epsilon_{\text{inf}}^* = \text{const.}$ when ϕ_0 , ϕ_1 are constant. By making t_1 , ϕ_0 , ϕ_1 suitably dependent upon the stress σ one could also construct cases for which the family of creep curves would look not unlike those illustrated in Fig. 3 and observed by P. G. McVetty in certain cases of creep.

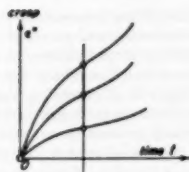


FIG. 2 CREEP CURVES

INFLUENCE OF STRAIN-HARDENING ON CREEP AND RELAXATION

Leaving aside the influence of the decrease of the cross-sectional areas of a tensile specimen elongating under a constant load $\sigma_0 = \text{const}$ on the shape of the creep curves quoted under (a) in the preceding section, the long-time creep tests under a constant stress σ and the relaxation tests $\epsilon = \epsilon' + \epsilon'' = \text{const}$ may be correlated with each other if the form of the stress surface is known. Assuming first that the time t does not enter in its equation, after solving Equation [1] for $u^* = d\epsilon^*/dt$, the differential equation of the long-time creep curves may be obtained in

$$u^* = \frac{d\epsilon^*}{dt} = f(\sigma, \epsilon^*) \quad [22]$$

by assuming here $\sigma = \text{const}$ and the differential equation of the relaxation tests after introducing in Equation [22] the condition

$$E(\epsilon'' - \epsilon_1'') = \sigma_1 - \sigma \quad [22a]$$

the subscript 1 referring to the initial values at the time $t = 0$ at the beginning of relaxation. From Equation [22a] also

$$\frac{d\sigma}{dt} = -E \frac{d\epsilon''}{dt} = -Eu^* \quad [22b]$$

Thus the equation for the relaxation test may be expressed either by using the values of σ and $d\sigma/dt$ taken from Equations [22a] and [22b], or by expressing ϵ'' and $d\epsilon''/dt$ by means of σ from these latter equations and substituting them in Equation [22], resulting in a differential equation of first order for ϵ'' or for σ , respectively. An equation of second order is, however, obtained, if the form of the stress surface is not a priori known or if such an equation does not exist and only the differential form Equation [2] can be utilized

$$\frac{d\sigma}{dt} = \psi u^* + \phi \frac{du^*}{dt} \quad [23]$$

ψ , ϕ being essentially positive quantities, since during relaxation $u^* > 0$, $d\sigma/dt < 0$, after solving the last equation for du^*/dt , using Equation [22b] we see that

$$\frac{du^*}{dt} = - \frac{(E + \psi)u^*}{\phi} \quad [23a]$$

always $du^*/dt < 0$. Since the first term ψu^* in the right side of Equation [23] is positive and the second term negative, the stress

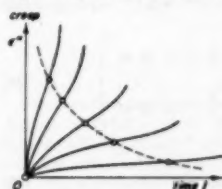


FIG. 3 CREEP CURVES AFTER P. G. McVETTY

σ in a strain-hardening material must decrease at a smaller rate $d\sigma/dt$ than in a substance which does not strain-harden. Strain-hardening slows down relaxation.⁸

⁸ This is illustrated in Fig. 4 in the relaxation curves for an elastic-viscous substance with linear strain-hardening. The stress surface for such a substance has the linear equation

$$\sigma = \psi \epsilon^* + \phi u^* \quad [23b]$$

The stress σ relaxes in it according to Equation [46g] (see next section). The stress follows the lowest of the curves in Fig. 4 when $\psi = 0$. With increasing values of ψ it decreases less rapidly and it approaches a greater final value when $t = \infty$.

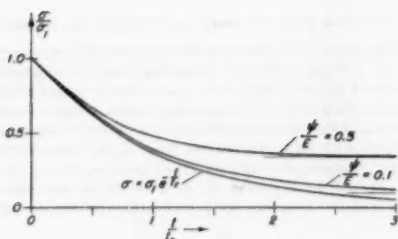


FIG. 4 RELAXATION CURVES FOR ELASTICO-VISCOUS SUBSTANCE WITH LINEAR STRAIN-HARDENING
($\sigma = \psi \epsilon^{1/2} + \phi u''$)

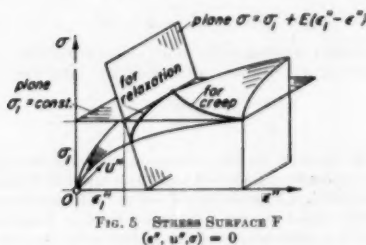


FIG. 5 STRESS SURFACE F
($\epsilon'', u'', \sigma = 0$)

If the stress surface is not known analytically, it may be represented by a block diagram like the one reproduced in Fig. 5 which may have been constructed by its contour lines $\sigma = \text{const.}$ or its sections $u'' = \text{const.}$ (constant plastic strain-rate tests). Relaxation tests would be represented by the intersection of a steeply inclined plane $\sigma = \sigma_1 + E(\epsilon'' - \epsilon^*)$ with the stress surface.

Plausible forms of Equation [1] have been considered by various investigators. Space prohibits their general discussion here, but for the ductile metals experiments have indicated that three speed relations are important for expressing the dependence of the resistance to flow σ on the rates of strain u'' , which should be listed here, namely

$$\sigma = \sigma_0 \left(\frac{u''}{u_0} \right)^m, \quad (0 < m \leq 1) \quad [24]$$

$$\left. \begin{aligned} \sigma &= \sigma_0 \frac{u''}{u_0} \dots \dots \dots 0 \leq u'' \leq u_0 \\ \sigma &= \sigma_0 \left(1 + \ln \frac{u''}{u_0} \right) \dots \dots \dots u_0 \leq u'' \end{aligned} \right\} \quad [25]$$

and

$$u'' = u_0 \sinh \frac{\sigma}{\sigma_0} \quad [26]$$

representing the power function, the logarithmic and the hyperbolic-sine speed laws,³ respectively. σ_0, u_0 are material constants.

If one or the other of the three preceding functions (Equations [24] to [26]) represents the complete equation of state for a metal,

³"The Influence of Time Upon Creep and the Hyperbolic-Sine Creep Law," in Stephen Timoshenko 60th Anniversary Volume, The Macmillan Company, New York, N. Y., 1938, pp. 155-170.

"Interpretation of Creep Test Data," by P. G. McVetty, Proceedings of the ASTM, vol. 43, 1943, pp. 707-727.

"Creep of Metals at Elevated Temperatures—the Hyperbolic-Sine Relation Between Stress and Creep Rate," by P. G. McVetty, Trans. ASME, vol. 65, 1943, pp. 761-767.

the flow stress σ depends only on the rates of strain u'' but not on the strains themselves. The creep curves for $\sigma = \text{const.}$ are then a family of straight lines $\epsilon'' = ct$, the constant c being the value of u'' computed from one or the other of the foregoing equations.

It may be of interest to evaluate the equations expressing the dependence of the stress σ on the time t in relaxation tests corresponding to these three speed laws. The computation was carried out denoting by σ_1 the initial value of stress at time $t = 0$ causing the initial elastic strain $\epsilon_1 = \sigma_1/E$.

For the power function law, Equation [24], one obtains

$$\sigma = \frac{\sigma_1}{\left[1 + \frac{(1-m)}{m} \frac{E}{\sigma_1} \left(\frac{\sigma_1}{\sigma_0} \right)^{\frac{1}{m}} u''_0 t \right]^{\frac{m}{1-m}}} \quad [24a]$$

This equation becomes indeterminate when $m = 1$, i.e., when $\sigma = \sigma_0 u''/u_0$ defining the elastico-viscous substance, for which, by direct computation

$$\sigma = \sigma_1 e^{-\frac{t}{t_0}}, \quad \left(t_0 = \frac{\sigma_0}{E u_0} \right) \quad [24b]$$

defining the Maxwell relaxation law.

For the logarithmic law, Equation [25], one obtains two branches of the stress-time curves with the equations

$$\left. \begin{aligned} \sigma &= \sigma_1 - \sigma_0 \ln \left(1 + \frac{t}{t_0} \right) \dots \text{for } 0 \leq t \leq t_0, u_0 \leq u'' \\ \sigma &= \sigma_0 e^{-\frac{(t-t_0)}{t_0}} \dots \text{for } t_0 \leq t, 0 \leq u'' \leq u_0 \end{aligned} \right\} \quad [25a]$$

where $t_0 = \sigma_0/(E u_0)$ and

$$t_0 = t_1 \left[1 - e^{-\frac{\sigma_1 - \sigma_0}{\sigma_0}} \right]$$

the constant t_0 denoting the time required to reach the transition value of stress $\sigma = \sigma_0$ at which the logarithmic speed law changes to the linear speed law.

For the hyperbolic-sine speed law, Equation [26], the stress decreases with the time according to the relaxation law¹⁰

$$\tanh \frac{\sigma}{2\sigma_0} = e^{-\frac{t}{t_0}} \tanh \frac{\sigma_1}{2\sigma_0} \quad [26a]$$

reverting, when σ becomes small to Equation [24b] and when σ has large values, to the first of the Equations [25a], provided that the constants σ_0 and u_0 in Equations [26] and [25]), respectively, are chosen properly to match with each other.

The three speed laws, Equations [24] to [26], have been verified during the past 30 years by many observations on flow and creep of metals over certain ranges of the rates of strain. They seem to provide the first basis for a working theory of creep and relaxation at elevated temperatures in engineering applications. This latter theory postulates the minimum creep rate $u''_{\min} = f(\sigma)$ as active over the entire time range. It is well known that this is not the case within the primary creep period with its continuously decreasing creep rates. The introduction of the quantities $\psi = \partial \sigma / \partial \epsilon''$ and $\chi = \partial \sigma / \partial t$ in the equation of state, formulated in the preceding section, offers a means for dealing also with cases of relaxation in which strain-hardening and softening must be considered.

For physical reasons, one should expect that at elevated temperatures the stress surface $F(\epsilon'', u'', \sigma) = 0$ should pass at least through the ϵ'' -axis, considering that how small a stress σ may act, if a sufficient time is allowed for its action, a very small, but

¹⁰"The Creep of Metals Under Various Stress Conditions," in Theodore von Kármán Anniversary Volume, California Institute of Technology, Pasadena, Calif., 1941, pp. 237-257.

finite creep rate may be observable.¹¹ At lower temperatures one may assume that the stress surface intersects both the σ , ϵ^* and σ , u^* planes along curves having finite ordinates σ . These latter would represent limits of yield stress, below which no permanent distortions could be produced. In such cases the hodographs $\phi(\epsilon^*, u^*) = 0$ for the constant stress and the relaxation test terminate at the ϵ^* axis—the creep curves approach finite creep limits, and the stress σ in relaxation tests cannot drop below the values of σ found along the ϵ^* axis.

If the surface $F = 0$ is not strongly curved, one may replace the function $F(\epsilon^*, u^*, \sigma) = 0$ by its tangent plane at the initial state of strain to be considered (Fig. 6)

$$\sigma = \sigma_1 + \psi \epsilon^* + \phi u^* \dots \dots \dots [27]$$

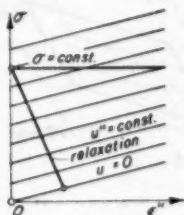


Fig. 6

where ψ , ϕ are assumed constant.¹²

If the metal strain-hardens at a small rate $\psi = \partial\sigma/\partial\epsilon^*$ but $\phi = \partial\sigma/\partial u^*$ varies rapidly corresponding to one of the three speed laws formulated in Equations [24] to [26], one sees that strain-hardening can have but little effect on the relaxation of stresses. On the contrary, relaxation is retarded more effectively, if ψ has a magnitude comparable to the modulus of elasticity E . An example illustrating such a case is treated in the following.

Suppose that the stress surface has the equation

$$\sigma = \sigma_0 \left(1 + \frac{\epsilon^*}{\epsilon_0} \right) \left(\frac{u^*}{u_0} \right)^m \quad (0 < m \leq 1) \dots \dots \dots [28]$$

σ_0 , u_0 , ϵ_0 , m being material constants. Let $c = \sigma_0/u_0^m$. The differential equation for the long-time creep curves is obtained after assuming in Equation [28], $\sigma = \text{const}$ and solving for u^*

$$u^* = \frac{d\epsilon^*}{dt} = \left(\frac{\sigma}{c} \right)^{\frac{1}{m}} \left(\frac{\epsilon_0}{\epsilon_0 + \epsilon^*} \right)^{\frac{1}{m}} \dots \dots \dots [29]$$

having

$$\epsilon^* = \epsilon_0 \left[\left(1 + \frac{t}{t_0} \right)^{\frac{m}{m+1}} - 1 \right], \quad t_0 = \frac{m\epsilon_0}{(m+1)u_0} \left(\frac{\sigma_0}{\sigma} \right)^{\frac{1}{m}} \dots \dots \dots [30]$$

as integral satisfying the initial condition $t = 0$, $\epsilon^* = 0$. The constant t_0 has the dimensions of a time. The initial rate with which creep starts is

$$u_1^* = \left(\frac{\sigma}{c} \right)^{\frac{1}{m}}$$

and u^* decreases while ϵ^* increases with time, neither approaching a limit at finite times t .

¹¹ A stress surface passing through the ϵ^* axis with a steep slope $\partial\sigma/\partial\epsilon^*$ near it and a gentle slope far from it would correspond to the regions in which "micro" and "macro" creep were distinguished in the tests described by B. Chalmers (Proceedings of the Royal Society of London, series A, vol. 156, 1936, p. 427).

¹² Such cases were treated in the second paper quoted in Footnote 2. Their hodographs consist of straight lines.

For the relaxation test we have to substitute in Equation [29] for $\sigma = \sigma_1 - E\epsilon^*$. Assuming that $\sigma = \sigma_1$ and $\epsilon = \epsilon_1 = \sigma_1/E$ represent the initial values of the stress and strain at the time $t = 0$, this then leads to the differential equation

$$\frac{d\epsilon^*}{dt} = c_0 \left(\frac{\epsilon_1 - \epsilon^*}{\epsilon_0 + \epsilon^*} \right)^{\frac{1}{m}} \dots \dots \dots [31]$$

where c_0 denotes the constant

$$c_0 = u_0 \left(\frac{E\epsilon_0}{\sigma_0} \right)^{\frac{1}{m}}$$

or this equation may be expressed in terms of the stress σ after substituting for $\epsilon^* = \epsilon_1 - (\sigma/E)$. It may be integrated by using a series development, after changing the variable ϵ^* to

$$v = \frac{\epsilon_0 + \epsilon^*}{\epsilon_0 + \epsilon_1} \dots \dots \dots [32]$$

When $0 < t < \infty$ varies between the limits

$$\frac{\epsilon_0}{\epsilon_0 + \epsilon_1} = v_1 < v < 1$$

From Equation [31]

$$\frac{dv}{dt} = \frac{1}{t_1} \left(\frac{1-v}{v} \right)^{\frac{1}{m}} \dots \dots \dots [33]$$

where $t_1 = (\epsilon_0 + \epsilon_1)/c_0$. The stress σ may be expressed as a function of the time t after integration as follows

$$\left. \begin{aligned} \sigma &= E(\epsilon_0 + \epsilon_1)(1-v) \\ t &= t_1 [v^k S(v) - v_1^k S(v_1)] \end{aligned} \right\} \dots \dots \dots [34]$$

where $k = 1/m$, ($1 < k < \infty$) and S denotes the infinite series

$$S(v) = \frac{v}{k+1} - \left(\frac{-k}{1} \right) \frac{v^2}{(k+2)} + \left(\frac{-k}{2} \right) \frac{v^3}{(k+3)} - \dots \dots \dots [35]$$

in which $\left(\frac{-k}{1} \right)$, $\left(\frac{-k}{2} \right)$, ... are the binomial coefficients

$$-k, \frac{(-k)(-k-1)}{1 \cdot 2}, \dots$$

The constant v_1 depends on the initial stress $\sigma = \sigma_1$ at time $t = 0$ and is equal to

$$v_1 = \frac{1}{1 + \frac{\sigma_1}{E\epsilon_0}}$$

The preceding equations describe the decrease in stress in a relaxation test for a metal which strain-hardens rapidly and linearly with the strain ϵ^* but in which the flow stress σ varies with the rates u^* , according to the power-function law, Equation [24], which has been verified empirically in many long-time creep tests made on metals. They bring out the effect of strain-hardening on relaxation in metals which have steeply rising stress-strain curves (at constant strain rates $u^* = \text{const}$) for small permanent strains ϵ^* . It is here assumed that the intercept ϵ_0 in Fig. 7 defining point A is comparable in magnitude with the initial elastic strain $\epsilon_1 = \sigma_1/E$.

As a second example, consider a metal in which the flow stress σ increases monotonically with the strains ϵ^* and with the rates of strain u^* according to

$$\sigma = c\epsilon^m u^{*n} \quad (0 < m, n \leq 1) \dots \dots \dots [36]$$

The stress-strain curves taken at constant strain rates u^* for this

metal are represented by a family of affine power-function curves of the permanent strain ϵ^* . Assuming $\sigma = \text{const}$, the corresponding creep curves have the equation

$$\epsilon^* = \left(\frac{n+m}{m} \right) \frac{1}{n+m} \left(\frac{\sigma}{c} \right)^{\frac{1}{n+m}} t^{\frac{n+m}{n+m}} \dots [37]$$

showing that creep now increases according to the $m/(n+m)$

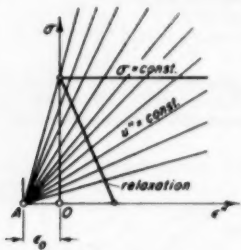


FIG. 7

power of the time t . The relaxation curve corresponding to Equation [36] can be determined in a way similar to that indicated in the preceding example by using a series development.¹³

INFLUENCE OF TIME RATE OF CHANGE OF FLOW RESISTANCE ON CREEP

Unfortunately, few observations are available on the magnitudes and variations with time t of the rate of change of resistance to flow $\chi = \partial\sigma/\partial t$ which has seldom been considered if at all by experimenters on creep of metals.

To illustrate the quantitative influence of a term containing $\chi = \partial\sigma/\partial t$ on the flow, consider the simple case that the equation of state is linear in the three terms¹⁴

$$\sigma = \psi\epsilon^* + \phi u^* + \chi t \dots [38]$$

where ψ , ϕ , χ are constants. After replacing u^* by $d\epsilon^*/dt$, assuming that $\sigma = \text{const}$, this gives the linear differential equation of first order for the creep test $\sigma = \text{const}$

$$\frac{d\epsilon^*}{dt} + \frac{\psi}{\phi} \epsilon^* = \frac{\sigma - \chi t}{\phi} \dots [39]$$

¹³ We may note that the stress surface, Equation [28], in the preceding example in fact represents the developable surface which is tangent to the stress surface, Equation [36], in the second example along the profile in which the latter surface is intersected by a plane $\epsilon^* = \text{const}$. In fact Equation [28] represents a strip made tangent along a profile in a plane $\epsilon^* = \text{const}$ in the double power surface, Equation [36]. Both these may characterize the behavior of a ductile metal having strain-hardening properties associated with an appreciable dependence of the flow stresses on the speeds of strain.

If the exponent n in Equation [36] is equal to zero, this reverts to Equation [24] and to the case when the flow stress σ is a power function of the rate of strain u^* , the creep curves become the straight lines

$\epsilon^* = (\sigma/c)^{1/n}$. The foregoing Equations [28] to [37] thus bring out the effect of strain-hardening on the shapes of the creep curves (Equations [30] and [37]) and of the relaxation curve (Equation [34]).

¹⁴ By adding a constant σ_0 on the right side of Equation [38] materials having a finite yield stress $\sigma = \sigma_0$ at the time $t = 0$ when $\epsilon^* = u^* = 0$ might also be included in the above considerations. These could be characterized as "Bingham substances"—to follow terminology used by the rheologists—having apart from elasticity, constant viscosity and linear strain-hardening and in which the "yield value" $\sigma_0 + \chi t$ would be subject to an increase or decrease due to age-hardening or softening with the time t (Fig. 8).

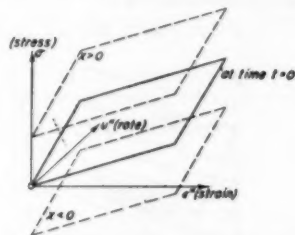
having the integral satisfying the initial condition $t = 0$, $\epsilon^* = 0$

$$\epsilon^* = -\frac{\chi}{\psi} t + \left(\frac{\sigma}{\psi} + \frac{\phi\chi}{\psi^2} \right) \left(1 - e^{-\frac{\psi}{\phi} t} \right) \dots [40]$$

expressing the equation of the creep-time curves at constant stress. The creep rates are

$$u^* = \frac{d\epsilon^*}{dt} = -\frac{\chi}{\psi} + \left(\frac{\sigma}{\psi} + \frac{\phi\chi}{\psi^2} \right) e^{-\frac{\psi}{\phi} t} \dots [41]$$

This last equation shows that when $t = 0$, $u^* = \sigma/\phi$, that the

FIG. 8 STRESS SURFACE $\sigma = \psi\epsilon^* + \phi u^* + \chi t$

creep curves, Equation [40], have the same initial slope for a given stress σ independently of the values of ψ and χ , independently of the rate of strain-hardening and of softening or aging. With the abbreviations

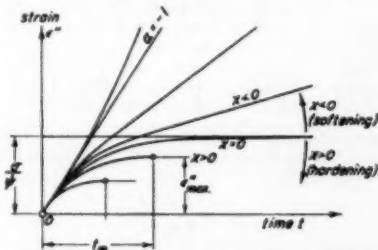
$$t_0 = \frac{\phi}{\psi}, \quad \alpha = \frac{\chi\phi}{\psi\sigma} \dots [42]$$

where α is negative for a material which softens with time and positive for an age-hardening material, Equations [40] and [41] take the simpler form

$$\epsilon^* = \frac{\sigma}{\psi} \left[-\alpha \frac{t}{t_0} + (1 + \alpha) \left(1 - e^{-\frac{t}{t_0}} \right) \right] \dots [43]$$

$$u^* = \frac{\sigma}{\phi} \left[-\alpha + (1 + \alpha)e^{-\frac{t}{t_0}} \right] \dots [44]$$

The creep curves, Equation [43], are exponential curves approach-

FIG. 9 INFLUENCE OF TIME RATE OF CHANGE OF FLOW RESISTANCE $\chi = \partial\sigma/\partial t$ ON SHAPE OF CREEP CURVES

ing asymptotically a family of inclined straight lines (Fig. 9), having the equation

$$\epsilon^* = \frac{\sigma}{\psi} \left[1 + \alpha - \alpha \frac{t}{t_0} \right] = a + bt \dots [45]$$

with the intercepts

$$a = (1 + \alpha)\sigma/\psi = \left(1 + \frac{\chi\phi}{\psi}\right)\frac{\sigma}{\psi} \quad [45a]$$

and the slopes representing the final values of the rate of creep u^* for $t = \infty$

$$b = -\frac{\alpha\sigma}{\psi} = -\frac{\chi}{\psi} \quad [45b]$$

When the material neither softens, nor hardens $\alpha = \chi = 0$, the creep curve has a horizontal asymptote (Fig. 9) with a creep limit $\epsilon^* = \sigma/\psi$. Table I contains a few values of a and b for the values of α , given in the first column.

TABLE I VALUES OF α , a and b

Rate of change of flow resistance	Intercept of asymptote	Slope of asymptote
$\alpha = \frac{\chi\phi}{\psi}$	$a = (1 + \alpha)\frac{\sigma}{\psi}$	$b = -\frac{\alpha\sigma}{\psi}$
Material softens		
$\left\{ \begin{array}{l} -2 \\ -3/2 \\ -1 \\ -2/3 \\ -1/3 \end{array} \right.$	$\left\{ \begin{array}{l} -1.0 \times \frac{\sigma}{\psi} \\ -0.500 \\ 0.0 \\ +0.333 \\ 0.667 \end{array} \right.$	$\left\{ \begin{array}{l} +2.0 \times \frac{\sigma}{\psi} \\ 1.500 \\ 1.0 \\ 0.667 \\ 0.333 \end{array} \right.$
0	1.0	0.0
Material hardens		
$\left\{ \begin{array}{l} 1/3 \\ 2/3 \\ 1 \\ 3/2 \\ 2 \end{array} \right.$	$\left\{ \begin{array}{l} 1.333 \\ 1.667 \\ 2.0 \\ 2.500 \\ 3.0 \end{array} \right.$	$\left\{ \begin{array}{l} -0.333 \\ -0.667 \\ -1.0 \\ -1.500 \\ -2.0 \end{array} \right.$

When the rate of softening is equal to $\chi = -\psi\sigma/\phi$, $\alpha = -1$, the creep curve is a straight line as for a purely viscous substance. In fact, this represents the special case for which, at the given stress, the rate of increase of the flow resistance due to strain-hardening ψ is just equal to the rate of decrease of resistance due to softening of the material, i.e., for which the condition of minimum creep rate is satisfied continuously from the beginning of the creep test during the entire extension.¹⁵ This has been illustrated also in the creep curves reproduced in Fig. 9, plotted for a few values of α .

The relaxation problem corresponding to the linear equation of state, Equation [39], is solved by remarking that if the condition of relaxation $E(\epsilon^* - \epsilon^s) = \sigma_1 - \sigma$ is introduced in Equation [39] and the decrease of stress $\sigma_1 - \sigma$ considered as the dependent variable, a differential equation results

$$\frac{d}{dt} \left(\frac{\sigma_1 - \sigma}{E} \right) + \frac{(E + \psi)}{\phi} \left(\frac{\sigma_1 - \sigma}{E} \right) = \frac{\sigma_1 - \sigma}{\phi} \quad [46a]$$

which has the same form as the differential equation for the creep test under a constant stress, Equation [39]. Also, the initial conditions $t = 0$, $\sigma_1 - \sigma = 0$ and $t = 0$, $\epsilon^* = 0$, respectively, have the same form. Therefore, if we replace in Equation [39] the quantities

$$\epsilon^*, \psi, \sigma, t_0 = \frac{\phi}{\psi}, \alpha = \frac{\chi\phi}{\psi} \quad [46b]$$

by the quantities

¹⁵ If $\chi < 0$, and $|\chi| > \psi\sigma/\phi$, $\alpha < -1$, creep develops first under accelerating rates, because the material softens too fast. On the contrary, if $\chi > 0$, $\alpha > 0$, i.e., when the material hardens, creep will stop after a certain time t_m , when ϵ^* reaches an analytic maximum ϵ_{max}^* and, consequently, u^* vanishes. Creep stops at the values

$$t_m = t_0 \ln \frac{1 + \alpha}{\alpha}, \quad \epsilon_{max}^* = \frac{\sigma}{\psi} \left(1 - \alpha \ln \frac{1 + \alpha}{\alpha} \right) \quad [46c]$$

$$\frac{\sigma_1 - \sigma}{E}, \psi + E, \sigma_1, t_0 = \frac{\phi}{\psi + E}, \alpha = \frac{\chi\phi}{(\psi + E)\sigma_1} \quad [46c]$$

in the same order, Equation [46a] results, having thus the solution (corresponding to Equation [43]) for the decrease of stress

$$\frac{\sigma_1 - \sigma}{E} = \frac{\sigma_1}{(\psi + E)} \left[-\frac{\alpha t}{t_0} + (1 + \alpha) \left(1 - e^{-\frac{t}{t_0}} \right) \right] \quad [46d]$$

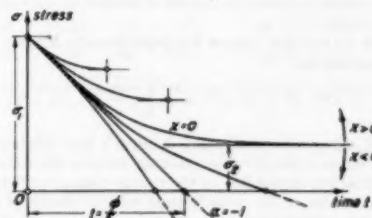
which, after rearranging terms may be written also as follows

$$\sigma = \sigma_1 + \frac{E\sigma_1}{\psi + E} \left[\frac{\alpha t}{t_0} - (1 + \alpha) \left(1 - e^{-\frac{t}{t_0}} \right) \right] \quad [46e]$$

where for t_0 , α the values of Equation [46c] have to be taken, σ_1 denoting the initial value of the stress at time $t = 0$ at which relaxation starts.

We note the interesting fact that the set of stress-time curves characterizing the relaxation of stress for a material having the linear equation of state, Equation [38], for the various values of the rate of change of the flow resistance χ is represented by the mirror image of the figure of the long-time creep curves. This is obtained by reflecting the curves in Fig. 9 along the time axis, resulting in Fig. 10 representing the corresponding relaxation curves. Thus we see also from Equation [46e] that all relaxation curves for various values of χ (and of ψ) have the same initial slope at time $t = 0$

$$\left(\frac{d\sigma}{dt} \right)_{t=0} = -\frac{E\sigma_1}{\phi} \quad [46f]$$

FIG. 10 RELAXATION CURVES FOR VARIOUS RATES OF CHANGE OF FLOW RESISTANCE χ

When $\chi = 0$, i.e., in a strain-hardening elasto-viscous material which neither softens nor hardens with time, the stress

$$\sigma = \frac{\sigma_1}{\psi + E} \left[\psi + E e^{-\frac{t}{t_0}} \right] \quad [46g]$$

drops from σ_1 to a finite value

$$\sigma_2 = \frac{\sigma_1\psi}{E + \psi}$$

which is reached asymptotically with the time t . When $\chi > 0$ (age-hardening) the relaxation curves terminate abruptly with horizontal tangents at finite ordinates after finite times, but when $\chi < 0$ (softening) the stress σ gradually drops to zero in finite times. In the special case $\alpha = -1$, $\chi = -(E + \psi)\sigma_1/\phi$, the exponential function in Equation [46e] cancels out and the stress decreases according to

$$\sigma = \sigma_1 \left(1 - \frac{E}{\phi} t \right) \quad [46h]$$

in a straight line, vanishing at the time $t = \phi/E$ (Fig. 10).

CREEP RECOVERY

The foregoing assumptions are not sufficient for the treatment of a phenomenon which is sometimes associated with the creep of solids, namely, of the recovery of strain after unloading. This is a negative strain which has been observed after a rapid unloading from a positive stress. It has the character of an aftereffect, usually requiring a considerable time for its full development. Recovery strains are less pronounced in metals than in certain high polymers¹⁶ but they have been observed definitely in careful measurements of creep in ductile metals at high temperatures. Their influence on the shape of creep and relaxation curves might be considered briefly in this section.

It has been pointed out² that whereas generalized elastico-viscosity is characterized by assuming a principle of superposition of two types of strains

$$\epsilon = \epsilon' + \epsilon'', \quad \epsilon' = \frac{\sigma}{E} \frac{d\epsilon''}{dt} = f(\sigma) \dots [47]$$

a corresponding principle of superposition of two types of stresses

$$\sigma = \sigma^* + \sigma^{**}, \quad \sigma^* = E\epsilon, \quad \sigma^{**} = f\left(\frac{d\epsilon}{dt}\right) \dots [48]$$

defines generalized recovery-viscosity in materials exhibiting recovery strains. This was termed "firmo-viscosity" by H. Jeffreys¹⁷ for the case in which $f(d\epsilon/dt)$ is a linear function. The part σ^* of the stress is carried by those elements in the microstructure of the material that are capable of responding elastically and the part σ^{**} by an internal resistance of the structure of generally viscous nature dependent on the rate of strain $d\epsilon/dt$ and vanishing with this latter.

Let us, for example, express this dependence by a power function, assuming that

$$\sigma = \sigma^* + \sigma^{**}, \quad \sigma^* = E\epsilon, \quad \sigma^{**} = \sigma_0 \left(l_0 \frac{d\epsilon}{dt} \right)^{\frac{1}{m}}, \quad (m > 1) \dots [49]$$

where E , σ_0 , l_0 , m are constants. A stress σ held constant generates a strain ϵ that develops gradually because the major part of the stress σ is carried first by the viscous resistance σ^{**} having large values due to the initially large rates of change of strain $d\epsilon/dt$ and because the part $\sigma^* = E\epsilon$ of the stress can only grow on the expense of σ^{**} , since the sum $\sigma^* + \sigma^{**}$ remains constant and equal to the applied stress σ . The strain ϵ increases as if it were an aftereffect according to the differential equation

$$\sigma_0 \left(l_0 \frac{d\epsilon}{dt} \right)^{\frac{1}{m}} + E\epsilon = \sigma = E\epsilon_0 = \text{const} \dots [50]$$

which is satisfied by

$$\epsilon = \epsilon_0 - \left[1 + (m-1) \left(\frac{E}{\sigma_0} \right) \left(\frac{\sigma}{\sigma_0} \right)^m \frac{t}{l_0} \right]^{\frac{1}{m-1}} \dots [51]$$

The strain approaches $\epsilon_0 = \sigma/E$ as t becomes infinite. The three terms appearing in this last equation after multiplication by E are

¹⁶ Certain plastics, after a rapid loading in compression to finite strains, may recover nearly completely their former initial strain after sufficient time. Concerning the theory of recovery, see H. Lederman: "Elastic and Creep Properties of Filamentous Materials and Other High Polymers," Textile Foundation, Washington, D. C., 1943, 278 pp.; and T. M. Burgers (1 and 2 Report on Viscosity and Plasticity, Academy of Sciences, Amsterdam, Holland, 1935, and 1938, see 1, Report pp. 5-64).

¹⁷ "The Earth," by H. Jeffreys, second edition, Cambridge University Press, London, England, 1929; also Proceedings of the Royal Society of London, series A, vol. 138, 1932, p. 283, and others of his papers.

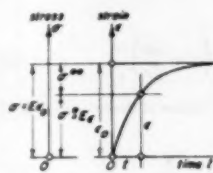


FIG. 11 UNDER CONSTANT STRESS $\sigma = \text{CONST}$

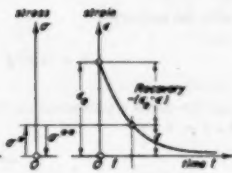


FIG. 12 AFTER UNLOADING

$E\epsilon = \sigma^*$, $E\epsilon_0 = \sigma$ and $-\sigma^{**}$ in the order from left to right (Fig. 11).

After sudden unloading from an initial stress σ and strain $\epsilon_0 = \sigma/E$ the strain is found from Equation [48] and the condition $\sigma^* + \sigma^{**} = 0$ as

$$\epsilon = \left[1 + (m-1) \left(\frac{E}{\sigma_0} \right) \left(\frac{\sigma}{\sigma_0} \right)^m \frac{t}{l_0} \right]^{\frac{1}{m-1}} \dots [52]$$

This expression is identical with the second term on the right side of Equation [51]. When $t = \infty$ the strain ϵ vanishes, and thus the original strain ϵ_0 under the stress σ is gradually recovered. The material exhibits at time t a recovery equal to $-\epsilon_0 + \epsilon$ becoming equal to $-\epsilon_0$ at time $t = \infty$ (Fig. 12).

If, after a constant stress σ acted for a certain time t_0 , during which the strain increased to the value ϵ_0 , the specimen is held at $\epsilon = \epsilon_0 = \text{const}$ the stress will suddenly drop at $t = t_0$ from its original value σ to a value $\sigma_1 = E\epsilon_0$ since for the times $t > t_0$ $d\epsilon/dt = 0$ and hence $\sigma^{**} = 0$. This sudden relaxation in the value of the stress by the amount

$$\sigma - \sigma_1 = \sigma - E\epsilon_0 \dots [53]$$

(where $\epsilon_0 = (\epsilon)_0$, is given by Equation [51]) occurs unless $\epsilon_0 < \epsilon_0 = \sigma/E$, i.e., unless the strain during the preceding period of loading $t < t_0$ has not reached its asymptotic value ϵ_0 .

The two superposition principles, expressed in the Equations [47] and [48] may be combined to include the case of slowly recoverable strains in the phenomena which were previously discussed. This leads us to propose that the total strain ϵ shall be considered as the sum of three types of strains

$$\epsilon = \epsilon' + \epsilon'' + \epsilon''' \dots [54]$$

namely, the elastic strain $\epsilon' = \sigma/E$ instantaneously carried, a permanent strain ϵ'' , and a recoverable strain ϵ''' . The last is assumed to be caused by the interaction of two stresses $\sigma^* = E\epsilon''$ and

$$\sigma^{**} = f\left(\frac{d\epsilon'''}{dt}\right)$$

the sum of which is equal to the externally produced stress σ .

Although special cases of the following synthesis of strains, assuming linear stress-rate of strain relations for the strains ϵ'' and ϵ''' have been discussed previously by authors, particularly by those who illustrated their action by means of certain mechanical models (consisting of elastic springs and dashpots¹⁸), it was considered worth while to evaluate here the complete equations for relaxation.

A substance having linear elastico and recovery-viscosity is characterized by the equation

$$\epsilon' = \frac{\sigma}{E}, \quad \frac{d\epsilon''}{dt} = \frac{\sigma}{3\mu}, \quad \epsilon''' = \frac{\sigma^*}{E}, \quad \frac{d\epsilon'''}{dt} = \frac{\sigma^{**}}{3\mu} \dots [55]$$

¹⁸ See the second group of papers quoted in Footnote 16.

The material constants E , μ , which may refer to a mechanism in the microstructure of the material contributing to the recoverable strains ϵ''' need not be equal to the modulus of elasticity E and the coefficient of viscosity μ of the substance, respectively. The strain is given by the sum Equation [54] and the stress by the sum

$$\sigma = \sigma^* + \sigma^{**} = E_s \epsilon''' + 3\mu_s \frac{d\epsilon'''}{dt} \quad [56]$$

Let

$$t_r = \frac{3\mu}{E}, \quad t_s = \frac{3\mu_s}{E_s} \quad [57]$$

where t_r , t_s have the dimension of time.

For the creep test Equations [55] and [56] give

$$3\mu \frac{d\epsilon''}{dt} = \sigma, \quad E_s \epsilon''' + 3\mu_s \frac{d\epsilon'''}{dt} = \sigma \quad [58]$$

where σ is constant.

The strains

$$\epsilon' = \frac{\sigma}{E}, \quad \epsilon'' = \frac{\sigma}{3\mu} t, \quad \epsilon''' = \frac{\sigma}{E_s} \left(1 - e^{-\frac{t}{t_s}}\right) \quad [59]$$

add up to the total strain

$$\epsilon = \frac{\sigma}{E} \left[1 + \frac{t}{t_r} + \frac{E}{E_s} \left(1 - e^{-\frac{t}{t_s}}\right)\right] \quad [60]$$

The strain after sudden unloading from a stress σ and an initial strain ϵ_1 is given by

$$\epsilon = \epsilon_1 - \frac{\sigma}{E} - \frac{\sigma}{E_s} \left(1 - e^{-\frac{t}{t_s}}\right) \quad [61]$$

where the creep recovery is given by the last one of the three terms on the right-hand side of this equation.

For the relaxation test

$$\epsilon' + \epsilon'' + \epsilon''' = \epsilon_1 = \text{const} \quad [62]$$

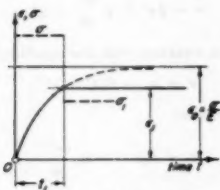


FIG. 13 RELAXATION

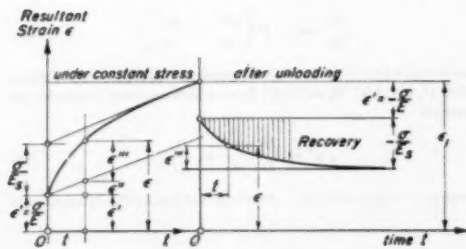


FIG. 14 STRAIN ϵ

ϵ_1 denotes the resultant strain to be held constant during relaxation. In reference to what has been said about Equation [53] it is of interest to distinguish two special cases in the initial conditions which might now be satisfied: (a) The case in which the load is applied instantaneously so that no permanent strains ϵ'' and ϵ''' are permitted to develop before the specimen starts to relax; this is expressed by the initial conditions $t = 0$, $\sigma = \sigma_1$, and $\epsilon'' = \epsilon''' = 0$, ($\epsilon' = \sigma_1/E = \epsilon_1$); (b) The case in which, on the contrary, the specimen has been held under a constant load for such a long time that the strain ϵ , representing its resultant extension, follows the inclined straight-line asymptote in Fig. 14, i.e., that the recoverable strain ϵ''' has increased already to the maximum value $\epsilon''' = \sigma_1/E_s$ it can attain before the relaxation test starts. The initial conditions in this second case are $t = 0$, $\sigma = \sigma_1$, $\epsilon''' = \sigma_1/E_s$; also, since $\epsilon = \epsilon_1$, $\epsilon' = \sigma_1/E$

$$\epsilon'' = \epsilon_1 - \sigma_1 \left(\frac{1}{E} + \frac{1}{E_s} \right)$$

After differentiating Equation [62] with respect to the time t

$$\frac{1}{E} \frac{d\sigma}{dt} + \frac{d\epsilon''}{dt} + \frac{d\epsilon'''}{dt} = 0 \quad [63]$$

substituting here for $(d\epsilon'')/(dt) = \sigma/(3\mu)$ from Equations [63] and [56]

$$\frac{d\epsilon'''}{dt} = -\frac{1}{E} \frac{d\sigma}{dt} - \frac{\sigma}{3\mu} = \frac{\sigma - E_s \epsilon'''}{3\mu_s} \quad [64]$$

is obtained, showing that also

$$\frac{d}{dt} \left(\frac{1}{E} \frac{d\sigma}{dt} + \frac{\sigma}{3\mu} + \frac{\sigma}{3\mu_s} \right) = -\frac{E_s}{3\mu_s} \left(\frac{1}{E} \frac{d\sigma}{dt} + \frac{\sigma}{3\mu} \right)$$

or that the stress σ must satisfy the differential equation of second order

$$\frac{d^2\sigma}{dt^2} + \left[\frac{1}{t_r} + \frac{1}{t_s} \left(1 + \frac{E}{E_s} \right) \right] \frac{d\sigma}{dt} + \frac{\sigma}{t_r t_s} = 0 \quad [65]$$

With the abbreviations

$$\left. \begin{aligned} \frac{1}{T} &= \frac{1}{t_r} \left(1 + \frac{E}{E_s} \right), \quad \lambda_0 = \frac{1}{2t_r} \left(1 + \frac{t_r}{T} \right) \\ \lambda &= \frac{1}{2t_r} \sqrt{\left(1 + \frac{t_r}{T} \right)^2 - \frac{4t_r}{t_s}}, \quad \lambda_1 = \lambda - \lambda_0, \quad \lambda_2 = -\lambda - \lambda_0 \end{aligned} \right\} \quad [66]$$

the integral of Equation [65] is expressed by

$$\sigma = A e^{\lambda_1 t} + B e^{\lambda_2 t} \quad [67]$$

λ_1 , λ_2 are the roots of

$$\lambda^2 + b\lambda + c = 0, \quad b = \frac{1}{t_r} + \frac{1}{T}, \quad c = \frac{1}{t_r t_s} \quad [68]$$

The discriminant being always positive and $\lambda_0 > \lambda$, both roots λ_1 and λ_2 must be negative.

Using the first set of initial conditions (case a)

$$t = 0, \quad \sigma = \sigma_1, \quad \epsilon'' = \epsilon''' = 0 \quad [69]$$

the constants of integration are found equal to

$$A = \frac{\sigma_1}{2} \left[1 - \frac{\left(\lambda_0 - \frac{1}{t_s} \right)}{\lambda} \right], \quad B = \frac{\sigma_1}{2} \left[1 + \frac{\left(\lambda_0 - \frac{1}{t_s} \right)}{\lambda} \right] \quad [70]$$

Substitution in Equation [67] gives for the relaxation of stress with time

$$\sigma = \sigma_1 e^{-\lambda t} \left[\cosh \lambda t - \frac{\left(\lambda_0 - \frac{1}{t_r} \right)}{\lambda} \sinh \lambda t \right] \dots [71]$$

When using the second set of initial conditions (case b)

$$t = 0, \sigma = \sigma_1, \epsilon''' = \frac{\sigma_1}{E_s} \dots [72]$$

the constants of integration are found equal to

$$A = \frac{\sigma_1}{2} \left[1 - \frac{\left(\lambda_0 - \frac{1}{T} \right)}{\lambda} \right], B = \frac{\sigma_1}{2} \left[1 + \frac{\left(\lambda_0 - \frac{1}{T} \right)}{\lambda} \right] \dots [73]$$

leading to

$$\sigma = \sigma_1 e^{-\lambda t} \left[\cosh \lambda t - \frac{\left(\lambda_0 - \frac{1}{T} \right)}{\lambda} \sinh \lambda t \right] \dots [74]$$

The initial rate of decrease of stress $d\sigma/dt$ when $t = 0$ may be computed as follows: For the first set of initial conditions, (case a) at $t = 0$, $\sigma'' = E\epsilon''' = 0$, $\sigma''' = \sigma_1 = 3\mu_s(d\epsilon'''/dt)$, from Equation [63] for $t = 0$

$$\text{Case a} \dots \frac{d\sigma}{dt} = -\sigma_1 \left(\frac{1}{t_r} + \frac{1}{t_s} \right) \dots [75]$$

For the second set of initial conditions (case b), at $t = 0$, $\sigma'' = 0$, $(d\epsilon''')/(dt) = 0$, $\sigma' = \sigma_1 = E_s\epsilon'''$, the initial rate of decrease of stress is found equal to

$$\text{Case b} \dots \frac{d\sigma}{dt} = -\frac{\sigma_1}{t_r} \dots [76]$$

For comparison, the elastico-viscous substance not exhibiting recovery strains relaxes according to

$$\frac{d\sigma}{dt} + \frac{\sigma}{t_r} = 0 \dots [77]$$

$$\sigma = \sigma_1 e^{-\frac{t}{t_r}} \dots [78]$$

under the initial rate

$$(t = 0) \quad \frac{d\sigma}{dt} = -\frac{\sigma_1}{t_r}$$

This rate is the same as in case b. However, the stress σ in case a decreases at a much faster rate when t_r and t_s are of the same order of magnitude or when t_r is smaller than t_s . We note that if a specimen has not had time to recover from the disturbance caused through a sudden application of its load, the recovery strains ϵ''' will exert a strong influence on the initial decrease of stress in a relaxation test, causing the load to drop faster than in the corresponding type of substance not having recovery properties.

Furthermore, at large values of the time t , since $|\lambda_1| > |\lambda_2|$, after considerable time has elapsed, the second term containing the integration constant B in Equation [67] decreases much

faster than the term containing A , when t approaches ∞ the stress varies as

$$\sigma = A e^{\lambda_1 t} \dots [79]$$

This function in case a overtakes after some time the function expressed by Equation [78] because

$$|\lambda_1| < \frac{1}{t_r}$$

as one easily verifies in spite of the originally faster rates $d\sigma/dt$ of Equation [71]. Thus the stress σ in a relaxation test of a substance, in which also the recovery strains ϵ''' are active, finally decreases at slower rates and under higher stresses than in an elastico-viscous material. This is illustrated by the following three numerical examples of exponential curves toward which the relaxing stress σ asymptotically converges at large values of the time t

$$\begin{array}{lll} \frac{E_s}{E} = \frac{1}{3}, \frac{\mu}{\mu_s} = \frac{3}{2}, \sigma = 0.122\sigma_1 e^{-0.177 \frac{t}{t_r}} \\ 1, 1, \sigma = 0.277\sigma_1 e^{-0.382 \frac{t}{t_r}} \\ 3, \frac{1}{2}, \sigma = 0.500\sigma_1 e^{-0.634 \frac{t}{t_r}} \end{array}$$

Elastico-viscous substance

$$\sigma = \sigma_1 e^{-\frac{t}{t_r}}$$

This last example is perhaps at least qualitatively indicative of what might be expected in reference to the influence of the recovery strains on relaxation in metals.

In order to generalize further the assumptions on which Equation [65] was based, one may include in the equation of the stress surface two more terms to express also strain-hardening and softening with time in the substance. This would define the most general case of flow based on a linear equation of state

$$\sigma = \psi \epsilon'' + \phi \frac{d\epsilon''}{dt} + \chi t \dots [80]$$

Combining this last equation with the condition of relaxation

$$\sigma = \sigma_1 - E(\epsilon'' + \epsilon''') \dots [81]$$

the condition of recovery

$$\sigma = E_s \epsilon''' + \phi_s \frac{d\epsilon'''}{dt} \dots [82]$$

and the equation obtained by differentiating Equation [81] with respect to the time t

$$\frac{d\sigma}{dt} = -E \left(\frac{d\epsilon''}{dt} + \frac{d\epsilon'''}{dt} \right) \dots [83]$$

one obtains four linear, nonhomogeneous equations for the quantities ϵ'' , ϵ''' , $(d\epsilon''/dt)$, $(d\epsilon'''/dt)$ from which one may compute, for example

$$\epsilon'' = \frac{D_1}{D} \frac{d\epsilon''}{dt} = \frac{D_2}{D} \dots [84]$$

in terms of σ and $(d\sigma)/(dt)$. D_1 , D_2 , and D denote the determinants

$$D_1 = \begin{vmatrix} \sigma_1 - \sigma & E & 0 & 0 \\ \sigma - \chi t & 0 & \phi & 0 \\ \sigma & E_s & 0 & \phi_s \\ -\frac{d\sigma}{dt} & 0 & E & E \end{vmatrix}, \quad D_2 = \begin{vmatrix} E & E & \sigma_1 - \sigma & 0 \\ \psi & 0 & \sigma - \chi t & 0 \\ 0 & E_s & \sigma & \phi_s \\ 0 & 0 & -\frac{d\sigma}{dt} & E \end{vmatrix}, \quad D = \begin{vmatrix} E & E & 0 & 0 \\ \psi & 0 & \phi & 0 \\ 0 & E_s & 0 & \phi_s \\ 0 & 0 & E & E \end{vmatrix} \dots [85]$$

Differentiating $\epsilon'' = D_1/D$ with respect to the time and equating this to $d\epsilon''/dt = D_2/D$ leads to the second-order linear equation for the stress σ

$$t_s t_s \frac{d\sigma^2}{dt^2} + \left[\left(1 + \frac{E}{E_s} \right) t_s + \left(1 + \frac{\psi}{E} \right) t_s \right] \frac{d\sigma}{dt} + \left[1 + \left(1 + \frac{E}{E_s} \right) \frac{\psi}{E} \right] \sigma = \frac{\psi \sigma_1}{E} + \chi \left(\frac{\phi_s}{E_s} + t \right) \dots [86]$$

This equation governs the relaxation of stress in the case of flow

with recovery strains corresponding to the most general equation of state, Equation [80], of linear form covering the phenomena of viscosity, of strain-hardening, and of softening with time. Equation [65] appears as the special case of Equation [86] when $\psi = \chi = 0$.

CONCLUSION

Analytical expressions were derived for describing the influence of strain-hardening, of the time rate of change of the flow resistance, and of recovery strains on the creep and relaxation of metals under uniaxial stress.



Automatic Flight Control—Analysis and Synthesis of Lateral-Control Problem

By R. N. BRETOI,¹ MINNEAPOLIS, MINN.

The author presents a method which is useful in the analysis and synthesis of the aircraft lateral-control problem. Consideration is given to establishing autopilot requirements necessary to accomplish fast, stable, and co-ordinated (zero sideslip) response. Charts are derived whereby responses of the controlled variables are plotted as a function of dimensionless time for systems represented by a second-order (e.g., simplified roll or simplified one-degree-of-freedom-yaw response), or by a third-order (e.g., simplified-co-ordinated directional control) linear-differential equation. Included is the derivation of a method for establishing autopilot requirements necessary for dynamic and steady-state co-ordination. The use of the analog computer in aiding the analysis and the effects of control lags are discussed briefly. Comparisons are made between aircraft responses calculated by means of the simplified equations, aircraft responses obtained from simulated flight recordings on the analog computer, and aircraft responses recorded during flight tests.

NOMENCLATURE

The following nomenclature is used in the paper:

- β = sideslip angle, positive for slip toward starboard, radians
 δ_a = differential aileron deflection (unless otherwise noted), right aileron down positive, radians
 δ_r = rudder deflection, left rudder positive, radians
 ϵ = turn-control signal, right turn positive, radians
 ζ = damping ratio; also a parameter in third-order equation
 θ = pitch attitude, nose up positive, radians
 $\varphi = \int p dt$, right roll positive, radians
 $\psi = \int r dt$, nose right positive, radians
 ω_n = undamped natural frequency for second-order system; also parameter in third-order equation, radians per sec
 A_2 = directional stiffness parameter appearing in third-order heading equation
 A_2/ω_n^2 = dimensionless directional stiffness parameter appearing in dimensionless third-order heading equation
 g = gravitational constant, f/psps
 I_{xx}, I_{yy} = moments of inertia about roll and yaw axes, respectively, slug sq ft
 I_{zz} = product of inertia about pitch axis, slug sq ft

¹ Research Engineer, Aeronautical Division, Minneapolis-Honeywell Regulator Company.

Contributed by the Industrial Instruments and Regulators Division of THE AMERICAN SOCIETY OF MECHANICAL ENGINEERS and presented at the Instrument Society of America—Instruments and Regulators Division Conference, Houston, Texas, September 10-14, 1951.

NOTE: Statements and opinions advanced in papers are to be understood as individual expressions of their authors and not those of the Society. Manuscript received at ASME Headquarters, April 25, 1951. Paper No. 51-11RD-1.

K = constant of proportionality in second-order roll equation

$$= \frac{-L_{\delta a} f_{\varphi}}{-L_{\delta a} f_{\varphi} - L_{\varphi}(g/U)} \approx 1$$

L = rolling moment per unit roll moment of inertia, sec^{-2}

$$L_{\varphi}, L_p, L_{\dot{r}} = \frac{\partial L}{\partial \varphi}, \frac{\partial L}{\partial p}, \frac{\partial L}{\partial \dot{r}}, \text{ etc.}$$

N = yawing moment per unit yaw moment of inertia, sec^{-2}

$$N_{\varphi}, N_p, N_{\dot{r}} = \frac{\partial N}{\partial \varphi}, \frac{\partial N}{\partial p}, \frac{\partial N}{\partial \dot{r}}, \text{ etc.}$$

p = perturbation roll angular velocity

r = perturbation yaw angular velocity

s = differential operator, sec^{-1}

z = dimensionless operator = $\frac{s}{\omega_n}$

t = time, sec

l = dimensionless time = $\omega_n t$, normalized seconds (norse)

U_1 = steady-state forward velocity, ft/sec⁻¹

v = perturbation sideslip velocity, ft/sec⁻¹

W_1 = steady-state normal velocity, ft/sec⁻¹

Y = lateral force per unit mass of aircraft, sec^{-2}

$$Y_{\varphi}, Y_p, Y_{\dot{r}} = \frac{\partial Y}{\partial \varphi}, \frac{\partial Y}{\partial p}, \frac{\partial Y}{\partial \dot{r}}, \text{ etc.}$$

$$f_{\varphi} = \frac{\partial \delta_a}{\partial \varphi}$$

$$f_{\dot{\varphi}} = \frac{\partial \delta_a}{\partial \dot{\varphi}}$$

$$f_{\psi} = \frac{\partial \delta_r}{\partial \psi}$$

$$f_{\dot{\psi}} = \frac{\partial \delta_r}{\partial \dot{\psi}}$$

$$f_{\dot{r}} = \frac{\partial \delta_a}{\partial \dot{r}}$$

$$f_{\dot{\varphi}} = \frac{\partial \delta_r}{\partial \dot{\varphi}}$$

$$f_{\dot{\psi}} = \frac{\partial \delta_a}{\partial \dot{\psi}}$$

$$f_{\dot{r}} = \frac{\partial \delta_r}{\partial \dot{r}}$$

$$f_{\dot{\varphi}} = \frac{\partial \delta_a}{\partial \dot{\varphi}}$$

$$f_{\dot{\psi}} = \frac{\partial \delta_r}{\partial \dot{\psi}}$$

$$f_{\dot{r}} = \frac{\partial \delta_a}{\partial \dot{r}}$$

$$f_{\dot{\varphi}} = \frac{\partial \delta_r}{\partial \dot{\varphi}}$$

$$F_{\varphi} = \frac{f_{\varphi}}{f_{\dot{\varphi}}}$$

Axis	x	y	z
Designation	Roll	Pitch	Yaw
Angular velocity	$P_1 + p$	$Q_1 + q$	$R_1 + r$
Linear velocity	$U_1 + u$	$V_1 + v$	$W_1 + w$
Moment per unit Moment of inertia	L	M	N

(With stability axes $W_1 = 0$.)

NOTE: The parameters $f_{\varphi}, f_{\dot{\varphi}}, f_{\psi}, f_{\dot{\psi}}$ act on φ and ψ directly as distinguished from $(\varphi_1 - \varphi)$ and $(\psi_1 - \psi)$, the roll and yaw errors.

INTRODUCTION

During recent years tremendous progress has been made in the advancement of aircraft speed, range, capacity, and handling qualities. As one result, autopilot functional and performance requirements have increased greatly. This has put a premium on obtaining a better understanding of the dynamics of the airplane-autopilot system.

Analysis of the dynamic behavior of the aircraft is as old as the aircraft itself. The basic equations of motion presented by Bryan¹ in 1911, are still being used. Subsequent work between 1911 and World War II was directed primarily toward the calculation of the motion of the free airplane, toward the development of dimensionless stability charts and criteria, and toward the evaluation of the aerodynamic stability derivatives. Most of this work entailed the use of theoretical calculations and the development of techniques for testing wind-tunnel models; a relatively small amount was directed toward obtaining data from a completely instrumented aircraft in flight or toward the analysis of the automatically controlled aircraft.

After 1940, German, British, and American engineers directed an increasing portion of their efforts toward the analysis of the motion of the automatically controlled aircraft, probably more from necessity than for abstract reasons. In this country a substantial part of the analytical work was conducted by NACA and the guided-missile manufacturers.

In developing higher performance automatic flight-control equipment the autopilot manufacturer has found, in the last few years, that available automatic aircraft-control design techniques were inadequate. In addition, the background of flight data was neither sufficiently adequate for determining whether the equations of motion presented by Bryan in 1911, accurately described the dynamics of the airplane, nor was it apparent to what degree of accuracy the stability derivatives could be determined.

A method for obtaining quantitative stability and control information for an aircraft by flight-test methods was suggested by O. Johnston and R. Kutzler in 1944;² the use of a precision autopilot as part of the instrumentation was recommended. Subsequent work directed by W. F. Milliken at Cornell Aeronautical Laboratory, did make use of an autopilot in obtaining recorded aircraft responses from which the aerodynamic stability derivatives could be checked for accuracy or even modified to match the calculated and experimental response data more closely.³

In 1948 the Aero Research group of the author's company directed its efforts toward attaining a better correlation of predicted and measured aircraft control. Since some concern was expressed of the ability to calculate aircraft motions, the initial phase of the program was directed toward establishing the relationship between calculated aircraft responses and those obtained from flight test.

Initial research work was conducted with a DC-3 type aircraft. Necessary coefficients and derivatives were obtained from the manufacturer (Douglas), and the equations of motion were solved for aircraft responses to sinusoidal control-surface motions. In flight the control surfaces were forced to oscillate sinusoidally at each of a number of forcing frequencies corresponding to periods ranging from about 0.5 sec to about 150 sec; recordings were made of resultant motions. Correlation between calculated fre-

quency responses and flight-test results appeared quite satisfactory and gave confidence that the aircraft itself could be expected to behave in accordance with theory, see Figs. 15(a) and (b). Hence the aircraft equations of motion were supplemented to include automatic control of surface positions and analyzed further to determine autopilot requirements to give desired over-all performance.⁴

The methods described in the next section were first used in the application of an experimental autopilot to an R4D (DC-3) type aircraft on a project involving automatic approach, landing, and cruise control. Its resulting performance in automatic flight showed close agreement with predictions, and bolstered faith in the analytical approach. Since then this approach has been used on several Air Force and Navy aircraft with gratifying effectiveness.

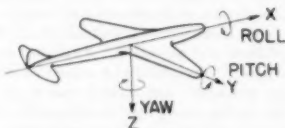


FIG. 1 AXIS SYSTEM

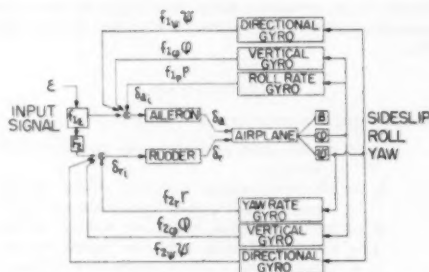


FIG. 2 SIMPLIFIED BLOCK DIAGRAM OF BASIC AUTOPILOT

War-time and subsequent experience—together with that just mentioned—certainly indicates that in order to meet present-day flight-control performance requirements it is necessary to analyze each aircraft design separately to allow "tailoring" the autopilot and aircraft to each other. The advantages of an analytical approach to this tailoring process are as follows:

- 1 Autopilot requirements can be established before the aircraft is ready for delivery.
- 2 A completed autopilot design can be made available for the early testing of the aircraft.
- 3 The number of flight-test hours can be greatly reduced by using precomputed settings. Because of the cost of keeping a newly designed aircraft flying, a substantial saving in cost and time is realized.
- 4 System malfunctions can be detected more easily since effects are produced which are at variance with the calculated results.
- 5 Greater safety for flight-test personnel is assured since con-

¹ "Stability in Aviation," by G. H. Bryan, The Macmillan Company, London, England, 1911.

² "The Use of a Precision Automatic Pilot in Recording Aircraft Performance Data," by R. Kutzler and O. Johnston, *Aeronautical Engineering Review*, vol. 4, March, 1945, pp. 17, 19, 21, 23, 25-27, 29, 31-32, 35, and 37.

³ "Progress in Dynamic Stability and Control Research," by W. F. Milliken, Jr., *Journal of the Aeronautical Sciences*, vol. 14, 1947, pp. 493-519.

⁴ During the various phases of this work computing facilities were used at the Reeves Instrument Corporation (courtesy Special Devices Center, ONR), Office of Air Research (Air Force), and the University of Minnesota.

roll-system adjustments can be kept within the predicted limits of safe operation. The adjustment and calibration of the autopilot on the ground and the following of a definite flight plan also make important contributions to safety in flight.

6 Near optimum performance can be achieved, and system limitations can be anticipated.

7 The capability of the autopilot in controlling the airplane under any critical modes of flight can be established.

8 From a psychological viewpoint, flight personnel have greater confidence in a program if performance characteristics have already been calculated.

9 The necessary close co-operation between the airframe manufacturer and the autopilot manufacturer facilitates the handling of many installation and service problems.

With these advantages in mind, considerable time and effort have been directed toward development of practical techniques for establishing autopilot requirements. Application of these techniques results in airplane-autopilot systems capable of stable, fast, and co-ordinated performance throughout the range of operating conditions encountered.

METHOD OF ANALYSIS

Performance Requirements. System performance requirements are dictated by the type of mission which the aircraft must accomplish. For example, performance requirements for a relief autopilot (cross-country flying) are relatively low compared to performance requirements for an autopilot used during combat or during an automatic landing. From a consideration of the aircraft's mission, an indication of desired aircraft responses to step input signals to the autopilot can be obtained. The requirements may be spelled out in the form of damping ratio or its equivalent and a time to reach a steady-state condition.

Hence, in using the methods described in this paper, it is assumed that desired system damping characteristics and desired system response times have been selected on the basis of the aircraft type and its mission.

If these desired response characteristics are known then the basic autopilot feedback parameters can be determined by using the relationships derived in the sections which follow.

Outline of Analysis. The lateral control analysis is divided into two phases. During the first phase, the autopilot feedback parameters are calculated using the assumptions and procedures to be outlined. During the second phase of the analysis the analog computer is used to obtain simulated flight recordings of the response of the aircraft to step roll (turn control) or heading input signals. The use of the analog computer and the assumptions made for this second phase of the analysis are discussed in the next section.

The assumptions made are as follows:

1 Aircraft motions are represented by linearized differential equations; this means that variations of motions from steady-state values are small.

2 The lateral equations of motion (roll, yaw, and sideslip) are separable from the longitudinal equations of motion (motions in the plane of symmetry of the aircraft).

3 Effects of structure dynamics are negligible (i.e., the equations of motion for the rigid airplane structure are applicable).

4 Nonlinearities in the control system are negligible.

Derivation of Second- and Third-Order Charts. In the preliminary analysis the aircraft is assumed to be in level flight and perfectly co-ordinated (zero sideslip). By initially assuming perfect co-ordination and no control-system lags, the equations of motion are simplified to the point where some of the basic autopilot feedback parameters are readily determined. The remaining

feedback parameters are then adjusted to fulfill requirements for dynamic and steady-state co-ordination. Effects of a first-order control-system lag will be considered later.

The aircraft lateral equations of motion are as follows:

Sideslip

$$[s - Y_\beta]r + [-W_\beta - Y_\beta]p - g \cos \theta_1 s^{-1}p + [U_1 - Y_\beta]r - g \sin \theta_1 s^{-1}r = Y_{\beta\delta} \delta_a + Y_{\beta\delta_r} \delta_r \dots [1a]$$

Roll

$$-L_\beta r + [s - L_\beta]p + \left[-\frac{I_{xx}}{I_y} s - L_r \right] r = L_{\beta\delta} \delta_a + L_{\beta\delta_r} \delta_r \dots [1b]$$

Yaw

$$-N_\beta r + \left[-\frac{I_{xx}}{I_z} s - N_r \right] p + [s - N_r] r = N_{\beta\delta} \delta_a + N_{\beta\delta_r} \delta_r \dots [1c]$$

Assume for the time being that control lags are negligible, then the generalized control-system equations are written (sideslip feedbacks are not considered)

$$\delta_a = f_{1\phi} \phi + f_{1\psi} \psi + f_{1p} p + f_{1r} r + f_{1\epsilon} \epsilon \dots [2a]$$

$$\delta_r = f_{2\phi} \phi + f_{2\psi} \psi + f_{2p} p + f_{2r} r + f_{2\epsilon} \epsilon \dots [2b]$$

Where $f_{1\phi}, f_{1\psi}, f_{1p}, \dots$ are constants. The quantity ϵ is an arbitrary input signal. If directional feedback is not present, ϵ may be considered to be a roll-input signal. If directional feedback is present, ϵ may be considered to be a heading-input signal ψ_c .

During the initial portion of the analysis, sideslip and product of inertia I_{xz} are assumed to be negligible. As a result, the lateral equations of motion simplify to

$$(s^2 - L_{\beta\beta})\phi - L_{\beta r} r = L_{\beta\delta} \delta_a \dots [3a]$$

$$r = s\psi = \frac{g}{U_1} \phi \dots [3b]$$

The simplified control-system equation is then written

$$\delta_a = (f_{1\phi} + f_{1r}s)\phi + f_{1\psi}\psi \dots [4]$$

Combining Equation [3] and Equation [4]

$$\left[s^2 + (-L_{\beta\beta} - L_{\beta\delta} f_{1\phi})s + (-L_{\beta\delta} f_{1\phi} - L_r \frac{g}{U_1}) \right] \phi = 0 \dots [5a]$$

$$\left[s^2 + (-L_{\beta\beta} - L_{\beta\delta} f_{1\phi})s^2 + (-L_{\beta\delta} f_{1\phi} - L_r \frac{g}{U_1}) s + \frac{g}{U_1} (-L_{\beta\delta} f_{1\psi}) \right] \psi = 0 \dots [5b]$$

In Equation [5a] directional feedback is zero.

If a turn control (roll input) signal is used, the roll equation is written

$$\left[s^2 + (-L_{\beta\beta} - L_{\beta\delta} f_{1\phi})s + (-L_{\beta\delta} f_{1\phi} - L_r \frac{g}{U_1}) \right] \phi = -L_{\beta\delta} f_{1\phi} \phi_c \dots [6]$$

If a directional input signal is used, the yaw equation is written

$$\left[s^2 + (-L_p - L_{\dot{\delta}p})s^2 + \left(-L_{\dot{\delta}p}f_{\dot{\delta}p} - L_r \frac{g}{U_1} \right) s + \frac{g}{U_1} (-L_{\dot{\delta}p}f_{\dot{\delta}p}) \psi = \frac{g}{U_1} (-L_{\dot{\delta}p}f_{\dot{\delta}p}) \psi_i \dots [7] \right]$$

Equations [6] and [7] are of the general form

$$[s^2 + 2\zeta\omega_n s + \omega_n^2] \varphi = K\omega_n^2 \varphi_i \dots [8a]$$

$$[s^2 + 2\zeta\omega_n s + \omega_n^2 + A_2] \psi = A_1 \psi_i \dots [8b]$$

where

ω_n = undamped natural frequency of second-order roll equation, radian per sec

ζ = damping ratio (ratio of actual damping to that necessary for critical damping; if $\zeta < 1$ some overshoot exists)

$$K = \frac{-L_{\dot{\delta}p}f_{\dot{\delta}p}}{-L_{\dot{\delta}p}f_{\dot{\delta}p} - L_r g/U_1} \approx 1$$

For convenience the coefficients in Equations [8] are tabulated

$$\left. \begin{aligned} \omega_n^2 &= \left(-L_{\dot{\delta}p}f_{\dot{\delta}p} - L_r \frac{g}{U_1} \right) \\ \zeta &= \frac{1}{2} \left(\frac{-L_p - L_{\dot{\delta}p}f_{\dot{\delta}p}}{\omega_n} \right) \\ K &= \frac{-L_{\dot{\delta}p}f_{\dot{\delta}p}}{\omega_n^2} \\ A_2 &= \frac{g}{U_1} (-L_{\dot{\delta}p}f_{\dot{\delta}p}) \end{aligned} \right\} [9]$$

Now it would be convenient to reduce Equations [8] to a dimensionless form. Select a dimensionless time, $t = \omega_n t$; then

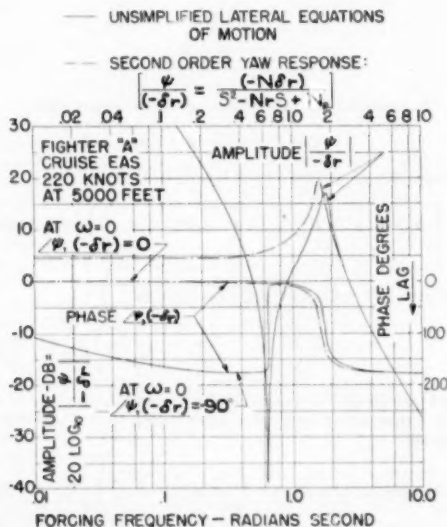


FIG. 3(a) COMPARISON OF SECOND-ORDER YAW RESPONSE TO RUDDER WITH RESPONSE OBTAINED BY USING UNIMPLIFIED LATERAL EQUATIONS OF MOTION

$$\begin{aligned} \frac{d\psi}{dt} &= \omega_n \frac{d\psi}{dt} \\ \frac{d^2\psi}{dt^2} &= \omega_n^2 \frac{d^2\psi}{dt^2} \\ \frac{d^3\psi}{dt^3} &= \omega_n^3 \frac{d^3\psi}{dt^3} \end{aligned}$$

— SECOND ORDER RESPONSE
— UNIMPLIFIED RESPONSE

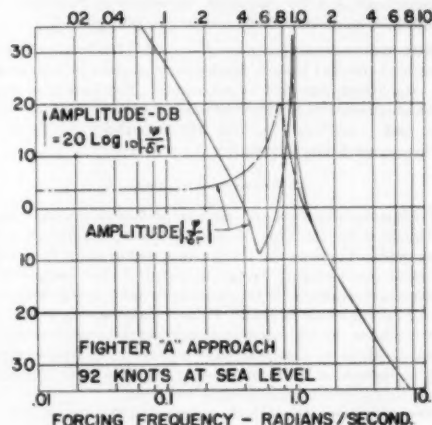


FIG. 3(b) COMPARISON OF SECOND-ORDER YAW RESPONSE TO RUDDER WITH RESPONSE OBTAINED BY USING UNIMPLIFIED LATERAL EQUATIONS OF MOTION

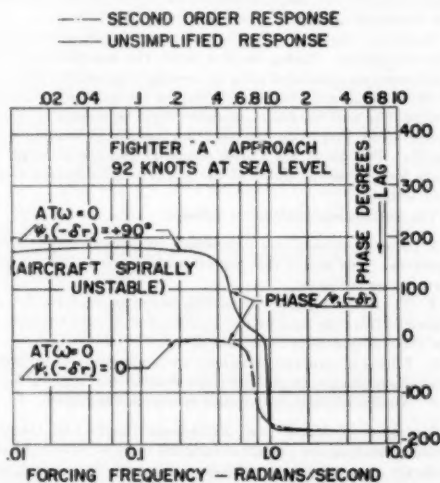


FIG. 3(c) COMPARISON OF SECOND-ORDER YAW RESPONSE TO RUDDER WITH RESPONSE OBTAINED BY USING UNIMPLIFIED LATERAL EQUATIONS OF MOTION

$$\begin{aligned}s\psi &= \omega_n \zeta \psi \\ s^2\psi &= \omega_n^2 \zeta s\psi \\ s^3\psi &= \omega_n^2 \zeta^2 s\psi\end{aligned}$$

Similarly

$$\begin{aligned}s\varphi &= \omega_n \zeta \varphi \\ s^2\varphi &= \omega_n^2 \zeta^2 s\varphi\end{aligned}$$

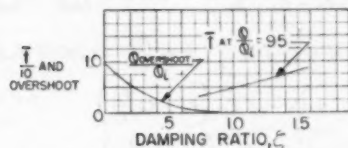
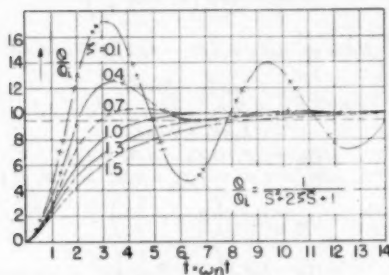


FIG. 4 SECOND-ORDER CHART—ROLL RESPONSE TO STEP-TURN CONTROL INPUT



Substituting into Equations [8]

$$(J^2 + 2\zeta^2 J + 1)\varphi = K\varphi, \dots \dots \dots [10a]$$

$$(J^2 + 2\zeta^2 J + J + A_2/\omega_n^2)\psi = A_2/\omega_n^2 \psi, \dots \dots \dots [10b]$$

Solutions for the roll equation are plotted in Fig. 4 for various values of damping ratio ζ . Solutions for the heading equation are plotted against dimensionless time in Fig. 5 for various values of heading gain factor A_2/ω_n^2 and roll damping ratio ζ . Because there are advantages in working with logarithmic expressions for amplitude data, amplitude ratios are expressed in decibels where $A_{db} = 20 \log_{10} A$. To convert to real time, $t = l/\omega_n$.

It may be well at this time to point out the significance of the various parameters appearing in Equations [10]. The roll-damping ratio ζ determines the roll-damping characteristics of the air-

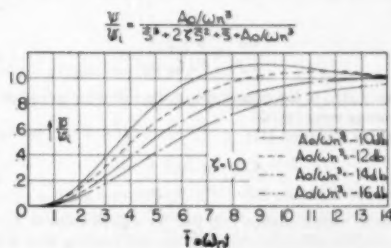


FIG. 5(c) THIRD-ORDER CHART—DIRECTIONAL RESPONSE TO STEP HEADING INPUT

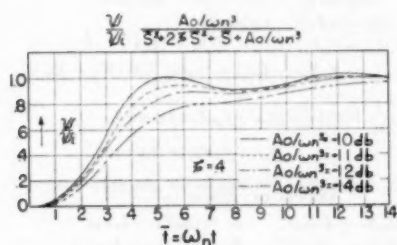


FIG. 5(b) THIRD-ORDER CHART—DIRECTIONAL RESPONSE TO STEP HEADING INPUT

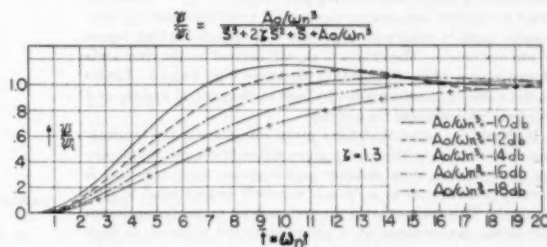


FIG. 5(d) THIRD-ORDER CHART—DIRECTIONAL RESPONSE TO STEP HEADING INPUT

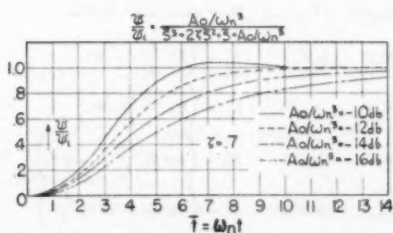


FIG. 5(b) THIRD-ORDER CHART—DIRECTIONAL RESPONSE TO STEP HEADING INPUT

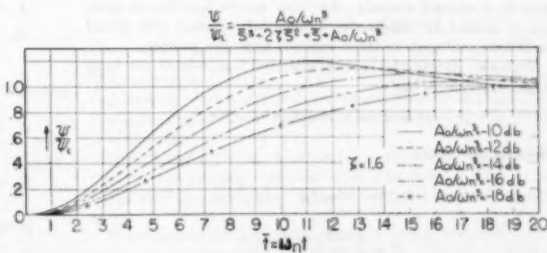


FIG. 5(e) THIRD-ORDER CHART—DIRECTIONAL RESPONSE TO STEP HEADING INPUT

craft. When directional feedback is zero, the amount of overshoot is a function of the roll-damping ratio only (for these simplified equations).

The undamped natural frequency in roll is a measure of roll stiffness. A change in ω_n , while holding the heading-gain factor A_0/ω_n^3 and the roll-damping ratio ζ constant, has the effect of shortening or elongating the time scale.

The heading-gain factor A_0/ω_n^3 is a measure of directional stiffness. Increasing this factor beyond a certain point may result in overshoot or instability. By Routh's criteria, stability exists if $A_0/\omega_n^3 < 2\zeta$.

From the definition of A_0 and ω_n , it follows that

$$\frac{A_0}{\omega_n^3} = \frac{-(g/U_1 L_{\delta\delta} f_{\psi})}{\omega_n (-L_{\delta\delta} f_{\psi} - I_x g/U_1)}$$

Normally, $I_x (g/U_1)$ is much less than $L_{\delta\delta} f_{\psi}$. Then, approximately

$$\frac{A_0}{\omega_n^3} \approx \frac{g f_{\psi}}{U_1 f_{\psi} \omega_n} \quad [11]$$

The ratio f_{ψ}/f_{ψ} is the magnitude of the called-for roll angle per unit heading error $|\varphi_r/\psi|$.

Rewriting Equation [11]

$$\frac{A_0}{\omega_n^3} \approx \frac{g}{U_1} \left| \frac{\varphi_r}{\psi} \right| \frac{1}{\omega_n} \quad [12]$$

It is evident from Equation [12] that for a given value of A_0/ω_n^3 , the permissible called-for roll angle per unit heading error is proportional to the true airspeed and undamped natural frequency in roll.

Since l equals $\omega_n t$, speed of response to a step input signal is proportional to undamped natural frequency in roll ω_n (for a given roll damping ratio ζ and heading-gain factor A_0/ω_n^3). Hence, in order to achieve fast, stable response, ω_n (and therefore f_{ψ}) necessarily must be relatively large (this corresponds to a high degree of roll stiffness). The choice of ω_n will depend on the time scale chosen from a study of the curves plotted in Figs. 4 and 5. Limits on the value of f_{ψ} are imposed by lags in the control system and physical limitations of the aircraft.

It should be noted that for a given roll stiffness the heading-gain factor A_0/ω_n^3 (which for a given roll stiffness and roll damping determines system stability and response characteristics) is directly proportional to $|\varphi_r/\psi|$ and inversely proportional to true airspeed. This means that if the system is set up to give optimum directional performance at a given indicated airspeed at high altitude (which means relatively high true airspeed), then for the same indicated airspeed at low altitude (relatively low true airspeed) overshoot or possibly instability is likely to occur.

The solutions plotted in Figs. 4 and 5 are not restricted to the analysis of aircraft motions; they also may be used for the solution of second or third-order differential equation with initial conditions analogous to those imposed upon the aircraft.

Example. Recall the second-order roll equation of the form (neglecting control lags)

$$(s^2 + 2\zeta\omega_n s + \omega_n^2)\varphi \approx \omega_n^2 \varphi_r$$

where for roll control

$$\omega_n^2 = -L_{\delta\delta} f_{\psi} - I_x \frac{g}{U_1}$$

$$\zeta = \frac{1}{2} \frac{-L_{\delta\delta} f_{\psi}}{\omega_n}$$

Now, ω_n and ζ depend upon the aerodynamic characteristics of

TABLE 1(a) SIDESLIP RESPONSE COEFFICIENTS WITH CONTROL FEEDBACKS BUT NEGLECTING CONTROL-SYSTEM LAGS

$$\beta = \frac{C_{\delta\delta\delta} + C_{\delta\delta\delta} + C_{\delta\delta\delta} + C_{\delta\delta} + C_{-1\delta\delta}^{-1}}{\Delta}$$

$$\frac{1}{f_{\psi}} U_1 C_{\delta\delta} = Y_{\delta\delta} \left(1 - \frac{I_{xx}}{I_x I_z} \right) + F_x Y_{\delta\delta} \left(1 - \frac{I_{xz}}{I_x I_z} \right)$$

$$\frac{1}{f_{\psi}} U_1 C_{\delta\delta} = -B_2 + C_4 + B_1 \frac{I_{xx}}{I_x} - C_2 \frac{I_{xz}}{I_x} - L_{\delta\delta} E_1 - N_{\delta\delta} E_2$$

$$+ F_x \left(-B_2 + C_4 + B_1 \frac{I_{xx}}{I_x} - C_2 \frac{I_{xz}}{I_x} - L_{\delta\delta} E_1 - N_{\delta\delta} E_2 \right)$$

$$+ (f_{\delta\delta} - f_{\delta\delta} F_x) \left(B_2 + C_4 \frac{I_{xx}}{I_x} \right)$$

$$+ (f_{\delta\delta} - f_{\delta\delta} F_x) \left(C_4 + B_1 \frac{I_{xx}}{I_x} \right)$$

$$\frac{1}{f_{\psi}} U_1 C_{\delta\delta} = -L_{\delta\delta} C_4 + N_{\delta\delta} B_1 - A_{\delta}(Y_{\delta} + W_1) + A_2 U_1$$

$$+ L_{\delta\delta} g E_1 + N_{\delta\delta} g E_2$$

$$+ F_x [-L_{\delta\delta} C_4 + N_{\delta\delta} B_1 - A_{\delta}(Y_{\delta} + W_1) + A_2 U_1$$

$$+ L_{\delta\delta} g E_1 + N_{\delta\delta} g E_2]$$

$$+ (f_{\delta\delta} - f_{\delta\delta} F_x) [L_{\delta\delta} C_4 - N_{\delta\delta} B_1 - A_{\delta}(U_1 - Y_r)]$$

$$+ (f_{\delta\delta} - f_{\delta\delta} F_x) [-L_{\delta\delta} C_4 + N_{\delta\delta} B_1 - A_{\delta}(W_1 + Y_{\delta})]$$

$$+ (f_{\delta\delta} - f_{\delta\delta} F_x) \left(B_2 + C_4 \frac{I_{xx}}{I_x} \right)$$

$$+ (f_{\delta\delta} - f_{\delta\delta} F_x) \left(C_4 + B_1 \frac{I_{xx}}{I_x} \right)$$

$$\frac{1}{f_{\psi}} U_1 C_{\delta\delta} = -A_{\delta\delta} \cos \theta_1 - A_{\delta\delta} \sin \theta_1 + F_x (-A_{\delta\delta} \cos \theta_1$$

$$- A_{\delta\delta} \sin \theta_1) + (f_{\delta\delta} - f_{\delta\delta} F_x) (A_{\delta\delta} \sin \theta_1)$$

$$(f_{\delta\delta} - f_{\delta\delta} F_x) (-A_{\delta\delta} \cos \theta_1)$$

$$(f_{\delta\delta} - f_{\delta\delta} F_x) [L_{\delta\delta} C_4 - N_{\delta\delta} B_1 - A_{\delta}(U_1 - Y_r)]$$

$$(f_{\delta\delta} - f_{\delta\delta} F_x) [-L_{\delta\delta} C_4 + N_{\delta\delta} B_1 - A_{\delta}(W_1 + Y_{\delta})]$$

$$\frac{1}{f_{\psi}} U_1 C_{-1\delta} = (f_{\delta\delta} - f_{\delta\delta} F_x) (A_{\delta\delta} \sin \theta_1)$$

$$(f_{\delta\delta} - f_{\delta\delta} F_x) (-A_{\delta\delta} \cos \theta_1)$$

TABLE 1(b) EXPANSION OF TERMS IN SIDESLIP COEFFICIENTS OF TABLE 1(a)

$$A_1 = (L_{\delta\delta} N_r - L_{\delta\delta} N_p) \quad B_1 = (L_{\delta\delta} Y_r - L_{\delta\delta} Y_p)$$

$$A_2 = (L_{\delta\delta} N_{\delta\delta} - L_{\delta\delta} N_{\delta\delta}) \quad B_2 = (L_{\delta\delta} Y_{\delta\delta} - L_{\delta\delta} Y_{\delta\delta})$$

$$A_3 = (L_{\delta\delta} N_{\delta r} - L_{\delta\delta} N_{\delta p}) \quad B_3 = (L_{\delta\delta} Y_{\delta r} - L_{\delta\delta} Y_{\delta p})$$

$$A_4 = (L_{\delta\delta} N_r - L_{\delta\delta} N_{\delta\delta}) \quad B_4 = (L_{\delta\delta} Y_r - L_{\delta\delta} Y_{\delta\delta})$$

$$A_5 = (L_{\delta\delta} N_r - L_{\delta\delta} N_{\delta r}) \quad B_5 = (L_{\delta\delta} Y_r - L_{\delta\delta} Y_{\delta r})$$

$$A_6 = (L_{\delta\delta} N_{\delta r} - L_{\delta\delta} N_{\delta\delta}) \quad B_6 = (L_{\delta\delta} Y_{\delta r} - L_{\delta\delta} Y_{\delta\delta})$$

$$C_1 = (N_p Y_r - N_r Y_p) \quad E_1 = \left(U_1 \frac{I_{xx}}{I_x} - W_1 \right)$$

$$C_2 = (N_p Y_{\delta\delta} - N_{\delta\delta} Y_p) \quad E_2 = \left(U_1 - \frac{I_{xz}}{I_x} W_1 \right)$$

$$C_3 = (N_p Y_{\delta r} - N_{\delta r} Y_p) \quad E_3 = \left(\cos \theta_1 \frac{I_{xz}}{I_x} + \sin \theta_1 \right)$$

$$C_4 = (N_{\delta\delta} Y_r - N_r Y_{\delta\delta}) \quad E_4 = \left(\cos \theta_1 + \sin \theta_1 \frac{I_{xz}}{I_x} \right)$$

$$C_5 = (N_{\delta r} Y_r - N_r Y_{\delta r})$$

$$C_6 = (N_{\delta\delta} Y_{\delta r} - N_{\delta r} Y_{\delta\delta})$$

the airplane and on the control-feedback parameters $f_{1\psi}$ and $f_{1\dot{\psi}}$. For a specific flight condition ζ and ω_n can be calculated if the control-feedback parameters are given. Conversely, if desired values for ω_n and ζ are known, the control-feedback parameters can be determined.

Consider now the rolling motion of fighter "A" in its approach configuration (EAS = 92 knots at SL) for which the stability coefficients appear in Table 2 (for this discussion neglect control lags).

TABLE 2 FIGHTER "A" STABILITY COEFFICIENTS

IAS	Knots	92	220
Altitude	Ft	0	5000
$Y_{1\dot{\psi}}$	ft sec ⁻²	4.3	28.0
$Y_{1\psi}$	ft sec ⁻¹	0.29	0.621
$Y_{1\dot{\psi}}$	sec ⁻¹	-0.101	-0.210
$L_{1\dot{\psi}}$	sec ⁻²	0	1.18
$L_{1\psi}$	sec ⁻¹	-1.064	-5.90
$L_{1\dot{\psi}}$	sec ⁻¹	-1.194	-2.54
$L_{1\psi}$	sec ⁻¹	0.454	0.305
$L_{1\dot{\psi}}$	ft ⁻¹ sec ⁻²	-0.0121	-0.040
$N_{1\dot{\psi}}$	sec ⁻²	-0.861	-4.5
$N_{1\psi}$	sec ⁻¹	0	0
$N_{1\dot{\psi}}$	sec ⁻¹	-0.0832	-0.0387
$N_{1\psi}$	sec ⁻¹	-0.1335	-0.286
$N_{1\dot{\psi}}$	ft ⁻¹ sec ⁻¹	0.00372	0.00675
$U_{1\dot{\psi}}$	ft sec ⁻¹	156	400
$g_{1\dot{\psi}}$	ft sec ⁻²	32.2	32.2
$\theta_{1\dot{\psi}}$		0	0
Gross weight = 19000 lb			

Assume the control parameters

$$f_{1\dot{\psi}} = 3, f_{1\psi} = 6, f_{1\dot{\psi}} = 1.5$$

$$\frac{\dot{\psi}}{\psi} = \frac{f_{1\dot{\psi}}}{f_{1\psi}} = 2$$

Substituting into Equations [9] and solving for ω_n and ζ

$$\begin{aligned}\omega_n &= \left(-L_{1\dot{\psi}} f_{1\dot{\psi}} - L_{1\psi} \frac{g}{U_1} \right)^{1/2} \\ &= 1.77 \text{ rad/sec} \\ \zeta &= \frac{-L_{1\dot{\psi}} - L_{1\psi} f_{1\dot{\psi}}}{2\omega_n} \quad (\text{roll case}) \\ &= 0.79\end{aligned}$$

Solutions corresponding to the foregoing values appear in Fig. 4 as a function of dimensionless time ($t = \omega_n t$) for various damping ratios ζ . From Fig. 4 it is found that time for roll angle to reach 95 per cent of its final value is

$$\begin{aligned}t_{95} &= 3.5 \text{ nsec} \\ t_{95} &= 1.98 \text{ sec}\end{aligned}$$

Consider now the heading response. Solving for the heading-gain factor (refer to Equation [12])

$$\frac{A_0}{\omega_n^2} = \frac{g}{U_1} \frac{\dot{\psi}}{\psi} \frac{1}{\omega_n} = 0.233 \text{ or } -12.6 \text{ db} \quad \left(\frac{A_0}{\omega_n^2} \text{ db} = 20 \log_{10} \frac{A_0}{\omega_n^2} \right)$$

We now have

$$\zeta = 0.79, \omega_n = 1.77 \text{ rad/sec}, A_0/\omega_n^2 = -12.6 \text{ db}$$

for which response to a step heading input is plotted in Fig. 5. Here it is found that time for heading to achieve 90 per cent of its final value is

$$\begin{aligned}t_{90} &= 7.1 \text{ nsec} \\ t_{90} &= 4 \text{ sec}\end{aligned}$$

Yaw-Damping Requirements. In establishing yaw-damping requirements the aircraft is considered to be constrained to pure rotation about the yaw axis. (The lateral-force equation is not considered and coupling between roll and yaw is neglected.) A study of amplitude and phase response of yaw angle to a sinusoidal rudder deflection indicates fair agreement at frequencies in the region of the natural frequency in yaw and above (for example, see Fig. 3). From experience it is found that a fairly good approximation of yaw-damping requirements is obtained in this way.

The single-degree-of-freedom-in-yaw equation is written

$$(s^2 - N_{\dot{\psi}} s + N_{\psi})\psi = N_{\dot{\psi}}\delta \dots \dots \dots [13]$$

Writing the simplified control-system equation (neglecting control lags)

$$\delta = f_{1\dot{\psi}}\dot{\psi} + f_{1\psi}\psi \dots \dots \dots [14]$$

Combining Equations [13] and [14]

$$[s^2 + (-N_{\dot{\psi}} - N_{\dot{\psi}}f_{1\dot{\psi}})s + (N_{\psi} - N_{\psi}f_{1\psi})]\psi = 0 \dots [15]$$

Equation [13] is of the form

$$(s^2 + 2\zeta\omega_n s + \omega_n^2)\psi = 0 \dots \dots \dots [16]$$

Now $f_{1\dot{\psi}}$ is dependent upon $f_{1\psi}$ ($f_{1\dot{\psi}}$ is determined from directional control requirements by methods described under "derivation of second- and third-order charts," and on requirements for dynamic co-ordination described in the section which follows this. Hence the undamped natural frequency about the yaw axis will be unavailable for adjusting yaw damping. Consequently, the one remaining variable in Equation [15] is rudder deflection per unit yaw rate $f_{1\dot{\psi}}$.

From Equations [15] and [16]

$$f_{1\dot{\psi}} = \frac{2[\zeta\omega_n - N_{\dot{\psi}}]}{-N_{\dot{\psi}}} \dots \dots \dots [17]$$

For a particular flight condition, ω_n will be determined from considerations other than yaw damping. Hence a satisfactory value of $f_{1\dot{\psi}}$ can be calculated by using Equation [17] and letting ζ be somewhere in the neighborhood of 0.7 to 1.5.

The effects of control-system lags on yaw damping are discussed briefly later.

Autopilot Requirements for Dynamic Co-Ordination. In order to establish autopilot requirements for dynamic co-ordination, it is necessary to refer to the complete lateral equations of motion, Equations [1] and the control-system equations (Equations [2]).

Combining Equations [1] and [2] and solving for sideslip response to the signal ϵ , in operational form

$$\frac{\beta}{\epsilon} = \frac{C_{1\dot{\psi}}s^2 + C_{1\psi}s^2 + C_{1\dot{\psi}}s + C_{1\psi} + C_{1\dot{\psi}}s^{-1}}{D_{1\dot{\psi}}s^2 + D_{1\psi}s^2 + D_{1\dot{\psi}}s + D_{1\psi} + D_{1\dot{\psi}}s^{-1}} \dots [18]$$

The coefficients $C_{1\dot{\psi}}, C_{1\psi}, \dots, D_{1\dot{\psi}}, D_{1\psi}$ are functions of the aircraft stability derivatives and of the control-feedback parameters. Equations describing the numerator coefficients appear in Tables 1(a) and 1(b).

Now, in order to achieve dynamic co-ordination, it is necessary that the numerator coefficients be minimized. This is accomplished through proper choice of autopilot feedback parameters.

For the case with directional feedback, steady-state sideslip response to the signal ϵ is given by $\beta/\epsilon = C_{1\dot{\psi}}/D_{1\dot{\psi}}$. Without directional feedback $\beta/\epsilon = C_{1\dot{\psi}}/D_{1\dot{\psi}}$ (when $f_{1\dot{\psi}} = f_{1\psi} = 0$, then $C_{1\dot{\psi}} = D_{1\dot{\psi}} = 0$).

TABLE 3 FIGHTER "A" SLIDESLIP-RESPONSE COEFFICIENTS

Approach EAS 92 knots at sea level

$$\begin{aligned}\frac{1}{f_{1s}} C_{1s} &= 0.027 F_s \\ \frac{1}{f_{1s}} C_{1p} &= -0.022 + 0.896 F_s - 0.029 (f_{1p} - f_{1p} F_s) \\ \frac{1}{f_{1s}} C_{1q} &= -0.334 + 1.031 F_s - 0.918 (f_{1q} - f_{1q} F_s) \\ &\quad + 0.003 (f_{1r} - f_{1r} F_s) - 0.029 (f_{1p} - f_{1p} F_s) \\ \frac{1}{f_{1s}} C_{1r} &= -0.027 - 0.081 F_s - 0.189 (f_{1r} - f_{1r} F_s) \\ &\quad - 0.918 (f_{1p} - f_{1p} F_s) + 0.003 (f_{1q} - f_{1q} F_s) \\ \frac{1}{f_{1s}} C_{-1\theta} &= -0.189 (f_{1\theta} - f_{1\theta} F_s)\end{aligned}$$

Cruise EAS 220 knots at 5000 ft

$$\begin{aligned}\frac{1}{f_{1s}} C_{1s} &= 0.070 F_s \\ \frac{1}{f_{1s}} C_{1p} &= -0.173 + 4.691 F_s - 0.413 (f_{1p} - f_{1p} F_s) \\ &\quad + 0.012 (f_{1r} - f_{1r} F_s) \\ \frac{1}{f_{1s}} C_{1q} &= -1.143 + 11.6 F_s - 26.42 (f_{1q} - f_{1q} F_s) \\ &\quad + 0.047 (f_{1r} - f_{1r} F_s) - 0.413 (f_{1p} - f_{1p} F_s) \\ &\quad + 0.012 (f_{1\theta} - f_{1\theta} F_s) \\ \frac{1}{f_{1s}} C_{1r} &= -0.131 - 0.083 F_s - 2.12 (f_{1r} - f_{1r} F_s) \\ &\quad - 26.42 (f_{1p} - f_{1p} F_s) + 0.047 (f_{1q} - f_{1q} F_s) \\ \frac{1}{f_{1s}} C_{-1\theta} &= -2.12 (f_{1\theta} - f_{1\theta} F_s)\end{aligned}$$

Once steady-state co-ordination is achieved, dynamic co-ordination is determined by the coefficients of the higher-order terms.

Example. Consider the fighter "A" approach configuration for which simplified sideslip coefficients appear in Table 4.

From previous considerations assume

$$f_{1\varphi} = 3, f_{1\psi} = 6$$

$$f_{1p} = 1.5, \text{ and assume } f_{1r} = 0$$

Examination of the simplified sideslip coefficients in Table 4 indicates that the airplane should be well co-ordinated dynamically if, with the foregoing values of $f_{1\varphi}$, f_{1p} , and $f_{1\psi}$

$$\begin{aligned}F_s &= \frac{f_{1\psi}}{f_{1\psi}} = 0.025 \text{ (assuming no control lags)} \\ f_{1p} &= -0.317 \\ f_{1q} &= -0.3 \\ f_{1r} &= 0.15\end{aligned}$$

With these values for the autopilot feedback parameters

$$\begin{aligned}C_{1s} &= 0.000675 \\ C_{1p} &= 0 \\ C_{1q} &= 0\end{aligned}$$

At this point it is possible to calculate a value for $f_{1\theta}$ from yaw-damping requirements. With $f_{1\psi} = 0.15$ and $f_{1r} = 1.75$, the yaw-damping ratio is 1.0. In this case steady-state co-ordination exists in a steady-state turn if $f_{1\theta} = -0.317$ (giving $C_{1\theta} = 0$).

TABLE 4 SIMPLIFIED FIGHTER "A" SIDESLIP-RESPONSE COEFFICIENTS

Approach EAS 92 knots at sea level

$$\begin{aligned}\frac{1}{f_{1s}} C_{1s} &= 0.027 F_s \\ \frac{1}{f_{1s}} C_{1p} &= -0.022 + 0.896 F_s \\ \frac{1}{f_{1s}} C_{1q} &= -0.334 - 0.918 f_{1p} + F_s (1.031 + 0.918 f_{1p}) \\ \frac{1}{f_{1s}} C_{1r} &= -0.027 - 0.189 f_{1r} - 0.918 f_{1p} \\ &\quad + F_s (-0.081 + 0.189 f_{1r} + 0.918 f_{1p}) \\ \frac{1}{f_{1s}} C_{-1\theta} &= -0.189 (f_{1\theta} - f_{1\theta} F_s)\end{aligned}$$

Cruise EAS 220 knots at 5000 ft

$$\begin{aligned}\frac{1}{f_{1s}} C_{1s} &= 0.07 F_s \\ \frac{1}{f_{1s}} C_{1p} &= -0.173 + 4.69 F_s \\ \frac{1}{f_{1s}} C_{1q} &= -1.143 - 26.4 f_{1p} + F_s (11.6 + 26.4 f_{1p}) \\ \frac{1}{f_{1s}} C_{1r} &= -0.131 - 2.12 f_{1r} - 26.4 f_{1p} \\ &\quad + F_s (-0.083 + 2.12 f_{1r} + 26.4 f_{1p}) \\ \frac{1}{f_{1s}} C_{-1\theta} &= -2.12 (f_{1\theta} - f_{1\theta} F_s)\end{aligned}$$

Effect of Control-System Lags on Roll Control. In the practical case, control-system lags are not always negligible. In a preliminary analysis a first-order approximation for the lag is usually sufficient, depending upon the magnitude of the lag at the natural frequencies of the aircraft.

In operational form the simplified control-system response to an input signal is considered to be of the form

$$\delta a = \frac{1}{1 + T_1 s} \delta a_i$$

where T_1 is a time constant.

Recall the simplified roll Equation [3]

$$(s^2 - L_{\dot{\psi}} s - L_{\dot{\psi}}/U_1) \varphi = L_{\dot{\psi}} \delta a$$

Let the aileron input signal be proportional to roll error and roll rate. Then

$$\delta a_i = f_{1\varphi} (\varphi - \varphi_i) + f_{1p} \dot{\varphi}$$

Combining (neglect effect of L_r)

$$\begin{aligned}\left[s^2 + \left(\frac{1}{T} - L_p \right) s + \left(\frac{-L_{\dot{\psi}} - L_{\dot{\psi}} f_{1p}}{T} \right) \right] \varphi \\ - \frac{L_{\dot{\psi}} f_{1\varphi}}{T} \varphi = \frac{-L_{\dot{\psi}} f_{1\varphi}}{T} \varphi_i \dots [19]\end{aligned}$$

Equation [19] is of the general form

$$(s^2 + 2\zeta \omega_n s + \omega_n^2 + A_0) \varphi = A_1 \varphi_i \dots [20]$$

for which solutions have already been plotted in Fig. 5 as a function of dimensionless time.

In selecting the feedback parameters f_{ψ} and $f_{\dot{\psi}}$, it is simpler to neglect control lags and use the method described previously under "Derivation of Second and Third-Order Charts." After selecting values for f_{ψ} and $f_{\dot{\psi}}$ a check of effects of control-system lags on roll control may be made by using Equations [19] and [20] and the third-order charts. If performance is found to be unsatisfactory because of the control-system lags, then modification of f_{ψ} and $f_{\dot{\psi}}$ is necessary.

Effect of Control Lags on Yaw Damping. Consideration will now be given to damping of the motion about the yaw axis. The assumptions here are the same as in the simplified analysis of the yaw-axis equation, except that a first-order control-system lag will now be considered.

Consider the second-order yaw equation

$$(s^2 - N_{\dot{\psi}} + N_{\psi})\dot{\psi} = N_{\dot{\psi}}\delta r$$

The control-system equations are written

$$\begin{aligned}\delta r &= \frac{1}{1 + T_2 s} \delta r_i \\ \delta r_i &= f_{\dot{\psi}} r + f_{\psi}(\dot{\psi} - \dot{\psi}_i)\end{aligned}$$

where T_2 is a time constant.

Combining

$$\left[s^2 + \left(-N_{\dot{\psi}} + \frac{1}{T} \right) s^2 + \left(N_{\psi} + \frac{-N_{\dot{\psi}} - N_{\dot{\psi}} f_{\dot{\psi}}}{T} \right) + \frac{N_{\psi} - N_{\dot{\psi}} f_{\dot{\psi}}}{T} \right] \dot{\psi} = \frac{-N_{\dot{\psi}} f_{\dot{\psi}}}{T} \dot{\psi}_i, \dots [21]$$

Again, Equation [21] is of the form

$$(s^2 + 2\zeta\omega_n s + \omega_n^2 + A_0)\dot{\psi} = K A_0 \dot{\psi}_i$$

where K is a constant.

As in the case described in the analysis of control-lag effects on roll control, the third-order charts can be used to estimate the effects of control-system lags on yaw-damping characteristics. Modification of $f_{\dot{\psi}}$ may be found to be desirable.

Effect of Control-System Lags on Dynamic Co-Ordination. Examination of the terms appearing in the equations for the sideslip coefficients, Table 3, indicates that the equations can be simplified to those appearing in Table 4 by omitting relatively small terms. The general form of these simplified equations is written

$$\left. \begin{aligned}\frac{1}{f_{\dot{\psi}}} C_{1\beta} &= c_1 F_e \\ \frac{1}{f_{\dot{\psi}}} C_{1\dot{\beta}} &= a_1 + c_1 F_e \\ \frac{1}{f_{\dot{\psi}}} C_{1\beta} &= a_1 + b_1 f_{\dot{\psi}} + F_e [c_1 - b_1 f_{1\dot{\psi}}] \\ \frac{1}{f_{\dot{\psi}}} C_{1\dot{\beta}} &= a_0 + d_0 f_{\dot{\psi}} + b_1 f_{\dot{\psi}} + F_e [c_0 - b_1 f_{1\dot{\psi}} - d_0 f_{1\dot{\psi}}] \\ \frac{1}{f_{\dot{\psi}}} C_{-1\beta} &= d_0 [f_{\dot{\psi}} - f_{1\dot{\psi}} F_e]\end{aligned} \right\} \dots [22]$$

Where c_1, c_0, b_1, \dots etc., are constants. If a first-order control lag is introduced such that

$$\left. \begin{aligned}\delta a_i &= \frac{1}{1 + T_1 s} \delta a_i \\ \delta r_i &= \frac{1}{1 + T_2 s} \delta r_i\end{aligned} \right\} \dots [23]$$

and if

$$\delta a_i = (f_{1\dot{\beta}} + f_{1\dot{\psi}})\dot{\psi} + (f_{1\dot{\beta}} + f_{1\dot{\psi}})\dot{\psi} + f_{1\dot{\beta}} \dots [24a]$$

$$\delta r_i = (f_{1\dot{\beta}} + f_{1\dot{\psi}})\dot{\psi} + (f_{1\dot{\beta}} + f_{1\dot{\psi}})\dot{\psi} + f_{1\dot{\beta}} \dots [24b]$$

Then the sideslip coefficients are written

$$\left. \begin{aligned}\frac{1}{f_{\dot{\psi}}} C'_{1\dot{\beta}} &= T_1 F_e c_1 \\ \frac{1}{f_{\dot{\psi}}} C'_{1\beta} &= T_2 a_1 + F_e (c_1 + T_1 c_1) \\ \frac{1}{f_{\dot{\psi}}} C'_{1\dot{\beta}} &= a_1 + T_2 a_1 + F_e (c_1 + T_1 c_1) \\ \frac{1}{f_{\dot{\psi}}} C'_{1\beta} &= a_1 + T_2 a_1 + b_1 f_{\dot{\psi}} + F_e (c_1 + T_1 c_1 - b_1 f_{1\dot{\psi}}) \\ \frac{1}{f_{\dot{\psi}}} C'_{1\dot{\beta}} &= a_0 + d_0 f_{\dot{\psi}} + b_1 f_{\dot{\psi}} + F_e (c_0 + b_1 f_{1\dot{\psi}} - d_0 f_{1\dot{\psi}}) \\ \frac{1}{f_{\dot{\psi}}} C'_{-1\beta} &= d_0 (f_{\dot{\psi}} - f_{1\dot{\psi}} F_e)\end{aligned} \right\} \dots [25]$$

and sideslip response to an externally applied autopilot signal is written

$$\frac{\beta}{s} = \frac{C'_{1\dot{\beta}} s^2 + C'_{1\beta} s^2 + C'_{1\dot{\beta}} s + C'_{1\beta} s + C'_{1\dot{\beta}} s + C'_{-1\beta} s^{-1}}{D'_{1\dot{\beta}} s^2 + D'_{1\beta} s^2 + D'_{1\dot{\beta}} s + D'_{1\beta} s + D'_{-1\beta} s^{-1}}$$

In the general case the time constant defining lag in the aileron-control system is not necessarily equal to that for the rudder-control system. For fighter "A" these constants are considered to be equal to each other.

Again, for dynamic co-ordination $C'_{1\dot{\beta}}, C'_{1\beta}, \dots, C'_{-1\beta}$ are minimized by proper choice of autopilot feedback parameters.

Example. Presented in Table 5 are the sideslip coefficients for the fighter "A" approach condition. Included is the effect of a first-order time lag in the aileron and rudder. The time constant used is $T = 0.2$ sec. From previous considerations

$$\begin{aligned}f_{1\dot{\beta}} &= 3.0 \\ f_{1\beta} &= 1.5 \\ f_{1\dot{\psi}} &= 6.0 \\ f_{1\psi} &= 0 \\ f_{1\dot{\psi}} &= 1.75\end{aligned}$$

For this case if

$$\begin{aligned}f_{1\dot{\beta}} &= -0.157 \\ f_{1\beta} &= -0.152 \\ F_e &= 0.08\end{aligned}$$

Then

$$\begin{aligned}C'_{-1\beta} &= C'_{1\dot{\beta}} = C'_{1\beta} = C'_{1\dot{\beta}} = 0 \\ C'_{1\dot{\beta}} &= 0.0137 \\ C'_{1\beta} &= 0.000475\end{aligned}$$

The phasing of these coefficients is in such a direction that adverse yaw tendencies of the aircraft are characterized by predominantly negative values of the coefficients, or, skidding turns are character-

TABLE 5 SIMPLIFIED FIGHTER "A" SIDESLIP-RESPONSE COEFFICIENTS WITH FIRST-ORDER TIME LAG OF 0.2 SEC IN AILERON AND RUDDER-CONTROL SYSTEMS

Approach EAS 92 knots at sea level

$$\begin{aligned}\frac{1}{f_{\delta}} C'_{\delta\beta} &= 0.0054 F_s \\ \frac{1}{f_{\delta}} C'_{\delta\dot{\beta}} &= -0.0044 + 0.206 F_s \\ \frac{1}{f_{\delta}} C'_{\delta\ddot{\beta}} &= -0.088 + 1.102 F_s \\ \frac{1}{f_{\delta}} C'_{\delta\dot{r}} &= -0.339 - 0.918 f_{\dot{r}} + F_s (1.105 + 0.918 f_{\dot{r}}) \\ \frac{1}{f_{\delta}} C'_{\delta\ddot{r}} &= -0.027 - 0.189 f_{\dot{r}} - 0.918 f_{\ddot{r}} \\ &\quad + F_s (-0.081 + 0.189 f_{\dot{r}} + 0.918 f_{\ddot{r}}) \\ \frac{1}{f_{\delta}} C'_{\delta\dot{\beta}} &= -0.189 (f_{\dot{\beta}} - f_{\dot{\beta}} F_s) \\ \text{Cruise EAS 220 knots at 5000 ft} \\ \frac{1}{f_{\delta}} C'_{\delta\beta} &= 0.014 F_s \\ \frac{1}{f_{\delta}} C'_{\delta\dot{\beta}} &= -0.0346 + 1.08 F_s \\ \frac{1}{f_{\delta}} C'_{\delta\ddot{\beta}} &= -0.401 + 6.9 F_s \\ \frac{1}{f_{\delta}} C'_{\delta\dot{r}} &= -1.169 - 26.4 f_{\dot{r}} + F_s (11.6 + 26.4 f_{\dot{r}}) \\ \frac{1}{f_{\delta}} C'_{\delta\ddot{r}} &= -0.131 - 2.12 f_{\dot{r}} - 26.4 f_{\ddot{r}} \\ &\quad + F_s (-0.083 + 2.12 f_{\dot{r}} + 26.4 f_{\ddot{r}}) \\ \frac{1}{f_{\delta}} C'_{\delta\dot{\beta}} &= -2.12 (f_{\dot{\beta}} - f_{\dot{\beta}} F_s)\end{aligned}$$

ized by positive values. The positive values for $C'_{\delta\beta}$ and $C'_{\delta\dot{\beta}}$ indicate a slight skid during the initial portion of the turn entry.

Study of the sideslip coefficients indicates that adverse yaw tendencies are overcome by increasing F_s (proportion of turn-control signal to rudder), or increasing $-f_{\dot{r}}$ (negative roll-rate signal to rudder).

The introduction of control-system lags effects an increase in F_s and a change in $f_{\dot{r}}$ in a positive direction if dynamic co-ordination is to be maintained. Hence, if control lags are increased, it is necessary to increase turn-control signal to rudder and adjust roll rate to rudder in a positive direction. (The sign convention is such that negative roll rate to rudder indicates that roll rate toward the right calls for right rudder.) It is found in some cases, where $f_{\dot{r}}$ is small, that the system can be simplified by eliminating roll angle to rudder ($f_{\dot{\beta}}$) and adjusting turn-control signal and perhaps roll rate to rudder a slight amount for co-ordination. In some cases it is possible to eliminate roll-rate feedback to rudder also. A slight increase in skid during turn entries usually is not serious.

Use of Electronic Analog Computer. The electronic analog computer is a system of electronic networks arranged in such a manner that the equations defining a physical system can be solved electronically. The physical variables such as velocity, acceleration, and position are represented by voltages. It is possible on

some analog computers to achieve a one-to-one time correspondence between the computer and the physical system which it represents and to record the results graphically. Hence simulated flight-test data can be obtained.

It is advantageous to solve the complete aircraft-autopilot equations of motion including control lags on the computer after the preliminary analysis is completed. In this way the results can be checked for errors, a more intelligent approach to the problem can be conducted, and, in general, more efficient use can be made of computer time.

Consider now fighter "A" for which aerodynamic data appear in Table 1. Consider the level flight condition and neglect $Y_{\dot{\beta}}$, $Y_{\dot{r}}$, and $Y_{\ddot{r}}$. Then the equations of motion are written

$$(s - Y_{\dot{\beta}})p - g s^{-1} \dot{p} + U_1 r = Y_{\delta} \delta r \dots \dots \dots [26a]$$

$$-L_{\dot{\beta}} v + (s - L_{\dot{r}})p - L_{\dot{r}} r = L_{\delta\beta} \delta \dot{\beta} + L_{\delta r} \delta r \dots \dots [26b]$$

$$-N_{\dot{\beta}} p - N_{\dot{r}} \dot{p} + (s - N_{\dot{r}})r = N_{\delta\beta} \delta \dot{\beta} + N_{\delta r} \delta r \dots \dots [26c]$$

The autopilot signals to the aileron and rudder controls are

$$\delta a_i = f_{\dot{\beta}} \dot{\beta} + f_{\dot{r}} \dot{r} + f_{\dot{r}} p + f_{\dot{r}} r + f_{\dot{r}} \ddot{r} \dots \dots \dots [27a]$$

$$\delta r_i = f_{\dot{\beta}} \dot{\beta} + f_{\dot{r}} \dot{r} + f_{\dot{r}} p + f_{\dot{r}} r + f_{\dot{r}} \ddot{r} \dots \dots \dots [27b]$$

The responses of surface deflections to control signals are approximately

$$\delta a_i = \frac{1}{(1 + 0.2s)(1 + 0.07s + 0.008s^2)} \delta a_i \dots \dots [28a]$$

$$\delta r_i = \frac{1}{(1 + 0.2s)(1 + 0.07s + 0.008s^2)} \delta r_i \dots \dots [28b]$$

Equations [28] were estimated from sinusoidal forcing-function tests on a control system similar to that in fighter "A."

The performance of the aircraft is defined by Equations [26], [27], and [28] for given values of the control-feedback parameters. A typical solution which was recorded on the Reeves electronic analog computer appears in Fig. 6.

Scheduling of Autopilot Feedback Parameters. By analyzing each of several flight conditions, autopilot feedback parameters can be calculated for satisfactory performance of the aircraft through its range of operating conditions. Where the range of airspeeds and altitudes is great, and if a high degree of control performance is desired at each of several conditions, then it may be necessary to schedule the feedback parameters with airspeed, Mach number, and altitude.

It may be advantageous to select a most important operating condition for the aircraft for which a near optimum control-system configuration is obtained, then schedule the feedback parameters in some relatively simple manner to obtain satisfactory performance at other operating conditions. Usually roll and heading control does not suffer appreciably if the simplified scheduling is chosen skillfully; co-ordination may suffer slightly.

The condition considered to be the most important for fighter "A" autopilot was the approach condition. The cruise configuration (EAS 220 knots at 5000 ft) was chosen with an eye toward simplifying the scheduling. With the scheduling chosen, a slight skid is expected during turn entries, but this is not considered to be serious. The approach condition was of great importance because of automatic take-off and landing requirements; during cruising flight autopilot performance requirements were not quite so high in this particular case.

Scheduling of feedback parameters of course does complicate the system somewhat. However, it was felt that the improvement

in system performance was well worth the small amount of additional equipment required.

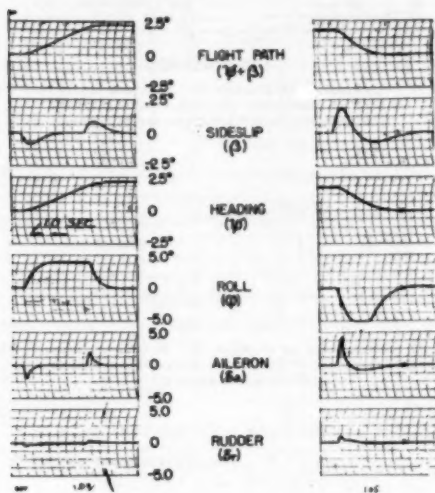


FIG. 6 TYPICAL SOLUTIONS OBTAINED ON ELECTRONIC ANALOG COMPUTER

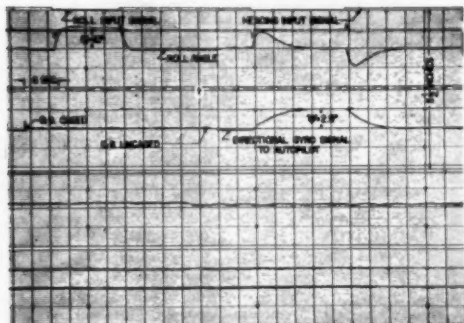


FIG. 7 TYPICAL FLIGHT-TEST RECORDING USING EIGHT-CHANNEL GRAPHIC RECORDER

Performance in Rough Air. The method derived does not consider performance of the autopilot-airplane system in turbulent air.

However, flight experience gained with autopilot configurations selected by the methods presented in this paper, indicates that satisfactory performance can be achieved during straight and level flight in rough air. This information is based to a great extent upon pilot opinion, since a concentrated study of this problem has not been made.

COMPARISON OF RESULTS OBTAINED FROM SIMPLIFIED ANALYSIS, ANALOG COMPUTER, AND FLIGHT TEST

Comparisons of results obtained by the analysis presented with those obtained by flight test appear in Figs. 8 to 14. These comparisons represent four aircraft designs—two fighters and two bombers—with flight conditions ranging from approach to high speed at high altitude. Fighter "A" and fighter "B" are fighters of conventional design. Bomber "A" is a high-speed bomber. Bomber "B" is a heavy bomber.

The small-amplitude oscillation evident at approach speeds, Figs. 9 and 12, is believed to be caused by a combination of the aircraft's poorer stability characteristics at low speeds (which is

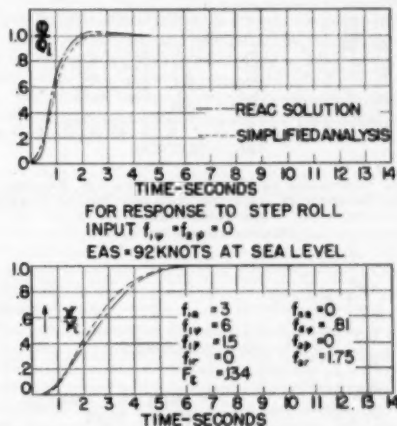


FIG. 8 COMPARISON OF FIGHTER "A" ROLL AND HEADING RESPONSES OBTAINED BY SIMPLIFIED ANALYSIS AND ANALOG COMPUTER—APPROACH CONFIGURATION

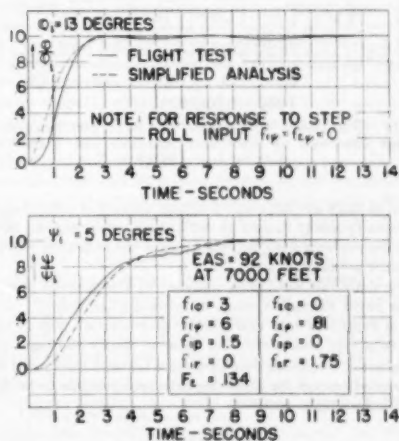


FIG. 9 COMPARISON OF FIGHTER "A" ROLL AND HEADING RESPONSES OBTAINED BY SIMPLIFIED ANALYSIS AND FLIGHT TEST—APPROACH CONFIGURATION

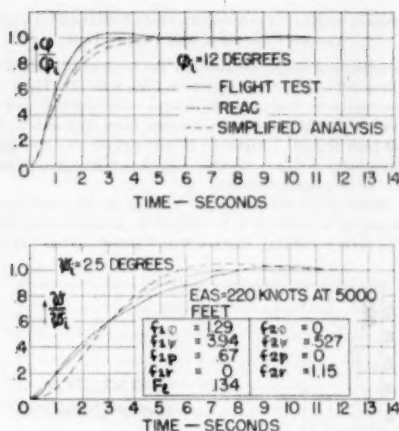


FIG. 10 COMPARISON OF FIGHTER "A" ROLL AND HEADING RESPONSES OBTAINED BY SIMPLIFIED ANALYSIS, ANALOG COMPUTER, AND FLIGHT TEST (EAS 220 knots at 5000 ft.)

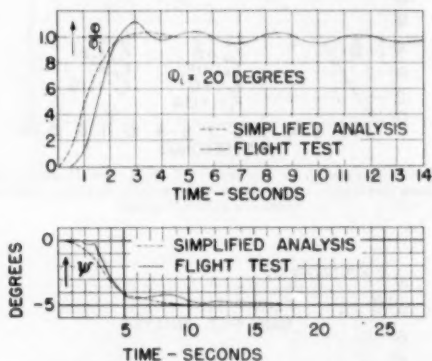


FIG. 11 COMPARISON OF BOMBER "A" ROLL AND HEADING RESPONSES OBTAINED BY SIMPLIFIED ANALYSIS AND FLIGHT TEST (EAS 390 mph at 35,000 ft.)

typical of most aircraft), and a certain amount of control-system dead spot (possibly caused by cable slack, cable friction, threshold of the yaw-rate gyro, nonlinearities in the hydraulic valve if a hydraulic actuator is used, etc.).

Several aircraft have been analyzed by the methods described in this paper through a range of operating conditions. On the basis of flight-test data available for these aircraft, Fig. 11 represents relatively poor correlation between theory and flight test.

In general, it appears that agreement between theory and flight test is good enough for control-system requirements to be determined before flight test.

CONCLUSIONS

The following conclusions have been drawn for the control system represented by the basic block diagram in Fig. 2:

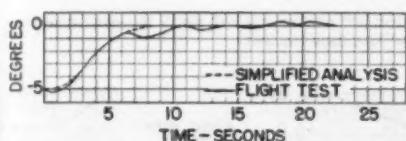


FIG. 12 COMPARISON OF BOMBER "A" HEADING RESPONSES OBTAINED BY SIMPLIFIED ANALYSIS AND FLIGHT TEST (EAS 160 mph at 10,000 ft with gear and flaps down.)

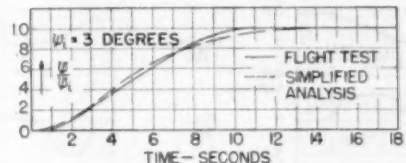


FIG. 13 COMPARISON OF BOMBER "B" ROLL AND HEADING RESPONSES OBTAINED BY SIMPLIFIED ANALYSIS AND FLIGHT TEST (EAS 170 mph at 40,000 ft.)

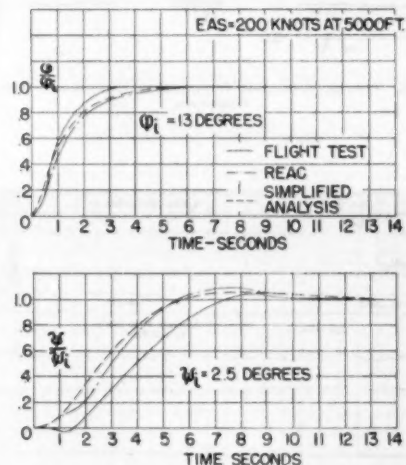


FIG. 14 COMPARISON OF FIGHTER "B" ROLL AND HEADING RESPONSES OBTAINED BY SIMPLIFIED ANALYSIS, ELECTRONIC ANALOG COMPUTER, AND FLIGHT TEST (EAS 200 knots at 5000 ft.)

The simplified analysis presented in this paper is useful in establishing control-system requirements.

The analog computer is useful in obtaining reasonably accurate simulated flight-test data.

If control lags are not excessive in the region of the aircraft natural frequencies, effects of control lags on roll control, directional control, and dynamic co-ordination can be approximated by the methods described in this paper.

By analyzing each of several flight conditions, autopilot feedback parameters can be calculated for satisfactory performance of the aircraft through its range of operating conditions. Where

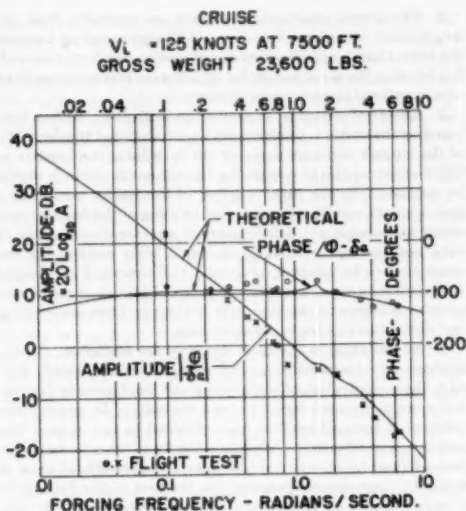


FIG. 15(a) DC-3 ROLL RESPONSE TO AILERON DEFLECTION
 (Flight test points and calculated curves.)

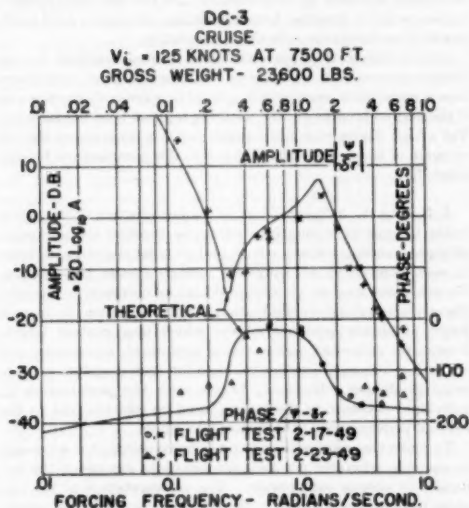


FIG. 15(b) DC-3 HEADING RESPONSE TO RUDDER DEFLECTION
 (Flight test points and calculated curves.)

the range of operating conditions is great, and if a high degree of control performance is desired through the range of operating conditions, then it is necessary to schedule the feedback parameters with airspeed, Mach number, and altitude.

Discussion

W. BOLLAY.⁶ The results presented in the paper represent an interesting addition to the currently available data on dynamic performance of aircraft. The correlation obtained between the results of the flight tests and the simplified dynamic analysis indicate that the simple theory gives a good first approximation. For more complicated problems the analog-computer technique used by the author is probably the most useful tool.

When an analog computer is not available a new method of analysis developed by W. R. Evans⁷ has proved to be very convenient even for relatively complicated systems of equations. This method, called the "root-locus" method, is a graphical one which permits the step-by-step calculation of the dynamic performance of a system. It starts with the simplified equations used by the author, and then computes successive approximations by introducing more and more of the coupling terms, time delays, and so forth, which were omitted in the first approximation. This method has the great practical advantage that it develops in the engineer a good feeling for the relative importance of these various secondary terms in the equations.

B. G. BROMBERG.⁸ The problem of providing automatic flight control, especially for the lateral modes of motion, is a particularly intricate one and one of current necessity. This paper indicates and substantiates means of obtaining first-order performance effects of the combination of airframe and automatic controls. As such, the paper is indeed welcome in that it is another accounting of a rather elaborate mathematical analysis substantiated by actual flight tests.

The author approaches the analysis of his automatic control problem from the so-called classical method of analysis, i.e., the solution of the pertinent differential equations of motion. By simplifying these equations by ignoring one or two degrees of freedom of the airframe and idealizing the control system, the mathematics becomes amenable to manual solution. To obtain a somewhat more rigorous solution, the author describes an electronic-analog procedure wherein the three degrees of freedom of the airframe are considered, and wherein the time lag of the control system is idealized as a cascaded system of a pure second-order system and a simple first-order time delay. Comparison of the simplified analysis, analog studies, and flight test shows that a fair correlation among the three methods is obtained. The most serious discrepancy is that neither the simplified analysis nor the analog studies were able to indicate the small, rather high-frequency residual oscillation which proves so bothersome to aircraft inhabitants, to fire-control apparatus, and to target-tracking radars.

The analysis and synthesis of automatic flight control for conventional aircraft and for guided missiles carried out under the direction of the writer differs significantly from the approach used by the author, and therefore a general comparison of these methods may serve a useful purpose. The general approach to the automatic control problem used by the writer is that of the servomechanism engineer. The system is delineated in block-diagram form and suitable transfer functions are assigned to the various blocks. The transfer functions can appear in the form of idealized equations or in the form of experimentally derived frequency-response curves. The frequency response of the entire

⁶ Address: 17411 Posetano Road, Pacific Palisades, Calif.

⁷ "Graphical Analysis of Control Systems," by W. R. Evans, Trans. AIEE, vol. 67, 1948, pp. 547-551.

⁸ "Aerodynamic Stability and Automatic Control," by William Bollay (1950 Wright Brother Lecture), *Journal of Aeronautical Sciences*, vol. 18, September, 1951, pp. 569-617.

⁹ Missile Chief Engineer, Missile Engineering Division, McDonnell Aircraft Corporation, St. Louis, Mo.

system can then be obtained by cascading the various functions numerically according to the algebra of closed loops. The overall response of the system can then be deduced from the frequency response or the related Nyquist diagrams; or if desired, the frequency response can be converted directly⁹ to the response to some standard test input such as a step function, pulse function, or ramp function.

It is felt that a number of advantages exist in the use of the servomechanism technique as contrasted to the classical means of solution. The number of degrees of freedom that can be handled by the servomechanism approach is practically unlimited without the addition of severe complications, and this method is as accurate as the classical method. Further, a physical feel of the effects of each component in the loop is obtained, as compared to interpretation of the algebraic characteristic equation which contains the parameters of each component of the loop combined in a seemingly indiscriminate manner. The effect of varying the value of a parameter, so important in the synthesis problem, requires obtaining a completely new solution of the characteristic equation before the change in performance can be seen.

In the light of the writer's recent experience, the basic assumptions made by the author and most other workers in the field of automatic flight control will be discussed. These assumptions are as follows:

1 Aircraft motions are represented by linearized differential equations. The calculation of airframe motions is based on an extension of the theory of dynamical stability studies originated around 1900 by Lanchester and first published in the form generally used at the present time by Bryan in 1911. There is little doubt as to the validity of the theoretical basis for the stability calculations. Although theoretically the calculations apply only to vanishingly small motions, the linear laws of aerodynamic reactions as a function of airplane motion do yield a fairly good approximation for airframe motion associated with ordinary maneuvers. However, the accuracy involved in computing the motion of an airframe is admittedly approximate, owing to the difficulty in determining the numerical values of the stability derivatives. Several of the derivatives such as $L_{\dot{u}}$, $N_{\dot{u}}$, $L_{\dot{w}}$, $L_{\dot{p}}$, $N_{\dot{p}}$, $N_{\dot{r}}$ can be found from wind-tunnel tests. However, some of these derivatives are quite susceptible to compressibility effects, and corrections for Mach number must be included. Other derivatives such as L_p , L_r , N_p , N_r require special tests—and in most cases are never determined experimentally by wind-tunnel tests. Some derivatives are affected seriously by propeller effects and there are not enough generalized data available which yield reasonable accuracy in computing motion of airplanes with propeller power.

It has been found necessary by the writer's company to establish the actual characteristics of the airframe by flight test, especially for those flight regimes near the critical Mach number. These tests involve applying pulse functions of a predetermined magnitude to the rudder and recording the resulting airframe motion. By back-figuring through the use of the linear equations of motion and the measured responses, the important stability derivatives can be determined. Of course the stability derivatives and differential equations of motion so used are bound together by the measured response and hence can produce accurate results for computations in connection with automatic controls. This procedure is required, however, only when accurate control response is required. When coarse results are desired, the stability derivatives as derived by competent aerodynamicists are usually satisfactory.

2 The lateral equations of motion are separable from the longitudinal equations of motion. Although coupling between the lateral and longitudinal modes of motion has been observed, it is felt that the use of uncoupled equations of motion for analysis of conventional airplanes is satisfactory.

3 Effects of structure dynamics are negligible. It has been found by the writer's company and elsewhere¹⁰ that the flexibility of the aircraft structure is important in defining the location in which the components comprising the automatic controls should be installed. In one case, coupling of the rudder motion to a gyro with the resulting bending and twisting of the fuselage produced high-frequency, lightly damped structural oscillations of wing and fuselage. Although the rigid body motion was not considered to be affected adversely, the structural oscillations were definitely unacceptable. Methods of including elastic and aeroelastic effects on the automatic control problem are evolving and should be available in the near future.

4 Nonlinearities in the control system are negligible. In the applications of automatic control to airplanes and guided missiles, the consideration of nonlinearity and dead spots in the control system has been found to be a necessity. In general, the solution of the problem has been obtained in two steps. The first is a manual solution wherein a family of transfer functions derived from laboratory tests for various amplitudes of input is utilized. Considerable judgment on the part of the dynamicist is required in order to obtain a realistic solution, for it is very easy to declare a system unstable on the basis of an improper choice or linearization of the control-transfer function, when flight tests later will indicate stability. The second step in the solution is to utilize an analog computer in which the airframe is simulated, but as much of the actual control system as practicable is utilized as inputs to the computer. In this way such nonlinearities as speed limiting, torque limiting, saturation, dead spots, actual time delays are considered accurately.

In conclusion, it appears that the methods outlined by the author are useful in establishing the broad range of control-system requirements, especially if control lags are not excessive and if the desired accuracy of the resulting solution need not be exact. For a high degree of control performance it is necessary that all or some of the considerations given in this commentary be considered.

J. B. REA.¹¹ As pointed out in the introduction of the paper, it has become increasingly important to consider the autopilot-airplane combination as a whole, and to tailor the characteristics of each component for optimum over-all system performance. From an even broader viewpoint, it may be necessary to consider the airplane-autopilot combination as only an element in an even larger automatic guidance system which may contain target-interceptor geometry, radar-sensing equipment, computers, and so forth. The optimization problem for such a system can become prodigious. However, in all cases the performance of individual elements in the system must be subordinated to the over-all performance of the system as a whole.

To make the solution of such problems possible, it is necessary to simplify, wherever possible, the equations describing the dynamics of system components. The representation of the airplane itself as a component in the system by simplified equations has long been a matter of conjecture, since until recently reliable test data have not been available to compare with analytical results. The recent dynamic flight test work on a DC-3 airplane, cited by the author, has been a step forward in clarifying the

⁹ "Application of the Performance Operation to Aircraft Automatic Control," by R. C. Seamans, Jr., B. G. Bromberg, and L. E. Payne, *Journal of Aeronautical Sciences*, vol. 15, September, 1948, pp. 535-555.

¹⁰ "Investigation of Lateral Dynamic Stability in the XB-47 Airplane," by R. J. White, *Institute of Aeronautical Sciences*, Preprint No. 241.

¹¹ President, J. B. Rea Company, Inc., Los Angeles, Calif.

questions of validity which have so long clouded the analytical approach to aircraft dynamics.

Recent developments in the application of servomechanism techniques and matrix methods to the analysis of aircraft systems, having large numbers of degrees of freedom, also have provided important contributions to the solution of these increasingly complex problems. Such methods have become particularly useful in the analysis of aeroelastic aircraft, where many additional degrees of freedom may be introduced by elastic deformation of components. Further, the analysis of aeroelastic aircraft has brought forth the requirement for extensive application of nonstationary aerodynamics to the problem of control-systems studies. Thus it can be seen that the development of a complete system for automatic control of aircraft cannot be performed satisfactorily by a group of unrelated people, but must be the combined, co-ordinated effort of a group of specialists, each of whom is cognizant of the influence of his particular phase of development on the system performance as a whole.

It is particularly interesting to note the comments of the author regarding the necessity of changing autopilot parameters during flight to obtain optimum performance for all operating conditions. This requirement becomes increasingly important with the advent of airplanes that have extremely wide ranges of operating conditions of speed and altitude, and becomes almost mandatory in cases where the aircraft is required to operate at both subsonic and supersonic speeds.

C. L. SEACORD, JR.¹³ It is in the practical application of the second and third-order approximation for airplane response that the only word of criticism to this paper is offered. The characteristics of many newly designed aircraft are such that appreciable deviations will occur between the exact and approximate airplane responses. It is probable that, while these deviations might not affect seriously the time constants of the composite airplane, they could cause appreciable errors in the stability of the airplane-autopilot combination. If the use of such approximations is limited, as the author suggests, to the estimation of approximate autopilot settings which are used as a starting point for more exact solutions, the errors are not important. It is doubtful, however, that the making of such approximations will result in any appreciable saving of time when an electronic differential analyzer is to be used to obtain the final solution.

The use of the transient approach to the solution of the airplane automatic-stabilization problem is particularly significant in that it appears to offer definite advantages over the present popular frequency-response techniques. It is true that most of these advantages depend for their existence upon the availability of a good electronic differential analyzer, but the number of such analyzers in use and being offered for sale indicates that they will be available in sufficient quantity to make transient analyses quite practical. The foregoing advantages of the transient method resolves themselves into, (a) more exact solutions, (b) a large saving in man-hours, and (c) a more easily interpreted result.

The increased accuracies accrue chiefly from the ability to include nonlinearities, such as control surface deflection limits, dead spots, and variable aerodynamic quantities. There also are certain cases in which the system equations themselves become inherently nonlinear. None of the currently well-known frequency-response methods offers simple means of handling such items.

The time-saving feature of the transient method results entirely from the use of electronic differential analyzers, and is apparent even when digital computers are used to calculate frequency-response functions.

¹³ Project Aerophysics Engineer, Consolidated Vultee Aircraft Corporation, Fort Worth, Texas.

In the matter of interpretation of results, the advantages of the transient method stem from the type of maneuvers usually desired when an autopilot is used to control an airplane. The airplane is expected to stay on a given heading until a command signal to change heading is introduced and then to establish the new heading as quickly as possible with the maneuvering limitation of the airplane. This definitely involves a transient occurring between two steady-state conditions, and the exact behavior of all variables may be noted from the record of the differential-analyzer solution.

The wide use of any engineering method depends of course upon the existence of a body of practical, well-written literature on the subject. This paper is an excellent example of the type, and it is hoped that others on different applications of the transient analysis of dynamic systems will follow.

R. J. WHITE.¹⁴ The aerodynamicist and servomechanism engineer are slowly but surely beginning to understand each other. This paper is a welcome contribution in this direction, as he has reduced the directional control problem to fundamental equations, void of log-decibel plots and Nyquist diagrams which the aerodynamicist, in general, does not take time to understand.

The introduction mentions work done in comparing calculated airplane response with that measured in flight. Fine work along this line has been done by the Minneapolis-Honeywell Company and others, all indicating that the calculated airplane stability coefficients based upon fundamental aerodynamics is good enough. The consideration of nonstationary aerodynamic effects when calculating stability coefficients is believed to be purely academic in most cases.¹⁵ One problem with which the writer's company has been concerned is that of how to represent the airplane response when aeroelastic effects become important. Here the calculated stability coefficients are more accurate than the assumptions that must be made regarding the elastic behavior of the airplane. In this case extra degrees of freedom of the airplane must be added to the present stability equations, making necessary the use of analog computing machines.

The author refers to the necessity of tailoring the autopilot to fit the airplane. This process also has been referred to as marrying the airplane and autopilot, which is probably correct, as any incompatibility must be worked out properly if the airplane is to fly successfully on the autopilot.

In analyzing the lateral control problem the author has certainly simplified the airplane equations of motion in going from Equations [1] to [3]. This has been done by neglecting the effects of side slip and specifying a co-ordinated turn. Equation [3b] specifies the co-ordinated turn and gives a definite relation between the yaw ψ and roll ϕ . It should be pointed out that the author has the choice of using either the yaw Equation [1c], or the roll Equation [1b], which actually is used to define the motion. Had the yaw Equation [1c] been used, then all of the specified constants of the simple solution would involve the N_{ζ} coefficients instead of the L_{ζ} coefficients. This is mentioned because at first glance one wonders what happened to the yawing-moment coefficients. The choice of using the roll equation is believed to be based upon a physical reason which points out a feature that some people do not realize, which is that the aileron control is more important in making a heading change than the rudder. Here the time required for the autopilot to respond to a heading change depends upon how fast the airplane may be rolled into, and out of the turn. Neglecting the yawing-moment equation in the simple analysis implies that the autopilot must operate the

¹³ Aerodynamicist, Boeing Airplane Company, Seattle, Wash.

¹⁴ "Dynamic Stability at High Speeds From Unsteady Flow Theory," by I. C. Statler, *Journal of Aeronautical Sciences*, vol. 17, April, 1950, pp. 232-242 and 255.

rudder to keep the yawing moments zero. If it is assumed that the aileron motion has only a small influence on the airplane yaw, then for a co-ordinated turn Equation [1c] indicates that the roll circuit of the autopilot must give a displacement and rate correction to the rudder specified by

$$f_{\phi} = \frac{-N_{\phi}}{N_{\phi}U_1}, \quad f_{\dot{\phi}} = \frac{-N_{\dot{\phi}}}{N_{\phi}} + \frac{g}{N_{\phi}U_1}$$

In discussing the yaw requirements the author indicates that the equation for the single degree of freedom in yaw given by Equation [13] is a good approximation to the exact solution, because of the agreement shown in Fig. 3 of the paper. This may be so, in so far as adjusting the autopilot; however, from the airplane standpoint the resonant peak in Fig. 3(b), determines the airplane stability. For example, using the stability coefficients of Table 2, fighter A requires 31 sec to damp to one-half amplitude. This is unsatisfactory for the airplane when the autopilot is not used. Equation [13] indicates that fighter A requires only 10 sec to damp to one-half amplitude, which is certainly a lot different. If it is desired to represent the airplane yawing motion by a second-order equation, it is suggested that the quartic lateral stability equation first be factored into two quadratic equations and modified values of N_{ϕ} and $N_{\dot{\phi}}$ be found and substituted in Equation [13]. This method has been used successfully by the British.¹³

In discussing the requirements for dynamic co-ordination of the autopilot, the author suggests that the numerator coefficients of Equation [18] be minimized. The method for minimizing these coefficients has not been explained sufficiently. The method implied, however, may be a cut-and-try problem that must be worked out for a particular installation.

The author points out that the setting for one flight condition may not be desirable for another condition. This problem also depends upon the type of flight controls used on the airplane. Certain modern high-speed airplanes require control-surface movements to improve their stability prior to using the autopilot. An example of this is the electronic yaw damper used in the Boeing B-47 airplane. This was developed jointly by Boeing and Minneapolis-Honeywell Company and operates only while the autopilot is off. Recent studies for another airplane indicate that a mechanical-type yaw damper, forming part of the control system, is possible. This when used with the autopilot is expected to improve the autopilot operation.

It is felt that the present paper gives to the aerodynamicist an idea of how the servomechanism engineer attempts to fit an autopilot to the lateral control system of an airplane.

AUTHOR'S CLOSURE

In reading through the discussions there appears to be a dif-

ference of opinion about the relative merits of the so-called classical method preferred to some extent by the aeronautical engineer, and the use of log-decibel plots and Nyquist diagrams preferred by most servomechanism engineers. This author belongs to that group of aeronautical engineers who have been exposed to the thinking of the servomechanism engineer and his log-decibel and Nyquist diagrams.

The author's philosophy in the use of the various methods is to use that method which is simplest and yet adequate. In the case of automatic flight control the simplified methods described in the paper appear adequate in selecting a preliminary autopilot configuration; the procedure is quite straightforward and can be applied by most aeronautical engineers. Extension can be made to cases where lagged turn-control signals are used or where cross-feeds of various types from the aileron surface deflection to the rudder-control system are used.

In the autopilot considered in the paper there were approximately eight autopilot feedback parameters. To determine these parameters by trial-and-error-methods such as may be necessary on the analog computer or by use of the frequency response or the root-locus methods would be relatively difficult. It is felt that the simplified method has merit in that autopilot requirements for co-ordination can be determined with relative ease. Of course, in order to obtain more accurately the system-response characteristics one should reconsider the assumptions made in the analysis and apply one or more of the methods suggested by the discussers. If the results obtained are at great variance with each other it is possible that some error exists in the calculations or that the assumptions made are not valid.

In answer to Mr. White's comment on achieving co-ordination, it has been found desirable to reduce to zero the coefficients in the following manner (see Table 4):

Select F_{ϕ} such that $C_{1\phi} = 0$.

Having selected F_{ϕ} , and since $f_{\dot{\phi}}$ has already been selected on the basis of roll-performance requirements, determine f_{ϕ} such that $C_{1\phi} = 0$.

In the case of $C_{1\phi}$, $f_{\dot{\phi}}$ is normally assumed zero; f_{ϕ} has already been determined from yaw damping requirements; $f_{\dot{\phi}}$ has already been determined from roll-performance requirements; F_{ϕ} was determined above. This leaves f_{ϕ} for minimizing $C_{1\phi}$.

For minimizing $C_{1\phi}$, $f_{\phi}/f_{\dot{\phi}} = F_{\phi}$.

It is evident that $C_{1\phi} \neq 0$. However, in the cases considered by the author this has been found to have relatively little effect.

When a first-order control lag is considered (see Table 5) it is usually desirable to follow the procedure mentioned above and reduce $C_{1\phi}$, $C_{1\phi}'$, $C_{1\phi}''$, and $C_{1\phi}'''$ to zero. In this case $C_{1\phi}'$ and $C_{1\phi}''$ are not zero, but usually are small enough to have little over-all effect.

The author wishes to thank the discussers, Messrs. Bollay, Bromberg, Res, Seacord, and White for their interesting and constructive comments.

¹³ "A Simplified Theory of the Lateral Oscillations of an Aircraft With Rudder Free, Including the Effect of Friction in the Control System," by S. Neumark, British R & M 2259, 1948.





AN ASME PAPER

Its Preparation, Submission and Publication, and Presentation

To a large degree the papers prepared and presented under the ASME sponsorship are evidence by which its professional standing and leadership are judged. It follows, therefore, that to qualify for ASME sponsorship, a paper must not only present suitable subject matter, but it must be well written and conform to recognized standards of good English and literary style.

The pamphlet on "AN ASME PAPER" is designed to aid authors in meeting these requirements and to acquaint them with rules of the Society relating to the preparation and submission of manuscripts and accompanying illustrations. It also includes suggestions for the presentation of papers before Society meetings.

CONTENTS

PREPARATION OF A PAPER—

General Information—Style, Preferred Spelling, Length Limitation, Approvals and Clearance.

Contents of the Paper—Title, Author's Name, Abstract, Body of Paper, Appendixes, Acknowledgments, Bibliographies, Tables, Captions, Photographs, Other Illustrations.

Writing the Paper—Outline Tabulations, Tables, Graphs, Charts for Computation, Drawings, Mathematics, Accuracy, Headings and Numbering, Lantern Slides, Motion Pictures, Typing, Number of Copies.

SUBMISSION AND PUBLICATION OF A PAPER—

Intention to Submit Paper Required in Advance, Meeting Dates, Due Dates for Manuscript, Discussers, Review and Acceptance, Proceeds, Advance Copies and Reprints, Discussion and Closure, Publication by Others.

PRESENTATION OF A PAPER—

Time Limit, Addressing Your Audience, Public Address Systems, Use of Slides.

REFERENCES—

References on Writing and Speaking, Engineering Standards.

Price 40¢. No discount allowed. A remittance must accompany all orders for \$5.00 or less. U. S. Postage Stamps are acceptable.

THE AMERICAN SOCIETY OF MECHANICAL ENGINEERS
29 West 39th Street, New York 18, N. Y.

The MAGAZINE

experts consult for an expert
appraisal of world literature
in applied mechanics
and related fields

THEY READ EVERY ISSUE FOR THE FOLLOWING REASONS:

Applied Mechanics Reviews offers the only practical way of keeping well informed.

Applied Mechanics Reviews is unsurpassed for accuracy and impartiality.

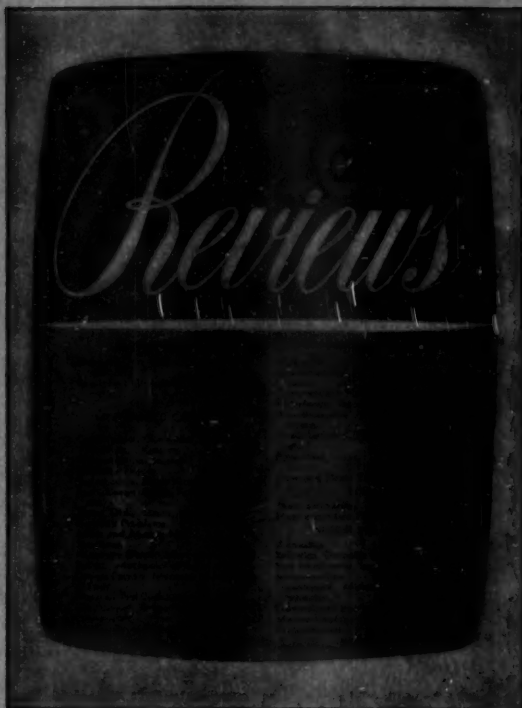
Applied Mechanics Reviews enables them to critically survey, within a relatively short time, the important literature contained in 525 engineering and scientific journals, in new books and in reports of research programs of 28 countries.

Applied Mechanics Reviews is prepared by well-known engineers and scientists who have been chosen for their knowledge of the subjects involved.

Applied Mechanics Reviews contains more information than they can get anywhere else.

Applied Mechanics Reviews is inexpensive—less than 3¢ a day for a world-wide reviewing service that costs thousands of dollars to produce.

**FILL IN AND MAIL
THIS COUPON TODAY**



In whatever branch of the field you are **APPLIED MECHANICS REVIEWS** can serve you. Every issue brings you 300 appraisals of the best articles and books in current applied mechanics literature, all written concisely for fast reading and grouped under 36 classifications for ready reference. Each issue also surveys progress in a particular field, summarizes the important factors responsible for advances therein, interprets developments, and assesses their prospects.

So that you may see for yourself how easy it is to have the broadest grasp of developments and progress in the whole field with the help of **APPLIED MECHANICS REVIEWS** the next seven issues are being made available to you at a special introductory price of \$4.50. Arrange to send for them. You will be glad you did.

Amer. Soc. Mech. Engrs.
29 W. 39 St., New York 18, N. Y.

Date.....

You may send me the next seven issues of **APPLIED MECHANICS REVIEWS** at the special introductory rate of \$4.50.

..... My check is enclosed. \$60 mo.

Name.....

Address.....

City..... Zone..... State.....